17 December 2010 | $10

Science

INSIGHTS OF THE DECADE

& Breakthrough of the Year

AAAS

SPECIAL SECTION

Insights of the Decade

page 1597

CONTENTS continued >>

COVER

In the first decade of the millennium, rapid progress has transformed whole areas of research (see the Insights of the Decade section on page 1612). Meanwhile, the Breakthrough of the Year goes to the first mechanical devices to reach the quantum ground state, a feat achieved by physicists at the University of California, Santa Barbara (see the Breakthrough section on page 1604). Also see related online content at www.sciencemag.org/special/insights2010/.

***Credit: Yael Fitzpatrick and Matthew Twombly*/Science**

DEPARTMENTS

Published by AAAS

REPORTS

CONTENTS continued >>

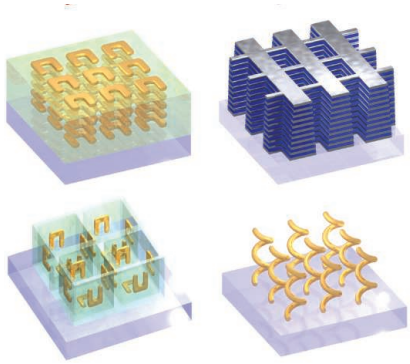

page 1633

pages 1636 & 1663

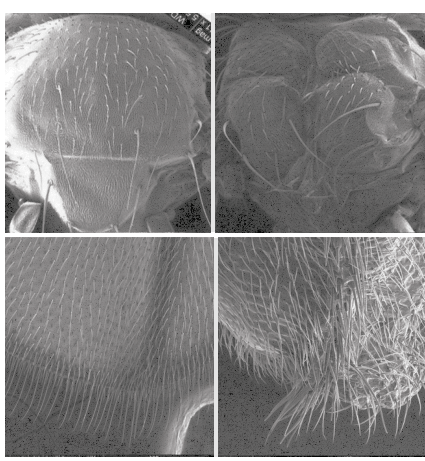

page 1682

Published by AAAS

SCIENCEONLINE

SCIENCEXPRESS
www.sciencexpress.org

Quantitative Analysis of Culture Using Millions of Digitized Books
J.-B. Michel et al.
Linguistic and cultural changes are revealed through the analyses of words appearing in books.
10.1126/science.1199644
>> News story p. 1600

The Genetic Landscape of the Childhood Cancer Medulloblastoma
D. Williams Parsons et al.
Genomic analysis of a childhood cancer reveals markedly fewer mutations than what is typically seen in adult cancers.
10.1126/science.1198056

Structure of DNMT1-DNA Complex Reveals a Role for Autoinhibition in Maintenance DNA Methylation
J. Song et al.
The eukaryote maintenance DNA methyltransferase discriminates against de novo CpG methylation sites.
10.1126/science.1195380

Passive Origins of Stomatal Control in Vascular Plants
T. J. Brodribb and S. A. M. McAdam
The transition from passive to active metabolic control of stomata and plant water balance occurred about 360 million years ago.
10.1126/science.1197985

Time-Resolved Holography with Photoelectrons
Y. Huismans et al.
The intefererence pattern produced by photoelectrons provides holographic snapshots of the photoionization process.
10.1126/science.1198450

TECHNICALCOMMENTS

Comment on "The Incidence of Fire in Amazonian Forests with Implications for REDD"
J. K. Balch et al.
Full text at www.sciencemag.org/cgi/content/full/330/6011/1627-b

Response to Comment on "The Incidence of Fire in Amazonian Forests with Implications for REDD"
L. E. O. C. Aragão and Y. E. Shimabukuro
Full text at www.sciencemag.org/cgi/content/full/330/6011/1627-c

SCIENCENOW
www.sciencenow.org
Highlights From Our Daily News Coverage

Cosmic Radiation Features Could Suggest Our Universe Is Not Alone
Data may provide evidence of a 'multiverse.'

Sperm May Hold Cure for Diabetes
Researchers grow insulin-producing cells from sperm stem cell precursors.

Violent Origin for Saturn's Rings
New study may have solved a centuries-old mystery.

SCIENCESIGNALING
www.sciencesignaling.org
The Signal Transduction Knowledge Environment

RESEARCH ARTICLE: A Conceptual Molecular Network for Chemotactic Behaviors Characterized by Feedback of Molecules Cycling Between the Membrane and the Cytosol
M. Otsuji et al.
Simulations and observations of migrating cells suggest a model for feedback loops that regulate chemotaxis.

PERSPECTIVE: Aspasing Out Metacaspases and Caspases—Proteases of Many Trades
P. V. Bozhkov et al.
The substrates of the metacaspase type of proteases are beginning to be identified.

PERSPECTIVE: Myc-Nick—The Force Behind c-Myc
K. Mousavi and V. Sartorelli
A cytoplasmic form of c-Myc promotes microtubule stability and cell differentiation.

REVIEW: INTERSECTINg Pathways in Cell Biology
J. P. O'Bryan
The intersectin family of scaffolding proteins links signaling and endocytic pathways.

SCIENCECAREERS
www.sciencecareers.org/career_magazine
Free Career Resources for Scientists

Breakthrough of the Year: Bridging the Quantum and the Classical Worlds
E. Pain
Ph.D. student Aaron O'Connell was able to induce and measure quantum effects in the motion of a micrometer-sized mechanical oscillator.
>> Breakthrough of the Year section p. 1604 and www.sciencemag.org/special/insights2010/

Engineering Solutions to Biomedical Problems
N. Volkers
There are many ways for classically trained engineers to work at the interface of engineering and medicine.

Tooling Up: Little 'r,' Big 'D'
D. Jensen
If you want to work in industry in this economy, tweak your CV to emphasize the 'development' side of R&D.

SCIENCETRANSLATIONAL MEDICINE
www.sciencetranslationalmedicine.org
Integrating Medicine and Science

RESEARCH ARTICLE: Genetic Correction of PSA Values Using Sequence Variants Associated with PSA Levels
J. Gudmundsson et al.

PERSPECTIVE: Personalized Prostate Cancer Screening—Improving PSA Tests with Genomic Information
J. S. Witte
Sequence variants in the human genome are associated with serum levels of prostate-specific antigen.
>> News story p. 1602

RESEARCH ARTICLE: Frequent and Focal *FGFR1* Amplification Associates with Therapeutically Tractable FGFR1 Dependency in Squamous Cell Lung Cancer
J. Weiss et al.

PERSPECTIVE: A Therapeutic Target for Smoking-Associated Lung Cancer
N. C. Turner and M. J. Seckl
A new oncogenic aberration in smoking-associated lung cancer may be the disease's first relatively high-frequency therapeutic target.

SCIENCEPODCAST
www.sciencemag.org/multimedia/podcast
Free Weekly Show

Download the 17 December *Science* Podcast to hear about the top scientific breakthrough of 2010 and some of the big ideas of the past decade.

VIDEOFEATURE
video.sciencemag.org

Breakthrough of the Year 2010: The First Quantum Machine
A video introduction to the top scientific achievement of 2010: putting a humanmade object into its quantum ground state.
>> Breakthrough of the Year section p. 1604; Insights of the Decade section p. 1612; and www.sciencemag.org/special/insights2010/

SCIENCEINSIDER
news.sciencemag.org/scienceinsider
Science Policy News and Analysis

SCIENCE (ISSN 0036-8075) is published weekly on Friday, except the last week in December, by the American Association for the Advancement of Science, 1200 New York Avenue, NW, Washington, DC 20005. Periodicals Mail postage (publication No. 484460) paid at Washington, DC, and additional mailing offices. The title SCIENCE is a registered trademark of the AAAS. Domestic individual membership and subscription (51 issues): $146 ($74 allocated to subscription). Domestic institutional subscription (51 issues): $910; Foreign postage extra: Mexico, Caribbean (surface mail) $55; other countries (air assist delivery) $85. First class, airmail, student, and emeritus rates on request. Canadian rates with GST available upon request, GST #1254 88122. Publications Mail Agreement Number 1069624. **Printed in the U.S.A.**

Change of address: Allow 4 weeks, giving old and new addresses and 8-digit account number. **Postmaster:** Send change of address to AAAS, P.O. Box 96178, Washington, DC 20090–6178. **Single-copy sales:** $10.00 current issue, $15.00 back issue prepaid includes surface postage; bulk rates on request. The identification code for *Science* is 0036-8075. *Science* is indexed in the *Reader's Guide to Periodical Literature* and in several specialized indexes.

AAAS
ADVANCING SCIENCE, SERVING SOCIETY

Published by AAAS

<< Size Matters

Animals regulate their growth so that all organs are mutually proportional, even when growth occurs at different times. However, the mechanism by which this occurs is unknown. **Nijhout and Grunert** (p. 1693, published online 25 November) performed an analysis of relative wing growth in the tobacco hornworm, *Manduca*. Animals that were small owing to starvation had smaller wings, due to their slower growth rate, and they also stopped growing earlier than large, well-fed larvae. The insect hormone ecdysone was implicated in the process that governs this scaling relationship between adult wings and body size.

Unlikely Planet

Most known extrasolar planets orbit stars similar to the Sun. Very few planets have been detected around metal-poor stars whose abundances of elements other than hydrogen and helium are much lower than those of the Sun, or around stars that are at a late stage in their evolution. **Setiawan *et al.*** (p. 1642, published online 18 November) report the detection of a close-in giant planet around a metal-poor star belonging to a group of stars that formed in a satellite galaxy of the Milky Way. The star has gone past the red giant phase of stellar evolution, when stars like the Sun expand up to many times their original size, and so it is unclear why the planet was not engulfed by the star as it expanded.

Spin Control

Controlling and manipulating the spin of an electron is a central requirement for applications in spintronics. Some of the challenges researchers are facing include efficient creation of spin currents, minimization of Joule heating, and extending the lifetime of electronic spins, which is especially important for quantum information applications. **Costache and Valenzuela** (p. 1645) address the first challenge by designing and fabricating an efficient and simple superconducting-based single-electron transistor that can produce spin current with controlled flow. Key to the design is asymmetric tunneling, which leads to a ratchet effect (or diode-like behavior), allowing the separation of up and down spins. **Jonietz *et al.*** (p. 1648) use electric currents five orders of magnitude smaller than those used previously in nanostructures to manipulate magnetization in a bulk material, MnSi, pointing the way toward decreased Joule heating in spintronic devices. This so-called spin-torque effect causes the rotation of the skyrmion lattice of spins, characteristic of MnSi, which is detected by neutron scattering. Finally, **McCamey *et al.*** (p. 1652) extend the short lifetime of an electronic spin of a phosphorous dopant by mapping it onto the much longer lived nuclear spin of the atom. Mapping the nuclear spin back onto the electronic spin allows production of a spin memory with a storage time exceeding 100s, which should prove useful for future practical applications.

Better Imaging When Separated

A fluorescent probe works better if its absorption and emission wavelengths are well separated; otherwise, the probe tends to reabsorb its own emission. **Ghosh *et al.*** (p. 1656, published online 25 November) found that oxygen doping of semiconducting single-wall carbon nanotubes (SWCNTs) improved the characteristics of these materials as imaging probes in the near-infrared. Exposure of SWCNTs to ozone and then to visible light caused the emission wavelength to be 10 to 15% longer than the absorption wavelength. They imaged these probes and untreated SWCNTs in cultured human cells and found an ~20-fold improvement in contrast.

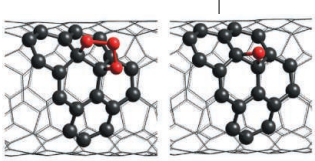

Metabolism Without Modification

Obesity-associated metabolic disease has rapidly become a public health priority in the developed world and is being addressed through prevention strategies aimed at lifestyle changes and through pharmacological approaches. **Barnett *et al.*** (p. 1689, published online 18 November) designed a drug that inhibits the action of ghrelin, a circulating peptide hormone that increases fat mass and food intake. The drug, a bisubstrate analog called GO-CoA-Tat, is a selective antagonist of ghrelin O-acyltransferase (GOAT), an enzyme that catalyzes a posttranslational modification that is essential for ghrelin activity. Injection of GO-CoA-Tat into wild-type mice on a high-fat diet improved glucose tolerance and reduced weight gain, probably through changes in metabolic activity. Because GO-CoA-Tat is a peptide-based drug that requires repeated injection, it is unsuitable for clinical use, but GOAT does represent a potentially valuable target for future drug development efforts in metabolic disease.

Burn, Baby, Burn

The atmospheric trace gas, carbon monoxide, has important effects on methane and on ozone, and is important both in atmospheric chemistry and for its indirect influence on climate. Little is known about the abundance and sources of CO prior to the industrial age, or about the importance of anthropogenic activities on its budget. **Wang *et al.*** (p. 1663, published online 2 December; see the Perspective by **Prentice**) present a 650-year-long record of CO atmospheric concentration and isotopic composition, using samples from Antarctic ice cores, in order to begin to reconstruct past CO variability and its causes. The concentration of CO decreased by ~25% from the mid-1300s to the 1600s, and then recovered completely by the late 1800s. Large variations in the degree of biomass burning in the Southern Hemisphere are likely to have been primarily responsible for the observed changes.

Continued on page 1585

Continued from page 1583

A Hot Dipole

In a ferroelectric material, there is an alignment of local electric dipole moments that produces a net overall electric polarization. This state is accompanied by a decrease in symmetry, which can be restored by heating above a critical temperature. In contrast, through a combination of theory and experiments, **Božin *et al.*** (p. 1660) now show that with increasing temperature, rock-salt–structured lead telluride and lead sulfide go through a phase transition from a high symmetry phase to a low symmetry phase with an associated dipole moment. Paradoxically, the dipoles are stabilized in the disordered state at high temperature, even though the undistorted structure has lower internal energy.

Dissecting Nitric Oxide Reductase

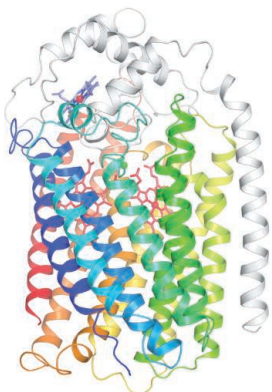

Bacterial breakdown of nitrogen compounds in soil and the oceans provides the largest emission source of the greenhouse gas, nitrous oxide (N_2O). A key enzyme in this process is nitric oxide reductase (NOR), which catalyzes the reduction of nitric oxide (NO) to N_2O. **Hino *et al.*** (p. 1666, published online 25 November; see the Perspective by **Moënne-Loccoz and Fee**) now describe the crystal structure of NOR from *Pseudomonas aeruginosa*. Consistent with their evolutionary relatedness, the transmembrane region topology and arrangement of metal centers in NOR are similar to those in cytochrome oxidases, key enzymes in aerobic respiration.

Few But Powerful

Drug activation of the different types of acetylcholine receptors in cholinergic neurons often generates opposing or conflicting effects. Using optogenetic techniques in transgenic mice, **Witten *et al.*** (p. 1677) investigated the function of a rather enigmatic subpopulation of cholinergic neurons, the giant interneurons of the nucleus accumbens. Their excitation paradoxically reduced neighboring medium spiny neuron firing, while their inhibition increased medium spiny neuron firing. Furthermore, the giant interneurons were directly activated by cocaine, and silencing their drug-induced activity during cocaine exposure in freely behaving animals disrupted cocaine reward.

Making a Germ Cell

When it comes to generating the germ line, animals fall into two classes: those, like mammals, which use inductive interactions to specify the germ line and those, like nematodes, which use germ plasm—a specialized egg cytoplasm that segregates asymmetrically in embryos. Germ plasm contains germ, or P, granules—RNA-protein aggregates that have been thought to harbor the germ line determinants. Now, **Gallo *et al.*** (p. 1685, published online 2 December) describe a *Caenorhabditis elegans* mutant that challenges this belief. The germ line still formed even when germ granule components were missegregated. Thus, even in animals with germ plasm, germ granules appear to be a consequence, not a cause, of germ cell specification.

Lymphocytes Layer It On

Cells of the immune system begin to develop from hematopoietic stem cells (HSCs) during fetal life. In the adult, HSCs continue to produce immune cells to replenish dying cells or in response to an infection. In mice and birds, immune cell development occurs in a "layered" manner, whereby distinct populations of HSCs that arise at different times during development generate distinct immune cell lineages. In contrast, development of human immune cells, and T lymphocytes in particular, is thought to be linear. **Mold *et al.*** (p. 1695; see the Perspective by **Betz**) now show that T lymphocyte development in humans is also "layered," and strategically so. T cells that arise from fetal HSCs are enriched in regulatory T cells, which promote immune tolerance, rather than classical T cells, which readily respond to foreign antigen. By favoring the development of regulatory T cell populations during fetal life, the immune system is perhaps better able to keep responses to maternal antigens in check. The development of large numbers of classical T cells is delayed until after birth when infectious agents represent a more imminent threat.

CREDIT: HINO *ET AL.*

Bruce Alberts is Editor-in-Chief of *Science*.

Is the Frontier Really Endless?

IN THIS ISSUE, THE NEWS TEAM AT *SCIENCE* NAMES ITS ANNUAL BREAKTHROUGH OF THE YEAR (see p. 1604). This year the honor goes to the first quantum machine—a microscopic cantilever ingeniously lowered to its lowest possible energy, the quantum ground state. The result may lead to ultrasensitive force detectors and to ways of controlling an object's mechanical vibrations as deftly as we now control electricity and light. It also heralds further investigations of one of the great mysteries of physics: the chasm separating the world of familiar objects from the bizarre realm of quantum mechanics.

There were other remarkable achievements this year, including the first cell with a synthetic genome and the deciphering of much of the genome sequence of our close, long-extinct relative, the Neandertal. And at long last, in the fight against AIDS, a new microbicidal gel that reduces a woman's risk of being infected with HIV.

This issue also adds something new: a look back over the past 10 years, highlighting 10 great scientific "insights of the decade" (see p. 1612). As emphasized, most of the insights have relied on the continued development of ever more powerful methods for investigating the world. Aided by new tools for peering out into space and for analyzing the molecules from which humans are made, among many others, the pace of scientific discovery is constantly accelerating. But most amazingly, it seems that whenever science increases our comprehension of the world, great new mysteries arise that need to be deciphered; from "dark energy" to the "dark genome" in the past decade alone. Moreover, discoveries in one domain can create new possibilities for breakthroughs in another. Thus, the discovery of water on Mars opens up the exciting possibility of discovering a form of primitive life on that planet, which may produce a better understanding of our own origins.

The question arises whether there will always be surprises, or if someday, perhaps thousands of years from now, there will be nothing left to discover. Can we ever expect to reach a complete understanding—an end of humanity's quest to understand the world through science?

Consider, for example, the grand challenge of deciphering how a multitude of cells cooperate with each other to form the human body. A cell is the fundamental unit of life, just as an atom is the fundamental unit of matter, and we have attained a highly sophisticated, but far from complete, understanding of its mechanisms. Loosely speaking, a cell is a collection of catalysts that, acting as a group, cause a complicated series of chemical reactions that end up duplicating all of the catalysts in the set. These are then divided into two sets, and the process starts over again with each daughter set.

But despite gaining an increasingly detailed understanding of the chemistry that underlies fundamental processes such as cell division, there are huge swathes of biology that puzzle us. The simplest cell known, a bacterium, contains about 500 types of catalysts in its set; the set in human cells is much more complex, with about 50 times the number of different types. In the year 2000, we thought that this added complexity was enough to allow the 100,000 billion human cells produced from a single fertilized egg cell to form the cell collaborative that we call a human being. Today we recognize that there are many more players in human cells, and that, amazingly, a total of about two-thirds of our essential genetic information—our "dark genome"—is needed for processes whose nature mostly remains a mystery.

Was Vannevar Bush right in 1945 when he described science as the "endless frontier"? Can we assume that if we solve the mysteries of the dark genome, new puzzles will arise? One can certainly hope so, because life would lose much of its grandeur and joy if we ever reached the finish line, with no further frontiers to challenge us.

– Bruce Alberts

10.1126/science.1201539

Published by AAAS

EDITED BY KRISTEN MUELLER AND JAKE YESTON

MICROBIOLOGY

Easy Riders

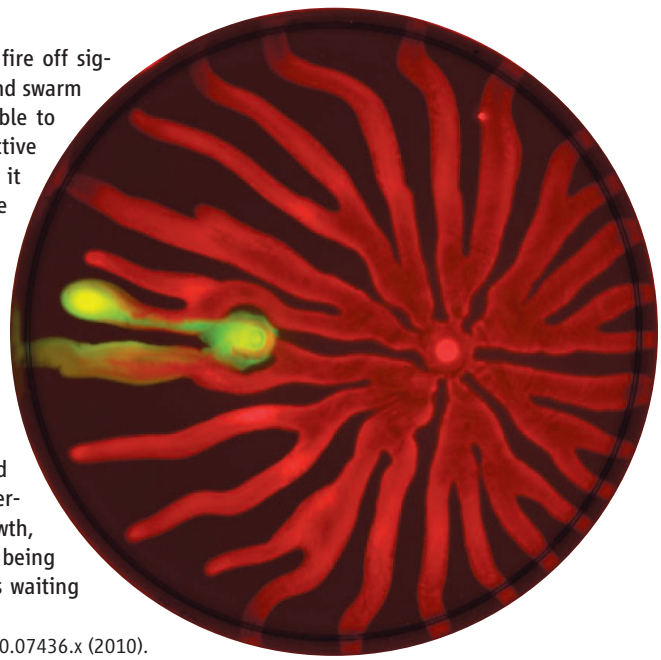

Microorganisms rarely act alone, and bacterial cells continually fire off signaling molecules, behave cooperatively, exchange metabolites, and swarm together. Despite its many advantages, collaboration is vulnerable to cheaters who may exploit the advantages generated by the collective without contributing themselves. Once cheating gains a foothold, it is difficult to eradicate. Xavier *et al.* have explored the occurrence of cheating in the bacterium *Pseudomonas aeruginosa,* which forms motile swarms that move on a self-produced, copious film of rhamnolipid surfactant. A mutant rendered incapable of emitting surfactant (green) could swarm along the film from a wild-type strain (red) without adversely affecting the producer, yet it overwhelmed a different strain engineered to produce surfactant continuously with no regulation. So how do colonies of wild-type producers avoid such takeover? Rhamnolipid production is costly; thus it is only synthesized when carbon is abundantly available and when growth is limited by a lack of nitrogen. In this scenario, perhaps bacteria need to be motile to find better food to resume growth, at which point surfactant production is switched off. Hence, by being frugal with surfactant production, producers can escape cheaters waiting for a free ride. — CA

Mol. Microbiol. 10.1111/j.1365-2958.2010.07436.x (2010).

CHEMISTRY

Agile CO_2 Catchers

There is vigorous ongoing research to develop sorbents that efficiently capture CO_2 generated through coal combustion and thereby keep it out of the atmosphere, where its infrared absorption would contribute to global warming. It's critical to bind the gas rapidly and selectively, but not too tightly, as release for concentrated sequestration should also be facile. Aqueous amines are promising compounds for this purpose, though ionic liquids (ILs), with their low volatility and high stability, might offer even better prospects. Unfortunately, in preliminary studies, introduction of CO_2 has led to an impractical rise in IL viscosity, attributed to the formation of salt bridge networks. To skirt this drawback, Gurkan *et al.* performed simulations on a distinct IL class comprising pyrrolide anions (charge balanced by tetraalkyl phosphonium) that could covalently capture CO_2 without involving network-forming protons. They then went on to synthesize a 2-cyanopyrrolide IL, and as predicted, the medium absorbed superstoichiometric quantities of CO_2 with minimal viscosity increase and even tolerated the presence of water. A variant based on a pyrazolide, rather than pyrrolide, framework confirmed the tunability of the approach. — JSY

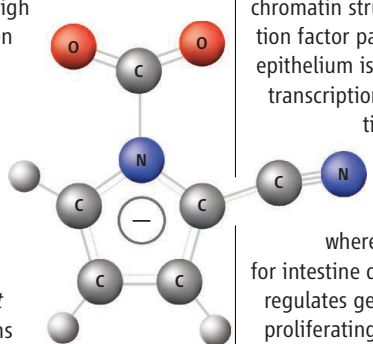

J. Phys. Chem. Lett. **1**, 3494 (2010).

DEVELOPMENT

Protein in Context

Proper cell differentiation requires permissive chromatin structure and specific transcription factor participation. The adult intestinal epithelium is an excellent model for studying transcriptional regulation during differentiation. The homeodomain protein CDX2 is expressed in progenitor and differentiated cells of the mammalian intestinal epithelium, where it likely acts as a master regulator for intestine development. Whether this factor regulates genes in the same way in both the proliferating and differentiated cells, however, is unclear. Verzi *et al*. now show that CDX2 is needed for appropriate chromatin modifications in intestinal epithelium; however, rather than showing a conserved mode of regulation, CDX2 associates with different binding sites and participates with variable chromatin and transcription factors among progenitor and differentiated intestinal cells. Hence, temporal function and cellular context dictate the mechanism of action of CDX2. — BAP

Dev. Cell **19**, 713 (2010).

MOLECULAR BIOLOGY

High Fidelity Required

Covalent modifications of histones in nucleosomes can determine characteristic gene expression states for specific cells and tissues. These marks are thought to be maintained through cell division and DNA replication by the close coordination of histone eviction from the parental DNA with the transfer of the "parental" histones onto the nascent daughter DNA strands. The modifications on these recycled histones are then copied to new nucleosomes added to counter the twofold dilution on the daughter DNA. The fidelity of histone transfer depends on its close coordination with DNA replication.

Sarkies *et al*. find that the normally silent [rho]-globin gene, which contains G quadruplex (G4) sequences that disrupt DNA replication, becomes activated in chicken cells lacking the specialized DNA polymerase REV1. REV1 helps the DNA replication machinery bypass G4 DNA. In the absence of REV1, post-replicative

Published by AAAS

gaps are suggested to form in the vicinity of the G4 DNA, which are filled in later, thereby uncoupling replication and parental histone transfer. In the absence of the coupled transfer, new histones are used to populate the repaired gaps. New histones bear activating marks—not the repressive marks of the [rho]-globin parental nucleosomes—resulting in [rho]-globin gene activation. Many of the genes activated in cells lacking REV1 also have G4 consensus sequences close to their promoters, suggesting that histone recycling is critical for maintaining epigenetic states. — GR

Mol. Cell **40**, 1 (2010).

BIOPHYSICS

Shining Light on Tendonitis

Athletes, whether two- or four-legged, can develop tendonitis, a painful condition that requires a long recovery period. Fundamental imaging studies of damage to collagen in tendon often exploit its birefringence, but polarized light imaging usually requires chemical staining of the fibers. Sivaguru *et al.* exploited collagen's noncentrosymmetric organization to perform direct imaging through second-harmonic generation. In their technique, two near-infrared photons (780 nm wavelength) from an ultrashort pulsed laser combine in the sample to produce a photon at 390 nm. The resulting images, which were taken both with light transmitted through the sample (forward scans) and with reflected light (backward scans), were then Fourier-transformed to determine fiber orientations. They compared normal tendon from horse with tendon that had undergone a model for injury—degradation with collagenase. Degradation led to a decrease in fiber orientation and better spread in the forward and backward scan ratios. Such strain-free methods lend themselves to endoscopic approaches for assessing tendon damage. — PDS

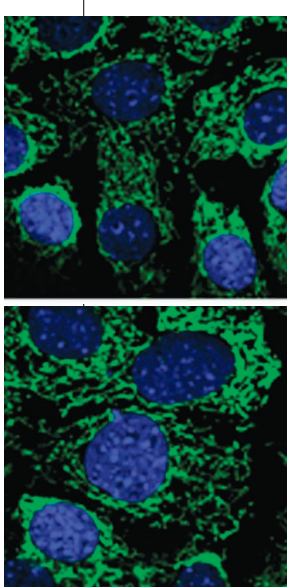

Opt. Express **18**, 24983 (2010).

COMPUTER SCIENCE

Sensing Worms

Arrays of small remote sensors are increasingly being used to gather fundamental data in many fields. Examples range from medical monitoring within and beyond hospitals to assessing energy usage. New sensors communicate wirelessly, are battery-powered, and have their own small processors and memory. For simplicity, they typically lack much security, but it has been considered difficult to infect a network through a few sensors. Giannetsos *et al.* explore how one common type of sensor, using the Van Neumann architecture, can be infected with a worm that will spread through the sensor network. In this architecture, the instructions and data share the same memory, and multiple packets of the virus can be uploaded into the buffer overload; once assembled, they override the instructions. Regular automatic communication with other sensors spreads the worm. The authors also explore how to protect sensor networks from this kind of attack. — BH

Comput. J. **53**, 1576 (2010).

SIGNAL TRANSDUCTION

Getting Apoptosis Started

Activation of the Bak and Bax proteins in response to apoptotic stimuli initiates the cascade of events that commit the cell to death. Bak and Bax activation requires a conformational change followed by multimerization, and now Fox *et al*. provide evidence for an additional layer of regulation. The authors identified a specific tyrosine residue, Y^{108}, on Bak that is phosphorylated in healthy human cells but was dephosphorylated during apoptosis. Dephosphorylation of Bak led to a conformational change and was necessary but not sufficient to cause Bak activation. A siRNA screen identified the protein tyrosine phosphatase PTPN5 as a major contributor to Bak activation in response to apoptotic stimuli. PTPN5 was regulated by the mitogen-activated protein (MAP) kinases ERK1 and ERK2. MAP kinase activation generally promotes cell survival, and MAP kinase activity was transiently decreased in cells treated with an apoptotic stimulus. This corresponded with increased dephosphorylation of Y^{108} by PTPN5. Thus, Bak may act as a point of integration of MAP kinase signaling with other pathways that influence the association of Bak with proapoptotic proteins. These results also suggest that by default, cells are programmed to survive and require multiple positive signals to initiate apoptosis. — LBR

EMBO J. **29**, 3853 (2010).

CREDIT: FOX *ET AL.*, *EMBO J.* **29**, 3853 (2010)

Published by AAAS

www.sciencemag.org

Science

1200 New York Avenue, NW
Washington, DC 20005
Editorial: 202-326-6550, FAX 202-289-7562
News: 202-326-6581, FAX 202-371-9227
Bateman House, 82-88 Hills Road
Cambridge, UK CB2 1LQ
+44 (0) 1223 326500, FAX +44 (0) 1223 326501

Subscription Services For change of address, missing issues, new orders and renewals, and payment questions: 866-434-AAAS (2227) or 202-326-6417, FAX 202-842-1065. Mailing addresses: AAAS, P.O. Box 96178, Washington, DC 20090-6178 or AAAS Member Services, 1200 New York Avenue, NW, Washington, DC 20005

Institutional Site Licenses please call 202-326-6755 for any questions or information

Reprints: Author Inquiries 800-635-7181
Commercial Inquiries 803-359-4578

Permissions 202-326-7074, FAX 202-682-0816

Member Benefits AAAS/Barnes&Noble.com bookstore www.aaas.org/bn; AAAS Online Store www.apisource.com/aaas/ code MKB6; AAAS Travels: Betchart Expeditions 800-252-4910; Apple Store www.apple.com/eppstore/aaas; Bank of America MasterCard 1-800-833-6262 priority code FAA3YU; Cold Spring Harbor Laboratory Press Publications www.cshlpress.com/affiliates/aaas.htm; GEICO Auto Insurance www.geico.com/landingpage/go51.htm?logo=17624; Hertz 800-654-2200 CDP#343457; Office Depot https://bsd.officedepot.com/portalLogin.do; Seabury & Smith Life Insurance 800-424-9883; Subaru VIP Program 202-326-6417; VIP Moving Services www.vipmayflower.com/domestic/index.html; Other Benefits: AAAS Member Services 202-326-6417 or www.aaasmember.org.

science_editors@aaas.org	(for general editorial queries)
science_letters@aaas.org	(for queries about letters)
science_reviews@aaas.org	(for returning manuscript reviews)
science_bookrevs@aaas.org	(for book review queries)

Published by the American Association for the Advancement of Science (AAAS), *Science* serves its readers as a forum for the presentation and discussion of important issues related to the advancement of science, including the presentation of minority or conflicting points of view, rather than by publishing only material on which a consensus has been reached. Accordingly, all articles published in *Science*—including editorials, news and comment, and book reviews—are signed and reflect the individual views of the authors and not official points of view adopted by AAAS or the institutions with which the authors are affiliated.

AAAS was founded in 1848 and incorporated in 1874. Its mission is to advance science, engineering, and innovation throughout the world for the benefit of all people. The goals of the association are to: enhance communication among scientists, engineers, and the public; promote and defend the integrity of science and its use; strengthen support for the science and technology enterprise; provide a voice for science on societal issues; promote the responsible use of science in public policy; strengthen and diversify the science and technology workforce; foster education in science and technology for everyone; increase public engagement with science and technology; and advance international cooperation in science.

Information for Authors
See pages 352 and 353 of the 15 January 2010 issue or access www.sciencemag.org/about/authors

EDITED BY LAUREN SCHENKMAN

Magic Mint

Salvia divinorum may be this generation's answer to magic mushrooms. A hallucinogenic member of the mint family, it has been used for centuries by Mexican shamans for spiritual purposes. Within the past decade it's become popular as a legal high—at least where its use hasn't been outlawed. Now researchers at Johns Hopkins University have conducted the first human laboratory study on the plant, published online 4 December in *Drug and Alcohol Dependence*.

Salvia's active ingredient, salvinorin A, binds to a different receptor than do drugs such as LSD or marijuana, which affect serotonin and endocannabinoid receptors. The effect is both much briefer and much more intense—enough to shake up the study subjects, who had all used other hallucinogenic drugs. "People were saying it was like opening a portal to another dimension," says the study's lead author, Matthew Johnson. They also encountered the same hallucinated beings from session to session. Salvinorin A could potentially become a research tool for conditions such as schizophrenia and dementia, Johnson says. Meanwhile, given the intensity of its effects, the classic caveat still applies: Kids, don't try this at home.

Million-Dollar Bird

Last week, this hand-painted print and the 434 others in John James Audubon's mid–19th century book *The Birds of America* sold at Sotheby's in London for $11.6 million to an anonymous bidder. Just 120 copies are known to exist.

Unlike other bird illustrators, Audubon "wanted to present them lifelike" and life-size, says curator Charles Aston of the University of Pittsburgh in Pennsylvania, who maintains that library's copy. So he shot birds—"he was an excellent marksman, and some of these are tiny birds"—posed them, and painted them in botanically accurate backgrounds. Audubon's field notes, published separately in *Ornithological Biography*, might shock a modern ornithologist, Aston says. "Often you get the startling comment such as, 'They're very good roasted.' "

Faster, Better, Smaller

Jonathan Rothberg is betting that $3 million will get labs around the world working on how to speed up the already rapid ascent of his new DNA sequencing technology. On 14 December, Rothberg, founder of Ion Torrent, which uses semiconductor know-how to build miniature sequencing machines, announced three $1 million prizes for researchers who can make his chip technology "faster, more accurate, and even more scalable."

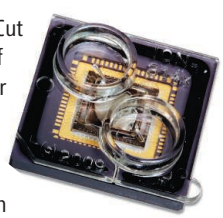

One way to earn a million: Cut sample preparation time in half so that, independent of whether the starting point is human spit or bacteria, sequences start rolling off the machine within 5 hours. A second million is for tweaking the chemical processes used to decode DNA so that the chip can churn through twice as much sequence at a time. The third rewards software that can identify bases more accurately from the Ion Torrent chip's raw data.

The funds are the first committed from a $7 million program by Ion Torrent's parent company, Life Technologies Corp., to encourage outside involvement in improving the company's products. "It's an interesting and very innovative approach and is going to get the research community excited about this technology," says Ulrich Broeckel, a complex-diseases geneticist at the Medical College of Wisconsin in Milwaukee. His lab is one of about a half-dozen to have an Ion Torrent machine, and he plans to go after a prize. Given the funding climate, $1 million "is a nice incentive," he adds.

AQUA BOT

Anyone who has taken a marine biology course is familiar with wading into the muck to collect samples. Christopher Scholin, president of the Monterey Bay Aquarium Research Institute in Moss Landing, California, spent 20 years searching for a better way. He came up with the Environmental Sample Processor (ESP), a "lab in a can" that can gather, prepare, and test water samples for microorganism DNA all on its own. Scientists can place the device anywhere from a freshwater marsh to the deep ocean and view the results remotely over the Internet—no galoshes required.

"It's a very promising and unique piece of equipment," says Don Anderson of the Woods Hole Oceanographic Institution in Massachusetts, who is testing the first ESP commercial prototype. Instruments that measure salinity, temperature, and current are standard, he says, "but it's a rare and unique sensor that can give you information about individual species."

Anderson will use the ESP to collect data on "red tide" blooms of toxin-producing *Alexandrium fundyense* algae in New England coastal waters. Other applications for the ESP, which was partly funded by NASA, could include monitoring drinking water quality and detecting microbial life in space, Scholin says. "Now that we've created a device to do remote analysis, we would welcome partnerships."

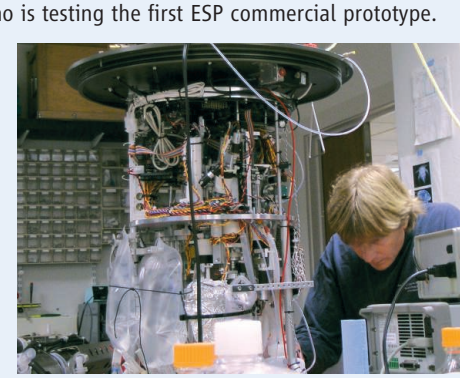

Scholin with the ESP.

Published by AAAS

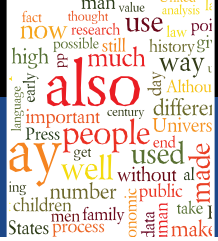

The debut of culturomics 1600

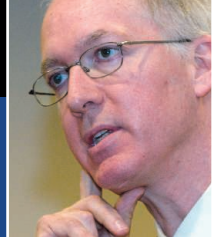

Parting thoughts from a physicist-congressman 1601

U.S. SCIENCE POLICY

NSF Won't Build Underground Lab; Scientists Hope That DOE Will

Plans to convert an abandoned gold mine in South Dakota into the world's largest underground lab may have to be scaled back and could fall apart entirely after the National Science Foundation's (NSF's) oversight board rejected the current proposal.

On 30 November, the National Science Board (NSB), which sets policy for NSF, turned down the agency's own request for additional money to support development through 2011 of the $875 million Deep Underground Science and Engineering Laboratory (DUSEL) at the Homestake mine in Lead, South Dakota. That puts the onus on the Department of Energy (DOE), NSF's partner in the project, to pay for whatever it wants to build.

Supporters are putting the best light on the board's decision. "This is not the end of the project," says Kevin Lesko, a physicist at the University of California, Berkeley, who leads the design team. "We are continuing conversations with the NSB, NSF, and DOE to resolve their issues and to maintain the project's momentum." But Edward Seidel, who leads NSF's mathematical and physical sciences directorate, says that the 10-year campaign to build the underground facility has entered uncharted waters: "One option that's no longer open is that the NSF would steward the facility." In other words, NSF may support experiments to be done at DUSEL, but it won't build the lab itself.

Researchers in Italy and Japan have enormous underground labs, and earlier this week China opened the world's deepest lab, 2500 meters down in a tunnel through Jinping Mountain in Sichuan Province (*Science*, 5 June 2009, p. 1246). DUSEL was supposed to be the biggest lab and, with a chamber at 2250 meters, among the deepest (*Science*, 12 November, p. 904). The great depth would shelter experiments from cosmic rays, and the huge capacity would allow for a suite of physics experiments whose results could be revolutionary, such as searches for particles of the mysterious dark matter whose gravity binds the galaxies and for a kind of radioactivity that would blur the distinction between matter and antimatter. The lab would also give geophysicists and microbiologists rare access to Earth's innards.

DUSEL began its rocky journey in 2001, when researchers tried and failed to win a congressional earmark to prevent the then-functioning Homestake mine from filling with water after it was shut down. NSF then held a site competition and in July 2007 chose Homestake, by then under water, based on a conceptual design. In September 2009, NSB approved $29 million to support a detailed preliminary design to be finished this year.

But that money didn't cover what's needed to continue operations, a key consideration because the pumps must keep running to keep the partially drained mine from filling up again. In March, South Dakota appropriated $5.4 million to keep things going through May 2011. NSF and the research team requested $19 million to tide them over until NSB could evaluate the design late next year, with the expectation that the board would provide $10 million more in the spring.

Instead, the NSB panel decided that the current plan was "unacceptable." Members objected to the two agencies' plan to share responsibilities and costs, says Mark Abbott, chair of the NSB committee that took action last month. Under that "stewardship model," NSF would have borne the $480 million expense of developing DUSEL's infrastructure, while DOE took the lead for the lab's biggest experiment, a particle detector called the Long-Baseline Neutrino Experiment (LBNE) weighing up to 200,000 metric tons and costing at least $660 million. That experiment would snare neutrinos fired through Earth from DOE's Fermi National Accelerator Laboratory in Batavia, Illinois, and would be Fermilab's flagship project in coming decades.

The NSB panel also questioned whether the massive infrastructure project fits the mission of NSF, which ordinarily builds scientific instruments such as telescopes. "We're a science agency, not a mission agency, or a facilities agency, or a big infrastructure agency," says Abbott, a biological oceanographer at Oregon State University, Corvallis. In contrast, DOE's Office of Science supports a network of national labs and user facilities specifically chosen to further DOE's mission.

NSB's decision affects the particle physics programs at both NSF and DOE. LBNE designers aren't wedded to a site, says Robert Tschirhart, a physicist at Fermilab, and an alternative could be the Sanford Underground Laboratory, the portion of Homestake that South Dakota has opened with $34.2 million of its own money and $70 million from philanthropist T. Denny Sanford in preparation for DUSEL approval.

The good news for DUSEL developers is that DOE seems willing to try to salvage the project. "We have not made any decisions yet, but we are trying not to lose all the effort that has been put into the project so far," says William Brinkman, head of DOE's Office of Science. In the meantime, there is only enough money to keep the water pumps running for a few more months.

–ADRIAN CHO

With reporting by Jeffrey Mervis.

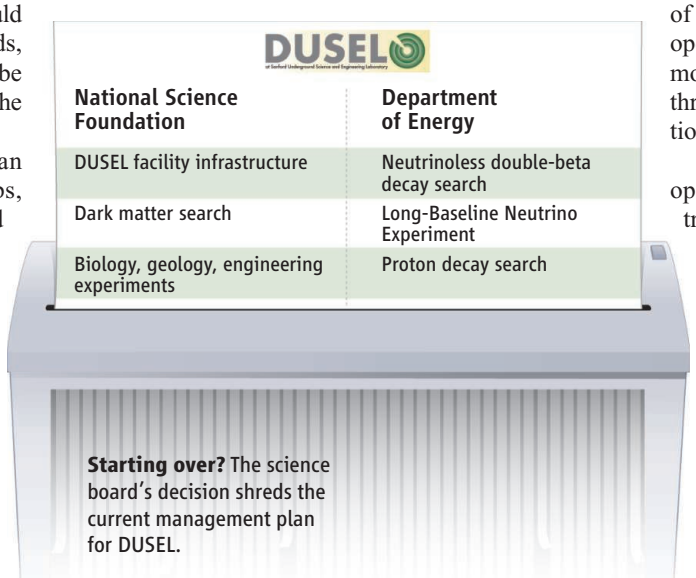

Starting over? The science board's decision shreds the current management plan for DUSEL.

SOURCE: DUSEL

Published by AAAS

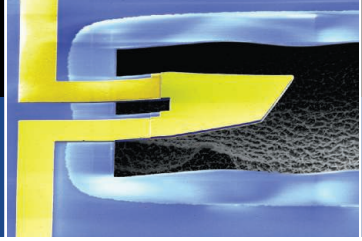

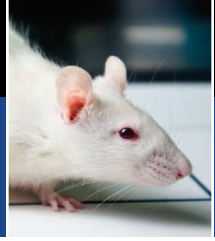

CLIMATE NEGOTIATIONS

Cancún Delegates See the Trees Through a Forest of Hot Air

A new deal inked last week at the United Nations climate talks in Mexico paves the way for rewarding nations for maintaining their forests. A central facet of the agreement, which puts the protection of trees at the vanguard of climate negotiations, is a call for developing countries to begin calculating national totals for emissions from forest loss and to adopt systems to begin monitoring deforestation.

The deal, which rests upon years of research and political maneuvering, opens the door for future trading of forest credits. Paying poor nations to preserve trees is considered a key component of any long-term strategy to reduce emissions. It also enshrines the scientific finding that carbon in forests can and should be measured at national scales. "Once you have the science demonstrating how it can work, it makes it possible politically," says Paulo Moutinho, executive director of Brazil's Instituto de Pesquisa Ambiental da Amazônia.

Deforestation, whether trees are felled or burned, contributes as much as a quarter of greenhouse gas emissions from human activity worldwide. The agreement on reducing emissions from deforestation and forest degradation, known as REDD, sets the stage for an arrangement in which countries would be compensated for slowing deforestation. Nations that keep trees standing might then sell credits to developed countries, or even individual polluters. The agreement does not, however, spell out a compensation mechanism. "How this stuff will be funded has been kicked down the road," says Steve Schwartzman of the Environmental Defense Fund (EDF) in Washington, D.C.

REDD was a high point among a series of modest achievements forged in the 2-week meeting in Cancún that ended on 11 December. Another agreement is a $100-billion-per-year green fund for developing nations to adapt to climate change and promote clean energy, although as with REDD, no one knows how that money will be raised. Negotiators also made progress on rules for sharing technology and monitoring emissions reductions. Mexican President Felipe Calderón said the meeting removed the "inertia of mistrust" that has existed, particularly between poor and rich countries.

Lumbering giant. Agreement highlights the role of forests in reducing carbon emissions.

Climate negotiations nearly broke down a decade ago over the REDD question. Negotiators initially wanted to allot credits to small-acreage conservation projects that could be carefully monitored. But protecting trees in one place might simply cause them to be cut down elsewhere.

Forest scientists and policy experts have since crafted the national-scale strategy at the heart of the REDD deal. One key step was a proposal in a 2005 paper by Brazilian and U.S. researchers, including Schwartzman, for "compensated reduction," a process in which countries could be rewarded for stemming deforestation at a national level.

In a series of meetings since then, remote-sensing experts determined that tools to calculate national totals do exist. Those workshops "showed the U.N. parties that you could actually measure this stuff," says Annie Petsonk, a forest expert with EDF.

The ability to monitor its forests has been a boon to Brazil, where, until a few years ago, deforestation was a source of shame and raw data were confidential. "Five or 6 years ago, Brazil's government didn't want to discuss deforestation, so they would say we didn't know how much carbon there was in the forest," says Moutinho. "Now it's hard to find anyone who questions the measurement technology." After building up the largest remote-sensing agency of any tropical nation, Brazil officials arrived at Cancún touting the lowest rate of national deforestation in more than 2 decades.

Researchers have also made progress in understanding the most effective ways to preserve forests. One powerful tool, they say, is demarcating territory for indigenous groups, which has occurred throughout Latin America in the past few years by the millions of hectares. "Before, that was just an argument. Now there is economic and remote-sensing data that backs up" that approach, says David Kaimowitz of the Ford Foundation in Mexico City.

Some researchers have also argued that REDD may be the cheapest way to reduce carbon emissions. That "created [the] political will," says Kaimowitz.

Scientists are already plotting their next steps, including how to merge remote-sensing data with on-the-ground monitoring. The biggest near-term challenge, scientists say, will be helping developing countries put in place the "robust and transparent" national forest-monitoring systems stipulated under the agreement. The Cancún deal requires countries to propose rules "for measuring, reporting and verifying anthropogenic forest-related emissions" before next year's meeting in Durban, South Africa.

Some solutions are already coming into view. At Cancún, the charity arm of the search company Google unveiled Google Earth Engine, which will allow users to study deforestation using its computing power. And a group at the Carnegie Institution for Science in Stanford, California, has been training hundreds of experts from several countries to analyze deforestation data.

Despite having a general framework for REDD, it will take years of negotiations to fill in the details. One especially sticky question is setting the baseline year against which to measure progress. Still, remote-sensing and forestry experts came away from Cancún revitalized. "It makes me feel that the last 5 years of not sleeping has been worth it," says Carnegie tropical ecologist Greg Asner. "We'll keep being sleepless, but we're going to be celebrating this."

–ELI KINTISCH AND ANTONIO REGALADO

CREDIT: GALEN ROWELL/CORBIS

Published by AAAS

Going critical. A worker pours the rare earth metal lanthanum into molds at a workshop in China.

CREDIT: DAVID GRAY/REUTERS

HIGH TECHNOLOGY

Haunted by 'Specter of Unavailability,' Experts Huddle Over Critical Materials

When shipments of rare earth metals from China to Japan temporarily stopped in the wake of a territorial spat this autumn, high-tech companies around the world got an uncomfortable reminder that China owns a stranglehold on supplies of the coveted commodities. The episode might have attracted more attention than China hoped for. The U.S. Department of Energy (DOE) and counterparts in Japan and Europe have held workshops in recent weeks bringing materials scientists and policymakers together to brainstorm on how to ensure supplies of rare earths and other strategic minerals and to stimulate research on alternatives.

The meetings, at Lawrence Livermore National Laboratory in California in November and at the Massachusetts Institute of Technology in Cambridge, Massachusetts, earlier this month, are expected to help DOE chart a strategy for critical materials, participants say. The quickest fix for restricted supply would be boosting production outside of China. But no one expects breakthroughs on supply or alternative materials overnight.

Rare earths—elements 57 through 71 on the periodic table plus scandium and yttrium—are key components in products such as solar panels and hybrid cars. Around 95% of the current supply comes from China, which is holding back an increasingly large share of production for its own use (*Science*, 11 September 2009, p. 1336). The recent controversy over shipments to Japan has observers worried about China's willingness to squeeze supplies for political purposes.

"The specter of mineral unavailability" due to geopolitical risks or market imbalances haunts other elements as well, says Roderick Eggert, a mineral resources economist at the Colorado School of Mines in Golden. Most of the world's lithium, a key component in batteries for consumer electronics and electric vehicles, is mined in Bolivia. Congo and Zambia are the main sources of cobalt, used in high-strength alloys and as an industrial catalyst. Indium and tellurium, ingredients of photovoltaic cells and flat panel displays, are byproducts of, respectively, zinc and copper processing. Because availability of indium and tellurium depends on demand for copper and zinc, supplies of the two won't necessarily increase with increasing prices, Eggert says.

Even before China flexed its muscles, experts in other countries were fretting over critical materials. A few years ago, Toru Nakayama, who manages materials research programs for the New Energy and Industrial Technology Development Organization (NEDO) in Kawasaki, Japan, drafted a rare metal substitute development project while at the Ministry of Economy, Trade and Industry. Since 2007, NEDO has organized consortia of researchers from companies, universities, and institutes to work on reducing or replacing indium, dysprosium, platinum group metals, and four other elements in high-tech products. NEDO has provided $82 million over the past 4 years for these efforts. As that effort was getting started, the U.S. National Research Council warned in 2008 that a looming shortage of critical minerals could hinder adoption of emerging clean energy technologies. And last June, the European Commission released a report citing concerns over access to 14 critical raw materials.

On the rare earth supply issue, workshop participants agreed that immediate relief would come from "getting rare earth mines outside of China up to speed as fast as you can," says Karl Gschneidner Jr., a metallurgist at DOE's Ames Laboratory and Iowa State University. Two rare earth mines—one in the United States and another in Australia—could come on stream in 2011, says Eggert. In the meantime, he says, manufacturers will be working to make more efficient use of the scarce minerals. Several NEDO projects aim to optimize manufacturing processes or tweak materials to get the same performance out of less mineral.

The toughest challenge may be to replace rare elements (*Science*, 26 March, p. 1597). Some materials have been in use for several decades, and "nobody has found substitutes yet," says Gschneidner. For example, he says, phosphors in lighting and optics applications have unique properties difficult to find in other materials.

The workshops showcased some progress on replacements. One NEDO-funded group has produced a trial liquid crystal display that uses zinc oxide instead of indium tin oxide for some electrodes, reducing indium use by 45%. Dysprosium, used in the magnets in motors powering electric and hybrid vehicles, is another target. Several groups have developed dysprosium-free magnets, but they weaken at car motor operating temperatures, says Kunihiro Ozaki, a materials scientist at Japan's National Institute of Advanced Industrial Science and Technology. By tweaking grain properties and strictly controlling manufacturing, researchers hope to strengthen these magnets' thermal resistance—but that could take 5 years or more, Ozaki says.

Workshop participants came away with a clearer picture of what colleagues are doing in other countries. "It was very valuable to understand the extent of the program that's ongoing in Japan," says John Hryn, a materials scientist at Argonne National Laboratory in Illinois. The first cooperative effort is likely to be between the geological surveys of the United States and Japan to assess rare mineral deposits around the world, Eggert says. Beyond that, Hryn says there are a number of ongoing projects at Argonne focused on magnets, phosphors, and catalysts that use rare earths, creating "opportunities for future collaborations." These will take time to coalesce and bear fruit. In the meantime, China is sitting pretty with most of the rare earth cards.

–DENNIS NORMILE

DEMOGRAPHIC RESEARCH

Asia's Looming Social Challenge: Coping With the Elder Boom

BEIJING—Asia is graying fast. The portion of the population age 65 or older will more than triple in China, India, and Indonesia—and more than double in Japan—between 2000 and 2050, according to United Nations projections. That's a triumph of civil society and medical science, but it also poses stiff challenges to Asian nations trying to create or strengthen social safety nets. "Responding to these challenges will be one of the most difficult tasks facing governments in the first half of this century," warns a report* released here last week by five science academies.

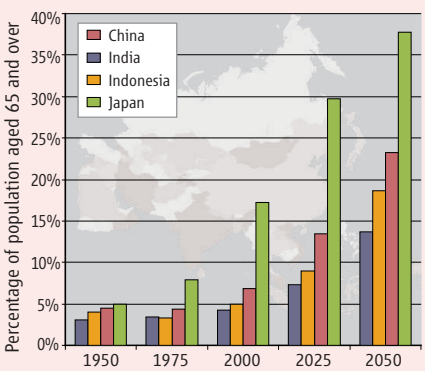

Country-Level Longitudinal Population Studies in Asia

Name	Status
China Health and Retirement Longitudinal Study (CHARLS)	Pilot survey in 2008 Baseline wave in 2011
Health, Aging and Retirement in Thailand (HART)	Pilot survey in 2009 Next wave in 2011
Indonesian Family Life Survey (IFLS)	Started in 1993 Fourth wave in 2008
Japanese Study of Aging and Retirement (JSTAR)	Baseline survey in 2007
Korean Longitudinal Study of Aging (KLoSA)	Started in 2006 Third wave under way
Longitudinal Aging Study in India (LASI)	Pilot survey in 2010 Next wave in 2012
Study on Global AGEing and Adult Health (SAGE)	Baseline survey in 2002 First wave in 2007–09

Long-term population studies under way or about to begin will chart demographic, economic, and health transitions—and give governments worldwide clues about how to cope with the aging boom. One hallmark of the studies is that all will put data in the public domain—not a common practice in Asia. "This is a scientific revolution," says James P. Smith, a senior economist at RAND Corp. in Santa Monica, California. "There are no secrets anymore. This is our version of WikiLeaks."

Asia's demographic shift is happening at a torrid clip. In the United States, it will take approximately 70 years for the percentage of the population age 65 and older to rise from 7% to 14%. Such a doubling is expected to occur in only about 25 years in China, India, and Indonesia, according to the report. "The growth in the number of the elderly will speed up very fast, and we are not prepared," says Mayling Oey-Gardiner, an economics professor at the University of Indonesia in Jakarta. "There are no social safety nets in Indonesia."

That's also true in China, where several factors—including its 30-year-long one-child policy and a tide of young migrant workers seeking their fortunes in cities—will increasingly leave elderly people to fend for themselves, especially in the countryside. In a revealing survey in 72 villages in Shandong Province, Wang Guangzhou and his colleagues at the Chinese Academy of Social Sciences' Institute of Population and Labor Economics here found that more than 80% of the elderly were in debt. Most could not afford medical care and lived in dilapidated housing.

A new generation of population studies (see table) modeled after the 20-year-old U.S. Health and Retirement Study will document, among other things, to what extent children will support elderly parents, how much money older Asians have put away for retirement or receive from pensions or governments, and how medical systems will manage. "We will learn what the myths are and what the facts are—what's happening in people's lives," says Smith.

It will be up to policymakers to implement the lessons. And the longer Asian governments wait to craft policies to care for graying populations, the more constrained their choices will be, says the report. Asia may not want to look to the United States for answers, says Robert Hauser of the National Academies. "We don't have a good model," he says. "We have a terrible situation with respect to [overreliance on] institutional care of the elderly." The population studies may not offer ready solutions, but they will give a vivid picture of the transformation of Asian societies.

–RICHARD STONE

Preparing for the Challenges of Population Aging in Asia, the Chinese Academy of Social Sciences, the Indian National Science Academy, the Indonesian Academy of Sciences, the National Research Council of the U.S. National Academies, and the Science Council of Japan.

ScienceInsider

From the *Science* Policy Blog

The FBI has belatedly provided an expert panel with new information that will **delay a long-awaited report** on the scientific merits of the government's investigation **into the deadly 2001 anthrax mailings**. Five weeks after getting a draft report, FBI officials provided new material and asked to appear before the committee. http://scim.ag/anthrax_report_delay

Political leaders in three western states are seeking help from Congress to **remove the northern Rocky Mountain gray wolf from protection** under the Endangered Species Act. "There do need to be discussions," says one California wildlife biologist. "But this needs to be done with the best science possible, not with legislation." http://scim.ag/wolf_politics

Eight bioethicists at the University of Minnesota are charging that their own institution has committed an "**alarming series of ethical violations**" in a clinical trial during which a young man committed suicide in 2004. They say that his death wasn't adequately investigated. http://scim.ag/minnesota_bioethics

The Irish government has **increased its funding for research** in 2011 by 12% despite being forced to make €6 billion in cuts following its recent bailout. But an emphasis on commercial research has some scientists concerned that funding for basic science will suffer. http://scim.ag/ireland_bucks_trend

European nuclear physicists released a long-range plan that sets as their top priorities completion of the Facility for Antiproton and Ion Research in Darmstadt, Germany, and of SPIRAL2, a complementary machine at France's GANIL lab in Caen. http://scim.ag/nupecc_report

A new **test for tuberculosis that is cheaper, faster, and more accurate** than standard tests has received an important thumbs-up from the World Health Organization. http://scim.ag/better_tb_test

For more science policy news, visit **http://news.sciencemag.org/scienceinsider**.

Published by AAAS

DIGITAL DATA

Google Opens Books to New Cultural Studies

In March 2007, a young man with dark, curly hair and a Brooklyn accent knocked on the door of Peter Norvig, the head of research at Google in Mountain View, California. It was Erez Lieberman Aiden, a mathematician doing a Ph.D. in genomics at Harvard University, and he wanted some data. Specifically, Lieberman Aiden wanted access to Google Books, the company's ambitious—and controversial—project to digitally scan every page of every book ever published.

By analyzing the growth, change, and decline of published words over the centuries, the mathematician argued, it should be possible to rigorously study the evolution of culture on a grand scale. "I didn't think the idea was crazy," recalls Norvig. "We were doing the scanning anyway, so we would have the data."

The first explorations of the Google Books data are now on display in a study published online this week by *Science* (www.sciencemag.org/content/early/2010/12/16/science.1199644.abstract). The researchers have revealed 500,000 English words missed by all dictionaries, tracked the rise and fall of ideologies and famous people, and, perhaps most provocatively, identified possible cases of political suppression unknown to historians. "The ambition is enormous," says Nicholas Dames, a literary scholar at Columbia University.

The project almost didn't get off the ground because of the legal uncertainty surrounding Google Books. Most of its content is protected by copyright, and the entire project is currently under attack by a class action lawsuit from book publishers and authors. Norvig admits he had concerns about the legality of sharing the digital books, which cannot be distributed without compensating the authors. But Lieberman Aiden had an idea. By converting the text of the scanned books into a single, massive "n-gram" database—a map of the context and frequency of words across history—scholars could do quantitative research on the tomes without actually reading them. That was enough to persuade Norvig.

Lieberman Aiden teamed up with fellow Harvard Ph.D. student Jean-Baptiste Michel. The pair were already exploring ways to study written language with mathematical techniques borrowed from evolutionary biology. Their 2007 study of the evolution of English verbs, for example, made the cover of *Nature*. But they had never contended with the amount of data that Google Books offered. It currently includes 2 trillion words from 15 million books, about 12% of every book in every language published since the Gutenberg Bible in 1450. By comparison, the human genome is a mere 3-billion-letter poem.

Michel took on the task of creating the software tools to explore the data. For the analysis, they pulled in a dozen more researchers, including Harvard linguist Steven Pinker. The first surprise, says Pinker, is that books contain "a huge amount of lexical dark matter." Even after excluding proper nouns, more than 50% of the words in the n-gram database do not appear in any published dictionary. Widely used words such as "deletable" and obscure ones like "slenthem" (a type of musical instrument) slipped below the radar of standard references. By the research team's estimate, the size of the English language has nearly doubled over the past century, to more than 1 million words. And vocabulary seems to be growing faster now than ever before.

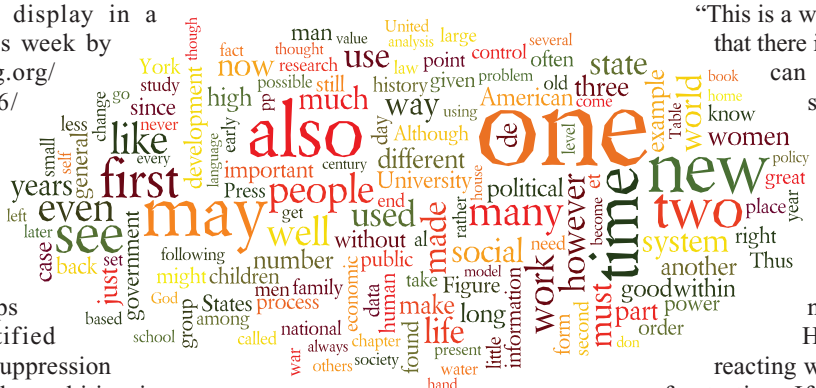

It was also possible to measure the cultural influence of individual people across the centuries. For example, notes Pinker, tracking the ebb and flow of "Sigmund Freud" and "Charles Darwin" reveals an ongoing intellectual shift: Freud has been losing ground, and Darwin finally overtook him in 2005.

Analysis of the n-gram database can also reveal patterns that have escaped the attention of historians. Aviva Presser Aiden led an analysis of the names of people that appear in German books in the first half of the 20th century. (She is a medical student at Harvard and the wife of Erez Lieberman Aiden.) A large number of artists and academics of this era are known to have been censored during the Nazi period, for being either Jewish or "degenerate," such as the painter Pablo Picasso. Indeed, the n-gram trace of their names in the German corpus plummets during that period, while it remains steady in the English corpus.

Once the researchers had identified this signature of political suppression, they analyzed the "fame trace" of all people mentioned in German books across the same period, ranking them with a "suppression index." They sent a sample of those names to a historian in Israel for validation. Over 80% of the people identified by the suppression index are known to have been censored—for example, because their names were on blacklists—proving that the technique works. But more intriguing, there is now a list of people who may have been victims of suppression unknown to history.

"This is a wake-up call to the humanities that there is a new style of research that can complement the traditional styles," says Jon Orwant, a computer scientist and director of digital humanities initiatives at Google. In a nod to data-intensive genomics, Michel and Lieberman Aiden call this nascent field "culturomics." Humanities scholars are reacting with a mix of excitement and frustration. If the available tools can be expanded beyond word frequency, "it could become extremely useful," says Geoffrey Nunberg, a linguist at the University of California, Berkeley. "But calling it 'culturomics' is arrogant." Nunberg dismisses most of the study's analyses as "almost embarrassingly crude."

Although he applauds the current study, Dames has a score of other analyses he would like to perform on the Google Books corpus that are not yet possible with the n-gram database. For example, a search of the words in the vicinity of "God" could reveal "semantic shifts" over history, Dames says. But the current database only reveals the five-word neighborhood around any given term.

Orwant says that both the available data and analytical tools will expand: "We're going to make this as open-source as possible." With the study's publication, Google is releasing the n-gram database for public use. The current version is available at www.culturomics.org.

–JOHN BOHANNON

CREDITS: J. B. MICHEL *ET AL.*; WORDLE.COM

Published by AAAS

U.S. SCIENCE POLICY

Leaving Congress, Physicist Bill Foster Calls for Reinforcements

A month after losing his seat in the U.S. House of Representatives, physicist-turned-lawmaker Bill Foster has a parting message for his fellow scientists: Replace me in Congress. And he's eager to help them do it.

Foster, 55, is a Democrat from an Illinois district that includes the Fermi National Accelerator Laboratory, where he spent 22 years as an experimental physicist. In 2006, he decided to "try to do something" about what he saw as "poor decisions" by Washington politicians. In March 2008, he was the surprise winner in a special election held to replace former Speaker Dennis Hastert, a Republican who retired a year after the Democrats won control of the House in November 2006.

Foster's allies portrayed him as an anti-politician with business savvy—he started and ran a successful company making lighting equipment. But after winning a full term in November 2008, his support for the president's $800 billion stimulus package and health care reform bill put him at odds with his traditionally conservative district. On 2 November, he lost 51% to 45% to Republican Randy Hultgren, a state legislator and lawyer who lambasted "Bill's boondoggle." The high unemployment rate doomed him, Foster says: "People were looking for someone to blame."

Despite his defeat, Foster thinks his scientific training helped him as a legislator. He pushed his staff to delve into the details of policy issues, polling data, and even get-out-the-vote efforts on Election Day, recalls Thomas Bowen, a former aide. "As chief of staff, I was always forced to 'show my work,'" says Bowen. During the yearlong debate over health care, Foster says, he would call experts to chase down numbers "that seemed fishy."

"An engineer or scientist can cut through the sound-bite level of debate that is common in politics," says Foster. That skill was especially useful in scrutinizing the complex financial products, many designed by scientists, whose failure contributed to the meltdown on Wall Street. "It takes a physicist to unwind what physicists did to structured finance," he says.

Using his perch on the House Committee on Financial Services, Foster persuaded colleagues to include six amendments in the Dodd-Frank financial reform bill passed earlier this year, including studies on derivatives and steps to compel banks to act less recklessly. Even so, his colleagues declined to adopt one idea that grew out of his years as an experimental physicist: a rule that complex derivatives—often spelled out in reams of legalese—be expressed as algorithms so that their possible impacts could be modeled on computers. The approach, he says, would mirror "very sophisticated software tools that get shared across experiments."

The need for more legislators with scientific backgrounds—"More than 80% of the people running China are engineers, and you see it in their [economic] behavior," Foster says—may even serve as the basis for the next stage of his career. "One of the things I've been contemplating [launching] is called Albert's list," he says. (The name comes from arguably the greatest physicist of all time.) It would be modeled on EMILY's List, the successful pro-choice political action committee formed in 1985, and it would go where previous efforts to get scientists politically involved have feared to tread.

> ***"More than 80% of the people running China are engineers, and you see it in their [economic] behavior."***
>
> **—REPRESENTATIVE BILL FOSTER**

Scientists and Engineers for America "never actively recruited and developed candidates the way EMILY's List does," Foster says about SEA, which has conducted workshops and offered fellowships since being formed in 2004. "EMILY's List very consciously identifies promising candidates, trains them, and gives them [help in] public fundraising."

One issue that must be resolved before any organization is created, Foster says, is whether to make the group partisan. "[Another is] whether you concentrate on only federal candidates or work on a state-by-state basis, or whether you recruit people to go into the federal bureaucracy." Then there's the question of applying a scientific litmus test. "You could imagine insisting, or not, that they have a science-based attitude about climate change, or, more controversially, about evolution," he says.

What type of person is Foster hoping to attract? Potential recruits would have to decide "what fraction of your life you should spend serving your fellow man," he says. And he thinks the best candidates would "have a sincere desire to serve and not to become famous. Voters detect that very rapidly."

As for his own political aspirations, there's talk that a Democratic-controlled state legislature in Illinois could create a congressional district next year that would be more compatible with Foster's liberal views. "It's way too early to think about that," he says. But Bowen thinks it could happen. "This may not be the last we hear from Bill Foster," he says.

If Albert's List becomes a reality, Foster could return to a Congress with more members who are scientists—and one that is more capable of dealing with an increasingly complex world.

–ELI KINTISCH

Training camp. Bill Foster wants to start an organization to help scientists run for office.

CREDIT: LLOYD DEGRANE

Published by AAAS

CANCER SCREENING

Genetic Analysis Points the Way to Individualized PSA Tests

In cancer research, one never-ending quest is the hunt for biomarkers, proteins in the blood that reveal tumors deep in the body. The goal is to find a reliable predictor that enables early diagnosis and better treatment of disease. Most biomarkers identified so far have been disappointing, but millions of men are tested for one of them: PSA, or prostate-specific antigen, which cells in the prostate gland churn out at higher levels when cancer is present.

But some men with high PSA levels don't have the disease, leading to unnecessary biopsies, and some with low PSA levels do. PSA testing is routine in some places, yet large clinical trials in the United States and Europe are questioning how big an impact it has on reducing cancer deaths. This week, a group in Iceland suggests a new way to assess PSA results: Acknowledge that under normal circumstances some men produce more (and some produce less) PSA, and individualize healthy and high levels for each man tested by focusing on genetic variants that affect PSA levels.

"Let's say that a PSA level of 4 is considered worrisome," says William Catalona of Northwestern University Feinberg School of Medicine in Chicago, Illinois. He developed the original PSA test and is a co-author of the new work, published in *Science Translational Medicine*. "You might be able to take something like a tongue depressor and scrape a man's cheek," and with DNA testing "you might find out this man is a high PSA secretor" normally, reducing concern.

The researchers on the PSA study, led by geneticists Julius Gudmundsson and Kari Stefansson of deCODE Genetics in Reykjavik, began by scanning the genomes of about 16,000 men to identify places in the genome that modify the PSA level in blood. They found six, including three that were previously identified. Then the group compared more than 5000 men with prostate cancer and 41,000 without. They assessed whether variants at the six sites modified PSA and prostate cancer risk. Although it's difficult to disentangle genetic effects on PSA levels from those on prostate cancer risk, the researchers concluded that two of the variants influenced only PSA levels and two others had only a marginal effect on cancer, making all four useful for testing.

> *"Basically what we're talking about is changing the parameters of detection of disease."*
>
> —RICHARD HAYES, NEW YORK UNIVERSITY

PSA levels for the men in the study varied widely. The key was whether genetic analysis would shift the men into different categories—for example, whether a man whose PSA level might merit a prostate biopsy would escape biopsy once his genes were taken into account. The numbers here were modest: About 6% had their PSA measurement reclassified as either safe or unsafe based on their genetics. "Basically what we're talking about is changing the parameters of detection of disease," says Richard Hayes, an epidemiologist at New York University who has studied some of these gene variants. In theory, the approach could be applied to biomarkers for other cancers, too, making them more precise and more clinically useful.

The study looked back in time, so the genes didn't influence health care decisions. And Hayes and others agree that although the concept of using genetics to make PSA tests more meaningful holds promise, these specific variants aren't ready for prime time. The finding "is a good start, but it's not sufficient to introduce this extensive genetic screening to everybody," says Fritz Schröder, a urologist at Erasmus Medical Center in Rotterdam, the Netherlands.

A valid gene-based PSA analysis could help, Stefansson claims, by, for example, enabling some men with high PSA results to avoid a biopsy. But genetic analysis cannot yet be used to tackle a different puzzle: Many men with high PSA results do have cancer but an "indolent" form that grows so slowly that it's unlikely to kill them if left untreated.

There is currently no way to distinguish the men at high risk of dying from their prostate cancer from those with a minimal risk of dying. The deCODE study didn't examine whether adding genetics to the mix could help reduce mortality. The deCODE group and others now need to examine "how many people they can help," says Stacy Loeb, chief resident in urology at Johns Hopkins University in Baltimore, Maryland, who has studied PSA genetics.

Two large U.S. and European clinical trials underscore this need. Both trials randomly assigned tens of thousands of men to get regular PSA testing, or not, and then followed them to see who developed prostate cancer and who died of it. Last year in *The New England Journal of Medicine*, the U.S. study reported no difference in mortality between the group that had regular PSA screening and the one that did not. The European team, led by Schröder, found that those who got PSA screening were 20% more likely to survive prostate cancer. Schröder attributes the contrasting results to different study designs; both groups are continuing to follow the men.

Meanwhile, PSA testing is in flux. Earlier this month, a cancer screening committee in the United Kingdom advised against routine PSA testing, citing concerns about overdiagnosis of slow-moving cancers. In other European countries, the popularity of PSA testing varies, says Schröder. It remains routine in the United States.

"I'm reluctant to make any predictions" about how PSA genetics might help guide early detection of prostate cancer, says Stephen Chanock, chief of the laboratory of translational genomics at the National Cancer Institute in Bethesda, Maryland, who works in this area. While he commends the deCODE group for pushing the ball forward, he says, "one really would want to see further confirmation and precision" in the number of men affected by these gene variants and the effect each variant has on PSA.

–JENNIFER COUZIN-FRANKEL

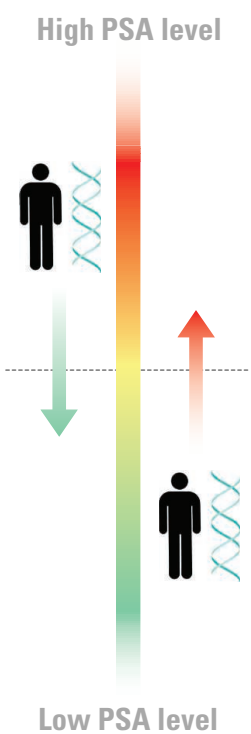

Adjustable baseline. A man's genes affect normal PSA levels. The border marking the danger zone for cancer risk (dotted line) may shift, depending on an individual's DNA.

Published by AAAS

The Top 10 *Science*NOWs of 2010

Here's a look back at some of our favorite and most popular stories of the year. As in previous years, the 2010 batch is an eclectic mix. And it contains something special: our most popular story of all time.

THE SECRET OF TURTLE ISLAND

10 In the Mediterranean Sea off the coast of Libya, there's an area local fishermen call "Turtle Island." It's real enough, but you'd be foolish to try to set foot on it. That's because it's composed of groups of loggerhead turtles. Biologists think they now know why the reptiles cluster like this.

SUPERACCURATE CLOCKS CONFIRM YOUR HAIR IS AGING FASTER THAN YOUR TOENAILS

9 According to Einstein's theory of relativity, a clock on the floor ought to run very slightly slower than an identical one on top of a step stool because the lower clock nestles deeper into Earth's gravitational field. Now, physicists have demonstrated this effect using two superaccurate clocks and hoisting one several centimeters above the other. It's the first time scientists have used clocks to show that time flies faster for your nose than for your navel.

THE SHOCKING TRUTH ABOUT RUNNING SHOES

8 Haile Gebrselassie, the world's fastest marathoner, once said of his early career, "When I wore shoes, it was difficult." A new study reveals why: Humans run differently in bare feet. Researchers have discovered that sneakers and other sports shoes alter our natural gait, which normally protects us from the impact of running. The finding offers new insight on how early humans ran and raises concerns that sports shoes may promote more injuries than they prevent.

HOW TO TRAIN YOUR ROBOT (TO LIE)

7 Just what the world needs: lying robots. Well, at least these guys don't look dangerous. Researchers have programmed small machines to trick each other—the first time scientists have deliberately implanted deceit.

THE SPIKY PENIS GETS THE GIRL

6 When it came to insect penises, Charles Darwin had it right. The famed naturalist suspected that insect genitalia, which are frequently festooned with bizarre combinations of hooks, spines, and knobs, essentially functioned like peacock tails. That is, they helped males beat out their rivals for females. Now, researchers have confirmed this hypothesis by zapping fly penises with a laser.

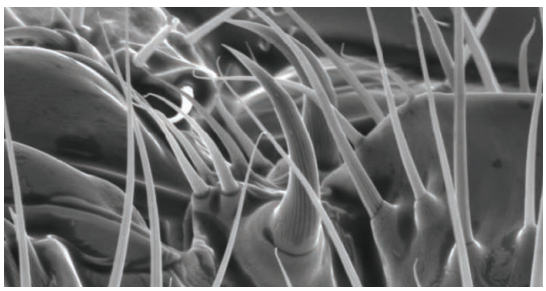

TINY 'FLYING SAUCERS' COULD SAVE EARTH FROM GLOBAL WARMING

5 Geoengineering—the concept of tinkering with the atmosphere to curb climate change—has seen some wacky ideas. But this may be the most bizarre of them all. Using a trick of sunlight itself, a researcher says tiny metallic disks could be levitated to the stratosphere, where they would shade Earth's surface and counteract the effects of global warming.

IS YOUR DOG PESSIMISTIC?

4 Why do dogs yowl when their owners leave home? According to this study, it's because they're down on life. The finding could help owners find ways to improve their dogs' mood.

OIL DROP NAVIGATES COMPLEX MAZE

3 Here's an ego crusher for mice. Scientists have found a way to make simple droplets of oil navigate complex labyrinths with the same skill as laboratory rodents. The advance could help researchers devise better ways to solve other mazelike problems, from rooting out cancer in the body to mapping paths through traffic jams.

THESE DANCE MOVES ARE IRRESISTIBLE

2 Hey, guys, want to impress ladies on the dance floor? Keep your head and torso moving and don't flail your arms and legs. This useful advice comes courtesy of a new study, which finds that women are more attracted to computer avatars that rock these moves.

1 ... AND THE TOP *SCIENCE*NOW OF 2010—AND THE MOST POPULAR OF ALL TIME—IS ...

Here's a hint:

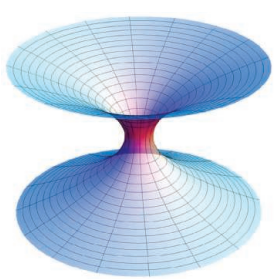

Go to **http://scim.ag/top10-2010** to find out the answer.

Daily postings, comments, and more are available at **http://news.sciencemag.org/sciencenow**.

CREDITS (FROM TOP): M. POLAK AND N. KAVAL; F. MAFFUCCI; GEORGIA INSTITUTE OF TECHNOLOGY; WIKIMEDIA COMMONS; D. LIEBERMAN/HARVARD UNIVERSITY; WIKIPEDIA; PHOTOS.COM

Published by AAAS

BREAKTHROUGH OF THE YEAR

The First Quantum Machine

A humanmade object that moves in ways that can be described only by quantum mechanics might lead to tests of our notion of reality

IT MAY NOT PROVE AS HANDY AS THE Model T, but, conceptually, a tiny machine unveiled this year blows the doors off Henry Ford's famous car or any other previous machine. Until now, all machines have moved according to the not-surprising laws of classical mechanics, which govern the motion of everyday objects. In contrast, the new gizmo jiggles in ways explicable only by the weird rules of quantum mechanics, which ordinarily govern molecules, atoms, and subatomic particles. The proto-quantum machine opens the way to myriad experimental devices and perhaps tests of our sense of reality. That potential and the ingenuity of the experiment make it the Breakthrough of the Year.

Thanks to quantum mechanics, the realm of the extremely small looks nothing like our everyday world. Quantum theory dictates that a very tiny thing can absorb energy only in discrete amounts, can never sit perfectly still, and can literally be in two places at once. Scientists have observed such quantum effects and weirder ones in countless experiments with atoms, molecules, subatomic particles, light, electric currents, and even liquid helium. But nobody had seen such effects in the motion of a humanmade object.

Not that physicists weren't trying. Researchers have fashioned tiny beams of semiconductor nanometers wide and micrometers long. Such a beam, or "oscillator," will vibrate at a set frequency like a guitar string, and according to quantum theory, it can absorb or emit energy only in dollops or quanta whose size is proportional to the beam's frequency. To see such effects, physicists first have to suck out every possible quantum and leave a beam in its least-energetic "ground state." Even then, a beam can't stand perfectly still, as quantum uncertainty requires it to hold an irretrievable half-quantum of energy and dance with unquenchable "zero-point motion."

To reach the ground state, physicists had to cool their beams to nearly absolute zero. They also had to make the quanta as large as possible by making a beam stiffer to increase its frequency. But that also reduces the amplitude of the motion, making it harder to detect. So several teams are using laser light or microwaves to cool a beam and detect its motion, getting them within a few quanta of the promised land.

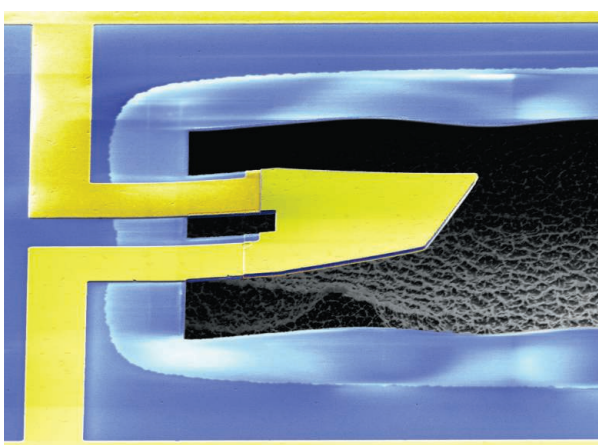

Springboard. Scientists achieved the simplest quantum states of motion with this vibrating device, which is as long as a hair is wide.

A team of American physicists found a quicker route, as they reported in March. Instead of a beam, they fashioned a tiny diving board of aluminum nitride plated with aluminum that vibrated by getting thinner and thicker. As the doohickey hummed away at a very high frequency—a whopping 6 billion cycles per second—the "piezoelectric" material in it produced a warbling electric field that was easy to detect. Most important, through that field, the physicists managed to "couple" the mechanical device to an electronic one called a "phase qubit," a ring of superconductor that itself has one low-energy and one high-energy quantum state.

Manipulating the qubit with microwaves, the researchers could use it to feed energy quanta into the oscillator or pull them out of it, as one might use an ATM to deposit a $20 bill to a bank account or withdraw one. First they showed that when they cooled the oscillator to a few hundredths of a degree they could get no quanta out of it. That meant it had to be in the cashed-out ground state, jiggling with only zero-point motion. The researchers then put the oscillator in a state with exactly one more quantum of energy. They even coaxed it into both states at once, so that it was literally moving two different amounts simultaneously.

The ingenuity in this scheme lay in the design of the oscillator and the use of a qubit to control it. In fact, in 2009, the team used a phase qubit to feed quanta into a long strip of superconducting metal that would ring with microwaves much as an organ pipe rings with sounds. Once they worked the kinks out, they replaced the microwave cavity with their clever mechanical oscillator, a move that had other physicists slapping their foreheads for not having seen it coming.

What use is it? In basic research, simple quantum machines might make ultrasensitive force detectors or serve to generate quantum states of light. Most grandly, they might help test the bounds of quantum theory and our sense of reality. Why can't a car or a person be in two slightly different places at once? Does some principle forbid it? One way to find out would be to try to put ever larger things in such states.

Such a test of quantum mechanics is a long way off. Still, other groups are already working toward quantum control of the motion of human-scale objects. In fact, after it is upgraded over the next 5 years, the Laser Interferometer Gravitational-Wave Observatory, which has sites in Livingston, Louisiana, and Hanford, Washington, will feature pairs of 40-kilogram mirrors laser-cooled to their ground states of motion, which may give physicists an opportunity to attempt an experiment on a very large scale.

But first, physicists had to achieve a quantum state of motion for a mechanical object. And in 2010 they did just that.

–ADRIAN CHO

Online

sciencemag.org

Expanded versions of Breakthrough of the Year and Insights of the Decade, plus podcast, video, reader picks, and more, at www.scim.ag/2010btoy

CREDIT: AARON D. O'CONNELL AND ANDREW N. CLELAND/UNIVERSITY OF CALIFORNIA, SANTA BARBARA

Published by AAAS

THE RUNNERS-UP >>

Build Your Own Genome

A technical tour de force grabbed headlines around the world for synthetic biology this year. In what was hailed as a defining moment for biology and for biotechnology, researchers at the J. Craig Venter Institute (JCVI) in Rockville, Maryland, and San Diego, California, built a synthetic genome and inserted it into a bacterium in place of the organism's original DNA. The new genome caused the bacterium to produce a new set of proteins.

The synthetic genome was an almost identical copy of a natural genome, but ultimately, researchers envision synthetic genomes custom-designed to produce biofuels, pharmaceuticals, or other useful chemicals. Also this year, researchers at Harvard University improved their high-throughput method of modifying existing genomes for such purposes, and other synthetic biologists showed that RNA-based "switches" can get cells to behave differently in response to certain signals.

J. Craig Venter and his team built its $40 million genome from smaller pieces of store-bought DNA. First they stitched the synthetic DNA together in stages in yeast; then they transplanted it into a bacterium, where it replaced the native genome.

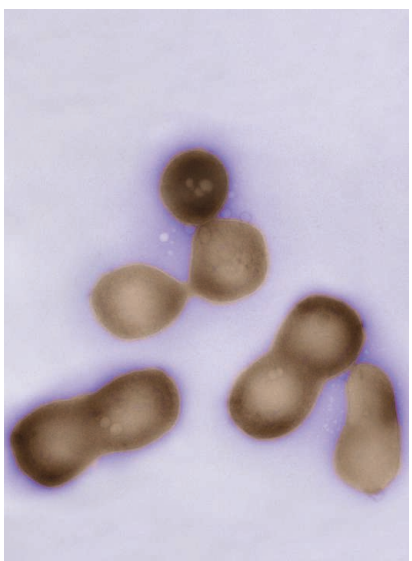

Life recreated. Scanning electron microscope image of bacteria with synthetic genomes.

Although not truly "artificial life," as some media declared, this success prompted a congressional hearing and a review by a presidential commission on the ethics of synthetic biology.

It's far from the only synthetic biology game in town, however. In 2009, Harvard's George Church introduced a technique called multiplex genome engineering, which adds multiple strands of DNA to bacteria every couple of hours, rapidly generating genetically engineered organisms with extensively revamped genomes. This year, his team came up with a cheaper way to produce the DNA strands used to modify the genome, in hopes of making this approach cost-effective for industrial use.

Teams led by Caltech's Niles Pierce, Stanford University's Christina Smolke, and Boston University's James Collins have come up with ways to change a cell's behavior by modifying its regulatory pathways. In some cases, they add specially designed RNA molecules that can sense molecules in the cell associated with, say, cancer or inflammation. Once that happens, they cause the cell to produce a protein that may sensitize the cell to drugs or cause it to undergo programmed cell death. Another team made a riboswitch that caused bacteria to seek out and destroy the herbicide atrazine. Such devices are much closer than synthetic and modified genomes to having practical applications.

In the DNA. Some living humans may have Neandertal ancestors.

Reading the Neandertal Genome

Thirteen years ago, when researchers sequenced just a few snippets of mitochondrial DNA from a Neandertal, the breakthrough made headlines worldwide. This year, researchers published a draft of the Neandertal nuclear genome—and their first analysis of what these 3 billion bases of DNA reveal about the evolution of these extinct humans and us.

Using new methods to sequence degraded fragments of ancient DNA (see "Insights of the Decade," p. 1616), researchers spliced together a composite sequence from three female Neandertals who lived in Croatia 38,000 to 44,000 years ago, to reconstruct about two-thirds of the entire Neandertal genome. For the first time, scientists could compare in detail the genomes of Neandertals and of modern humans.

Reading this sequence, the researchers concluded that modern Europeans and Asians—but not Africans—have inherited between 1% and 4% of their genes from Neandertals. Apparently, Neandertals interbred with modern humans after they left Africa at least 80,000 years ago but before they spread into Europe and Asia. If correct, this stunning discovery challenges a model that says that as modern humans swept out of Africa, they completely replaced archaic humans such as Neandertals without interbreeding.

The Neandertal genome also gives researchers a powerful new tool to fish for genes that have evolved recently in humans, since they split from Neandertals. The catalog includes 78 differences in genes that encode proteins that are important for wound healing, the beating of sperm flagella, and gene transcription. Several encode proteins expressed in the skin, sweat glands, and inner sheaths of hair roots, as well as skin pigmentation—all differences that reflect adaptations to new climates and environments as modern humans spread around the globe.

The researchers have also identified 15 regions of interest that differ between humans and Neandertals, including genes that are important in cognitive and skeletal development. When mutated in humans, some of these genes contribute to diseases such as schizophrenia, Down syndrome, and autism, or to skeletal abnormalities such as misshapen clavicles and a bell-shaped rib cage.

As researchers close in on the few genes that separate us from Neandertals, they are also trying to decipher how differences in genetic code alter proteins produced in the lab. This year, scientists inserted 11 pairs of single peptides into eukaryote cells to test for differences in gene expression. With luck, they may pinpoint some of the genes that equipped us to survive while Neandertals went extinct.

Published by AAAS

Next-Generation Genomics

Genomics researchers savored the fruits of massively parallel sequencing in 2010. Cheaper, faster "next generation" machines have taken hold over the past 5 years; this year they yielded important results from several large projects.

One ambitious effort, the 1000 Genomes Project, seeks to find all single-base differences—or single-nucleotide polymorphisms (SNPs)—present in at least 1% of humans. It completed three pilot studies this year, which together identified 15 million SNPs—including 8.5 million novel ones. The information will help scientists track down mutations that cause diseases.

Researchers also finished cataloging all the functional elements in the genomes of the fruit fly *Drosophila melanogaster* and the nematode *Caenorhabditis elegans*; the results are expected to be published by year's end. In human DNA, the complete genome sequences of two Africans from hunter-gatherer tribes, the oldest known lineages of modern humans, confirmed the extensive genetic diversity within those groups. Researchers also produced a draft of the Neandertal genome (see p. 1605) and deciphered the genome from 4000-year-old hair preserved in Greenland's permafrost.

The cornucopia of results also included surveys of all the transcribed DNA—the so-called transcriptome—and of protein-DNA interactions, as well as assessments of gene expression and the identification of rare disease genes.

Souped-Up Cellular Reprogramming

Changing a cell's fate by adding extra copies of a few genes has become routine in labs around the world. The technique, known as cellular reprogramming, allows scientists to turn back a cell's developmental clock, making adult cells behave like embryonic stem cells (see "Insights of the Decade," p. 1612). The resulting induced pluripotent stem cells (iPSCs) are helping scientists to study a variety of diseases and may someday help to treat patients by supplying them with genetically matched replacement cells.

This year, scientists found a way to make reprogramming even easier using synthetic RNA molecules. The synthetic RNAs are designed to elude the cell's antiviral defenses, which usually attack foreign RNA. The technique is twice as fast and 100 times as efficient as standard techniques. And because the RNA quickly breaks down, the reprogrammed cells are genetically identical to the source cells, making them potentially safer for use in therapies.

Early evidence suggests that the RNA approach reprograms the cell more thoroughly than other methods do, yielding a closer match to embryonic stem cells. The method can also prompt cells to become nonembryonic cell types. By inserting synthetic RNA into a cell that codes for a key gene in muscle tissue, for example, the researchers could turn both fibroblasts and iPSCs into muscle cells.

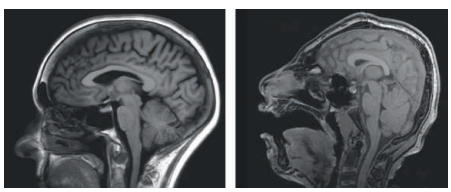

Homing In on Errant Genes

Scientists who study rare genetic disorders hit on a powerful strategy for finding the culprit DNA this year. Using cheap sequencing techniques and a shortcut—sequencing just the 1% of the genome that tells cells how to build proteins—they cracked several diseases that had eluded researchers until now.

The old way to track down the cause of Mendelian disorders, or diseases caused by a mutation in a single gene, was to study DNA inheritance patterns in families. That approach doesn't work when few relatives with the disease can be found or when a mutation isn't inherited but instead crops up spontaneously.

In late 2009, geneticists began sequencing just the exons, or protein-coding DNA, of patients with Mendelian disorders. (A few teams sequenced the patients' entire genome.) This "exome" sequencing yielded a long list of mutations that the scientists then winnowed, for example, by ignoring those that don't change protein structure or that many people carry. The end result: the faulty DNA underlying at least a dozen mystery diseases—including genes that lead to severe brain malformations, very low cholesterol levels, and facial deformities that look like a made-up Japanese Kabuki performer.

Finding the gene behind a rare disease can lead to better diagnosis and treatments and to new insights into human biology. Scientists hope to use exome sequencing to tick off the causes of more than half of some 7000 known or suspected Mendelian diseases that still don't have a genetic explanation.

Quantum Simulators Pass First Key Test

Like a student who sneaks a calculator into a test, physicists have found a quick way to solve tough mathematical problems. This year, they showed that quantum simulators—typically, simulated crystals in which spots of laser light play the role of the crystal's ions and atoms trapped in the spots of light play the role of electrons—can quickly solve problems in condensed-matter physics.

Physicists usually invent theoretical models to explain experiments. They might approximate a magnetic crystal as a three-dimensional array of points with electrons on the points interacting through their magnetic fields. Theorists can jot down a mathematical function called a Hamiltonian encoding such an idealization. But "solving" a Hamiltonian to reveal how a system behaves—for example, under what conditions the electrons align to magnetize the crystal—can be daunting.

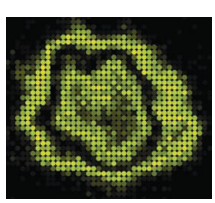

CREDITS (TOP TO BOTTOM): STEVEN EVANS/WIKIPEDIA; MURAT GUNEL; W. S. BAKR *ET AL.*, *SCIENCE* **329**, 547 (30 JULY 2010)

Published by AAAS

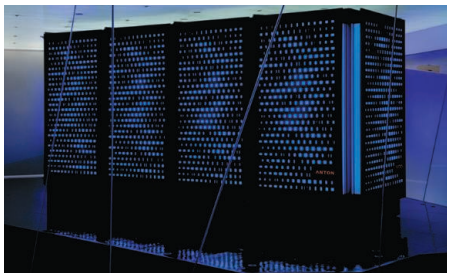

Molecular Dynamics Simulations

Sometimes brute force is the way to go, particularly when using computers to simulate the gyrations proteins make as they fold. Such simulations are a combinatorial nightmare. Each two neighboring amino acids in a protein chain can bind to one another at two different angles, each of which can have three conformations. So a simple protein with 100 amino acids can fold in 3^{198} different ways. Getting at the atomic detail is even scarier. Proteins sort through all these possibilities in milliseconds or less. Computers take far longer.

Protein-folding experts have long turned to supercomputers for help. But even these behemoths struggle to track the motions long enough to simulate the complete folding process. Two years ago, researchers in the United States unveiled a new supercomputer hardwired with 512 computer chips tailor-made to speed the calculations of the way neighboring atoms in a protein and the surrounding water interact. That enabled them to gain another burst in speed. As a result, the group reported this year that they've been able to track the motion of atoms in a small protein 100 times longer than previous efforts could do—long enough to see the protein wind its way through 15 cycles of folding and unfolding. Next up, the group is already turning to novel machines with 1024 and 2048 chips to improve simulations of larger proteins.

However, physicists can tailor a quantum simulator to a particular Hamiltonian and let the experiment solve the theoretical problem. Five groups reproduced the results for four previously solved Hamiltonians. Three even mapped "phase diagrams" akin to the one that shows the temperatures and pressures at which water becomes a gas, liquid, or solid.

Physicists hope quantum simulators will crack Hamiltonians that have not been solved—such as one for high-temperature superconductors. But first they had to show that the things could reproduce known results. Check.

Rats Redux

Today, most lab cages house mice, but the tenant of choice used to be rats. The reason: Rats are more like us. The human heart, for example, beats about 70 times a minute; a rat's heart, 300 times; a mouse's, 700. Electrical signal patterns in rat and human hearts are also similar. Rats, being more intelligent than mice, might also be better models of human neural diseases such as Alzheimer's and Parkinson's. And rats are bigger and easier to handle for lab work.

Then, in 1989, researchers learned to delete specific genes to make "knockout mice." The technique they used, called homologous recombination of embryonic stem cells, didn't work in rats. So mice became the preferred experimental animal in various studies, from developmental biology to drug development.

That too may pass. In 2009, researchers adapted to rats a method, previously used in fruit flies and zebrafish, that uses enzymes called zinc finger nucleases to knock out genes. In August, another group announced a tweak that produced "knockout rats" by the same genetic trick used for knockout mice. Also this year, several groups reported advances in using transposons, DNA sequences that jump from one location to another within a genome, to generate rats with genetic mutations—animals useful for developmental biology and disease research. As a result of such techniques, knockout and genetically modified rats may soon displace their smaller cousins in lab cages around the world.

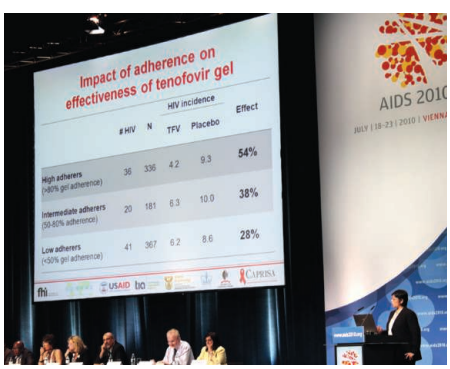

HIV Prophylaxis

From the start of the AIDS epidemic through 2009, only five of 37 large-scale studies that attempted to prevent HIV yielded convincing, positive results. Then, this past July and November, two trials of different, novel HIV-prevention strategies unequivocally reported success. AIDS researchers all but danced with joy.

The first result stole the show at the jam-packed XVIII International AIDS Conference held in Vienna, Austria. A vaginal gel that contains the anti-HIV drug tenofovir reduced HIV infections in high-risk women by 39% over a 30-month period. Nearly 900 South African women participated in the study, half receiving the microbicide and the others an inert gel. Among "high adherers," women who used the microbicide exactly as instructed, its efficacy reached 54%.

Last month, the first-ever study of oral pre-exposure prophylaxis made headlines with results even more encouraging. The subjects, 2499 men and transgender women who have sex with men, were recruited from six countries. Half were asked to take Truvada, a combination of tenofovir and emtricitabine, each day. After an average of 1.2 years, the treated group had 43.8% fewer infections than the group that took a placebo. Again, better adherence equaled better efficacy: In a small substudy, efficacy increased to 92% in participants who had measurable levels of Truvada in their blood.

Neither approach is a magic bullet, AIDS researchers say. But in combination with other measures, they could usher in a new era of HIV prevention.

CREDITS (TOP TO BOTTOM): © 2009 MATTHEW MONTEITH; ISTOCKPHOTO; JON COHEN

Published by AAAS

Diving Into the Oil Spill

During the massive, 3-month oil spill in the Gulf of Mexico this year, scientists were quick to offer help. It wasn't always easy. Many researchers in the region at first felt unwanted; there were rough patches in coordinating academic and government scientists; and clashes over when to release data sometimes sent the public mixed messages. But through improved communication, researchers ultimately helped devise ways to deal with the leaking well and assessed the scale of the spill.

One early source of confusion was the conflicting estimates of the amount of oil flowing from the well. At first, BP estimated 1000 barrels per day. Academic scientists accused the company of low-balling, and a National Oceanic and Atmospheric Administration (NOAA) scientist studying a video figured the rate was roughly five times higher. The resulting scientific debate and public confusion over the flow rate—which will be crucial for determining BP's fine—might have been lessened if the various groups had shared their methods and data. Eventually, an ad hoc task force of government scientists estimated the flow at 35,000 to 60,000 barrels per day, a figure made more rigorous by sensors added to the wellhead.

As the oil continued to gush, academic scientists hopped on boats and rearranged their research plans to investigate the extent of the spill and the damage to wetlands and wildlife. But lack of coordination bred tensions, and researchers clashed over when to release preliminary data and how much to speculate on their meaning. The highest-profile example was the surprise discovery on 15 May of what appeared to be oil plumes. When NOAA Administrator Jane Lubchenco tried to sound a note of caution about the preliminary results, researchers and media blasted her for squelching the discovery (*Science*, 2 July, p. 22). In June, NOAA confirmed the plumes.

One of the most controversial decisions was to use dispersants to keep oil from reaching wetlands and islands. A group of experts convened to advise the government approved the unprecedented use of dispersants at depth, which appears to have worked.

Overall, the spill appears to have been less of an environmental disaster than first feared, at least for the wetlands and barrier islands. But it will take years before the toll is fully known, especially for deep-sea organisms. A $500 million research fund, set up by BP, will help scientists gauge the long-term impact.

–ERIK STOKSTAD

SCORECARD

Rating Last Year's Areas to Watch

IPS CELLS

Last year, we predicted that the ability to reprogram adult skin cells into induced pluripotent stem cells (iPSCs) would usher in a new wave of research based on patient-specific cell lines. In 2010, researchers made new cell lines from hundreds of patients with dozens of disorders. Patient-derived iPSCs, which can be coaxed to become various mature cell types, have helped scientists better understand Rett syndrome and genetic heart defects, among other conditions. But finding new treatments for more common conditions, say, Parkinson's disease or diabetes, is still a work in progress.

COSMIC EYE

The Alpha Magnetic Spectrometer (AMS) particle detector didn't make it into space aboard NASA's space shuttle as planned, but it had an interesting year nevertheless. Destined for the international space station, AMS received a last-minute design change in April that delayed its launch by 4 months until November. Then, in July, NASA delayed its shuttle schedule for other reasons, pushing the launch into 2011. AMS is now scheduled to go up on 1 April. No fooling.

AREAS TO WATCH

THE LARGE HADRON COLLIDER

The first really interesting results will come out of the LHC this year, and dollars to doughnuts they'll have nothing to do with the search for the Higgs boson or supersymmetric particles with the collider's two big detectors, ATLAS and CMS. Rather, look for results from a smaller detector called LHCb, which will study familiar particles called B mesons in great detail with an eye to probing a slight asymmetry between matter and antimatter called CP violation. CP violation in ordinary B mesons seems to conform to physicists' standard theory. This year, however, researchers at Fermi National Accelerator Laboratory in Batavia, Illinois, reported hints that there could be extra CP violation in a subspecies called Bs mesons—a possible sign of new particles on the horizon. Collecting data at a massive rate, LHCb should test those claims in short order.

ADAPTATION GENES

Ecologists and evolutionary biologists are busy harnessing the faster, cheaper sequencing technologies to learn which genes help organisms, from bacteria to butterflies, thrive in the natural world. Until now, such genome scans were very difficult to do in organisms that weren't also already well studied in the lab. But new techniques, such as one called RAD tag sequencing, should lead to the discovery of many more genes contributing to adaptation in the coming year.

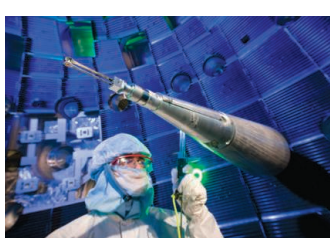

LASER FUSION

The National Ignition Facility (NIF) at Lawrence Livermore National Laboratory in California will make an end run in 2011 for a long-sought goal of energy research: an ignited fusion burn. Shots from NIF's 192 laser beams will pump energy into a peppercorn-sized target containing deuterium and tritium. The ensuing implosion compresses and heats the nuclei until they begin to fuse, releasing

CREDITS (TOP TO BOTTOM): AP; © 2009, JAY MATTERNES; LAWRENCE LIVERMORE NATIONAL LABORATORY

Published by AAAS

Diving Into the Oil Spill

During the massive, 3-month oil spill in the Gulf of Mexico this year, scientists were quick to offer help. It wasn't always easy. Many researchers in the region at first felt unwanted; there were rough patches in coordinating academic and government scientists; and clashes over when to release data sometimes sent the public mixed messages. But through improved communication, researchers ultimately helped devise ways to deal with the leaking well and assessed the scale of the spill.

One early source of confusion was the conflicting estimates of the amount of oil flowing from the well. At first, BP estimated 1000 barrels per day. Academic scientists accused the company of low-balling, and a National Oceanic and Atmospheric Administration (NOAA) scientist studying a video figured the rate was roughly five times higher. The resulting scientific debate and public confusion over the flow rate—which will be crucial for determining BP's fine—might have been lessened if the various groups had shared their methods and data. Eventually, an ad hoc task force of government scientists estimated the flow at 35,000 to 60,000 barrels per day, a figure made more rigorous by sensors added to the wellhead.

As the oil continued to gush, academic scientists hopped on boats and rearranged their research plans to investigate the extent of the spill and the damage to wetlands and wildlife. But lack of coordination bred tensions, and researchers clashed over when to release preliminary data and how much to speculate on their meaning. The highest-profile example was the surprise discovery on 15 May of what appeared to be oil plumes. When NOAA Administrator Jane Lubchenco tried to sound a note of caution about the preliminary results, researchers and media blasted her for squelching the discovery (*Science*, 2 July, p. 22). In June, NOAA confirmed the plumes.

One of the most controversial decisions was to use dispersants to keep oil from reaching wetlands and islands. A group of experts convened to advise the government approved the unprecedented use of dispersants at depth, which appears to have worked.

Overall, the spill appears to have been less of an environmental disaster than first feared, at least for the wetlands and barrier islands. But it will take years before the toll is fully known, especially for deep-sea organisms. A $500 million research fund, set up by BP, will help scientists gauge the long-term impact.

–ERIK STOKSTAD

SCORECARD

Rating Last Year's Areas to Watch

IPS CELLS

Last year, we predicted that the ability to reprogram adult skin cells into induced pluripotent stem cells (iPSCs) would usher in a new wave of research based on patient-specific cell lines. In 2010, researchers made new cell lines from hundreds of patients with dozens of disorders. Patient-derived iPSCs, which can be coaxed to become various mature cell types, have helped scientists better understand Rett syndrome and genetic heart defects, among other conditions. But finding new treatments for more common conditions, say, Parkinson's disease or diabetes, is still a work in progress.

COSMIC EYE

The Alpha Magnetic Spectrometer (AMS) particle detector didn't make it into space aboard NASA's space shuttle as planned, but it had an interesting year nevertheless. Destined for the international space station, AMS received a last-minute design change in April that delayed its launch by 4 months until November. Then, in July, NASA delayed its shuttle schedule for other reasons, pushing the launch into 2011. AMS is now scheduled to go up on 1 April. No fooling.

AREAS TO WATCH

THE LARGE HADRON COLLIDER

The first really interesting results will come out of the LHC this year, and dollars to doughnuts they'll have nothing to do with the search for the Higgs boson or supersymmetric particles with the collider's two big detectors, ATLAS and CMS. Rather, look for results from a smaller detector called LHCb, which will study familiar particles called B mesons in great detail with an eye to probing a slight asymmetry between matter and antimatter called CP violation. CP violation in ordinary B mesons seems to conform to physicists' standard theory. This year, however, researchers at Fermi National Accelerator Laboratory in Batavia, Illinois, reported hints that there could be extra CP violation in a subspecies called Bs mesons—a possible sign of new particles on the horizon. Collecting data at a massive rate, LHCb should test those claims in short order.

ADAPTATION GENES

Ecologists and evolutionary biologists are busy harnessing the faster, cheaper sequencing technologies to learn which genes help organisms, from bacteria to butterflies, thrive in the natural world. Until now, such genome scans were very difficult to do in organisms that weren't also already well studied in the lab. But new techniques, such as one called RAD tag sequencing, should lead to the discovery of many more genes contributing to adaptation in the coming year.

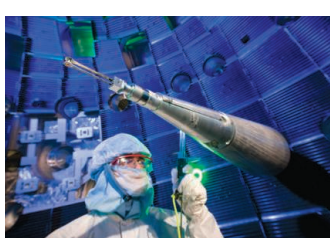

LASER FUSION

The National Ignition Facility (NIF) at Lawrence Livermore National Laboratory in California will make an end run in 2011 for a long-sought goal of energy research: an ignited fusion burn. Shots from NIF's 192 laser beams will pump energy into a peppercorn-sized target containing deuterium and tritium. The ensuing implosion compresses and heats the nuclei until they begin to fuse, releasing

CREDITS (TOP TO BOTTOM): AP; © 2009, JAY MATTERNES; LAWRENCE LIVERMORE NATIONAL LABORATORY

Published by AAAS

EXOME STUDIES

This new way of gene hunting—sequencing just protein-coding DNA—revealed the errant DNA underlying a dozen or so rare diseases (see Runner-Up, p. 1606). But exome sequencing hasn't yet found the elusive mutations that geneticists hope will explain much of the missing heritability for common disorders, such as Alzheimer's disease, diabetes, and heart disease. These studies require thousands of patients' exomes, and at year's end, researchers were still collecting data and analyzing their results.

BIOCHEMISTRY BEATS CANCER?

Safety has been the stumbling block for treatments that tamper with cancer metabolism. But this year, a preliminary trial gave the compound dichloroacetate a passing grade. Researchers also exposed new metabolic eccentricities of cancer cells that might inspire fresh avenues of attack.

HUMAN SPACE FLIGHT

As forecast, President Obama set a new direction for the U.S. space program. But the plan drew fire from Congress, which eventually accepted it only in part. Obama wanted to scrap the Bush Administration's $3.5-billion-a-year Constellation program and invest $3.3 billion over the next 3 years in the development of commercial spacecraft. In an authorization measure, Congress allowed NASA to spend $1.3 billion on commercial spacecraft development and required that the agency start building a heavy-lift rocket next year, instead of after 2015, as Obama had proposed. Congress also gave the space shuttle one more flight next year, instead of retiring it in 2010.

energy. If that self-heating causes a sustained fusion burn with energy gain, NIF will have finally shown that generating power from fusion is at least possible.

HAMMERING VIRUSES

Most antibodies are quite specific, derailing only viruses that look alike. But broadly neutralizing antibodies (bNAbs) are immune system generalists, capable of disabling a wide range of viral variants. Recent progress in identifying bNAbs effective against HIV and in developing a flu vaccination strategy in animals that elicits these generalists have brought us closer to harnessing these molecules. In 2011, researchers hope to come up with the viral pieces—the main vaccine ingredients—that trigger the immune system to make bNAbs.

ELECTRIC CARS

Toyota's Prius and other gas-electric hybrids have been on the market for years. But in 2011, plug-in hybrid electric cars that charge a car's batteries from a wall socket are set to go mainstream. These cars make a marked shift in the demands put on battery technology to take consumers where they want to go. For now, battery-powered cars cost more than their gasoline-powered alternatives. Will consumers give up their long-distance driving range and the convenience of a quick fill-up to produce less carbon emissions? Doesn't seem like a sure bet.

MALARIA SHOTS

Scientists can't wait for the results of the first phase III trial of a malaria vaccine. Up to 16,000 children in seven African countries are taking part in the study; the results for almost 9000 of them—the cohort aged 5 to 17 months—will be announced late in 2011. The vaccine, called RTS,S, offered roughly 50% protection in phase II studies. That's not spectacular, but given the field's frustrating history, expect elation—and a speedy application for regulatory approval—if the phase III study does equally well.

Whiplash for Stem Cell Researchers

The field of stem cell research in the United States was shaken to its core last summer when a federal court banned taxpayer-funded research on human embryonic stem cells (hESCs). Although a higher court soon allowed the research to continue temporarily, the ongoing lawsuit, *Sherley* v. *Sebelius*, has cast a shadow over the area that could linger well into 2011.

Stem cell scientists began the year on a high note, after the Obama Administration lifted Bush-era limits on which cell lines could be used in studies funded by the National Institutes of Health (NIH). Government lawyers and NIH weren't terribly worried about a lawsuit challenging the agency's July 2009 embryonic stem cell guidelines filed last year by two scientists, Christian groups, and an embryo adoption agency on behalf of embryos. And Chief Judge Royce Lamberth of the U.S. District Court in Washington, D.C., soon threw the suit out because the plaintiffs had not demonstrated they were harmed by the NIH policy.

The suit got a second wind last summer when an appeals court reversed Lamberth's ruling about the legal standing of the two scientists, James Sherley and Theresa Deisher, who claimed that the NIH guidelines made it harder for them to win grants to study adult stem cells. Lamberth then considered Sherley and Deisher's argument that the guidelines violated the Dickey-Wicker Amendment, which bans the use of federal funds for research that destroys embryos (a step necessary to derive hESCs). On 23 August, Lamberth ruled that NIH-funded hESC research likely violated the amendment and issued a preliminary injunction blocking it.

Brakeman. Judge Royce Lamberth's ruling threw hESC research into turmoil.

NIH Director Francis Collins said he was "stunned"; NIH suspended hESC grant payments and peer review and stopped research on the NIH campus. Lamberth's decision, Collins said, threw "sand into that engine of discovery." Researchers got a reprieve on 9 September, when the U.S. Court of Appeals for the District of Columbia Circuit lifted the ban while it considered the government's appeal of Lamberth's preliminary injunction. A three-judge panel that heard oral arguments on 6 December is expected to rule by mid-January—and no one is making bets on the outcome. Meanwhile, Lamberth could issue a permanent ban any day if he decides federally funded hESC research violates Dickey-Wicker. Any decision will likely be appealed, ultimately to the Supreme Court.

Since the September stay, it's officially been business as usual at NIH. But researchers say damage has already been done. The uncertainty about whether hESC research will be halted again—and the fading hope that Congress will pass a law allowing hESC research—has many scientists rethinking their work. U.S. postdocs are thinking twice about venturing into the field, and foreign graduate students are hesitating to take postdoc positions in U.S. labs. The legal tangle is yet another low point in the roller-coaster history of hESC research in the United States. **–JOCELYN KAISER**

CREDITS (TOP TO BOTTOM): AP; JAMES D. GATHANY/WIKIPEDIA

Published by AAAS

EXOME STUDIES

This new way of gene hunting—sequencing just protein-coding DNA—revealed the errant DNA underlying a dozen or so rare diseases (see Runner-Up, p. 1606). But exome sequencing hasn't yet found the elusive mutations that geneticists hope will explain much of the missing heritability for common disorders, such as Alzheimer's disease, diabetes, and heart disease. These studies require thousands of patients' exomes, and at year's end, researchers were still collecting data and analyzing their results.

BIOCHEMISTRY BEATS CANCER?

Safety has been the stumbling block for treatments that tamper with cancer metabolism. But this year, a preliminary trial gave the compound dichloroacetate a passing grade. Researchers also exposed new metabolic eccentricities of cancer cells that might inspire fresh avenues of attack.

HUMAN SPACE FLIGHT

As forecast, President Obama set a new direction for the U.S. space program. But the plan drew fire from Congress, which eventually accepted it only in part. Obama wanted to scrap the Bush Administration's $3.5-billion-a-year Constellation program and invest $3.3 billion over the next 3 years in the development of commercial spacecraft. In an authorization measure, Congress allowed NASA to spend $1.3 billion on commercial spacecraft development and required that the agency start building a heavy-lift rocket next year, instead of after 2015, as Obama had proposed. Congress also gave the space shuttle one more flight next year, instead of retiring it in 2010.

energy. If that self-heating causes a sustained fusion burn with energy gain, NIF will have finally shown that generating power from fusion is at least possible.

HAMMERING VIRUSES

Most antibodies are quite specific, derailing only viruses that look alike. But broadly neutralizing antibodies (bNAbs) are immune system generalists, capable of disabling a wide range of viral variants. Recent progress in identifying bNAbs effective against HIV and in developing a flu vaccination strategy in animals that elicits these generalists have brought us closer to harnessing these molecules. In 2011, researchers hope to come up with the viral pieces—the main vaccine ingredients—that trigger the immune system to make bNAbs.

ELECTRIC CARS

Toyota's Prius and other gas-electric hybrids have been on the market for years. But in 2011, plug-in hybrid electric cars that charge a car's batteries from a wall socket are set to go mainstream. These cars make a marked shift in the demands put on battery technology to take consumers where they want to go. For now, battery-powered cars cost more than their gasoline-powered alternatives. Will consumers give up their long-distance driving range and the convenience of a quick fill-up to produce less carbon emissions? Doesn't seem like a sure bet.

MALARIA SHOTS

Scientists can't wait for the results of the first phase III trial of a malaria vaccine. Up to 16,000 children in seven African countries are taking part in the study; the results for almost 9000 of them—the cohort aged 5 to 17 months—will be announced late in 2011. The vaccine, called RTS,S, offered roughly 50% protection in phase II studies. That's not spectacular, but given the field's frustrating history, expect elation—and a speedy application for regulatory approval—if the phase III study does equally well.

Whiplash for Stem Cell Researchers

The field of stem cell research in the United States was shaken to its core last summer when a federal court banned taxpayer-funded research on human embryonic stem cells (hESCs). Although a higher court soon allowed the research to continue temporarily, the ongoing lawsuit, *Sherley* v. *Sebelius*, has cast a shadow over the area that could linger well into 2011.

Stem cell scientists began the year on a high note, after the Obama Administration lifted Bush-era limits on which cell lines could be used in studies funded by the National Institutes of Health (NIH). Government lawyers and NIH weren't terribly worried about a lawsuit challenging the agency's July 2009 embryonic stem cell guidelines filed last year by two scientists, Christian groups, and an embryo adoption agency on behalf of embryos. And Chief Judge Royce Lamberth of the U.S. District Court in Washington, D.C., soon threw the suit out because the plaintiffs had not demonstrated they were harmed by the NIH policy.

The suit got a second wind last summer when an appeals court reversed Lamberth's ruling about the legal standing of the two scientists, James Sherley and Theresa Deisher, who claimed that the NIH guidelines made it harder for them to win grants to study adult stem cells. Lamberth then considered Sherley and Deisher's argument that the guidelines violated the Dickey-Wicker Amendment, which bans the use of federal funds for research that destroys embryos (a step necessary to derive hESCs). On 23 August, Lamberth ruled that NIH-funded hESC research likely violated the amendment and issued a preliminary injunction blocking it.

Brakeman. Judge Royce Lamberth's ruling threw hESC research into turmoil.

NIH Director Francis Collins said he was "stunned"; NIH suspended hESC grant payments and peer review and stopped research on the NIH campus. Lamberth's decision, Collins said, threw "sand into that engine of discovery." Researchers got a reprieve on 9 September, when the U.S. Court of Appeals for the District of Columbia Circuit lifted the ban while it considered the government's appeal of Lamberth's preliminary injunction. A three-judge panel that heard oral arguments on 6 December is expected to rule by mid-January—and no one is making bets on the outcome. Meanwhile, Lamberth could issue a permanent ban any day if he decides federally funded hESC research violates Dickey-Wicker. Any decision will likely be appealed, ultimately to the Supreme Court.

Since the September stay, it's officially been business as usual at NIH. But researchers say damage has already been done. The uncertainty about whether hESC research will be halted again—and the fading hope that Congress will pass a law allowing hESC research—has many scientists rethinking their work. U.S. postdocs are thinking twice about venturing into the field, and foreign graduate students are hesitating to take postdoc positions in U.S. labs. The legal tangle is yet another low point in the roller-coaster history of hESC research in the United States. **–JOCELYN KAISER**

CREDITS (TOP TO BOTTOM): AP; JAMES D. GATHANY/WIKIPEDIA

Published by AAAS

The Year in News

2010 was a busy year for science and science policy. Here are some developments that tested the limits of our knowledge and influenced thinking about the global research enterprise

January: A magnitude-7.0 earthquake in a long-recognized seismic zone kills more than 200,000 people in a highly vulnerable population.

February: A magnitude-8.8 quake results in fewer than 500 deaths thanks to quake-resistant building construction and an offshore epicenter.

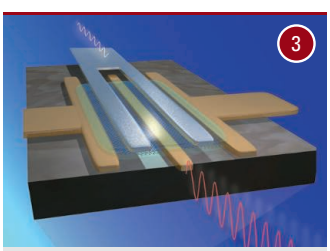

February: IBM researchers create graphene transistors that switch on and off at 100 billion times per second.

April: Arizona State University agrees to return DNA samples to the Havasupai tribe following questions about informed consent.

April: Explosion of *Deepwater Horizon* drilling platform triggers release of 205 million gallons of oil in the Gulf of Mexico—and research on effects that could last for decades.

April: Researchers evaluate the first data from the NEPTUNE project, an undersea cable network of sensors.

May: J. Craig Venter's group incorporates a synthetic genome into a microbe.

October: Four people die in helicopter crash involving employees at the French Polar Institute Paul Émile Victor.

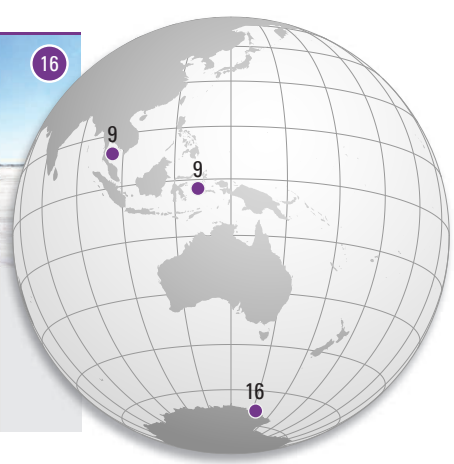

August: Federal judge blocks U.S. government funding of stem cell research.

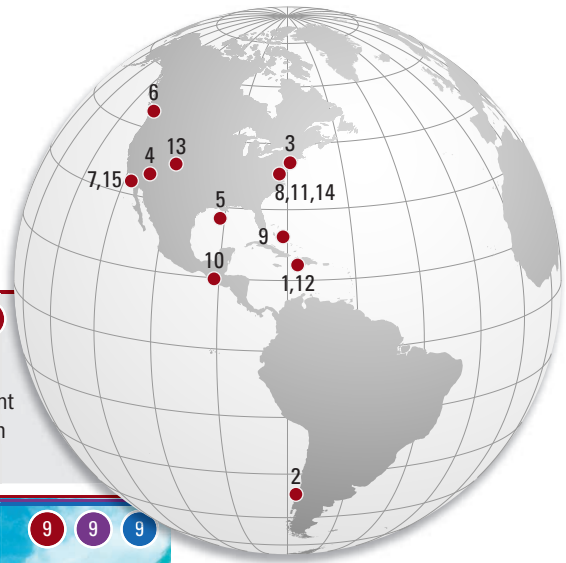

Summer/Fall: What may prove to be the worst coral bleaching on record devastates reefs in the Caribbean, the Indian Ocean, and the tropical Pacific.

September: Historian uncovers a syphilis study in Guatemala from the 1940s, and the U.S. government apologizes for its ethical lapses.

September: The U.S. and European governments sharply restrict use of the diabetes drug Avandia because of safety concerns, capping a long controversy.

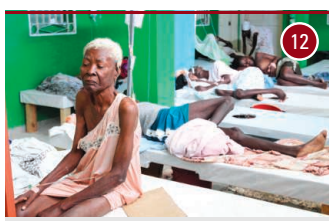

October: Explosive cholera outbreak erupts and spirals out of control.

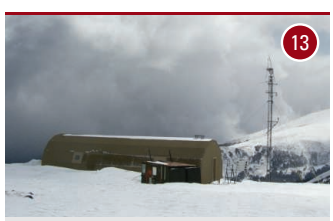

October: Construction completed on prototype site for NEON, an ecological observatory network to monitor long-term change on continental scales.

November: Study finds that CT exams cut death from lung cancer 20% among smokers—but screening has major costs.

November: Long-delayed NASA Stratospheric Observatory for Infrared Astronomy (SOFIA) completes first science flight.

CREDITS (TOP TO BOTTOM): AP; ISTOCKPHOTO; AP; NEPTUNE CANADA; E. PENNISI/*SCIENCE*; NEWSCOM; COURTESY OF WELLESLY COLLEGE; THINKSTOCK; NASA PHOTO/JIM ROSS

Published by AAAS

January: The Intergovernmental Panel on Climate Change offers "regrets" about overstating the rate of glacier melting in the Himalayas. 17

February: Government rejects commercial release of genetically modified brinjal (eggplant). 18

March: Eruption of Eyjafjallajökull volcano leads to the greatest disruption to air travel since World War II.

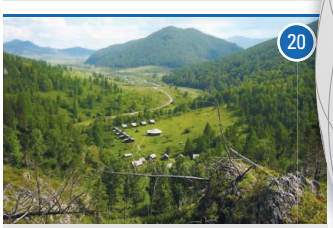

March: New species of human discovered from ancient DNA.

March: Science ministers declare 2011–2020 as the "Decade of Science in Africa." 21

April: Research center opens to develop technologies for a post-ITER fusion reactor. 22

April: Chinese Family Panel Studies survey, the largest long-term social science study in the developing world, begins. 23

May: Neandertal genome sequenced.

June: The Hayabusa spacecraft capsule lands in Australia with dust from asteroid Itokawa.

September: China's one-child policy turns 30.

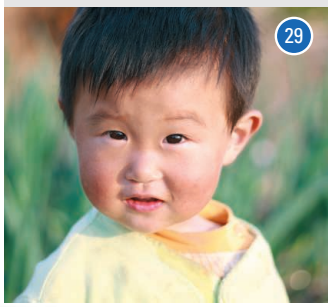

July: Funding profile approved for ITER fusion reactor project. 26

July: First positive HIV microbicide results from South Africa announced at international AIDS meeting. 27

August: Wildfires across Russia reach the region heavily affected by the Chornobyl nuclear disaster, raising fears that they could spread radiation.

October: Parties to the Convention on Biological Diversity adopt new targets to protect biodiversity and urge caution on geoengineering. 30

October: Plan to honor presidency of Teodoro Obiang with UNESCO science prize is put on ice after human rights protests.

October: Results of the first Census of Marine Life presented.

October: U.K. science avoids sharp cuts in government research spending. 33

October: The U.N. Food and Agriculture Organization proclaims end to rinderpest, a deadly cattle disease.

November: China unveils world's fastest supercomputer.

December: Launch of new, affordable meningitis vaccine to protect 450 million people. 36

Ongoing: BGI-Shenzhen enhances its reputation as world's largest sequencing center, deciphering an ant, a paleo-Eskimo, the human methylome, and a gene catalog of the human gut microbiome. 37

–JEFFREY MERVIS

CREDITS (TOP TO BOTTOM): AP; WHIT WELLES/WIKIPEDIA; GETTY IMAGES/ISTOCKPHOTO; AP; THINKSTOCK; JOHANNES KRAUSE; AP (2); EL SIDRON RESEARCH TEAM; WIKIPEDIA

Published by AAAS

INSIGHTS OF THE DECADE

INTRODUCTION

Stepping Away From the Trees For a Look at the Forest

***Science*'s news staff takes a break from reporting to review some big ideas of the past 10 years and the technologies that made them possible**

TEN YEARS AGO, KARL DEISSEROTH WAS stuck. A psychiatrist and neuroscientist, he wanted to learn how different brain circuits affect behavior—and what went awry in the brains of his patients with schizophrenia and depression. But the tools of his trade were too crude: Electrodes inserted into the brain would stimulate too many cells in their vicinity. So in 2004, Deisseroth and his students invented a new tool. They inserted a gene for a light-activated algal protein into mice brains, where it entered nerve cells. By stimulating those cells with a laser, the researchers could control the activity of specific nerve circuits with millisecond precision and study the effects.

The technique, called optogenetics, took the field by storm. Today, thousands of scientists in hundreds of labs are using optogenetics to probe how brains work. They have examined which cells in the brain's reward pathway get hijacked by cocaine, and how deep brain stimulation relieves the symptoms of Parkinson's disease. The list of questions that can now be addressed is endless.

Deisseroth's story repeats itself everywhere in science: An ingenious new tool triggers a cascade of new insights. In this special section, *Science*'s news reporters and editors mark the end of the current decade by stepping back from weekly reporting to take a broader look at 10 insights that have changed science since the dawn of the new millennium. This survey covers only a small fraction of the decade's scientific advances, of course; many others could have filled these pages.

First, however, a shout-out to some of the tools that made those insights possible. In the past 10 years, new ways of gathering, analyzing, storing, and disseminating information have transformed science. Researchers generate more observations, more models, and more automated experimentation than ever before, creating a data-saturated world. The Internet has changed how science is communicated and given nonscientists new opportunities to take part in research. Whole new fields, such as network science, are arising, and science itself is becoming more of a network—more collaborative, more multidisciplinary—as researchers recognize that it takes many minds and varied expertise to tackle complex questions about life, land, and the universe.

Seeing and sensing

Many of the decade's most useful new tools, like optogenetics, were advances in sensing and imaging. Cryoelectron tomography brought into focus the cell's components, allowing scientists to get atomic-level detail of whole-cell organization. The technique builds up a three-dimensional image from a series of two-dimensional slices of a flash-frozen cell, a computer-intensive process.

In 2002, intravital scanning two-photon confocal microscopy revolutionized immunology when it was applied to lymph nodes, showing immune cells in intact tissue in real time. The work opened the door to understanding the interactions among immune cells and the body and changed how researchers thought about immune responses.

Developmental biology has also made huge leaps since 2000 thanks to new microscopy techniques. Now researchers can keep samples alive and have longer-lasting fluorescent tags to track specific cells. They can follow whole-organ and whole-animal development in movies that follow cells as they divide and move around. Other microscopy techniques have been able to sidestep a fundamental limit of optics to look at proteins and the fine structure of cells smaller than the diffraction limit—half the wavelength of the light being used.

Not only can we see better, but we can also send our eyes to hard-to-reach places. On Mars, for example, the Spirit and Opportunity rovers marked a big step up from earlier spacecraft: able to roam for kilometers instead of meters and carrying more capable instruments to analyze the chemical and physical properties of rock. Their observations rewrote the history of water on Mars. Closer to home, torpedolike robots with no connection to the surface searched for

Published by AAAS

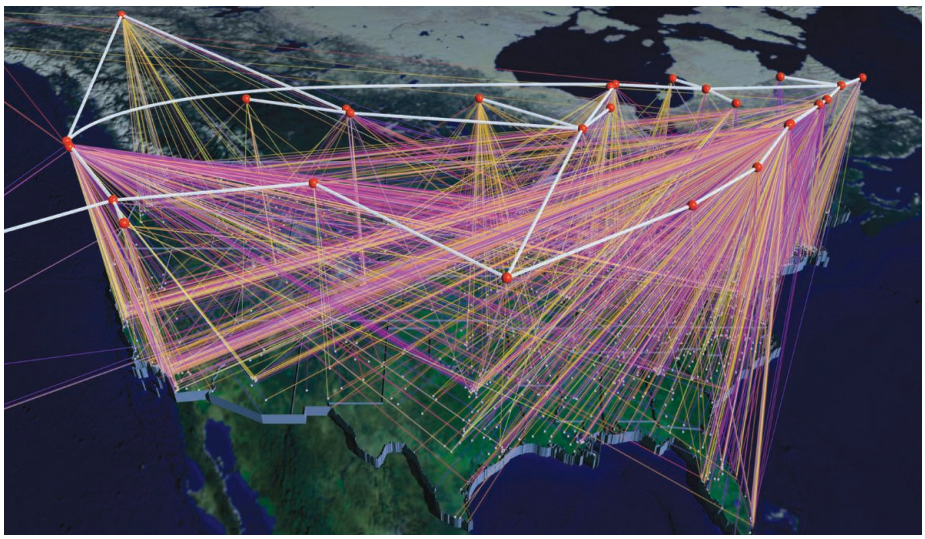

Emphasizing connections. Thanks to computers, the Internet, and new ways of looking at links among everything from genes to people, network science is flourishing.

CREDIT: D. COX AND R. PATTERSON/NCSA, UIUC

oil in the Gulf of Mexico and explored the water under glacial ice shelves in Antarctica. Remotely operated planes, some the size of model airplanes and some the size of military Predators and Hawks, routinely monitor sunlight passing through clouds and fly over hurricanes. Thousands of oceangoing floats send back data on water properties and, therefore, currents. These mobile sensing devices, along with stationary counterparts on land and in the sea, will soon monitor the state of the planet around the clock, making ecology and environmental science almost as data-rich as astronomy and particle physics are.

The indispensable machine

Key to handling such unprecedented torrents of data, of course, have been ever more powerful and more affordable computers. No field has benefited more than genomics. A decade ago, sequencing a human genome took years, hundreds of people, hundreds of machines, and endless hours of sample preparation to generate the pieces of DNA to be deciphered, one at a time. Some researchers favored a shotgun approach—cutting up whole genomes, then sequencing and assembling them all at once—but available computers weren't up to the task. Proponents had to build a massive supercomputer and laboriously program it for the job. Now whole-genome shotgun is de rigueur, and efficient software abounds. In the past 5 years, new "next-generation" sequencing technologies have streamlined the work even more. Today, a single machine can decipher three human genomes in little more than a week.

Sequencing is getting so cheap that researchers are using it to study gene expression and protein-DNA interactions on an unprecedented scale. Geneticists now depend on sequencing to track down the genetic causes of rare diseases. In 2008, 10 countries set up the International Cancer Genome Consortium, which aims to catalog mutations and other DNA and epigenetic changes for about 50 types of cancer by sequencing part or all of 25,000 genomes.

Computers aren't limited to piecing genomes back together. With their help, genomics researchers predict gene locations and compare, say, chimp and human genomes to identify sequences of evolutionary importance—deriving new insights about how genomes work. The Web has served as a vital link between researchers and publicly accessible databases of genome information.

In biochemistry, computer technology has led to huge strides in understanding proteins. To help with the calculations needed to model the jumps and squiggles proteins make as they fold into their "final" shape, scientists beefed up their hardware with graphics processing units used to render 3D images in video games.

Computational chemistry also got a boost from field programmable gate arrays: chips that allow users to essentially design their own hardware to streamline their simulations. And one research team built a supercomputer with customized integrated circuits that dramatically speed protein-folding calculations, allowing simulations on the time scale of milliseconds.

In some cases, computing power is transforming the basic way researchers work together. In astronomy, for example, the Sloan Digital Sky Survey is cataloging everything that can be seen in a fifth of the sky using a 2.5-meter telescope at the Apache Point Observatory in New Mexico. Researchers will tap into the masses of data over the Web. Similar "data utilities" are business as usual in particle physics and seismology, but they are a far cry from the way small teams of observers have divided up telescope time in the past. Europe's CERN laboratory has gone even further. To handle the petabytes of data its Large Hadron Collider (LHC) will generate every year, CERN has set up a computing "grid" system—a virtual organization that pools and shares the computer processing power of each member institution. The grid also makes it possible for thousands of scientists to access LHC data and work together in unprecedented ways.

Other organizations are harnessing the power of networking through crowdsourcing, in which large numbers of researchers (even nonscientists) can contribute to solving problems, setting policy, or forecasting the future. An Internet company called InnoCentive, for example, posts problems online and offers rewards of up to $1 million for their solution. It boasts that 200,000 people have weighed in on more than 1000 problems in fields as wide-ranging as drug synthesis and brick manufacture and have solved two-thirds of them.

Networking programs also enable volunteers around the world to donate idle time on home computers for protein-folding calculations, to search for comets in images from the SOHO satellite, and to classify galaxy types in data from the Sloan Digital Sky Survey.

To get a handle on all this interconnectedness and grasp the ways information travels through complex systems, theorists have spawned a new field called network science. The field took off about 10 years ago, after physicists developed mathematical models to explain some of the network phenomena sociologists had observed. Now, thanks to technologies that make possible measurements on thousands of genes or proteins at once and to computers that can track and analyze the movements, voting habits, or shopping preferences of millions of people, the network approach is bursting into full flower. A host of new insights are bound to lie just ahead.

But that is a tale for another decade.

–THE NEWS STAFF

Published by AAAS

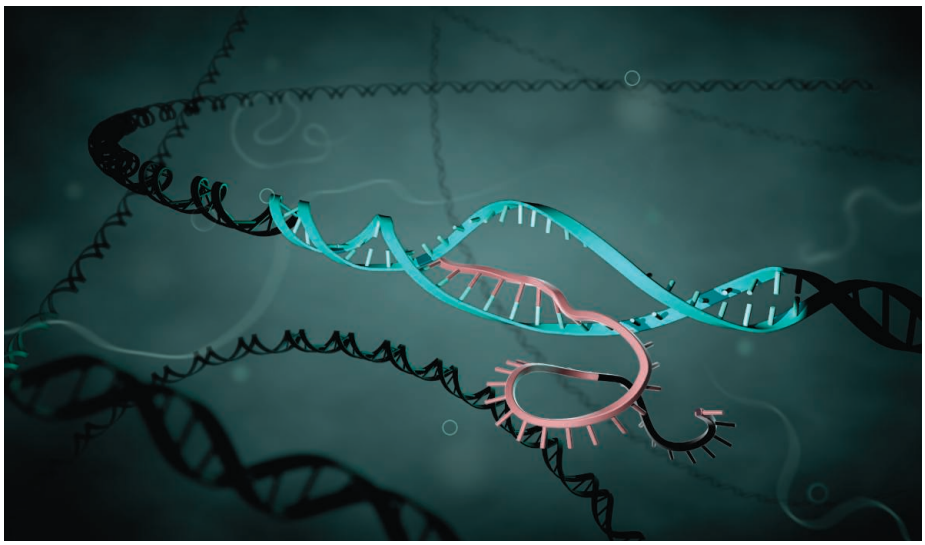

Shining a Light on the Genome's 'Dark Matter'

IT USED TO SEEM SO STRAIGHTFORWARD. DNA told the body how to build proteins. The instructions came in chapters called genes. Strands of DNA's chemical cousin RNA served as molecular messengers, carrying orders to the cells' protein factories and translating them into action. Between the genes lay long stretches of "junk DNA," incoherent, useless, and inert.

That was then. In fact, gene regulation has turned out to be a surprisingly complex process governed by various types of regulatory DNA, which may lie deep in the wilderness of supposed "junk." Far from being humble messengers, RNAs of all shapes and sizes are actually powerful players in how genomes operate. Finally, there's been increasing recognition of the widespread role of chemical alterations called epigenetic factors that can influence the genome across generations without changing the DNA sequence itself.

The scope of this "dark genome" became apparent in 2001, when the human genome was first published. Scientists expected to find as many as 100,000 genes packed into the 3 billion bases of human DNA; they were startled to learn that there were fewer than 35,000. (The current count is 21,000.) Protein-coding regions accounted for just 1.5% of the genome. Could the rest of our DNA really just be junk?

The deciphering of the mouse genome in 2002 showed that there must be more to the story. Mice and people turned out to share not only many genes but also vast stretches of noncoding DNA. To have been "conserved" throughout the 75 million years since the mouse and human lineages diverged, those regions were likely to be crucial to the organisms' survival.

Edward Rubin and Len Pennacchio of the Joint Genome Institute in Walnut Creek, California, and colleagues figured out that some of this conserved DNA helps regulate genes, sometimes from afar, by testing it for function in transgenic mouse embryos. Studies by the group and others suggested that noncoding regions were littered with much more regulatory DNA than expected.

Further evidence that noncoding DNA is vital has come from studies of genetic risk factors for disease. In large-scale searches for single-base differences between diseased and healthy individuals, about 40% of the disease-related differences show up outside of genes.

Genetic dark matter also loomed large when scientists surveyed exactly which DNA was being transcribed, or decoded, into RNA. Scientists thought that most RNA in a cell was messenger RNA generated by protein-coding genes, RNA in ribosomes, or a sprinkling of other RNA elsewhere. But surveys by Thomas Gingeras, now at Cold Spring Harbor Laboratory in New York, and Michael Snyder, now at Stanford University in Palo Alto, California, found a lot more RNA than expected, as did an analysis of mouse RNA by Yoshihide Hayashizaki of the RIKEN Omics Science Center in Japan and colleagues. Other researchers were skeptical, but confirmation soon came from Ewan Birney of the European Bioinformatics Institute and the Encyclopedia of DNA Elements project, which aims to determine the function of every base in the genome. The 2007 pilot results were eye-opening: Chromosomes harbored many previously unsuspected sites where various proteins bound—possible hotbeds of gene regulation or epigenetic effects. Strikingly, about 80% of the cell's DNA showed signs of being transcribed into RNA. What the RNA was doing was unclear.

Other studies revealed that RNA plays a major role in gene regulation and other cellular functions. The story started to unfold in the late 1990s, when plant researchers and nematode biologists learned to use small RNA molecules to shut down genes. Called RNA interference (RNAi), the technique has become a standard way to control gene activity in a variety of species, earning a Nobel Prize in 2006.

To understand RNAi and RNA in general, researchers began isolating and studying RNA molecules just 21 to 30 bases long. It turned out that such "small RNAs" can interfere with messenger RNA, destabilizing it. Four papers in 2002 showed that small RNAs also affect chromatin, the complex of proteins and DNA that makes up chromosomes, in ways that might further control gene activity. In one study, yeast missing certain small RNAs failed to divide properly. Other studies have linked these tiny pieces of RNA to cancer and to development.

The surprises didn't stop at small RNAs. In 2007, a group led by Howard Chang of Stanford and John Rinn, now at Beth Israel Deaconess Medical Center in Boston, pinned down a gene-regulating function by so-called large intervening noncoding RNAs. Rinn and colleagues later determined that the genome contained about 1600 of these lincRNAs. They and other researchers think this type of RNA will prove as important as protein-coding genes in cell function.

Many mysteries about the genome's dark matter are still under investigation. Even so, the overall picture is clear: 10 years ago, genes had the spotlight all to themselves. Now they have to share it with a large, and growing, ensemble.

–ELIZABETH PENNISI

CREDIT: Y. HAMMOND/*SCIENCE*

Published by AAAS

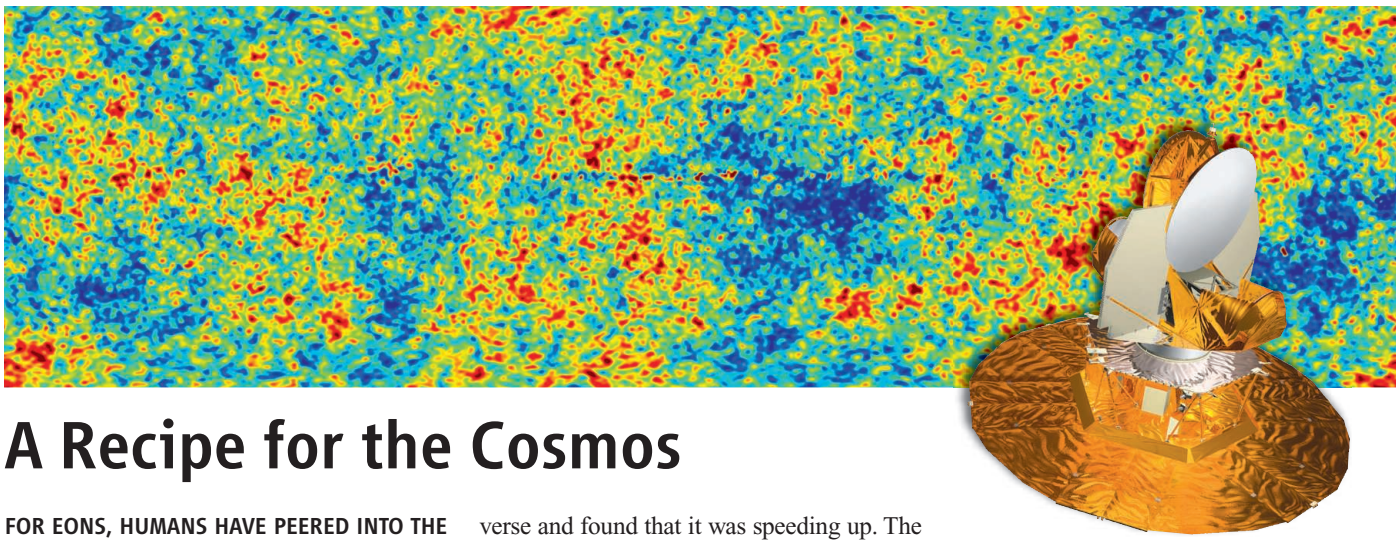

A Recipe for the Cosmos

FOR EONS, HUMANS HAVE PEERED INTO THE starry sky and wondered, "Where did it all come from?" Cosmologists still don't have a solid answer, but in the past decade they have deduced a very precise recipe for the content of the universe, as well as instructions for putting it together. The advance has transformed cosmology from a largely qualitative endeavor to a precision science with a standard theory that provides little wiggle room for other ideas, even as it leaves obvious questions unanswered. Like it or not, cosmologists are now more or less stuck with the theory.

If you are cooking along at home, you'll need three ingredients: ordinary matter such as that in stars and planets, mysterious "dark matter" whose gravity binds the galaxies, and even weirder "dark energy" that's stretching space and accelerating the expansion of the universe. According to the latest numbers, the proportions are 4.56% ordinary matter, 22.7% dark matter, and 72.8% dark energy.

Here's how they went together: The universe emerged, superhot and ultradense, in the instant of the big bang. For a tiny fraction of a second it expanded at faster-than-light speed. Known as "inflation," that growth spurt stretched tiny quantum fluctuations in the density of the newborn universe to colossal scales. The gravity of these "overdense" regions pulled in dark matter, which drew along with it ordinary matter, initially a soup of subatomic particles. Slowly, a vast "cosmic web" of filaments and clumps of dark matter formed, and within them, the galaxies.

Before the turn of the millennium, cosmologists had narrowed the list of cosmic ingredients. Many had suspected the presence of dark matter for decades. Dark energy made a splashy entrance in 1998, when astronomers used stellar explosions called type Ia supernovae to trace the rate of expansion of the universe and found that it was speeding up. The idea of inflation emerged in the 1980s to solve various conceptual puzzles. But only recently have observations enabled scientists to weave these threads into a rigorous theory.

Much of the progress has come through studies of the afterglow of the big bang, radiation known as the cosmic microwave background (CMB). In 2000, an experiment known as Balloon Observations of Millimetric Extragalactic Radiation and Geophysics measured the CMB in detail in patches of the sky; a year later, so did the ground-based Degree Angular Scale Interferometer at the South Pole. Then in 2003, NASA's space-based Wilkinson Microwave Anisotropy Probe (WMAP) mapped the CMB across the sky, producing an exquisite baby picture of the cosmos.

It's the myriad dimples in that picture that count. The temperature of the CMB varies by about one part in 100,000 from point to point on the sky, with the hotter spots corresponding to the denser regions in the primordial universe. By measuring the distribution of the spots' sizes and fitting it with their theoretical model, scientists can probe the interplay and amounts of ordinary and dark matter in the early universe. They can also measure the geometry of space. That allows them to deduce the total density of energy and matter in the universe and infer the amount of dark energy.

CMB studies show that the universe is flat. That means that if you draw parallel lines in space, then they will remain the same distance apart along their infinite lengths instead of converging or diverging. Such flatness is a central prediction of inflation, so the measurements bolster that wild idea. So does a particular randomness seen in the hot and cold spots. The WMAP team released its latest results in January, 9 months before the satellite shut down.

First light. The afterglow of the big bang as charted by the WMAP spacecraft (*inset*).

The most jaw-dropping thing about the CMB results is that the cosmologists' model, which has only a half-dozen adjustable parameters, fits the data at all. This isn't some marginal approximation; the theory fits the data like the casing on a sausage. That makes it hard to argue that dark matter and dark energy are not real and to explain them away by, for example, modifying Einstein's theory of gravity. Other cosmological data, such as measurements of the distribution of the galaxies, also jibe nicely with the model.

All of this leaves cosmologists in a peculiar situation: They have the precise proportions of the ingredients of the universe, but they still do not know what two of the three ingredients—dark matter and dark energy—really are. It's as if they've been handed a brownie recipe that calls for a "sweet granular substance" and a "white powder that mixes with water to make a paste," instead of specifying sugar and flour.

Cosmologists may have a better idea of what they're talking about by the end of the next decade. A particle theory called "supersymmetry" predicts the existence of weakly interacting massive particles (WIMPs), which could be the particles of dark matter. Researchers are optimistic that they may soon detect WIMPs bumping into sensitive detectors deep underground, emerging from high-energy particle collisions at an atom smasher, or producing telltale gamma rays in space. Numerous astronomical surveys will probe space-stretching dark energy, although figuring out what it is could take much longer than another decade. **–ADRIAN CHO**

CREDITS: NASA/WMAP SCIENCE TEAM

INSIGHTS OF THE DECADE

Tiny Time Machines Revisit Ancient Life

FOR HUNDREDS OF YEARS, HUMANS studying ancient life had to rely on stones and bones for hard evidence about what extinct creatures looked like. In the past decade, powerful new x-ray scans and three-dimensional computer models have transformed the analysis of bones, teeth, and shells. But something even more revolutionary has been afoot: a new kind of analysis capable of revealing anatomical adaptations that skeletal evidence can't provide, such as the color of a dinosaur's feathers or how woolly mammoths withstood the cold.

The new views of the prehistoric world hinge on the realization that "biomolecules" such as ancient DNA and collagen can survive for tens of thousands of years and give important information about long-dead plants, animals, and humans. In the past 10 years, this field has surged forward beyond expectation. In 1997, the sequencing of the first snippet of DNA from a Neandertal by a team at the Max Planck Institute of Evolutionary Anthropology in Leipzig, Germany, was hailed as a major milestone. But this year, the same lab published the nuclear genome of Neandertals, representing 10 million times as much DNA (see "Breakthrough of the Year," p. 1605). Over the past decade, these molecules have painted the past in living color: Ancient genes have shown that some Neandertals had red hair and pale skin, and ancient pigment-bearing organelles called melanosomes have revealed the chestnut color of a *Sinosauropteryx* dinosaur's downy tail.

Ancient molecules can also expose relationships among long-dead species; for example, showing that the amino acid sequence of collagen from a dinosaur more closely resembled that of living birds than that of reptiles. Ancient DNA from woolly mammoths revealed that their blood contained special cold-adapted hemoglobin, which researchers reproduced in bacteria this year. DNA has even shown that a few Neandertals interbred with our ancestors.

Ancient-DNA research began in the mid-1980s. But its early promise faded amid a series of spectacular but unfounded claims, such as supposed 80-million-year-old dinosaur DNA that was actually from a human. Ancient DNA was so often contaminated with DNA from bacteria or scientists themselves that no one trusted (or published) the findings. Funding dried up, and only a few labs survived, mostly in Europe.

But over the past 10 years, new tools developed for exploring the human genome gave ancient DNA research a lifesaving infusion. For example, new high-throughput sequencers turned out to work best with small fragments of DNA—just what degraded ancient samples yield. The technology enabled scientists to sequence every bit of extracted DNA relatively cheaply. So they were able to develop methods to recognize and sort short bits of ancient DNA from longer chunks of contaminant DNA and also to fish out gene regions of interest.

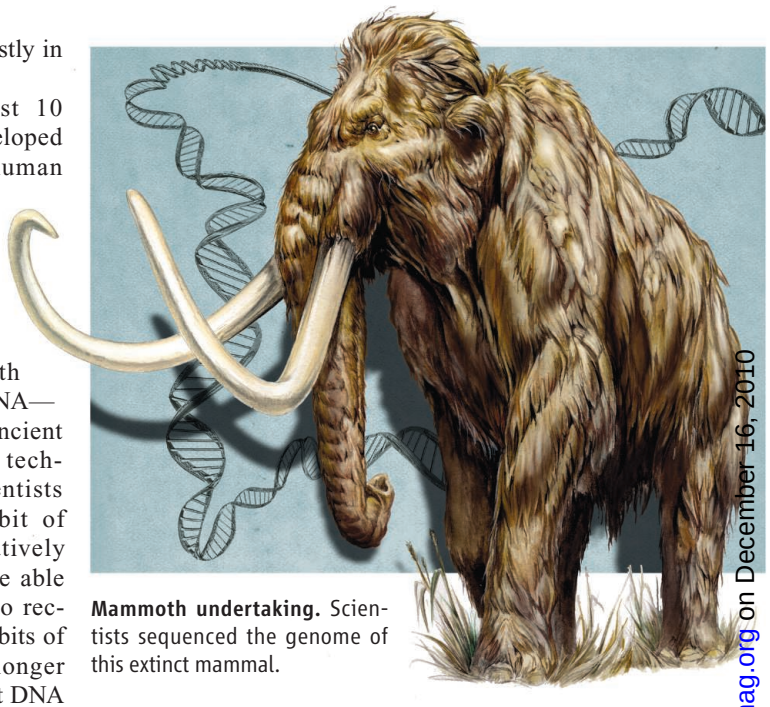

Mammoth undertaking. Scientists sequenced the genome of this extinct mammal.

As sequencing power leapt forward, researchers began making discoveries at a record-breaking clip. In 2005, two teams worked together to sequence 27,000 bases of ancient cave bear DNA. Six months later, another team generated a remarkable 28 million bases of DNA from a mammoth bone and showed that mammoths split from Afri-

Code-buster. A researcher extracts DNA from ancient bone.

can elephants about 6 million years ago. In 2008, that same team bought mammoth hair on eBay and sequenced the entire mammoth genome—the first genome of an extinct animal. That same year, the first complete mitochondrial genome of a Neandertal was published; five others soon followed. In 2010, that work culminated in the publication of the Neandertal genome.

Also this year, the Max Planck team achieved a feat that many researchers a decade ago would have dismissed as impossible: They identified a previously unknown species of human by its DNA alone. They sequenced the mitochondrial genome of a single human finger from a Siberian cave. The finger was neither Neandertal nor human; it apparently belonged to a new species that lived in Central Asia just 40,000 years ago.

Meanwhile, researchers are also zeroing in on other ancient molecules, such as RNA and collagen. Researchers at North Carolina State University in Raleigh made the spectacular claim that they had isolated collagen from a 68-million-year-old *Tyrannosaurus rex* and from an 80-million-year-old hadrosaur. Some scientists suspect that the collagen comes from bacteria rather than dinosaurs, but others are investigating collagen as a way to bar-code scraps of unidentifiable bone. A few are even looking at RNA—which is far more fragile than DNA—in ancient seeds to learn about gene expression in early crops.

Unlocking the secret lives of long-dead organisms may have practical implications in today's world, too. Some researchers hope to use ancient DNA to introduce genetic diversity back into threatened populations, for example, those of polar bears. If they succeed, molecules of long-dead organisms may one day help save living ones.

–ANN GIBBONS

Published by AAAS

A Roller-Coaster Plunge Into Martian Water—and Life?

IT'S BEEN A HECK OF A RIDE. FROM civilization-sustaining canals early in the past century to Mariner 9's barren, lunarlike terrain of the 1970s to shallow, salty seas on early Mars in this decade, the search for water on the Red Planet—and the life that liquid water would permit—has had its ups and downs.

The ballyhooed shallow seas evaporated from scientists' view of early Mars within a few years, but even so, the past decade's half-dozen martian missions have finally delivered. It is now clear that early in Mars history, liquid water on or just inside the planet did indeed persist long enough to alter rock and, possibly, sustain the origin of life. There is now even enough moisture to encourage those who seek living, breathing alien microbes—organisms that, if they exist, could hold the key to explaining how life on our own planet got its start.

At the turn of the millennium, experts knew early Mars hadn't been bone dry. News headlines of the day spoke of "A Dripping Wet Early Mars" and suggested that "Mars Is Getting Wetter and Wetter" (to cite two examples from *Science*). Cameras on spacecraft following Mariner 9 had revealed landscapes sculpted by catastrophic floods. Layered sediments evoked long-past crater lakes, and there were even hints of ancient shorelines that had encompassed a great northern ocean. But as far as anyone knew, all of those reservoirs could have been too ephemeral to give life a start.

A soaking splash of martian water came in early 2004 when the Opportunity rover discovered signs of long-lived seas, or at least broad lakes, on early Mars. Opportunity was investigating a splotch of spectral color, seen from orbit, that connoted the water-related iron mineral hematite. From close up, the landing site appeared to be the salty remains of a shallow sea or lake. *Science* proclaimed the find—along with the discovery of cryptic water-rotted rocks on the other side of the planet by the Spirit rover—the Breakthrough of the Year for 2004.

The excitement was short-lived. Opportunity never found much more evidence that surface waters had rippled the sediments. Instead of a sea, rare puddles of salty, acidic groundwater may have oozed up between arid dunes of salt sand. Such intensely briny, corrosive water would have been inimical to Earth-like life.

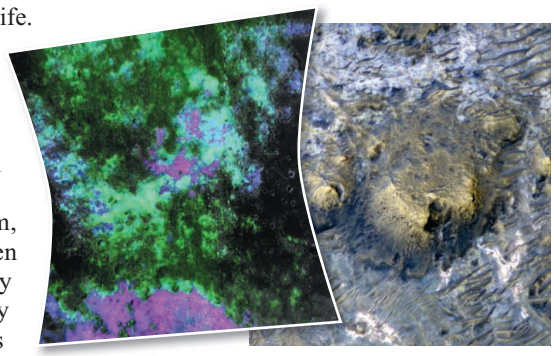

Pointers. Clay's spectral blues and greens (*above, left*) will guide the Curiosity rover (*below*).

Not to worry. Spectrometers flying on Mars Reconnaissance Orbiter and Mars Express the past half-dozen years are far more capable of spying out water-altered minerals, especially clays. Astrobiologists love clays. Their formation requires prolonged contact of water and rock under mild, life-favoring conditions, and they are great for preserving the remnant organic matter of past life. Researchers have now turned up water-generated clays in so many places on Mars that the scientists and engineers contemplating where to send the next rover—the high-powered Curiosity, a.k.a. Mars Science Laboratory—had scores of choices.

Orbiting instruments have also turned up ice buried within centimeters of the soil surface and in now-stagnant, debris-covered glaciers hundreds of meters thick. Ice near the martian surface can't melt today, but because Mars wobbles wildly on its axis, its climate has swung through warmer spells lasting hundreds of thousands of years many times in the past.

Early in the decade, planetary scientists started finding signs that some of this ice may have been liquid within geologically recent times. Sharper imaging revealed gullies on crater walls that look as if they were cut by water gushing down the slope, perhaps from melting snow. In October, team members from the Phoenix lander mission reported evidence that liquid water—perhaps little more than a damp film—had percolated through the upper few centimeters of far-north soil. And Spirit team members earlier this year suggested a similar seeping near the equator where the rover has become stuck.

As a result of such discoveries, the search for life on Mars now means more than merely groping in the dirt for long-decayed molecular remains. For the first time, many scientists think they might realistically find actual microorganisms, either living or recently deceased. To biologists, that prospect is incalculably exciting. If such micro-martians turn up, will they be products of a separate origin, with their own distinctive biochemistry and genetic code? Or will they be related to life on Earth—perhaps precursors such as a hypothesized "RNA world"—carried from one planet to another by spaceborne debris?

It's possible. Meteorites from Mars, knocked off the surface by asteroid impacts, have been found on Earth. Sometimes those rocks might make the trip quickly enough for bacterial hitchhikers to survive the crossing. Mars was wet enough early enough and long enough; if it turns out to harbor life as we know it, then life on Earth could well have started there.

–RICHARD A. KERR

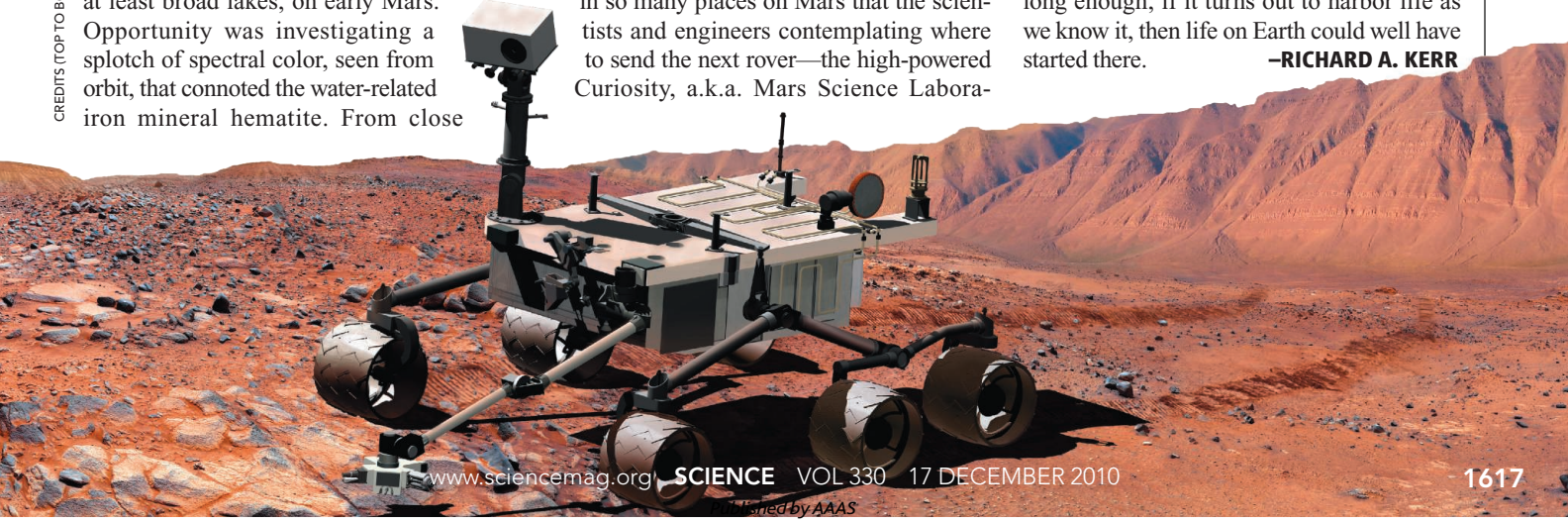

CREDITS (TOP TO BOTTOM): NASA/JPL/JHUAPL (INSET); NASA/JPL/UNIVERSITY OF ARIZONA; NASA/JPL

Reprogrammed. Adding extra copies of a few genes turns the developmental clock backward, producing induced pluripotent stem cells.

Cells Rewrite Their Own Destiny

A CLASSIC METAPHOR IN BIOLOGY PICTURES an embryonic cell at the top of a hill. As the embryo develops, the cell rolls downhill into a series of branching valleys. Once a cell enters, say, the valley that leads to becoming a skin cell, it cannot suddenly change course and become a neuron. When developmental biologist Conrad Waddington came up with the image in the 1950s, the message was clear: Development is a one-way trip.

Not so. In the past decade, scientists have figured out how to push differentiated cells back up the hill and, perhaps even more surprising, directly from one valley to the next. By prompting a cell to overexpress a few genes, researchers can turn a skin or blood cell into a pluripotent cell: one that has regained the potential to become any number of cells in the body. Other genes can prompt skin cells to turn directly into neurons or blood cells. Scientists are already using the technique to make cell lines from patients with hard-to-study diseases, and ultimately they hope to grow genetically matched replacement cells and tissues—perhaps even entire organs.

The foundation for this groundbreaking insight was built over several decades of research. John Gurdon laid the cornerstone in the 1960s, when he cloned frogs from adult cells by transferring the cell's nucleus into an enucleated egg. For the first time, a scientist had coaxed an adult cell's genetic material into starting over to make an entire new individual. In 1996, Dolly the sheep extended this "nuclear transfer" to mammalian cells. That work raised hopes that researchers could figure out how oocytes can reset the cellular clock of introduced adult DNA, allowing development to begin afresh in defiance of Waddington's metaphor.

In 2006, however, Shinya Yamanaka stunned the world when he showed that simply by adding extra copies of four genes to adult mouse cells, he could prompt them to become pluripotent—no help from oocytes necessary. He called the resulting cells "induced pluripotent stem" cells (iPSCs).

A year later, two groups—one led by Yamanaka, the other by James Thomson—independently created iPSCs from human skin cells. The groups used slightly different combinations of genes, demonstrating that there are alternative ways to make the process work. Soon thereafter, several groups showed that it was possible to reprogram one adult cell type directly into another, turning fibroblasts into neurons and fibroblasts into blood cells, among other results.

The breakthrough offered a way around some of the sticky ethical and political issues that have dogged research with human embryonic stem cells, which are taken from early embryos. Suddenly, scientists had a source of human pluripotent cells free of special rules and regulations.

Early reprogramming techniques did have several drawbacks, however. First, they permanently inserted the extra genes into the reprogrammed cell's genome. Although the genes seemed to turn back off once the cells were pluripotent, it wasn't clear how they might influence the cells' later behavior. Second, at least one of the genes Yamanaka used was known to trigger cancer, and indeed it soon became clear that mice grown from iPSCs frequently developed tumors. Finally, the process was inefficient, reprogramming only about one in 5000 of the treated cells.

Many of those problems have now been addressed. Some labs have reprogrammed cells using viruses that don't insert themselves into the genome. Others have used small rings of DNA called episomes that don't replicate when the cell divides. Other researchers have found small molecules that can substitute for some of the genetic factors, and they have found ways to insert reprogramming proteins directly into a cell. A few months ago, one group described how to use modified RNA to reprogram cells faster and more efficiently than the original technique.

At the same time, scientists have been eagerly reprogramming cells from hundreds of patients and healthy controls, in an effort to uncover the origins of various diseases and perhaps find new treatments. Labs are using such cells to study amyotrophic lateral sclerosis, Parkinson's disease, Huntington's disease, and even autism. Pharmaceutical companies are using heart cells grown from iPSCs to test drugs for cardiac side effects, a common reason that promising drugs fail.

Researchers are also working to understand exactly how reprogramming works. The evidence so far suggests that a bit of luck is involved: A cell has to receive the right dose of each factor at the right time. That could explain why the process is so inefficient: Only a small fraction of cells happens to receive the correct dose. Nuclear transfer is much more efficient, and some researchers are still working to piece together how the oocyte works its magic, in the hope that it might provide clues to make reprogramming work better.

Reprogramming has reshaped the developmental biology landscape, both for cells and for researchers. Scientists hope that in the coming decades it will reshape medicine as well.

–GRETCHEN VOGEL

CREDIT: COURTESY OF SHINYA YAMANAKA, KYOTO UNIVERSITY

Published by AAAS

Body's Hardworking Microbes Get Some Overdue Respect

HUMANS HAVE BEEN DOING BATTLE WITH bacteria since the 1800s, thwarting disease with antibiotics, vaccines, and good hygiene with mixed success. But in 2000, Nobel laureate Joshua Lederberg called for an end to the "We good; they evil" thinking that has fueled our war against microbes. "We should think of each host and its parasites as a superorganism with the respective genomes yoked into a chimera of sorts," he wrote in *Science* in 2000.

His comments were prescient. This past decade has seen a shift in how we see the microbes and viruses in and on our bodies. There is increasing acceptance that they are us, and for good reason. Nine in 10 of the cells in the body are microbial. In the gut alone, as many as 1000 species bring to the body 100 times as many genes as our own DNA carries. A few microbes make us sick, but most are commensal and just call the human body home. Collectively, they are known as the human microbiome. Likewise, some viruses take up residence in the body, creating a virome whose influence on health and disease is just beginning to be studied.

Their genes and ours make up a metagenome that keeps the body functioning. This past decade we've begun to see how microbial genes affect how much energy we absorb from our foods and how microbes and viruses help to prime the immune system. Viewing the human and its microbial and viral components as intimately intertwined has broad implications. As one immunologist put it, such a shift "is not dissimilar philosophically from the recognition that the Earth is not the center of the solar system."

This appreciation has dawned gradually, as part of a growing recognition of the key role microbes play in the world. Microbiologists sequencing DNA from soil, seawater, and other environments have discovered vast numbers of previously undetected species. Other genomics research has brought to light incredible intimacies between microbes and their hosts—such as a bacterium called *Buchnera* and the aphids inside which it lives. A study in 2000 found that each organism has what the other lacks, creating a metabolic interdependency.

One of the first inklings that microbiologists were missing out on the body's microbial world came in 1999, when David Relman of Stanford University in Palo Alto, California, and colleagues found that previous studies of bacteria cultured from human gums had seriously undercounted the diversity there. Turning to samples taken from the gut and from stools, the researchers identified 395 types of bacteria, two-thirds of them new to science.

In 2006, Steven Gill of the University at Buffalo in New York and colleagues did a metagenomics study of the gut, analyzing all the genes they could find in the 78 million bases sequenced. They found metabolic genes that complemented the human genome, including ones that break down dietary fiber, amino acids, or drugs, and others that produce methane or vitamins. This and a more comprehensive survey in 2010 by Jun Wang of BGI-Shenzhen in China and colleagues provided support for the concept of the microbe-human superorganism, with a vast genetic repertoire. Now, large-scale studies have surveyed the microflora in the gut, skin, mouth, nose, and female urogenital tract. The Human Microbiome Project has sequenced 500 relevant microbial genomes out of a planned 3000.

Some of these microbes may play important roles in metabolic processes. In 2004, a team led by Jeffrey Gordon of Washington University School of Medicine in St. Louis, Missouri, found that germ-free mice gained weight after they were supplied with gut bacteria—evidence that these bacteria helped the body harvest more energy from digested foods. Later studies showed that both obese mice and obese people harbored fewer Bacteroidetes bacteria than their normal-weight counterparts.

The microbiome is also proving critical in many aspects of health. The immune system needs it to develop properly. What's more, to protect themselves inside the body, commensal bacteria can interact with immune cell receptors or even induce the production of certain immune system cells. One abundant gut bacterium, *Faecalibacterium prausnitzii*, proved to have anti-inflammatory properties, and its abundance seems to help protect against the recurrence of Crohn's disease. Likewise, Sarkis Mazmanian of the California Institute of Technology in Pasadena showed that the human symbiont *Bacteroides fragilis* kept mice from getting colitis. And inserting bacteria isolated from healthy guts restored the microbial communities, curing chronic diarrhea in a patient infected with *Clostridium difficile*.

Herbert Virgin of Washington University School of Medicine finds a similar role for the virome. In mice, his team found that dormant herpesviruses revved up the immune system just enough to make the mice less susceptible to certain bacterial infections.

The ideas of a microbiome and a virome didn't even exist a decade ago. But now researchers have reason to hope they may one day manipulate the body's viral and microbial inhabitants to improve health and fight sickness.

–ELIZABETH PENNISI

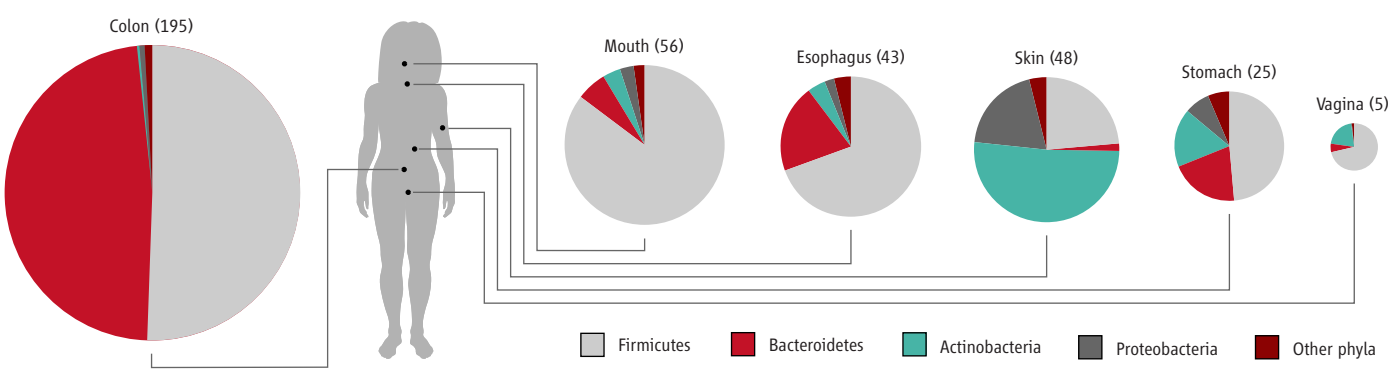

Invisible partners. The roster of bacteria varies among body sites.

CREDIT: ADAPTED FROM L. DETHLEFSEN *ET AL.*, *NATURE* **449** (18 OCTOBER 2007)

Plural worlds. The Kepler space telescope (*below*) has already spotted hundreds of candidate planets around other stars.

Alien Planets Hit the Commodities Market

There are countless suns and countless earths all rotating around their suns in exactly the same way as the seven planets of our system. We see only the suns because they are the largest bodies and are luminous, but their planets remain invisible to us because they are smaller and non-luminous. —*Giordano Bruno, 1584*

FOR HOLDING FIRM TO THIS IDEA OF PLURAL worlds, Giordano Bruno spent 7 years in a dungeon; then, on 17 February 1600, he was led to a public square in Rome and burned at the stake. If Bruno had had the power to summon the future, his best shot at survival might have been to show his inquisitors the Web page of the Extrasolar Planets Encyclopedia, circa 2010. Evidence from the year 2000, when the planets in the encyclopedia numbered a mere 26, might not have done the trick. But the latest tally, 505 and counting, surely would have stayed their torches.

In the past decade, astronomers have discovered so many planets outside of the solar system that only the weirdest of them now make the mainstream news—such as WASP-17, a giant planet discovered in August 2009, which orbits "backward," or counter to the spin of its parent star. A software application for iPhones and iPads keeps track of exoplanet discoveries; the score crossed 500 as this article was being written. Hundreds more may soon follow as astronomers pursue some 700 candidates that NASA's Kepler space telescope detected in the first few months after its launch in March 2009.

Although most of the planets discovered so far are gas giants, an analysis of the Kepler data has convinced researchers that smaller Earth-like planets abound in the universe and that improved detection capabilities in the coming years will turn up scores of them just in our galactic backyard. This insight has opened up the possibility of detecting life elsewhere in the universe within the lifetimes of young astronomers entering the field, if not sooner. Meanwhile, the sizes and orbits of planets already discovered are revolutionizing researchers' understanding of how planetary systems form and evolve.

The discovery of exoplanets began as a trickle in the previous decade, starting with the detection of "51 Pegasi b" in 1995 by a Swiss team led by Michel Mayor, followed the next year by the discoveries of five planets by U.S. astronomers Geoffrey Marcy, Paul Butler, and their colleagues. By 2001, several other teams had joined the quest, and the pace of discovery quickened.

The oldest and most popular technique for finding planets has been the use of Doppler spectroscopy—the blue-ward or red-ward shift in the light of a star as it wobbles under the gravitational tug of its orbiting planet. In 1999, astronomers also began detecting exoplanets by the transit technique, watching for a star to dim slightly as its planet travels across its face. Transits have yielded the discovery or confirmation of more than 100 planets to date.

Since 2001, planet-hunters have added two more techniques to their toolbox. One is microlensing, in which a star briefly brightens as the gravity of another star in the foreground bends its light; changes in the brightening can reveal a planet orbiting the foreground star. Researchers led by Ian Bond of the Royal Observatory, Edinburgh, in the United Kingdom announced the first discovery of a planet through microlensing in 2004; the technique has led to 10 more finds since.

In 2008, astronomers published the first direct images of exoplanets: tiny pinpricks of light close to a nearby star. With advances in adaptive optics, the technology that corrects for the blurring effect of the atmosphere on ground telescopes, and the development of better coronagraphs—devices that help block out the direct light from a star—astronomers hope to image many more planets directly.

The diversity of planetary systems discovered to date has forced astronomers to revise their theories of how these systems arise and develop. The discovery of hot Jupiters orbiting very close to their parent star suggests that gas giants—thought to form far out from the star—can migrate inward over time. And the discovery of planets dancing around their stars in tilted or even retrograde orbits suggests that planets can be wrenched from their original birthplaces into odd orbits that astronomers could not have predicted.

Astronomers expect Kepler to find several Earth-like planets in the next few years. Already, researchers are planning new ground- and space-based instruments to take spectra of the atmospheres of some of those habitable planets. Those atmospheres may bear signatures of life, such as oxygen, which researchers believe can be produced only by biological processes. If and when that happens, it would be the ultimate vindication of Bruno's fatal vision of a cosmos teeming with worlds.

–YUDHIJIT BHATTACHARJEE

CREDITS: ESO; NASA (INSET)

Published by AAAS

Inflammation Bares a Dark Side

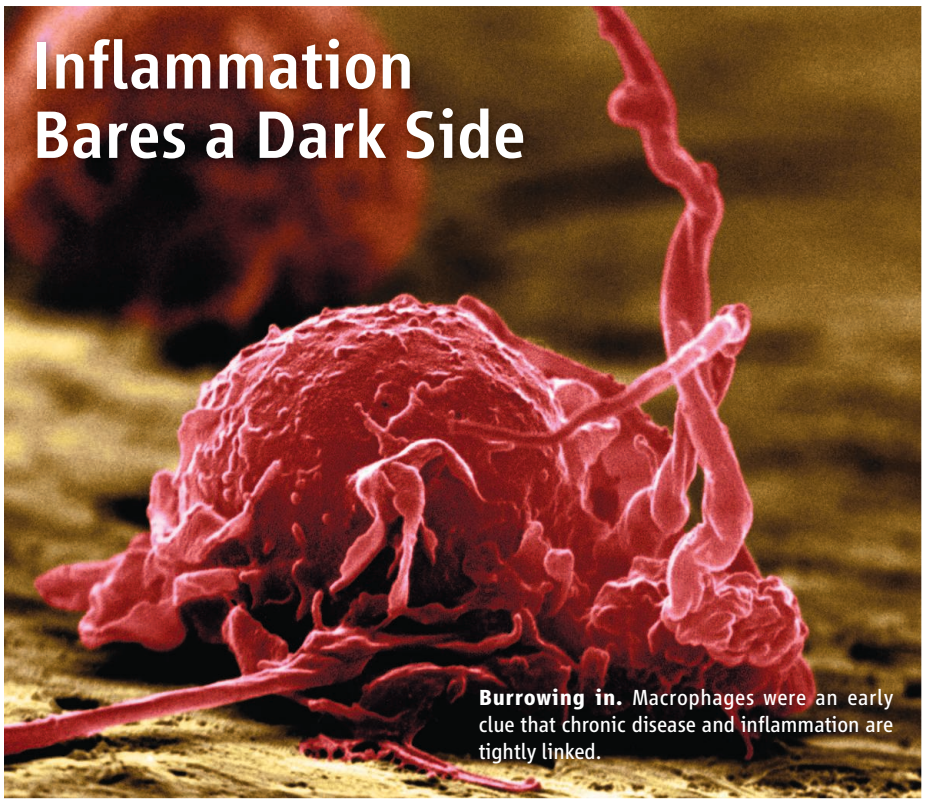

Burrowing in. Macrophages were an early clue that chronic disease and inflammation are tightly linked.

NOT LONG AGO, INFLAMMATION HAD A CLEAR role: It was a sidekick to the body's healers, briefly setting in as immune cells rebuilt tissue damaged by trauma or infection. Today, that's an afterthought. Inflammation has hit the big time. Over the past decade, it has become widely accepted that inflammation is a driving force behind chronic diseases that will kill nearly all of us. Cancer. Diabetes and obesity. Alzheimer's disease. Atherosclerosis. Here, inflammation wears a grim mask, shedding its redeeming features and making sick people sicker.

When a kitchen knife slips while you're chopping vegetables, the body reacts swiftly. White blood cells swoop in and sterilize the injury, and the tissue-repair effort begins. This inflammatory response does have its downsides, causing swelling, redness, and pain. (Indeed, "inflammation" derives from the Latin verb *inflammare*, which means to set on fire.) But there's no question that acute inflammation is a net positive, a response to trauma that evolved millennia ago to keep us alive and healthy.

A darker story began to emerge in the 1990s. Researchers peering at apparently unrelated diseases noticed that immune cells congregate at disease sites. Atherosclerosis, in which fatty plaques build up in the arteries, was among the first to make the list. In the 1980s, the late Russell Ross of the University of Washington, Seattle, saw macrophages in atherosclerotic tissue; these white blood cells are a hallmark of inflammation. Slowly, as more people parsed arterial tissue, more came to agree that an inflammatory response was under way. There were T cells. There was interferon-γ, which the immune system produces as part of its inflammatory efforts. Also in the mix were gene variants identified by the Icelandic company deCODE that predispose people to heart attacks by fueling inflammation in plaques. And then this April, researchers used a new microscopic technique to describe, in *Nature*, tiny crystals of cholesterol in arteries that induce inflammation at the earliest stages of disease in mice.

Other conditions unrolled parallel story lines. In 1993, a group at Harvard University found that fat tissue in obese mice was churning out a classic inflammatory protein. Ten years later, back-to-back papers showed a correlation between macrophage infiltration of fat tissue in rodents and people and how obese they were. Newcomers to the inflammatory story include neurodegenerative diseases such as Alzheimer's and Parkinson's. Here, it's murkier whether inflammation is perpetuating disease or just along for the ride.

In most chronic illnesses for which inflammation has been fingered, it appears to drive ill health but not initiate it. In cancer, for example, papers published over the past decade suggest that tumors and inflammation dance together toward disaster: Tumors distort healthy tissue, setting off tissue repair, which in turn promotes cell proliferation and blood vessel growth, helping cancers expand. And although it's genetic mutations in tumor cells that initiate cancer, there's evidence that inflammation in surrounding tissue helps coax those cells along.

In cancer, inflammation shows up at least partly for the same reasons it normally does: tissue injury. Elsewhere, its appearance is more mysterious. In neurodegenerative conditions, for example, there's some tissue damage from loss of neurons, which could prod inflammation—but there's evidence, too, that inflammation is helping kill neurons. Inflammation also seems to promote two components of type 2 diabetes: insulin resistance and the death of pancreatic beta cells that produce insulin.

When it comes to obesity, it's unclear why inflammation permeates fat tissue. But theories are percolating. One cites a misguided immune response: Fat cells in obese individuals are not metabolically normal, and the immune system perceives them as needing help and sends macrophages to the rescue, even though they only do harm.

The surest way to prove that inflammation is driving any disease is by blocking it and testing whether that helps, and experiments are under way. In 2007, Marc Donath of University Hospital of Zurich in Switzerland and his colleagues described results from a clinical trial of type 2 diabetes that had once been dismissed as crazy. Seventy patients received either a placebo or anakinra, a drug used occasionally to treat rheumatoid arthritis that blocks interleukin-1. IL-1 is a proinflammatory cytokine, a protein that promotes inflammation; it's been found in beta cells from people with type 2 diabetes. In Donath's small study, published in *The New England Journal of Medicine*, the drug helped control the disease. Anakinra is not a good option for long-term diabetes treatment, so several companies are racing to develop alternatives.

Mediating inflammation in chronic diseases is a new frontier, its success still uncertain. But after inflammation eluded them for so long, researchers are chasing lead after lead, trying to stay a step ahead and discern when its fires need putting out.

–JENNIFER COUZIN-FRANKEL

Strange New Tricks With Light

Now you see it. Metamaterials make it possible to steer light around an object, creating an artificial blind spot (*below*). A disk version works with microwaves (*left*).

THREE CENTURIES AFTER ISAAC NEWTON published his *Opticks*, that ages-old science got really weird. In the past decade, physicists and engineers pioneered new ways to guide and manipulate light, creating lenses that defy the fundamental limit on the resolution of an ordinary lens and even constructing "cloaks" that make an object invisible—sort of.

The feats sprang from a roughly 50–50 mixture of a new technology and one oh-so-clever idea. The technology was "metamaterials": assemblages of little rods, rings, and wires that act like materials with bizarre optical properties. The idea was transformation optics, a scheme that tells scientists how to tailor the properties of a metamaterial to achieve an effect like cloaking.

Metamaterials work by steering light and other electromagnetic waves. When light waves enter normal materials such as glass, the material alters the electric and magnetic fields in the light, slowing the waves to a particular new speed. The deceleration gives the new medium a different refractive index. This effect explains why a straw in a glass of water appears to bend at the surface of the water. In natural materials, light waves entering at an angle always bend to plunge more steeply into the material—the hallmark of a refractive index greater than 1.

Back in 1968, Victor Veselago, a Russian physicist, reasoned that a material might be engineered to create a negative index of refraction and bend light waves more radically. If water had a negative index of refraction, then a straw placed in a glass would appear to bend back under itself. Such a material, Veselago determined, could form a superlens: a flat sheet capable of focusing light even better than curved lenses do. The notion sat dormant for decades. Then, in the late 1990s, John Pendry, a physicist at Imperial College London, and colleagues determined that the long, thin shape of carbon nanotubes helped them absorb radio waves.

Pendry started pondering how other artificial materials might affect electromagnetic waves. Copper wires and slitted rings will ring, or "resonate," with electric and magnetic fields of specific frequencies, and Pendry realized that by playing with those resonances he could tune the electric and magnetic properties of a metamaterial independently to achieve a negative refractive index for microwaves. He also reasoned that it should be possible to build Veselago's superlens to see objects smaller than one-half the wavelength of the light it transmits. No conventional lens can beat that "diffraction limit." But metamaterials, Pendry realized, might do it by amplifying tiny resonances, called evanescent waves, that light creates under certain conditions.

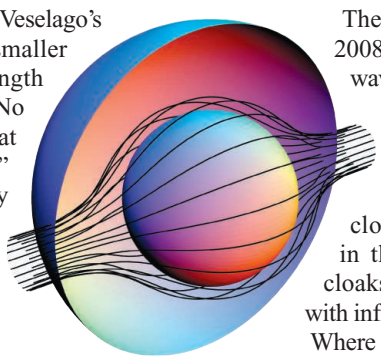

Pendry's ideas touched off a torrent of experiments. In 2001, Pendry teamed up with physicist David Smith, then at the University of California (UC), San Diego, and now at Duke University in Durham, North Carolina, to build Pendry's negative-refractive-index material for microwaves—although it took them a few years to convince the scientific community that it worked. Just a few years later, other teams reported initial success in making a superlens and related devices called hyperlenses.

Then things got really strange. In May 2006, Pendry and colleagues and, independently, Ulf Leonhardt, a theorist at the University of St. Andrews in the United Kingdom, reported that metamaterials could be used to render an object invisible by steering light around it the way water streams around a boulder. Just 5 months later, Smith, his postdoc David Schurig (now at North Carolina State University in Raleigh), and other colleagues unveiled such a ring-shaped cloaking device.

The device wasn't perfect; it worked only for microwaves of a specific frequency. The real advance lay in the concept behind it. In his theory of general relativity, Einstein realized that space and time can stretch and warp in ways that change the trajectory of light. So Leonhardt and Pendry imagined bending space to steer light around a circular region, making anything inside that hole invisible.

The theorists realized that they could mimic this extreme stretching of space by filling an unwarped region of space with a metamaterial whose electric and magnetic properties vary in a specific way. They laid out the mathematical theory for making that transformation. In principle, that theory enables experimenters to bend light pretty much any way they want, provided they can sculpt a metamaterial accordingly.

The wonders keep coming. In 2008, researchers built a microwave cloak that works over a range of wavelengths. That same year, UC Berkeley physicist Xiang Zhang and colleagues created the first cloaking device that worked in three dimensions. Related cloaks have been made to work with infrared rays and visible light.

Where all of this will lead is hard to say. Much to the disappointment of Harry Potter fans, cloaking a human-sized object at visible wavelengths seems like a long shot. But metamaterials for microwaves could have myriad practical uses. And the idea of transformation optics is so beautiful that it would seem a profligate waste of inspiration if it didn't lead to something useful.

–ROBERT F. SERVICE AND ADRIAN CHO

CREDITS: DAVID SCHURIG, J.B. PENDRY *ET AL.*, *SCIENCE* **312** (23 JUNE 2006)

Published by AAAS

Both sides now. Global warming's impacts—both drying and wetting—have come sooner than expected.

Climatologists Feel the Heat As Science Meets Politics

MOST INSIGHTS COME AS A SURPRISE: a burst of understanding, an elegant solution to a problem. This decade's main insight in climate science was a different breed. For 40 years, researchers had wrestled with three big questions: Is the world warming? If so, are humans behind the warming? And are natural processes likely to rein it in? In the past few years, climate scientists finally agreed on solid answers: yes, yes, and no—just as they had suspected.

There were surprises, and they were bad ones. The effects of rising greenhouse gases on oceans and polar ice were swifter than models had predicted. Yet, faced with the obvious remedy—cutting carbon emissions—the world balked. In the United States, even as the science grew stronger, a political backlash forced climate scientists to defend their credibility and motives.

The sudden reversal blindsided global-warming researchers. They had been issuing assessments of the state of greenhouse-warming science under the aegis of one organization or another since 1979; in 1990, the new United Nations Intergovernmental Panel on Climate Change (IPCC) took the lead. IPCC's second assessment, released in 1995, asserted mildly that "the balance of evidence suggests" that humans were influencing global climate. But by 2007, IPCC had reached a solid scientific consensus: Warming was "unequivocal," it was "very likely" due mostly to human beings, and natural processes were "very unlikely" to blunt its strength. The breadth and depth of the IPCC process seemed to drown out the small but well-publicized chorus of climate contrarians.

Developments around the globe amplified the message. In the 1980s and '90s, most researchers thought the projected impacts of rising greenhouse gases wouldn't hit hard until well into the 21st century. But by the mid-2000s, summertime Arctic sea ice was obviously disappearing, ice shelves were falling apart, and Greenland and West Antarctic glaciers were rushing to the sea. Hurricane Katrina inundated New Orleans just as scientists were debating how the greenhouse could intensify and multiply hurricanes. Even ocean acidification was an observational fact by decade's end. In April 2006, a cover story in *Time* magazine treated global warming as a given and warned starkly: "Be Worried. Be Very Worried."

But powerful nations were acting anything but. As a presidential candidate in 2000, George W. Bush had pledged to regulate CO_2; as president, he swiftly reneged and refused to sign the Kyoto Protocol, an emissions-limiting treaty that 187 countries had ratified 3 years earlier. There followed years of efforts by the Bush Administration to alter a handful of climate science reports to downplay the possible effects of climate change, while lawmakers in Washington and negotiators overseas repeatedly failed to pass comprehensive U.S. or international regulations. Europe had some initial success with its cap-and-trade system, but even the World Wildlife Fund says there is "no indication that the scheme is as yet influencing longer-term investment decisions."

A new Administration in Washington brought a change in tone but not in course. During the 2008 presidential campaign, Barack Obama pledged to cut U.S. emissions 80% by 2050 relative to 1990; after the election, the U.S. House of Representatives passed a law that did basically that. But the bill died in the Senate this year, after President Obama failed to secure a binding treaty on emissions at key negotiations in Copenhagen in December 2009.

That November, the release of e-mail correspondence among scientists, taken from the servers of the University of East Anglia in the United Kingdom, had given climate science a jolt of bad publicity. Five panels of experts later absolved the scientists of scientific malfeasance. Even so, the event may have profoundly damaged public views of climate science, with political repercussions yet to unfold. Last month's U.S. congressional elections may hint at things to come: Most Republicans who won election to the House and nearly all Republican Senate candidates have questioned the fundamental science behind climate change, and a few of them denounce the entire field as a conspiracy. "The war on climate science and scientists that's going on now makes the Bush Administration look moderate," says Rick Piltz, a White House climate official from 1995 to 2005 who now heads the watchdog group Climate Science Watch in Washington, D.C.

There are hints of movement. The U.S. Environmental Protection Agency is girding for battle to cut emissions of big power plants, and China, Indonesia, Brazil, and India have recently made their first-ever commitments to tackle emissions. But "climate hawks" have lost time and momentum, and many experts now think that adapting to a warming planet, not mitigating emissions, will dominate policy discussions in the decade ahead.

–RICHARD A. KERR AND ELI KINTISCH

CREDITS (FROM LEFT TO RIGHT): © JP LAFFONT/SYGMA/CORBIS; KONRAD STEFFEN, UNIVERSITY OF COLORADO/CIRES

LETTERS

edited by Jennifer Sills

China's Plan Flawed But Courageous

IN HER NEWS FOCUS STORY "HAS CHINA OUTgrown the one-child policy?" (17 September, p. 1458), M. Hvistendahl explores the consequences of China's fertility policies. Overall, the story presents the one-child policy in a negative light, buttressed by statistical data, such as the current gender ratio of 119:100 at birth and the projected graying of the Chinese population. These data are accurate but misleadingly incomplete. The single most relevant statistic is the one that drove the original decision to implement the policy: the total population of China as a function of time. Even with the reduced population growth that came with the one-child policy and with China's rapid shift toward an urbanized and export-driven economy, those numbers are sobering. In 1960, China had a population of 646 million; in 1980, it was 981 million; by 2000, it had grown to 1.267 billion; and in 2010, it is projected to be 1.354 billion (*1*). In the past 50 years, China's population has increased by an amount equal to or greater than the population of all of Central and North America (~500 million). Without defending or criticizing the one-child policy, we can at least recognize that it stands as a brave attempt by the inhabitants of an overcrowded planet to create a more livable future for our children and grandchildren.

JEREMY NATHANS

Department of Molecular Biology and Genetics, The Johns Hopkins Medical School, Baltimore, MD 21205, USA.
E-mail: jnathans@jhmi.edu

Reference

1. United Nations, Department of Economic and Social Affairs, Population Division, Population Estimates and Projections Section, World Population Prospects: The 2008 Revision (http://esa.un.org/unpd/wpp2008/tab-sorting_population.htm).

Science TALK

Readers' Picks

Your Breakthrough Nominations

EVERY YEAR, THE EDITORS AT *SCIENCE* GET TOGETHER TO LOOK back and decide which scientific advances merit the title of Breakthrough of the Year. This year, we also asked you, our readers, to weigh in with your nominations on our Web site. You responded immediately with a wide range of worthy ideas, and your comments were still pouring in as the magazine went to press.

As it turned out, almost all of your nominations overlapped with our selections. However, you felt that our number-one pick, the first quantum machine, was a distant dark horse to the synthetic-biology results we deemed a runner-up.

You also pointed to some results that didn't make our list. Of these nominations, the overwhelming favorite was the arsenic-based bacterium that *Science* published online on 2 December. The News editors who selected our breakthroughs agree that the idea of a life form with arsenic in its DNA is, as one of you put it, "effing badass!" But because the paper ran late in the year, we feel it is prudent to allow for further analysis before giving it a nod. Other recent results you felt warranted attention, such as the apparent reversal of aging in genetically engineered mice by researchers at Harvard University, fell into our wait-and-see category as well. CERN physicists' success in trapping atoms of antihydrogen, reported in November, also justifiably impressed readers. We passed it over only because it's sure to be quickly overshadowed by follow-up experiments to measure critical properties of the mysterious antimatter.

The rest of your suggestions were all over the scientific map. They include basic research (the crystal structure of the eukaryotic ribosome and quantum entanglement in solid-state circuits); far-flung results such as the detection of free oxygen on Saturn's moon Rhea ("totally amazing"); various transformations of stem cells; and mind-boggling speculations from theoretical physics (the holographic universe). Only a couple of inventions crept in, notably a mechanical walker for paralyzed people. One tech-minded reader asked, "Is there any way we can sneak the commercial realization of memristors in here?" (That's not *Science*'s kind of breakthrough, but you could try *Business Week*.)

We thank the many readers who participated in our Breakthrough discussion. You can read all the suggestions sent by your fellow readers, including those sent after our press deadline, at *Science*'s Talk page (talk.sciencemag.org) and the Facebook page for our online news outlet, *Science*NOW.

***SCIENCE* NEWS STAFF**

Published by AAAS

Regulating Genetic Tests: Account for Benefits

THE POLICY FORUM "REGULATING DIRECT-TO-consumer personal genome testing" (A. L. McGuire *et al*., 8 October, p. 181) perpetuates the myth that risk-based stratification represents the best way to regulate direct-to-consumer genome tests. In fact, risk-based regulation fails to account for tolerability of risk (*1*), where the greater the expected benefit, the greater should be the tolerability of risk. The proposed method would likely delay access to all test results deemed high risk, regardless of the potential benefit of those results to the patient.

Sophisticated regulation based on tolerability of risk reduces the approval time and evidentiary requirements for the products with the highest potential for benefit. The U.S. Food and Drug Administration (FDA) already applies this strategy by granting an accelerated approval process for life-saving drugs, yet the agency often appears to take the opposite approach for diagnostic tests. This is an important issue as FDA considers expanding its reach into tests developed in laboratories. For many direct-to-consumer genetic tests, it is the absence of actionable benefit that appropriately reduces the tolerability of risk, not a high level of risk in absolute terms. The Policy Forum should have more explicitly stated that for patients, the harm caused by delaying a new test can be greater than the benefit of the regulation itself.

STEPHEN A. WILLIAMS

SomaLogic, 2945 Wilderness Place, Boulder, CO 80301, USA. E-mail: swilliams@somalogic.com

Reference

1. F. Bouder, D. Slavin, R. Lofstedt, *The Tolerability of Risk: A New Framework for Risk Management* (Earthscan, London, 2007).

Regulating Genetic Tests: Who Owns the Data?

DIRECT-TO-CONSUMER (DTC) GENETIC TESTing is not as dangerous as A. L. McGuire *et al*. suggest ("Regulating direct-to-consumer personal genome testing," Policy Forum, 8 October, p. 181). The belief that genetic information will compel consumers to behave unreasonably is unfounded.

Unlike the classical genetic tests that look for rare genetic abnormalities (such as Huntington's disease), genetic tests sold directly to consumers cannot diagnose a disease. They merely provide information about DNA sequence variations, or single-nucleotide polymorphisms (SNPs). Certain SNPs can be found more often among individuals with a particular disease or condition. For example, one particular combination of two SNPs in the APOE gene occurs 3 to 20 times more frequently in individuals with Alzheimer's (*1*). Consequently, a person with this particular combination of SNPs could be at a greater risk to develop Alzheimer's; the mere presence of these SNPs is not diagnostic.

There is no reason to require government approval before allowing a person to see his or her own genetic information. After receiving results that indicate a health-related risk, a person will likely see a doctor to determine the next appropriate step. This action would be no different from a person's response to learning that he or she has increased blood pressure, cholesterol, or weight. Should DTC sales of weight scales be regulated too?

The real question is what will happen if governments, big pharma, committees, and other faceless bodies gain control of our genetic information. College admissions based on genotype? Advertising geared to those with a particular SNP? This is a question for the ethicists to ponder.

ANDRIUS BASKYS

Department of Psychiatry and Human Behavior, University of California Irvine, Irvine, CA 92697, USA. E-mail: abaskys@uci.edu

Reference

1. L. Bertram *et al*., *Nat. Genet*. **39**, 17 (2007).

Response

IN OUR POLICY FORUM "REGULATING DIRECT-to-consumer personal genome testing" (8 October, p. 181), we recommend a risk-stratified regulatory approach for direct-to-consumer (DTC) genetic tests. If tests are low risk (as existing data indicate for the vast majority of tests sold DTC) then the oversight should be minimal and should focus on ensuring that consumers have accurate and truthful information. Only high-risk tests would be subject to greater oversight and enhanced scrutiny by agencies such as the U.S. Food and Drug Administration (FDA).

Williams argues that this type of risk-based strategy fails to account for the impact of benefit on the tolerability of risk. We agree that benefit is an important consideration. A high-risk test that has the potential to benefit consumers significantly, and thus has proven therapeutic utility, should be cleared or approved for distribution. In fact, the sort of external data-driven review that would be required to assess benefit is precisely what the FDA would provide when evaluating a high-risk new test product. However, the primary goal of regulatory oversight is to ensure consumer safety, so regardless of the potential for benefit, a test that poses significant risk ought to be subject to external review. The data required for the review in this circumstance allow regulators to take into account both risks and benefits.

Williams also argues that delayed access to a new test may prevent the introduction of life-saving diagnostics. We are not aware of any evidence that life-saving genetic tests, such as those used in newborn screening, are being delayed, but we agree that waiting for robust effectiveness data could effectively regulate DTC companies out of existence and should be avoided. We therefore believe that the FDA's premarket oversight should focus on the legitimacy of claims made and that there should be enhanced post-market data collection and surveillance. This approach is quite flexible in terms of the amount and type of evidence required for a test to move to market. It is more hospitable to innovative tests than is the case in many other countries, such as Germany, where DTC testing has been banned.

Baskys believes that all individuals have a right to receive their genetic information. We do not necessarily disagree. We simply argue that consumers need access to accurate and truthful information in order to make informed decisions. For tests that have the potential to influence important medical decisions, this includes contextual information about the individual's other risk factors, including family history, environmental exposures, and biological symptoms. We agree that there is a dearth of scientific evidence on the potential risks associated with receiving genetic information DTC; there is also a lack of evidence of the potential benefits. As noted by Baskys, there are few, if any, DTC tests that have as much predictive value as a blood pressure test or a weight scale. Indeed, available evidence tells us that genetic risk information does little to motivate healthy behavior change (*1*). Given this reality, it seems appropriate that the vast majority of

Published by AAAS

DTC tests will not require significant oversight, as per our stratified approach.

AMY L. MCGUIRE,[1]* BARBARA J. EVANS,[2] TIMOTHY CAULFIELD,[3] WYLIE BURKE[4]

[1]Center for Medical Ethics and Health Policy, Baylor College of Medicine, Houston, TX 77030, USA. [2]Health Law and Policy Institute, University of Houston Law Center, Houston, TX 77204, USA. [3]Health Law Institute, University of Alberta, Edmonton, AB T6G 2H5, Canada. [4]Department of Bioethics and Humanities, University of Washington School of Medicine, Seattle, WA 98195, USA.

*To whom correspondence should be addressed. E-mail: amcguire@bcm.edu

Reference

1. T. M. Marteau *et al*., "Effects of communicating DNA-based disease risk estimates on risk-reducing behaviours" (*Cochrane Database of Systematic Reviews*, issue 10, 10.1002/14651858.CD007275.pub2, 2010).

CORRECTIONS AND CLARIFICATIONS

Books *et al*.: "How neuromythologies support sex role stereotypes" by D. F. Halpern (3 December, p. 1320). An error was introduced during the production process. Reference 5 should read: R. A. Lippa, M. L. Collaer, M. Peters, *Arch. Sex. Behav*. **39**, 997 (2010).

Reports: "A low-magnetic-field soft gamma repeater" by N. Rea *et al*. (12 November, p. 944). Paolo Esposito's affiliation contained an error. He is at the Osservatorio Astronomico di Cagliari. The affiliation has been corrected in the HTML version online.

Random Samples: "What, us bitter?" (8 October, p. 157). The accompanying photograph mistakenly showed a scene in the Swiss Alps, not the Pamir Mountains.

Research Articles: "*Australopithecus sediba*: A new species of *Homo*-like Australopith from South Africa" by L. R. Berger *et al*. (9 April, p. 195). In the legend for Fig. 3, the mesiodistal diameter of the RM2 of the mandible of the adult individual MH2 should be 13.1 mm (not 14.1 mm). In Fig. 4, the specimen number of the pelvis of *Australopithecus afarensis* (Lucy) should be A.L. 288-1 (not A.L. 228-1). These errors do not affect the Research Article's conclusions.

TECHNICAL COMMENT ABSTRACTS

Comment on "The Incidence of Fire in Amazonian Forests with Implications for REDD"

Jennifer K. Balch, Daniel C. Nepstad, Paulo M. Brando, Ane Alencar

Aragão and Shimabukuro (Reports, 4 June 2010, p. 1275) reported that fires increase in agricultural frontiers even as deforestation decreases and concluded that these fires lead to unaccounted carbon emissions under the United Nations climate treaty's tropical deforestation and forest degradation component. Emissions from post-deforestation management activities are, in fact, included in these estimates—but burning of standing forests is not.

Full text at www.sciencemag.org/cgi/content/full/330/6011/1627-b

Response to Comment on "The Incidence of Fire in Amazonian Forests with Implications for REDD"

Luiz E. O. C. Aragão and Yosio E. Shimabukuro

Balch *et al*. suggest that the increased fire frequency reported in our study is principally due to post-deforestation activities. We present a new analysis demonstrating that for the majority of grid cells with positive fire trends, there is a low likelihood that these trends have resulted exclusively from post-deforestation activities. We therefore confirm that fires pose a growing threat to reducing emissions from deforestation and degradation (REDD) policies.

Full text at www.sciencemag.org/cgi/content/full/330/6011/1627-c

LETTERS

edited by Jennifer Sills

China's Plan Flawed But Courageous

IN HER NEWS FOCUS STORY "HAS CHINA OUTgrown the one-child policy?" (17 September, p. 1458), M. Hvistendahl explores the consequences of China's fertility policies. Overall, the story presents the one-child policy in a negative light, buttressed by statistical data, such as the current gender ratio of 119:100 at birth and the projected graying of the Chinese population. These data are accurate but misleadingly incomplete. The single most relevant statistic is the one that drove the original decision to implement the policy: the total population of China as a function of time. Even with the reduced population growth that came with the one-child policy and with China's rapid shift toward an urbanized and export-driven economy, those numbers are sobering. In 1960, China had a population of 646 million; in 1980, it was 981 million; by 2000, it had grown to 1.267 billion; and in 2010, it is projected to be 1.354 billion (*1*). In the past 50 years, China's population has increased by an amount equal to or greater than the population of all of Central and North America (~500 million). Without defending or criticizing the one-child policy, we can at least recognize that it stands as a brave attempt by the inhabitants of an overcrowded planet to create a more livable future for our children and grandchildren.

JEREMY NATHANS

Department of Molecular Biology and Genetics, The Johns Hopkins Medical School, Baltimore, MD 21205, USA.
E-mail: jnathans@jhmi.edu

Reference

1. United Nations, Department of Economic and Social Affairs, Population Division, Population Estimates and Projections Section, World Population Prospects: The 2008 Revision (http://esa.un.org/unpd/wpp2008/tab-sorting_population.htm).

Science TALK

Readers' Picks

Your Breakthrough Nominations

EVERY YEAR, THE EDITORS AT *SCIENCE* GET TOGETHER TO LOOK back and decide which scientific advances merit the title of Breakthrough of the Year. This year, we also asked you, our readers, to weigh in with your nominations on our Web site. You responded immediately with a wide range of worthy ideas, and your comments were still pouring in as the magazine went to press.

As it turned out, almost all of your nominations overlapped with our selections. However, you felt that our number-one pick, the first quantum machine, was a distant dark horse to the synthetic-biology results we deemed a runner-up.

You also pointed to some results that didn't make our list. Of these nominations, the overwhelming favorite was the arsenic-based bacterium that *Science* published online on 2 December. The News editors who selected our breakthroughs agree that the idea of a life form with arsenic in its DNA is, as one of you put it, "effing badass!" But because the paper ran late in the year, we feel it is prudent to allow for further analysis before giving it a nod. Other recent results you felt warranted attention, such as the apparent reversal of aging in genetically engineered mice by researchers at Harvard University, fell into our wait-and-see category as well. CERN physicists' success in trapping atoms of antihydrogen, reported in November, also justifiably impressed readers. We passed it over only because it's sure to be quickly overshadowed by follow-up experiments to measure critical properties of the mysterious antimatter.

The rest of your suggestions were all over the scientific map. They include basic research (the crystal structure of the eukaryotic ribosome and quantum entanglement in solid-state circuits); far-flung results such as the detection of free oxygen on Saturn's moon Rhea ("totally amazing"); various transformations of stem cells; and mind-boggling speculations from theoretical physics (the holographic universe). Only a couple of inventions crept in, notably a mechanical walker for paralyzed people. One tech-minded reader asked, "Is there any way we can sneak the commercial realization of memristors in here?" (That's not *Science*'s kind of breakthrough, but you could try *Business Week*.)

We thank the many readers who participated in our Breakthrough discussion. You can read all the suggestions sent by your fellow readers, including those sent after our press deadline, at *Science*'s Talk page (talk.sciencemag.org) and the Facebook page for our online news outlet, *Science*NOW.

***SCIENCE* NEWS STAFF**

Published by AAAS

Regulating Genetic Tests: Account for Benefits

THE POLICY FORUM "REGULATING DIRECT-TO-consumer personal genome testing" (A. L. McGuire *et al*., 8 October, p. 181) perpetuates the myth that risk-based stratification represents the best way to regulate direct-to-consumer genome tests. In fact, risk-based regulation fails to account for tolerability of risk (*1*), where the greater the expected benefit, the greater should be the tolerability of risk. The proposed method would likely delay access to all test results deemed high risk, regardless of the potential benefit of those results to the patient.

Sophisticated regulation based on tolerability of risk reduces the approval time and evidentiary requirements for the products with the highest potential for benefit. The U.S. Food and Drug Administration (FDA) already applies this strategy by granting an accelerated approval process for life-saving drugs, yet the agency often appears to take the opposite approach for diagnostic tests. This is an important issue as FDA considers expanding its reach into tests developed in laboratories. For many direct-to-consumer genetic tests, it is the absence of actionable benefit that appropriately reduces the tolerability of risk, not a high level of risk in absolute terms. The Policy Forum should have more explicitly stated that for patients, the harm caused by delaying a new test can be greater than the benefit of the regulation itself.

STEPHEN A. WILLIAMS

SomaLogic, 2945 Wilderness Place, Boulder, CO 80301, USA. E-mail: swilliams@somalogic.com

Reference

1. F. Bouder, D. Slavin, R. Lofstedt, *The Tolerability of Risk: A New Framework for Risk Management* (Earthscan, London, 2007).

Regulating Genetic Tests: Who Owns the Data?

DIRECT-TO-CONSUMER (DTC) GENETIC TESTing is not as dangerous as A. L. McGuire *et al*. suggest ("Regulating direct-to-consumer personal genome testing," Policy Forum, 8 October, p. 181). The belief that genetic information will compel consumers to behave unreasonably is unfounded.

Unlike the classical genetic tests that look for rare genetic abnormalities (such as Huntington's disease), genetic tests sold directly to consumers cannot diagnose a disease. They merely provide information about DNA sequence variations, or single-nucleotide polymorphisms (SNPs). Certain SNPs can be found more often among individuals with a particular disease or condition. For example, one particular combination of two SNPs in the APOE gene occurs 3 to 20 times more frequently in individuals with Alzheimer's (*1*). Consequently, a person with this particular combination of SNPs could be at a greater risk to develop Alzheimer's; the mere presence of these SNPs is not diagnostic.

There is no reason to require government approval before allowing a person to see his or her own genetic information. After receiving results that indicate a health-related risk, a person will likely see a doctor to determine the next appropriate step. This action would be no different from a person's response to learning that he or she has increased blood pressure, cholesterol, or weight. Should DTC sales of weight scales be regulated too?

The real question is what will happen if governments, big pharma, committees, and other faceless bodies gain control of our genetic information. College admissions based on genotype? Advertising geared to those with a particular SNP? This is a question for the ethicists to ponder.

ANDRIUS BASKYS

Department of Psychiatry and Human Behavior, University of California Irvine, Irvine, CA 92697, USA. E-mail: abaskys@uci.edu

Reference

1. L. Bertram *et al*., *Nat. Genet*. **39**, 17 (2007).

Response

IN OUR POLICY FORUM "REGULATING DIRECT-to-consumer personal genome testing" (8 October, p. 181), we recommend a risk-stratified regulatory approach for direct-to-consumer (DTC) genetic tests. If tests are low risk (as existing data indicate for the vast majority of tests sold DTC) then the oversight should be minimal and should focus on ensuring that consumers have accurate and truthful information. Only high-risk tests would be subject to greater oversight and enhanced scrutiny by agencies such as the U.S. Food and Drug Administration (FDA).

Williams argues that this type of risk-based strategy fails to account for the impact of benefit on the tolerability of risk. We agree that benefit is an important consideration. A high-risk test that has the potential to benefit consumers significantly, and thus has proven therapeutic utility, should be cleared or approved for distribution. In fact, the sort of external data-driven review that would be required to assess benefit is precisely what the FDA would provide when evaluating a high-risk new test product. However, the primary goal of regulatory oversight is to ensure consumer safety, so regardless of the potential for benefit, a test that poses significant risk ought to be subject to external review. The data required for the review in this circumstance allow regulators to take into account both risks and benefits.

Williams also argues that delayed access to a new test may prevent the introduction of life-saving diagnostics. We are not aware of any evidence that life-saving genetic tests, such as those used in newborn screening, are being delayed, but we agree that waiting for robust effectiveness data could effectively regulate DTC companies out of existence and should be avoided. We therefore believe that the FDA's premarket oversight should focus on the legitimacy of claims made and that there should be enhanced post-market data collection and surveillance. This approach is quite flexible in terms of the amount and type of evidence required for a test to move to market. It is more hospitable to innovative tests than is the case in many other countries, such as Germany, where DTC testing has been banned.

Baskys believes that all individuals have a right to receive their genetic information. We do not necessarily disagree. We simply argue that consumers need access to accurate and truthful information in order to make informed decisions. For tests that have the potential to influence important medical decisions, this includes contextual information about the individual's other risk factors, including family history, environmental exposures, and biological symptoms. We agree that there is a dearth of scientific evidence on the potential risks associated with receiving genetic information DTC; there is also a lack of evidence of the potential benefits. As noted by Baskys, there are few, if any, DTC tests that have as much predictive value as a blood pressure test or a weight scale. Indeed, available evidence tells us that genetic risk information does little to motivate healthy behavior change (*1*). Given this reality, it seems appropriate that the vast majority of

Published by AAAS

DTC tests will not require significant oversight, as per our stratified approach.

AMY L. MCGUIRE,[1]* BARBARA J. EVANS,[2] TIMOTHY CAULFIELD,[3] WYLIE BURKE[4]

[1]Center for Medical Ethics and Health Policy, Baylor College of Medicine, Houston, TX 77030, USA. [2]Health Law and Policy Institute, University of Houston Law Center, Houston, TX 77204, USA. [3]Health Law Institute, University of Alberta, Edmonton, AB T6G 2H5, Canada. [4]Department of Bioethics and Humanities, University of Washington School of Medicine, Seattle, WA 98195, USA.

*To whom correspondence should be addressed. E-mail: amcguire@bcm.edu

Reference

1. T. M. Marteau *et al*., "Effects of communicating DNA-based disease risk estimates on risk-reducing behaviours" (*Cochrane Database of Systematic Reviews*, issue 10, 10.1002/14651858.CD007275.pub2, 2010).

CORRECTIONS AND CLARIFICATIONS

Books *et al*.: "How neuromythologies support sex role stereotypes" by D. F. Halpern (3 December, p. 1320). An error was introduced during the production process. Reference 5 should read: R. A. Lippa, M. L. Collaer, M. Peters, *Arch. Sex. Behav*. **39**, 997 (2010).

Reports: "A low-magnetic-field soft gamma repeater" by N. Rea *et al*. (12 November, p. 944). Paolo Esposito's affiliation contained an error. He is at the Osservatorio Astronomico di Cagliari. The affiliation has been corrected in the HTML version online.

Random Samples: "What, us bitter?" (8 October, p. 157). The accompanying photograph mistakenly showed a scene in the Swiss Alps, not the Pamir Mountains.

Research Articles: "*Australopithecus sediba*: A new species of *Homo*-like Australopith from South Africa" by L. R. Berger *et al*. (9 April, p. 195). In the legend for Fig. 3, the mesiodistal diameter of the RM2 of the mandible of the adult individual MH2 should be 13.1 mm (not 14.1 mm). In Fig. 4, the specimen number of the pelvis of *Australopithecus afarensis* (Lucy) should be A.L. 288-1 (not A.L. 228-1). These errors do not affect the Research Article's conclusions.

TECHNICAL COMMENT ABSTRACTS

Comment on "The Incidence of Fire in Amazonian Forests with Implications for REDD"

Jennifer K. Balch, Daniel C. Nepstad, Paulo M. Brando, Ane Alencar

Aragão and Shimabukuro (Reports, 4 June 2010, p. 1275) reported that fires increase in agricultural frontiers even as deforestation decreases and concluded that these fires lead to unaccounted carbon emissions under the United Nations climate treaty's tropical deforestation and forest degradation component. Emissions from post-deforestation management activities are, in fact, included in these estimates—but burning of standing forests is not.

Full text at www.sciencemag.org/cgi/content/full/330/6011/1627-b

Response to Comment on "The Incidence of Fire in Amazonian Forests with Implications for REDD"

Luiz E. O. C. Aragão and Yosio E. Shimabukuro

Balch *et al*. suggest that the increased fire frequency reported in our study is principally due to post-deforestation activities. We present a new analysis demonstrating that for the majority of grid cells with positive fire trends, there is a low likelihood that these trends have resulted exclusively from post-deforestation activities. We therefore confirm that fires pose a growing threat to reducing emissions from deforestation and degradation (REDD) policies.

Full text at www.sciencemag.org/cgi/content/full/330/6011/1627-c

Comment on "The Incidence of Fire in Amazonian Forests with Implications for REDD"

Jennifer K. Balch,[1,2,3]* Daniel C. Nepstad,[1] Paulo M. Brando,[1] Ane Alencar[1,4]

Aragão and Shimabukuro (Reports, 4 June 2010, p. 1275) reported that fires increase in agricultural frontiers even as deforestation decreases and concluded that these fires lead to unaccounted carbon emissions under the United Nations climate treaty's tropical deforestation and forest degradation component. Emissions from post-deforestation management activities are, in fact, included in these estimates—but burning of standing forests is not.

Satellite-based observations of Earth's surface allow us to map active fires and smoke under a range of conditions, but do not reliably detect fires that burn beneath the canopies of standing moist tropical forests (*1*). Until we can quantify the types of human-caused fires across Amazonia (*2*), not just the occurrence of fire, the carbon consequences of fire-facilitated clearing and land use and associated accidental fires will be uncertain.

Our inability to fully differentiate among different types of vegetation fires detected by satellites can lead to potentially erroneous conclusions. Aragão and Shimabukuro (*3*) presented evidence that fire frequency can increase even as deforestation (forest felling and immediate burning events) decreases in Amazon frontier zones—an important finding. However, they go on to conclude that the observed increase in post-deforestation fire reverses the emissions reductions that might be achieved through the United Nations initiative for reducing emissions from deforestation and degradation (REDD). However, this conclusion is not justified by their data because they cannot say what proportion of the observed fires took place as part of the multiyear process to burn off unwanted forest biomass or what proportion, if any, occurred in otherwise intact, standing forests. Moreover, once an area is deforested, there is a high likelihood that management fires will follow, particularly in pastures.

Aragão and Shimabukuro (*3*) measured fire occurrence using temperature threshold data from the National Oceanic and Atmospheric Administration's Advanced Very High Resolution Radiometer (AVHRR) and Moderate Resolution Imaging Spectroradiometer (MODIS). These data principally provide information on clearing and management fires ignited by farmers and ranchers to remove brush and organic debris from their land and on unintentional fires that burn across cleared land (*4*). The carbon emissions from these repeated fires, including "slash-and-burn" fires, take place over a several-year period after forest felling (*5*) and, contrary to Aragão and Shimabukuro's statement, are already included in carbon emissions estimates from deforestation (*6*, *7*). Because the authors do not characterize the different types of fires, they could not quantify the proportion of fires that are part of the normal post-felling process and those that escaped into surrounding forest.

Fires that burn standing forests, referred to here as understory fires, are not included in most estimates of carbon emissions from deforestation, even though they can affect more than twice the area deforested annually (*8*). These fires kill many trees, from 8 to 64% of mature individuals across Amazon forest sites (*9*), and burn biomass (*10*)—thereby reducing forest carbon stocks. Understory fires represent a threat to the "permanence" of carbon that could eventually be compensated through a REDD program.

REDD+, as currently negotiated, will provide benefits to nations that decrease carbon emissions from deforestation and forest degradation and that enhance forest carbon (*11*). Prevention of forest degradation from fire will not be rewarded under REDD+, in part because robust methods for quantifying emissions from degradation have only recently become available (*12*). Nations that do not succeed in implementing wildfire control programs to protect forest carbon will therefore likely be penalized (*11*). Fire represents an important threat to the permanence of forest carbon stocks, and in this sense the Aragão and Shimabukuro study (*3*) is a welcome contribution.

In 2010, the pattern documented by Aragão and Shimabukuro (*3*) may have appeared on the scale of the Brazilian Amazon. By 3 October 2010, more than 104,000 active fires had already been detected in Brazil, which is 14% higher than the average between 2005 and 2009 for this same 9-month period (*13*). Total deforestation detected within Brazil's legal Amazon was only 925 km^2 between January and August 2010 (*14*). If this rate continues, total forest loss for 2010 will be even lower than the record low of 7464 km^2 detected for the period from August 2008 to August 2009 (*15*).

Future research will need to find ways of differentiating between those fires that are the result of intentional clearing, continued land management, or unintentional, escaped wildfires. Further, we need to better understand how fire management decisions and drought can lead to extensive and sustained wildfires. New remote-sensing technologies such as burned-area mapping and quantification of fire radiative power will enable better understanding of the diversity of intentional and unintentional anthropogenic fires across this region. But in the meantime, as 2010 demonstrates, Brazil needs a strong national firefighting plan for Amazonia and a new model of rural development that encourages more sustainable and fire-sensitive investments—especially if it is to defend its remarkable progress in slowing deforestation (*16*).

[1]Amazon Environmental Research Institute (IPAM), Brasília, DF 71.503-505, Brazil. [2]Woods Hole Research Center, Woods Hole, MA 02540, USA. [3]National Center for Ecological Analysis and Synthesis, University of California–Santa Barbara, CA 93101, USA. [4]School of Forest Resources and Conservation, University of Florida, Gainesville, FL 32611, USA.

*To whom correspondence should be addressed. E-mail: balch@nceas.ucsb.edu

References

1. D. C. Nepstad *et al.*, *Nature* **398**, 505 (1999).
2. D. Nepstad *et al.*, *For. Ecol. Manage.* **154**, 395 (2001).
3. L. E. O. C. Aragão, Y. E. Shimabukuro, *Science* **328**, 1275 (2010).
4. W. Schroeder *et al.*, *Earth Interact.* **9**, 1 (2005).
5. D. C. Morton *et al.*, *Glob. Change Biol.* **14**, 2262 (2008).
6. R. A. Houghton *et al.*, *Nature* **403**, 301 (2000).
7. P. M. Fearnside, *Clim. Change* **35**, 321 (1997).
8. A. Alencar, D. C. Nepstad, M. C. V. Diaz, *Earth Interact.* **10**, 1 (2006).
9. J. Barlow, C. A. Peres, in *Emerging Threats to Tropical Forests,* W. F. Laurance, C. A. Peres, Eds. (Univ. of Chicago Press, Chicago, 2006), pp. 225–240.
10. J. K. Balch *et al.*, *Glob. Change Biol.* **14**, 2276 (2008).
11. C. M. Stickler *et al.*, *Glob. Change Biol.* **15**, 2803 (2009).
12. G. P. Asner *et al.*, *Proc. Natl. Acad. Sci. U.S.A.* **107**, 16738 (2010).
13. Instituto Nacional de Pesquisas Espaciais (INPE), *Annual Accumulation of NOAA-15 Active Fire Detections by Country from 01 January to 03 October 2010: Project Queimadas*; http://sigma.cptec.inpe.br/queimadas.
14. S. Hayashi, C. Souza, M. Sales, A. Veríssimo, *IMAZON Boletim Transparência Florestal: January–August 2010*; www.imazon.org.br.
15. Instituto Nacional de Pesquisas Espaciais (INPE), *Monitoring of the Brazilian Amazon Forest by Satellite: Project PRODES*; www.obt.inpe.br/prodes/prodes_1988_2009.htm.
16. D. Nepstad *et al.*, *Science* **326**, 1350 (2009).

21 June 2010; accepted 23 November 2010
10.1126/science.1194032

Response to Comment on "The Incidence of Fire in Amazonian Forests with Implications for REDD"

Luiz E. O. C. Aragão[1]* and Yosio E. Shimabukuro[2]

Balch *et al*. suggest that the increased fire frequency reported in our study is principally due to post-deforestation activities. We present a new analysis demonstrating that for the majority of grid cells with positive fire trends, there is a low likelihood that these trends have resulted exclusively from post-deforestation activities. We therefore confirm that fires pose a growing threat to reducing emissions from deforestation and degradation (REDD) policies.

Balch *et al*. (*1*) challenge our conclusion (*2*) that the widespread increase in fire incidence across Amazonia, which has occurred despite a reduction in deforestation rates, poses an emerging threat to the efficacy of reducing emissions from deforestation and degradation (REDD) policy. We address their objections and present new evidence to support our conclusions.

The criticisms of Balch *et al*. (*1*) arise from an inaccurate interpretation of our conclusions. We did not claim that post-deforestation fires reverse emission reductions achieved through REDD but, instead, that there is an increased risk of carbon losses resulting from increased fire frequency, even with the reduction in deforestation rates, because of ongoing enlargement of forest edges, secondary forest cover, and fragmentation, favoring the leakage of accidental fires from farms. Balch *et al*. appear to suggest that the observed fire trends are the product of post-deforestation activities alone. Their proposition is grounded on two studies (*3*, *4*) that have not evaluated this issue. Our conclusions are based on the fact that active fires data, in addition to post-deforestation fires, capture high-energy fires in forest edges, degraded forests, and forest crown (*5*). Active fire data are likely to underestimate understory fires and, therefore, our conclusions are rather conservative (*2*). Agreeing on methods for monitoring, reporting, and verifying emissions (MRV) from these areas within the REDD framework is thus urgently required.

Balch *et al*. do raise an interesting question about the extent to which active fire detections capture fires other than post-deforestation fires. In response, we have performed a further evaluation of the patterns found in our study (*2*). Despite our inability to detect fire types, if it is assumed that active fire detections are proportional to the biomass available to burn (fuel loads) in a given location (*6*), then the temporal trends in fuel loads, after successive deforestation, incomplete combustion, and vegetation regrowth in a grid cell, can provide an estimation of the likelihood of post-deforestation fire trajectories in that grid cell.

To verify whether post-deforestation activities can generate positive trends in fuel loads and, hence, sustain an increase in fire incidence along an 8-year time frame, we conducted 250 simulations (four experiments, Fig. 1) based on 110 deforestation scenarios with negative temporal trends. For each scenario, annual frac-

[1]Landscape and Ecosystem Dynamics Group, Department of Geography, School of Life and Environmental Sciences, University of Exeter, Amory Building, Rennes Drive, Exeter, Devon, EX4 4RJ, UK. [2]Remote Sensing Division, National Institute for Space Research, Avenue dos Astronautas, 12227-010, São José dos Campos, SP, Brazil.

*To whom correspondence should be addressed. E-mail: l.aragao@exeter.ac.uk

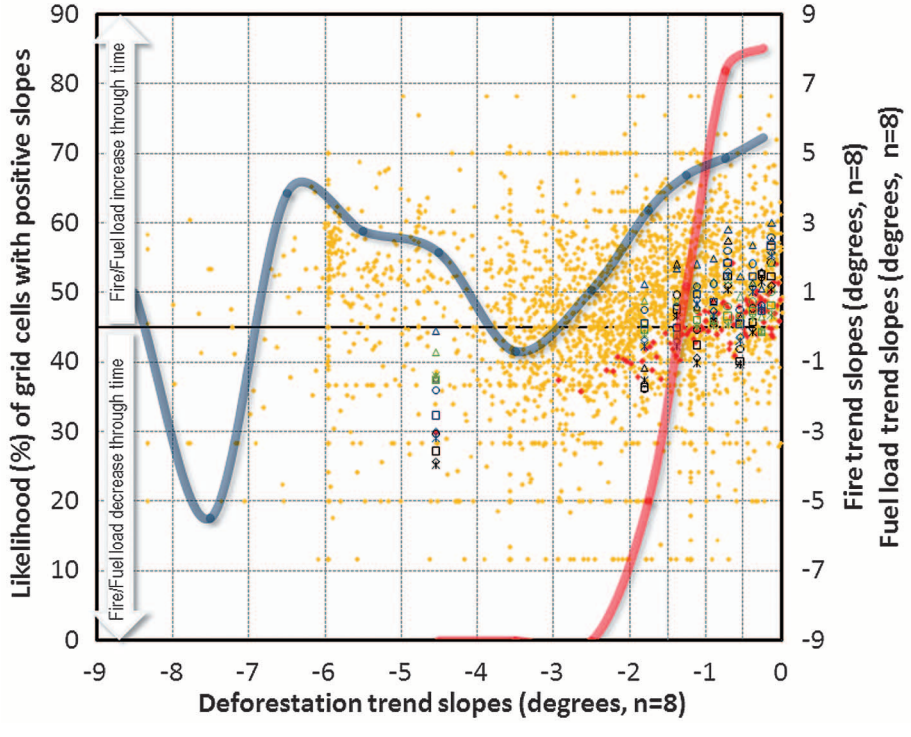

Fig. 1. Scatter plot of trend slopes of fire and fuel load across the range of deforestation. All slopes presented in the figure were calculated using normalized values of deforestation, fuel loads, and fire. Yellow diamonds correspond to the slopes derived from the original fire (AVHRR/NOAA-12) and deforestation (PRODES) data presented in (*2*). Different colors represent fuel load slopes for three simulations (experiments), based on 10 random deforestation scenarios, using a regrowth rate R_b = 15 t ha^{-1} year^{-1} (*16*), and with varying levels of fractional area deforested (A_f). Experiment 1 assumes A_f = 20% (black), experiment 2 assumes A_f = 40% (green), and experiment 3 assumes A_f = 100% (blue). Symbols represent the five levels of *CC* used in each experiment: *CC* = 20% (open triangle), *CC* = 30% (open circle), *CC* = 40% (open square), *CC* = 50% (open diamonds), and *CC* = 60% (asterisks). Experiment 4 is the most likely scenario (red diamonds) for fuel load calculations. It is based on 100 random deforestation scenarios. For experiment 4, fuel loads were calculated assuming *CC* = 40% [approximate mean value of values reported for Amazonia (*7*)], A_f = 40% (encompass 96% of all values for annual fractional area deforested in Amazonia) and R_b = 8 t ha^{-1} yr^{-1} [average net primary production for grasslands in Amazonia (*7*)]. Lines indicate the likelihood (percentage of all simulation results in each class of deforestation slopes) of obtaining positive fire (original data, blue line) and fuel loads (simulations, red line) slopes in each category of deforestation slopes (0.0 to –0.5, –0.5 to –1.0, –1.0 to –1.5, –1.5 to –2.0, –2.0 to –3.0, –3.0 to –4.0, –4.0 to –5.0, –5.0 to –6.0, –6.0 to –7.0, –7.0 to –8.0, and –8.0 to –9.0). Categories match with the vertical grid lines.

tional deforestation in a 5 × 5 grid cell (total of 25 subcells) was randomly assigned following a normal distribution. The simulations included five levels of combustion completeness (CC), three levels of fractional area deforested (A_f), and two levels of biomass regrowth rate (R_b). CC was calculated as a proportion of the initial biomass, which ranges from 19.5% to 61.5% in Amazonia (*7*). For each deforestation event, we assumed an average initial biomass (B_i) of 300 t ha^{-1}. The biomass remaining at each time interval t ($B_{r,t}$) was calculated as $B_{r,t} = B_{r,t-1} - (B_i \times CC) + R_b$. Cumulative annual fuel load was estimated as the sum of $B_{r,t}$ in each of the 25 subcells. Trend slopes were calculated using normalized values of deforestation, fuel loads, and fire. The likelihood of obtaining positive fuel load (simulations) and fire (data) slopes was crudely estimate as a proportion of all simulation results in each class of deforestation slopes (Fig. 1).

Considering all simulations, 57% of the grid cells with positive fire slope fall in a region with less than 30% likelihood of positive fuel load trend. This value increases to 77% considering the most likely scenario alone (experiment 4). The likelihood of extra biomass burning from secondary forests, adjacent forest edges, and disturbed forests is therefore high for the majority of the grid cells. Conversely, as deforestation slopes approach zero, fires associated exclusively with clearing and management are more likely to occur. Other than emissions from primary forest clearance and maintenance fires, none of the above processes are fully considered in previous basin-wide net carbon emission estimates (*7*–*11*).

Balch *et al*. highlight the contribution and difficulties in reporting understory fires emissions under REDD. This was also a central point of our discussion (*2*). Emissions from understory forest fires [0.01 to 0.2 Gt C year^{-1} (*9*, *12*)] and long-term changes in fire-affected forest carbon pools (*13*) are likely to be unaccounted for, not only because of the lack of agreement on methods to quantify and monitor these events (*14*) but also if the MRV processes mirror the guidelines on land use, land-cover change, and forestry used by Annex I countries (*15*).

There is a high probability that fires other than those from post-deforestation activities have an important contribution to the increased fire incidence in Amazonia, confirming our conclusion that REDD benefits may be undermined by the increased risk of unaccounted fire emissions. We hope that this exchange advances the discussions on tropical forest fires and spurs urgent actions to place REDD as an efficient climate change mitigation policy.

References and Notes

1. J. K. Balch, D. C. Nepstad, P. M. Brando, A. Alencar, *Science* **330**, 1627 (2010); www.sciencemag.org/cgi/content/full/330/6011/1627-b.
2. L. E. O. C. Aragão, Y. E. Shimabukuro, *Science* **328**, 1275 (2010).
3. D. C. Nepstad *et al*., *Nature* **398**, 505 (1999).
4. W. Schroeder *et al*., *Earth Interact.* **9**, 1 (2005).
5. M. J. Wooster, Y. H. Zhang, *Geophys. Res. Lett.* **31**, L20505 (2004).
6. D. C. Morton *et al*., *Glob. Change Biol.* **14**, 2262 (2008).
7. G. R. van der Werf *et al*., *Biogeosciences* **6**, 235 (2009).
8. P. M. Fearnside, *Clim. Change* **35**, 321 (1997).
9. R. A. Houghton *et al*., *Nature* **403**, 301 (2000).
10. R. S. DeFries *et al*., *Proc. Natl. Acad. Sci. U.S.A.* **99**, 14256 (2002).
11. N. Ramankutty *et al*., *Glob. Change Biol.* **13**, 51 (2007).
12. A. Alencar, D. C. Nepstad, M. C. V. Diaz, *Earth Interact.* **10**, 1 (2006).
13. J. Barlow, C. A. Peres, B. O. Lagan, T. Haugaasen, *Ecol. Lett.* **6**, 6 (2003).
14. Intergovernmental Panel on Climate Change (IPCC), Good Practice Guidance for Land Use, Land-Use Change and Forestry (2003); www.ipcc-nggip.iges.or.jp/public/gpglulucf/gpglulucf_contents.html.
15. Intergovernmental Panel on Climate Change (IPCC), Definitions and Methodological Options to Inventory Emissions from Direct Human-Induced Degradation of Forests and Devegetation of Other Vegetation Types (2003); www.ipcc-nggip.iges.or.jp/public/gpglulucf/degradation.html.
16. R. I. Barbosa, P. M. Fearnside, *J. Geophys. Res.* **101**, (D20), 25847 (1996).

17. We thank the U.K. Natural Environment Research Council for providing funds to L. E. O. C. Aragão (NE/F015356/2).

13 July 2010; accepted 23 November 2010
10.1126/science.1195063

NETWORK ANALYSIS

Exploring Links to Improve Health

Jimi Adams

Networks are everywhere. Over the past several decades, social networks have garnered increasing attention, leading people to craft languages illustrating their essential elements, develop strategies to harness their power (e.g., Facebook), and devote considerable efforts to systematically describe the salient characteristics of network structure and dynamics. Network-based perspectives have so permeated our lives and shaped scientific thinking that few would question Thomas Valente's claim that "Today, network analysis represents a full-grown paradigm of research and constitutes a perspective that is increasingly difficult to ignore." Thus it is no surprise that health researchers such as Valente (University of Southern California) are exploring how social networks influence our health-related behaviors and outcomes along with ways our health shapes the formation, maintenance, and dissolution of social relationships.

Some of the network approach's roots developed in health-related fields, and in *Social Networks and Health*, Valente demonstrates how the usefulness of the approach can reach far beyond its current application in medicine and public health. Sketching much of the state of the art in current social network research, he devotes the bulk of the book to adeptly providing the foundations for effectively carrying out social network analyses. He describes the major theoretical perspectives, outlines the primary ways they have been implemented in empirical research, details the important methodological basis of those contributions, and acknowledges several aspects that have limited advances. Although many of these topics are addressed in other sources, Valente's focus on health-based examples is unique. This simultaneously serves to highlight the range of health-related topics to which networks can be applied and to demonstrate how aspects specific to health research require particular adaptations of the general network approach.

Social Networks and Health
Models, Methods, and Applications
by Thomas W. Valente
Oxford University Press, New York, 2010. 291 pp. $49.95, £32.50. ISBN 9780195301014.

Perhaps the book's most important insights appear in the chapters detailing research on network interventions and diffusion of innovations. Appropriately, these two chapters also highlight areas where the author's own work has made substantial contributions. Within the general social networks literature, these topics are comparatively less understood than many others, but they likely have the broadest appeal for anyone interested in understanding and improving the health of human populations.

Diffusion research captures the capacity for networks to either promote or constrain the spread of "things." This network property can be leveraged to quickly disseminate important scientific breakthroughs or exploited to limit widespread epidemics. Research has demonstrated considerable ability to pinpoint relevant elements of network structure that contributed to the successful spread of ideas through a population, such as how central actors helped promote adoption of particular family-planning practices during the transitions from high to low fertility in several countries. We even understand how those network characteristics relate to the form those innovation trajectories take (S-curve growth). However, our ability to predict which networks will generate those ideas that will take off or to accurately predict when a breakthrough will occur has not yet similarly advanced.

Beyond simply observing networks, researchers have developed a widespread interest in being able to identify aspects of networks that are potentially susceptible to targeted change. Such change can take a range of forms, from leveraging knowledge of existing network structure with the goal of promoting particular behaviors to modifying existing networks by adding new people or connections at strategic locations within them. Other interventions involve rewiring connections within networks in attempts to make them more efficient (e.g., for spreading news across an organization) or trying to disrupt existing networks by removing particular members (e.g., combating terrorism). For example, Valente has demonstrated the importance of identifying and targeting "opinion leaders" for evincing health-promoting behavioral changes among teens, such as reduced substance abuse and slowed taking up of smoking. However, targeted network interventions have had widely varying success. Although some work as desired, others have shown virtually no effect, and still others have even produced significant results opposite the intended effect. As a future aim for network research, interventions may be an area ripe for advance. Nonetheless, with the present state of the field we can do little more than conclude that "purposively changing networks, in many cases, is likely to be very difficult since people have the relationships they have for very good reasons."

Recent advances in computation have played an important role in developing our capacity to examine the complexities inherent in networks-based research. This enlarged capacity has enabled a shift from a nearly exclusive focus on the static prop-

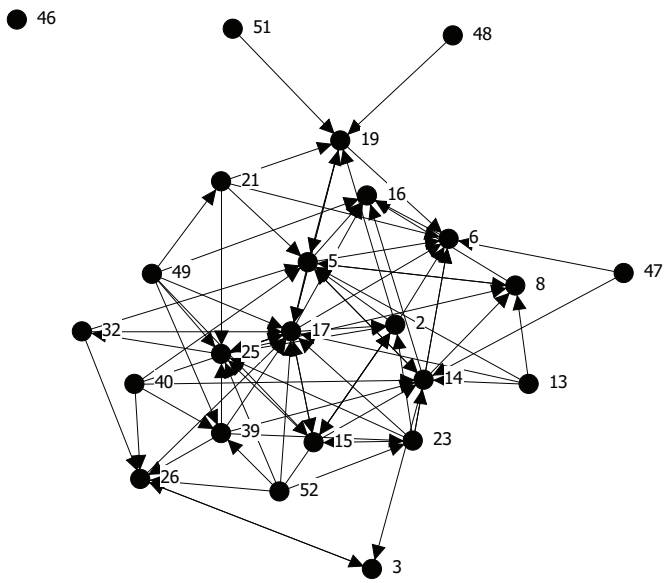

Mapping guidance. This network of a community coalition designed to promote substance abuse prevention activities illustrates who went to whom for advice.

CREDIT: FROM *SOCIAL NETWORKS AND HEALTH*/COURTESY THOMAS VALENTE

The reviewer is at the School of Social and Family Dynamics, Arizona State University, Tempe, AZ 85287–3701, USA. E-mail: jadams27@asu.edu

Published by AAAS

erties of networks to examining patterns of network change. Recent years have also seen the development of statistical approaches for examining networks, both for static and dynamic network characteristics (through exponential random graph models and actor-oriented models of network evolution, respectively). Several similar future steps will likely influence how broadly networks can influence health research. We need to consider ways to more systematically integrate network-based approaches into new data collection efforts (especially in large, population-based samples) and to effectively combine network advances with other analytic approaches (e.g., spatial analytic methods). As Valente's book indicates, the confluence of widespread interest, a relatively established research "canon," and recent advances in the field has laid the grounds for the network approach to make important contributions to science, in health and writ large, in the coming years.

10.1126/science.1197365

SYNTHETIC BIOLOGY

Inventive Constructions Using Biobricks

Valda Vinson

In early November, 118 teams (wearing group colors and, some, shouting team cheers) from 26 countries descended on the MIT campus for the grand finale of the 2010 International Genetically Engineered Machine (iGEM) competition. The undergraduate students had plunged into their projects at the beginning of the summer, when teams received a kit of "biobricks" from the Registry of Standard Biological Parts. They were to use these to design and build simple biological systems and operate them in living cells. In addition to the existing standard parts, their projects could involve new parts that they created and would contribute to the registry. Under the mentorship of faculty sponsors (who helped them obtain research space, funding, equipment, and expert advice), the students worked through the summer, recording their progress on team wikis. On 27 October, the wikis were frozen, and evaluation of the teams' efforts began. The iGEM Jamboree offered students the opportunity to present their work to the judges, their competitors, and other interested observers. And present they did.

Meeting at MIT. The iGEM 2010 teams gathered for the Jamboree.

CREDIT: COURTESY IGEM AND JUSTIN KNIGHT

Arriving at the Jamboree on Saturday evening, I felt a little weary and was bracing myself for the task of viewing more than 60 posters. But I was soon energized by the enthusiasm of the young presenters. Entire teams greeted me, eager to explain their creations—such as an "*E. coli* pen," which produced different colors in response to a gradient of hydroperoxide, and a hydrophobic biofilm, touted as a potential alternative to chemical coatings. Through the poster sessions and oral presentations on Saturday and Sunday, the joy of scientific discovery was on display. Dreams were big, with the students undaunted as they described the sometimes small steps they had taken toward large goals. Among those small steps, 1863 new parts were added to the registry. One of the goals of iGEM is to teach, and the students were certainly learning—engaged in their own projects but also eagerly absorbing the details about those of their peers. Message boards were full of congratulatory and encouraging comments between teams (and offers to swap T-shirts). Most projects involved modeling and experimentation, so teams were interdisciplinary, comprising computer scientists, bioengineers, and molecular biologists, among others. I found myself wondering whether this model of "teamwork," rather than the more distant "collaboration," could be applied more broadly.

Excitement peaked on Monday, when everyone gathered to hear the announcement of the six finalists: BCCS-Bristol, who built a soil fertility sensor into *Escherichia coli*; Cambridge, with their bioluminescent bacteria *E. glowli*; Imperial College London, who engineered *Bacillus subtilis* to detect the waterborne *Schistosoma* parasite; Peking, for designing bacteria that could detect and absorb heavy metals; Slovenia, who built a system to control the sequence of steps in a multi-step biosynthetic pathway; and TUDelft, who designed a system that can sense and degrade hydrocarbons in aqueous environments. All finalists gave their presentations again, appearing unintimidated by the tens of judges sitting in the front rows. The judges retired to decide the winner, and the mood switched to celebratory as students shared YouTube videos highlighting talents that went beyond scientific. (Cambridge University's song extolling Gibson assembly was a particular hit.) The buzzing room quieted when the judges reentered; the runners up were announced, and then there were cheers for the winners of the golden biobrick trophy, Slovenia. This year's competition is over, but I'm sure discussions of next year's projects have already begun. With the level of enthusiasm, talent, and hard work demonstrated by these undergraduates, the future of synthetic biology looks bright.

iGEM 2010 Jamboree
Massachusetts Institute of Technology, Cambridge, MA.
6–8 November 2010.
http://2010.igem.org/

10.1126/science.1201091

Published by AAAS

erties of networks to examining patterns of network change. Recent years have also seen the development of statistical approaches for examining networks, both for static and dynamic network characteristics (through exponential random graph models and actor-oriented models of network evolution, respectively). Several similar future steps will likely influence how broadly networks can influence health research. We need to consider ways to more systematically integrate network-based approaches into new data collection efforts (especially in large, population-based samples) and to effectively combine network advances with other analytic approaches (e.g., spatial analytic methods). As Valente's book indicates, the confluence of widespread interest, a relatively established research "canon," and recent advances in the field has laid the grounds for the network approach to make important contributions to science, in health and writ large, in the coming years.

10.1126/science.1197365

SYNTHETIC BIOLOGY

Inventive Constructions Using Biobricks

Valda Vinson

In early November, 118 teams (wearing group colors and, some, shouting team cheers) from 26 countries descended on the MIT campus for the grand finale of the 2010 International Genetically Engineered Machine (iGEM) competition. The undergraduate students had plunged into their projects at the beginning of the summer, when teams received a kit of "biobricks" from the Registry of Standard Biological Parts. They were to use these to design and build simple biological systems and operate them in living cells. In addition to the existing standard parts, their projects could involve new parts that they created and would contribute to the registry. Under the mentorship of faculty sponsors (who helped them obtain research space, funding, equipment, and expert advice), the students worked through the summer, recording their progress on team wikis. On 27 October, the wikis were frozen, and evaluation of the teams' efforts began. The iGEM Jamboree offered students the opportunity to present their work to the judges, their competitors, and other interested observers. And present they did.

Meeting at MIT. The iGEM 2010 teams gathered for the Jamboree.

CREDIT: COURTESY IGEM AND JUSTIN KNIGHT

Arriving at the Jamboree on Saturday evening, I felt a little weary and was bracing myself for the task of viewing more than 60 posters. But I was soon energized by the enthusiasm of the young presenters. Entire teams greeted me, eager to explain their creations—such as an "*E. coli* pen," which produced different colors in response to a gradient of hydroperoxide, and a hydrophobic biofilm, touted as a potential alternative to chemical coatings. Through the poster sessions and oral presentations on Saturday and Sunday, the joy of scientific discovery was on display. Dreams were big, with the students undaunted as they described the sometimes small steps they had taken toward large goals. Among those small steps, 1863 new parts were added to the registry. One of the goals of iGEM is to teach, and the students were certainly learning—engaged in their own projects but also eagerly absorbing the details about those of their peers. Message boards were full of congratulatory and encouraging comments between teams (and offers to swap T-shirts). Most projects involved modeling and experimentation, so teams were interdisciplinary, comprising computer scientists, bioengineers, and molecular biologists, among others. I found myself wondering whether this model of "teamwork," rather than the more distant "collaboration," could be applied more broadly.

Excitement peaked on Monday, when everyone gathered to hear the announcement of the six finalists: BCCS-Bristol, who built a soil fertility sensor into *Escherichia coli*; Cambridge, with their bioluminescent bacteria *E. glowli*; Imperial College London, who engineered *Bacillus subtilis* to detect the waterborne *Schistosoma* parasite; Peking, for designing bacteria that could detect and absorb heavy metals; Slovenia, who built a system to control the sequence of steps in a multi-step biosynthetic pathway; and TUDelft, who designed a system that can sense and degrade hydrocarbons in aqueous environments. All finalists gave their presentations again, appearing unintimidated by the tens of judges sitting in the front rows. The judges retired to decide the winner, and the mood switched to celebratory as students shared YouTube videos highlighting talents that went beyond scientific. (Cambridge University's song extolling Gibson assembly was a particular hit.) The buzzing room quieted when the judges reentered; the runners up were announced, and then there were cheers for the winners of the golden biobrick trophy, Slovenia. This year's competition is over, but I'm sure discussions of next year's projects have already begun. With the level of enthusiasm, talent, and hard work demonstrated by these undergraduates, the future of synthetic biology looks bright.

iGEM 2010 Jamboree
Massachusetts Institute of Technology, Cambridge, MA.
6–8 November 2010.
http://2010.igem.org/

10.1126/science.1201091

Published by AAAS

INTELLECTUAL PROPERTY

Turning Patent Swords into Shares

Compulsory licenses and patent pools will assist modern patent law in fueling genetic test development.

Geertrui Van Overwalle

The decision earlier this year in the U.S. District Court to deny patent protection for isolated human genes and associated diagnostic methods (*1*) shocked the biotech community. The case related to genetic tests for familial breast and ovarian cancer developed by the company Myriad Genetics. The product claims (used to describe the compound in question) were directed to isolated DNA containing human *BRCA1* and *BRCA2* gene sequences. The method claims (used to describe the activity exercised upon the compound) covered the process of identifying certain mutations in the *BRCA* genes. The court held that the claimed isolated DNA "is not markedly different from native DNA as it exists in nature" and constitutes unpatentable subject matter (*1*). The court also ruled that the claimed method is "directed only to the abstract mental process of comparing or analyzing gene sequences," fails the so-called "machine or transformation test" (*2*), and is unpatentable as well (*1*).

Although the Myriad decision has been appealed (*3*) and may be reversed in light of the heavily criticized transformation test in the Bilski case (*4*) or arguments set forth by the U.S. Department of Justice (*5*), many public-policy issues relating to diagnostic gene patenting will persist. Development and accessibility of genetic tests has also been a central concern for the Secretary's Advisory Committee on Genetics, Health, and Society (SACGHS) of the U.S. National Institutes of Health and recently led to recommendations to the Secretary of Health and Human Services calling for focused legislative changes in this area (*6*).

Research and Clinical and Patient Access

The disputed issues in the Myriad case point to two distinct phenomena in the area of human genomic science and intellectual property. First, claims on genes are generally difficult, if not impossible, to circumvent, or "invent around" (*7*). Problems arise when gene patents are licensed too restrictively; this could hamper research and development (*8*), clinical access, and availability of high-quality tests for patients. The Myriad case exemplifies such a restrictive license policy, resulting

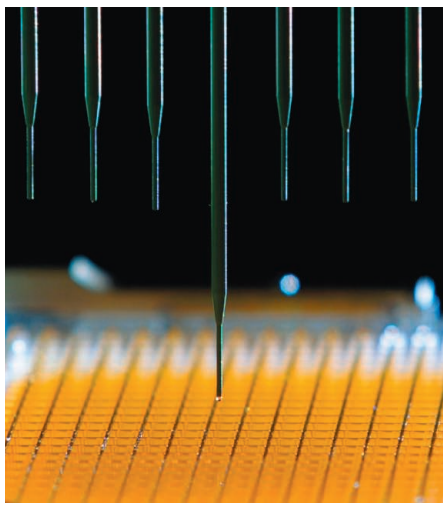

in public disapproval (*9*). Studies have documented similar restrictive licensing practices for other tests as well (*10*, *11*).

A second phenomenon relates to the dense and fragmented genetic patent landscape. Problems arise when "patent thickets" (a web of overlapping patents through which a company must "hack" in order to commercialize a technology) emerge (*12*). Accumulation, or "stacking," of royalties that have to be paid when confronted with a patent thicket may lead to a "tragedy of the anti-commons" (*13*), affecting research and development and harming clinical and patient access in the long run. Empirical data do not yet confirm existence of a patent thicket in genetics at large (*14*, *15*). However, thicket problems in genetic diagnostics could grow with shifts (i) from monogenetic to multifactorial testing (multiplex diagnostics) and (ii) toward diagnostics based on genome-wide association studies driven by the high-throughput of single nucleotide polymorphism platforms and next-generation sequencing possibilities (*6*, *16*). Although not an illustrative example of this phenomenon, the Myriad decision has invigorated concerns about potential negative effects of a dense and dispersed patent landscape.

Designing Solutions

It is widely accepted that patent systems are premised on an implicit "social contract" (*17*) aimed at balancing private and public interests. Changes to the system should acknowledge this social contract and explore options that preserve the positive incentive for the production of drugs and therapies and remedy some perceived hindrances in the field of genetic diagnostics.

The problems surfacing in the Myriad case can be tackled with legislative measures or court decisions—some of which may be inspired by European approaches (as described below). However, providing swift, flexible responses to changing conditions through such avenues may be hard because of legal complexity and political reality. In the meantime, or as a substitute, rules of contract may offer a partial solution, thereby turning patent "swords" (*18*) into commonly shared assets or shares.

Alleviating Restrictive Licensing

Current patent and antitrust law leave considerable freedom to patentees to set up licensing agreements and do not prohibit exclusive licensing. Legal measures may assist in tackling restrictive licensing practices. Recently, legislatures imposed compulsory licenses, forcing patent holders to grant use in the name of public health in Belgium, France, and Switzerland (*19*). Although none of these compulsory license mechanisms have yet been put to work, they may have an indirect, preventive effect on unduly restrictive licensing behavior by patent owners (*19*).

Another potential legislative measure is the introduction of a diagnostic-use exemption, shielding diagnostic testing from infringement. At present, blood or tissue sampling may fall within the "safe harbor" research exemption (i.e., use in research does not infringe the patent) appearing in many European countries, but it is unlikely that the subsequent diagnostic steps do (*20*). Hence, a separate statutory diagnostic exemption is necessary, as recognized by SACGHS (*6*). SACGHS recommends that this exemption would equally apply to (commercial and noncommercial) service providers using laboratory-developed tests and to test-kit makers. However, in view of the uncertain (and possibly stifling) impact of the exemption on kit development—requiring approval by the Food and Drug Administration, which would raise costs for entering the market—its scope should be restricted to clinicians using their own "homemade" gene-based tests.

To attenuate restrictive effects of diagnostic gene patents resulting from government research funding, agencies like the NIH could be encouraged to exercise so-called "march-

Centre for Intellectual Property Rights, University of Leuven, 3000 Leuven, Belgium; Tilburg Institute for Law, Technology, and Society, University of Tilburg, 5000 LE Tilburg, Netherlands. E-mail: geertrui.vanoverwalle@law.kuleuven.be

Published by AAAS

in" rights, provided by the Bayh-Dole Act (35 U.S. Code § 200–212), ignoring the patent to grant licenses to others. Although some believe this a valuable alternative (*21*), others have criticized it as inadequate (*22*).

Redressing Patent Thickets

Patent law may be altered to exclude genes from its field of application. Deeming gene patents ineligible for protection may be valuable in view of fostering (upstream) research and the provision of genetic testing, but may be detrimental to incentivizing (downstream) development of drugs and therapies. A more moderate alternative may be to focus on the scope of patent rights and to introduce a purpose-bound protection regime for gene patents. Under such a rule, a patent for a DNA sequence no longer encompasses all possible future applications but is restricted to the specific use described in the patent application. Such an approach seems to be supported by the Court of Justice of the European Union in the Monsanto case (*23*). However restrictive it may seem, purpose bound protection may still prevent free use of a gene patented for diagnostic applications.

Exclusion of patents for diagnostic methods can also be considered. A diagnostic method exclusion is different from a diagnostic exemption: The former prevents patenting in the first place; the latter allows the issuance of patents but exempts certain uses of the patent from infringement. A diagnostic method exclusion can be constructed rather narrowly, mirroring the European statutory example, which implies that the only methods excluded from patent protection are diagnostic methods practiced on the human body (*24*, *25*). However, a broader exclusion of all diagnostic methods, disregarding the fact whether the treatment was practiced on the human body or not (*26*), will have more effect in patent practice.

The feasibility and pace of changing statutory patent law will depend on processes at work for domestic and/or international patent law reform. Rather than statutory reform, judicial law-making may assist in shaping patent law to the particularities of the genetic diagnostics' sector (*27*). Navigating the landscape in genetic diagnostics may even be achieved more adequately and rapidly through private, collaborative efforts. These could take the form of specially tailored genetic patent pools and clearinghouses. The latter is inspired by the copyright collecting–society model, such as the American Society of Composers, Authors, and Publishers, which collects license fees from users and distributes them among those whose works were performed (*20*, *28*).

Some genetic pools and clearinghouses have been established for humanitarian purposes. For-profit initiatives, however, remain scarce, except MPEG LA, which recently launched a diagnostic genetics patent clearinghouse or "licensing supermarket" (*29*). More research is needed to assess the economic viability and commercial sustainability of collaborative models (*30*, *31*). Discussion is also required on the need for rules that permit the "visible hand" of government to stimulate or even force parties into such collaborative transactions (*32*).

Genetic patent pools—requiring as a matter of competition law an open and nondiscriminatory licensing policy—convert the exclusivity principle of patent protection into a liability or take-now-pay-later rule (where access and use of a patent are not dependent on the consent of the patent holder, but only conditioned upon payment of a fee) (*33*). In other words, patent pools turn exclusive patent rights into commonly shared assets or shares. This paradoxical effect of collaborative mechanisms on private entitlements has been seen before (*34, 35*) but has not been put into operation in diagnostic genetics yet. This sharing effect of collaborative models might safeguard the social contract in genetic diagnostics. It also has been suggested to restore trust in the patent system (*36*).

Patents as Temporary Privileges

In light of controversies surrounding gene patents and growing discontent with some undesirable effects of the current patent system, there is a need to reconceptualize patent rights. A patent can no longer be viewed as a title giving (almost) complete freedom to exclude others from use, but rather as a temporary permit to exploit monopoly rights under fair and reasonable conditions, investing technology owners with the authority to invent and share, in other words, as a "duty-bearing privilege" (*37*). A compulsory license for public health and a narrow diagnostic-use exemption can discourage exclusive or overly restrictive licensing. A purpose-bound protection regime, a broad diagnostic method exclusion, and genetic patent pools and clearinghouses may help deal with patent thickets. Such measures will assist modern patent law in preserving the underlying social contract with the advent of multifactorial testing and whole-genome sequencing.

References and Notes

1. *Association for Molecular Pathology* v. *U.S. Patent and Trademark Office*, Southern District of New York (29 March 2010).
2. As cited in (*4*) from In re Bilski (*39*): "[a] claimed process is surely patent-eligible under §101 if: (1) it is tied to a particular machine or apparatus, or (2) it transforms a particular article into a different state or thing."
3. The notice of appeal was filed on 16 June 2010.
4. *Bilski* v. *Kappos*, U.S. Supreme Court (28 June 2010).
5. Brief for the United States as Amicus Curiae in Support of Neither Party submitted to the U.S. Court of Appeals for the Federal Circuit, re (*1*) (29 October 2010).
6. SACGHS, *Revised Draft Report on Gene Patents and Licensing Practices and Their Impact on Patient Access to Genetic Tests* (SACGHS, NIH, Bethesda, MD, 2010).
7. I. Huys, N. Berthels, G. Matthijs, G. Van Overwalle, *Nat. Biotechnol.* **27**, 903 (2009).
8. In some empirical studies, a negative impact of patents could not be found [e.g., (*38*)]. However, these studies focused on biomedical research, not downstream product development.
9. E. R. Gold, J. Carbone, *Genet. Med.* **12** (suppl.), S39 (2010).
10. M. K. Cho, S. Illangasekare, M. A. Weaver, D. G. Leonard, J. F. Merz, *J. Mol. Diagn.* **5**, 3 (2003).
11. Patently Complicated: Case Studies on the Impact of Patenting and Licensing on Clinical Access to Genetic Testing in the United States. *Genet. Med.* **12** (4 suppl.), S1–S211 (2010).
12. C. Shapiro, in *Innovation Policy and the Economy*, vol. 1, A. B. Jaffe *et al*., Eds. (MIT Press, Cambridge, MA, 2001), pp. 119–150.
13. M. A. Heller, R. S. Eisenberg, *Science* **280**, 698 (1998).
14. M. M. Hopkins *et al.*, *Nat. Biotechnol.* **25**, 185 (2007).
15. K. Jensen, F. Murray, *Science* **310**, 239 (2005).
16. J. H. Barton, *Nat. Biotechnol.* **24**, 939 (2006).
17. L. H. Hoffmann, in *Kirin-Amgen* v. *Hoechst Marion Roussel*, House of Lords (21 October 2004).
18. "Sword" refers to use of patents to obtain royalties or damages (*39*).
19. E. van Zimmeren, G. Van Overwalle, http://ssrn.com/abstract=1717974.
20. G. Van Overwalle, E. van Zimmeren, B. Verbeure, G. Matthijs, *Nat. Rev. Genet.* **7**, 143 (2006).
21. C. H. Holman, *Biotech Brief.* **5**, 1 (2008); www.abanet.org/scitech/genepatents.html.
22. K. Rai, R. S. Eisenberg, *Law Contemp. Probl.* **66**, 289 (2003).
23. *Monsanto* v. *Cefetra* (6 July 2010).
24. Article 53 (c) of the European Patent Convention.
25. Such a restrictive approach has been reinforced by the European Patent Office in its recent case law (G 1/04, Enlarged Board of Appeal, 16 December 2005).
26. Mirroring article 27 (*3*) (a) of the Agreement on Trade-Related Aspects of Intellectual Property Rights (World Trade Organization, Geneva, 1994).
27. D. L. Burk, M. A. Lemley, *The Patent Crisis and How the Courts Can Solve It* (Univ. Chicago Press, Chicago, 2009).
28. G. Van Overwalle, Ed., *Gene Patents and Collaborative Licensing Models: Patent Pools, Clearing Houses, Open Source Models, and Liability Regimes* (Cambridge Univ. Press, Cambridge, 2009).
29. MPEG LA, news release, 8 April 2010; www.mpegla.com/main/Pages/Media.aspx.
30. And to ascertain that they do not merely create "markets for lemons" (*31*).
31. G. Akerlof, *Q. J. Econ.* **84**, 488 (1970).
32. R. P. Merges, in *Expanding the Boundaries of Intellectual Property*, R. Dreyfuss *et al*. Eds. (Oxford Univ. Press, Oxford, 2001), pp. 123–166.
33. G. Calabresi, A. D. Melamed, *Harv. Law Rev.* **85**, 1089 (1972).
34. R. P. Merges, *Calif. Law Rev.* **84**, 1293 (1996).
35. J. H. Reichman, *Va. Law Rev.* **53**, 1743 (2000).
36. T. Caulfield, E. Einsiedel, J. F. Merz, D. Nicol, *Nat. Biotechnol.* **24**, 1352 (2006).
37. P. Drahos, *A Philosophy of Intellectual Property* (Dartmouth Publishing, Sudbury, MA, 1996).
38. J. P. Walsh, C. Cho, W. M. Cohen, *Science* **309**, 2002 (2005).
39. *In re Bilski*, 545 F 3d **943**, 959–60 and n. 19 (CA Fed 2008).

40. The author thanks the Vancraesbeeck Fund for support and I. Huys and E. van Zimmeren for comments.

10.1126/science.1189592

BIOCHEMISTRY

Catalyzing NO to N_2O in the Nitrogen Cycle

A structure for the bacterial enzyme cNOR reveals a biochemical mechanism driving nitrous oxide emissions.

Pierre Moënne-Loccoz[1] and James A. Fee[2]

The great planetary nitrogen cycle, which includes the cyclic conversion of nitrogen gas (N_2) into "fixed" nitrogen that can be used by plants, is in large part mediated by metalloenzymes that catalyze the elementary chemical reactions. On page 1666 of this issue, Hino *et al*. (*1*) take an important step toward understanding the chemical function and evolution of one of these enzymes. They describe the structure of a nitric oxide reductase (NOR) from a common bacterium that plays an important role in the nitrogen cycle—and in human disease.

Today, human activities such as the widespread use of agricultural fertilizers and the burning of fossil fuels are influencing Earth's nitrogen cycle (*2*). Of considerable interest is the increasing release into the atmosphere of nitrous oxide (N_2O), a greenhouse gas (*3*) about 300 times as powerful, on an equimolar basis, as CO_2 (*2*). The vast majority of N_2O originates from microbes that break down nitrogen compounds in soil and water. Approximately equal quantities of N_2O come from two processes: nitrification (which converts ammonia into nitrite), in which N_2O is an unintended by-product of the oxidation of hydroxylamine (NH_2OH), and anaerobic denitrification, in which nitric oxide (NO) and N_2O are formed as diffusible intermediates (*2*, *4*).

Hino *et al*. studied cytochrome c–dependent nitric oxide reductase (cNOR), in which the cytochrome acts as the electron donor to an enzyme that catalyzes the reduction of NO in *Pseudomonas aeruginosa*, a ubiquitous, denitrifying bacterium. It is also a nasty pathogen, particularly among burn victims and patients with chronic infections of their airways (*5*, *6*). Similar infectious bacteria, such as *Neisseria meningitides* and *Neisseria gonorrhoeae*, depend on NOR activity to withstand the defenses of host cells (*7*). Hino *et al*. describe the x-ray structure of cNOR at 2.7 Å resolution. In addition to offering insight into the detailed chemical mechanisms that affect the nitrogen cycle, the structure offers evidence for the existence of a common ancestor connecting the NORs to the heme-copper oxidase (HCO) superfamily of enzymes, and raises intriguing questions about how one diverged from the other. Finally, the structure provides the basis for an atomic-level understanding of the chemistry of both NOR and HCO enzymes.

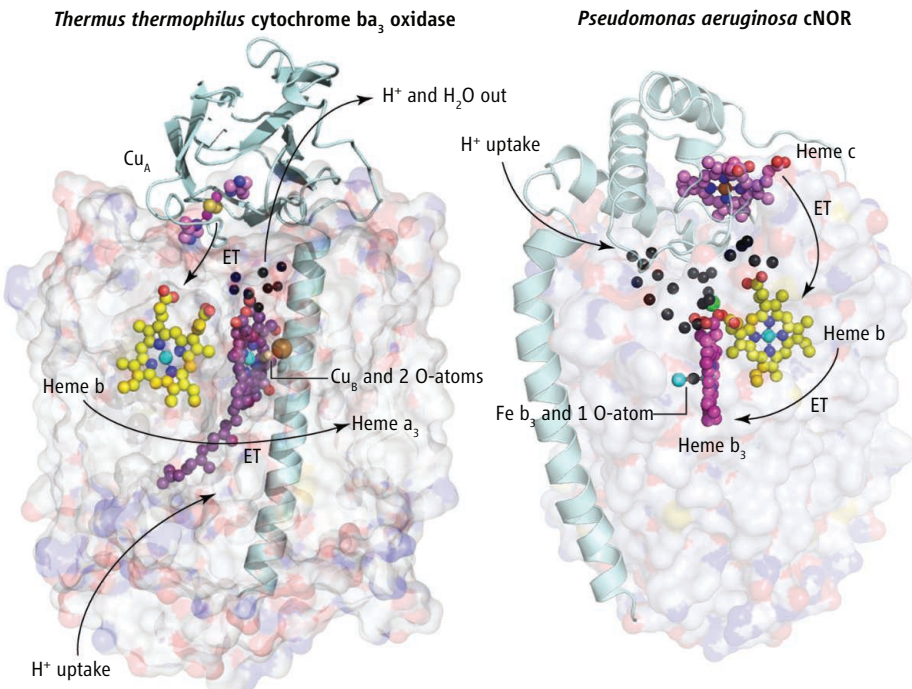

Compare and contrast. The structures of *T. thermophilus* (*Tt*) cytochrome ba_3 oxidase (**left**) and cNOR from *P. aeruginosa* (*Pa*) (**right**), with large subunits shown as transparent surfaces. The two structures are aligned vertically at the level of the b hemes and the cNOR structure is rotated approximately 180° about its vertical axis to bring the b-hemes into the same plane. Electrons flow from the subunit II of ba_3 that anchors the dinuclear copper cluster Cu_A, and from the cytochrome c in cNOR (ET, electron transfer). These two redox centers and globular domains exemplify the variability in redox partners in the oxidases and NO reductases, as evolution may allow for occasional interchange of large and small subunits. Electrons flow into the b hemes before passing to the binuclear active sites. Presumed proton flow in ba_3 oxidase and its water exit are represented by arrows. Black spheres represent crystallographically defined water molecules. The single Ca^{2+} ion is shown as a green sphere. In cNOR, protons appear to flow from the outside into the extensive water cluster, and from there into the binuclear heme b_3/Fe_B active site.

Both HCOs and NORs are integral membrane proteins. The HCO superfamily contains at least three types that share a common core structure but vary in the number of peripheral subunits, heme types, physiological electron donors, and proton pathways that can generate the heme-copper cluster (*8*). The NOR family is also composed of several types (*9*). *P. aeruginosa* cNOR consists of a small (NorC) and a large (NorB) subunit. Although NorB and the large subunits of HCOs are clearly homologs, both families show diversity in the smaller subunits (especially in the associated electron donor). It is hard to see how the predominantly β-sheet cupredoxin fold of subunit II containing Cu_A (see the figure, left panel) and the predominantly helical cytochrome c fold of NorC (right panel) could be linked evolutionarily via a series of mutations. Rather, it seems more likely that the smaller subunits evolve partly by "jumping" from one type of large subunit to another.

Hino *et al*. compare their structure to the simplest known HCO, the B-type cytochrome ba_3 oxidase from *Thermus thermophilus* (*8*, *10*), and a comparison to the C-type cbb_3

[1]Division of Environmental & Biomolecular Systems, Institute of Environmental Health, Oregon Health & Science University, Beaverton, OR 97006, USA. [2]Department of Molecular Biology, Scripps Research Institute, La Jolla, CA 92037, USA. E-mail: ploccoz@ebs.ogi.edu; jafee@scripps.edu

Published by AAAS

oxidase from *Pseudomonas stutzeri* (*11*) is also informative. Although the cbb_3 enzyme appears to be closer to cNOR than does ba_3, similarities in the amino acid sequences of NorB and subunit I of cbb_3 are low (<40%). Regardless, the two proteins exhibit highly similar three-dimensional structures. Specifically, 12 central transmembrane helices are conserved that share a topology of tightly packed helices arranged around a low-spin heme and a binuclear active site (i.e., a heme b_3/Fe_B or a heme a_3/Cu_B). In ba_3, the active-site heme a_3/Cu_B center is buried in the hydrophobic core of the enzyme, requiring that both polar (H^+, e^-, and H_2O) and lipophilic (O_2) reactants move along structurally specified pathways to their intended destinations. In cNOR, the active-site heme b_3/Fe_B is found essentially at the same location in the hydrophobic core. The three histidine side chains that coordinate the Cu_B in HCO are conserved in cNOR and are supplemented with a glutamyl carboxylate group, providing a favorable coordination shell for an iron ion at the Fe_B site.

The structure of cNOR also shows that transmembrane pathways (D- and K-paths) for proton uptake are absent; this supports previous findings that cNOR does not pump protons (*12*) and sheds light on how heme-Cu oxidases acts as a proton pump. Hino *et al.* also propose pathways for electron transfer from the cytochrome c via the low-spin heme and proton entries from the periplasmic side to the binuclear center. As in cbb_3, a Ca^{2+} ion bridges and may stabilize an efficient electron transfer route between the two hemes in NorB. Another remarkable feature of the cNOR structure is the presence of a Y-shaped hydrophobic channel similar to that reported by Luna *et al.* (*13*) in ba_3 and by Buschmann *et al.* (*11*) in cbb_3. In cNOR, this channel must serve to carry NO from the lipid bilayer to the active site.

The authors do not assign the exit route of the N_2O product, but the factor of 10 increase in water solubility of N_2O relative to O_2 or NO may allow this small molecule to diffuse through both hydrophobic and hydrophilic channels. A question worthy of future investigation is whether the exit route of N_2O from cNOR influences its capture by the periplasmic, copper-containing N_2O reductase, and its escape into the atmosphere. The structure also leaves two other questions unanswered: (i) How do the two NO molecules bind at the diiron site? (ii) How do the N-N bond formation and N-O bond cleavage occur? A distal glutamic acid within 5 Å of the iron cluster that appears conserved in NorB sequences may provide a proton to a putative hyponitrite anion ($N_2O_2^{2-}$) and facilitate N-O bond cleavage. Although most investigators might agree that the first NO binds to the ferrous heme b_3, the mode of addition of a second NO to this mononitrosyl complex remains to be defined, as do the respective roles of the two Fe ions (*14*). Bioengineering models of the heme b_3/Fe_B site in the simpler protein scaffold of myoglobin will be valuable tools for conducting these mechanistic investigations (*15*). Structural characterization of other transmembrane NORs in parallel with HCOs will further clarify evolutionary variation in Fe_B/Cu_B coordination spheres, electron and proton transfer pathways, and hydrophobic channels to the catalytic dinuclear center.

References

1. T. Hino *et al.*, *Science* **330**, 1666 (2010); 10.1126/science.1195591.
2. D. E. Canfield, A. N. Glazer, P. G. Falkowski, *Science* **330**, 192 (2010).
3. A. A. Lacis, G. A. Schmidt, D. Rind, R. A. Ruedy, *Science* **330**, 356 (2010).
4. A. Mosier *et al.*, *Nutr. Cycl. Agroecosyst.* **52**, 225 (1998).
5. N. Barraud *et al.*, *J. Bacteriol.* **188**, 7344 (2006).
6. T. Romeo, *J. Bacteriol.* **188**, 7325 (2006).
7. T. M. Stevanin, J. R. Laver, R. K. Poole, J. W. B. Moir, R. C. Read, *Microbes Infect.* **9**, 981 (2007).
8. M. M. Pereira, M. Santana, M. Teixeira, *Biochim. Biophys. Acta* **1505**, 185 (2001).
9. S. de Vries, I. Schröder, *Biochem. Soc. Trans.* **30**, 662 (2002).
10. L. M. Hunsicker-Wang, R. L. Pacoma, Y. Chen, J. A. Fee, C. D. Stout, *Acta Crystallogr. D.* **61**, 340 (2005).
11. S. Buschmann *et al.*, *Science* **329**, 327 (2010).
12. U. Flock *et al.*, *J. Biol. Chem.* **238**, 3839 (2008).
13. V. M. M. Luna, Y. Chen, J. A. Fee, C. D. Stout, *Biochemistry* **47**, 4657 (2008).
14. P. Moënne-Loccoz, *Nat. Prod. Rep.* **24**, 610 (2007).
15. N. Yeung *et al.*, *Nature* **462**, 1079 (2009).

10.1126/science.1200247

MATERIALS SCIENCE

Optical Metamaterials—More Bulky and Less Lossy

Advanced techniques for bulk fabrication and loss reduction provide good prospects for practical optical metamaterials.

Costas M. Soukoulis[1,2] and Martin Wegener[3]

Usually, investigators in materials science have asked: "What properties does a certain new material or structure have?" Now, the inverse problem arises: "I want to achieve certain—possibly unheard-of—material properties. How should the corresponding micro- or nanostructure look?" Examples could be: efficiently blocking acoustic noise due to a highway from a nearby village by a tailored wall, concentrating electromagnetic energy into as-tight-as-possible spaces, or avoiding reflections from a material's surface. The underlying common scheme is wave physics. Material properties that were otherwise unachievable, e.g., negative refraction and cloaking, may eventually be designed into optical metamaterials and photonic crystals. Both require tailoring of the properties (i.e., phase velocity and impedance) of an electromagnetic wave moving through the substance at the local level. In photonic crystals, the phase velocity of an electromagnetic wave moving through the crystal is controlled by tuning the photonic band structure; the impedance is determined by the electromagnetic field distributions throughout the material. In metamaterials, this amounts to tailoring the effective electric permittivity and magnetic permeability. In either case, introducing resonances is the key to controlling the local wave properties. The recent development of advanced fabrication techniques being applied to metamaterials and photonic crystals may lead to realization of such designer materials.

In photonic crystals, the focus has traditionally been on many wavelength-scale building blocks arranged on a dielectric lattice (generalized Bragg resonances) that produce collective resonances in response to an electromagnetic field, whereas researchers working with metamaterials started with

[1]Ames Laboratory and Department of Physics and Astronomy, Iowa State University, Ames, IA 50011, USA. [2]Institute of Electronic Structure and Laser–Foundation for Research and Technology Hellas, University of Crete, Heraklion, Crete, Greece. [3]Institute of Applied Physics, Institute of Nanotechnology, and Center for Functional Nanostructures, Karlsruhe Institute of Technology, Karlsruhe, Germany. E-mail: soukoulis@ameslab.gov

oxidase from *Pseudomonas stutzeri* (*11*) is also informative. Although the cbb_3 enzyme appears to be closer to cNOR than does ba_3, similarities in the amino acid sequences of NorB and subunit I of cbb_3 are low (<40%). Regardless, the two proteins exhibit highly similar three-dimensional structures. Specifically, 12 central transmembrane helices are conserved that share a topology of tightly packed helices arranged around a low-spin heme and a binuclear active site (i.e., a heme b_3/Fe_B or a heme a_3/Cu_B). In ba_3, the active-site heme a_3/Cu_B center is buried in the hydrophobic core of the enzyme, requiring that both polar (H^+, e^-, and H_2O) and lipophilic (O_2) reactants move along structurally specified pathways to their intended destinations. In cNOR, the active-site heme b_3/Fe_B is found essentially at the same location in the hydrophobic core. The three histidine side chains that coordinate the Cu_B in HCO are conserved in cNOR and are supplemented with a glutamyl carboxylate group, providing a favorable coordination shell for an iron ion at the Fe_B site.

The structure of cNOR also shows that transmembrane pathways (D- and K-paths) for proton uptake are absent; this supports previous findings that cNOR does not pump protons (*12*) and sheds light on how heme-Cu oxidases acts as a proton pump. Hino *et al.* also propose pathways for electron transfer from the cytochrome c via the low-spin heme and proton entries from the periplasmic side to the binuclear center. As in cbb_3, a Ca^{2+} ion bridges and may stabilize an efficient electron transfer route between the two hemes in NorB. Another remarkable feature of the cNOR structure is the presence of a Y-shaped hydrophobic channel similar to that reported by Luna *et al.* (*13*) in ba_3 and by Buschmann *et al.* (*11*) in cbb_3. In cNOR, this channel must serve to carry NO from the lipid bilayer to the active site.

The authors do not assign the exit route of the N_2O product, but the factor of 10 increase in water solubility of N_2O relative to O_2 or NO may allow this small molecule to diffuse through both hydrophobic and hydrophilic channels. A question worthy of future investigation is whether the exit route of N_2O from cNOR influences its capture by the periplasmic, copper-containing N_2O reductase, and its escape into the atmosphere. The structure also leaves two other questions unanswered: (i) How do the two NO molecules bind at the diiron site? (ii) How do the N-N bond formation and N-O bond cleavage occur? A distal glutamic acid within 5 Å of the iron cluster that appears conserved in NorB sequences may provide a proton to a putative hyponitrite anion ($N_2O_2^{2-}$) and facilitate N-O bond cleavage. Although most investigators might agree that the first NO binds to the ferrous heme b_3, the mode of addition of a second NO to this mononitrosyl complex remains to be defined, as do the respective roles of the two Fe ions (*14*). Bioengineering models of the heme b_3/Fe_B site in the simpler protein scaffold of myoglobin will be valuable tools for conducting these mechanistic investigations (*15*). Structural characterization of other transmembrane NORs in parallel with HCOs will further clarify evolutionary variation in Fe_B/Cu_B coordination spheres, electron and proton transfer pathways, and hydrophobic channels to the catalytic dinuclear center.

References

1. T. Hino *et al.*, *Science* **330**, 1666 (2010); 10.1126/science.1195591.
2. D. E. Canfield, A. N. Glazer, P. G. Falkowski, *Science* **330**, 192 (2010).
3. A. A. Lacis, G. A. Schmidt, D. Rind, R. A. Ruedy, *Science* **330**, 356 (2010).
4. A. Mosier *et al.*, *Nutr. Cycl. Agroecosyst.* **52**, 225 (1998).
5. N. Barraud *et al.*, *J. Bacteriol.* **188**, 7344 (2006).
6. T. Romeo, *J. Bacteriol.* **188**, 7325 (2006).
7. T. M. Stevanin, J. R. Laver, R. K. Poole, J. W. B. Moir, R. C. Read, *Microbes Infect.* **9**, 981 (2007).
8. M. M. Pereira, M. Santana, M. Teixeira, *Biochim. Biophys. Acta* **1505**, 185 (2001).
9. S. de Vries, I. Schröder, *Biochem. Soc. Trans.* **30**, 662 (2002).
10. L. M. Hunsicker-Wang, R. L. Pacoma, Y. Chen, J. A. Fee, C. D. Stout, *Acta Crystallogr. D.* **61**, 340 (2005).
11. S. Buschmann *et al.*, *Science* **329**, 327 (2010).
12. U. Flock *et al.*, *J. Biol. Chem.* **238**, 3839 (2008).
13. V. M. M. Luna, Y. Chen, J. A. Fee, C. D. Stout, *Biochemistry* **47**, 4657 (2008).
14. P. Moënne-Loccoz, *Nat. Prod. Rep.* **24**, 610 (2007).
15. N. Yeung *et al.*, *Nature* **462**, 1079 (2009).

10.1126/science.1200247

MATERIALS SCIENCE

Optical Metamaterials—More Bulky and Less Lossy

Advanced techniques for bulk fabrication and loss reduction provide good prospects for practical optical metamaterials.

Costas M. Soukoulis[1,2] and Martin Wegener[3]

Usually, investigators in materials science have asked: "What properties does a certain new material or structure have?" Now, the inverse problem arises: "I want to achieve certain—possibly unheard-of—material properties. How should the corresponding micro- or nanostructure look?" Examples could be: efficiently blocking acoustic noise due to a highway from a nearby village by a tailored wall, concentrating electromagnetic energy into as-tight-as-possible spaces, or avoiding reflections from a material's surface. The underlying common scheme is wave physics. Material properties that were otherwise unachievable, e.g., negative refraction and cloaking, may eventually be designed into optical metamaterials and photonic crystals. Both require tailoring of the properties (i.e., phase velocity and impedance) of an electromagnetic wave moving through the substance at the local level. In photonic crystals, the phase velocity of an electromagnetic wave moving through the crystal is controlled by tuning the photonic band structure; the impedance is determined by the electromagnetic field distributions throughout the material. In metamaterials, this amounts to tailoring the effective electric permittivity and magnetic permeability. In either case, introducing resonances is the key to controlling the local wave properties. The recent development of advanced fabrication techniques being applied to metamaterials and photonic crystals may lead to realization of such designer materials.

In photonic crystals, the focus has traditionally been on many wavelength-scale building blocks arranged on a dielectric lattice (generalized Bragg resonances) that produce collective resonances in response to an electromagnetic field, whereas researchers working with metamaterials started with

[1]Ames Laboratory and Department of Physics and Astronomy, Iowa State University, Ames, IA 50011, USA. [2]Institute of Electronic Structure and Laser–Foundation for Research and Technology Hellas, University of Crete, Heraklion, Crete, Greece. [3]Institute of Applied Physics, Institute of Nanotechnology, and Center for Functional Nanostructures, Karlsruhe Institute of Technology, Karlsruhe, Germany. E-mail: soukoulis@ameslab.gov

densely packed, ideally noninteracting resonances of individual subwavelength-size building blocks (generalized Mie resonances). Mie resonances are especially pronounced for metals. In general, both Bragg- and Mie-type resonances are advantageous.

In 2007, optical metamaterials (*1*) were not actually "materials" but were rather metafilms or metasurfaces—planar monolayers of meta-atoms. Today, various truly three-dimensional (3D) optical metamaterial structures have been reported (see the figure) (*2*–*5*). The larger the 3D metal-based metamaterial structures become and the more the "bulk" is approached, the more obvious it becomes that losses must be reduced. Otherwise, a large chunk of metamaterial will simply be black and opaque, rendering it useless. At optical frequencies, most of the losses result from the constituent metal. Thus, avoiding sharp edges for the current flow and/or avoiding nearby resonances can eliminate part of the losses. Superconductors may appear as a remedy for resistive losses, but their small superconducting band-gap frequency inherently prohibits operation at optical or even visible frequencies.

A different approach to reduce losses is to incorporate active gain materials to counteract the losses and achieve negative phase velocities of light. The fact that we are unable to change the past strongly connects losses and phase velocities of light. Combined with the condition of stability, this imposes rather stringent fundamental constraints on what is possible—regardless of the particular design (*6*, *7*). As in any laser, the system becomes intrinsically unstable for macroscopic metamaterial structures and for long times even if the gain exceeds the loss only at a single frequency. Thus, the effective loss can only be zero at a single frequency, for which the phase velocity of light may be negative. For all other frequencies, the losses remain finite. Spontaneous and stimulated emissions will occur and must be considered as intense sources of "noise" if the artificial material shall be used to guide, focus, and/or influence external light. This aspect might force a retraction from the exact gain-equals-loss condition, leaving behind losses that can still be orders of magnitude lower compared to those in the absence of gain material.

Recent experiments on gain have returned to metafilms to avoid tackling both the bulk and the loss challenges simultaneously. Only partial loss compensation has been obtained in experiments with quantum dots (*8*) and single quantum wells (*9*), whereas it was possible to compensate for losses completely in the visible range via dyes embedded in epoxy resin and pumped by picosecond pulses (*10*). The latter experiment and corresponding theory (*11*, *12*) have raised hopes, but it is not clear that this success can be translated to macroscopic 3D photonic metamaterials under steady-state conditions.

Three crucial aspects have already been demonstrated experimentally: (i) operation in the visible spectrum, (ii) truly 3D optical metamaterials, and (iii) loss-free metamaterials. Another crucial aspect for many applications that has only been achieved theoretically so far is isotropy (*13*, *14*). Realizing the ideal negative-index metamaterials, i.e., a 3D isotropic zero-loss negative-index metamaterials operating at visible wavelengths, requires the combination of all these aspects. It is unlikely that compensating loss via optical pumping will meet real-world requirements, whereas injecting an electrical current into a semiconductor through two wires coming out of a chunk of metamaterial is more practical. Once all of this has been achieved, the next frontier toward commercialization is bringing the fabrication cost down, e.g., with nanochemistry-based bottom-up self-assembly approaches (*13*). Another interesting though unexplored avenue is replacing the lithographically defined meta-atoms by tailored large molecules. Ideally, these molecules could be assembled to 3D molecular crystals.

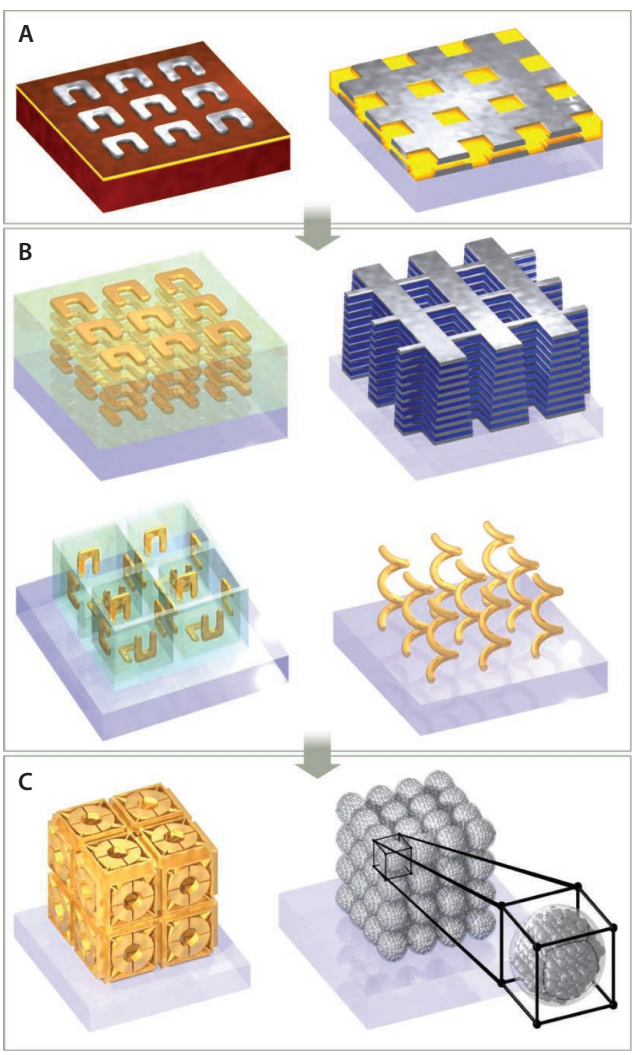

Bulking up. Metamaterials operating at optical frequencies have developed from planar monolayers of meta-atoms (**A**) to truly 3D nanostructures (*2*–*5*) (**B**). Incorporating gain materials (yellow in top box) led to loss reduction (*8*–*10*). (**C**) Blueprints for isotropic metamaterials based on bottom-up self-assembly (*13*) or direct laser writing (*14*) do exist. If all of these aspects could be combined, one of the early dreams of the field, namely, visible 3D isotropic zero-loss negative-index metamaterials, might eventually become reality.

CREDIT: MANUEL DOCKER

References and Notes

1. C. M. Soukoulis, S. Linden, M. Wegener, *Science* **315**, 47 (2007).
2. N. Liu *et al.*, *Nat. Mater.* **7**, 31 (2008).
3. J. Valentine *et al.*, *Nature* **455**, 376 (2008).
4. J. K. Gansel *et al.*, *Science* **325**, 1513 (2009).
5. D. B. Burckel *et al.*, *Adv. Mater.* **22**, 3171 (2010).
6. M. I. Stockman, *Phys. Rev. Lett.* **98**, 177404 (2007).
7. P. Kinsler, M. W. McCall, *Phys. Rev. Lett.* **101**, 167401 (2008).
8. E. Plum, V. A. Fedotov, P. Kuo, D. P. Tsai, N. I. Zheludev, *Opt. Express* **17**, 8548 (2009).
9. N. Meinzer *et al.*, *Opt. Express* **18**, 24140 (2010).
10. S. Xiao *et al.*, *Nature* **466**, 735 (2010).
11. S. Wuestner, A. Pusch, K. L. Tsakmakidis, J. M. Hamm, O. Hess, *Phys. Rev. Lett.* **105**, 127401 (2010).
12. A. Fang, Th. Koschny, C. M. Soukoulis, *Phys. Rev. B* **82**, 121102 (2010).
13. C. Rockstuhl, F. Lederer, C. Etrich, T. Pertsch, T. Scharf, *Phys. Rev. Lett.* **99**, 017401 (2007).
14. D. O. Güney, T. Koschny, C. M. Soukoulis, *Opt. Express* **18**, 12348 (2010).

15. We thank M. Decker for preparing the figure. Supported by the European Union FET project PHOME (contract 213390); by Ames Laboratory, U.S. Department of Energy (Basic Energy Sciences), under contract DE-AC02-07CH11358; by Office of Naval Research and Air Force Office of Scientific Research–Multidisciplinary University Research Initiative grants (C.M.S.); and by projects CFN A1.5 and METAMAT (M.W.).

10.1126/science.1198858

IMMUNOLOGY

Have You Seen Your Mother, Baby…

T cell development occurs in waves, involving distinct stem cell populations, throughout human fetal development.

Alexander G. Betz

In 1953, immunologist (and later, Nobel Laureate) Peter Medawar posed the question, "How does the pregnant mother contrive to nourish within itself, for many weeks or months, a fetus that is an antigenically foreign body?" (*1*). Although none of his proposed mechanisms stood the test of time, they nevertheless provided the intellectual framework for years to come in the study of how a fetus evades rejection by the mother's immune system (maternal fetal tolerance). Regulatory T cells are now recognized as key mediators of immunological tolerance. Although they are best known for preventing autoimmunity (*2*), development of an embryo inside the body of the mother (invasive placental viviparity) would not be possible without these immune cells (*3*). On page 1695 of this issue, Mold *et al*. (*4*) show that fetal and adult T cells, including regulatory T cells, are distinct populations that arise from different hematopoietic stem-progenitor cells (HSPCs) present at different stages of development. Moreover, the early fetal immune system appears to be biased toward tolerance. This not only has important implications for understanding how a fetus avoids launching an immune response against the mother (fetal maternal tolerance), but it also raises questions about how the human immune system is set up during fetal development and in adulthood.

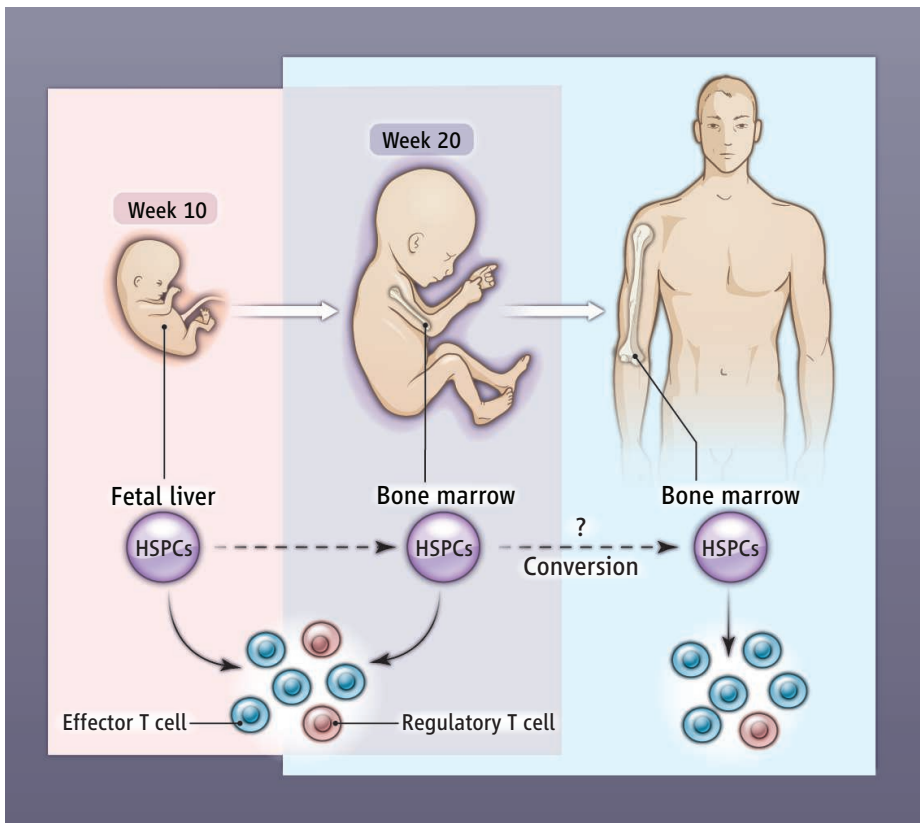

Layers of immunity. Fetal hematopoietic stem-progenitor cells (HSPCs) generate a higher number of regulatory T cells than adult HSPCs, leading to a bias toward immune tolerance. It is not clear whether the fetal and adult HSPCs are distinct lineages or whether the adult pool arises from the fetal source. It is also not known when the transition in the ratio of T cells occurs, once lymphocyte production migrates from the fetal liver to fetal bone marrow.

The concept of acquired immunological tolerance can be traced back to Medawar and colleagues when they set out to develop a "foolproof method" to distinguish nonidentical (dizygotic) from identical (monozygotic) cattle twins (*5*). Their idea to use skin transplant rejection to test for dizygosity was based on the knowledge that grafts between identical twins are readily accepted, whereas grafts between siblings are vigorously rejected. They were surprised to find that grafts between dizygotic twins, which are genetically no more closely related than siblings, failed to be rejected. They concluded that dizygotic twins somehow acquired tolerance to grafts of one another's skin. This puzzle led Medawar to also realize that placental viviparity in itself constitutes a problem to the mother's immune system (*1*). So-called suppressor T cells were suspected to prevent maternal rejection of the fetus, but because of a lack of experimental model systems, the connection remained correlative (*6*). With the demise of the suppressor T cell field in the late 1980s, this was all but forgotten.

A decade later, suppressor T cells were resurrected as regulatory T cells (*2*). With the discovery of the transcriptional regulatory protein Foxp3 as a lineage marker for regulatory T cells (*7*), it did not take long to demonstrate that they play a crucial role in maternal fetal tolerance in both mice and humans (*8*). There is now little doubt of the importance of regulatory T cells in immune tolerance.

In contrast to mice, in which the adaptive immune system only starts to develop around birth, T cells in humans can be detected as early as gestational week 10 (*9*). Thus, the human fetal immune system has the ability to recognize noninherited maternal alloantigens and must somehow tolerate them. What better way to do this than to use the mechanism that was already proven so successful for maternal fetal tolerance (*10*), especially given that regulatory T cells are required for preventing autoreactivity during the same time of fetal development. Mutations in the gene encoding Foxp3 (which resides on the inherited X chromosome) result in impaired regulatory T cell function, with disas-

Medical Research Council, Laboratory of Molecular Biology, Protein & Nucleic Acid Chemistry Facility, University of Cambridge, Cambridge CB2 0QH, UK. E-mail: betz@mrc-lmb.cam.ac.uk

Published by AAAS

trous consequences for the affected males. In many cases, they are born with raging autoimmune disease (*11*). Intriguingly, few if any of these patients carry a true null mutant (encoding a functionless form) of the *FOXP3* gene. The reason for this might be that the phenotype of such a mutant would be much more severe, resulting in the fetus not only developing autoimmunity, but also attacking the maternally derived portion of the placenta (the decidua). As a result, the affected fetus would cut off its own supply of nutrients and oxygen and thus might never see the light of day.

The data of Mold *et al*. suggest that hematopoiesis during fetal development occurs in waves, each generating distinct populations of T cells that may coexist for a period of time. T cells ($CD4^+$ subtype) originating from fetal liver HSPCs appear to have a propensity to adopt the fate of regulatory T cells ($Foxp3^+$), thereby biasing the fledgling immune system toward immune tolerance. As the source of hematopoiesis switches to the fetal bone marrow, the resulting effector T cell/regulatory T cell ratio gradually moves toward that found in adults. It will be interesting to examine whether the tendency of the early fetal immune system to promote tolerance is restricted to self antigens and noninherited maternal alloantigens, or whether it extends to foreign antigens encountered during development. The latter might have both beneficial and detrimental consequences on the immune system that reach far beyond pregnancy. Although the tendency toward tolerance might provide a window to educate the immune system not to respond to common allergens (*12*, *13*), it also provides an opportunity for exploitation by pathogens. Indeed, exposure of a fetus to malaria in utero, which leads to the accumulation of infected red blood cells in the placenta (placental malaria), results in the expansion of malaria-specific regulatory T cells. This might explain why children who have been infected as a result of placental malaria are more susceptible to subsequent malaria infections (*14*).

It remains to be resolved whether the fetal liver and adult HSPCs are distinct lineages, or whether the latter develops from the former (see the figure). A detailed analysis of the transcriptional profiles of these progenitor pools, in combination with an analysis of epigenetic modifications, should yield valuable information regarding their relationship.

References

1. P. B. Medawar, *Symp. Soc. Exp. Biol.* **7**, 320 (1953).
2. S. Sakaguchi, *Cell* **101**, 455 (2000).
3. V. R. Aluvihare, M. Kallikourdis, A. G. Betz, *Nat. Immunol.* **5**, 266 (2004).
4. J. E. Mold *et al*., *Science* **330**, 1695 (2010).
5. R. E. Billingham, L. Brent, P. B. Medawar, *Nature* **172**, 603 (1953).
6. G. Chaouat, G. A. Voisin, *J. Immunol.* **122**, 1383 (1979).
7. H. D. Ochs, S. F. Ziegler, T. R. Torgerson, *Immunol. Rev.* **203**, 156 (2005).
8. J. Trowsdale, A. G. Betz, *Nat. Immunol.* **7**, 241 (2006).
9. B. F. Haynes, M. E. Martin, H. H. Kay, J. Kurtzberg, *J. Exp. Med.* **168**, 1061 (1988).
10. J. E. Mold *et al*., *Science* **322**, 1562 (2008).
11. R. S. Wildin, S. Smyk-Pearson, A. H. Filipovich, *J. Med. Genet.* **39**, 537 (2002).
12. G. Wegienka *et al*., *J. Reprod. Immunol.* **81**, 74 (2009).
13. E. von Mutius, D. Vercelli, *Nat. Rev. Immunol.* **10**, 861 (2010).
14. K. L. Flanagan *et al*., *Eur. J. Immunol.* **40**, 1062 (2010).

10.1126/science.1200406

ATMOSPHERIC SCIENCE

The Burning Issue

Antarctic ice cores reveal a 650-year record of biomass burning in the Southern Hemisphere.

Iain Colin Prentice

Fortunately for us, carbon monoxide (CO)—a toxic gas—is a very minor constituent of the atmosphere. It is produced by incomplete burning of fossil fuels and biomass (such as dry leaves and wood) and by the oxidation of methane and other volatile hydrocarbons in the atmosphere. On page 1663 of this issue, Wang *et al*. (*1*) present high-precision measurements, taken from air trapped in Antarctic ice, of how atmospheric concentrations of CO have changed over the past 650 years. Their findings offer a striking and surprising look at the history of fire in the Southern Hemisphere, and some hints at future global fire trends.

In addition to CO concentrations, Wang *et al*. present the first record of changes in two stable isotopes—carbon-13 (^{13}C) and oxygen-18 (^{18}O)—which they use to estimate how much of the CO came from burning biomass. This is a notable feat, consid-

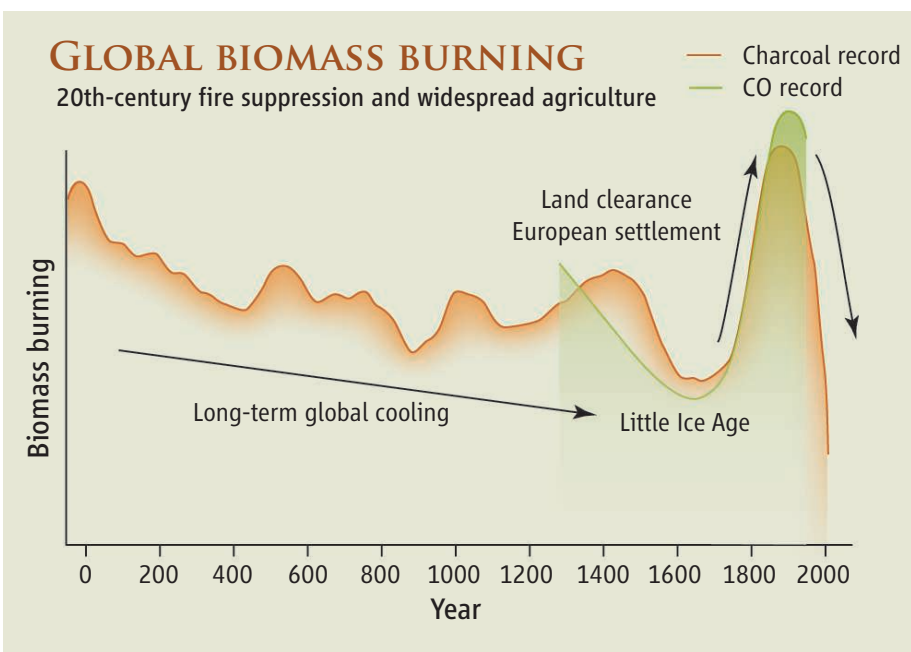

Burning history. Hypothesized causes of major long-term trends in global biomass burning, based on a synthesis of sedimentary charcoal records (orange) (*4*) and analyses of carbon monoxide trapped in Antarctic ice (green) (*1*).

Department of Biological Sciences, Macquarie University, Sydney, North Ryde, NSW 2109 Australia. E-mail: colin.prentice@mq.edu.au

trous consequences for the affected males. In many cases, they are born with raging autoimmune disease (*11*). Intriguingly, few if any of these patients carry a true null mutant (encoding a functionless form) of the *FOXP3* gene. The reason for this might be that the phenotype of such a mutant would be much more severe, resulting in the fetus not only developing autoimmunity, but also attacking the maternally derived portion of the placenta (the decidua). As a result, the affected fetus would cut off its own supply of nutrients and oxygen and thus might never see the light of day.

The data of Mold *et al*. suggest that hematopoiesis during fetal development occurs in waves, each generating distinct populations of T cells that may coexist for a period of time. T cells ($CD4^+$ subtype) originating from fetal liver HSPCs appear to have a propensity to adopt the fate of regulatory T cells ($Foxp3^+$), thereby biasing the fledgling immune system toward immune tolerance. As the source of hematopoiesis switches to the fetal bone marrow, the resulting effector T cell/regulatory T cell ratio gradually moves toward that found in adults. It will be interesting to examine whether the tendency of the early fetal immune system to promote tolerance is restricted to self antigens and noninherited maternal alloantigens, or whether it extends to foreign antigens encountered during development. The latter might have both beneficial and detrimental consequences on the immune system that reach far beyond pregnancy. Although the tendency toward tolerance might provide a window to educate the immune system not to respond to common allergens (*12*, *13*), it also provides an opportunity for exploitation by pathogens. Indeed, exposure of a fetus to malaria in utero, which leads to the accumulation of infected red blood cells in the placenta (placental malaria), results in the expansion of malaria-specific regulatory T cells. This might explain why children who have been infected as a result of placental malaria are more susceptible to subsequent malaria infections (*14*).

It remains to be resolved whether the fetal liver and adult HSPCs are distinct lineages, or whether the latter develops from the former (see the figure). A detailed analysis of the transcriptional profiles of these progenitor pools, in combination with an analysis of epigenetic modifications, should yield valuable information regarding their relationship.

References

1. P. B. Medawar, *Symp. Soc. Exp. Biol.* **7**, 320 (1953).
2. S. Sakaguchi, *Cell* **101**, 455 (2000).
3. V. R. Aluvihare, M. Kallikourdis, A. G. Betz, *Nat. Immunol.* **5**, 266 (2004).
4. J. E. Mold *et al*., *Science* **330**, 1695 (2010).
5. R. E. Billingham, L. Brent, P. B. Medawar, *Nature* **172**, 603 (1953).
6. G. Chaouat, G. A. Voisin, *J. Immunol.* **122**, 1383 (1979).
7. H. D. Ochs, S. F. Ziegler, T. R. Torgerson, *Immunol. Rev.* **203**, 156 (2005).
8. J. Trowsdale, A. G. Betz, *Nat. Immunol.* **7**, 241 (2006).
9. B. F. Haynes, M. E. Martin, H. H. Kay, J. Kurtzberg, *J. Exp. Med.* **168**, 1061 (1988).
10. J. E. Mold *et al*., *Science* **322**, 1562 (2008).
11. R. S. Wildin, S. Smyk-Pearson, A. H. Filipovich, *J. Med. Genet.* **39**, 537 (2002).
12. G. Wegienka *et al*., *J. Reprod. Immunol.* **81**, 74 (2009).
13. E. von Mutius, D. Vercelli, *Nat. Rev. Immunol.* **10**, 861 (2010).
14. K. L. Flanagan *et al*., *Eur. J. Immunol.* **40**, 1062 (2010).

10.1126/science.1200406

ATMOSPHERIC SCIENCE

The Burning Issue

Antarctic ice cores reveal a 650-year record of biomass burning in the Southern Hemisphere.

Iain Colin Prentice

Fortunately for us, carbon monoxide (CO)—a toxic gas—is a very minor constituent of the atmosphere. It is produced by incomplete burning of fossil fuels and biomass (such as dry leaves and wood) and by the oxidation of methane and other volatile hydrocarbons in the atmosphere. On page 1663 of this issue, Wang *et al*. (*1*) present high-precision measurements, taken from air trapped in Antarctic ice, of how atmospheric concentrations of CO have changed over the past 650 years. Their findings offer a striking and surprising look at the history of fire in the Southern Hemisphere, and some hints at future global fire trends.

In addition to CO concentrations, Wang *et al*. present the first record of changes in two stable isotopes—carbon-13 (^{13}C) and oxygen-18 (^{18}O)—which they use to estimate how much of the CO came from burning biomass. This is a notable feat, consid-

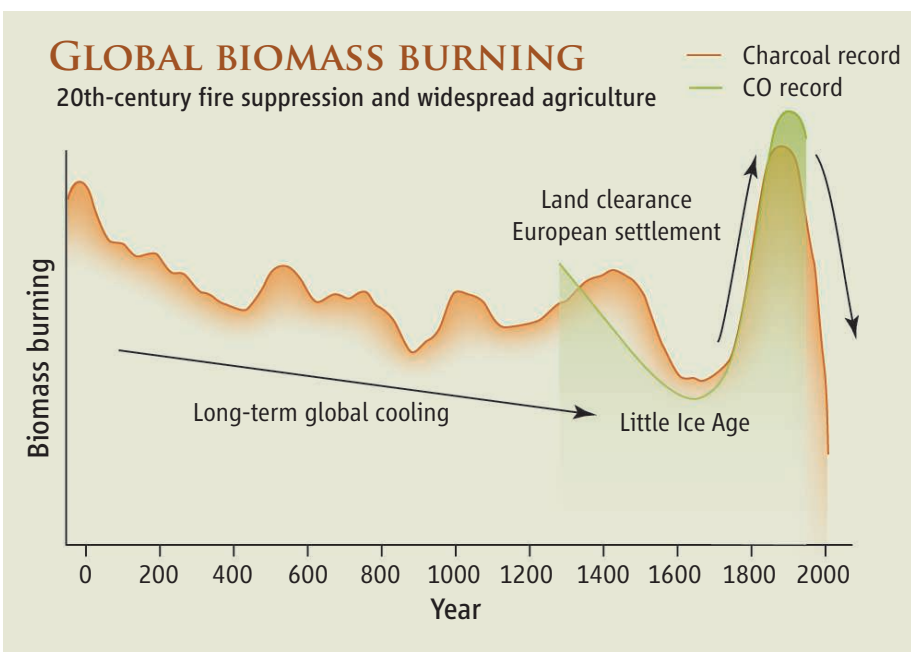

Burning history. Hypothesized causes of major long-term trends in global biomass burning, based on a synthesis of sedimentary charcoal records (orange) (*4*) and analyses of carbon monoxide trapped in Antarctic ice (green) (*1*).

Department of Biological Sciences, Macquarie University, Sydney, North Ryde, NSW 2109 Australia. E-mail: colin.prentice@mq.edu.au

ering the small amounts of air trapped in ice, the tiny amount of CO in the air (35 to 55 parts per billion), and the even smaller amounts of heavy isotopes in CO. A striking pattern emerged. Biomass burning declined steadily from the 1300s through the 1600s, in parallel with cooling that occurred from the Medieval Warm Period to the Little Ice Age. Then, some combination of warming and human activity drove a rapid increase in biomass burning, which peaked in the late 1800s before abruptly declining to a historic low in the present.

Wang *et al*.'s results add to a small but growing literature on the global history of fire. Studying fire from an "earth system" perspective is a relatively immature field, despite its enormous importance for carbon cycling, atmospheric composition, and human welfare (*2*). Until very recently, there were no large-scale data on fires, apart from records kept by firefighting agencies in a few countries. Two developments have changed that situation: the availability of data on active fires and burned areas from remote-sensing satellites (*3*) and the assembly of charcoal abundance records from stratified sediments (*4*). The remote-sensing data provide detailed information on the spatial patterns and interannual variability of fires. The stratigraphic records reveal longer-term regional trends. Researchers have also obtained evidence of long-term fire trends from the ^{13}C content of atmospheric methane (*5*), which is disproportionately influenced by changes in the frequency and extent of fires.

Wang *et al*.'s "top-down" observations dramatically confirm the recent history of global fire inferred from "bottom-up" charcoal records (*4*). Marlon *et al*. (*4*) show that a similar pattern, including the recent abrupt decline, was common to different regions of both hemispheres. The most plausible explanation for the decline is that it was a side effect of the spread of European-style intensive cropping and grazing, which dramatically reduced both fuel loads and connections between fire-prone habitats, inhibiting both the initiation and the spread of fires.

CREDIT: PETE STARMAN/CORBIS

Burning out. Studies of the recent history of fire, like this blaze in a California forest in 2009, suggest that total global biomass burning is now lower than at any time in the past 2000 years.

To bridge the gap between the uppermost ice-core measurements and the present day, Wang *et al*. include one crucial data point based on direct atmospheric measurements, and several more derived from firn air (firn is the mixture of air and snow that eventually consolidates to become ice). These data confirm that there has been a strong downward trend of biomass burning since the peak in the late 19th century and are consistent with the charcoal record (*4*).

These findings challenge some of the myths that abound in the fire literature. None is more persistent than the perception that fires are caused mainly by human activities. People start fires, it has been reasoned; therefore, in earlier times, when there were fewer people, there must have been less burning. This faulty assumption underlies several attempts, some of which are cited by Wang *et al*., to reconstruct changes in the composition of the atmosphere during the industrial era. The evidence, however, shows the opposite. In southern Africa, for instance, researchers using remote-sensing observations have found a negative relationship between human population density and burned area, with fire decreasing as population increases (*6*). And despite the high media profile of "deforestation fires" in places like Indonesia and Brazil, research demonstrates that these fires are spatially restricted and subject to strong climate control (*7*); total biomass burning during recent decades has been lower than at any time during the past 650 years (*1*) or even the past 2000 years (*4*). Climate change, on the other hand, has had a major impact—as shown in the long decline in biomass burning in response to natural global climate changes of the past millennium, which researchers believe had an amplitude of no more than a few tenths of a degree. It is reasonable to expect that future climate change will greatly increase the risks of wildfire (*2*), especially if the global mean temperature increases by several degrees (*8*–*10*) as suggested by many projections.

This new perspective on the recent history of fire brings both good news and bad. If biomass burning on a large scale is controlled mainly by climate, then this is bad news for Smokey the Bear (the U.S. advertising icon who says that "only you can prevent forest fires"). The good news is that, if we can predict fire risks by using process-based models (*11*–*13*), we should be able to reduce fires through land use and fuel management. This approach, however, will require a major shift of policy emphasis toward avoiding conditions that favor the spread of fire (*10*).

References

1. Z. Wang, J. Chappellaz, K. Park, J. E. Mak, *Science* **330**, 1663 (2010).
2. D. M. J. S. Bowman *et al*., *Science* **324**, 481 (2009).
3. L. Giglio *et al*., *Biogeosciences* **7**, 1171 (2010).
4. J. R. Marlon *et al*., *Nat. Geosci.* **1**, 697 (2008).
5. D. F. Ferretti *et al*., *Science* **309**, 1714 (2005).
6. S. Archibald, D. P. Roy, B. W. van Wilgen, R. J. Scholes, *Glob. Change Biol.* **15**, 613 (2009).
7. G. R. van der Werf *et al*., *Proc. Natl. Acad. Sci. U.S.A.* **105**, 20350 (2008).
8. M. Scholze, W. Knorr, N. W. Arnell, I. C. Prentice, *Proc. Natl. Acad. Sci. U.S.A.* **103**, 13116 (2006).
9. M. A. Krawchuk, M. A. Moritz, M.-A. Parisien, J. Van Dorn, K. Hayhoe, *PLoS ONE* **4**, e5102 (2009).
10. S. P. Harrison, J. R. Marlon, P. J. Bartlein, in *Changing Climates, Earth Systems and Society*, J. Dodson, Ed. (Springer, Dordrecht, 2010), pp. 21–48.
11. S. Kloster *et al*., *Biogeosciences* **7**, 1877 (2010).
12. O. Pechony, D. T. Shindell, *J. Geophys. Res.* **114**, D16115 (2009).
13. K. Thonicke *et al*., *Biogeosciences* **7**, 1991 (2010).

10.1126/science.1199809

Published by AAAS

mechanism by which Gwl controls mitotic entry and progression. Activation of Gwl by Cdk1 leads to direct phosphorylation of Ensa or Arpp19, either of which then blocks PP2A-B55δ. The consequence of this decrease in dephosphorylation is an increase in the net phosphorylation of mitotic substrates, resulting in entry into mitosis (see the figure).

These results raise new questions. Are Ensa and Arpp19 the only relevant substrates of Gwl? Depletion of these proteins in *Xenopus* and human cells supports this notion, and there is precedent for cell cycle–regulatory kinases (such as Wee1) phosphorylating a limited number of substrates. Gharbi-Ayachi *et al*. and Mochida *et al*. disagree about the relative importance of Ensa versus Arpp19 in *Xenopus* mitotic entry, and this will require further study.

How is the phosphorylation of Ensa and Arpp19 regulated? Although Gharbi-Ayachi *et al*. and Mochida *et al*. suggest a simple mechanism—phosphorylation of a single serine residue by Gwl—other potential phosphorylation sites in Ensa and Arpp19 have been identified by phosphoproteomic screens (*12*), including two tyrosine phosphorylation sites immediately adjacent to the Gwl site. Perhaps these additional phosphorylation events, catalyzed by other kinases, alter the affinity of Ensa and Arpp19 for PP2A-B55δ or other PP2A B subunits, or the activity of Gwl on Ensa and Arpp19.

If phosphorylation of Ensa and Arpp19 is important for mitotic entry, are both proteins inactivated at mitotic exit so that mitotic substrates can be dephosphorylated? PP2A-B55δ may not be required for dephosphorylating mitotic proteins at exit from mitosis; indeed, a screen of phosphatases by RNA interference identified a different PP2A heterotrimer, PP2A-B55α, as a regulator of mitotic exit (*13*). There may be additional PP2A inhibitors to be discovered, which are inactivated through as yet unknown mechanisms.

References

1. J. E. Ferrell Jr. *et al*., *FEBS Lett.* **583**, 3999 (2009).
2. A. Gharbi-Ayachi *et al*., *Science* **330**, 1673 (2010).
3. S. Mochida, S. L. Maslen, M. Skehel, T. Hunt, *Science* **330**, 1670 (2010).
4. L. Busino *et al*., *Nature* **426**, 87 (2003).
5. J. Yu *et al*., *J. Cell Biol.* **164**, 487 (2004).
6. J. Yu, Y. Zhao, Z. Li, S. Galas, M. L. Goldberg, *Mol. Cell* **22**, 83 (2006).
7. E. Voets, R. M. Wolthuis, *Cell Cycle* **9**, 3591 (2010).
8. P. K. Jackson, *Mol. Cell* **22**, 156 (2006).
9. P. V. Castilho, B. C. Williams, S. Mochida, Y. Zhao, M. L. Goldberg, *Mol. Biol. Cell* **20**, 4777 (2009).
10. S. Mochida, S. Ikeo, J. Gannon, T. Hunt, *EMBO J.* **28**, 2777 (2009).
11. S. Vigneron *et al*., *EMBO J.* **28**, 2786 (2009).
12. www.phosphosite.org
13. M. H. Schmitz *et al*., *Nat. Cell Biol.* **12**, 886 (2010).

10.1126/science.1199898

MATHEMATICS

Being Glassy Without Being Hard to Solve

The threshold for mathematical problems being easy or hard to solve can be extremely abrupt.

Federico Ricci-Tersenghi

The statistical mechanics that describes collective phenomena in disordered systems and solutions to large search problems have important mathematical connections. One of the models that describes disordered materials, the diluted p-spin model, is strongly related to the random XORSAT problem, a problem of finding variables that simultaneously satisfy a large number of logical constraints (*1*). This relation has provided insight into how small changes in a model can modify its computational difficulty.

Cooling a physical liquid creates an ordered crystal or a largely disordered configuration called a glass. Similarly, cooling a solid containing atoms with unpaired electron spins may lead to a spin-aligned state (for example, a ferromagnet) or to a disordered spin glass. Simple models of interacting particles or spins normally create the ordered state at low temperatures. Glass models, when cooled, form small regions of local order that mismatch at the boundaries, so that no ordered structure is evident on larger length scales.

A natural dynamics exists for these models: Particles or spins are allowed to move or flip according to the change in energy this would produce. In a glass model, a large amount of energy is needed to rearrange the local structures all along the boundaries; relaxation times become huge and diverge at the glass critical temperature T_g. Below T_g, the system will likely get trapped in one of many false local energy minima above the true equilibrium energy. In most models, when this situation occurs, the computation of the ground states can be unfeasibly long. However, there are glass models in which the relaxation dynamics indeed get stuck at a threshold energy value, yet a different algorithm can find all of the ground states in a very efficient way. Although such models (considered ideal glasses) are prototypes for complex systems, the problem of finding their ground state is easy to solve.

An example of these ideal glass models is the diluted p-spin model, which is defined in terms of N spins s that either point up or down (1 or –1). Their interactions are described by the Hamiltonian

$$H = -\sum_{\langle ijk \rangle}^{\alpha N} J_{ijk} s_i s_j s_k \qquad (1)$$

The sum runs over a set of αN randomly chosen triplets (i, j, k) of neighboring sites (so in this case, $p = 3$, only triplet interactions are included), and the couplings J_{ijk} are quenched random variables (e.g., they are randomly set to +1 or –1). The specifics will not matter in the limit of large N. Typically, the ratio α of interactions per variable is chosen so that not all sites interact, and some are more connected than others.

This model displays the desired dramatic increase of the relaxation times near T_g that reproduces glass phenomenology (*2*, *3*). Even when a spin configuration exists that satisfies all the interactions—which would favor ordering—a perfect glass still forms (*4*). This model has a mean-field nature—it reduces a difficult many-body problem to a simpler one-body problem—and could be solved analytically (*5*).

The figure summarizes the properties of the diluted p-spin model that are relevant for discussing possible relations between glassiness and computational hardness. In this sketch, potential energy E is shown as a function of α. The green region corresponds to energy values that can be reached by a stochastic algorithm—one with randomly cho-

Dipartimento di Fisica, Sapienza Università di Roma, Piazzale Aldo Moro 5, 00185 Roma, Italy. E-mail: federico.ricci@uniroma1.it

sen moves, such as a Monte Carlo Markov chain. These algorithms would get "stuck" at the threshold energy E_g separating the green from the red region. The red region is full of local minima (the glassy states) and large energy barriers (it looks like an "egg carton") and is hard to sample with stochastic local moves algorithms (and probably with any polynomial time algorithm). The blue line corresponds to unfrustrated ground states, that is, configurations with all interactions satisfied.

The search for the unfrustrated ground states of the Hamiltonian (Eq. 1) can be easily recast as solving a set of αN linear equations in N Boolean (true or false) variables of the type

$$x_i \text{ XOR } x_j \text{ XOR } x_k = c_{ijk} \qquad (2)$$

where XOR is the exclusive OR operation—the XOR statement is true if one but not both arguments are true. As before, the triplets are randomly chosen, and the known constants c_{ijk} are randomly fixed to true or false with probability 1/2. Equation 2 is a constraint satisfaction (SAT) problem (CSP)—each equation imposes a constraint on the Boolean variables—and is called a random XORSAT problem (*6*).

For small values of the ratio α of constraints per variable, true and false values can be found so that all αN linear equations are satisfied. However, as the ratio α increases, the random XORSAT problem becomes more and more difficult to solve and finally cannot be satisfied (UNSAT). The largest α value for which solutions exist is called SAT-UNSAT threshold. As long as α is smaller than this threshold, the problem is linear and all solutions can be found efficiently, for example, by the Gaussian elimination method, which takes a time of order N^3 in the worst case.

In a sense, the random XORSAT problem in computer science can be viewed as a limiting case (for temperature going to zero) of the diluted p-spin model in physics, and it is curious that its solution has been reached by the two communities independently and at the same time (*7*, *8*).

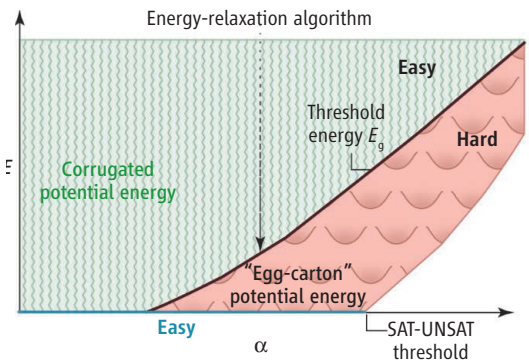

The line between easy and hard. A schematic picture for the potential energy E of a glass model (the diluted p-spin model) as a function of the ratio α of interactions or constraints per variable. The green region corresponds to configurations that can be easily sampled by a standard stochastic algorithm with local moves (e.g., Monte Carlo methods). In the red region, deep local minima separated by high energy barriers make the sampling of configurations a computationally hard problem. The zero-energy ground-state configurations along the blue line (at the horizontal axis) can be sampled efficiently, because this problem is not computationally hard before the satisfiability (SAT-UNSAT) threshold. However, configurations on the blue line cannot be accessed by cooling the glass model: In this case, a straightforward connection between physical glassiness and computational complexity cannot be made.

Returning to the figure, an important connection can be made about computational hardness. The blue line is computationally easy and can be sampled in polynomial time. However, it extends below the red hard region that cannot be accessed by the stochastic searches. The naïve connection between glassiness and hardness fails. Thus, it is not possible to say a priori that a complex physical problem does always correspond to a computationally hard problem. It is entirely possible to find an easy problem that looks "glassy" and difficult to solve if approached with a suboptimal algorithm.

Despite the existence of specific cases like the diluted p-spin model, scientists believe in a strong connection between the physical complexity of a model (i.e., the properties of its potential energy, which determine phase transitions) and the computational complexity of the corresponding CSP (*9*–*11*). Indeed, the peculiarity of the diluted p-spin model arises from an intrinsic symmetry in the model (*6*) that allows easy computation of configurations satisfying all interactions. As soon as this symmetry is broken, the computation of ground-state configurations becomes very difficult, even if these configurations satisfy all interactions (*12*).

In general, the connection between physical complexity and computational complexity may apply and may help in solving the following very important open problem. Computational problems fall into one of two complexity classes (*13*). The class P contains all of the problems for which a solving algorithm running in polynomial time is known, whereas the class NP contains all of the problems for which such an algorithm is not available, although a candidate solution can be checked in polynomial time. If the classes P and NP turn out to coincide—that is, if the "P = NP" conjecture is true—our world would change dramatically. For example, current cryptographic codes, based on the NP hardness of factoring large numbers, would be useless.

Scientists strongly believe P and NP classes to be different. In August 2010, some Internet blogs reported a claim of a proof that P ≠ NP by Vinay Deolalikar. A wiki site aggregates most of the information on the proof and the discussion about it (*14*). The proof tries to connect the complexity of the solution space of random CSPs (i.e., the structure of ground states of the corresponding physical model) and the complexity of algorithms for finding solutions to these problems.

In essence, Deolalikar tries to prove that those random CSPs in which solutions form clusters with frozen variables (that is, variables taking the same value for all solutions in the cluster) cannot be solved in polynomial time by any algorithm. However, the diluted p-spin model is a classical example that a simple connection cannot work. The solution space of random XORSAT problems shows clustering with frozen variables (*7*), but the problem is solvable in polynomial time. Certainly, we need to understand better this connection, and hopefully Deolalikar's work will help in this regard.

References and Notes

1. M. Mezard, A. Montanari, *Information, Physics, and Computation* (Oxford Univ. Press, Oxford, UK, 2009).
2. P. G. Debenedetti, F. H. Stillinger, *Nature* **410**, 259 (2001).
3. A. Cavagna, *Phys. Rep.* **476**, 51 (2009).
4. S. Franz, M. Mézard, F. Ricci-Tersenghi, M. Weigt, R. Zecchina, *Europhys. Lett.* **55**, 465 (2001).
5. A. Montanari, F. Ricci-Tersenghi, *Phys. Rev. B* **70**, 134406 (2004).
6. N. Creignou, H. Daude, *Discrete Appl. Math.* **96-97**, 41 (1999).
7. M. Mézard, F. Ricci-Tersenghi, R. Zecchina, *J. Stat. Phys.* **111**, 505 (2003).
8. O. Dubois, J. Mandler, in *Proceedings of the 43rd Annual IEEE Symposium on Foundations of Computer Science*, Vancouver, 16 to 19 November 2002, p. 769778.
9. R. Monasson *et al.*, *Nature* **400**, 133 (1999).
10. M. Mézard, G. Parisi, R. Zecchina, *Science* **297**, 812 (2002).
11. F. Krzakała, A. Montanari, F. Ricci-Tersenghi, G. Semerjian, L. Zdeborová, *Proc. Natl. Acad. Sci. U.S.A.* **104**, 10318 (2007).
12. W. Barthel *et al.*, *Phys. Rev. Lett.* **88**, 188701 (2002).
13. M. Garey, D. S. Johnson, *Computers and Intractability: A Guide to the Theory of NP-Completeness* (Freeman, New York, 1979).
14. "Deolalikar P vs NP paper"; http://michaelnielsen.org/polymath1/index.php?title=Deolalikar_P_vs_NP_paper.

10.1126/science.1189804

RETROSPECTIVE

Britton Chance (1913–2010)

A pioneering scientist and gold medal Olympian had unflagging energy and broad interests that fueled his research.

P. Leslie Dutton

Britton Chance was the Eldridge Reeves Johnson emeritus professor of biophysics, physical chemistry, and radiologic physics at the University of Pennsylvania. In a remarkable life, he was both a renowned biophysicist and a world-class yachtsman. Recognized for his pioneering research on how living organisms capture, manage, and produce cellular energy, he leaves a rich legacy of laboratory and clinical instrumentation and a wide range of discoveries and principles fundamental to biological catalysis and energetics, and biomedical application. Among his many honors was the National Medal of Science (1974). His parallel, lifelong love affair with sailing, mainly enjoyed in Barnegat Bay, New Jersey, culminated in his gold medal in the 1952 summer Olympics. Britton Chance pursued his research and sailing until his death on 16 November at age 97.

Chance graduated from the University of Pennsylvania with bachelor's and master's degrees in the 1930s, and a Ph.D. in physical chemistry and engineering in 1940. Apart from short periods at Cambridge University, England, where he earned a second Ph.D. in biology and physiology (1943), at the Massachusetts Institute of Technology (MIT) during World War II (1941 to 1945) where he worked on radar, and at Stockholm as a Guggenheim Fellow (1946 to 1948), his career was at Penn. He joined the Johnson Research Foundation in the School of Medicine in 1943 and became its director in 1949.

Chance's time at Penn from student to emeritus (1983) was marked by a succession of outstanding achievements, from novel instrumentation to biophysical research strategies. His capacity for innovation with mechanics, electronics, and optics was evident from an early age. During extended family sailing trips he became the qualified radio operator; at age 13, he built his first powerful radio transmitter and became a ham radio enthusiast. By age 17 he had built and patented an automatic ships-steering device incorporating a novel servomechanism. Interest in the device took him to England in 1938, and to Cambridge, where he extended his Ph.D. research in rapid flow/mixing techniques. Under contract from the British General Electric Company, he installed his automatic steering device in a 20,000-ton refrigerator ship and sailed with it from England to Australia. Back in Cambridge and supervised by Glenn Millikan, he moved from chemistry to enzyme mechanisms. In 1940, at the beginning of World War II in Europe, he returned to the United States and was admitted to the Johnson Research Foundation at Penn. But as the United States entry into the war loomed, Chance's reputation for imaginative and effective use of electricity, electronics, and light prompted his recruitment to the Radiation Laboratory at MIT. Early success there in developing submicrosecond circuits for radar directing guns and bombing elevated him to group leader and then the Steering Committee of the "Rad Lab," and by the end of the war he was in charge of a research team of 300. In looking back on this period, Chance reflected that he was happy to have played a part in the war effort.

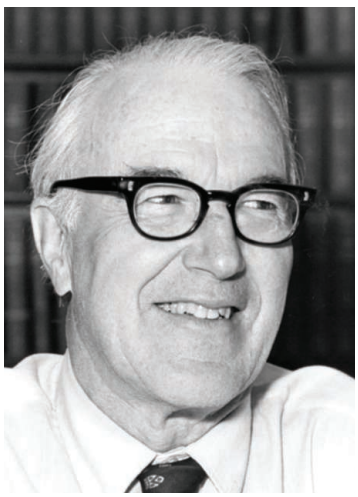

CREDIT: BRUCE ROSENBLUM/COURTESY OF PENN MEDICINE

Department of Biochemistry and Biophysics, University of Pennsylvania, Philadelphia, PA 19104, USA. E-mail: dutton@mail.med.upenn.edu

The ensuing three decades at Penn saw Chance's many discoveries in biological energetics. His 1930s miniaturized stopped-flow device demonstrated the long-predicted enzyme-substrate complex. In the 1950s, using the dual-wavelength spectrophotometer that he invented, Chance revealed many of the cellular redox cofactors of respiratory electron transfer that remain fundamental textbook knowledge. Moreover, in seminal work, he defined the energetic states and the reversibility of mitochondrial oxidative phosphorylation (state 3, state 4, etc.) that are essential descriptors for assessing health, damage, or disease in mitochondria. In the 1960s, using a ruby laser to activate photosynthetic bacteria at cryogenic temperatures, he discovered that biological electron transfer is governed by quantum-mechanical tunneling, a mechanism that underpins photosynthesis, respiration, and many of the most conspicuous oxidoreductase enzymes. In the 1970s, he discovered that superoxide and peroxide are generated by respiratory complex III (cytochrome bc_1) during normal energy-coupled respiratory electron transfer. Now recognized more widely and called reactive oxygen species, this phenomenon is the subject of intensive biomedical research on cellular regulation and in age-related diseases. In the late 1970s, Chance turned to pioneering magnetic resonance spectroscopy to track cellular energetics deep in live tissue through phosphorous compounds of oxidative phosphorylation. Magnets of ever-increasing bore size saw his research scale from mice to men en route to the now widely used magnetic resonance imaging, but in the 1990s he returned to his forte of small, inexpensive electro-optical instruments designed to analyze living tissue.

In his mid-70s, Chance (then emeritus) launched a new field of optical diagnostics that rests on the physics of light diffusion through scattering materials such as living tissue. He showed that scattered near-infrared light pulses could not only measure the dynamics of oxy- and deoxyhemoglobin levels in performing muscles, but also reveal and locate tumors and cancerous tissue in muscles and breast as well as injury in the brain. Because changing patterns of oxy- and deoxyhemoglobin in the brain reflect cognitive activity, the applications of his diagnostic approach widened to include assessing neuronal connectivity in premature babies.

In recent times, Chance's research focused on the possibility of analyzing the energy status of cells in living tissue in terms of the energy and redox states of mitochondria that he had described over half a century ago. The "metabolometer" that he and colleagues in Taiwan developed is small enough to be inserted into body cavities to make such measurements. Although the application of this device must still be tested, such visions for biomedical optics ensure that his work will be remembered well into the future.

10.1126/science.1200976

A Giant Planet Around a Metal-Poor Star of Extragalactic Origin

Johny Setiawan,[1]* Rainer J. Klement,[1] Thomas Henning,[1] Hans-Walter Rix,[1] Boyke Rochau,[1] Jens Rodmann,[2] Tim Schulze-Hartung[1]

Stars in their late stage of evolution, such as horizontal branch stars, are still largely unexplored for planets. We detected a planetary companion around HIP 13044, a very metal-poor star on the red horizontal branch, on the basis of radial velocity observations with a high-resolution spectrograph at the 2.2-meter Max-Planck Gesellschaft–European Southern Observatory telescope. The star's periodic radial velocity variation of P = 16.2 days caused by the planet can be distinguished from the periods of the stellar activity indicators. The minimum mass of the planet is 1.25 times the mass of Jupiter and its orbital semimajor axis is 0.116 astronomical units. Because HIP 13044 belongs to a group of stars that have been accreted from a disrupted satellite galaxy of the Milky Way, the planet most likely has an extragalactic origin.

In the past two decades, several hundred planets have been detected beyond our solar system. Most of these extrasolar planets orbit Sun-like stars. A small number have been detected around stars that are in their late evolutionary state, such as red giant branch (RGB) stars and pulsars. The phase directly after the RGB stage, the horizontal branch (HB), however, is still unexplored; therefore, there is no empirical evidence for whether close-in planets, i.e., those with semimajor axes less than 0.1 astronomical unit (AU), survive the giant phase of their host stars.

In addition to its evolutionary stage, a star's chemical composition appears to be a major indicator of its probability for hosting a planet. Previous studies [e.g., (*1*)] showed that main-sequence (MS) stars that host giant planets are metal-rich. This finding is supported by the large exoplanet search surveys around MS stars reporting a connection between planet frequency and metallicity (*2*, *3*), and a survey of 160 metal-poor MS stars finding no evidence for Jovian planets (*4*).

Until now, few planets have been detected around stars with metallicities as low as [Fe/H] = −1, i.e., 10% of the Sun's metallicity. The detection of PSR B1620 b, a Jovian planet orbiting a pulsar in the core of the metal-poor globular cluster M4 ([Fe/H] = −1.2), suggests, however, that planets may form around metal-poor stars (*5*, *6*), although the formation mechanism of this particular planet might be linked to the dense cluster environment (*7*).

We used the Fiber-fed Extended Range Optical Spectrograph (FEROS), a high-resolution spectrograph (resolution R = 48,000) attached to the 2.2-m Max-Planck Gesellschaft–European Southern Observatory telescope (*8*), to observe the star HIP 13044. This star is classified as a red HB (RHB) star (Fig. 1), and its metal content is $[Fe/H]_{mean}$ = −2.09 (*9*–*12*), i.e., about 1% that of the Sun. So far, HIP 13044 is not known as a binary system. Detailed stellar parameters can be found in Supporting Online Material (SOM) text 1.

Previous radial velocity (RV) measurements of HIP 13044 showed a systematic velocity of about 300 km s^{-1} with respect to the Sun, indicating that the star belongs to the stellar halo (*13*). Indeed, the star has been connected to the Helmi stream (*14*), a group of stars that share similar orbital parameters that stand apart from those of most other stars in the solar neighborhood. The Helmi stream stars move on prograde eccentric orbits [pericentric radius (R_{peri}) ~ 7 kiloparsec (kpc; 1 parsec = 3.26 light-years), apocentric radius (R_{apo}) ~ 16 kpc] that reach distances up to $|z|_{max}$ ~ 13 kpc above and below the galactic plane. From that, it has been concluded that these stars were once bound to a satellite galaxy of the Milky Way (*10*, *14*) that was tidally disrupted 6 to 9 billion years ago (*15*).

The variation of the RV between our observations at different epochs has a semi-amplitude (K) of 120 m s^{-1} (*16*) (Fig. 2). The generalized Lomb Scargle (GLS) periodogram (*17*) reveals a significant RV periodicity at P = 16.2 days with a false alarm probability (FAP) of 5.5 × 10^{-6}. Additional analysis, using a Bayesian algorithm (*18*), yields a similar period around 16 days. Such RV variation can be induced by an unseen orbiting companion, by moving or rotating surface inhomogeneities, or by nonradial stellar pulsations. Exploring both stellar rotational modulation and pulsations is critical when probing the presence of a planetary companion, because they can produce a similar or even the same RV variation, mimicking a Keplerian motion.

A well-established technique for detecting stellar rotational modulation is to investigate the line profile asymmetry or bisector (*19*) and Ca II lines (SOM text 3). Surface inhomogeneities, such as starspots and large granulation cells, produce asymmetry in the spectral line profiles.

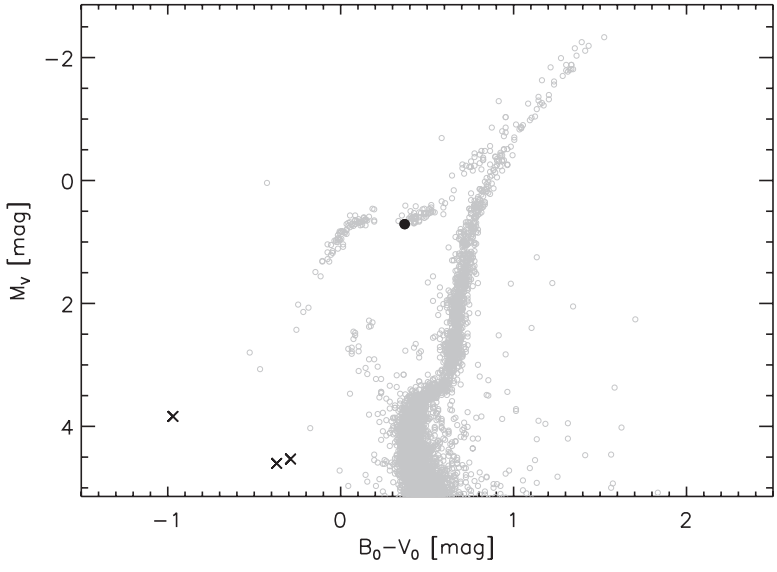

Fig. 1. Location of HIP 13044 in a M_V versus $B - V$ color-magnitude diagram (CMD) shown as a black dot superimposed to the CMD of Messier 3 (gray open circles) based on the photometry by (*46*). Apparent magnitudes have been converted to absolute magnitudes by considering the distance modulus and extinction given by Harris (*47*). The gap separating the blue and red horizontal branch (RHB) is due to RR Lyrae instability strip. The CMD location of HIP 13044 implies that it is a core He-burning star, located at the blue edge of the RHB. Further candidates for post-RGB stars hosting planets and/or brown dwarfs, V391 Peg, HW Vir, and HD 149382 (*31*–*33*), are displayed as crosses.

[1]Max-Planck-Institut für Astronomie, Königstuhl 17, 69117 Heidelberg, Germany. [2]European Space Agency, Space Environment and Effects Section, European Space Research and Technology Centre, Keplerlaan 1, 2201 AZ Noordwijk, Netherlands.

*To whom correspondence should be addressed. E-mail: setiawan@mpia.de

When a spotted star rotates, the barycenter of the line profiles moves periodically and the variation can mimic a RV variation caused by an orbiting companion. Instead of measuring the bisectors, one can equivalently use the bisector velocity spans (BVSs) to search for rotational modulation (*20*). Adopting this technique, we have measured BVSs from the stellar spectra. There is only a weak correlation between BVS and RV (correlation coefficient = −0.13), but the BVS variation shows a clear periodicity with P = 5.02 days (SOM text 3.1.1). No period around 16 days is found in the BVS variation.

In addition to the BVS analysis, we investigated the variation of the Ca II λ849.8 line, which is one of the Ca II infrared triplet lines. From the observed Ca II λ849.8 equivalent-width variations, we computed a mean period of 6.05 days (SOM text 3.1.2), which is on the same order of the period of the BVS variation. We adopted the mean period of both stellar activity indicators, P_{rot} = 5.53 ± 0.73 days, as the stellar rotation period of HIP 13044 and then calculated the inclination angle of the stellar rotation axis, which follows from $P_{rot}/\sin i = 2\pi R_* / v \sin i$. With a stellar radius R_* = 6.7 times the radius of the Sun (*21*) and our adopted value for the projected rotational velocity, $v \sin i$ = 10.25 km s^{-1}, which was derived from the observed line broadening (SOM text 1), we obtained an inclination angle i = 9.7° ± 1.3°. Thus, the real stellar rotation velocity is ~62 km s^{-1}, which is typical for an early F-type MS star but relatively high for HB stars.

An explanation for this high rotation velocity is the assumption that HIP 13044 has engulfed its close-in planets during the red giant phase. Infalling planets are able to spin-up their host star (*22*–*24*), and this mechanism has been suggested to explain the high $v \sin i$ values observed for many RGB and HB stars (*25*).

We observed variations of HIP 13044 in the photometric data from the Hipparcos satellite (*26*) and SuperWASP (*27*) (SOM text 3.2.4). Whereas the Hipparcos data show only a marginal significant periodicity of 7.1 hours (FAP = 1.8%), the SuperWASP data show few intraday periodicities with FAP ~ 1% and two significant periodicities at 1.39 (FAP = 5 × 10^{-4}) and 3.53 days (FAP = 2 × 10^{-4}). These two periods, however, are most likely harmonic to each other ($1.4^{-1} + 3.5^{-1} = 1$). It is expected that HIP 13044 oscillates only at pulsationally unstable overtones of high order (*28*). Observations of one RHB star in the metal-poor globular cluster NGC 6397 (*29*), as well as theoretical predictions (*28*), set these periods in the range of a few hours to a day. No clear theoretical predictions for a star with parameters similar to those for HIP 13044 exist, hence it is possible that some high-order oscillations can explain the 1.4- or 3.5-day signal. What is important, however, is that there is no signal of a period around 16.2 days in the photometric data.

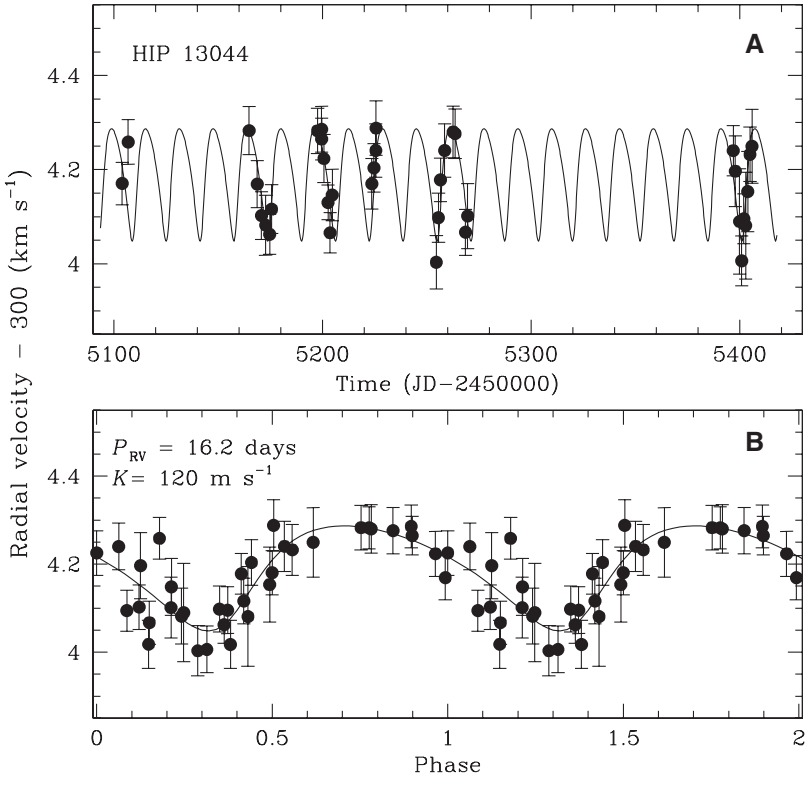

Fig. 2. (**A**) RV variation of HIP 13044. The RV values have been computed from the mean RVs of 20 usable echelle orders of the individual spectrum. The error bars have been calculated from the standard error of the mean RV of each order. (**B**) RV variation phase-folded with P = 16.2 days.

The arguments above show that neither stellar rotational modulation nor pulsations are plausible sources of the observed periodic RV variation. Therefore, the best explanation for the ~16-day period is the presence of an unseen companion. We computed its orbital solution (Table 1). Its minimum mass lies securely in the planetary mass domain, even with a plausible $\sin i$ uncertainty. With an eccentricity (e) of 0.25 and a semimajor axis (a) of 0.116 AU, the planet has a periastron distance of about 0.087 AU, which is ≈2.8 times the present stellar radius. The periastron is ~0.06 AU away from the stellar surface.

Because many known exoplanets have orbital semimajor axes between 0.01 and 0.06 AU, the distance between the periastron and the star HIP 13044 itself is not unusual. The noncircular orbit (e = 0.25), however, is not expected for a close-in giant planet around a post-RGB star.

In the case of HIP 13044, the original orbit could have been disturbed or changed during the evolution of the star-planet system, particularly during the RGB phase (*22*). Notably, the orbital period of HIP 13044 b is close to three times the stellar rotation period. A number of known planetary systems also have such a "coupling" between the stellar rotation and orbital periods, e.g., Tau Boo (1:1), HD 168433 (1:2), HD 90156 (1:2), and HD 93083 (1:3). Such planetary systems are particularly interesting for studying star-planet interactions (*30*).

So far, few planets or brown dwarfs have been detected around post-RGB stars besides the pulsar planets, namely V391 Peg (*31*), HW Vir (*32*), and HD 149382 (*33*) (Fig. 1). These are, however, substellar companions around subdwarf-B or Extreme Horizontal Branch (EHB) stars, i.e., the nature of their host stars differs from that of HIP 13044, an RHB star. Contrary to RGB stars, such as G and K giants (*34*–*37*), and subgiants, e.g., (*38*), HB stars have not yet been extensively surveyed for planets.

Although at least 150 MS stars bear close-in (a = 0.1 AU) giant planets, so far no such planets have been reported around RGB stars. A possible explanation is that the inner planets have been engulfed by the star when the stellar

Table 1. Orbital parameters of HIP 13044 b. ω, longitude of periastron; JD_0, Julian date of periastron passage; rms, root mean square deviation; M_{Jup}, mass of Jupiter.

P	16.2 ± 0.3	days
K	119.9 ± 9.8	m s^{-1}
e	0.25 ± 0.05	
ω	219.8 ± 1.8	degrees
JD_0 − 2,450,000	5,109.78 ± 0.02	days
χ^2	32.35	m s^{-1}
rms	50.86	m s^{-1}
$m_2 \sin i$	1.25 ± 0.05	M_{Jup}
a	0.116 ± 0.01	AU

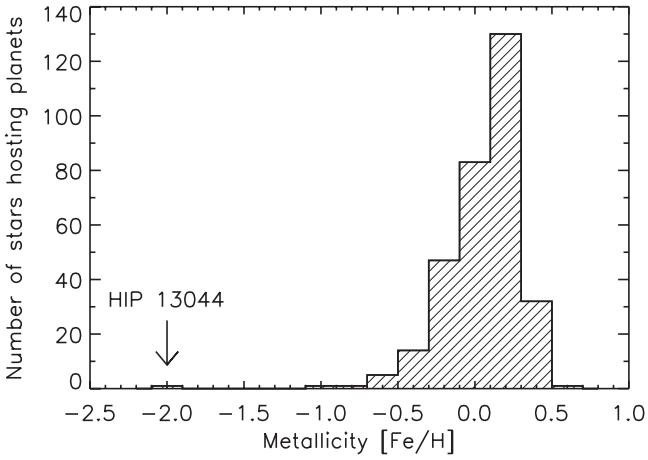

Fig. 3. Distribution of the metallicity [Fe/H] of planet-hosting stars.

atmosphere expanded during the giant phase. The survival of HIP 13044 b during that phase is theoretically possible under certain circumstances (*22*, *39*, *40*). It is also possible that the planet's orbit decayed through tidal interaction with the stellar envelope. However, a prerequisite to survival is then that the mass loss of the star stops before the planet would have been evaporated or accreted. Assuming asymmetric mass loss, velocity kicks could have increased the eccentricity of HIP 13044 b to its current, somewhat high value (*41*). The same could be achieved by interaction with a third body in the system.

A survey to characterize the multiplicity of EHB stars showed that more than 60% of the sample are close binaries (*42*). Their orbital radii are much smaller than the stellar radius in the RGB phase. This could be explained by the high friction in the interstellar medium, which would move a distant companion toward the primary. Such a spiral-in mechanism could also take place in the RGB-to-RHB transition phase. Similar to the binary case, a distant giant planet in the RGB phase can move toward the primary into a smaller orbit. Consequently, the resulting close orbiting planets will be engulfed when the stellar envelope expands again in the next giant phase. HIP 13044 b could be a planet that is just about to be engulfed by its star.

HIP 13044, with a mean metallicity estimate of [Fe/H] = −2.1, is far more metal-poor than any known exoplanet-hosting star (Fig. 3). For the existing theories of hot giant planet formation, metallicity is an important parameter; in particular, it is fundamental for the core-accretion planet formation model (*43*). It might be that initially, in the planet-formation phase, HIP 13044 had a higher metallicity, and that during its subsequent evolution, it lost its heavier elements. For example, during the giant phase, heavy elements could have had been incorporated into dust grains and then separated from the star's atmosphere (*44*). However, given the star's membership in the Helmi stream, in which the most metal-rich subdwarfs known so far have [Fe/H] ~ −1.5 (*45*), we do not expect its initial Fe abundance to exceed this value.

Finally, as a member of the Helmi stream, HIP 13044 most probably has an extragalactic origin. This implies that its history is likely different from those of most known planet-hosting stars. HIP 13044 was probably attracted to the Milky Way several billion years ago. Before that, it could have belonged to a satellite galaxy of the Milky Way similar to Fornax or the Sagittarius dwarf spheroidal galaxy (*14*). Because of the long galactic relaxation time scale, it is extremely unlikely that HIP 13044 b joined its host star through exchange with some Milky Way star, after the former had been tidally stripped. The planet HIP 13044 b could thus have a non-Galactic origin.

References and Notes

1. G. Gonzalez, *Mon. Not. R. Astron. Soc.* **285**, 403 (1997).
2. N. C. Santos, G. Israelian, M. Mayor, *Astron. Astrophys.* **415**, 1153 (2004).
3. J. A. Valenti, D. A. Fischer, *Astrophys. J.* **159** (suppl.), 141 (2005).
4. A. Sozzetti *et al.*, *Astrophys. J.* **697**, 544 (2009).
5. E. B. Ford, K. J. Joshi, F. A. Rasio, B. Zbarsky, *Astrophys. J.* **528**, 336 (2000).
6. S. Sigurdsson, H. B. Richer, B. M. Hansen, I. H. Stairs, S. E. Thorsett, *Science* **301**, 193 (2003).
7. M. E. Beer, A. R. King, J. E. Pringle, *Mon. Not. R. Astron. Soc.* **355**, 1244 (2004).
8. The observations of HIP 13044 were carried out from September 2009 to July 2010. The spectrograph covers a wavelength range from 350 to 920 nm (*48*). To measure the RV values of HIP 13044, we used a cross-correlation technique, in which the stellar spectrum is cross-correlated with a numerical template (mask) designed for stars of the spectral type F0 (SOM text 2).
9. T. C. Beers, J. A. Kage, G. W. Preston, S. A. Shectman, *Astron. J.* **100**, 849 (1990).
10. M. Chiba, T. C. Beers, *Astron. J.* **119**, 2843 (2000).
11. B. W. Carney *et al.*, *Astron. J.* **135**, 892 (2008).
12. I. U. Roederer, C. Sneden, I. B. Thompson, G. W. Preston, S. A. Shectman, *Astrophys. J.* **711**, 573 (2010).
13. B. W. Carney, D. W. Latham, *Astron. J.* **92**, 60 (1986).
14. A. Helmi, S. D. M. White, P. T. de Zeeuw, H. Zhao, *Nature* **402**, 53 (1999).
15. A. A. Kepley *et al.*, *Astron. J.* **134**, 1579 (2007).
16. To search for periodic variations, we used periodogram analysis techniques, which can treat missing values and unevenly spaced time points.
17. M. Zechmeister, M. Kürster, *Astron. Astrophys.* **496**, 577 (2009).
18. P. C. Gregory, *Bayesian Logical Data Analysis for the Physical Sciences: A Comparative Approach with 'Mathematica' Support* (Cambridge Univ. Press, Cambridge, UK, 2005).
19. D. F. Gray, B. W. Carney, D. Yong, *Astron. J.* **135**, 2033 (2008).
20. A. P. Hatzes, *Publ. Astron. Soc. Pac.* **108**, 839 (1996).
21. B. W. Carney, D. W. Latham, R. P. Stefanik, J. B. Laird, *Astron. J.* **135**, 196 (2008).
22. N. Soker, *Astron. J.* **116**, 1308 (1998).
23. B. Levrard, C. Winisdoerffer, G. Chabrier, *Astrophys. J.* **692**, L9 (2009).
24. J. K. Carlberg, S. R. Majewski, P. Arras, *Astrophys. J.* **700**, 832 (2009).
25. B. W. Carney, D. W. Latham, R. P. Stefanik, J. B. Laird, J. A. Morse, *Astron. J.* **125**, 293 (2003).
26. M. A. C. Perryman, European Space Agency, Eds., *The Hipparcos and Tycho Catalogues. Astrometric and Photometric Star Catalogues Derived from the ESA Hipparcos Space Astrometry Mission*, ESA Spec. Publ. Ser. 1200 (Noordwijk, Netherlands, 1997).
27. D. L. Pollacco *et al.*, *Publ. Astron. Soc. Pac.* **118**, 1407 (2006).
28. D. R. Xiong, Q. L. Cheng, L. Deng, *Astrophys. J.* **500**, 449 (1998).
29. D. Stello, R. L. Gilliland, *Astrophys. J.* **700**, 949 (2009).
30. E. Shkolnik, D. A. Bohlender, G. A. H. Walker, A. Collier Cameron, *Astrophys. J.* **676**, 628 (2008).
31. R. Silvotti *et al.*, *Nature* **449**, 189 (2007).
32. J. W. Lee *et al.*, *Astron. J.* **137**, 3181 (2009).
33. S. Geier, H. Edelmann, U. Heber, L. Morales-Rueda, *Astrophys. J.* **702**, L96 (2009).
34. G. A. H. Walker *et al.*, *Astrophys. J.* **396**, L91 (1992).
35. A. P. Hatzes, W. D. Cochran, *Astrophys. J.* **413**, 339 (1993).
36. J. Setiawan *et al.*, *Astron. Astrophys.* **421**, 241 (2004).
37. M. P. Döllinger *et al.*, *Astron. Astrophys.* **472**, 649 (2007).
38. J. A. Johnson *et al.*, *Publ. Astron. Soc. Pac.* **122**, 701 (2010).
39. M. Livio, N. Soker, *Astron. Astrophys.* **125**, L12 (1983).
40. E. Bear, N. Soker, http://arxiv.org/abs/1003.4884 (2010).
41. J. Heyl, *Mon. Not. R. Astron. Soc.* **382**, 915 (2007).
42. P. L. Maxted, U. Heber, T. R. Marsh, R. C. North, *Mon. Not. R. Astron. Soc.* **326**, 1391 (2001).
43. S. Ida, D. N. C. Lin, *Prog. Theor. Phys.* **158** (suppl.), 68 (2005).
44. J. S. Mathis, H. J. G. L. M. Lamers, *Astron. Astrophys.* **259**, L39 (1992).
45. R. Klement *et al.*, *Astrophys. J.* **698**, 865 (2009).
46. R. Buonanno *et al.*, *Astron. Astrophys.* **290**, 69 (1994).
47. W. E. Harris, *Astron. J.* **112**, 1487 (1996).
48. A. Kaufer *et al.*, in *Society of Photo-Optical Instrumentation Engineers* (*SPIE*) *Conference Series*, M. Iye, A. F. Moorwood, Eds., SPIE Conf. Ser. 4008, pp. 459–466.

49. We thank our colleagues at Max-Planck-Institut für Astronomie: W. Wang, C. Brasseur, R. Lachaume, M. Zechmeister, and D. Fedele for the spectroscopic observations with FEROS. We also thank M. Perryman, E. Bear, N. Soker, and P. Maxted for discussion, comments, and suggestions that improved this paper.

Supporting Online Material

www.sciencemag.org/cgi/content/full/science.1193342/DC1
SOM Text
Figs. S1 to S6
Tables S1 and S2
References

7 June 2010; accepted 10 November 2010
Published online 18 November 2010;
10.1126/science.1193342

Experimental Spin Ratchet

Marius V. Costache[1] and Sergio O. Valenzuela[1,2,3]*

Spintronics relies on the ability to transport and use the spin properties of an electron rather than its charge. We describe a spin ratchet at the single-electron level that produces spin currents with no net bias or charge transport. Our device is based on the ground-state energetics of a single-electron transistor comprising a superconducting island connected to normal leads via tunnel barriers with different resistances that break spatial symmetry. We demonstrate spin transport and quantify the spin ratchet efficiency by using ferromagnetic leads with known spin polarization. Our results are modeled theoretically and provide a robust route to the generation and manipulation of pure spin currents.

Brownian motors or ratchets refer to directed transport in the presence of a signal or perturbation that drives the system without an obvious bias in any preferred direction of motion. The perturbation generates useful work, for instance, the transport of particles, when combined with asymmetry, often realized by a so-called ratchet potential (Fig. 1A) (*1*–*3*). Experimental realizations of ratchets are spread over many different fields of biology, chemistry, and physics, where the perturbation may be external to the system (e.g., induced by an experimentalist) or intrinsic to it (e.g., nonthermal noise). In mesoscopic structures, experiments have demonstrated ratchets in both the quantum and classical limits (*4*–*6*). On such small scales, noise rectification with ratchets can be used to control particle transport and has become one of the most promising techniques for powering nanodevices (*3*).

Because of the growing interest in the spin degree of freedom as a carrier of information (*7*) as well as a means to address fundamental properties of quantum mechanics and quantum computation (*8*), a variety of ratchets have been proposed in pursuit of unidirectional spin currents and spin control (*9*–*12*). A pure spin ratchet (*11*) generalizes the particle ratchet mechanism (*1*–*3*), enabling pure spin currents by means of broken spatial symmetry (*9*–*12*). Thus, an indispensable hallmark for a spin ratchet is the breaking of the inversion symmetry for spin but not charge (*11*), whereby the ratchet-potential easy direction for one spin orientation is opposite to the ratchet-potential easy direction for the other spin orientation (Fig. 1A). Recent theoretical efforts use mesoscopic semiconductors and nonuniform magnetic fields (*9*), asymmetric periodic structures with Rashba spin-orbit interaction (*10*), and double-well structures combined with local external magnetic fields and resonant tunneling (*12*).

The concept of our spin ratchet is different from what has been proposed before. A small-volume superconducting (S) island is connected via tunnel junctions with two normal metal electrodes [N(l) and N(r)] to form an asymmetric single-electron transistor (SET) with different tunneling resistances (Fig. 1B). A voltage V applied across the SET drives the system, whereas a voltage on the back gate V_g sets the induced gate charge $Q = V_g C_g$ on the island, with C_g the capacitive coupling between the island and the gate.

At low temperatures, parity effects in the superconducting island are important (*13*–*16*). When the number of conduction electrons n is odd, there is necessarily one unpaired electron that is manifest as a quasiparticle excitation (*13*, *17*). The ground state energy of the system for odd n is higher than for even n by the superconducting gap Δ, which in our design is larger than the charging energy, E_c (Fig. 1C). In order to break the symmetry between spin-up and spin-down transport, a magnetic field B is applied in-plane along the axis of the electrodes [spin up refers to spins parallel to B, whereas spin down refers to spins antiparallel to B]. This field splits the quasiparticle levels (e.g., $n = 1^{\downarrow}$ and $n = 1^{\uparrow}$) by the Zeeman energy $E_Z = g\mu_B B$, where g is the g factor of the superconductor and μ_B the Bohr magneton, but it does not affect the Cooper-pair states (e.g., $n = 0$ and $n = 2$), which are singlet states, and it weakly reduces Δ because orbital depairing is minimized by an in-plane B (*18*) (Fig. 1, D and E). The $n = 1^{\downarrow}$ state shifts down continuously with increasing B and, at $B_{SR} = 2(\Delta - E_c)/(g\mu_B)$

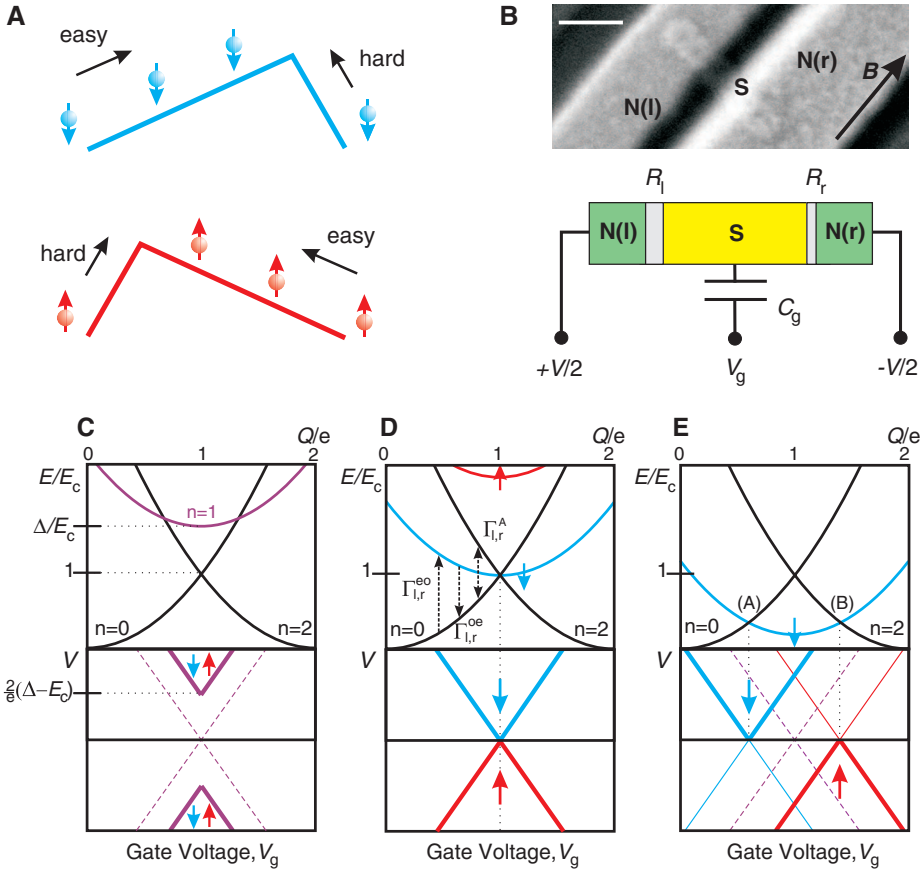

Fig. 1. SET spin ratchet. (**A**) In the presence of a ratchet potential and a driving force without a preferential direction, spin-down and spin-up electrons can be forced to move in opposite directions, giving rise to a spin current. (**B**) Scanning electron microscope image of an SET spin ratchet. A small-volume superconducting (S) island is contacted with two metal electrodes [N(l) and N(r)] via tunnel junctions with different tunnel resistances, $R_l > R_r$. The bar is 100 nm long. A voltage V is applied across the electrodes, and a voltage V_g on the back gate. (**C** to **E**) SET energetics of Cooper-pair and quasi-particle states (top) and associated below-gap voltage thresholds (bottom) for single- and two-electron transport at low temperatures for $B = 0$ (C), $B = B_{SR}$ (D) and $B > B_{SR}$ (E). Dashed and solid lines represent the positions of the Andreev and quasi-particle conductance thresholds, respectively.

[1]Institut Català de Nanotecnologia (ICN), Centre d'Investigació en Nanociència i Nanotecnologia (CIN2), Campus Universitat Autònoma de Barcelona, Bellaterra, Barcelona E-08913, Spain. [2]Institució Catalana de Recerca i Estudis Avançats (ICREA), Barcelona E-08010, Spain. [3]Department of Physics, Harvard University, Cambridge, MA 02138, USA.

*To whom correspondence should be addressed. E-mail: SOV@icrea.cat

(Fig. 1D), it becomes degenerate with both the zero ($n = 0$) and the one ($n = 2$) excess Cooper-pair states for $Q/e = 1$ (e is the electron charge).

The spin ratchet effect occurs at $B = B_{SR}$. Insight into the underlying mechanism can be gained by analyzing the relevant charge transport processes and their occurrence rates. Single-electron tunneling processes in the l and r junctions cause transitions between even (e) $n = 0,2$ and odd (o) $n = 1^{\downarrow}$ states with rates $\Gamma^{oe}_{l,r}$ and $\Gamma^{eo}_{l,r}$, whereas two-electron Andreev processes cause transitions between even $n = 0$ and $n = 2$ states with rates $\Gamma^{A}_{l,r}$ (Fig. 1D). For a spin ratchet, the rate hierarchy $\Gamma^{A}_{l,r} \ll \Gamma^{oe}_{l} < \Gamma^{oe}_{r} \ll \Gamma^{eo}_{l,r}$ is required, where the l junction transparency is chosen to be smaller than that of the r junction. There, driving single-particle cycles (subsequent addition and removal of an electron from the SET island) results in a net spin current into one preferred direction in the following manner. A cycle that only uses transitions between $n = 0$ and $n = 1^{\downarrow}$ (cycle 01) only transports spin-down electrons through the SET, whereas a cycle that only uses transitions between $n = 2$ and $n = 1^{\downarrow}$ (cycle 21) only transports spin-up electrons. The essential ingredient to the spin ratchet mechanism is that, for $\Gamma^{oe}_{l} < \Gamma^{oe}_{r}$, cycle 01 dominates at positive V, whereas cycle 21 dominates at negative V. Hence, in both cases there is a net spin-up current from, say, left to right through the SET. Because the charge transferred is null in average when a voltage V with zero mean is applied, the SET spin ratchet generates spin currents with no charge transport (*19*).

The thresholds for single- and two-electron Andreev events in an SET fulfilling the above rate hierarchy are shown schematically in Fig. 1, C, D, and E. At $B = 0$, single-electron transport sets in only for $V > 2(\Delta - E_c)/e$, when the odd state is reached ($Q/e = 1$). When B is applied, the Andreev and quasi-particle thresholds become closer, and, at B_{SR}, they coincide. There, single electron transport is possible even at $V \sim 0$, and the spin ratchet is effective for an unbiased V, where the spin orientation of moving electrons changes sign at $V = 0$. For larger B, the ground state energetics of the SET fully separates cycles 01 and 21 around the degeneracy points (A) and (B) (*18*). There, the asymmetric SET acts as a diode that resolves spin (*19*).

We have realized the proposed SET spin ratchet by using electron-beam lithography and shadow evaporation techniques (*20*). The small (6 nm thick by 40 nm wide by 250 nm long) superconducting island is made from aluminum, which is oxidized and contacted with two metal leads. Sequential deposition of the leads from two different angles allowed us to generate distinct tunneling resistances in the junctions (*19*). We verified the spin-ratchet mechanism in Fig. 1 by means of ferromagnetic (F) leads made of CoFe that were used as spin detectors (FSF device). The spin polarization sign change at $V = 0$ is preserved, as when using normal leads, but the effective polarization of the

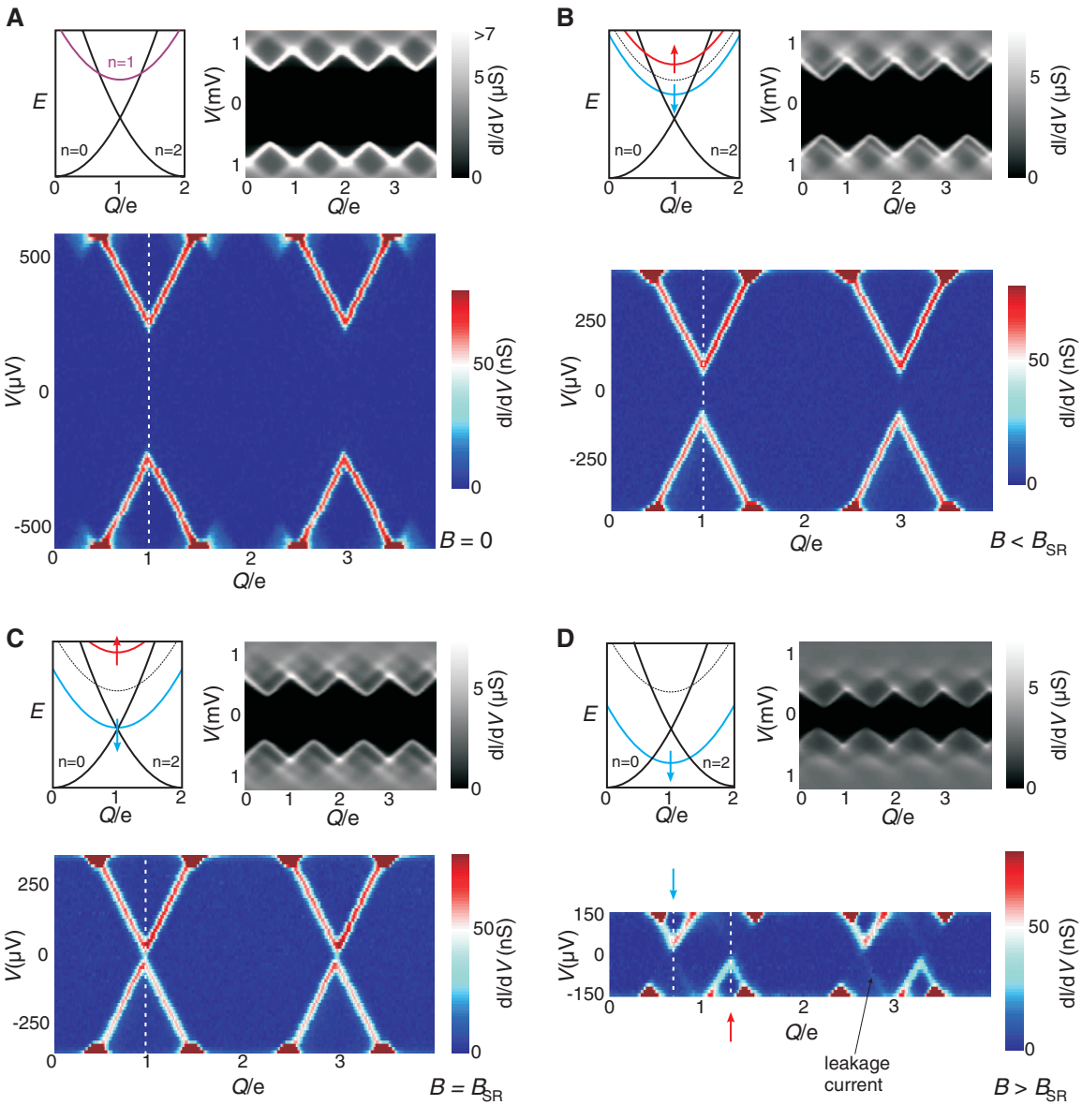

Fig. 2. Spin transport regimes in an applied magnetic field and characteristics of an SET spin ratchet. (**A**) $B = 0$. (**B**) $B = 1$ T. (**C**) $B = 1.5$ T. (**D**) $B = 2.5$ T. The top images represent the SET energetics of Copper-pair and quasi-particle states at the associated B (left) and show the above-gap response dI/dV versus V_g, which sets Q/e, and bias V (right). The bottom images show the below-gap transport in the SET (black area in the above-gap dI/dV plots), that is, dI/dV versus V_g, and bias V.

leads, P_F, measures the relative contribution of cycles 01 and 21. For a quantitative measurement of the spin-ratchet efficiency, we independently determined P_F. We accomplished this by using similarly fabricated junctions embedded in nonlocal spin devices, for which we obtained $P_F \sim 0.28$ (*20*, *21*).

The electron transport properties of such an FSF SET were fully characterized by means of differential conductance dI/dV measurements at above-gap voltage bias, from which we estimated $\Gamma_l^{oe} \approx 8 \times 10^6\ s^{-1} < \Gamma_r^{oe} \approx 4 \times 10^7\ s^{-1} << \Gamma_{l,r}^{eo} \approx 5 \times 10^9\ s^{-1}$ (*19*). Figure 2 shows the evolution of dI/dV as a function of the magnetic field at below-gap bias for this device. At $B = 0$, we observe a symmetric response about $V = 0$ (Fig. 2A). There, dI/dV is zero within the sensitivity of our measurements for voltage magnitudes below the gap, except at the quasi-particle thresholds, where it presents a peak whose intensity is nearly independent of V and V_g (*22*). The below-gap quasi-particle thresholds cross at about $V_0 = 259\ \mu V$ (Fig. 2A). This is in agreement with $V_0 \sim 2(\Delta - E_c)/e$ (Fig. 1C) when using $E_c = 170\ \mu eV$ and $\Delta \approx 303\ \mu eV$ as obtained from the above-gap thresholds [fig. S2 (*19*)]. At $B = 1$ T, V_0 decreases to 94 μV because of E_Z. At $B = 1.5$ T, V_0 becomes zero and the SET is in the pure spin ratchet regime (Fig. 1D) (*23*).

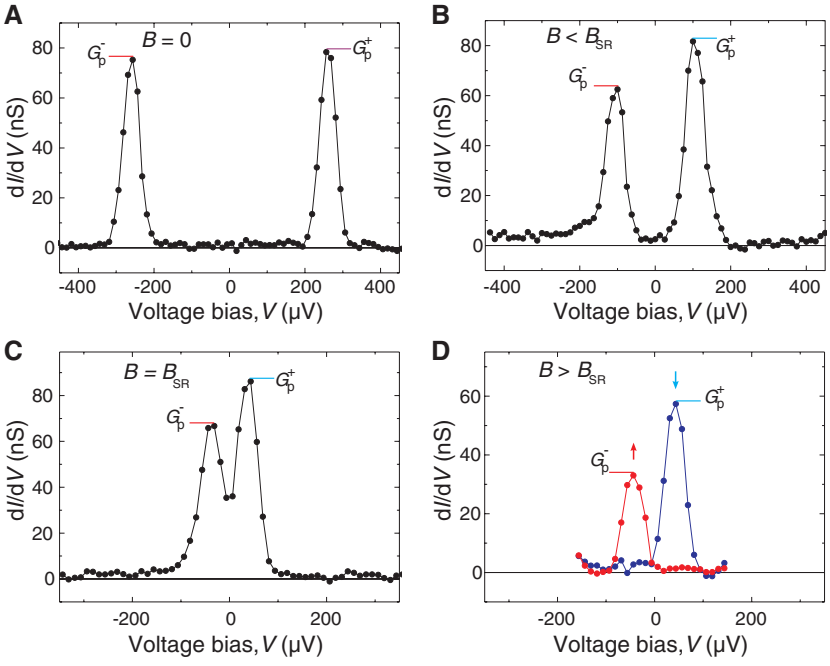

Fig. 3. Spin filtering. (**A**) $B = 0$. (**B**) $B = 1$ T. (**C**) $B = 1.5$ T. (**D**) $B = 2.5$ T. Differential conductance dI/dV versus V cross sections along the dotted white lines in Fig. 3. In (D), the red and blue curves are cross sections along the white lines indicated with red and blue, respectively, arrows in Fig. 2D.

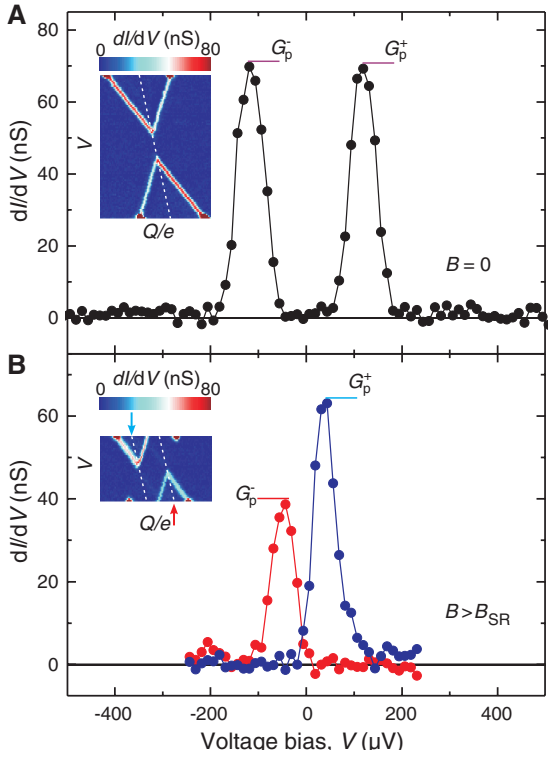

Fig. 4. Spin-filtering detection using an NSF sample. (**A**) $B = 0$. (**B**) $B = 2$ T. (Insets) dI/dV versus Q/e and bias V. The dI/dV versus V cross sections (main graphs) are taken along the corresponding dotted lines in the insets.

Of key importance, the differential conductance at $B \neq 0$ (Fig. 2, B and C) is no longer symmetric about $V = 0$, presenting a larger magnitude for $V > 0$ than for $V < 0$ along the below-gap quasi-particle thresholds. This observation is consistent with the description in Fig. 1 and represents an experimental confirmation of the spin ratchet effect. Indeed, the asymmetry results from P_F and the fact that the current across the SET for positive and negative V has opposite spin polarization. The leads are always magnetized parallel to each other along the B direction and, because $P_F > 0$, they favor the dominant spin-down current cycle 01 at $V > 0$ and hinder the dominant spin-up current cycle 21 at $V < 0$. We quantify such a transport asymmetry by using the parameter $\beta = (G_p^+ - G_p^-)/(G_p^+ + G_p^-)$, where $G_p^+ = dI/dV\rfloor_{peak}$ $(V > 0)$ and $G_p^- = dI/dV\rfloor_{peak}$ $(V < 0)$ are the values of the peak conductances along the dotted white lines in Fig. 2. At $B = 0$ (Figs. 2A and 3A), β is zero within the sensitivity of our measurements, as expected. At $B = 1$ T and $B = 1.5$ T (Fig. 2, B and C, and Fig. 3, B and C), the difference between G_p^+ and G_p^- becomes apparent, resulting in $\beta \sim 0.14$ in both cases.

We define the spin-ratchet efficiency η_{SET} as equal to the spin-filtering capability $\eta_{SET} \approx (1 - \alpha)/(1 + \alpha)$ of our device, where the ratio $\alpha = \Gamma_l^{oe}/\Gamma_r^{oe} \approx R_r/R_l$ measures the asymmetry of the SET and $R_{l,r}$ are the associated normal tunnel resistance of junctions l and r (Fig. 1B). For $\alpha \sim 0$, nearly perfect filtering, that is, $\eta_{SET} \sim 1$, is achieved. In such a scenario, β directly measures the effective polarization of the leads; that is, $\beta = P_F = 0.28$. For $\alpha > 0$, a decrease in filtering efficiency is expected, and therefore β should decrease accordingly as $\beta \approx \eta_{SET} P_F$. For our device, $R_l \approx 350\ k\Omega$ and $R_r \approx 70\ k\Omega$ and $\alpha \sim 0.2$. We thus estimate $\eta_{SET} \sim 0.67$ and $\beta \approx \eta_{SET} P_F \sim 0.19$, a value that is somewhat larger than that obtained with our measurements ($\beta \sim 0.14$), which results in $\eta_{SET} \approx 0.5$. This discrepancy could be related to the uncertainty in the estimation of $R_{l,r}$ or to Andreev reflections in one of the junctions, which could contribute an unpolarized component to the total current.

At magnetic fields $B > B_{SR}$, where the spin-up and spin-down quasi-particle thresholds are resolved, the SET behaves as a diode that filters spin-up or spin-down quasi-particles (Figs. 2D and 3D). Namely, the current should be polarized

fully spin-down for V_g about the degeneracy point (A) and fully spin-up for V_g about the degeneracy point (B) in Fig. 1E. Accordingly, we calculate β from the conductance peaks along the two dotted lines in Fig. 2D, obtaining β ~ 0.26, which is close to P_F ~ 0.28 and indicates a filtering efficiency larger than 0.9.

Lastly, we stress that the spin-ratchet effect is related to quasi-particle tunneling through the high-transparency junction (*22*). To further show this, we fabricated normal super conductor ferromagnet (NSF) devices with the normal metal lead made of Cu connected to the low-transparency junction. Here, $R_l \approx 650$ kΩ and $R_r \approx 70$ kΩ. Because the high-transparency tunnel barrier connected to the ferromagnetic lead controls the transport, β should remain close to P_F, when calculated as in Fig. 3D. Moreover, because R_r in this device is estimated to be of the same order of magnitude as that of the FSF device, the conductance peaks should not be substantially affected. Both these observations agree with the experimental *dI*/*dV* results shown in Fig. 4. At $B = 0$ (Fig. 4A), β is again zero within the sensitivity of our measurements and, at $B > B_{SR}$ (Fig. 4B), β ~ 0.25 ~ P_F, whereas the magnitudes of the conductance peaks compare well with those shown in Fig. 3.

Spin ratchets represent a fundamentally new approach for spin current generation and detection; thus, our research paves the way for a new means to study spin-related phenomena. Because the spin ratchets presented here work at the single-electron level, they can, for example, be used to initialize and read out the state of spin-based quantum bits (*8*) or to identify the spin orientation of single electrons in a test of the Einstein-Podolsky-Rosen paradox (*24*) with spin-entangled electrons (*25*–*29*).

References and Notes

1. P. Hänggi, F. Marchesoni, F. Nori, *Ann. Phys.* **14**, 51 (2005).
2. P. Reimann, *Phys. Rep.* **361**, 57 (2002).
3. P. Hänggi, F. Marchesoni, *Rev. Mod. Phys.* **81**, 387 (2009).
4. A. M. Song *et al.*, *Phys. Rev. Lett.* **80**, 3831 (1998).
5. H. Linke *et al.*, *Science* **286**, 2314 (1999).
6. J. E. Villegas *et al.*, *Science* **302**, 1188 (2003).
7. I. Žutić, J. Fabian, S. Das Sarma, *Rev. Mod. Phys.* **76**, 323 (2004).
8. D. D. Awschalom, D. Loss, N. Samarth, *Semiconductor Spintronics and Quantum Computation* (Springer-Verlag, Berlin, 2002).
9. M. Scheid, D. Bercioux, K. Richter, *N. J. Phys.* **9**, 401 (2007).
10. S. Smirnov, D. Bercioux, M. Grifoni, K. Richter, *Phys. Rev. Lett.* **100**, 230601 (2008).
11. M. E. Flatté, *Nat. Phys.* **4**, 587 (2008).
12. M. Scheid, A. Lassl, K. Richter, *EPL* **87**, 17001 (2009).
13. D. V. Averin, Y. V. Nazarov, *Phys. Rev. Lett.* **69**, 1993 (1992).
14. M. T. Tuominen, J. M. Hergenrother, T. S. Tighe, M. Tinkham, *Phys. Rev. Lett.* **69**, 1997 (1992).
15. T. M. Eiles, J. M. Martinis, M. H. Devoret, *Phys. Rev. Lett.* **70**, 1862 (1993).
16. F. W. J. Hekking, L. I. Glazman, K. A. Matveev, R. I. Shekhter, *Phys. Rev. Lett.* **70**, 4138 (1993).
17. G. Schön, in *Quantum Transport and Dissipation*, T. Dittrich *et al.*, Eds. (Wiley, Weinheim, Germany, 1998), chap. 3.
18. A. J. Ferguson, S. E. Andresen, R. Brenner, R. G. Clark, *Phys. Rev. Lett.* **97**, 086602 (2006).
19. Materials and methods are available as supporting material on *Science* Online.
20. S. O. Valenzuela, M. Tinkham, *Nature* **442**, 176 (2006).
21. S. O. Valenzuela, *Int. J. Mod. Phys. B* **23**, 2413 (2009).
22. A zero *dI*/*dV* below the quasi-particle thresholds suggests that the Andreev cycle (Fig. 1C) and cotunneling processes (*13*) are suppressed. Integration of *dI*/*dV* results in a current plateau I_p ~ 5.8 pA beyond the thresholds. Because the current is limited by Γ_r^{oe}, $I_p \approx e\Gamma_r^{oe}$ ~ 5 pA, which is in reasonable agreement with the measured value. This indicates that transport is dominated by tunneling events in the r junction.
23. The decrease in V_0 with increasing B is larger than expected if only E_Z is considered; in which case, the ratchet effect should occur at $B_{SR} \approx 2.3$ T. This is due to a reduction of Δ by residual orbital depairing. When such a reduction is considered, $\Delta(1\text{ T}) = 272$ μeV, $V_0(1\text{ T}) = 2[\Delta(1\text{ T}) - E_c]/e - E_Z/e \approx 88$ μV is close to the measured value. Moreover, considering $\Delta(1.5\text{ T}) = 256$ μeV, we estimate $B_{SR} = [\Delta(1.5\text{ T}) - E_c]/(g\mu_B) \approx 1.48$ T, in agreement with the observed result.
24. A. Einstein, B. Podolsky, N. Rosen, *Phys. Rev.* **47**, 777 (1935).
25. C. Bena, S. Vishveshwara, L. Balents, M. P. A. Fisher, *Phys. Rev. Lett.* **89**, 037901 (2002).
26. D. S. Saraga, D. Loss, *Phys. Rev. Lett.* **90**, 166803 (2003).
27. L. Hofstetter, S. Csonka, J. Nygård, C. Schönenberger, *Nature* **461**, 960 (2009).
28. P. Cadden-Zimansky, J. Wei, V. Chandrasekhar, *Nat. Phys.* **5**, 393 (2009).
29. L. G. Herrmann *et al.*, *Phys. Rev. Lett.* **104**, 026801 (2010).

30. We gratefully acknowledge discussions with and support from M. Tinkham and thank I. Žutić and Y. Tserkovnyak for discussions and W. D. Oliver, P. Gambardella, and A. Bachtold for a critical reading of the manuscript. This research was supported in part by the Spanish Ministerio de Ciencia e Innovación (MAT2010-18065, FIS2009-06671-E). Samples were made at the Center for Nanoscale Systems, Harvard University.

Supporting Online Material

www.sciencemag.org/cgi/content/full/330/6011/1645/DC1
Materials and Methods
SOM Text
Figs. S1 to S3
References

9 August 2010; accepted 9 November 2010
10.1126/science.1196228

Spin Transfer Torques in MnSi at Ultralow Current Densities

F. Jonietz,[1] S. Mühlbauer,[1,2] C. Pfleiderer,[1]* A. Neubauer,[1] W. Münzer,[1] A. Bauer,[1] T. Adams,[1] R. Georgii,[1,2] P. Böni,[1] R. A. Duine,[3] K. Everschor,[4] M. Garst,[4] A. Rosch[4]

Spin manipulation using electric currents is one of the most promising directions in the field of spintronics. We used neutron scattering to observe the influence of an electric current on the magnetic structure in a bulk material. In the skyrmion lattice of manganese silicon, where the spins form a lattice of magnetic vortices similar to the vortex lattice in type II superconductors, we observe the rotation of the diffraction pattern in response to currents that are over five orders of magnitude smaller than those typically applied in experimental studies on current-driven magnetization dynamics in nanostructures. We attribute our observations to an extremely efficient coupling of inhomogeneous spin currents to topologically stable knots in spin structures.

The discovery of the effect of giant magnetoresistance, now used commercially in the hard disk drive industry, is widely recognized as the starting point of the field of spintronics. It represents the first example of electric currents controlled efficiently by spin structures. The complementary process of so-called spin transfer torques, where magnetic structures and textures are manipulated by electric currents (*1*, *2*), appears to be even more promising. For instance, strong current pulses allow the movement of ferromagnetic domain walls (*3*, *4*), the switching of magnetic domains in multilayer devices (*5*, *6*), the induction of microwave oscillations in nanomagnets (*7*), and the switching of ferromagnetic semiconductor structures (*8*). However, the typical current densities required to create observable spin transfer torques in present-day studies exceed 10^{11} A m^{-2}. Because this implies extreme ohmic heating, it was generally believed that spin torque effects can be studied exclusively in nanostructures. We report the observation of spin transfer torques in a bulk material, the skyrmion lattice phase of MnSi. The spin transfer torques appear when the current density exceeds an ultralow threshold of ~10^6 A m^{-2}, five orders of magnitude smaller than those used typically in experimental studies on current-driven magnetization dynamics in ferromagnetic metals and semiconductors.

The skyrmion lattice in chiral magnets, like MnSi and related B20 compounds, was only recently discovered in neutron-scattering studies (*9*–*12*) and confirmed to exist in Lorentz force microscopy for $Fe_{1-x}Co_xSi$ (x = 0.5) (*13*). It represents a new form of magnetic order that may be viewed as a crystallization of topologically stable knots of the spin structure that shares remarkable similarities with the mixed state in type II superconductors. For zero magnetic field (Fig. 1A), helimagnetic order appears in MnSi below the critical temperature T_c = 29.5 K.

[1]Physik-Department E21, Technische Universität München, D-85748 Garching, Germany. [2]Forschungsneutronenquelle Heinz Maier-Leibnitz (FRM II), Technische Universität München, D-85748 Garching, Germany. [3]Institute for Theoretical Physics, Utrecht University, 3584 CE Utrecht, Netherlands. [4]Institute of Theoretical Physics, University of Cologne, D-50937 Cologne, Germany.

*To whom correspondence should be addressed. E-mail: christian.pfleiderer@frm2.tum.de

fully spin-down for V_g about the degeneracy point (A) and fully spin-up for V_g about the degeneracy point (B) in Fig. 1E. Accordingly, we calculate β from the conductance peaks along the two dotted lines in Fig. 2D, obtaining β ~ 0.26, which is close to P_F ~ 0.28 and indicates a filtering efficiency larger than 0.9.

Lastly, we stress that the spin-ratchet effect is related to quasi-particle tunneling through the high-transparency junction (*22*). To further show this, we fabricated normal super conductor ferromagnet (NSF) devices with the normal metal lead made of Cu connected to the low-transparency junction. Here, $R_l \approx 650$ kΩ and $R_r \approx 70$ kΩ. Because the high-transparency tunnel barrier connected to the ferromagnetic lead controls the transport, β should remain close to P_F, when calculated as in Fig. 3D. Moreover, because R_r in this device is estimated to be of the same order of magnitude as that of the FSF device, the conductance peaks should not be substantially affected. Both these observations agree with the experimental *dI*/*dV* results shown in Fig. 4. At $B = 0$ (Fig. 4A), β is again zero within the sensitivity of our measurements and, at $B > B_{SR}$ (Fig. 4B), β ~ 0.25 ~ P_F, whereas the magnitudes of the conductance peaks compare well with those shown in Fig. 3.

Spin ratchets represent a fundamentally new approach for spin current generation and detection; thus, our research paves the way for a new means to study spin-related phenomena. Because the spin ratchets presented here work at the single-electron level, they can, for example, be used to initialize and read out the state of spin-based quantum bits (*8*) or to identify the spin orientation of single electrons in a test of the Einstein-Podolsky-Rosen paradox (*24*) with spin-entangled electrons (*25*–*29*).

References and Notes

1. P. Hänggi, F. Marchesoni, F. Nori, *Ann. Phys.* **14**, 51 (2005).
2. P. Reimann, *Phys. Rep.* **361**, 57 (2002).
3. P. Hänggi, F. Marchesoni, *Rev. Mod. Phys.* **81**, 387 (2009).
4. A. M. Song *et al.*, *Phys. Rev. Lett.* **80**, 3831 (1998).
5. H. Linke *et al.*, *Science* **286**, 2314 (1999).
6. J. E. Villegas *et al.*, *Science* **302**, 1188 (2003).
7. I. Žutić, J. Fabian, S. Das Sarma, *Rev. Mod. Phys.* **76**, 323 (2004).
8. D. D. Awschalom, D. Loss, N. Samarth, *Semiconductor Spintronics and Quantum Computation* (Springer-Verlag, Berlin, 2002).
9. M. Scheid, D. Bercioux, K. Richter, *N. J. Phys.* **9**, 401 (2007).
10. S. Smirnov, D. Bercioux, M. Grifoni, K. Richter, *Phys. Rev. Lett.* **100**, 230601 (2008).
11. M. E. Flatté, *Nat. Phys.* **4**, 587 (2008).
12. M. Scheid, A. Lassl, K. Richter, *EPL* **87**, 17001 (2009).
13. D. V. Averin, Y. V. Nazarov, *Phys. Rev. Lett.* **69**, 1993 (1992).
14. M. T. Tuominen, J. M. Hergenrother, T. S. Tighe, M. Tinkham, *Phys. Rev. Lett.* **69**, 1997 (1992).
15. T. M. Eiles, J. M. Martinis, M. H. Devoret, *Phys. Rev. Lett.* **70**, 1862 (1993).
16. F. W. J. Hekking, L. I. Glazman, K. A. Matveev, R. I. Shekhter, *Phys. Rev. Lett.* **70**, 4138 (1993).
17. G. Schön, in *Quantum Transport and Dissipation*, T. Dittrich *et al.*, Eds. (Wiley, Weinheim, Germany, 1998), chap. 3.
18. A. J. Ferguson, S. E. Andresen, R. Brenner, R. G. Clark, *Phys. Rev. Lett.* **97**, 086602 (2006).
19. Materials and methods are available as supporting material on *Science* Online.
20. S. O. Valenzuela, M. Tinkham, *Nature* **442**, 176 (2006).
21. S. O. Valenzuela, *Int. J. Mod. Phys. B* **23**, 2413 (2009).
22. A zero *dI*/*dV* below the quasi-particle thresholds suggests that the Andreev cycle (Fig. 1C) and cotunneling processes (*13*) are suppressed. Integration of *dI*/*dV* results in a current plateau I_p ~ 5.8 pA beyond the thresholds. Because the current is limited by Γ_r^{oe}, $I_p \approx e\Gamma_r^{oe}$ ~ 5 pA, which is in reasonable agreement with the measured value. This indicates that transport is dominated by tunneling events in the r junction.
23. The decrease in V_0 with increasing B is larger than expected if only E_Z is considered; in which case, the ratchet effect should occur at $B_{SR} \approx 2.3$ T. This is due to a reduction of Δ by residual orbital depairing. When such a reduction is considered, $\Delta(1\text{ T}) = 272$ μeV, $V_0(1\text{ T}) = 2[\Delta(1\text{ T}) - E_c]/e - E_Z/e \approx 88$ μV is close to the measured value. Moreover, considering $\Delta(1.5\text{ T}) = 256$ μeV, we estimate $B_{SR} = [\Delta(1.5\text{ T}) - E_c]/(g\mu_B) \approx 1.48$ T, in agreement with the observed result.
24. A. Einstein, B. Podolsky, N. Rosen, *Phys. Rev.* **47**, 777 (1935).
25. C. Bena, S. Vishveshwara, L. Balents, M. P. A. Fisher, *Phys. Rev. Lett.* **89**, 037901 (2002).
26. D. S. Saraga, D. Loss, *Phys. Rev. Lett.* **90**, 166803 (2003).
27. L. Hofstetter, S. Csonka, J. Nygård, C. Schönenberger, *Nature* **461**, 960 (2009).
28. P. Cadden-Zimansky, J. Wei, V. Chandrasekhar, *Nat. Phys.* **5**, 393 (2009).
29. L. G. Herrmann *et al.*, *Phys. Rev. Lett.* **104**, 026801 (2010).

30. We gratefully acknowledge discussions with and support from M. Tinkham and thank I. Žutić and Y. Tserkovnyak for discussions and W. D. Oliver, P. Gambardella, and A. Bachtold for a critical reading of the manuscript. This research was supported in part by the Spanish Ministerio de Ciencia e Innovación (MAT2010-18065, FIS2009-06671-E). Samples were made at the Center for Nanoscale Systems, Harvard University.

Supporting Online Material

www.sciencemag.org/cgi/content/full/330/6011/1645/DC1
Materials and Methods
SOM Text
Figs. S1 to S3
References

9 August 2010; accepted 9 November 2010
10.1126/science.1196228

Spin Transfer Torques in MnSi at Ultralow Current Densities

F. Jonietz,[1] S. Mühlbauer,[1,2] C. Pfleiderer,[1]* A. Neubauer,[1] W. Münzer,[1] A. Bauer,[1] T. Adams,[1] R. Georgii,[1,2] P. Böni,[1] R. A. Duine,[3] K. Everschor,[4] M. Garst,[4] A. Rosch[4]

Spin manipulation using electric currents is one of the most promising directions in the field of spintronics. We used neutron scattering to observe the influence of an electric current on the magnetic structure in a bulk material. In the skyrmion lattice of manganese silicon, where the spins form a lattice of magnetic vortices similar to the vortex lattice in type II superconductors, we observe the rotation of the diffraction pattern in response to currents that are over five orders of magnitude smaller than those typically applied in experimental studies on current-driven magnetization dynamics in nanostructures. We attribute our observations to an extremely efficient coupling of inhomogeneous spin currents to topologically stable knots in spin structures.

The discovery of the effect of giant magnetoresistance, now used commercially in the hard disk drive industry, is widely recognized as the starting point of the field of spintronics. It represents the first example of electric currents controlled efficiently by spin structures. The complementary process of so-called spin transfer torques, where magnetic structures and textures are manipulated by electric currents (*1*, *2*), appears to be even more promising. For instance, strong current pulses allow the movement of ferromagnetic domain walls (*3*, *4*), the switching of magnetic domains in multilayer devices (*5*, *6*), the induction of microwave oscillations in nanomagnets (*7*), and the switching of ferromagnetic semiconductor structures (*8*). However, the typical current densities required to create observable spin transfer torques in present-day studies exceed 10^{11} A m^{-2}. Because this implies extreme ohmic heating, it was generally believed that spin torque effects can be studied exclusively in nanostructures. We report the observation of spin transfer torques in a bulk material, the skyrmion lattice phase of MnSi. The spin transfer torques appear when the current density exceeds an ultralow threshold of ~10^6 A m^{-2}, five orders of magnitude smaller than those used typically in experimental studies on current-driven magnetization dynamics in ferromagnetic metals and semiconductors.

The skyrmion lattice in chiral magnets, like MnSi and related B20 compounds, was only recently discovered in neutron-scattering studies (*9*–*12*) and confirmed to exist in Lorentz force microscopy for $Fe_{1-x}Co_xSi$ (x = 0.5) (*13*). It represents a new form of magnetic order that may be viewed as a crystallization of topologically stable knots of the spin structure that shares remarkable similarities with the mixed state in type II superconductors. For zero magnetic field (Fig. 1A), helimagnetic order appears in MnSi below the critical temperature T_c = 29.5 K.

[1]Physik-Department E21, Technische Universität München, D-85748 Garching, Germany. [2]Forschungsneutronenquelle Heinz Maier-Leibnitz (FRM II), Technische Universität München, D-85748 Garching, Germany. [3]Institute for Theoretical Physics, Utrecht University, 3584 CE Utrecht, Netherlands. [4]Institute of Theoretical Physics, University of Cologne, D-50937 Cologne, Germany.

*To whom correspondence should be addressed. E-mail: christian.pfleiderer@frm2.tum.de

In a small magnetic field, the skyrmion lattice stabilizes in a pocket below T_c, also known as the A phase. The spin structure of the skyrmion lattice in MnSi consists of a hexagonal lattice of magnetic vortex lines oriented parallel to the magnetic field **B** (Fig. 1A, inset).

Skyrmion lattices in chiral magnets are attractive for studies of spin torque effects, because they are coupled very weakly to the atomic crystal structure (*9*) and may be expected to pin very weakly to disorder. In addition, electric currents couple very efficiently to skyrmions as follows. When the conduction electrons in a metal move across a magnetic texture, their spin follows the local magnetization adiabatically. Spins that change their orientation pick up a quantum mechanical phase, the Berry phase, that may be viewed as an Aharonov-Bohm phase arising from a fictitious effective field (*14*–*16*) $\mathbf{B}^i_{\mathrm{eff}} = \frac{\Phi_0}{8\pi} D_{ijk}\hat{M}(\partial_j\hat{M} \times \partial_k\hat{M})$, where $\hat{M} = \mathbf{M}/|\mathbf{M}|$ is the direction of the local magnetization and $\Phi_0 = h/e$ is the flux quantum for a single electron (h is Planck's constant). In the skyrmion lattice, B_{eff} has a topologically quantized average strength of $-\Phi_0$ per area of the magnetic unit cell [for MnSi $B_{\mathrm{eff}} \approx 2.5$ T (*11*)]. B_{eff} induces an effective Lorentz force, which gives rise to an additional "topological" contribution to the Hall effect proportional to the product of B_{eff} and the local polarization of the conduction electrons as observed experimentally (*11*, *17*). Correspondingly, because the electrons are deflected, a force is exerted on the magnetic structure so that there is an efficient "gyromagnetic coupling" (*18*) of the current to the skyrmion lattice (*19*).

From an alternative point of view, the skyrmion lattice may be viewed as an array of circulating dissipationless spin currents, because the skyrmions are characterized by gradients in the spin orienta-

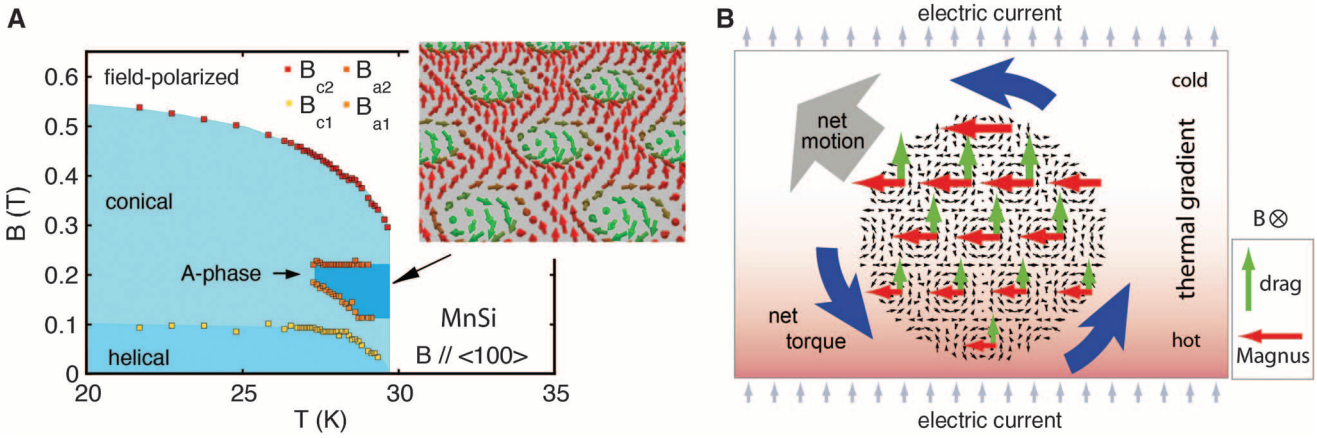

Fig. 1. (**A**) Magnetic phase diagram of MnSi. (Inset) Schematic spin structure of the skyrmion lattice in a plane perpendicular to the applied field. (**B**) Schematic depiction of the spin transfer torque effects on the skyrmion lattice. A temperature gradient induces inhomogeneous Magnus and drag forces and therefore a rotational torque.

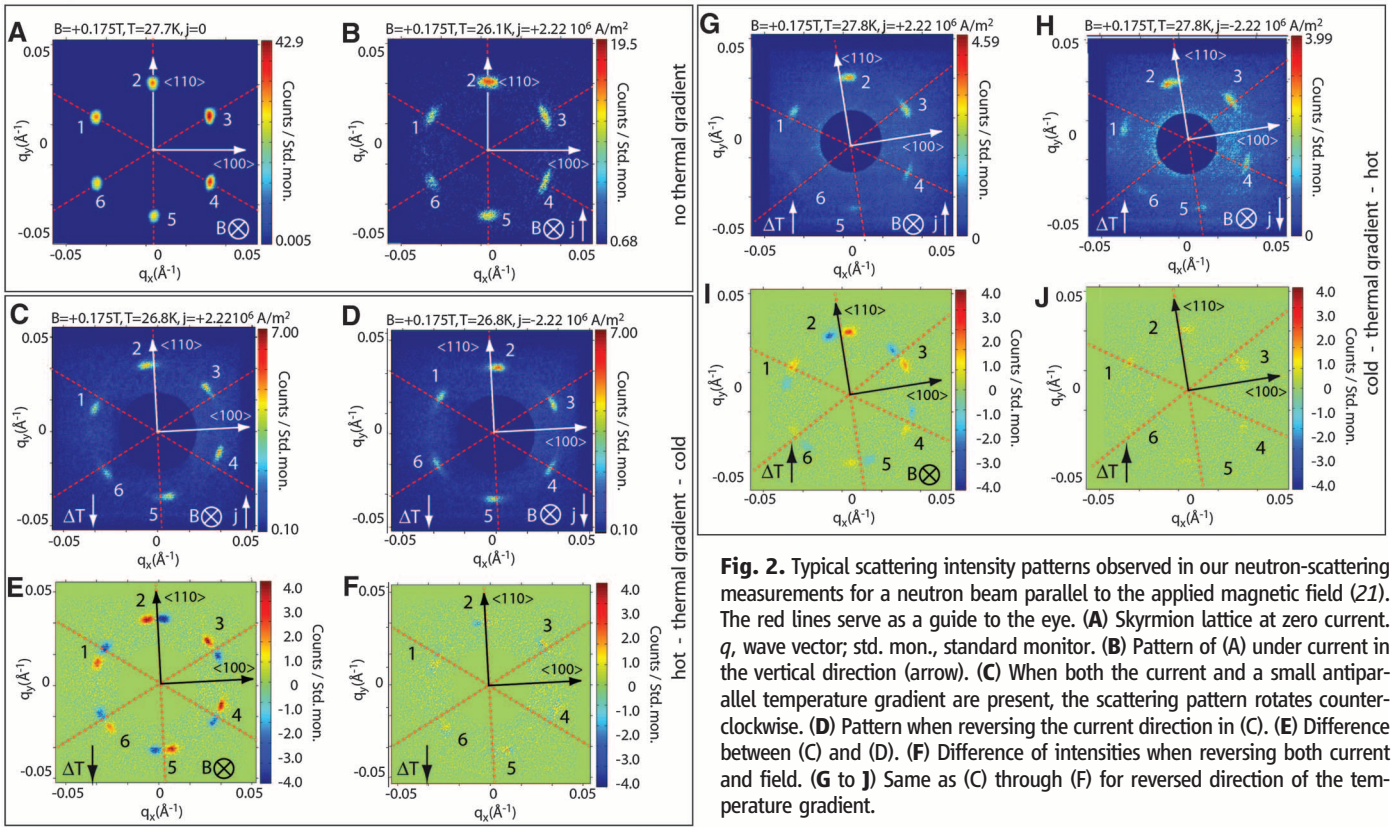

Fig. 2. Typical scattering intensity patterns observed in our neutron-scattering measurements for a neutron beam parallel to the applied magnetic field (*21*). The red lines serve as a guide to the eye. (**A**) Skyrmion lattice at zero current. *q*, wave vector; std. mon., standard monitor. (**B**) Pattern of (A) under current in the vertical direction (arrow). (**C**) When both the current and a small antiparallel temperature gradient are present, the scattering pattern rotates counterclockwise. (**D**) Pattern when reversing the current direction in (C). (**E**) Difference between (C) and (D). (**F**) Difference of intensities when reversing both current and field. (**G** to **J**) Same as (C) through (F) for reversed direction of the temperature gradient.

tion related to their quantized winding number. This is analogous to superconductors, where dissipationless charge currents flow around quantized vortices because of gradients of the phase. When an extra spin current is induced by driving an electric current through the magnetic metal, the spin currents on one side of the skyrmion are enhanced, while they are reduced on the other side. As for a spinning tennis ball, this velocity difference gives rise to a Magnus force acting on the skyrmions. Note, however, that spin (because of spin-orbit coupling) is in contrast to charge not conserved, and therefore this intuitive picture is incomplete. Most importantly, further dissipative forces also arise (*20*), which drag the skyrmions parallel to the current.

In Fig. 1B, this magnetic Magnus force, which is perpendicular to current and field direction, is sketched together with the additional drag forces. The Magnus and drag forces may lead to a translational motion of the skyrmion lattice. However, for the current densities used in our experiment the drift velocity of the electrons and therefore also the drift velocity of the skyrmions is not very large and thus very difficult to detect in a neutron scattering experiment.

In contrast to a translational motion, a rotation is much easier to measure in neutron scattering. Thus, we performed our experiment in the presence of a small temperature gradient parallel to the current, causing the magnetization and therefore the spin currents to vary in magnitude across the domains of the skyrmion lattice. In turn, the strength of the Magnus force varies across the skyrmion lattice (Fig. 1B), inducing a net torque. As estimated below, the torques are sufficiently strong to induce rotations that can be measured directly by neutron scattering.

For our measurements, an electric current was applied along bar-shaped single crystals, where the direction of the current was always perpendicular to the magnetic field and therefore to the skyrmion lines. In Fig. 2, the neutron beam was always collinear to the magnetic field (*21*). The sixfold diffraction pattern of the skyrmion lattice at zero current, $j = 0$ (Fig. 2A), can be compared to the same scattering pattern at a current density, $j = 2.22 \times 10^6$ A m^{-2}, first in a setup minimizing any thermal gradients along the current direction (Fig. 2B). The current was applied along the vertical $[1\bar{1}0]$ direction, whereas the field and the neutron beam were collinear to the line of sight and along [110] (the horizontal direction is along [001]). Under a current, the peaks of the diffraction spots remain in the same location and broaden azimuthally.

We next generated a small temperature gradient along the direction of the current as explained in (*21*). Figure 2C shows the diffraction pattern of the skyrmion lattice for this setup under an electrical current density, $j = 2.22 \times 10^6$ A m^{-2}, which shows a pronounced counterclockwise rotation as compared with Fig. 2, A and B (note that arrows show the technical current direction and the line of sight is opposite to the direction of the neutron beam, consistent with convention). When the current direction is reversed, the rotation changes sign, and the diffraction pattern turns clockwise (Fig. 2D).

There are several unusual aspects of this rotation. First, the entire scattering pattern rotates with respect to its center; that is, all spots move by the same angle even though the electric current has a distinct direction. Second, when reversing either the direction of the current or the direction of the applied field, the sense of the rotation changes sign. This is illustrated in Fig. 2, E and F, which shows the difference of intensity under current reversal and simultaneous reversal of current and field, respectively. For the latter case, the difference of intensities vanishes.

To confirm that the small temperature gradient along the current direction causes the rotation of the scattering pattern, we reversed the direction of the thermal gradient. As illustrated in Fig. 2, G and H, this reverses the sense of rotation with respect to the current and field direction applied in Fig. 2, C and D. Thus the differences of intensity under field reversal, shown in Fig. 2I, are reversed as compared with Fig. 2E (red and blue spots have changed location). When reversing both current and field direction, the difference of the patterns, Fig. 2J, vanishes as before. Lastly, when applying the current along a different crystallographic direction (we tested ⟨111⟩ and an arbitrarily cut sample), the same antisymmetric rotations of the diffraction pattern as a function of magnetic field, electric current, and temperature gradient are observed (*21*).

The detailed rotation as a function of the applied current was determined in systematic measurements for various temperatures and samples. Here, the temperature measured at a specific spot at the surface of the sample (*21*) was kept constant, and temperature gradients had always the same direction. The resulting current dependence of the azimuthal rotation angle ΔΦ, shown for three temperatures as a function of the applied current density in Fig. 3, exhibits a well-defined threshold of order $j_c \approx 10^6$ A m^{-2} above which the rotation begins. For $|j| > j_c$, the entire scattering pattern rotates, and ΔΦ increases steeply with increasing $|j| - j_c$.

Potential parasitic effects cannot explain the observed rotations. First, detailed studies show that there are no changes of orientation of the skyrmion lattice as a function of temperature at $j = 0$ (*10*, *12*, *13*). Second, the temperature difference ΔT between the sample surface and the sample support shows a smooth quadratic increase with current density independent of the direction of the current (Fig. 3B) in contrast to Fig. 3A. Third, for the current densities applied in our study, the Oersted field increases from zero (at the center of the sample) to a value of roughly 1 mT at the surface of the sample, much smaller than the applied magnetic field of 175 mT and therefore negligible. Lastly, for a current parallel to the skyrmion lines or the pristine helimagnetic state, neither a rotation nor a broadening was observed. Interestingly, recent numerical simulations (*22*, *23*) suggest that much larger current densities of the order 10^{12} A m^{-2} may change the orientation of helical magnetic structures.

To explain our experiments, the interplay of three tiny forces has to be considered: (i) spin transfer torques, that is, current induced forces; (ii) pinning forces; and (iii) anisotropy terms. These determine the origin of the rotation, the presence of a threshold, and the angle ΔΦ of the rotated diffraction pattern, respectively. The spin transfer torques can, for example, be described by a Landau-Lifshitz-Gilbert (LLG) equation or variants of Landau-Lifshitz Bloch equations (*24*), which include both reactive and dissipative components representing the Magnus and drag forces mentioned above, respectively. Both are expected to be of the same order of magnitude (*25*). Although the strength of the dissipative forces (related to the parameter β in the LLG equations) is not known, it is possible to estimate the strength of the reactive forces quantitatively.

The size of the Magnus force is given by the product of spin current and the fictitious effec-

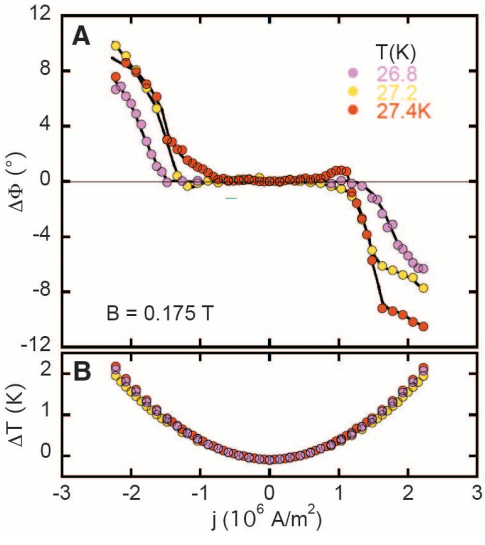

Fig. 3. (**A**) Change of the azimuthal angle of rotation of the scattering pattern as a function of current density for three different temperatures. Data were recorded in a magnetic field of 0.175 T. Above a threshold of 10^6 A m^{-2}, an increasingly strong rotation is observed, where the sign of the rotation depends on the direction of the current. (**B**) Temperature difference between the surface of the sample and the sample holder as a function of current density, where the temperature at the surface of the sample was kept constant for each of the three values given in (A).

tive magnetic field, $f_M \approx ej_s B_{eff}$, and may be estimated as

$$f_M \approx p(T)\frac{j}{10^6\ \mathrm{A\ m^{-2}}}\frac{2.5\times10^6\mathrm{N}}{\mathrm{m}^3}$$
$$\approx p(T)\frac{j}{10^6\ \mathrm{A\ m^{-2}}}\frac{2.7\times10^{-10}k_BT_c}{a^4} \quad (1)$$

where $a \approx 4.58$ Å is the lattice constant of MnSi, k_B is the Boltzmann constant, $T_c \approx 29.5$ K is the ordering temperature, and the local temperature-dependent polarization is defined as the ratio of the spin and charge current densities times the elementary charge, $p(T) = ej_s/j$. For the skyrmion phase, we estimate $p(T) \approx 0.1$ (*11*). The resulting forces at the current densities of 10^6 A m^{-2} studied are much larger than, for example, gravitational forces on the sample, but small when expressed in terms of the microscopic units, k_BT_c/a^4 (compare with Eq. 1), raising the question of why the critical currents j_c are so small.

For $j < j_c$ the current-induced forces are balanced by pinning forces caused by disorder and the underlying regular atomic crystal lattice. The latter may be neglected because of the small spin-orbit interaction (*26*). The discussion presented in (*21*) suggests that even a very strong defect, which locally destroys the magnetization completely, will result in a very small pinning force, less than a few $10^{-5}\ k_BT_c/a$ per impurity, mainly because the magnetization of the skyrmions varies very smoothly. Therefore the observed critical current density j_c together with our estimate, Eq. 1, is consistent with strong pinning defects with a density below 1 part per million. In fact, even though the real density of defects may be higher, their influence may be strongly reduced as the system is in the "collective pinning" regime known, for example, from vortices in superconductors (*27*). Here, pinning forces of random orientation average out to a large extent because of the rigidity of the skyrmion lattice.

The size of the rotation of the skyrmion lattice for $j > j_c$ reflects the balance of the torques τ_M and τ_L due to inhomogeneous Magnus forces and the atomic lattice, respectively. We start by noting, that by symmetry the orientation of a perfect skyrmion lattice (described by a third rank tensor) cannot couple linearly to the current j because of the sixfold rotational symmetry of the lattice. However, a small temperature gradient breaks this symmetry and generates sizable variations of the amplitude of the magnetization and associated polarization $p(T)$ of the electric currents, because the skyrmion phase is only stable close to T_c (compare with Fig. 1). As a result, the Magnus force, Eq. 1, which is proportional to the spin currents and therefore to $p(T)$, will be considerably larger at the "cold" side of the skyrmion lattice than at its "hot" side. This gives rise to a net torque per volume $\tau_M \sim \int \mathbf{r}\times\mathbf{f}_M(\mathbf{r})d^3r/V$. By using Eq. 1 with a spatially varying $p(T)$ and ignoring again dissipative forces for an order of magnitude estimate, we find that the rotational torque per volume, τ_M, in the direction of the fictitious field $\boldsymbol{B}_{eff}$ for a skyrmion lattice domain of size R is given by

$$\tau_M \sim 10^{-10}\frac{\mathbf{j}\cdot\nabla p}{10^6\ \mathrm{A\ m^{-2}}}\frac{R^2}{a}\frac{k_BT_c}{a^3}$$
$$\sim 10^{-5}\frac{k_BT_c}{a^3}\left(\frac{R}{1\ \mathrm{mm}}\right)^2 \quad (2)$$

where we assume $j \approx j_c$ and $\nabla p \approx 0.1/10$ mm.

Note that the effect is proportional to the gradient of the temperature parallel to the current as $\nabla p \approx \frac{\partial p}{\partial T}\nabla T$ (Fig. 1B). Thus τ_M changes sign when either current, magnetic field, or temperature gradient is reversed. The sign of τ_M and all other forces obtained from this analysis (Fig. 1B) is consistent with all our experiments taking into account that charge carriers are holelike as measured experimentally (*11*, *17*). This explains our main experimental results. According to this analysis, the rotational torques arise from temperature-gradient-induced gradients in the spin current. Interestingly, it is more difficult to generate an analogous effect for vortices in superconductors, because charge, as opposed to the spin in skyrmion lattices, is exactly conserved [in (*28*), a rotation of a superconducting vortex lattice has been induced with a bespoke current distribution].

For an estimate of the factor $(R/1\ \mathrm{mm})^2$ in Eq. 2, a lower limit $R > 1$ μm may be inferred from the resolution-limited rocking width of the magnetic Bragg peaks in the skyrmion phase when avoiding demagnetization fields (*21*). Yet, even a small torque τ_M may lead to large rotation angles, because the balancing torque, τ_L, which orients the skyrmion lattice relative to the atomic lattice, is tiny. Only anisotropy terms arising in high power of the spin orbit coupling λ_{SO} contribute to the torque per volume τ_L, which we estimate as (*21*)

$$\tau_L \sim -10^{-2}\lambda_{SO}^4\frac{k_BT_c}{a^3}\sin(6\Phi) \quad (3)$$

For small rotation angles, the torque τ_L grows linearly in the rotation angle Φ. However, in contrast to the torques arising from the inhomogeneous Magnus force, τ_L is independent of the size R of the domains. The rotation angle Φ is finally determined by the balance of τ_M and τ_L. Because of the small prefactor in Eq. 3, $10^{-2}\lambda_{SO}^4$, the large rotation angles observed in our experiments can be explained even for moderately large domains.

It is likely that for $j > j_c$ not only a rotation by an angle sets in but also a linear motion of the magnetic structure, because any rotation of a sizable magnetic domain requires a depinning from defects. For moving domains, spin currents in a frame of reference that is comoving with the domain enter in all formulas given above. Therefore the size of the rotation in the end also depends sensitively on the frictional forces that break Galilean invariance (*25*).

Our observations identify chiral magnets and systems with nontrivial topological properties as ideal systems to advance the general understanding of the effects of spin transfer torques. For instance, spin transfer torques may even be used to manipulate individual skyrmions, recently observed directly in thin samples (*13*). In fact, even complex magnetic structures at surfaces and interfaces may be expected to exhibit the spin torque effects we report here (*29*).

References and Notes

1. J. Slonczewski, *J. Magn. Magn. Mater.* **159**, L1 (1996).
2. L. Berger, *Phys. Rev. B* **54**, 9353 (1996).
3. J. Grollier *et al.*, *Appl. Phys. Lett.* **83**, 509 (2003).
4. M. Tsoi, R. Fontana, S. Parkin, *Appl. Phys. Lett.* **83**, 2617 (2003).
5. M. Tsoi *et al.*, *Phys. Rev. Lett.* **80**, 4281 (1998).
6. E. B. Myers, D. C. Ralph, J. A. Katine, R. N. Louie, R. A. Buhrman, *Science* **285**, 867 (1999).
7. S. I. Kiselev *et al.*, *Nature* **425**, 380 (2003).
8. M. Yamanouchi, D. Chiba, F. Matsukura, H. Ohno, *Nature* **428**, 539 (2004).
9. S. Mühlbauer *et al.*, *Science* **323**, 915 (2009).
10. W. Münzer *et al.*, *Phys. Rev. B* **81**, 041203 (2010).
11. A. Neubauer *et al.*, *Phys. Rev. Lett.* **102**, 186602 (2009).
12. C. Pfleiderer *et al.*, *J. Phys. Condens. Matter* **22**, 164207 (2010).
13. X. Z. Yu *et al.*, *Nature* **465**, 901 (2010).
14. J. Ye *et al.*, *Phys. Rev. Lett.* **83**, 3737 (1999).
15. G. Tatara, H. Kohno, J. Shibata, Y. Lemaho, K.-J. Lee, *J. Phys. Soc. Jpn.* **76**, 054707 (2007).
16. B. Binz, A. Vishwanath, *Physica B* **403**, 1336 (2008).
17. M. Lee, W. Kang, Y. Onose, Y. Tokura, N. P. Ong, *Phys. Rev. Lett.* **102**, 186601 (2009).
18. A. A. Thiele, *Phys. Rev. Lett.* **30**, 230 (1973).
19. C. Pfleiderer, A. Rosch, *Nature* **465**, 880 (2010).
20. S. Zhang, Z. Li, *Phys. Rev. Lett.* **93**, 127204 (2004).
21. Materials and methods are available as supporting material on *Science* Online.
22. O. Wessely, B. Skubic, L. Nordström, *Phys. Rev. Lett.* **96**, 256601 (2006).
23. K. Goto, H. Katsura, N. Nagaosa, Current-induced dynamics of spiral magnet (2008); http://arxiv.org/abs/0807.2901.
24. C. Schieback, D. Hinzke, M. Kläui, U. Nowak, P. Nielaba, *Phys. Rev. B* **80**, 214403 (2009).
25. J. He, Z. Li, S. Zhang, *Phys. Rev. B* **73**, 184408 (2006).
26. D. Belitz, T. R. Kirkpatrick, A. Rosch, *Phys. Rev. B* **73**, 054431 (2006).
27. G. Blatter, M. V. Feigel'man, V. B. Geshkenbein, A. I. Larkin, V. M. Vinokur, *Rev. Mod. Phys.* **66**, 1125 (1994).
28. D. López *et al.*, *Phys. Rev. Lett.* **82**, 1277 (1999).
29. M. Bode *et al.*, *Nature* **447**, 190 (2007).

30. We thank B. Binz, S. Dunsiger, E. M. Forgan, C. Franz, E. Hering, M. Janoschek, H. Kolb, M. Laver, S. Legl, T. Lorenz, A. H. MacDonald, T. Nattermann, J. Peters, S. M. Ramos da Silva, B. Russ, T. Schulz, R. Schwikowski, B. Spivak, A. Vishwanath, M. Vojta, M. Wagner, W. Zwerger, and the team of FRM II for discussions and support. We gratefully acknowledge financial support through SFB608 and TRR80, SFB/TR12 of the German Science Foundation (Deutsche Forschungsgemeinschaft), the Deutsche Telekom Stiftung (K.E.), NSF grant PHY05-51164 (A.R.), and by Stichting voor Fundamenteel Onderzoek der Materie, Nederlandse Organisatie voor Wetenschappelijk Onderzoek, and the European Research Council (R.A.D.).

Supporting Online Material

www.sciencemag.org/cgi/content/full/330/6011/1648/DC1
Materials and Methods
SOM Text
Figs. S1 to S8
Table S1
References

27 July 2010; accepted 18 November 2010
10.1126/science.1195709

Electronic Spin Storage in an Electrically Readable Nuclear Spin Memory with a Lifetime >100 Seconds

D. R. McCamey,[1]*† J. Van Tol,[2] G. W. Morley,[3] C. Boehme[1]

Electron spins are strong candidates with which to implement spintronics because they are both mobile and able to be manipulated. The relatively short lifetimes of electron spins, however, present a problem for the long-term storage of spin information. We demonstrated an ensemble nuclear spin memory in phosphorous-doped silicon, which can be read out electrically and has a lifetime exceeding 100 seconds. The electronic spin information can be mapped onto and stored in the nuclear spin of the phosphorus donors, and the nuclear spins can then be repetitively read out electrically for time periods that exceed the electron spin lifetime. We discuss how this memory can be used in conjunction with other silicon spintronic devices.

The ability to store and retrieve spin information in solid-state systems is important for the development of spin-based electronic devices for classical and quantum information processing. The ability to store spin information in situ enhances the ability to integrate spintronic and classical electronic systems, allows the stored spin to be used as an initialized classical or quantum register, and may provide the ability to perform quantum nondemolition readout on difficult-to-probe spin systems. Nuclear spins are an obvious candidate for implementing such a memory, because they tend to have extremely long spin lifetimes (*1*–*3*).

To date, implementations of quantum logic or memory devices directly involving nuclear spins have used optical or microwave detection in systems such as the nitrogen vacancy center of diamond (*4*–*6*). However, coupling these systems to classical electronic devices requires transduction between optical and electrical signals. We demonstrated electrical readout of a nuclear spin memory consisting of phosphorus donors in silicon. Previous work to electrically detect nuclear spin states has focused on continuous-wave spin resonance techniques, which are unsuitable for the manipulation required for nuclear spin storage (*7*), and on electrically detected nuclear magnetic resonance approaches using quantum Hall edge states in gallium arsenide heterostructures (*8*).

Phosphorus donors in silicon (Si:P) provide a number of advantages for the implementation of such a device. Si:P is widely used in the modern semiconductor industry, providing the ability to fabricate devices on the scale of a few nanometers (*9*). Recent work has demonstrated that ^{31}P-doped silicon can be used for spintronic applications (*10*), allowing long-distance spin transport with conduction electrons (*11*). Additionally, the phosphorus donor has long electron (*12*) and extremely long nuclear spin (*3*) coherence times, making it an ideal system for implementing such a device.

As a result of these properties, Si:P has been widely investigated for use in applications ranging from quantum information processing (*2*, *13*, *14*) to more "classical" spintronics (*10*, *11*), where the phase of the spin is less important. However, few advances related to the nuclear spin of donors have been reported (*2*, *15*–*17*). It has been demonstrated that an ensemble of coherent donor electron spin states could be stored in the nuclear spin for over a second, before being returned to the electrons and read out with conventional spin resonance techniques (*2*). Recently, it was also shown that the spin state of a single electron in silicon could be detected electrically with a single shot, although simultaneous control of the spin has yet to be demonstrated (*14*).

Previous attempts to use electrical spin readout of donors with the pulsed manipulation of their nuclear spins required for storage have proven challenging because of the small characteristic change in current seen at low magnetic fields. By using high magnetic fields (~8.59 T), we are able to obtain large electron spin polarization and a correspondingly large change in current (*18*). The difficulty with these large fields is that the frequencies required for electron spin manipulation are ~240 GHz. The recent development of pulsed spin resonance at these frequencies allows these measurements to be performed.

In high magnetic fields, the product states of the ^{31}P donor electron and nuclear spin system, $|\uparrow_e \uparrow_n\rangle$, $|\downarrow_e \uparrow_n\rangle$, $|\uparrow_e \downarrow_n\rangle$, and $|\downarrow_e \downarrow_n\rangle$ are very close to the eigenstates (↑ and ↓ represent the individual spin-up and spin-down eigenstates, respectively). Allowed transitions between these

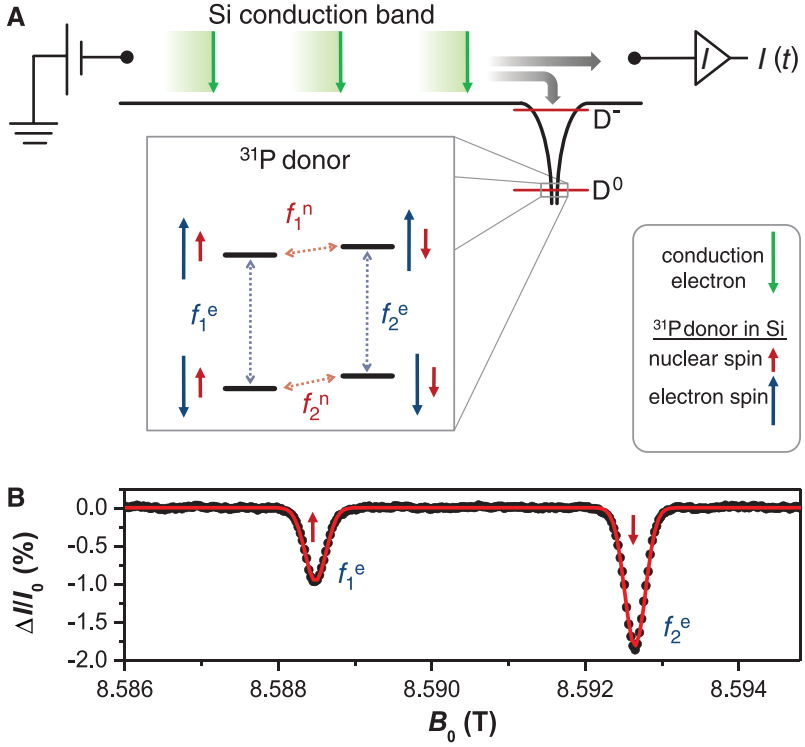

Fig. 1. The Si:P system used for implementing spin storage. (**A**) The singly occupied (D^0) state of the phosphorus donor in silicon may capture a conduction electron and form a doubly occupied (D^-) state only if they have opposite spin. Modifying the capture rate by manipulating the donor electron spin leads to a change in current through the silicon crystal. (**B**) Electron spin resonance reveals two resonances in the device current, due to the different donor nuclear-spin orientations, which couple to the electron spins through a contact hyperfine interaction.

[1]Department of Physics and Astronomy, University of Utah, Salt Lake City, UT, 84112, USA. [2]National High Magnetic Field Laboratory, Florida State University, Tallahassee, FL 32310, USA. [3]London Centre for Nanotechnology and Department of Physics and Astronomy, University College London, London WC1H 0AH, UK.

*Present address: School of Physics, University of Sydney, Sydney 2006, Australia.

†To whom correspondence should be addressed. E-mail: dane.mccamey@sydney.edu.au

states can be driven by spin resonance (Fig. 1A). The presence of a contact hyperfine interaction of 117.5 MHz between the electron and nucleus, along with the nonnegligible nuclear Zeeman energy (148.2 MHz at 8.59 T), lifts the degeneracy of the spin resonance conditions, allowing the four transitions to be independently addressed. We use a custom built 240 GHz pulsed spectrometer (*19*–*21*) to drive these transitions, at a temperature (T) = 3.5 ± 0.2 K. To read out the nuclear spin state, we use a spin trap method (*18*): If the conduction electrons are polarized in the spin-down state, the doubly occupied D^- state of the donor cannot be occupied if the donor electron also has spin down. However, if the donor electron is resonantly excited to the spin-up state, then the D^- state is able to trap an electron from the conduction band, thus reducing the conductivity of the silicon. This can be detected by measuring the change in the conductivity after resonant excitation, using the circuit

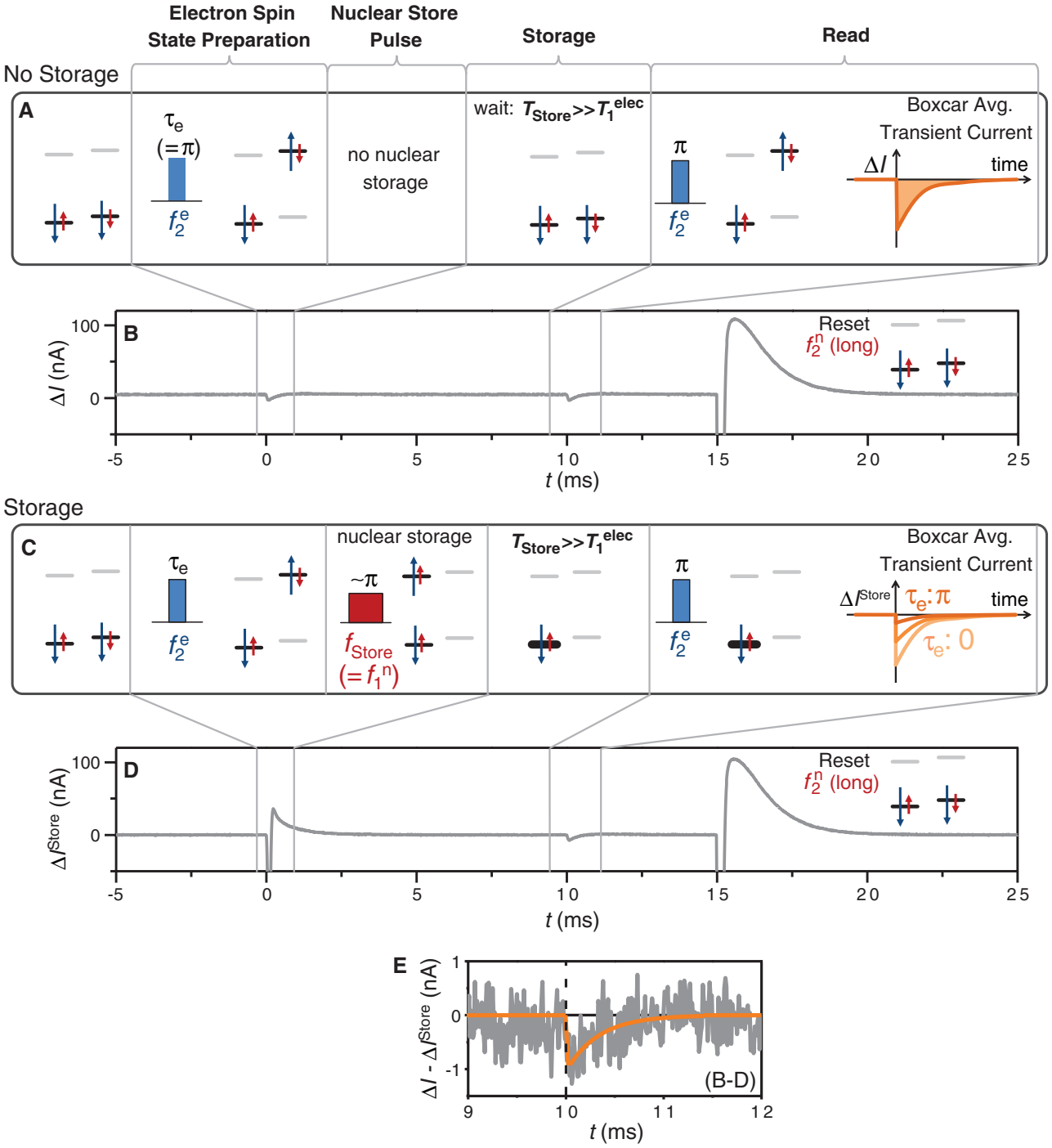

Fig. 2. Schematic of different storage pulse sequences. (**A**) The electron is prepared into a 1 state by applying a $\pi(f_2^e)$ pulse. If no nuclear spin storage is undertaken, the initial spin state has no impact on the final spin state obtained. (**B**) Transient current during the pulse sequence in (A). (**C**) However, if the electron is prepared into a 1 state then stored in the nuclear spin, the magnitude of the current change after the readout pulse is reduced. (**D**) The change in the current through the silicon sample during the application of a STORE-1 sequence. The large nonresonant current changes at 0 and 15 ms are due to nonresonant coupling of the radio frequency (rf) to the electrical contacts. (**E**) Difference between NO STORE and STORE transient current for the initial state 1. The solid orange line is a fit to the data for time (t) > 10 ms.

shown in Fig. 1A. Figure 1B shows the change in current after a 240-GHz π pulse was applied to the device as the external magnetic field B_0 was varied, bringing the f_1^e and f_2^e transitions on resonance at 8.5885 and 8.5927 T, respectively. The difference in amplitude is due to an Overhauser-mediated nuclear polarization effect (*15*) and is not important to the nuclear storage.

A nuclear storage and electrical readout experiment was performed using a modified Davies electron-nuclear double resonance (ENDOR) scheme (*22*–*24*), previously only demonstrated on a sample containing a large number of donors (>4 × 10^{12}) in a conventional ENDOR approach. Because of the large electron spin polarization, the initial state of the phosphorus donors is $|\downarrow_e \uparrow_n\rangle$ or $|\downarrow_e \downarrow_n\rangle$. In the experiments, P atoms in the $|\downarrow_e \uparrow_n\rangle$ state remain unchanged while those in the $|\downarrow_e \downarrow_n\rangle$ state are used for storage. If a pure initial state is required, the pulse sequence $[\pi(f_1^e) - \pi(f_2^n) -$ wait $> T_1^e]$ maps $|\downarrow_e \uparrow_n\rangle$ onto $|\downarrow_e \downarrow_n\rangle$ while leaving those donors initially in $|\downarrow_e \downarrow_n\rangle$ in that state. We prepared some arbitrary electronic spin state $|\downarrow_e \downarrow_n\rangle \xrightarrow{\tau_e(f_2^e)} \alpha|\downarrow_e \downarrow_n\rangle + \beta|\uparrow_e \downarrow_n\rangle$ by applying a $\tau_e(f_2^e)$ pulse of varying length (Fig. 2, A and C). Logical information can thus be encoded in the electron spins: Ensembles comprising spins in the spin-up eigenstates are assigned as "1" and in the spin-down eigenstate as "0".

The ensemble electron spin state can now be stored in a nuclear spin state by applying a controlled NOT (CNOT) gate [a $\pi(f_1^n)$ pulse] between the electronic and nuclear spin (Fig. 2C): $\alpha|\downarrow_e \downarrow_n\rangle + \beta|\uparrow_e \downarrow_n\rangle \xrightarrow{\pi(f_1^n)} \alpha|\downarrow_e \downarrow_n\rangle + \beta|\uparrow_e \uparrow_n\rangle$.

The nuclear spin state can then be read at later times by measuring the change in current after a $\pi(f_2^e)$ pulse (Fig. 2C). In an idealized single-spin system, this would result in a current change on resonance if the nuclear spin was in the $|\downarrow_n\rangle$ (or 0) configuration, and no change in the $|\uparrow_n\rangle$ (1) configuration (*25*). For the ensemble we investigated, we expect a current change after nuclear storage $\Delta I^\tau \propto \alpha^2 \Delta I$ determined by the rotation angle, where ΔI is the transient if there is no storage (Fig. 2B) or if the logical value 0 is stored (no preparation pulse). If the pulses applied to the system resulted in perfect π rotations of the electron and nuclear spins, we would expect $\Delta I^\tau = 0$; however, imperfections in the pulse duration and homogeneity, the incomplete electron spin polarization, and the inhomogeneous linewidth of the nuclear resonance all reduce the fidelity of our CNOT implementation, and thus some of the spins are not ideally stored. The transient current is therefore not completely eliminated (Fig. 2D) but is reduced as compared to the no-storage case (Fig. 2E). The system can be reset by applying a long pulse at f_2^n.

To confirm that the signal in Fig. 2E is due to storage in the phosphorus nuclear spin, we repeated the STORE-1 sequence while varying the frequency of the storage pulse. Figure 3A shows the boxcar-averaged change in ΔI after the readout pulse after storage for 10 ms. A resonance is clearly seen at 89.1 MHz, corresponding to the f_1^n transition. The resonance is a positive change in the current transient, corresponding to fewer electronic spins being excited during the readout pulse.

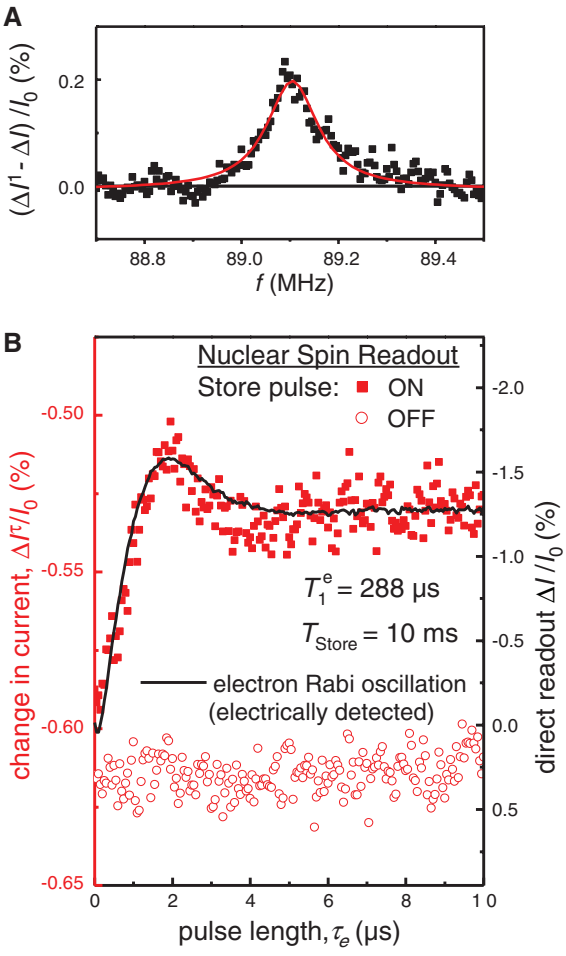

Fig. 3. (**A**) Applying the STORE-1 sequence, nuclear storage occurs only when the applied rf radiation is resonant with the f_1^n transition (Lorentzian fit). f, frequency. (**B**) By varying the length of the electron preparation pulse, an arbitrary electron spin state can be stored in the nuclear spin ensemble. The black line shows the prepared electronic spin state readout immediately after preparation (a single-pulse Rabi experiment, right axis), and the square red data points show the read from the nuclear spins after 10 ms of storage (the STORE-τ sequence for varying τ_e) (left axis). With no storage, the initial spin information is lost (open red circles).

Figure 3B shows an electron spin Rabi oscillation (black line), electrically detected immediately after a preparation pulse, $\tau_e(f_2^e)$. The oscillations, while visible, are damped with a Gaussian envelope of width 1.7 μs, due to spatial inhomogeneities in the oscillating magnetic field of the microwaves used to drive the electron spin resonance. By using a STORE-τ sequence, we are able to write an arbitrary electron state to the nuclear memory, store it there, and then use a read pulse to obtain the state from memory T_{Store} = 10 ms later (solid red squares, Fig. 3B). To confirm that the information is indeed stored in the nuclear spins, the experiment was repeated with no storage pulse (open red circles) and with a nonresonant storage pulse (not shown in Fig. 3B); in neither case is the initial electron state recovered. It is important to note that it is not the coherent electron state prepared by the initial pulse but the projection of this state onto the spin eigenstates (the coefficients α and β) that we are storing in the nuclear spin polarization. Including a $\pi(f_2^e)$ pulse after the store pulse would allow a coherent state to be stored and subsequently read out electrically. We expect, however, that such a stored state would decohere within $T_2^n \leq 2T_1^e = 576$ μs (*2*).

To determine the time scale on which the electron spin state can be stored in the nuclear spin, we stored a spin state, in this case 1, and watched its relaxation back to the steady state. Figure 4A shows the result of repeated storage and readout of the electron spin state 1. In Fig. 4B, the storage pulse is moved off resonance, and the nuclear spin memory slowly relaxes back to the initial 0 state with a time constant $T_{Store} = 112 \pm 2$ s. This is close to the 150 ± 20 s Overhauser relaxation rate (electron-nuclear spin flip-flops) previously seen in Si:P under illumination in similar high magnetic field conditions (*15*). We have thus been able to increase the spin storage time by a factor >3 × 10^5 as compared to T_1^e. By varying the experimental conditions, even longer storage times may be accessible: Nuclear spin lifetimes exceeding 10 hours at magnetic fields of around 0.3 T have been observed with conventional ENDOR experiments (*3*).

After relaxation, the store pulse frequency is moved back into resonance (Fig. 4C), and the signal returns to the value associated with storing a 1. A small number of repetitions are required to return to the 1 state because of the imperfect π rotations used in this experiment, and are not an intrinsic feature of this scheme. Figure 4, D and

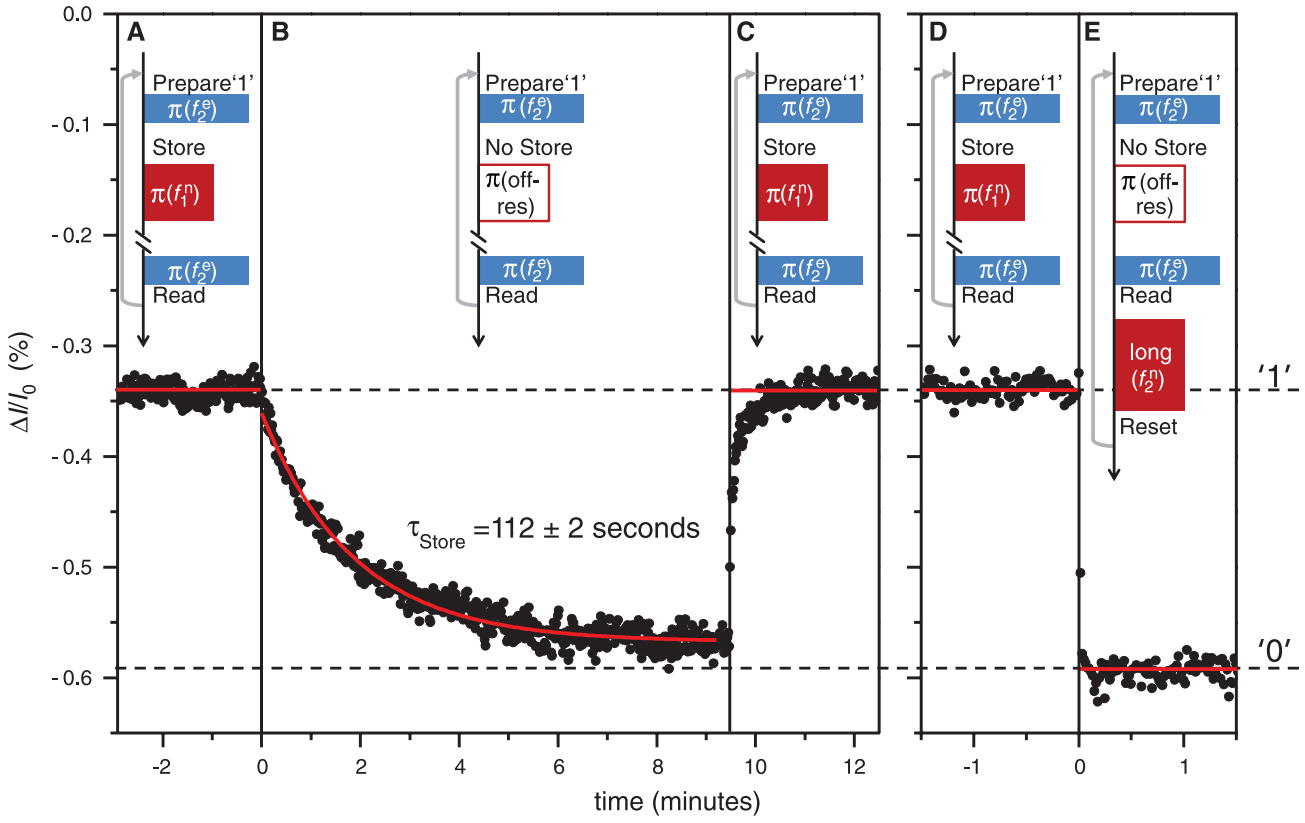

Fig. 4. (**A**) Repetitive application of STORE-1 (without a reset pulse) demonstrates the stability of the stored nuclear information (T_{Store} = 10 ms). (**B**) At t = 0, the frequency of the store pulse is detuned from the resonance by 300 kHz (from 89.1 to 88.8 MHz), and the stored information is repetitively read out. The stored spin state is lost from memory with an exponential time constant of 112 ± 2 s. (**C**) At $t \approx 9.5$ min, the store pulse is returned to the resonant frequency, and the 1 state is seen again. The nonzero recovery time of the stored state is due to the imperfection of the applied storage pulses. (**D**) To demonstrate the effectiveness of resetting the memory, a STORE-1 pulse without reset was applied. (**E**) At t = 0, the store pulse frequency was again moved off resonance and the reset pulse turned on. The read state quickly returned to the 0 state.

E, show a similar experiment: In Fig. 4D, a 1 is repetitively prepared, stored, and read out. The store pulse is again moved off resonance, but now a reset pulse is introduced (Fig. 4E); as can be seen, the stored signal is immediately destroyed, and the initial 0 state is recovered.

As well as allowing a measure of the storage lifetime, Fig. 4, B and D, reveal another advantage of the storage method demonstrated here: repetitive readout of the stored spin state (*6*, *25*). Most readout techniques for obtaining the spin state of a donor electron require that the state be destroyed (*13*, *14*, *18*, *26*). Here, however, we have shown that the electron spin state can be stored in the nuclear spins and that the state of the nuclear spin can then be repetitively read out without changing the state. We have measured the stored spin over 2000 times without any observable impact on its state (*27*).

The phosphorus nuclear spin is not the only relevant nucleus for the electrical readout approach demonstrated here. The storage and readout scheme described above was performed on natural silicon containing ~5% spin ½ ^{29}Si (fig. S1). As the hyperfine coupling between ^{29}Si nuclei and the ^{31}P donor electron varies depending on the relative position, an addressable nuclear spin register for the storage of multiple electron spin states in different ^{29}Si nuclear spins is obtained. ^{29}Si nuclear spins have extremely long lifetimes (*28*), making them another promising storage system. Donors such as Bi may also be amenable to such a scheme (*16*, *17*). Indeed, the approach presented here may have wide application in spectroscopic investigations of small-scale nuclear spin systems, where conventionally detected approaches are inapplicable.

It is possible to store logical information from donor electronic spins in donor nuclear spins for times exceeding 100 s. Previous work on phosphorus in silicon has demonstrated spin-conserved transport of polarized conduction electrons over long distances (*11*), local spin resonance on the micrometer scale (*29*), electrical detection of the spin resonance signal from as few as 50 donors (*26*), and single-shot detection of the state of a single spin (*14*). Combining these advances should enable the development of a practical spin memory in silicon, possibly at the single donor level.

References and Notes

1. W. M. Witzel, S. Das Sarma, *Phys. Rev. B* **76**, 045218 (2007).
2. J. J. L. Morton *et al.*, *Nature* **455**, 1085 (2008).
3. G. Feher, E. A. Gere, *Phys. Rev.* **114**, 1245 (1959).
4. L. Childress *et al.*, *Science* **314**, 281 (2006).
5. L. Jiang *et al.*, *Science* **326**, 267 (2009).
6. P. Neumann *et al.*, *Science* **329**, 542 (2010).
7. B. Stich, S. Greulich-Weber, J.-M. Spaeth, *Appl. Phys. Lett.* **68**, 1102 (1996).
8. G. Yusa, K. Muraki, K. Takashina, K. Hashimoto, Y. Hirayama, *Nature* **434**, 1001 (2005).
9. M. Fuechsle *et al.*, *Nat. Nanotechnol.* **5**, 502 (2010).
10. S. P. Dash, S. Sharma, R. S. Patel, M. P. de Jong, R. Jansen, *Nature* **462**, 491 (2009).
11. I. Appelbaum, B. Huang, D. J. Monsma, *Nature* **447**, 295 (2007).
12. A. Tyryshkin, S. Lyon, A. V. Astashkin, A. M. Raitsimring, *Phys. Rev. B* **68**, 193207 (2003).
13. B. E. Kane, *Nature* **393**, 133 (1998).
14. A. Morello *et al.*, *Nature* **467**, 687 (2010).
15. D. R. McCamey, J. van Tol, G. W. Morley, C. Boehme, *Phys. Rev. Lett.* **102**, 027601 (2009).
16. R. E. George *et al.*, *Phys. Rev. Lett.* **105**, 067601 (2010).
17. G. W. Morley *et al.*, *Nat. Mater.* **9**, 725 (2010).
18. G. W. Morley *et al.*, *Phys. Rev. Lett.* **101**, 207602 (2008).
19. J. van Tol, L.-C. Brunel, R. J. Wylde, *Rev. Sci. Instrum.* **76**, 074101 (2005).
20. G. W. Morley, L.-C. Brunel, J. van Tol, *Rev. Sci. Instrum.* **79**, 064703 (2008).
21. Supporting material on *Science* Online includes experimental methods and additional data.
22. A. M. Tyryshkin, J. J. L. Morton, A. Ardavan, S. A. Lyon, *J. Chem. Phys.* **124**, 234508 (2006).
23. G. W. Morley *et al.*, *Phys. Rev. Lett.* **98**, 220501 (2007).
24. J. J. L. Morton, N. S. Lees, B. M. Hoffman, S. Stoll, *J. Magn. Reson.* **191**, 315 (2008).
25. M. Sarovar, K. C. Young, T. Schenkel, K. B. Whaley, *Phys. Rev. B* **78**, 245302 (2008).
26. D. R. McCamey *et al.*, *Appl. Phys. Lett.* **89**, 182115 (2006).

27. The state 1 varied during nondemolition readout due to the intrinsic relaxation toward the steady state 0. No change was observed in the 0 state.
28. T. D. Ladd, D. Maryenko, Y. Yamamoto, E. Abe, K. M. Itoh, *Phys. Rev. B* **71**, 014401 (2005).
29. L. H. Willems van Beveren *et al*., *Appl. Phys. Lett.* **93**, 072102 (2008).
30. This work was supported in part by Visiting Scientist Program Grant 12488 from the National High Magnetic Field Laboratory (NHMFL). The NHMFL is funded by the State of Florida, the U.S. Department of Energy, and NSF through Cooperative Agreement DMR-0654118. D.R.M. acknowledges support through an Australian Research Council Postdoctoral Fellowship (DP1093526). G.W.M. acknowledges support from the Royal Commission for the Exhibition of 1851 and the EPSRC COMPASSS grant. C.B. acknowledges support from the NSF CAREER program (grant 953225).

Supporting Online Material
www.sciencemag.org/cgi/content/full/330/6011/1652/DC1
Materials and Methods
Figs. S1 to S3
References

17 September 2010; accepted 9 November 2010
10.1126/science.1197931

Oxygen Doping Modifies Near-Infrared Band Gaps in Fluorescent Single-Walled Carbon Nanotubes

Saunab Ghosh,[1] Sergei M. Bachilo,[1] Rebecca A. Simonette,[2] Kathleen M. Beckingham,[2] R. Bruce Weisman[1]*

Controlled chemical modifications of single-walled carbon nanotubes (SWCNTs) that tune their useful properties have been sought for multiple applications. We found that beneficial optical changes in SWCNTs resulted from introducing low concentrations of oxygen atoms. Stable covalently oxygen-doped nanotubes were prepared by exposure to ozone and then light. Treated samples showed distinct, structure-specific near-infrared fluorescence at wavelengths 10 to 15% longer than displayed by pristine semiconducting SWCNTs. Dopant sites harvest light energy absorbed in undoped nanotube regions by trapping mobile excitons. The oxygen-doped SWCNTs are much easier to detect and image than pristine SWCNTs because they give stronger near-infrared emission and do not absorb at the shifted emission wavelength.

One of the most remarkable characteristics of single-walled carbon nanotubes (SWCNTs) is their diversity of well-defined electronic and optical properties (*1*, *2*). Each SWCNT is composed of covalently bonded carbon atoms forming an ordered tubular structure with a specific diameter and roll-up angle, uniquely defined by a pair of integers called the (*n*,*m*) index. About two-thirds of SWCNT structures are semiconducting. Their intrinsic band gaps are determined by quantum confinement and linked to physical structure, with only slight alterations possible through environmental perturbation.

A variety of optical and electronic applications would benefit from the controlled modification of SWCNT band gaps in bulk samples, individual nanotubes, and even segments within nanotubes. Covalent sidewall reactions have been used to bond nanotubes to chemical groups having a range of selected electronic properties (*3*, *4*). However, to date such reactions have randomly eroded the highly ordered nanotube π-electron structure. The additional covalent bonds remove electrons from the π-system, broadening and suppressing the signature near-infrared (IR) fluorescence peaks of semiconducting SWCNTs (*5*). Here, we describe a different type of chemically modified SWCNT that is more analogous to dopant-tuned semiconductor materials. These stable and easily prepared oxygen-doped nanotubes are near-IR fluorophores that display distinct, structure-specific optical properties systematically shifted from those of the pristine parent. They are more readily detected than pristine nanotubes.

We produce these modified SWCNTs by exposing aqueous suspensions of pristine SWCNTs to low doses of ozone and then photolyzing the resulting product (*6*). Our studies rely on samples highly enriched in individual semiconducting (*n*,*m*) species through nonlinear density gradient ultracentrifugation (*7*). The simpler optical spectra of these sorted samples allow monitoring of the conversion reaction by fluorescence spectroscopy. Immediately after mild ozone exposure, the characteristic near-IR E_{11} fluorescence band shows small red shifts (~0.2) and appreciable broadening (~5%). Subsequent exposure to light induces a new emission feature, termed E_{11}*, that is red-shifted from E_{11}. Spectra measured during this transformation are shown for a (6,5)-enriched sample in Fig. 1A. During phototransformation by light from a desk lamp, 980-nm E_{11} emission diminishes as the 1120-nm E_{11}* feature increases (Fig. 1, A and B). However, except for some broadening, the absorption spectrum remains essentially unchanged by this conversion (Fig. 1C). The transformed nanotubes show very little absorption at their new emission peak, unlike pristine SWCNTs. We estimate that the photoconversion efficiency is quite low, requiring 10^7 to 10^9 absorbed photons per micrometer of SWCNT length. An excitation-emission contour plot demonstrates that near-IR emission from both the original and the transformed (6,5) sample is induced by absorption at the same E_{22} transition (Fig. 1D). The shifted emission from our converted SWCNTs differs in wavelength from the weak intrinsic satellite features observed in pristine samples (*8*–*10*). In addition to the prominent shifted emission band, a weak secondary shifted feature can also be seen (*6*).

Very low ozone doses followed by photoconversion are required to prepare such modified SWCNTs. They are qualitatively different from those prepared through more extensive nanotube ozonation (*11*–*17*), which quenches SWCNT near-IR fluorescence (*18*). Of several ionic surfactants used to suspend samples during ozonation treatment, we found that sodium tridecylbenzenesulfonate (STBS) gave the most reproducible results, presumably because it could be used at lower concentrations that compete less for reaction with ozone. Resonance Raman spectra revealed that the ozone-and-photolysis transformation was accompanied by the appearance of a sharp D-band near 1310 cm^{-1} (figs. S10 and S11) signifying covalent functionalization of the nanotube sidewall (*19*). The transformation reaction also occurred, although less efficiently, when weaker oxidants H_2O_2 or K_2CrO_4 were substituted for ozone (fig. S18) (*6*). We conclude that the transformed nanotubes incorporate covalently bonded oxygen. Similar but unintended oxidation may have led to the defect-induced emission reported from some individual SWCNTs exposed to intense pulsed laser light (*20*).

Other semiconducting (*n*,*m*) species also underwent oxygen doping. For example, bulk samples enriched in (6,4) and (8,3) showed reduced E_{11} emission and the growth of a new red-shifted E_{11}* emission band as they were treated with ozone and visible light (fig. S9). Spectral transformations were less efficient for larger-diameter SWCNTs (fig. S15) (*6*). We measured spectral positions and widths of E_{11}* peaks from 10 different oxygen-doped (*n*,*m*) species in STBS for comparison with their pristine forms (Table 1). The spectral red shifts between E_{11} and E_{11}* ranged from 106 to 214 meV and showed a strong positive correlation with E_{11} (Fig. 1E) (*21*). These doping-induced shifts represent optical band gap decreases of 10 to 15% from the pristine values.

Spectroscopic measurements on individual nanotubes revealed photophysical heterogeneity in the doped samples. The results are illustrated with fluorescence spectra acquired from three individual nanotubes in a (6,5)-enriched bulk sample (Fig. 2A). One nanotube was pristine and

[1]Department of Chemistry and R. E. Smalley Institute for Nanoscale Science and Technology, Rice University, Houston, TX 77005, USA. [2]Department of Biochemistry and Cell Biology and R. E. Smalley Institute for Nanoscale Science and Technology, Rice University, Houston, TX 77005, USA.

*To whom correspondence should be addressed. E-mail: weisman@rice.edu

27. The state 1 varied during nondemolition readout due to the intrinsic relaxation toward the steady state 0. No change was observed in the 0 state.
28. T. D. Ladd, D. Maryenko, Y. Yamamoto, E. Abe, K. M. Itoh, *Phys. Rev. B* **71**, 014401 (2005).
29. L. H. Willems van Beveren *et al*., *Appl. Phys. Lett.* **93**, 072102 (2008).
30. This work was supported in part by Visiting Scientist Program Grant 12488 from the National High Magnetic Field Laboratory (NHMFL). The NHMFL is funded by the State of Florida, the U.S. Department of Energy, and NSF through Cooperative Agreement DMR-0654118. D.R.M. acknowledges support through an Australian Research Council Postdoctoral Fellowship (DP1093526). G.W.M. acknowledges support from the Royal Commission for the Exhibition of 1851 and the EPSRC COMPASSS grant. C.B. acknowledges support from the NSF CAREER program (grant 953225).

Supporting Online Material
www.sciencemag.org/cgi/content/full/330/6011/1652/DC1
Materials and Methods
Figs. S1 to S3
References

17 September 2010; accepted 9 November 2010
10.1126/science.1197931

Oxygen Doping Modifies Near-Infrared Band Gaps in Fluorescent Single-Walled Carbon Nanotubes

Saunab Ghosh,[1] Sergei M. Bachilo,[1] Rebecca A. Simonette,[2] Kathleen M. Beckingham,[2] R. Bruce Weisman[1]*

Controlled chemical modifications of single-walled carbon nanotubes (SWCNTs) that tune their useful properties have been sought for multiple applications. We found that beneficial optical changes in SWCNTs resulted from introducing low concentrations of oxygen atoms. Stable covalently oxygen-doped nanotubes were prepared by exposure to ozone and then light. Treated samples showed distinct, structure-specific near-infrared fluorescence at wavelengths 10 to 15% longer than displayed by pristine semiconducting SWCNTs. Dopant sites harvest light energy absorbed in undoped nanotube regions by trapping mobile excitons. The oxygen-doped SWCNTs are much easier to detect and image than pristine SWCNTs because they give stronger near-infrared emission and do not absorb at the shifted emission wavelength.

One of the most remarkable characteristics of single-walled carbon nanotubes (SWCNTs) is their diversity of well-defined electronic and optical properties (*1*, *2*). Each SWCNT is composed of covalently bonded carbon atoms forming an ordered tubular structure with a specific diameter and roll-up angle, uniquely defined by a pair of integers called the (*n*,*m*) index. About two-thirds of SWCNT structures are semiconducting. Their intrinsic band gaps are determined by quantum confinement and linked to physical structure, with only slight alterations possible through environmental perturbation.

A variety of optical and electronic applications would benefit from the controlled modification of SWCNT band gaps in bulk samples, individual nanotubes, and even segments within nanotubes. Covalent sidewall reactions have been used to bond nanotubes to chemical groups having a range of selected electronic properties (*3*, *4*). However, to date such reactions have randomly eroded the highly ordered nanotube π-electron structure. The additional covalent bonds remove electrons from the π-system, broadening and suppressing the signature near-infrared (IR) fluorescence peaks of semiconducting SWCNTs (*5*). Here, we describe a different type of chemically modified SWCNT that is more analogous to dopant-tuned semiconductor materials. These stable and easily prepared oxygen-doped nanotubes are near-IR fluorophores that display distinct, structure-specific optical properties systematically shifted from those of the pristine parent. They are more readily detected than pristine nanotubes.

We produce these modified SWCNTs by exposing aqueous suspensions of pristine SWCNTs to low doses of ozone and then photolyzing the resulting product (*6*). Our studies rely on samples highly enriched in individual semiconducting (*n*,*m*) species through nonlinear density gradient ultracentrifugation (*7*). The simpler optical spectra of these sorted samples allow monitoring of the conversion reaction by fluorescence spectroscopy. Immediately after mild ozone exposure, the characteristic near-IR E_{11} fluorescence band shows small red shifts (~0.2) and appreciable broadening (~5%). Subsequent exposure to light induces a new emission feature, termed E_{11}*, that is red-shifted from E_{11}. Spectra measured during this transformation are shown for a (6,5)-enriched sample in Fig. 1A. During phototransformation by light from a desk lamp, 980-nm E_{11} emission diminishes as the 1120-nm E_{11}* feature increases (Fig. 1, A and B). However, except for some broadening, the absorption spectrum remains essentially unchanged by this conversion (Fig. 1C). The transformed nanotubes show very little absorption at their new emission peak, unlike pristine SWCNTs. We estimate that the photoconversion efficiency is quite low, requiring 10^7 to 10^9 absorbed photons per micrometer of SWCNT length. An excitation-emission contour plot demonstrates that near-IR emission from both the original and the transformed (6,5) sample is induced by absorption at the same E_{22} transition (Fig. 1D). The shifted emission from our converted SWCNTs differs in wavelength from the weak intrinsic satellite features observed in pristine samples (*8*–*10*). In addition to the prominent shifted emission band, a weak secondary shifted feature can also be seen (*6*).

Very low ozone doses followed by photoconversion are required to prepare such modified SWCNTs. They are qualitatively different from those prepared through more extensive nanotube ozonation (*11*–*17*), which quenches SWCNT near-IR fluorescence (*18*). Of several ionic surfactants used to suspend samples during ozonation treatment, we found that sodium tridecylbenzenesulfonate (STBS) gave the most reproducible results, presumably because it could be used at lower concentrations that compete less for reaction with ozone. Resonance Raman spectra revealed that the ozone-and-photolysis transformation was accompanied by the appearance of a sharp D-band near 1310 cm^{-1} (figs. S10 and S11) signifying covalent functionalization of the nanotube sidewall (*19*). The transformation reaction also occurred, although less efficiently, when weaker oxidants H_2O_2 or K_2CrO_4 were substituted for ozone (fig. S18) (*6*). We conclude that the transformed nanotubes incorporate covalently bonded oxygen. Similar but unintended oxidation may have led to the defect-induced emission reported from some individual SWCNTs exposed to intense pulsed laser light (*20*).

Other semiconducting (*n*,*m*) species also underwent oxygen doping. For example, bulk samples enriched in (6,4) and (8,3) showed reduced E_{11} emission and the growth of a new red-shifted E_{11}* emission band as they were treated with ozone and visible light (fig. S9). Spectral transformations were less efficient for larger-diameter SWCNTs (fig. S15) (*6*). We measured spectral positions and widths of E_{11}* peaks from 10 different oxygen-doped (*n*,*m*) species in STBS for comparison with their pristine forms (Table 1). The spectral red shifts between E_{11} and E_{11}* ranged from 106 to 214 meV and showed a strong positive correlation with E_{11} (Fig. 1E) (*21*). These doping-induced shifts represent optical band gap decreases of 10 to 15% from the pristine values.

Spectroscopic measurements on individual nanotubes revealed photophysical heterogeneity in the doped samples. The results are illustrated with fluorescence spectra acquired from three individual nanotubes in a (6,5)-enriched bulk sample (Fig. 2A). One nanotube was pristine and

[1]Department of Chemistry and R. E. Smalley Institute for Nanoscale Science and Technology, Rice University, Houston, TX 77005, USA. [2]Department of Biochemistry and Cell Biology and R. E. Smalley Institute for Nanoscale Science and Technology, Rice University, Houston, TX 77005, USA.

*To whom correspondence should be addressed. E-mail: weisman@rice.edu

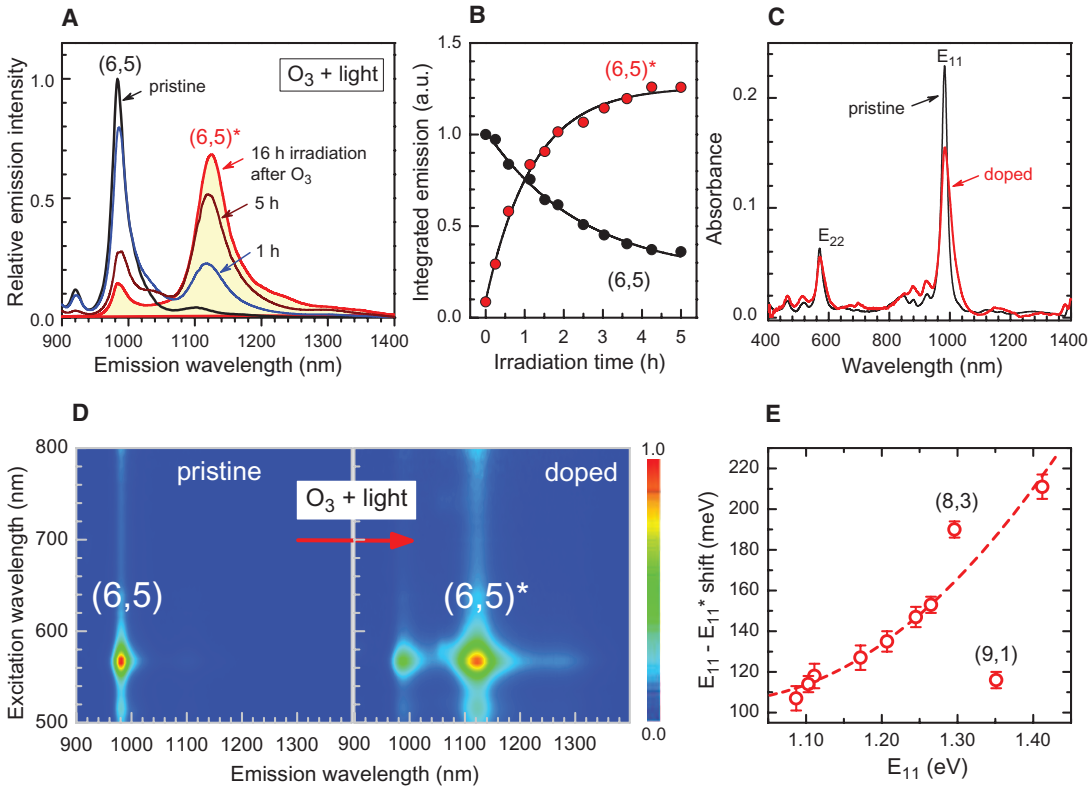

Fig. 1. Spectral changes in a (6,5)-enriched SWCNT dispersion exposed to ozone and light. (**A**) Emission spectra measured with 785-nm excitation after a single treatment with ozone and 1 to 16 hours of white-light irradiation. (**B**) Spectrally integrated emission under the (6,5) main band (black) and side band (red) versus irradiation time with a desk lamp. (**C**) Absorption spectra (path length 1 cm) of the SWCNT sample before (black) and after (red) treatment with ozone and light. (**D**) Photoluminescence excitation-emission contour plots from the (6,5)-enriched sample before and after treatment. The (6,5)* emission feature shows the same excitation peak wavelength as the (6,5) feature. (**E**) Measured photon energy differences between the unshifted and shifted fluorescence peaks of 10 different bulk (*n*,*m*) species as a function of unshifted emission energy. Points show experimental data; the dashed line is a quadratic function drawn to guide the eye. Two points far from the line are labeled with their (*n*,*m*) values.

the other two had been oxygen-doped. One of the two doped nanotubes showed an intense shifted emission band and nearly complete depletion of the normal band; the other emitted both shifted and normal bands with similar peak intensities. These observations demonstrate that the extent of oxygen doping can vary among nanotubes within the same bulk sample. Moreover, the bimodal emission traces imply that individual nanotubes can contain both pristine and doped regions with independent fluorescence spectra. We have compared the polarization of E_{11} and E_{11}* emission from an individual SWCNT whose spectrum is shown in Fig. 2A. The integrated intensities of the two bands measured through a linear polarizer both follow a $\cos^2$ pattern with matching phase angles (Fig. 2B). This result demonstrates that E_{11}* emission arises from a transition dipole oriented parallel to that of the normal E_{11} emission, which is known to lie along the nanotube axis.

Oxygen-doped SWCNTs showed good stability. Transformed bulk samples have been stored under ambient conditions for several months with no change in spectral properties. To check photostability, we measured the E_{11}* emission spectrum of an individual doped (6,4) nanotube at 1-min intervals while irradiating it with 775-nm light at 150 W/cm^2. The emission remained constant in peak position and shape but showed a slight (~3%) decrease in intensity over the 10-min irradiation period (Fig. 2C). The E_{11}* emission intensity remained proportional to excitation intensity at levels up to several kW/cm^2 (fig. S20).

Table 1. Comparative spectral characteristics of pristine and oxygen-doped SWCNTs (*35*). Precise E_{11}* peak positions depend on the extent of doping.

(*n*,*m*)	Pristine E_{11} peak (nm)	Treated E_{11} peak (nm)	Treated E_{11}* peak (nm)	Treated E_{11}-E_{11}* shift (meV)	Pristine E_{11} width (meV)	Treated E_{11} width (meV)	Treated E_{11}* width (meV)
(6,4)	878	889	1050	214	35	45	77
(7,3)	996	1012	1150	147	34	39	75
(9,1)	918	924	1012	117	26	43	73
(6,5)	980	983	1120	154	28	43	50
(8,3)	957	960	1125	189	26	31	48
(9,2)	1141	1147	1272	106	25	28	62
(7,5)	1027	1033	1155	127	23	41	56
(8,4)	1116	1125	1258	117	24	42	72
(10,2)	1058	1070	1190	117	22	24	56
(7,6)	1124	1135	1266	113	28	45	80

We propose a photophysical model in which oxygen doping of a SWCNT at low doses creates sparse perturbed regions that have locally reduced band gaps. Because the great majority of carbon atoms are remote from the doping sites, the overall absorption spectrum remains nearly unchanged and shows no appreciable component at the E_{11}* emission wavelength. However, excitons generated by light absorption in undoped regions are mobile, as in pristine nanotubes (*22*–*24*), and may diffuse during their lifetimes to doped sites where they are stabilized by the local potential minimum. Radiative recombination of these trapped excitons gives the E_{11}* emission characteristic of the doped nanotubes. A single treated nanotube may show both E_{11} and E_{11}* emission because excitons can radiate in pristine or doped locations. Higher doping levels increase the E_{11}*/E_{11} intensity ratio by raising the probability of trapping before emission. Assuming irreversible trapping and mean exciton ranges somewhat below pristine values, we estimate that SWCNTs with intensity ratios near 1 contain approximately one oxygen atom per few thousand carbon atoms.

We used quantum chemical modeling to predict the most stable product of O_3 reaction with SWCNTs and the resulting wave function perturbations over nanotube segments 2 to 3 nm in length, representing the axial size of an exciton

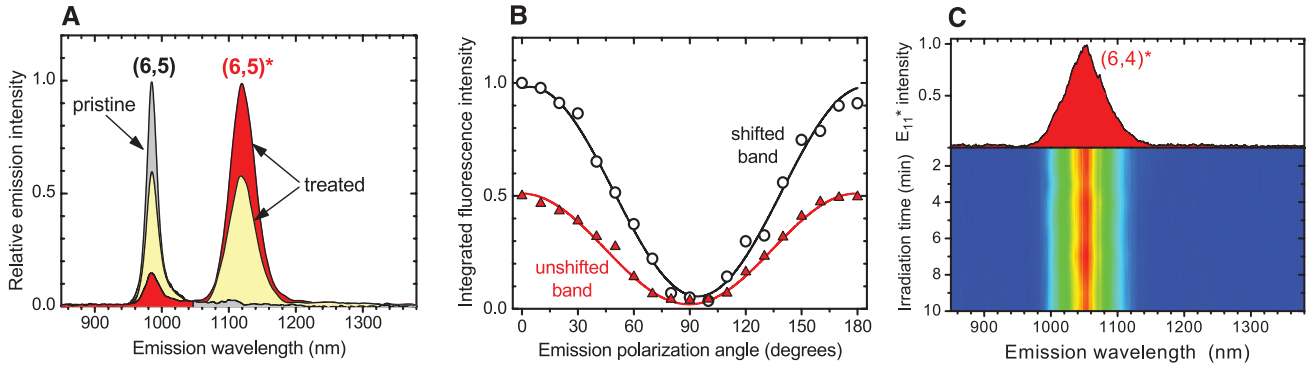

Fig. 2. Spectral characterization of individual oxygen-doped SWCNTs. (**A**) Fluorescence emission spectra of three individual (6,5) nanotubes. The gray trace is from a pristine SWCNT; the red and yellow traces are from different treated nanotubes in the same bulk sample. (**B**) Spectrally integrated intensities from the nanotube giving the yellow trace in (A) as a function of emission polarization angle. (**C**) Emission spectrum (top) and contour plot of successive emission spectra (bottom) from a single heavily treated (6,4) SWCNT continuously irradiated at an intensity of 150 W/cm^2. Spectra were acquired each minute.

(*25*, *26*). Such segments include ~200 carbon atoms, making them very challenging subjects for ab initio studies. We therefore applied a semi-empirical model (PM3) instead. In agreement with previous reports (*27*–*30*), our computations point to formation of an ozonide adduct in which O_3 covalently bridges two adjacent carbon atoms (Fig. 3A, left). Exothermicities vary from 20 to 40 kcal/mol, depending on SWCNT species and orientation of the O_3 addend (fig. S2). The most stable adducts predicted for smaller-diameter nanotubes tend to have O_3 groups oriented nearly parallel to the tube axis. In a process analogous to that experimentally observed in fullerene ozonides (*31*–*33*), subsequent loss of O_2 from the ozonide leaves an epoxide with an oxygen atom bridging the same adjacent sp^3 carbon atoms (Fig. 3A, center). However, our calculations show this epoxide adduct to be less stable [by more than 20 kcal/mol for a (6,5) nanotube] than an isomer in which the oxygen atom links two sp^2 carbon atoms nearly perpendicular to the nanotube axis through C-O-C ether bonds (Fig. 3A, right). We propose that the light-induced step in our treatment is irreversible photoisomerization of the epoxide adduct into this much more stable ether structure. Similar results for the relative stabilities of SWCNT oxide isomers were recently reported by Johnson and co-workers from density functional theory (DFT) ab initio calculations (*28*).

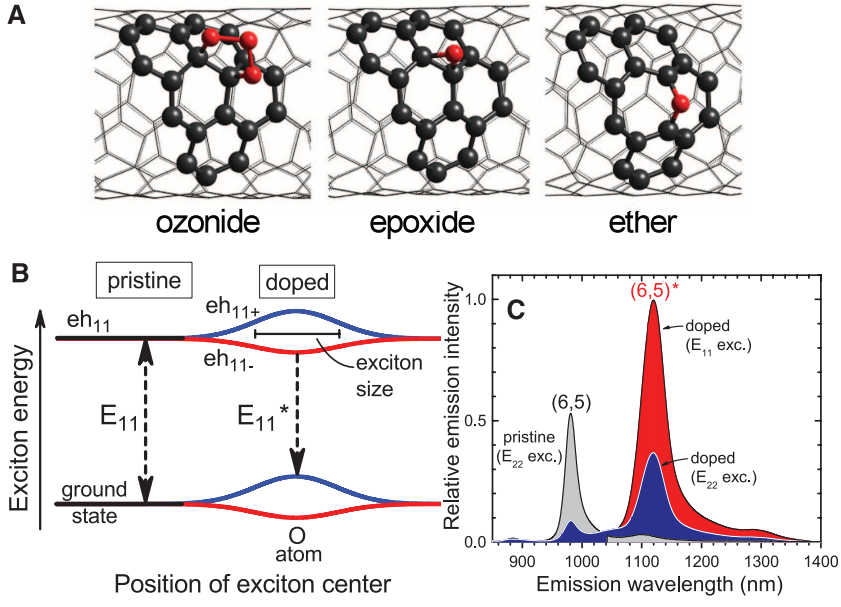

Fig. 3. (**A**) PM3-computed structures of the most stable ozonide (left), epoxide (center), and ether (right) adducts of a segment of (6,5) SWCNT. (**B**) Sketch of qualitative energy levels, showing oxygen-induced perturbations to the ground and lowest "bright" exciton states as a function of axial distance from the dopant atom. Dashed arrows indicate relevant allowed optical transitions. (**C**) Bulk emission spectra of (6,5) SWCNTs: a pristine sample excited at its E_{22} absorption (gray), an oxygen-doped sample excited at its E_{22} absorption (blue), and the same oxygen-doped sample excited at its E_{11} absorption (red).

The two oxide isomers cause quite different perturbations to the nanotube π-electron system. In the epoxide adduct, both carbon atoms bonded to the oxygen are converted to sp^3 hybridization, and five C-C bonds are appreciably lengthened and angularly distorted. By contrast, in the ether adduct, sp^2 carbon hybridization is maintained, only one C-C bond lengthens (the broken one under the ether bridge), and angular distortions are smaller. The electronic and spectroscopic characters of the ether adduct should be much more similar than the epoxide to the pristine SWCNT. An analogous result was demonstrated in earlier experimental studies of C_{60} and C_{70} treated with ozone (*31*, *32*, *34*). After the initially formed fullerene ozonides lost O_2 to form oxides, those with ether bridges and sp^2 carbon hybridization could be distinguished from fullerene epoxides because they resembled the pristine parent fullerene in electronic absorption spectroscopy. Optical excitation of several C_{70} oxides converted them into other isomers through shifts of the oxygen atom on the cage surface (*32*). We propose that the light-induced process observed in our treated SWCNTs is a related photoisomerization.

A comparison of computed wave functions for doped and pristine SWCNTs helps us to interpret the observed optical properties. The highest occupied and lowest unoccupied molecular orbitals (HOMO and LUMO) for a perfect, infinitely long semiconducting SWCNT are both doubly degenerate. To model the optical perturbations caused by sparse doping, we considered short SWCNT segments having lengths comparable to exciton sizes (a few nanometers). For such segments, the degenerate HOMO and LUMO orbitals of chiral nanotubes show a small end-effect splitting on the order of 0.01 meV. By contrast, an ether group oriented across the tube axis induces a far larger perturbation of 100 to 200 meV (figs. S4, S7, and S8). This splits the ground-state and excited-state (eh_{11}) energies in the vicinity of the doping site to give four distinct levels (Fig. 3B). Dipole selection rules allow optical transitions between the upper excited-state sublevel and the lower ground-state sublevel, and also between the lower excited-state and upper ground-state sublevels. The latter transition repre-

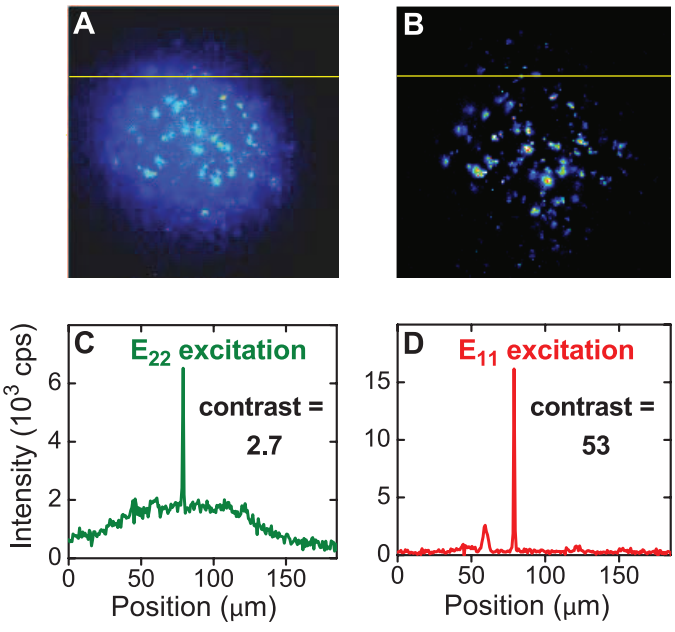

Fig. 4. Comparative near-IR fluorescence micrographs (100-ms exposures) of a cultured human uterine adenocarcinoma cell specimen containing oxygen-doped (6,5) SWCNTs. (**A** and **B**) Excitation was at the E_{22} transition (A) and the E_{11} transition (B) under matched conditions. (**C** and **D**) Intensity profiles and peak/background contrast ratios along the yellow horizontal lines in the images. The sharp peaks near 80 μm are from a single nanotube.

sents the red-shifted fluorescence (E_{11}*) observed from oxygen-doped SWCNTs. Our calculations also predict that the allowed transition dipoles remain parallel to the nanotube axis, in agreement with polarization measurements (Fig. 2B).

Absorption spectroscopy of our lightly doped nanotubes reveals neither of the distinctly shifted, allowed transitions between split levels because the strong electronic perturbation from oxygen doping is local and affects only a small fraction of the carbon atoms. However, we observe broadening of E_{11} and E_{22} absorptions, probably from a distribution of small excitonic energy shifts extending to longer distances from doping sites. After light absorption, some of the excitons from undoped regions diffuse to doped centers, become trapped by the reduced potential, and emit in the red-shifted (E_{11}*) transition involving the lower LUMO and upper HOMO components. Trapping will be reversible if the potential well is not deep relative to the thermal energy k_BT, and the ratio of E_{11}* to E_{11} emission intensities will decrease as temperature increases. We measured these ratios over a limited temperature range and constructed van't Hoff plots to deduce well depths of 40 meV for (8,3) and 61 meV for (6,5) (fig. S12) (*6*). Consistent with the sketch of Fig. 3B, these values are less than half of the red shift between E_{11}* and E_{11} peaks because they represent only the trapping energy, (the difference between the levels marked eh_{11} and eh_{11-}). By assuming that the E_{11}*/E_{11} intensity ratio reflects an equilibrium distribution of exciton locations, we estimate a carbon/oxygen ratio of ~2000 for (6,5) SWCNTs with equal emission intensities (*6*).

After light energy is harvested throughout the nanotube by strong E_{11} and E_{22} absorption bands comparable to those of pristine SWCNTs, mobile excitons transfer the absorbed energy to doping sites that can emit red-shifted E_{11}* fluorescence. This spectral separation of intense near-IR absorption and emission, which is absent in pristine SWCNTs, allows greatly improved optical imaging and detection of the doped nanotubes. Three factors contribute. First, excitation light can be tuned to a sample's E_{11} peak, which has greater absorptivity than the E_{22} peak that must be excited in a pristine sample. Second, emission efficiency is also improved, as spectrally integrated E_{11}* emission exceeds E_{11} emission of the pristine SWCNT under equivalent excitation conditions. These differences are illustrated by three spectra recorded from the same (6,5)-enriched sample excited at its E_{22} peak before doping, at its E_{22} peak after doping, and at its E_{11} peak after doping (Fig. 3C). The third factor is that excitation with longer-wavelength, near-IR light generates far less background emission from biological or environmental specimens.

We demonstrated this enhanced detectivity by near-IR fluorescence microscopy of cultured human uterine adenocarcinoma cells incubated in growth medium containing oxygen-doped (6,5) SWCNTs coated with Pluronic F127 surfactant. For comparison, 100-ms fluorescence images of the same specimen were recorded using E_{22} excitation (as for pristine samples) and E_{11} excitation of matched intensity. Optical filters blocked wavelengths below 1050 nm in the imaging path. The resulting images are shown (false-colored) in Fig. 4, A and B, along with intensity profile plots along the horizontal lines drawn through the image frames (Fig. 4, C and D). Most individual spots represent single nanotubes. The profile plots show that E_{11} excitation provides more than 3 times the emission intensity with one-sixth the background level compared to E_{22} excitation. This improves image contrast by a factor of ~20.

Oxygen doping of SWCNTs is a simple chemical treatment that spectrally separates near-IR emission from absorption bands. This makes doped SWCNTs superior near-IR fluorophores and suggests the prospect of a family of near-IR SWCNT lasers pumped by optical excitation, energy transfer, or charge injection.

References and Notes

1. S. Reich, C. Thomsen, J. Maultzsch, *Carbon Nanotubes: Basic Concepts and Physical Properties* (Wiley-VCH, Weinheim, 2004).
2. S. M. Bachilo *et al.*, *Science* **298**, 2361 (2002); 10.1126/science.1078727.
3. S. Banerjee, T. Hemraj-Benny, S. S. Wong, *Adv. Mater.* **17**, 17 (2005).
4. A. Hirsch, O. Vostrowsky, *Top. Curr. Chem.* **245**, 193 (2005).
5. S. Qin *et al.*, *Macromolecules* **37**, 3965 (2004).
6. See supporting material on *Science* Online.
7. S. Ghosh, S. M. Bachilo, R. B. Weisman, *Nat. Nanotechnol.* **5**, 443 (2010).
8. O. Kiowski, K. Arnold, S. Lebedkin, F. Hennrich, M. M. Kappes, *Phys. Rev. Lett.* **99**, 237402 (2007).
9. Y. Murakami *et al.*, *Phys. Rev. B* **79**, 195407 (2009).
10. O. N. Torrens, M. Zheng, J. M. Kikkawa, *Phys. Rev. Lett.* **101**, 157401 (2008).
11. D. B. Mawhinney *et al.*, *J. Am. Chem. Soc.* **122**, 2383 (2000).
12. S. Banerjee, S. S. Wong, *J. Phys. Chem. B* **106**, 12144 (2002).
13. L. T. Cai, J. L. Bahr, Y. X. Yao, J. M. Tour, *Chem. Mater.* **14**, 4235 (2002).
14. Z. Chen, K. J. Ziegler, J. Shaver, R. H. Hauge, R. E. Smalley, *J. Phys. Chem. B* **110**, 11624 (2006).
15. D. Ogrin, J. Chattopadhyay, A. K. Sadana, W. E. Billups, A. R. Barron, *J. Am. Chem. Soc.* **128**, 11322 (2006).
16. J. M. Simmons *et al.*, *J. Phys. Chem. B* **110**, 7113 (2006).
17. M. Li, M. Boggs, T. P. Beebe, C. P. Huang, *Carbon* **46**, 466 (2008).
18. K. Tsvaygboym, thesis, Rice University (2007).
19. See fig. S9 for additional Raman data.
20. H. Harutyunyan *et al.*, *Nano Lett.* **9**, 2010 (2009).
21. Positions of shifted peaks depend somewhat on extent of doping.
22. L. Cognet *et al.*, *Science* **316**, 1465 (2007).
23. A. J. Siitonen, D. A. Tsyboulski, S. M. Bachilo, R. B. Weisman, *Nano Lett.* **10**, 1595 (2010).
24. A. J. Siitonen, D. A. Tsyboulski, S. M. Bachilo, R. B. Weisman, *J. Phys. Chem. Lett.* **1**, 2189 (2010).
25. V. Perebeinos, J. Tersoff, Ph. Avouris, *Phys. Rev. Lett.* **92**, 257402 (2004).
26. L. Lüer *et al.*, *Nat. Phys.* **5**, 54 (2009).
27. S. Picozzi, S. Santucci, L. Lozzi, L. Valentini, B. Delley, *J. Chem. Phys.* **120**, 7147 (2004).
28. W. L. Yim, J. K. Johnson, *J. Phys. Chem. C* **113**, 17636 (2009).
29. X. Lu, L. Zhang, X. Xu, N. Wang, Q. Zhang, *J. Phys. Chem. B* **106**, 2136 (2002).
30. B. Akdim, T. Kar, X. Duan, R. Pachter, *Chem. Phys. Lett.* **445**, 281 (2007).
31. D. Heymann *et al.*, *J. Am. Chem. Soc.* **122**, 11473 (2000).
32. D. Heymann, S. M. Bachilo, R. B. Weisman, *J. Am. Chem. Soc.* **124**, 6317 (2002).
33. D. Heymann, R. B. Weisman, *C. R. Chim.* **9**, 1107 (2006).
34. R. B. Weisman, D. Heymann, S. M. Bachilo, *J. Am. Chem. Soc.* **123**, 9720 (2001).
35. Samples suspended in aqueous sodium tridecylbenzenesulfonate.

36. Supported by NSF grant CHE-0809020, Welch Foundation grants C-0807 and C-1119, and NASA grant NNX09AH43G. We thank J. K. Johnson for unpublished computational results, and C. Farach-Carson and D. Carson for providing the cultured cell line.

Supporting Online Material

www.sciencemag.org/cgi/content/full/science.1196382/DC1
Materials and Methods
Figs. S1 to S20
Table S1
References

11 August 2010; accepted 14 October 2010
Published online 25 November 2010;
10.1126/science.1196382

Entropically Stabilized Local Dipole Formation in Lead Chalcogenides

Emil S. Božin,[1] Christos D. Malliakas,[2] Petros Souvatzis,[3] Thomas Proffen,[4] Nicola A. Spaldin,[5] Mercouri G. Kanatzidis,[2,6] Simon J. L. Billinge[1,7]*

We report the observation of local structural dipoles that emerge from an undistorted ground state on warming, in contrast to conventional structural phase transitions in which distortions emerge on cooling. Using experimental and theoretical probes of the local structure, we demonstrate this behavior in binary lead chalcogenides, which were believed to adopt the ideal, undistorted rock-salt structure at all temperatures. The behavior is consistent with a simple thermodynamic model in which the emerging dipoles are stabilized in the disordered state at high temperature due to the extra configurational entropy despite the fact that the undistorted structure has lower internal energy. Our findings shed light on the anomalous electronic and thermoelectric properties of the lead chalcogenides. Similar searches may show that the phenomenon is more widespread.

Ferroelectric materials are characterized by a spontaneous alignment of static local dipole moments leading to a net electric polarization that can be switched by an applied electric field (*1*). Above their critical Curie temperature, T_c, they undergo a phase transition to a higher symmetry, nonpolar state, which by analogy with ferromagnets is called paraelectric. Although the question of whether the paraelectric phase consists of fluctuating local dipole moments or entirely centrosymmetric arrangements of atoms remains open (and likely depends on material, temperature, and length scale), the transition from paraelectric to ferroelectric on cooling always involves a lowering in symmetry that is well described within the traditional Landau picture of phase transitions, for example, in $BaTiO_3$ (*2*). In PbTe and PbS, we have observed the existence at high temperature of such a paraelectric phase of disordered, fluctuating dipoles, but the ground state rather than being the ferroelectric state is a dielectric with no local dipoles. There is no macroscopic symmetry change associated with the spontaneous local dipole formation, so the behavior is invisible to conventional crystallographic techniques. We detect the local atomic off-centering at high temperature using recently developed local structural probes.

Lead chalcogenides such as PbTe and the mineral galena (PbS) have been known and exploited since ancient times (*3*). They are particularly important today, with PbTe currently the leading thermoelectric material in applications just above room temperature (*4*). Despite their long history, their nanoscale structure has only recently been studied in detail (*5*–*7*), motivated by the realization that intrinsic nanoscale structural modulations are helpful in producing low thermal conductivity and, therefore, high thermoelectric figures of merit (*4*, *8*). Such studies of the nanostructure have been enabled by powerful synchrotron-based local structure probes, such as atomic pair distribution function (PDF) analysis (*9*, *10*). The PDF is obtained by Fourier transforming appropriately collected and corrected x-ray or neutron powder diffraction data (*9*) and has peaks at positions corresponding to interatomic distances in the solid. We show in Fig. 1B the PDF of the simple rock-salt structure (Fig. 1A) that the lead chalcogenides were previously believed to adopt at all temperatures. Because both Bragg and diffuse scattering signals are used, the PDF yields local structural information rather than just the average crystallographic structure.

Our main results, obtained from temperature-dependent neutron diffraction studies, are summarized in Fig. 1, C to I. Because PbTe and PbS behave qualitatively similarly, we present only the PbTe results in the figure; data for PbS are contained in figs. S1 and S2 in the supporting online material (*11*). The dramatic effect of temperature on the structure of PbTe is evident in the powder diffraction pattern, shown in the form of the corrected and normalized diffraction intensity function $F(Q)$ (*11*) in Fig. 1C. This figure also serves to illustrate the high quality and good statistics of the neutron powder diffraction data collected over a wide range of momentum transfer, Q ($Q = 4\pi\sin\theta/\lambda$, where θ is the Bragg angle and λ the wavelength of the x-rays or neutrons). The dramatic loss of intensity in the Bragg peaks at high Q in the 500 K data (red) compared with the 15 K data (blue) is clear. The attenuation is due in part to the usual Debye-Waller effects (*12*) from increased thermal motion; however, the extent of the changes is extraordinarily large. In Fig. 1, D and E, we show the PDFs at 15 K and 500 K, respectively; the effect of temperature on the PDFs is anomalous, with notable broadening evident at 500 K compared with 15 K. (The scale in Fig. 1E is one-fifth that in Fig. 1D.)

To study the temperature-induced local structural effects in more detail, we next analyze the temperature dependence of the low-r region, where r is the interatomic pair separation distance, of the PDF (Fig. 1F), where measured PDFs are shown every 50 K from 15 K to 500 K. The PDF peak broadening is reflected in the drop in the maxima of the peaks. Particularly striking is the drop in the nearest-neighbor peak, which occurs as rapidly as those in the higher-neighbor peaks. This strong broadening of the nearest-neighbor PDF peak does not occur in conventional materials. This is because of the highly correlated dynamics of nearest-neighbor atoms (*13*), which results in the relative motion of directly bonded atom pairs having a much smaller temperature dependence than the higher-neighbor pairs.

In Fig. 1, G and H, we show the Pb-Te nearest-neighbor peak on an expanded scale. At 15 K (Fig. 1G), the peak appears as a sharp, single-Gaussian function with small ripples coming from the finite Q range of the Fourier transform, so-called termination ripples (*9*). The red line is a calculated PDF peak with a pure Gaussian line-shape, convoluted with a sinc function to simulate the effects of the finite Fourier transform (*9*). This is characteristic of a single average bond length with harmonic motion taking place around that position, indicating that the ground state of PbTe at 15K is ideal rock-salt in both the local and average structures, as expected. However, at 500 K (Fig. 1H), the peak is considerably broadened and qualitatively non-Gaussian, with extra intensity apparent on the high-r side of the peak. This unambiguously indicates the appearance of nonharmonic effects with increasing temperature.

We have quantified the asymmetry of this peak, and in Fig. 1I we plot the temperature dependence of a PDF peak asymmetry parameter, ΔR_{ASYMM} (*11*). It has a value of zero for a perfectly symmetric peak such as a Gaussian, and its numerical value increases as the peak becomes more asymmetric. As evident in Fig. 1I, the asymmetric nature of the first PDF peak increases continuously from 15 K to ~250 K, where it saturates.

The non-Gaussian asymmetry can be interpreted either in terms of strong anharmonicity in a single-welled potential probed by the atomic motions or by the appearance of multiple, incompletely resolved, short and long bond lengths under the nearest-neighbor PDF peak, characteristic of quasistatic structural dipoles in materials studied using the PDF (*14*, *15*). Figure 1F points to the latter interpretation because it is evident that higher-neighbor peaks are also losing their Gaussian character at high temperature. Despite being globally rock-salt, characteristic of lone-pair–inactive Pb^{2+} compounds (*6*), the local structure behaves like that in ferroelectrically distorted lone-pair–active Pb^{2+} compounds such as $PbTiO_3$ (*14*). The off-centered ions are disordered

[1]Condensed Matter Physics and Materials Science Department, Brookhaven National Laboratory, Upton, NY 11973, USA. [2]Department of Chemistry, Northwestern University, Evanston, IL 60208, USA. [3]Theoretical Division, Los Alamos National Laboratory, Los Alamos, NM 87545, USA. [4]Lujan Neutron Scattering Center, Los Alamos National Laboratory, Los Alamos, NM 87545, USA. [5]Department of Materials, ETH, Zurich, Switzerland. [6]Materials Science Division, Argonne National Laboratory, Argonne, IL 60439, USA. [7]Department of Applied Physics and Applied Mathematics, Columbia University, New York, NY 10027, USA.

*To whom correspondence should be addressed. E-mail: sb2896@columbia.edu

among symmetry-equivalent displaced sites similar to the Ti in the high-temperature phases of $BaTiO_3$ (*14*). Although the PDF does not yield information directly on the dynamics, it is likely that the local dipole moments are fluctuating between the symmetry equivalent displaced sites.

Further confirmation of this unexpected result has been obtained by modeling the PDF using a least-squares fitting procedure (*11*). In Fig. 2A, the reduced χ^2 (goodness of fit) values of a number of competing models are shown as a function of temperature. Undistorted models give the best agreement at low temperature, but above 100 K distorted models give better agreement, with a model including displacements along ⟨100⟩ crystallographic directions being clearly preferred.

In Fig. 2, B and C, we show the T dependence of Pb isotropic atomic displacement parameters (ADPs) and the lattice parameter, respectively, refined from the simplest undistorted model. In this model, any off-centering must be accommodated in the refined ADP. The temperature dependence of both lattice parameters and the ADPs are linear, as expected, in the high-temperature region. In contrast, both properties show a downward deviation from this linear behavior below room temperature, precisely in the region where the PDF peak asymmetry is changing. This cannot be explained in any harmonic or quasiharmonic model for the lattice dynamics, such as the Debye model (*16*), shown as solid lines in the figure. The combined temperature dependences of the PDF peak asymmetry and the ADPs suggest that local ferroelectric-like Pb^{2+} off-center displacements, absent at T = 0 K, gradually emerge over the temperature range up to 250 K. At higher temperatures, the displaced ions show more conventional dynamics, resulting in a linear ADP and lattice expansion. The amplitude of the Pb^{2+} ion off-centering distortion, refined in the favored ⟨100⟩-displacements model, is shown in Fig. 2E. The refined distortion saturates at a maximum value of 0.24 Å. This is comparable in magnitude to ferroelectric displacements in, for example, $BaTiO_3$ (*2*). The vicinity of a ferroelectric instability is also implicated in first-principles electronic structure calculations (*7*), including our recently developed self-consistent ab initio lattice dynamical (SCAILD) method (*17*), as evident in fig. S3 (*11*).

Although the behavior observed in the PDF is highly unusual—we know of no other observation of local dipoles emerging from an undistorted ground state on heating—we rationalize it using a simple thermodynamic argument. In Fig. 3A, we plot the familiar schematic of the thermodynamic free energy, F, versus temperature for a series of phases.

The curves slope downward with increasing temperature, T, due to the increased contribution of the entropy term in the free energy at higher temperature: $F = U - TS$, where U is the internal energy. Phases with higher entropies, S, slope down more steeply and may cross below phases, with lower internal energy becoming the stable phase at high temperature. This is the classic explanation of the solid-liquid phase transition. In Fig. 3A, we represent the free energy of an ordered ferroelectric phase as a light blue line and that of the disordered paraelectric phase in olive green. In the absence of competing phases, the ferroelectric phase transition occurs at T_F, where these lines cross as indicated in the figure. Above T_F, the stable state is the paraelectric phase.

Another metastable state may exist that is undistorted but has a higher internal energy than the distorted phase. This is represented as a dashed gray line in Fig. 3B. Its configurational entropy should be the same as the ordered ferroelectric phase (light blue curve), so in the schematic we give these a similar slope, although factors such as vibrational entropy differences will change this somewhat in practice. Because it is higher in energy and has a similar slope, the free energy of this phase never crosses the ferroelectric phase, and it is never the stable state. However, consider the special situation in which this competing undistorted state is very close but slightly lower in energy than the ferroelectric state at T = 0. This situation is depicted as the red line in the figure. In this case,

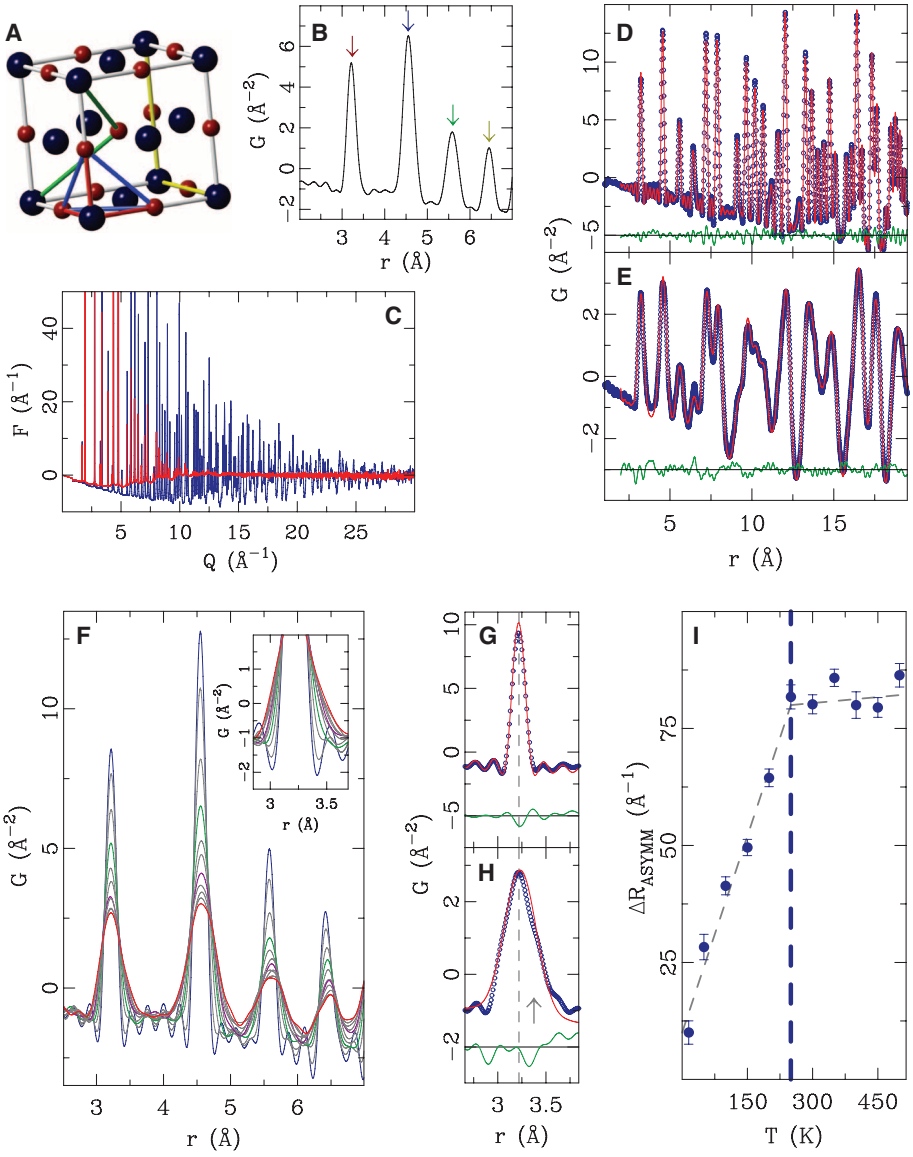

Fig. 1. (**A**) The rock-salt structure of PbTe with various interatomic distances color coded and (**B**) the respective PDF peaks marked with arrows using the same color code to illustrate how the PDF is built up from atom-pair distances in the structure. (**C**) Experimental total scattering structure function $F(Q)$ at T = 15 K (blue) and T = 500 K (red), with the corresponding PDFs (open symbols) shown in (**D**) and (**E**). The PDF of the rock-salt structure model is superimposed as a solid red line, with the difference curve (green) offset for clarity. (**F**) A stack of experimental PDFs from 15 K (blue) to 500 K (red) in ~50 K increments. The 150 K data set is highlighted in green, and the 300 K data are in purple. The inset focuses on the behavior of the nearest-neighbor PDF peak. (**G**) Fit of the rock-salt crystallographic model to the near-neighbor PDF peak data at 15 K and (**H**) at 500 K. (**I**) Asymmetry of the near-neighbor PDF peak.

the ground state is undistorted, but on warming the stable state becomes the paraelectric phase, and local fluctuating dipoles emerge out of an undistorted ground state. This crossover is indicated by T_E in the figure. These thermodynamic arguments do not explain the phenomenon, but they give an intuitive rationalization for this behavior and suggest that it may be more widespread than in the PbQ compounds studied here.

The thermodynamic arguments do not address the microscopic mechanisms that could give rise to this situation, nor do they address the precise nature of the transition from the undistorted to the paraelectric phase, that is, whether it is an abrupt transition or a diffuse crossover. The short-range nature of the dipole fluctuations suggests the latter, although characterizing this will require further study. Although there is no change in crystal symmetry, so it is not possible to identify a macroscopic order parameter, there is evidence for the transition in a macroscopic structural parameter: An anomaly is evident in the temperature dependence of the lattice parameter (Fig. 2B), which shows a similar negative deviation from linear behavior at 250 K.

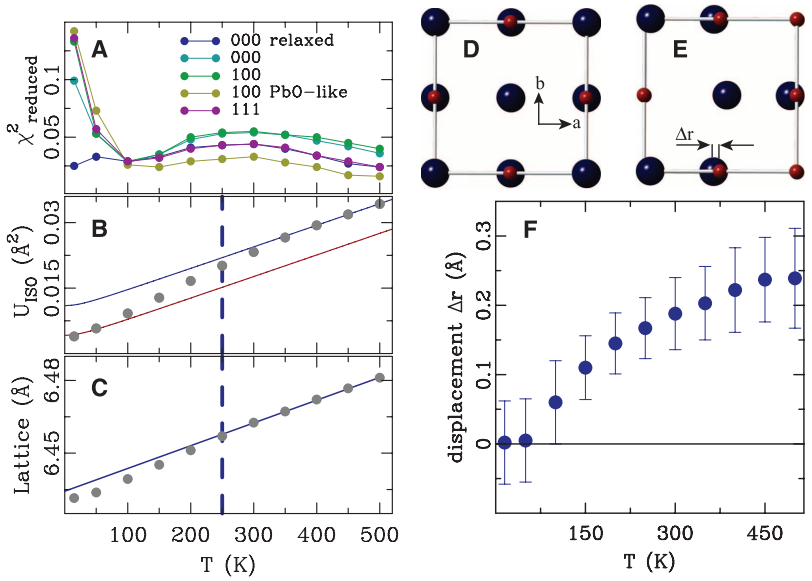

Fig. 2. (**A**) Reduced χ^2 of best fits for competing models of the local structure (*11*). (**B**) The gray dots are the isotropic ADPs for Pb refined from the undistorted model. The solid lines represent the behavior expected from the Debye model, using the same Debye temperature, but with different offset parameters, accounting for static disorder, for the red and blue lines. (**C**) The PbTe lattice parameter (gray dots) as obtained from Rietveld refinement. The vertical dashed line indicates the temperature 250 K where the asymmetry of the nearest-neighbor peak saturates (Fig. 1I). (**D**) Schematic of the rock-salt structure shown in projection down the *c* axis, showing Pb (blue) and Te (red). (**E**) Same view of the proposed model for the distorted rock-salt structure above room temperature. The amplitude of the Pb displacements have been highly exaggerated to show the displacements more clearly. (**F**) Amplitude of Pb local off-centering refined from the ⟨100⟩ displaced model.

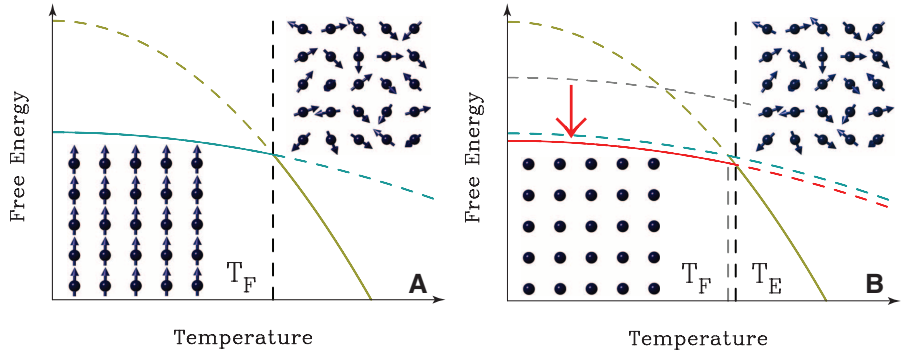

Fig. 3. Schematics of the temperature dependence of the thermodynamic free energy *F*. (**A**) The light blue curve represents *F*(*T*) for a ferroelectric state with ordered dipole moments (shown schematically as blue arrows), and the olive green curve is for the paraelectric state where the dipoles are fluctuating and only short-range ordered at best. It is more steeply sloping because of the extra configurational entropy. Where these curves cross is the ferroelectric transition temperature, labeled T_F. The blue arrows show schematically the ordered dipole moments in the ferroelectric phase and disordered moments in the paraelectric phase. (**B**) As in (A) but superimposed are additional free-energy curves for putative undistorted states. The gray dashed curve represents *F*(*T*) for a metastable undistorted state. The red curve shows the case where the competing undistorted state is slightly lower in energy than the ferroelectric state. In this case, there is a crossover from an undistorted to a paraelectric phase at a temperature T_E, as shown schematically. In the insets, the blue dots indicate the absence of dipoles at low temperature and the blue arrows the disordered fluctuating dipoles at high temperature.

The structural effects we report should be considered in future explanations of the peculiar properties of these materials; for example, the very low lattice thermal conductivity (*18*) at elevated temperatures. The ferroelectric-like moment fluctuations would also explain the well-known strong temperature dependence of carrier scattering, which is unique in PbQ and not found in other semiconductors such as Si, Ge, and Bi_2Te_3. This dependence causes the rapid degradation of carrier mobility with rising temperature with a $T^{-2.5}$ dependence (*19*). Generally, the power exponent for the mobility in semiconductors is $\sim T^{-1.5}$, and it is due to the increase in vibrational amplitude of the lattice. The high power exponent in PbQ implies additional scattering mechanisms for the carriers that would come from the local off-centering fluctuations of the Pb^{2+} ions. Similarly, our electronic structure calculations (*11*) find an enhanced band gap for the locally distorted structure, indicating that the observed anomalous increase in the band gap, E_g, with increasing temperature observed in PbTe (*20*), may be explained by the appearance of the local distortions.

The emergence of structural dipoles from normal, undistorted states in materials may be more ubiquitous than currently recognized. There are some similarities of the present situation to the search for a hidden broken symmetry in the pseudogap phase of high-temperature superconductors, where a short-range nematic orbital ordering may be relevant but is only apparent in probes of local structure (*21*). The PDF is a powerful experimental tool for probing these effects. Finally, we may now begin to contemplate new ways to control these fluctuations through appropriate chemical modifications that could lead to large increases in the thermoelectric performance of PbTe-based materials. We suggest in particular that new thermoelectrics should be sought among materials that, like PbTe, are close to a ferroelectric instability. It is remarkable that binary compounds with such simple structures, which have been known about and exploited for thousands of years, can still harbor surprises when studied using modern experimental and theoretical tools.

References and Notes

1. F. Jona, G. Shirane, *Ferroelectric Crystals* (Dover, New York, 1993).
2. G. H. Kwei, A. C. Lawson, S. J. L. Billinge, S.-W. Cheong, *J. Phys. Chem.* **97**, 2368 (1993).
3. P. Walter *et al.*, *Nano Lett.* **6**, 2215 (2006).

4. Z. H. Dughaish, *Physica B* **322**, 205 (2002).
5. H. Lin, E. S. Bozin, S. J. L. Billinge, E. Quarez, M. G. Kanatzidis, *Phys. Rev. B* **72**, 174113 (2005).
6. U. V. Waghmare, N. A. Spaldin, H. C. Kandpal, R. Seshadri, *Phys. Rev. B* **67**, 125111 (2003).
7. J. M. An, A. Subedi, D. J. Singh, *Solid State Commun.* **148**, 417 (2008).
8. J. R. Sootsman *et al.*, *Angew. Chem. Int. Ed.* **47**, 8618 (2008).
9. T. Egami, S. J. L. Billinge, *Underneath the Bragg Peaks: Structural Analysis of Complex Materials* (Pergamon Press, Elsevier, Oxford, England, 2003).
10. S. J. L. Billinge, I. Levin, *Science* **316**, 561 (2007).
11. Materials and methods are available as supporting material on *Science* Online.
12. B. E. Warren, *X-ray Diffraction* (Dover, New York, 1990).
13. I.-K. Jeong, T. Proffen, F. Mohiuddin-Jacobs, S. J. L. Billinge, *J. Phys. Chem. A* **103**, 921 (1999).
14. G. H. Kwei, S. J. L. Billinge, S.-W. Cheong, J. G. Saxton, *Ferroelectrics* **164**, 57 (1995).
15. H. D. Rosenfeld, T. Egami, *Ferroelectrics* **164**, 133 (1995).
16. P. Debye, *Ann. Phys.-Berlin* **39**, 789 (1912).
17. P. Souvatzis, O. Eriksson, M. I. Katsnelson, S. P. Rudin, *Phys. Rev. Lett.* **100**, 095901 (2008).
18. A. F. Joffé, *Can. J. Phys.* **34**, (12A), 1342 (1956).
19. B. A. E. Yu, I. Ravich, I. A. Smirnov, *Semiconducting Lead Chalcogenides*, vol. 5 (Plenum, New York, 1970).
20. R. N. Tauber, A. A. Machonis, I. B. Cadoff, *J. Appl. Phys.* **37**, 4855 (1966).
21. T. M. Chuang *et al.*, *Science* **327**, 181 (2010).
22. S.J.B. and E.B. thank J. Richardson for his early support and enthusiasm for the project and dedicate the paper to him. We acknowledge useful discussions with A. Millis, P. Allen, R. Cohen, C. Farrow, and J. Hill. Work in the Billinge group was supported by the U.S. Department of Energy, Office of Basic Energy Sciences (DOE-BES), under contract DE-AC02-98CH10886. Work in the Kanatzidis group was supported by the Office of Naval Research. Work in the Spaldin group was supported by the NSF under award DMR-0940420. The neutron diffraction measurements were carried out at the Lujan Center at Los Alamos National Laboratory, and the x-ray experiments were carried out at the Advanced Photon Source, Argonne National Laboratory, both of which are supported by DOE-BES, and the calculations were performed at the San Diego Supercomputer Center, which is supported by NSF.

Supporting Online Material

www.sciencemag.org/cgi/content/full/330/6011/1660/DC1
Materials and Methods
SOM Text
Figs. S1 to S4
References

24 May 2010; accepted 16 November 2010
10.1126/science.1192759

Large Variations in Southern Hemisphere Biomass Burning During the Last 650 Years

Z. Wang,[1] J. Chappellaz,[2] K. Park,[1] J. E. Mak[1]*

We present a 650-year Antarctic ice core record of concentration and isotopic ratios ($\delta^{13}C$ and $\delta^{18}O$) of atmospheric carbon monoxide. Concentrations decreased by ~25% (14 parts per billion by volume) from the mid-1300s to the 1600s then recovered completely by the late 1800s. $\delta^{13}C$ and $\delta^{18}O$ decreased by about 2 and 4 per mil (‰), respectively, from the mid-1300s to the 1600s then increased by about 2.5 and 4‰ by the late 1800s. These observations and isotope mass balance model results imply that large variations in the degree of biomass burning in the Southern Hemisphere occurred during the last 650 years, with a decrease by about 50% in the 1600s, an increase of about 100% by the late 1800s, and another decrease by about 70% from the late 1800s to present day.

Carbon monoxide (CO) plays a key role in the chemistry of the troposphere, largely determining the oxidation potential of the atmosphere through its interaction with hydroxyl radical (OH). CO also interacts with atmospheric methane, a gas whose preindustrial variability is the topic of continuing debate (*1*, *2*). Little is known about the variability of CO before the industrial age (*3*) or about the anthropogenic impact on its budget, although both affect atmospheric CH_4 and O_3 budgets and related climate-chemistry interactions.

The main sources of atmospheric CO include atmospheric oxidation of methane and nonmethane hydrocarbons (NMHCs), biomass burning, and fossil fuel combustion (*4*). These sources account for about 90% of today's global CO budget (*4*). Stable isotopic ratios ($\delta^{13}C$ and $\delta^{18}O$) in atmospheric CO help to resolve the relative contributions of these sources and thus to better estimate the global CO budget (*5*). To date, no isotopic ratios from CO in ice have been reported, and few CO mixing ratio measurements have been reported (*1*, *3*, *6*). Through use of a recently developed analytical technique (*7*), we present measurements of CO concentration ([CO]), $\delta^{13}C$, and $\delta^{18}O$ from a South Pole ice core [89°57'S 17°36'W; 2800 m above sea level (asl)] and from the D47 ice core (67°23'S 154°03'E; 1550 m asl) in Antarctica (Fig. 1).

The combined changes in [CO], $\delta^{13}C$, and $\delta^{18}O$ during the past 650 years should reflect variations in both total CO flux and a shift in relative source strengths over time. [CO] shows a decreasing trend from 53 ± 5 parts per billion by volume (ppbv) in the mid-1300s to a minimum of 38 ± 5 ppbv in the 1600s. CO mixing ratio then increases to a relatively constant value of 55 ± 5 ppbv in the late 1800s. Good agreement was observed between our [CO] data and previous measurements on Antarctic ice samples (*3*, *6*). Trends in both $\delta^{13}C$ and $\delta^{18}O$ look similar to the [CO] record up to the late 1800s. $\delta^{13}C$ [Vienna Pee Dee belemnite (VPDB)] and $\delta^{18}O$ [Vienna standard mean ocean water (VSMOW)], respectively, decreased from –28.0 ± 0.3‰ and 0.6 ± 0.7‰ in the mid-1300s to –30.2 ± 0.3‰ and –3.4 ± 0.7‰ in the 1600s, then increased to –27.4 ± 0.3‰ and 0.8 ± 0.7‰ by the late 1800s. Minimum values of [CO], $\delta^{13}C$, and $\delta^{18}O$ roughly coincide with the Little Ice Age (LIA; circa 1500–1800), as defined in the Northern Hemisphere.

Observations from Berkner Island (79°32.90'S 45°40.7'W; 890 m asl) firn and present day samples are also shown in Fig. 1. The slight decrease of [CO] from the late 1800s to present day is thus accompanied by large shifts in both $\delta^{13}C$ and $\delta^{18}O$, which is a result of variations in relative source strengths during the past century. In particular, methane-derived CO, which is dependent upon methane concentration and depleted in both $\delta^{13}C$ and $\delta^{18}O$, increased dramatically—by 13 ppbv—during this time (Fig. 2). Because there was little difference in overall [CO] between the late 1800s and present day, contributions from other CO sources must have decreased by a similar amount. Data from Berkner Island firn air show an increase in [CO] and a decrease in $\delta^{13}C$ since 1970 (*8*), reflecting the increase in atmospheric methane (*9*).

The contribution from fossil fuel combustion is negligible before the 1900s according to historic CO_2 emissions data (*10*). In addition, simulations from the Model for Ozone and Related chemical Tracers (MOZART-4) (*11*) show the fossil fuel combustion contribution to today's CO budget in Antarctica is only 2 to 3 ppbv. Thus, the main sources of CO able to explain our signals are biomass burning and NMHC oxidation.

We can use isotopic compositions to help distinguish combustion-derived CO (such as biomass burning) from noncombustion-derived CO (such as hydrocarbon oxidation). $C^{18}O$ is a useful tracer for this because of large differences in the oxygen isotopic composition between combustion and noncombustion sources of CO (*12*). The $\delta^{18}O$ signature from combustion sources is significantly enriched as compared with the $\delta^{18}O$ signature from hydrocarbon oxidation processes (*12*, *13*). The $\delta^{18}O$ value for biomass burning–derived CO is generally between 15 and 22‰, depending on specific combustion conditions (*13*–*15*).

We used an isotope mass balance model to estimate the ratio of combustion to noncombustion

[1]Institute for Terrestrial and Planetary Atmospheres/School of Marine and Atmospheric Sciences, Stony Brook University, Stony Brook, NY 11794–5000, USA. [2]Laboratoire de Glaciologie et Géophysique de l'Environnement (LGGE), CNRS, University of Grenoble, BP 96, 38402 St. Martin d'Hères Cedex, France.

*To whom correspondence should be addressed. E-mail: john.mak@stonybrook.edu

4. Z. H. Dughaish, *Physica B* **322**, 205 (2002).
5. H. Lin, E. S. Bozin, S. J. L. Billinge, E. Quarez, M. G. Kanatzidis, *Phys. Rev. B* **72**, 174113 (2005).
6. U. V. Waghmare, N. A. Spaldin, H. C. Kandpal, R. Seshadri, *Phys. Rev. B* **67**, 125111 (2003).
7. J. M. An, A. Subedi, D. J. Singh, *Solid State Commun.* **148**, 417 (2008).
8. J. R. Sootsman *et al.*, *Angew. Chem. Int. Ed.* **47**, 8618 (2008).
9. T. Egami, S. J. L. Billinge, *Underneath the Bragg Peaks: Structural Analysis of Complex Materials* (Pergamon Press, Elsevier, Oxford, England, 2003).
10. S. J. L. Billinge, I. Levin, *Science* **316**, 561 (2007).
11. Materials and methods are available as supporting material on *Science* Online.
12. B. E. Warren, *X-ray Diffraction* (Dover, New York, 1990).
13. I.-K. Jeong, T. Proffen, F. Mohiuddin-Jacobs, S. J. L. Billinge, *J. Phys. Chem. A* **103**, 921 (1999).
14. G. H. Kwei, S. J. L. Billinge, S.-W. Cheong, J. G. Saxton, *Ferroelectrics* **164**, 57 (1995).
15. H. D. Rosenfeld, T. Egami, *Ferroelectrics* **164**, 133 (1995).
16. P. Debye, *Ann. Phys.-Berlin* **39**, 789 (1912).
17. P. Souvatzis, O. Eriksson, M. I. Katsnelson, S. P. Rudin, *Phys. Rev. Lett.* **100**, 095901 (2008).
18. A. F. Joffé, *Can. J. Phys.* **34**, (12A), 1342 (1956).
19. B. A. E. Yu, I. Ravich, I. A. Smirnov, *Semiconducting Lead Chalcogenides*, vol. 5 (Plenum, New York, 1970).
20. R. N. Tauber, A. A. Machonis, I. B. Cadoff, *J. Appl. Phys.* **37**, 4855 (1966).
21. T. M. Chuang *et al.*, *Science* **327**, 181 (2010).
22. S.J.B. and E.B. thank J. Richardson for his early support and enthusiasm for the project and dedicate the paper to him. We acknowledge useful discussions with A. Millis, P. Allen, R. Cohen, C. Farrow, and J. Hill. Work in the Billinge group was supported by the U.S. Department of Energy, Office of Basic Energy Sciences (DOE-BES), under contract DE-AC02-98CH10886. Work in the Kanatzidis group was supported by the Office of Naval Research. Work in the Spaldin group was supported by the NSF under award DMR-0940420. The neutron diffraction measurements were carried out at the Lujan Center at Los Alamos National Laboratory, and the x-ray experiments were carried out at the Advanced Photon Source, Argonne National Laboratory, both of which are supported by DOE-BES, and the calculations were performed at the San Diego Supercomputer Center, which is supported by NSF.

Supporting Online Material

www.sciencemag.org/cgi/content/full/330/6011/1660/DC1
Materials and Methods
SOM Text
Figs. S1 to S4
References

24 May 2010; accepted 16 November 2010
10.1126/science.1192759

Large Variations in Southern Hemisphere Biomass Burning During the Last 650 Years

Z. Wang,[1] J. Chappellaz,[2] K. Park,[1] J. E. Mak[1]*

We present a 650-year Antarctic ice core record of concentration and isotopic ratios ($\delta^{13}C$ and $\delta^{18}O$) of atmospheric carbon monoxide. Concentrations decreased by ~25% (14 parts per billion by volume) from the mid-1300s to the 1600s then recovered completely by the late 1800s. $\delta^{13}C$ and $\delta^{18}O$ decreased by about 2 and 4 per mil (‰), respectively, from the mid-1300s to the 1600s then increased by about 2.5 and 4‰ by the late 1800s. These observations and isotope mass balance model results imply that large variations in the degree of biomass burning in the Southern Hemisphere occurred during the last 650 years, with a decrease by about 50% in the 1600s, an increase of about 100% by the late 1800s, and another decrease by about 70% from the late 1800s to present day.

Carbon monoxide (CO) plays a key role in the chemistry of the troposphere, largely determining the oxidation potential of the atmosphere through its interaction with hydroxyl radical (OH). CO also interacts with atmospheric methane, a gas whose preindustrial variability is the topic of continuing debate (*1*, *2*). Little is known about the variability of CO before the industrial age (*3*) or about the anthropogenic impact on its budget, although both affect atmospheric CH_4 and O_3 budgets and related climate-chemistry interactions.

The main sources of atmospheric CO include atmospheric oxidation of methane and nonmethane hydrocarbons (NMHCs), biomass burning, and fossil fuel combustion (*4*). These sources account for about 90% of today's global CO budget (*4*). Stable isotopic ratios ($\delta^{13}C$ and $\delta^{18}O$) in atmospheric CO help to resolve the relative contributions of these sources and thus to better estimate the global CO budget (*5*). To date, no isotopic ratios from CO in ice have been reported, and few CO mixing ratio measurements have been reported (*1*, *3*, *6*). Through use of a recently developed analytical technique (*7*), we present measurements of CO concentration ([CO]), $\delta^{13}C$, and $\delta^{18}O$ from a South Pole ice core [89°57'S 17°36'W; 2800 m above sea level (asl)] and from the D47 ice core (67°23'S 154°03'E; 1550 m asl) in Antarctica (Fig. 1).

The combined changes in [CO], $\delta^{13}C$, and $\delta^{18}O$ during the past 650 years should reflect variations in both total CO flux and a shift in relative source strengths over time. [CO] shows a decreasing trend from 53 ± 5 parts per billion by volume (ppbv) in the mid-1300s to a minimum of 38 ± 5 ppbv in the 1600s. CO mixing ratio then increases to a relatively constant value of 55 ± 5 ppbv in the late 1800s. Good agreement was observed between our [CO] data and previous measurements on Antarctic ice samples (*3*, *6*). Trends in both $\delta^{13}C$ and $\delta^{18}O$ look similar to the [CO] record up to the late 1800s. $\delta^{13}C$ [Vienna Pee Dee belemnite (VPDB)] and $\delta^{18}O$ [Vienna standard mean ocean water (VSMOW)], respectively, decreased from –28.0 ± 0.3‰ and 0.6 ± 0.7‰ in the mid-1300s to –30.2 ± 0.3‰ and –3.4 ± 0.7‰ in the 1600s, then increased to –27.4 ± 0.3‰ and 0.8 ± 0.7‰ by the late 1800s. Minimum values of [CO], $\delta^{13}C$, and $\delta^{18}O$ roughly coincide with the Little Ice Age (LIA; circa 1500–1800), as defined in the Northern Hemisphere.

Observations from Berkner Island (79°32.90'S 45°40.7'W; 890 m asl) firn and present day samples are also shown in Fig. 1. The slight decrease of [CO] from the late 1800s to present day is thus accompanied by large shifts in both $\delta^{13}C$ and $\delta^{18}O$, which is a result of variations in relative source strengths during the past century. In particular, methane-derived CO, which is dependent upon methane concentration and depleted in both $\delta^{13}C$ and $\delta^{18}O$, increased dramatically—by 13 ppbv—during this time (Fig. 2). Because there was little difference in overall [CO] between the late 1800s and present day, contributions from other CO sources must have decreased by a similar amount. Data from Berkner Island firn air show an increase in [CO] and a decrease in $\delta^{13}C$ since 1970 (*8*), reflecting the increase in atmospheric methane (*9*).

The contribution from fossil fuel combustion is negligible before the 1900s according to historic CO_2 emissions data (*10*). In addition, simulations from the Model for Ozone and Related chemical Tracers (MOZART-4) (*11*) show the fossil fuel combustion contribution to today's CO budget in Antarctica is only 2 to 3 ppbv. Thus, the main sources of CO able to explain our signals are biomass burning and NMHC oxidation.

We can use isotopic compositions to help distinguish combustion-derived CO (such as biomass burning) from noncombustion-derived CO (such as hydrocarbon oxidation). $C^{18}O$ is a useful tracer for this because of large differences in the oxygen isotopic composition between combustion and noncombustion sources of CO (*12*). The $\delta^{18}O$ signature from combustion sources is significantly enriched as compared with the $\delta^{18}O$ signature from hydrocarbon oxidation processes (*12*, *13*). The $\delta^{18}O$ value for biomass burning–derived CO is generally between 15 and 22‰, depending on specific combustion conditions (*13*–*15*).

We used an isotope mass balance model to estimate the ratio of combustion to noncombustion

[1]Institute for Terrestrial and Planetary Atmospheres/School of Marine and Atmospheric Sciences, Stony Brook University, Stony Brook, NY 11794–5000, USA. [2]Laboratoire de Glaciologie et Géophysique de l'Environnement (LGGE), CNRS, University of Grenoble, BP 96, 38402 St. Martin d'Hères Cedex, France.

*To whom correspondence should be addressed. E-mail: john.mak@stonybrook.edu

sources over the time period of interest (*11*). Steady-state atmospheric conditions were assumed on the basis of the relatively short lifetime of CO (weeks to months) as compared with the integrated sampling time for a typical ice core sample (~10 years for the D47 ice core and ~30 years for the South Pole ice core). Resulting source emission estimates are shown in Fig. 2. Also shown are source emission estimates over the last three decades and those in present day. CO from NMHC oxidation did not change significantly, whereas CO from biomass burning showed a large "saddle" trend, with maxima in both the mid-1300s and the late 1800s and a minimum in the 1600s. The observed trend in [CO], $\delta^{13}C$, and $\delta^{18}O$ was therefore mostly driven by variations in biomass burning, and compared with present day, biomass burning was almost the same in the late 1800s as that in the mid-1300s. This is consistent with the correlation observed between $\delta^{18}O$ and CO concentration (fig. S1). The *y* intercept of 9‰, corrected for the inverse mass-dependent kinetic isotope effect (KIE) for CO+OH (*16*) during atmospheric transport, leads to a mean oxygen isotopic signature of the source of 15 to 18‰, which indicates a predominant combustion source.

We have assumed that the observations were driven by variations in CO source strengths. It is possible, however, that the removal rate of CO by OH could have changed. However, if that were the case, then a slight enrichment in $\delta^{13}C$ should be observed because of the KIE (*16*). This is contrary to the observations. The second largest loss mechanism known for CO (but only accounting for 10%) is uptake by soils, which is largely dependent on soil surface area and mean temperature (*17*), both of which have not changed much in the Southern Hemisphere during the past several hundred years (*18*).

Satellite data combined with biogeochemical models to interpret the interannual variability of global biomass burning emissions show that from 1997 to 2004, lower temperature and higher precipitation correlated with reduced biomass burning emission (*19*). On longer time scales, biomass burning was shown to increase with the rapid Dansgaard/Oeschger warmings of the last glacial, probably because of increased vegetation productivity and fuel availability for burning (*20*).

Our calculated biomass burning trend (Fig. 2) is generally consistent with the tropical charcoal index (Fig. 3) (*21*). The charcoal index, which is a proxy for biomass burning, suggests a decline from ~0 to ~1750 followed by a sharp increase between 1750 and 1870 and a substantial decrease during the past century (*21*). Because of the fast deposition of charcoal particles, the charcoal index reflects a more regional component of biomass burning as compared with CO; however, the general trends for the two records are consistent within the range of calculated uncertainty, with perhaps the exception of the period of 1600–1700. The initial decline in biomass burning occurred in concert with a global cooling trend, reflecting the impact of climate change (*21*). The cooling was more muted on average in the Southern Hemisphere (*22*). But in a region such as southern South America, warm episodes are recorded before 1350 and in the early 19th century (*23*), coinciding with the stronger biomass burning emissions of CO deduced from our record. Since the 1700s, the increase of biomass burning has probably been influenced by both natural and anthropogenic forcings. This trend is also consistent with Berkner Island firn air data from ~1970 to present day. Such a reduction may result from a shift toward intensive grazing and fire management (*24*), which could lead to a change in landscape makeup and subsequently less biomass availability in some regions (*25*).

Biomass burning changes during the last two millennia have also been evaluated by using $[CH_4]$ and $\delta^{13}CH_4$ records from the Law Dome ice core (*1*). These investigators conclude that the pyrogenic emissions of CH_4 decreased by ~40% on the

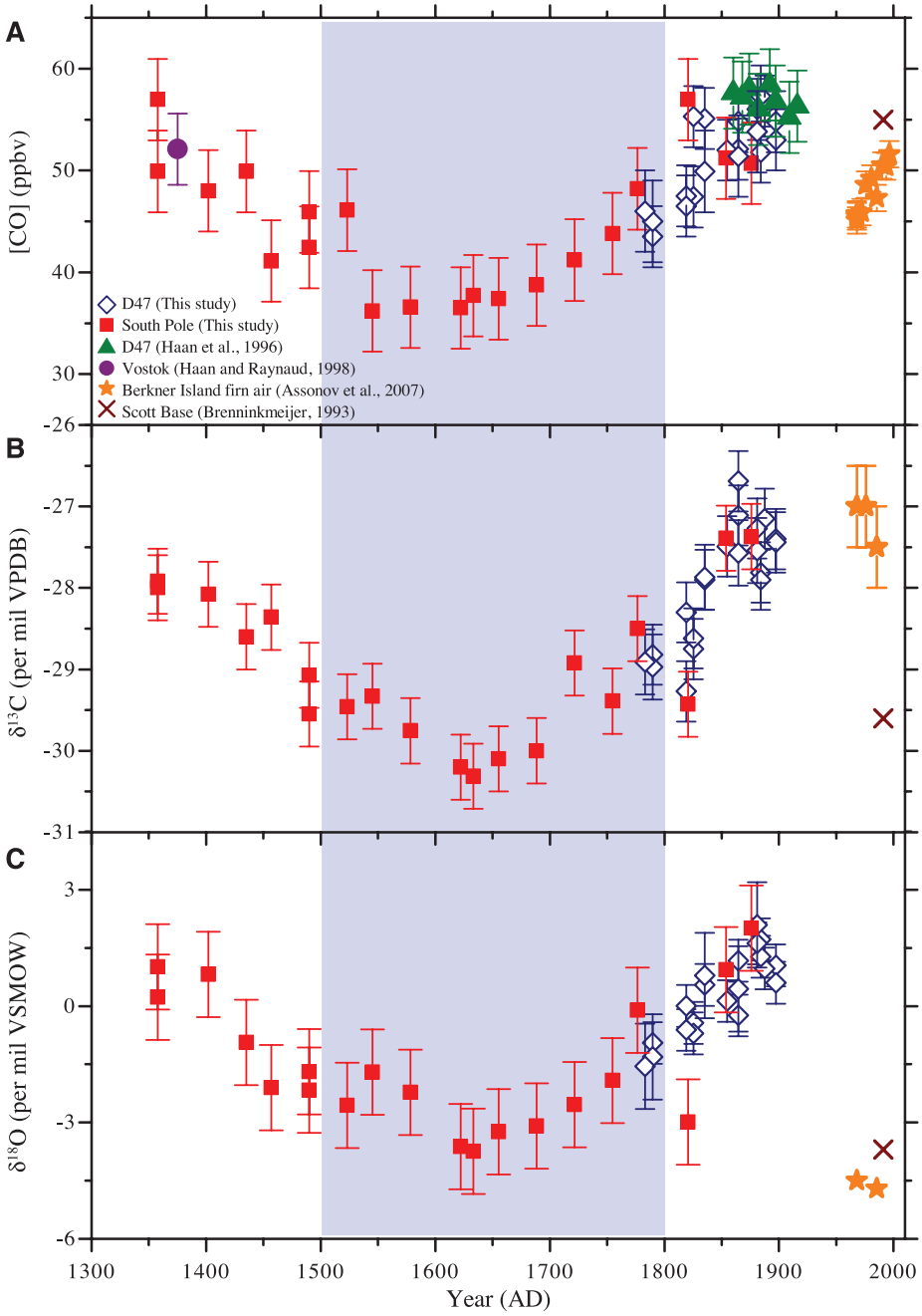

Fig. 1. The 650-year records of [CO], $\delta^{13}C$, and $\delta^{18}O$ from two ice cores: D47 ice core (diamonds) and South Pole ice core (squares). (**A**) [CO]. (**B**) $\delta^{13}C$. (**C**) $\delta^{18}O$. Error bars represent analytical uncertainties. The shaded area shows the timing of the LIA. Also shown are observations of annually averaged [CO], $\delta^{13}C$, and $\delta^{18}O$ of atmospheric CO (crosses) at Scott Base in 1991 (*13*). Berkner Island firn air data (stars) (*8*) roughly covering the last three decades of the 20th century show a 5 ppbv increase of [CO], 2.5‰ decrease of $\delta^{13}C$, and a slight increase in $\delta^{18}O$ since the late 1960s.

global scale in 1700 relative to the emissions from 0 to 1000, a figure that is consistent with our calculated ~50% drop of biomass burning emissions of CO during the 1600s in the Southern Hemisphere. Furthermore, recent research based on the stable isotopic ratios of methane in the West Antarctic Ice Sheet (WAIS) Divide ice core (79°27.7'S 112°7.51'W; 1759 m asl) also indicates that the median biomass burning source strength decreased by 38 ± 1% from the period of 990–1460 to 1689–1730 (*26*).

Long-term variations in atmospheric circulation could have partly modulated the long-range transport of biomass burning CO from the tropics to the high-latitude Southern Hemisphere (*27*), thus contributing in part to the calculated CO variability. For instance, a strengthened polar vortex could inhibit latitudinal exchanges and extratropical CO intrusion into the Antarctic atmosphere. However, the last period of intensification of southern circumpolar westerlies and accompanying relatively cooler conditions over East Antarctica (*28*) and West Antarctica occurred ~1200 to 1000 years ago (*29*), well before the period of this study. Although it cannot be entirely ruled out, indications are that circumpolar circulation did not change significantly during this period and did not have a large impact on CO large-scale transport.

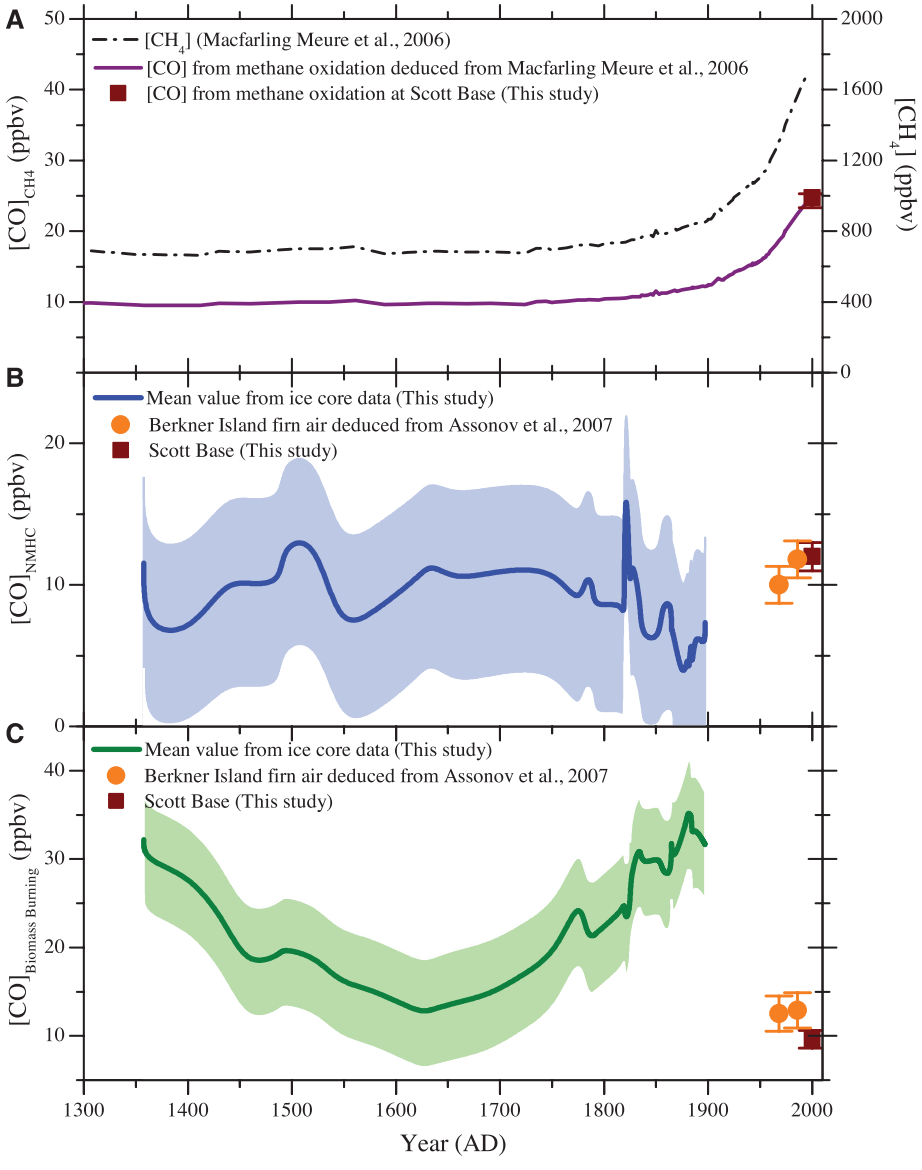

Fig. 2. Modeled CO source partitioning based on observations and an isotope mass balance model. (**A**) [CO] from methane oxidation. (**B**) [CO] from NMHC oxidation. (**C**) [CO] from biomass burning. Different scenarios have been tested in the model to show the sensitivity of minor sources (*11*). Thick lines in (B) and (C) represent the mean values of different scenarios, and shaded areas represent different scenario run results and uncertainties. [CH_4] data are from the Law Dome record (*9*). [CO] derived from the three major sources since the late 1960s was calculated based on Berkner Island firn air data (*8*) and an isotope mass balance model (orange circles). CO source partitioning at present day was calculated based on MOZART-4 simulation and CO measurements (annually averaged, 1997–2004) at Scott Base (red squares).

Another possible process that has a major effect on the meridional transport of CO is the movement of the Intertropical Convergence Zone (ITCZ) (*30*). Paleoclimatic evidence from continental Asia (*31*), Africa (*32*), the Americas (*33*), and the Pacific Ocean (*34*) suggests that a southward shift of the ITCZ occurred during the past millennium, reaching its southernmost position some time during the LIA (*34*). As the ITCZ shifts southward, less CO produced from biomass burning will be transported to the Southern Hemisphere. This would have reduced the contribution of Southern Hemisphere biomass burning to [CO] observed in Antarctica during the LIA. A southward shift of the ITCZ position would also shift rainfall patterns southward because precipitation follows the ITCZ (*35*). A southward shift of precipitation could also contribute to a decrease in biomass burning during the LIA because dry conditions favor biomass burning.

Previous modeling studies suggest that preindustrial biomass burning was much lower than today, with a reduction of up to 90% (*36*–*38*). This is the common assumption in climate model simulations. However, our results show that present-day CO from Southern Hemisphere biomass burning is lower than at any other time during the last 650 years. This is particularly relevant because assumptions on preindustrial [CO] are an important component for correctly estimating the radiative forcing of tropospheric ozone in preindustrial times (*39*). [CO] changes due to biomass burning also suggest that there were decadal and centennial scale variations in average concentrations of black carbon, which is another major atmospheric constituent produced with burning, leading to the unanswered question of its potential role in long-term climate variability.

References and Notes

1. D. F. Ferretti *et al.*, *Science* **309**, 1714 (2005).
2. J. R. Petit *et al.*, *Nature* **399**, 429 (1999).
3. D. Haan, P. Martinerie, D. Raynaud, *Geophys. Res. Lett.* **23**, 2235 (1996).
4. W. Seiler, *Tellus* **26**, 116 (1974).
5. P. Bergamaschi, R. Hein, C. A. M. Brenninkmeijer, P. J. Crutzen, *J. Geophys. Res.* **105** (D2), 1929 (2000).
6. D. Haan, D. Raynaud, *Tellus* **50**, 253 (1998).
7. Z. Wang, J. E. Mak, *Atmos. Meas. Tech.* **3**, 1307 (2010).
8. S. S. Assonov *et al.*, *Atmos. Chem. Phys.* **7**, 295 (2007).
9. C. M. Macfarling Meure *et al.*, *Geophys. Res. Lett.* **33**, L14810 (2006).
10. G. Marland, T. A. Boden, R. J. Andres, "Global, Regional, and National Fossil-Fuel CO_2 Emissions," in *Trends: A Compendium of Data on Global Change* (Carbon Dioxide Information Analysis Center, Oak Ridge National Laboratory, U.S. Department of Energy, Oak Ridge, TN, 2008).
11. Materials and methods are available as supporting material on *Science* Online.
12. C. A. M. Brenninkmeijer, T. Rockmann, *J. Geophys. Res.* **102** (D21), 25477 (1997).
13. C. A. M. Brenninkmeijer, *J. Geophys. Res.* **98**, 10595 (1993).
14. S. Kato, H. Akimoto, T. Rockmann, M. Braunlich, C. A. M. Brenninkmeijer, *Atmos. Environ.* **33**, 4357 (1999).
15. C. M. Stevens, A. F. Wagner, *Z. Naturforsch. A* **44**, 376 (1989).
16. C. M. Stevens *et al.*, *Int. J. Chem. Kinet.* **12**, 935 (1980).
17. R. E. Inman, R. B. Ingersoll, E. A. Levy, *Science* **172**, 1229 (1971).

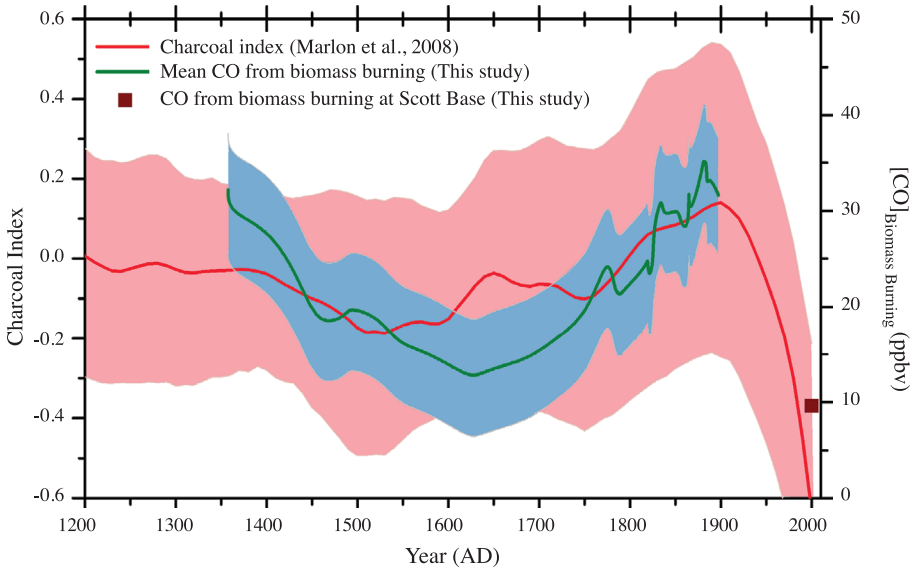

Fig. 3. Correlation between the derived CO from biomass burning (green line) and the sedimentary charcoal record compilation in the tropics (30°N–20°S) (red line) (*21*). The red shaded area represents charcoal index measurement uncertainties. The blue shaded area is the same as that in Fig. 2C. Also shown is the MOZART-4–simulated CO from biomass burning emission at Scott Base for the modern atmosphere.

18. M. E. Mann, P. D. Jones, *Geophys. Res. Lett.* **30**, 1820 (2003).
19. G. R. van der Werf *et al.*, *Atmos. Chem. Phys.* **6**, 3423 (2006).
20. A.-L. Daniau, S. P. Harrison, P. J. Bartlein, *Quat. Sci. Rev.* **29**, 2918 (2010).
21. J. R. Marlon *et al.*, *Nat. Geosci.* **1**, 697 (2008).
22. M. E. Mann *et al.*, *Science* **326**, 1256 (2009).
23. R. Neukom *et al.*, *Clim. Dyn.* (2010).
24. K. K. Goldewijk, *Global Biogeochem. Cycles* **15**, 417 (2001).
25. S. J. Pyne, *World Fire: The Culture of Fire on Earth* (Univ. of Washington Press, Seattle, 1995).
26. J. A. Mischler *et al.*, *Global Biogeochem. Cycles* **23**, Gb4024 (2009).
27. D. P. Edwards *et al.*, *J. Geophys. Res.* **111** (D14), D14312 (2006).
28. V. Masson *et al.*, *Quat. Res.* **54**, 348 (2000).
29. P. A. Mayewski *et al.*, *Rev. Geophys.* **47**, RG1003 (2009).
30. W. Seiler, H. Giehl, E. G. Brunke, E. Halliday, *Tellus* **36**, 219 (1984).
31. D. M. Anderson, J. T. Overpeck, A. K. Gupta, *Science* **297**, 596 (2002).
32. D. Verschuren, K. R. Laird, B. F. Cumming, *Nature* **403**, 410 (2000).
33. G. H. Haug, K. A. Hughen, D. M. Sigman, L. C. Peterson, U. Röhl, *Science* **293**, 1304 (2001).
34. J. P. Sachs *et al.*, *Nat. Geosci.* **2**, 519 (2009).
35. J. C. Stager, C. Cocquyt, R. Bonnefille, C. Weyhenmeyer, N. Bowerman, *Quat. Res.* **72**, 47 (2009).
36. P. J. Crutzen, P. H. Zimmermann, *Tellus* **43**, 136 (1991).
37. A. Ito, J. E. Penner, *Global Biogeochem. Cycles* **19**, GB2028 (2005).
38. F. Mouillot, A. Narasimha, Y. Balkanski, J. F. Lamarque, C. B. Field, *Geophys. Res. Lett.* **33**, L01801 (2006).
39. M. Gauss *et al.*, *Atmos. Chem. Phys.* **6**, 575 (2006).

40. We thank C. A. M. Brenninkmeijer for useful help and discussions. South Pole ice core samples were provided by the National Ice Core Laboratory (NICL) and drilled by J. Cole-Dai and colleagues. We greatly thank M. Twickler for ice allocation and thank B. Bencivengo, E. Cravens, and G. Hargreaves for cutting and shipping ice. We thank the drillers (LGGE) and logistics (French polar institute) who made D47 drilling possible. We also thank E. Brook and J. E. Lee from Oregon State University for providing bubble-free ice and M. Montagnat, LGGE, CNRS for providing monocrystalline and polycrystalline bubble-free ice. We also thank L. Emmons for useful help on MOZART-4 simulation and NCAR for providing a supercomputing environment for MOZART-4 simulation. Z.W. strongly thanks P. Martinerie for logistical support in Grenoble. We are grateful to M. Zhang, D. Black, V. Masson-Delmotte, and D. Knopf for their useful comments. We thank A. Matthews from Mt. Sinai High School for providing a walk-in freezer in which to prepare some ice core samples. This work was supported by NSF grant OCE0731406, the European Science Foundation (ESF) EURO-CORES Programme EuroCLIMATE (contract ERAS-CT-2003-980409 of the European Commission, DG Research, FP6), Institut National des Sciences de l'Univers (INSU) project ISOTRACE-FP21, and the French ANR NEEM (ANR-O7-VULN-09-001).

Supporting Online Material

www.sciencemag.org/cgi/content/full/science.1197257/DC1
Materials and Methods
Figs. S1 to S4
Tables S1 to S3
References

1 September 2010; accepted 1 November 2010
Published online 2 December 2010;
10.1126/science.1197257

Structural Basis of Biological N_2O Generation by Bacterial Nitric Oxide Reductase

Tomoya Hino,[1,2,3] Yushi Matsumoto,[1,4] Shingo Nagano,[1,5] Hiroshi Sugimoto,[1] Yoshihiro Fukumori,[6] Takeshi Murata,[2,3] So Iwata,[2,3,7] Yoshitsugu Shiro[1]

Nitric oxide reductase (NOR) is an iron-containing enzyme that catalyzes the reduction of nitric oxide (NO) to generate a major greenhouse gas, nitrous oxide (N_2O). Here, we report the crystal structure of NOR from *Pseudomonas aeruginosa* at 2.7 angstrom resolution. The structure reveals details of the catalytic binuclear center. The non-heme iron (Fe_B) is coordinated by three His and one Glu ligands, but a His-Tyr covalent linkage common in cytochrome oxidases (COX) is absent. This structural characteristic is crucial for NOR reaction. Although the overall structure of NOR is closely related to COX, neither the D- nor K-proton pathway, which connect the COX active center to the intracellular space, was observed. Protons required for the NOR reaction are probably provided from the extracellular side.

Nitrous oxide gas (N_2O) is now the greatest threat to the ozone layer and also induces climate change as a greenhouse gas more powerful than carbon dioxide and methane (*1*). Agricultural fertilizers, fossil fuel combustion, biomass burning, and animal waste contribute to N_2O production. However, the largest emission source of N_2O into the atmosphere is bacterial breakdown of nitrogen compounds in soils and in the oceans. Denitrifiers perform the step-by-step chemical reduction of nitrogen oxides (NO_3^- and NO_2^-) to N_2, producing N_2O as an intermediate by-product: $NO_3^- \rightarrow NO_2^- \rightarrow NO \rightarrow N_2O \rightarrow N_2$. The key enzyme in N_2O production is nitric oxide reductase (NOR), which catalyzes the reduction of nitric oxide (NO) with two electrons and two protons: $2NO + 2e^- + 2H^+ \rightarrow N_2O + H_2O$. The NOR reaction is also of interest to synthetic chemists because it involves N-O bond cleavage and N-N bond formation (Scheme 1). Structural and functional models of the active site of NOR have been syn-

[1]RIKEN SPring-8 Center, 1-1-1 Kouto, Sayo, Hyogo 679-5148, Japan. [2]Japan Science and Technology Agency, Exploratory Research for Advanced Technology, Human Receptor Crystallography Project, Yoshida-Konoe-cho, Sakyo-ku, Kyoto 606-8501, Japan. [3]Department of Cell Biology, Graduate School of Medicine, Kyoto University, Yoshida-Konoe-cho, Sakyo, Kyoto 606-8501, Japan. [4]Division of Protein Chemistry, Post-Genome Science Center, Medical Institute of Bioregulation, Kyushu University, Fukuoka 812-8552, Japan. [5]Department of Chemistry and Biotechnology, Graduate School of Engineering, Tottori University, Tottori 680-8552, Japan. [6]Graduate School of Natural Science and Technology, Kanazawa University, Kanazawa, Ishikawa 920-1192, Japan. [7]Division of Molecular Bioscience, Membrane Protein Crystallography Group, Imperial College London, Exhibition Road, London SW7 2AZ, UK.

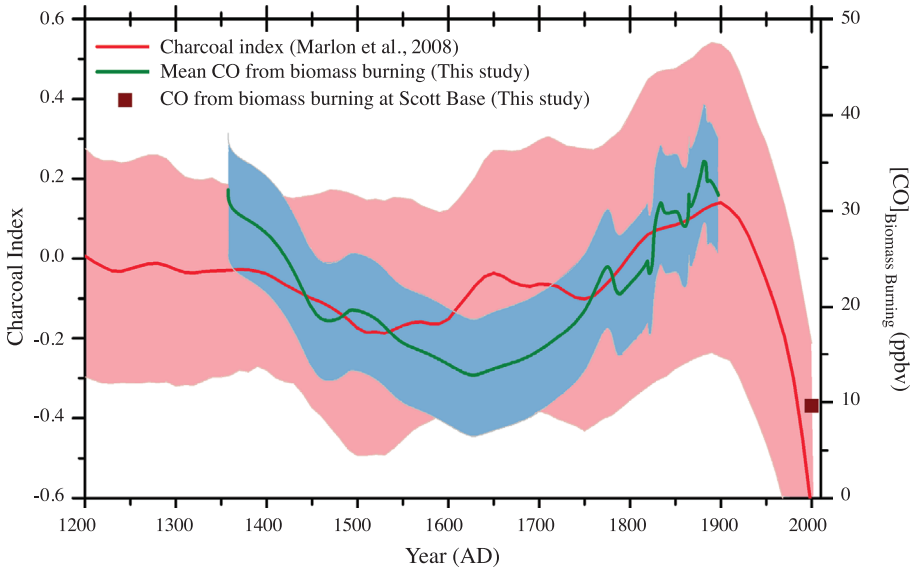

Fig. 3. Correlation between the derived CO from biomass burning (green line) and the sedimentary charcoal record compilation in the tropics (30°N–20°S) (red line) (*21*). The red shaded area represents charcoal index measurement uncertainties. The blue shaded area is the same as that in Fig. 2C. Also shown is the MOZART-4–simulated CO from biomass burning emission at Scott Base for the modern atmosphere.

18. M. E. Mann, P. D. Jones, *Geophys. Res. Lett.* **30**, 1820 (2003).
19. G. R. van der Werf *et al.*, *Atmos. Chem. Phys.* **6**, 3423 (2006).
20. A.-L. Daniau, S. P. Harrison, P. J. Bartlein, *Quat. Sci. Rev.* **29**, 2918 (2010).
21. J. R. Marlon *et al.*, *Nat. Geosci.* **1**, 697 (2008).
22. M. E. Mann *et al.*, *Science* **326**, 1256 (2009).
23. R. Neukom *et al.*, *Clim. Dyn.* (2010).
24. K. K. Goldewijk, *Global Biogeochem. Cycles* **15**, 417 (2001).
25. S. J. Pyne, *World Fire: The Culture of Fire on Earth* (Univ. of Washington Press, Seattle, 1995).
26. J. A. Mischler *et al.*, *Global Biogeochem. Cycles* **23**, Gb4024 (2009).
27. D. P. Edwards *et al.*, *J. Geophys. Res.* **111** (D14), D14312 (2006).
28. V. Masson *et al.*, *Quat. Res.* **54**, 348 (2000).
29. P. A. Mayewski *et al.*, *Rev. Geophys.* **47**, RG1003 (2009).
30. W. Seiler, H. Giehl, E. G. Brunke, E. Halliday, *Tellus* **36**, 219 (1984).
31. D. M. Anderson, J. T. Overpeck, A. K. Gupta, *Science* **297**, 596 (2002).
32. D. Verschuren, K. R. Laird, B. F. Cumming, *Nature* **403**, 410 (2000).
33. G. H. Haug, K. A. Hughen, D. M. Sigman, L. C. Peterson, U. Röhl, *Science* **293**, 1304 (2001).
34. J. P. Sachs *et al.*, *Nat. Geosci.* **2**, 519 (2009).
35. J. C. Stager, C. Cocquyt, R. Bonnefille, C. Weyhenmeyer, N. Bowerman, *Quat. Res.* **72**, 47 (2009).
36. P. J. Crutzen, P. H. Zimmermann, *Tellus* **43**, 136 (1991).
37. A. Ito, J. E. Penner, *Global Biogeochem. Cycles* **19**, GB2028 (2005).
38. F. Mouillot, A. Narasimha, Y. Balkanski, J. F. Lamarque, C. B. Field, *Geophys. Res. Lett.* **33**, L01801 (2006).
39. M. Gauss *et al.*, *Atmos. Chem. Phys.* **6**, 575 (2006).

40. We thank C. A. M. Brenninkmeijer for useful help and discussions. South Pole ice core samples were provided by the National Ice Core Laboratory (NICL) and drilled by J. Cole-Dai and colleagues. We greatly thank M. Twickler for ice allocation and thank B. Bencivengo, E. Cravens, and G. Hargreaves for cutting and shipping ice. We thank the drillers (LGGE) and logistics (French polar institute) who made D47 drilling possible. We also thank E. Brook and J. E. Lee from Oregon State University for providing bubble-free ice and M. Montagnat, LGGE, CNRS for providing monocrystalline and polycrystalline bubble-free ice. We also thank L. Emmons for useful help on MOZART-4 simulation and NCAR for providing a supercomputing environment for MOZART-4 simulation. Z.W. strongly thanks P. Martinerie for logistical support in Grenoble. We are grateful to M. Zhang, D. Black, V. Masson-Delmotte, and D. Knopf for their useful comments. We thank A. Matthews from Mt. Sinai High School for providing a walk-in freezer in which to prepare some ice core samples. This work was supported by NSF grant OCE0731406, the European Science Foundation (ESF) EURO-CORES Programme EuroCLIMATE (contract ERAS-CT-2003-980409 of the European Commission, DG Research, FP6), Institut National des Sciences de l'Univers (INSU) project ISOTRACE-FP21, and the French ANR NEEM (ANR-O7-VULN-09-001).

Supporting Online Material

www.sciencemag.org/cgi/content/full/science.1197257/DC1
Materials and Methods
Figs. S1 to S4
Tables S1 to S3
References

1 September 2010; accepted 1 November 2010
Published online 2 December 2010;
10.1126/science.1197257

Structural Basis of Biological N_2O Generation by Bacterial Nitric Oxide Reductase

Tomoya Hino,[1,2,3] Yushi Matsumoto,[1,4] Shingo Nagano,[1,5] Hiroshi Sugimoto,[1] Yoshihiro Fukumori,[6] Takeshi Murata,[2,3] So Iwata,[2,3,7] Yoshitsugu Shiro[1]

Nitric oxide reductase (NOR) is an iron-containing enzyme that catalyzes the reduction of nitric oxide (NO) to generate a major greenhouse gas, nitrous oxide (N_2O). Here, we report the crystal structure of NOR from *Pseudomonas aeruginosa* at 2.7 angstrom resolution. The structure reveals details of the catalytic binuclear center. The non-heme iron (Fe_B) is coordinated by three His and one Glu ligands, but a His-Tyr covalent linkage common in cytochrome oxidases (COX) is absent. This structural characteristic is crucial for NOR reaction. Although the overall structure of NOR is closely related to COX, neither the D- nor K-proton pathway, which connect the COX active center to the intracellular space, was observed. Protons required for the NOR reaction are probably provided from the extracellular side.

Nitrous oxide gas (N_2O) is now the greatest threat to the ozone layer and also induces climate change as a greenhouse gas more powerful than carbon dioxide and methane (*1*). Agricultural fertilizers, fossil fuel combustion, biomass burning, and animal waste contribute to N_2O production. However, the largest emission source of N_2O into the atmosphere is bacterial breakdown of nitrogen compounds in soils and in the oceans. Denitrifiers perform the step-by-step chemical reduction of nitrogen oxides (NO_3^- and NO_2^-) to N_2, producing N_2O as an intermediate by-product: $NO_3^- \rightarrow NO_2^- \rightarrow NO \rightarrow N_2O \rightarrow N_2$. The key enzyme in N_2O production is nitric oxide reductase (NOR), which catalyzes the reduction of nitric oxide (NO) with two electrons and two protons: $2NO + 2e^- + 2H^+ \rightarrow N_2O + H_2O$. The NOR reaction is also of interest to synthetic chemists because it involves N-O bond cleavage and N-N bond formation (Scheme 1). Structural and functional models of the active site of NOR have been syn-

[1]RIKEN SPring-8 Center, 1-1-1 Kouto, Sayo, Hyogo 679-5148, Japan. [2]Japan Science and Technology Agency, Exploratory Research for Advanced Technology, Human Receptor Crystallography Project, Yoshida-Konoe-cho, Sakyo-ku, Kyoto 606-8501, Japan. [3]Department of Cell Biology, Graduate School of Medicine, Kyoto University, Yoshida-Konoe-cho, Sakyo, Kyoto 606-8501, Japan. [4]Division of Protein Chemistry, Post-Genome Science Center, Medical Institute of Bioregulation, Kyushu University, Fukuoka 812-8552, Japan. [5]Department of Chemistry and Biotechnology, Graduate School of Engineering, Tottori University, Tottori 680-8552, Japan. [6]Graduate School of Natural Science and Technology, Kanazawa University, Kanazawa, Ishikawa 920-1192, Japan. [7]Division of Molecular Bioscience, Membrane Protein Crystallography Group, Imperial College London, Exhibition Road, London SW7 2AZ, UK.

thesized (*2*), and recently a construction of the active site of NOR in myoglobin through biomolecular engineering techniques was reported (*3*, *4*). In addition, NOR is clinically and pharmaceutically important as well because pathogens such as *Pseudomonas aeruginosa*, which are known to be a major opportunistic pathogen that causes acute and chronic infection, have NOR to detoxify cytotoxic NO produced in anaerobic respiration in cystic fibrosis lung (*5*). Accordingly, the molecular mechanism of the NO reduction by NOR have been extensively studied through chemical, biochemical, and physicochemical techniques (*2*, *6*–*8*), but a structure of NOR enzyme has been lacking.

Here, we report the structure of cNOR, which has a cytochrome c subunit as the electron donor for the catalytic reaction at the active center. The enzyme was isolated from *P. aeruginosa* and crystallized in the presence of the cNOR antibody (Fab), which was essential for obtaining high-quality crystals (table S1) (*9*). Compared with the amino acid sequences of cNOR from *Paracoccus denitrificans* and *Pseudomonas stutzeri*, both of which have been comprehensively studied (*6*, *7*), the amino acid sequence of *P. aeruginosa* cNOR has 75 and 94% homology, respectively (fig. S1). *P. aeruginosa* cNOR also has five well-conserved Glu residues (Glu^{135}, Glu^{138}, Glu^{211}, Glu^{215}, and Glu^{280}) that have been shown to be functionally important (*10*–*12*). In addition, the NO reduction activity (433 ± 70 μM NO/min/μM enzyme) is comparable, and the spectroscopic properties are also identical among the cNORs (*13*, *14*).

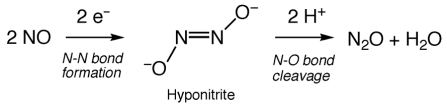

Scheme 1.

P. aeruginosa cNOR is an integral membrane and iron-containing heterodimeric enzyme consisting of small (NorC) and large (NorB) subunits (Fig. 1). The NorB subunit has 12 α-helices and interacts with one α-helix of the NorC subunit. These 13 helices span the transmembrane (TM) region. The TM domain of the NorB subunit contains two heme irons in hemes *b* and b_3 and one non-heme iron, Fe_B (Fig. 1B). As predicted (*15*), three His residues (His^{60}, His^{347}, and His^{349}) are ligands for the two b-type hemes. The globular hydrophilic domain of the NorC subunit contains heme *c*, which has His^{65} and Met^{112} as axial iron ligands. Consistent with the previous prediction that NOR is an evolutionary progenitor of cytochrome oxidases, the topology of the TM region and the arrangement of the metal centers in cNOR are similar to those of cytochrome oxidases, a superfamily of enzymes that act as the terminal oxidases in aerobic respiratory transport chains (Fig. 1C and fig. S2) (*15*, *16*).

Non-heme iron Fe_B and heme b_3 constitute the binuclear center that serves as the catalytic site of cNOR (Fig. 2A and fig. S3). For this analysis, cNOR was crystallized in a purified ferric resting form (fig. S3) (*8*, *17*). Three His residues (His^{207}, His^{258}, and His^{259}) coordinate the non-heme Fe_B, and Glu^{211} also serves as a ligand, as was proposed for the homologous Glu^{198} in *P. denitrificans* cNOR (*4*, *10*, *18*). The Fe_B site has a slightly distorted trigonal-bipyramidal coordination geometry that differs from the geometry observed at the Cu_B site in cytochrome oxidase (Fig. 2). The Glu^{211} coordination position of Fe_B in cNOR is occupied by a His ligand (His^{233}) of Cu_B in cytochrome oxidases; this His ligand is covalently attached to a highly conserved Tyr residue (Tyr^{237} of *Thermus thermophilus* cytochrome oxidase) (fig. S4B) (*19*–*21*). The carboxylate of the coordinated Glu^{211} is hydrogen-bonded to Glu^{280}. Glu^{215} and Glu^{280}, both of which are also conserved Glu residues in NORs, are near the binuclear center, indicating a large electro-negative environment at the active site, as predicted on the basis of resonance Raman studies (*8*). This electro-negative environment results in a redox potential of heme b_3 iron (60 mV) that is lower than those of hemes b (345 mV) and c (310 mV) irons and thus contributes to activation of the NO molecule bound to the heme b_3 and Fe_B irons (*3*, *4*). In addition, the hydrogen-bonding network involving the three Glu residues can serve as a terminal proton-donating system to facilitate N-O bond cleavage in N_2O and H_2O production (*10*, *12*).

Three possible mechanisms have been proposed for the reduction of NO by NOR: the *trans* mechanism (*8*, *14*, *22*), the *cis* Fe_B mechanism (*23*, *24*), and the *cis* heme b_3 mechanism (*25*, *26*). Because two NO molecules are required for NOR reaction, the heme b_3 and Fe_B binuclear pocket allows two NO molecules to bind in all three proposed mechanisms. This is in sharp contrast with the heme a_3 and Cu_B binuclear center of

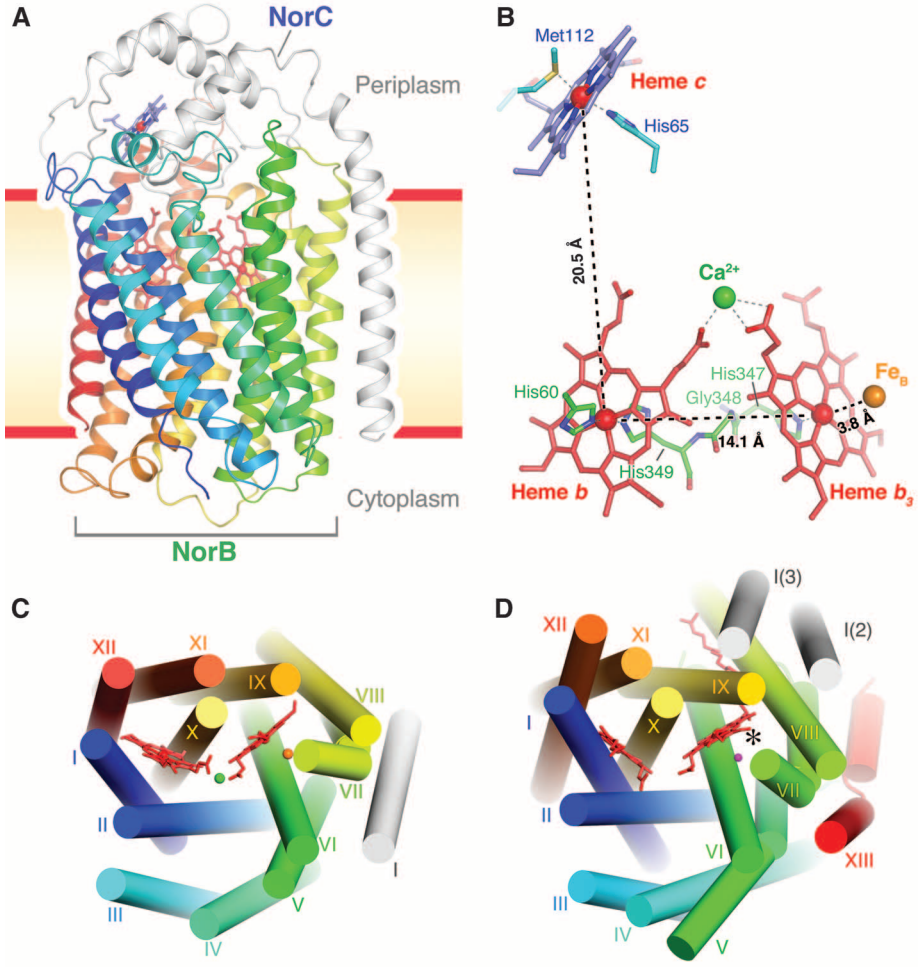

Fig. 1. (**A**) Overall structures of cNOR from *P. aeruginosa* viewed parallel to the membrane. The NorB and NorC subunits are shown as ribbon in various colors and white, respectively. Heme c is shown as blue sticks, and hemes b and b_3 are shown as red sticks. Fe_B and calcium ions are represented as orange and green spheres, respectively. (**B**) Arrangement of metal centers of cNOR. Distances between redox centers are shown. (**C**) Arrangement of membrane-spanning helices of cNOR viewed from the periplasmic side. Transmembrane helices are indicated with Roman numerals. (**D**) Cytochrome ba_3 oxidase from *T. thermophilus* (PDB code 1EHK). Subunit 1 with helices I ~ XII is shown in color. Helix I of subunit 2 and helix I of subunit 3 are shown in gray. The position of the K-pathway is marked with an asterisk.

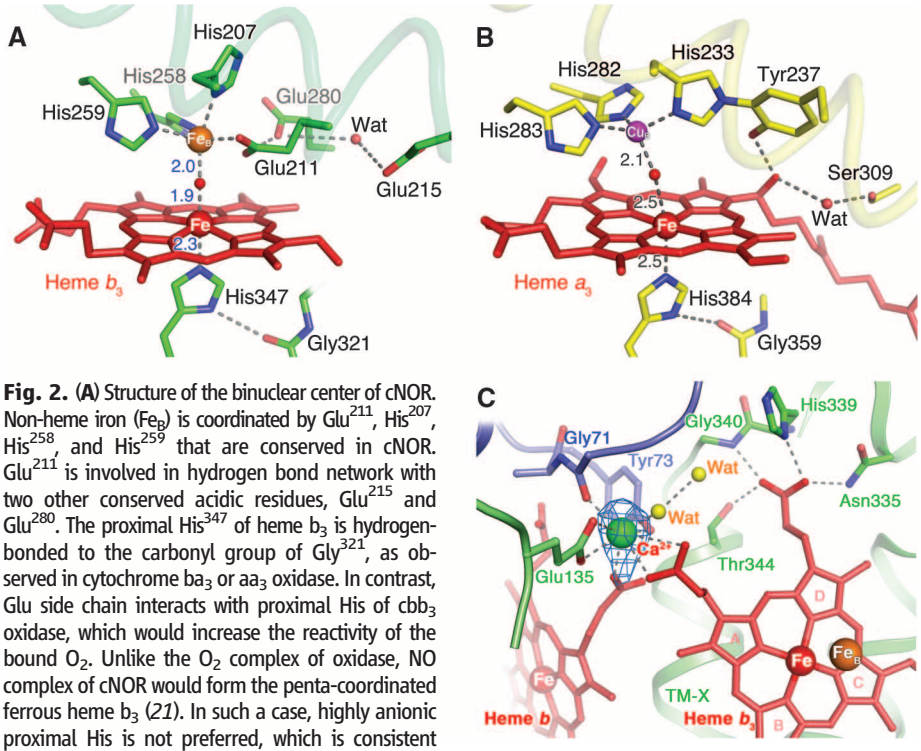

Fig. 2. (**A**) Structure of the binuclear center of cNOR. Non-heme iron (Fe_B) is coordinated by Glu^{211}, His^{207}, His^{258}, and His^{259} that are conserved in cNOR. Glu^{211} is involved in hydrogen bond network with two other conserved acidic residues, Glu^{215} and Glu^{280}. The proximal His^{347} of heme b_3 is hydrogen-bonded to the carbonyl group of Gly^{321}, as observed in cytochrome ba_3 or aa_3 oxidase. In contrast, Glu side chain interacts with proximal His of cbb_3 oxidase, which would increase the reactivity of the bound O_2. Unlike the O_2 complex of oxidase, NO complex of cNOR would form the penta-coordinated ferrous heme b_3 (*21*). In such a case, highly anionic proximal His is not preferred, which is consistent with the present structure. (**B**) Structure of the binuclear center of ba_3 oxidase (PDB code 1XME). His^{233} and Tyr^{237} are connected by a covalent bond. (**C**) Coordination structure of calcium and the interaction of the heme propionates. An anomalous difference Fourier map calculated from the low-energy data set collected at wavelength of 1.9 Å is contoured at 5 σ and shown as blue mesh. One of the calcium ligands (Glu135) and the residues interacting with the D-ring propionate of heme b_3 (Asn^{335}, His^{339}, Gly^{340}, and Thr^{344}) are conserved in the amino acid sequence of other cNOR and cbb_3 oxidase, whereas cbb_3 oxidase structure lacks the interaction with Gly or Thr.

cytochrome oxidases, which can accommodate a single O_2 molecule. Slightly larger space near the catalytic binuclear center for substrate-binding is created by the residues of Fe_B ligand residues and hydrophobic residues in cNOR as compared with cytochrome oxidases (fig. S4), although the size of the space in cNOR is not opened enough to accommodate two NO molecules. This is caused by the short distance between the two irons of cNOR (3.9 Å) in comparison with the distance between the heme a_3 iron and Cu_B in cytochrome oxidase (4.4 Å) and by the ligation of the Glu^{211} to Fe_B. When the iron is reduced from the ferric state to the ferrous state, the μ-oxo ligand dissociates, and the distance between the two irons probably increases. Upon NO binding to reduced iron during the catalytic cycle of cNOR, further conformational changes of the binuclear center and its protein ligands might be required to locate the two NO molecules suitable for N-N bond formation. To study this issue, we need to determine structures of cNOR in several oxidation and ligand-coordination states.

The electrons used in the NO reduction are donated from cytochrome c_{551} to the heme c, which is covalently attached at Cys^{61} and Cys^{64} in the globular domain of the NorC subunit (fig. S5). The binding site of cytochrome c_{551} probably overlaps Fab binding site on cNOR (fig. S6) because Fab can inhibit cytochrome c_{551}-supported NO reduction but not phenazine methosulfate (PMS)–supported NO reduction (fig. S7 and table S2). Electrons thus donated are transferred from the heme c iron to the heme b iron (20.5 Å distance)

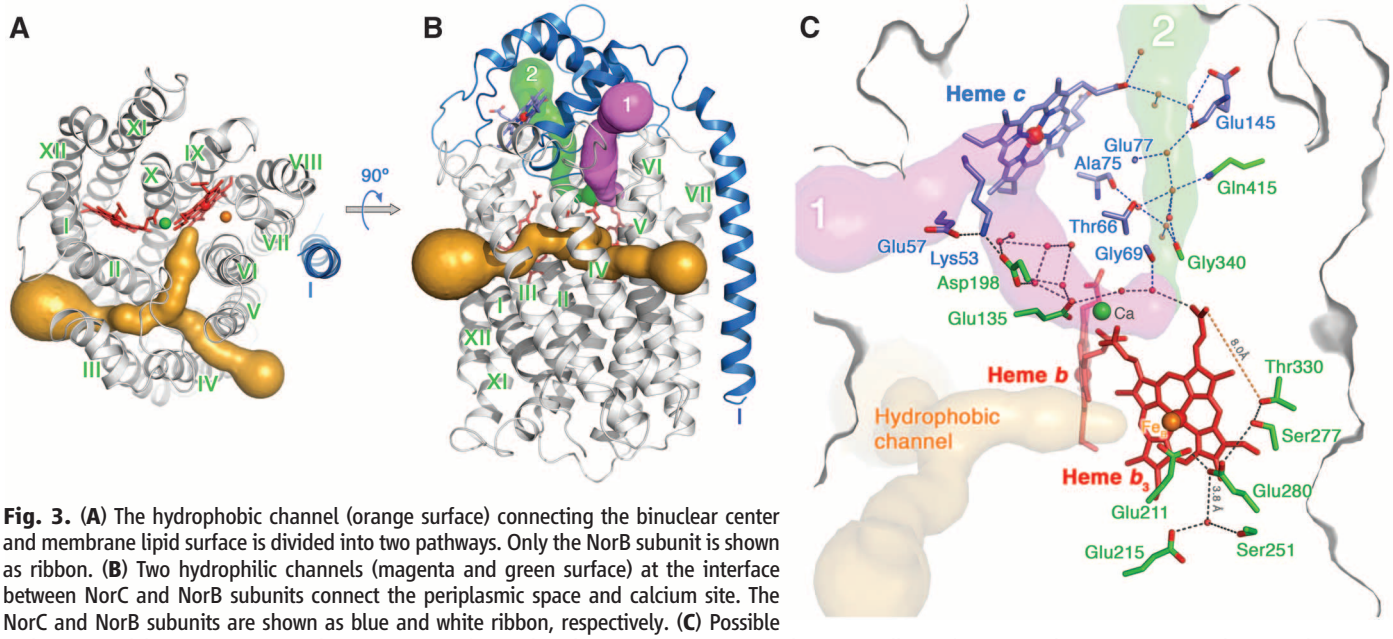

Fig. 3. (**A**) The hydrophobic channel (orange surface) connecting the binuclear center and membrane lipid surface is divided into two pathways. Only the NorB subunit is shown as ribbon. (**B**) Two hydrophilic channels (magenta and green surface) at the interface between NorC and NorB subunits connect the periplasmic space and calcium site. The NorC and NorB subunits are shown as blue and white ribbon, respectively. (**C**) Possible pathways for delivering protons and water. Waters observed in the crystal structure are shown as yellow spheres. Residues from NorC and NorB subunits are shown as blue and green stick models. The first hydrophilic channel in the subunit interface, represented by a magenta surface in panel (B), starts from Glu^{57} and ends at the propionate of heme b_3. Seven waters are observed in this channel and generate the hydrogen-bonding network involving the side chains of the residues (Lys^{53} and Glu^{57} of NorC and Glu^{135} and Asp^{198} of NorB) that are highly conserved in cNOR. The second hydrophilic channel between Gly^{340} and the heme c propionate, shown as a green surface in (B), contains nine waters that interact with the main chain carbonyl group or the side chain of the conserved residues. This hydrogen-bonding network is separated by 8.0 Å from another network involving the Fe_B ligand Glu^{211}.

through the NorC/NorB interface (fig. S8). The iron-to-iron distance between the hemes b and b_3 in cNOR is 14.1 Å, which is comparable with that between hemes a and a_3 in cytochrome oxidase, and Gly^{348} is present between the two hemes in cNOR (Fig. 1B) in place of conserved Phe on cytochrome oxidases (*19*). A calcium ion (Ca) was identified in cNOR (Fig. 2C, fig. S2, and table S3) at the same position of microaerobic respiratory enzyme, cbb_3 oxidase (*27*). Because the plausible electron transfer pathway in cNOR (figs. S8 and S9) from the heme c to the binuclear center (heme b_3 and Fe_B) appears similar to the pathway from Cu_A to heme a in cytochrome oxidases (*19*, *21*, *28*), Ca possibly acts as a factor maintaining protein and heme structures suitable for the intramolecular electron transfer.

In the proposed mechanism of NO reduction (*8*, *14*, *22*–*26*), a hyponitrite ($^-ONNO^-$) is plausibly formed as a transient species after the N-N bond formation between the two bound NO molecules (Scheme 1). To facilitate N-O bond cleavage of the transient species to produce N_2O and H_2O, protons must be transferred from bulk water to the buried active site, possibly through a water channel and a hydrogen-bonding network. We identified two channels extending from the NorB/NorC interface to the periplasmic side of the enzyme (Fig. 3B), which connect the bulk water and the catalytic center of the enzyme through a possible hydrogen-bonding network (Fig. 3C). Although a long gap between Thr^{330} and the propionate of heme b_3 (8.0 Å) is observed in the channels and hydrogen-bonding network, introduction of one or two water molecules in the gap would facilitate proton transfer to the binuclear center through Glu^{211}, Glu^{215}, and Glu^{280}. A branched hydrophobic channel extending from the binuclear center to the surface in the membrane-spanning region that could provide a means of NO entry was identified (Fig. 3, orange), but neither an obvious channel nor a hydrogen-bonding network from the active site of the cNOR to the cytoplasmic region was identified (Fig. 4), which is in sharp contrast to the K- and the D-channel of cytochrome oxidases, which are considered as possible proton transfer channels (*19*–*21*).

In 1985, the first data showing that the protons required for NO reduction are supplied from the periplasmic space were obtained from whole-cell measurements (*29*). Membrane potential measurements of *Rhodobacter capsulatus* by using endogenous carotenoid pigments indicated that the NOR reaction is not electrogenic (*30*). Since then, extensive evidence including electrochemical, biochemical, and flow-flash kinetic data have been obtained, all of which unambiguously indicate that electrons and protons are supplied from the periplasmic space. Therefore, we propose that the channels and hydrogen-bonding network identified in the *P. aeruginosa* cNOR structure serve as the pathway for proton transfer in the catalytic reduction of NO at the binuclear center. Asp^{198} (NorB) and Glu^{57} (NorC) at the protein surface are probably the proton entry site, because both acidic residues are highly conserved in NORs (fig. S1).

Glu^{135} in *P. aeruginosa* cNOR, which is one of the conserved Glu residues (fig. S10), participates in the formation of the proposed proton transfer network (Fig. 3C). This is consistent with the proposal by Reimann *et al.* for the corresponding Glu^{122} in *P. denitrificans* cNOR (*31*). Glu^{135} also serves as a Ca ligand (Fig. 2C), suggesting that it is a key residue in determining the structural and functional properties of cNOR. Indeed, Flock *et al.* reported that upon mutation of Glu^{122} in *P. denitrificans* cNOR, the NO reduction activity was significantly decreased (*11*). This mutation effect might be caused by Ca dissociation, disturbance of electron transfer between the hemes, and disturbance of proton transfer to the binuclear center.

Similarity in the overall structure, the hydrogen-bond network from heme b_3 propionate to periplasmic space, metal configuration, and Ca ligation between cNOR and cbb_3 oxidase suggests that two enzymes are very close in the phylogenetic tree, although it does not necessarily support the notion that aerobic respiration evolved from nitrate respiration. Structural differences of the binuclear center, however, provide insight into conversion of the chemical reactivity of the enzymes from the NO reduction to the O_2 reduction. The Glu^{211} in cNOR is a better ligand for Fe, whereas the His-Tyr covalent bond in cytochrome oxidases would restrain the geometry of non-heme metal to a more planar form that is favorable for Cu atom coordination. Thus, the amino acid substitution determines the selectivity of non-heme metal, which could lead to the conversion of respiratory substrate. This functional conversion of respiratory enzyme must have played a key role in the evolution of life to adjust to the environmental change of earth.

Considering the regions of cNOR that correspond to the K- and D-proton–pumping pathways proposed for cytochrome oxidases (Fig. 4), there are many hydrophobic residues, but neither an obvious channel nor a hydrogen-bonding network can be identified (comparison with cytochrome oxidases is shown in fig. S11), indicating no connection between the cytoplasm and periplasm (*32*). This observation is consistent with the absence of proton-pumping ability of cNOR. However, near the terminal proton donor Glu^{211}, cNOR contains a small charged region generated by Glu^{215}, Glu^{280}, and water (Fig. 4A) that partly overlaps with the K-pathway of cytochrome oxidases. This region of cNOR might reflect the first step in the evolution to acquire a proton delivery pathway from cytoplasm to the binuclear center. Indeed, in the structure of cbb_3 oxidase (*27*) the proton permeable route between the active site and cytoplasm is found at the region equivalent to the K-pathway, whereas the putative D-pathway is blocked by hydrophobic residues. Further structural, biochemical, and chemical studies that are based on the structural characterization of cNOR and cbb_3 oxidase are expected to elucidate the evolutionary history of the heme copper oxidase superfamily.

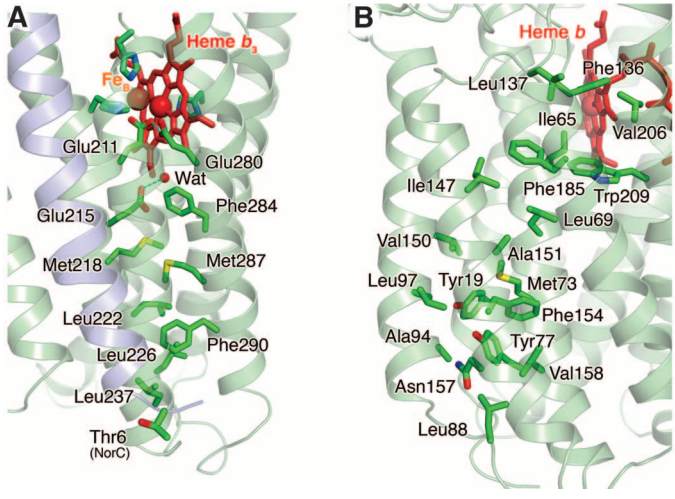

Fig. 4. Residues of cNOR corresponding to the (**A**) K-pathway and (**B**) D-pathway of cytochrome aa_3 oxidase are mostly hydrophobic. The main chain of NorC and NorB subunits is shown as blue and green ribbons, respectively. Comparisons with the residues of cbb_3, aa_3, or ba_3 oxidase in the same region are shown in fig. S11.

References and Notes

1. D. J. Wuebbles, *Science* **326**, 56 (2009).
2. J. P. Collman *et al.*, *Proc. Natl. Acad. Sci. U.S.A.* **105**, 15660 (2008).
3. N. Yeung *et al.*, *Nature* **462**, 1079 (2009).
4. Y. W. Lin *et al.*, *Proc. Natl. Acad. Sci. U.S.A.* **107**, 8581 (2010).
5. K. Kakishima, A. Shiratsuchi, A. Taoka, Y. Nakanishi, Y. Fukumori, *Biochem. Biophys. Res. Commun.* **355**, 587 (2007).
6. A. P. de Boer *et al.*, *Eur. J. Biochem.* **242**, 592 (1996).
7. W. G. Zumft, C. Braun, H. Cuypers, *Eur. J. Biochem.* **219**, 481 (1994).
8. P. Moenne-Loccoz, S. de Vries, *J. Am. Chem. Soc.* **120**, 5147 (1998).
9. Materials and methods are available as supporting material on *Science* Online.
10. G. Butland, S. Spiro, N. J. Watmough, D. J. Richardson, *J. Bacteriol.* **183**, 189 (2001).
11. U. Flock *et al.*, *J. Biol. Chem.* **283**, 3839 (2008).
12. U. Flock, P. Lachmann, J. Reimann, N. J. Watmough, P. Adelroth, *J. Inorg. Biochem.* **103**, 845 (2009).
13. B. Heiss, K. Frunzke, W. G. Zumft, *J. Bacteriol.* **171**, 3288 (1989).
14. P. Girsch, S. de Vries, *Biochim. Biophys. Acta* **1318**, 202 (1997).

15. M. Saraste, J. Castresana, *FEBS Lett.* **341**, 1 (1994).
16. J. van der Oost *et al.*, *FEMS Microbiol. Lett.* **121**, 1 (1994).
17. P. Moenne-Loccoz *et al.*, *J. Am. Chem. Soc.* **122**, 9344 (2000).
18. K. L. Grönberg *et al.*, *Biochemistry* **38**, 13780 (1999).
19. S. Iwata, C. Ostermeier, B. Ludwig, H. Michel, *Nature* **376**, 660 (1995).
20. T. Soulimane *et al.*, *EMBO J.* **19**, 1766 (2000).
21. T. Tsukihara *et al.*, *Science* **272**, 1136 (1996).
22. H. Kumita *et al.*, *J. Biol. Chem.* **279**, 55247 (2004).
23. R. W. Ye, B. A. Averill, J. M. Tiedje, *Appl. Environ. Microbiol.* **60**, 1053 (1994).
24. C. S. Butler, H. E. Seward, C. Greenwood, A. J. Thomson, *Biochemistry* **36**, 16259 (1997).
25. L. M. Blomberg, M. R. Blomberg, P. E. Siegbahn, *Biochim. Biophys. Acta* **1757**, 240 (2006).
26. P. Moënne-Loccoz, *Nat. Prod. Rep.* **24**, 610 (2007).
27. S. Buschmann *et al.*, *Science* **329**, 327 (2010).
28. J. J. Regan, B. E. Ramirez, J. R. Winkler, H. B. Gray, B. G. Malmström, *J. Bioenerg. Biomembr.* **30**, 35 (1998).
29. J. P. Shapleigh, W. J. Payne, *J. Bacteriol.* **163**, 837 (1985).
30. L. C. Bell, D. J. Richardson, S. J. Ferguson, *J. Gen. Microbiol.* **138**, 437 (1992).
31. J. Reimann, U. Flock, H. Lepp, A. Honigmann, P. Adelroth, *Biochim. Biophys. Acta* **1767**, 362 (2007).
32. J. Hemp, H. Han, J.-H. Roh, S. Kaplan, *Biochemistry* **46**, 9963 (2007).
33. Atomic coordinates and structure factors have been deposited to the Protein Data Bank (PDB) with code 3O0R. We thank T. Tosha for measurements of the enzymatic activity of cNOR under various conditions and the staff of the SPring-8 beamlines for their help with diffraction measurements. S.N., H.S., and Y.S. are supported by grants from the Ministry of Education, Culture, Sports, Science and Technology (MEXT), and Y.S. also acknowledges financial support from the Structural Biology and Molecular Ensemble projects of RIKEN. A part of this work was also supported by a grant from the ERATO IWATA Human Receptor Crystallography Project from the Japan Science and Technology Agency.

Supporting Online Material

www.sciencemag.org/cgi/content/full/science.1195591/DC1
Materials and Methods
Figs. S1 to S11
Tables S1 to S3
References

26 July 2010; accepted 1 November 2010
Published online 25 November 2010;
10.1126/science.1195591

Greatwall Phosphorylates an Inhibitor of Protein Phosphatase 2A That Is Essential for Mitosis

Satoru Mochida,[1,2] Sarah L. Maslen,[1] Mark Skehel,[1] Tim Hunt[1]*

Entry into mitosis in eukaryotes requires the activity of cyclin-dependent kinase 1 (Cdk1). Cdk1 is opposed by protein phosphatases in two ways: They inhibit activation of Cdk1 by dephosphorylating the protein kinases Wee1 and Myt1 and the protein phosphatase Cdc25 (key regulators of Cdk1), and they also antagonize Cdk1's own phosphorylation of downstream targets. A particular form of protein phosphatase 2A (PP2A) containing a B55δ subunit (PP2A-B55δ) is the major protein phosphatase that acts on model CDK substrates in *Xenopus* egg extracts and has antimitotic activity. The activity of PP2A-B55δ is high in interphase and low in mitosis, exactly opposite that of Cdk1. We report that inhibition of PP2A-B55δ results from a small protein, known as α-endosulfine (Ensa), that is phosphorylated in mitosis by the protein kinase Greatwall (Gwl). This converts Ensa into a potent and specific inhibitor of PP2A-B55δ. This pathway represents a previously unknown element in the control of mitosis.

Progression from interphase to mitosis requires that a large number of proteins be phosphorylated to bring about processes such as nuclear-envelope breakdown, chromosome condensation, and spindle assembly (*1*). Cyclin-dependent kinase 1 (Cdk1)–cyclin B, also called maturation-promoting factor (MPF), is the main (but not the sole) protein kinase that catalyzes these modifications (*2*). The activation of MPF requires that Cdc25, a phosphatase for the phospho-Tyr^{15} residue of Cdk1, is active, whereas Wee1 and Myt1, the protein kinases that phosphorylate Tyr^{15}, must be turned off. This is achieved by multisite phosphorylation of Cdc25, Wee1, and Myt1 (*3*–*5*), mainly catalyzed by MPF itself (*6*), and is opposed by protein phosphatase 2A (PP2A)–B55δ (PP2A-B55δ) (*7*). This form of PP2A is a major phosphatase for model CDK substrates (*8*), and depletion of PP2A-B55δ accelerates mitotic progression in *Xenopus* extracts (*8*), partly by promoting the activity of Cdc25 and the inactivity of Wee1 and Myt1, and partly by reducing antagonizing phosphatase activity against the substrates of CDKs and other mitotic kinases (*9*). Crucially, the activity of PP2A-B55δ fluctuates during the cell cycle, being high in interphase and low in mitosis (*10*). This presumably accentuates the switchlike behavior of the system; when a kinase is active, the opposing phosphatase is inactive and vice versa. This behavior also avoids futile cycles. But how PP2A-B55δ phosphatase is regulated was not known.

An important clue to the control of PP2A-B55δ has recently emerged from studies of the protein kinase Greatwall (Gwl) (*11*). In *Xenopus* egg extracts, Gwl is activated in mitosis and is essential for both entry into mitosis and maintenance of the mitotic state (*11*). Gwl apparently promotes mitosis by inactivating PP2A (*9*, *12*). We were unable to detect substantial phosphorylation of the components of PP2A-B55δ in vitro (*13*); hence, we suspected that Gwl might instead act by phosphorylating and activating some as-yet unidentified PP2A-B55δ–specific inhibitor protein. We therefore searched for Gwl substrates with the KESTREL (kinase substrate tracking and elucidation) method (*14*) in which active Gwl was incubated with extracts containing potential substrates, under conditions where endogenous protein kinase activity was suppressed. Several proteins in interphase egg extracts were phosphorylated by Gwl (Fig. 1A), and two prominent substrates of small apparent molecular size (arrows in Fig. 1A) were heat stable (*15*). The boiled extract was fractionated on a Mono-Q column, and fractions containing the major substrate were analyzed by mass spectrometry. We detected about 80 different *Xenopus* proteins, but no Gwl-dependent phosphorylated peptides emerged from the analysis. Thus, we choose 29 proteins with molecular sizes between 10 and 30 kD from the list and expressed them in bacteria (Fig. 1B). Seventeen of them were soluble after boiling, and these proteins were further tested as substrates for Gwl in vitro. One protein—cyclic adenosine monophosphate (cAMP)–regulated phosphoprotein-19 (Arpp-19)—was a better substrate for Gwl than any of the others (Fig. 1B, lane 22). Arpp-19 is a major substrate for cAMP-activated protein kinase (PKA) in postsynaptic neurons (*16*). Arpp-19 is a close relative of α-endosulfine (Fig. 1C), which was identified as an endogenous ligand of sulfonylurea receptor K^+ channels in the pancreas (*17*), although this idea seems to have been abandoned by its original proponents (*18*). Recombinant endosulfine (Ensa), like Arpp-19, was a good substrate for Gwl. Substitution of alanine for all of the potential conserved phosphorylation sites in Arpp-19 and Ensa (11 in the former and 7 in the latter) abolished phosphorylation by Gwl (Fig. 1D and fig. S1). In contrast, mutants of Arpp-19 and of Ensa that retained Ser^{67} in the highly conserved sequence FDSGDY (*19*) were phosphorylated by Gwl to a similar degree as the wild-type (WT) proteins. Because these proteins also have conserved CDK (S/T-P-X-K/R) and PKA (K/R-K/R-X-S/T) consensus sites, we tested to see whether they were substrates for these kinases in vitro. Indeed, Ser^{28} of Arpp-19 and Thr^{28} of Ensa were strongly phosphorylated by Cdk2-cyclin A (and Thr^{99} residues of both proteins phosphorylated weakly). Ser^{109} of both pro-

[1]Cancer Research UK, London Research Institute, Clare Hall Laboratories, South Mimms, Herts EN6 3LD, UK. [2]Priority Organization for Innovation and Excellence, Kumamoto University, 2-2-1 Honjo, Kumamoto, Kumamoto 860-0811, Japan.

*To whom correspondence should be addressed. E-mail: tim.hunt@cancer.org.uk

15. M. Saraste, J. Castresana, *FEBS Lett.* **341**, 1 (1994).
16. J. van der Oost *et al.*, *FEMS Microbiol. Lett.* **121**, 1 (1994).
17. P. Moenne-Loccoz *et al.*, *J. Am. Chem. Soc.* **122**, 9344 (2000).
18. K. L. Grönberg *et al.*, *Biochemistry* **38**, 13780 (1999).
19. S. Iwata, C. Ostermeier, B. Ludwig, H. Michel, *Nature* **376**, 660 (1995).
20. T. Soulimane *et al.*, *EMBO J.* **19**, 1766 (2000).
21. T. Tsukihara *et al.*, *Science* **272**, 1136 (1996).
22. H. Kumita *et al.*, *J. Biol. Chem.* **279**, 55247 (2004).
23. R. W. Ye, B. A. Averill, J. M. Tiedje, *Appl. Environ. Microbiol.* **60**, 1053 (1994).
24. C. S. Butler, H. E. Seward, C. Greenwood, A. J. Thomson, *Biochemistry* **36**, 16259 (1997).
25. L. M. Blomberg, M. R. Blomberg, P. E. Siegbahn, *Biochim. Biophys. Acta* **1757**, 240 (2006).
26. P. Moënne-Loccoz, *Nat. Prod. Rep.* **24**, 610 (2007).
27. S. Buschmann *et al.*, *Science* **329**, 327 (2010).
28. J. J. Regan, B. E. Ramirez, J. R. Winkler, H. B. Gray, B. G. Malmström, *J. Bioenerg. Biomembr.* **30**, 35 (1998).
29. J. P. Shapleigh, W. J. Payne, *J. Bacteriol.* **163**, 837 (1985).
30. L. C. Bell, D. J. Richardson, S. J. Ferguson, *J. Gen. Microbiol.* **138**, 437 (1992).
31. J. Reimann, U. Flock, H. Lepp, A. Honigmann, P. Adelroth, *Biochim. Biophys. Acta* **1767**, 362 (2007).
32. J. Hemp, H. Han, J.-H. Roh, S. Kaplan, *Biochemistry* **46**, 9963 (2007).
33. Atomic coordinates and structure factors have been deposited to the Protein Data Bank (PDB) with code 3O0R. We thank T. Tosha for measurements of the enzymatic activity of cNOR under various conditions and the staff of the SPring-8 beamlines for their help with diffraction measurements. S.N., H.S., and Y.S. are supported by grants from the Ministry of Education, Culture, Sports, Science and Technology (MEXT), and Y.S. also acknowledges financial support from the Structural Biology and Molecular Ensemble projects of RIKEN. A part of this work was also supported by a grant from the ERATO IWATA Human Receptor Crystallography Project from the Japan Science and Technology Agency.

Supporting Online Material

www.sciencemag.org/cgi/content/full/science.1195591/DC1
Materials and Methods
Figs. S1 to S11
Tables S1 to S3
References

26 July 2010; accepted 1 November 2010
Published online 25 November 2010;
10.1126/science.1195591

Greatwall Phosphorylates an Inhibitor of Protein Phosphatase 2A That Is Essential for Mitosis

Satoru Mochida,[1,2] Sarah L. Maslen,[1] Mark Skehel,[1] Tim Hunt[1]*

Entry into mitosis in eukaryotes requires the activity of cyclin-dependent kinase 1 (Cdk1). Cdk1 is opposed by protein phosphatases in two ways: They inhibit activation of Cdk1 by dephosphorylating the protein kinases Wee1 and Myt1 and the protein phosphatase Cdc25 (key regulators of Cdk1), and they also antagonize Cdk1's own phosphorylation of downstream targets. A particular form of protein phosphatase 2A (PP2A) containing a B55δ subunit (PP2A-B55δ) is the major protein phosphatase that acts on model CDK substrates in *Xenopus* egg extracts and has antimitotic activity. The activity of PP2A-B55δ is high in interphase and low in mitosis, exactly opposite that of Cdk1. We report that inhibition of PP2A-B55δ results from a small protein, known as α-endosulfine (Ensa), that is phosphorylated in mitosis by the protein kinase Greatwall (Gwl). This converts Ensa into a potent and specific inhibitor of PP2A-B55δ. This pathway represents a previously unknown element in the control of mitosis.

Progression from interphase to mitosis requires that a large number of proteins be phosphorylated to bring about processes such as nuclear-envelope breakdown, chromosome condensation, and spindle assembly (*1*). Cyclin-dependent kinase 1 (Cdk1)–cyclin B, also called maturation-promoting factor (MPF), is the main (but not the sole) protein kinase that catalyzes these modifications (*2*). The activation of MPF requires that Cdc25, a phosphatase for the phospho-Tyr^{15} residue of Cdk1, is active, whereas Wee1 and Myt1, the protein kinases that phosphorylate Tyr^{15}, must be turned off. This is achieved by multisite phosphorylation of Cdc25, Wee1, and Myt1 (*3*–*5*), mainly catalyzed by MPF itself (*6*), and is opposed by protein phosphatase 2A (PP2A)–B55δ (PP2A-B55δ) (*7*). This form of PP2A is a major phosphatase for model CDK substrates (*8*), and depletion of PP2A-B55δ accelerates mitotic progression in *Xenopus* extracts (*8*), partly by promoting the activity of Cdc25 and the inactivity of Wee1 and Myt1, and partly by reducing antagonizing phosphatase activity against the substrates of CDKs and other mitotic kinases (*9*). Crucially, the activity of PP2A-B55δ fluctuates during the cell cycle, being high in interphase and low in mitosis (*10*). This presumably accentuates the switchlike behavior of the system; when a kinase is active, the opposing phosphatase is inactive and vice versa. This behavior also avoids futile cycles. But how PP2A-B55δ phosphatase is regulated was not known.

An important clue to the control of PP2A-B55δ has recently emerged from studies of the protein kinase Greatwall (Gwl) (*11*). In *Xenopus* egg extracts, Gwl is activated in mitosis and is essential for both entry into mitosis and maintenance of the mitotic state (*11*). Gwl apparently promotes mitosis by inactivating PP2A (*9*, *12*). We were unable to detect substantial phosphorylation of the components of PP2A-B55δ in vitro (*13*); hence, we suspected that Gwl might instead act by phosphorylating and activating some as-yet unidentified PP2A-B55δ–specific inhibitor protein. We therefore searched for Gwl substrates with the KESTREL (kinase substrate tracking and elucidation) method (*14*) in which active Gwl was incubated with extracts containing potential substrates, under conditions where endogenous protein kinase activity was suppressed. Several proteins in interphase egg extracts were phosphorylated by Gwl (Fig. 1A), and two prominent substrates of small apparent molecular size (arrows in Fig. 1A) were heat stable (*15*). The boiled extract was fractionated on a Mono-Q column, and fractions containing the major substrate were analyzed by mass spectrometry. We detected about 80 different *Xenopus* proteins, but no Gwl-dependent phosphorylated peptides emerged from the analysis. Thus, we choose 29 proteins with molecular sizes between 10 and 30 kD from the list and expressed them in bacteria (Fig. 1B). Seventeen of them were soluble after boiling, and these proteins were further tested as substrates for Gwl in vitro. One protein—cyclic adenosine monophosphate (cAMP)–regulated phosphoprotein-19 (Arpp-19)—was a better substrate for Gwl than any of the others (Fig. 1B, lane 22). Arpp-19 is a major substrate for cAMP-activated protein kinase (PKA) in postsynaptic neurons (*16*). Arpp-19 is a close relative of α-endosulfine (Fig. 1C), which was identified as an endogenous ligand of sulfonylurea receptor K^+ channels in the pancreas (*17*), although this idea seems to have been abandoned by its original proponents (*18*). Recombinant endosulfine (Ensa), like Arpp-19, was a good substrate for Gwl. Substitution of alanine for all of the potential conserved phosphorylation sites in Arpp-19 and Ensa (11 in the former and 7 in the latter) abolished phosphorylation by Gwl (Fig. 1D and fig. S1). In contrast, mutants of Arpp-19 and of Ensa that retained Ser^{67} in the highly conserved sequence FDSGDY (*19*) were phosphorylated by Gwl to a similar degree as the wild-type (WT) proteins. Because these proteins also have conserved CDK (S/T-P-X-K/R) and PKA (K/R-K/R-X-S/T) consensus sites, we tested to see whether they were substrates for these kinases in vitro. Indeed, Ser^{28} of Arpp-19 and Thr^{28} of Ensa were strongly phosphorylated by Cdk2-cyclin A (and Thr^{99} residues of both proteins phosphorylated weakly). Ser^{109} of both pro-

[1]Cancer Research UK, London Research Institute, Clare Hall Laboratories, South Mimms, Herts EN6 3LD, UK. [2]Priority Organization for Innovation and Excellence, Kumamoto University, 2-2-1 Honjo, Kumamoto, Kumamoto 860-0811, Japan.

*To whom correspondence should be addressed. E-mail: tim.hunt@cancer.org.uk

teins was the major site targeted by PKA (Fig. 1D and fig. S1A) (*20*).

We raised antibodies against Arpp-19 and Ensa in rabbits and used them to measure the concentrations of Arpp-19 and Ensa in *Xenopus* egg extracts. Arpp-19 was hardly detectable, despite its presence in the original mass spectrometric analysis. On the other hand, Ensa was present at ~150 to 300 nM in egg extracts, in excess of PP2A-B55δ, whose concentration we measured at ~50 to 70 nM.

We tested whether Ensa affected the phosphatase activity of PP2A-B55δ. Although dephosphorylated Ensa did not inhibit any form of PP2A, Ensa phosphorylated by Gwl strongly inhibited the PP2A-B55δ heterotrimer holocomplex (Fig. 2A), but not the monomeric catalytic subunit or the dimer comprising the A scaffold and C catalytic subunits (AC). Phosphorylation of Ensa by CDK or PKA alone did not generate any inhibitory activity against PP2A-B55δ. Similar results were obtained for Arpp-19 (fig. S1B). These results indicate that Arpp-19 and Ensa are converted into inhibitors of PP2A-B55δ by phosphorylation on Ser^{67}.

We tested the specificity of Ensa's interactions with various forms of PP2A and other protein phosphatases by making affinity matrices covalently conjugated with Ensa. Gwl-phosphorylated Ensa strongly bound PP2A-B55δ from interphase egg extracts, but no other B subunits, nor the PP1 or PP5 catalytic subunit, were retained by Ensa beads (Fig. 2B). Mock- and PKA-phosphorylated Ensa bound PP2A-B55δ only weakly. These results suggest that Ensa inhibits PP2A-B55δ by a Ser^{67} phosphorylation-dependent physical interaction, which makes it a highly specific inhibitor of PP2A-B55δ. Neither Ensa nor Arpp-19 inhibited PP1, regardless of their phosphorylation state (fig. S1C).

Antibodies specific for phospho-Ser^{67} reacted with Ensa in mitotic extracts much more strongly than in interphase extracts (Fig. 3A). Using Phos-Tag acrylamide gels, which specifically retard phosphorylated proteins (*21*), we confirmed that the majority of Ensa became phosphorylated in mitotic extracts (Fig. 3A) and that Ser^{67} was required for the observed phosphorylation-dependent shift in migration on polyacrylamide gel electrophoresis (Fig. 3A). These results show that Ensa is quantitatively phosphorylated at its Ser^{67} residue in mitosis, which leads to the inhibition of PP2A-B55δ. The timing of Ensa phosphorylation in relation to that of a number of other cell-cycle markers is shown in fig. S2. The phosphorylation of anaphase-promoting complex 3 (Apc3), Cdc25, Wee1, and Gwl all took place at the same time at the resolution of this experiment.

We tested the effects of Ensa depletion on "cycling" frog egg extracts (*22*, *23*). In this experiment, the control (Fig. 3C) performed two cycles of entry into and exit from mitosis, whereas the Ensa-depleted extract (Fig. 3D) never entered M phase, despite larger amounts of histone H1 kinase activity than in the control. Apc3 was never fully phosphorylated, and mitotic phosphoproteins showed only slightly increased intensity (fig. S3C). Cyclin destruction was not activated in the Ensa-depleted extract. Adding back WT recombinant Ensa to depleted extracts restored induction of mitosis (Fig. 3E), whereas the Ser^{67}→Ala^{67} (S67A) mutant protein did not

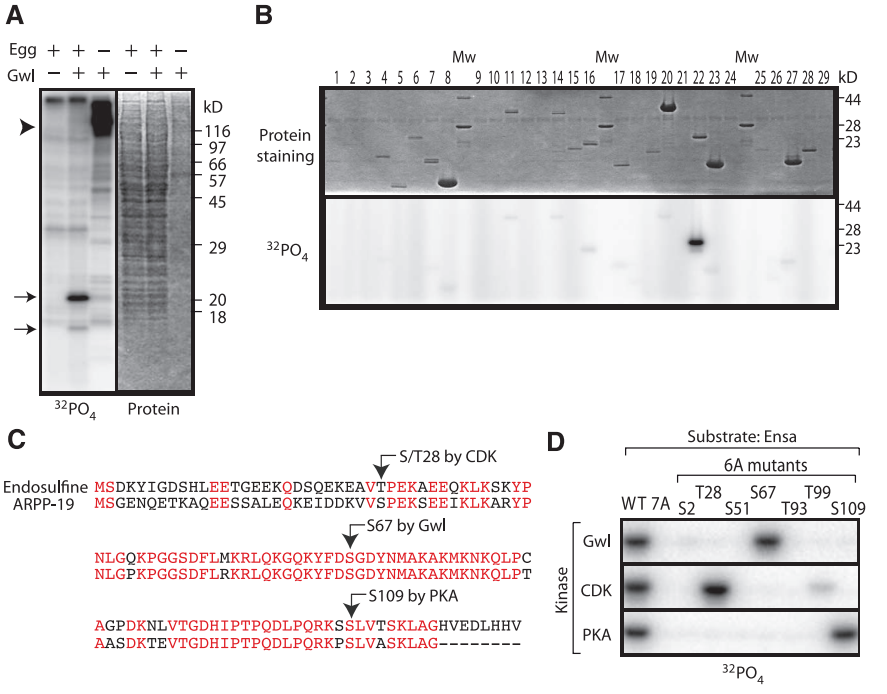

Fig. 1. Ensa and ARPP-19 are substrates of Gwl. (**A**) Phosphorylation of two small proteins in *Xenopus* interphase egg extract to which Gwl was added. Coomassie blue staining (right) and autoradiography (left). The positions of the two candidates and of Gwl are indicated with arrows and an arrowhead, respectively. (**B**) In vitro phosphorylation of candidate substrates by Gwl. Lanes marked "Mw" are molecular size markers. (**C**) Sequence alignment of *X. laevis* Ensa and Arpp-19. Conserved residues are shown in red. (**D**) In vitro phosphorylation of Ensa by Gwl. WT Ensa and mutants were phosphorylated by Gwl kinase (top), CDK (middle), or PKA (bottom). In the 7A mutant, Ser^{2}, Thr^{28}, Ser^{51}, Ser^{67}, Thr^{93}, Thr^{99}, and Ser^{109} of Ensa were all substituted by alanine. In the 6A mutants, one of these seven residues was restored to its original state as indicated.

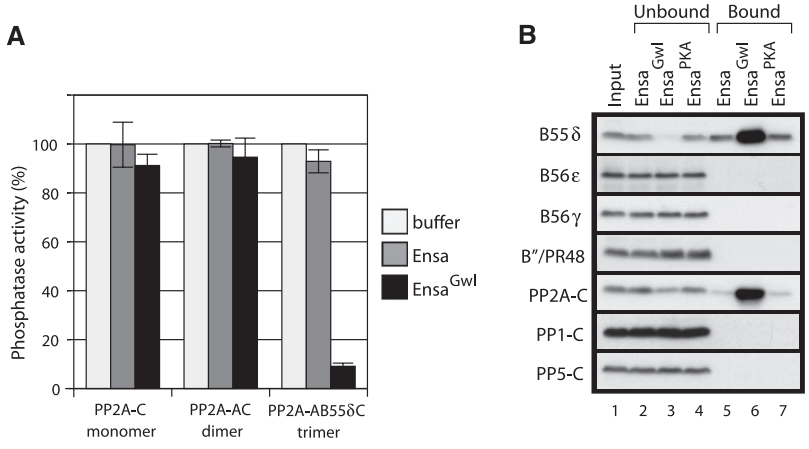

Fig. 2. Regulation of PP2A-B55δ by Ensa. (**A**) Phosphatase activities of recombinant PP2A-C monomer, AC dimer, and AB55δC trimer complexes were analyzed with and without Ensa using $^{32}PO_4$-labeled maltose binding protein fused to a 25-residue peptide containing Ser^{50} of Fizzy (MBP-Fizzy-Ser50) as a substrate (*10*). Results are the means ± range for three experiments. The activities are expressed as percentages of controls. Open bars, buffer; gray bars, Ensa; black bars, Ensa thiophosphorylated by Gwl. Error bars indicate the range from three independent experiments. (**B**) Physical interaction between Ensa and PP2A subunits in *Xenopus* interphase egg extract. Fractions bound to (lanes 5 to 7) and not retained by (lanes 2 to 4) Ensa beads were analyzed for PP1, PP2A, and PP5 subunits.

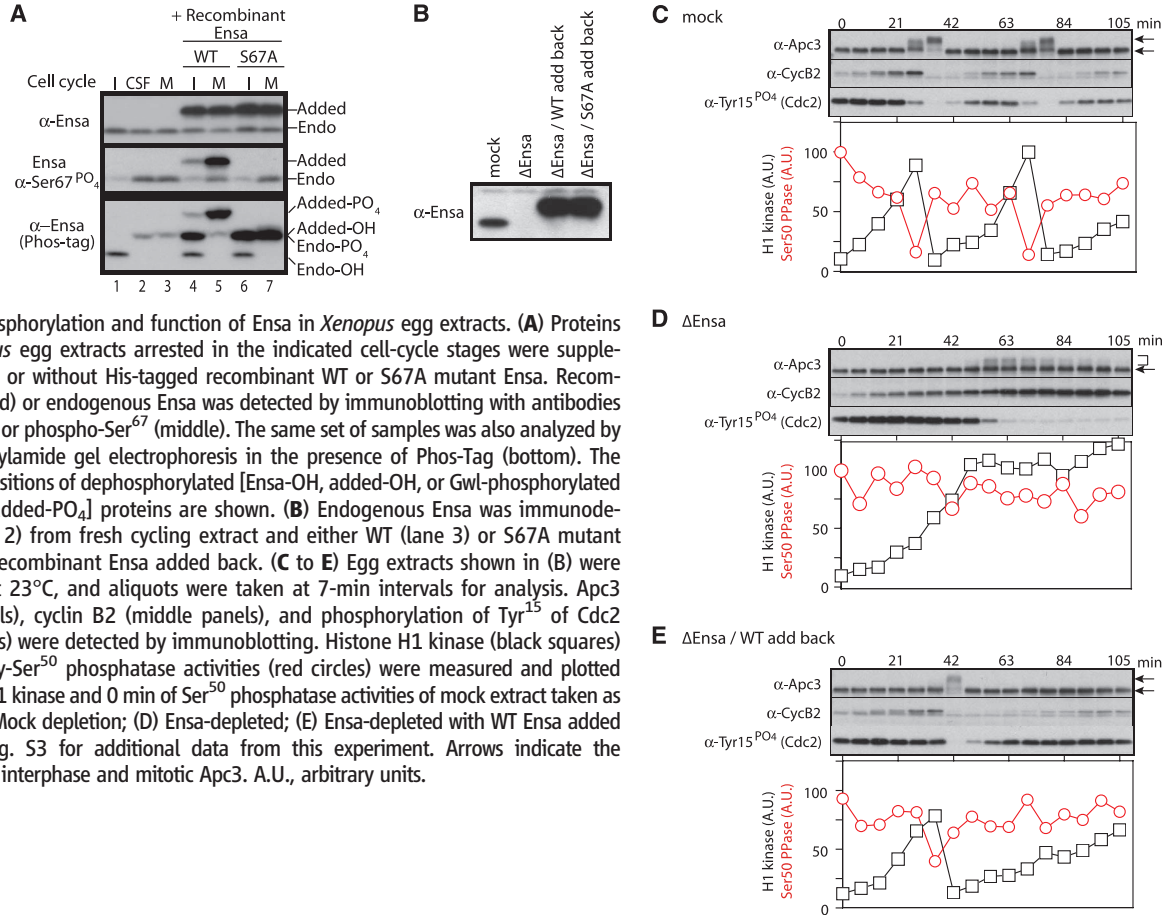

Fig. 3. Phosphorylation and function of Ensa in *Xenopus* egg extracts. (**A**) Proteins from *Xenopus* egg extracts arrested in the indicated cell-cycle stages were supplemented with or without His-tagged recombinant WT or S67A mutant Ensa. Recombinant (added) or endogenous Ensa was detected by immunoblotting with antibodies to Ensa (top) or phospho-Ser^{67} (middle). The same set of samples was also analyzed by SDS–polyacrylamide gel electrophoresis in the presence of Phos-Tag (bottom). The migration positions of dephosphorylated [Ensa-OH, added-OH, or Gwl-phosphorylated (Ensa-PO_4, added-PO_4] proteins are shown. (**B**) Endogenous Ensa was immunodepleted (lane 2) from fresh cycling extract and either WT (lane 3) or S67A mutant (lane 4) of recombinant Ensa added back. (**C** to **E**) Egg extracts shown in (B) were incubated at 23°C, and aliquots were taken at 7-min intervals for analysis. Apc3 (upper panels), cyclin B2 (middle panels), and phosphorylation of Tyr^{15} of Cdc2 (lower panels) were detected by immunoblotting. Histone H1 kinase (black squares) and MBP-Fzy-Ser^{50} phosphatase activities (red circles) were measured and plotted (70 min of H1 kinase and 0 min of Ser^{50} phosphatase activities of mock extract taken as 100%). (C) Mock depletion; (D) Ensa-depleted; (E) Ensa-depleted with WT Ensa added back. See fig. S3 for additional data from this experiment. Arrows indicate the mobilities of interphase and mitotic Apc3. A.U., arbitrary units.

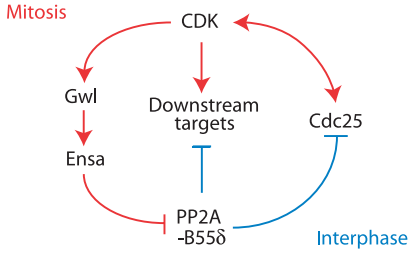

Pathways in red are active in mitosis; lines in blue are dominant in interphase

Fig. 4. Diagram of how PP2A-B55δ is inactivated by CDK via the Gwl and Ensa pathway. Pathways in blue are active in interphase; pathways in red denote those active during mitosis.

(fig. S3A), indicating that residue Ser^{67} of Ensa is crucial for proper cell-cycle control. Tyr^{15} of Cdk1 was dephosphorylated in all three conditions, but in the Ensa-depleted extract, Tyr^{15} remained dephosphorylated for the duration of the incubation, whereas in the controls, Tyr^{15} was rephosphorylated. This experiment implies that the main effect of not inhibiting PP2A-B55δ is in antagonizing Cdk1 phosphorylation of downstream target proteins, rather than on the control of Cdk1 activity. Somehow, Cdc25 or an equivalent activity that dephosphorylated Tyr^{15} was activated in the Ensa-depleted extract, yet despite strong histone H1 kinase activity, the extract failed to enter mitosis.

We tested the results of adding thiophosphorylated Ensa to egg extracts. Supplemental fig. S4 shows that when extra Ensa was added to interphase extracts supplemented with cycloheximide and a small amount of recombinant stable cyclin B (not enough to induce mitosis by itself), phosphorylation events typical of mitotic extracts were induced when Gwl-thiophosphorylated Ensa was added. Dephosphorylated Ensa or Ensa thiophosphorylated by PKA did not show any effect. These results are all consistent with the idea that Gwl inhibits PP2A-B55δ by phosphorylating Ensa, thereby both activating Cdk1 (by inhibiting Wee1 and turning on Cdc25) and allowing Cdk1 to efficiently phosphorylate its target proteins in mitosis by suppressing the activity of the main opposing protein phosphatase.

In this paper, we identify Ensa and Arpp-19 as phosphorylation-dependent inhibitors of PP2A-B55δ and physiological substrates of Gwl kinase. In *Drosophila*, Ensa is required for proper spindle assembly and oocyte maturation; endosulfine-deficient oocytes are unable to pass between prophase of first meiosis into metaphase (*24*–*26*). Tellingly, these oocytes have high Cdk1 activity yet display little phosphorylation of mitotic substrates, exactly as we observed in *Xenopus* extracts, consistent with a failure to shut off protein phosphatase(s) upon entry into M phase (*25*). The Gwl-Arpp-Ensa module appears to be active in human cells, because reduction of Gwl levels by RNA interference blocks cells in G_2 phase of the cell cycle (*27*).

It is still difficult to understand the details of how gradually accumulating cyclin levels are converted into the sharp activation of MPF at the G_2-to-M transition. Gwl appears to require activation by MPF (*11*), and once it is turned on, it phosphorylates Ensa, which, in turn, switches off PP2A-B55δ (Fig. 4). This promotes the activation of MPF by increasing phosphorylation of Wee1, Myt1, and Cdc25, and it also assists entry into mitosis by reducing the dephosphorylation of MPF targets. This is an example of a "coherent feed-forward loop" (*28*), because Cdk1 phosphorylates its own activation module in a positive feedback loop, it phosphorylates its mitotic target proteins, and it indirectly inactivates the antagonizing protein phosphatase by activating Gwl and the downstream phosphatase inhibitor Ensa. Clearly, once this system is active, the cell switches completely into mitosis in a kind of latch mechanism. Thus, both Gwl and Ensa are essential for the maintenance of the mitotic state, implying that inhibition of protein phosphatases is critically important for this process. How the return to interphase is brought about is unclear. When cyclins are degraded and Cdk1 levels fall, Gwl and

Ensa are dephosphorylated, presumably by protein phosphatase(s) other than PP2A-B55δ, such as PP1 (*29*, *30*). The threshold for activation of Gwl and entry into mitosis depends on the balance of activities of these as-yet unidentified phosphatases and that of MPF.

References and Notes

1. D. O. Morgan, in *The Cell Cycle: Principles of Control (Primers in Biology)* (New Science Press, London, 2007), p. 297.
2. A. Lindqvist, V. Rodríguez-Bravo, R. H. Medema, *J. Cell Biol.* **185**, 193 (2009).
3. A. Kumagai, W. G. Dunphy, *Cell* **70**, 139 (1992).
4. P. R. Mueller, T. R. Coleman, W. G. Dunphy, *Mol. Biol. Cell* **6**, 119 (1995).
5. S. Y. Kim, E. J. Song, K. J. Lee, J. E. Ferrell Jr., *Mol. Cell. Biol.* **25**, 10580 (2005).
6. S. L. Harvey, A. Charlet, W. Haas, S. P. Gygi, D. R. Kellogg, *Cell* **122**, 407 (2005).
7. G. Pal, M. T. Paraz, D. R. Kellogg, *J. Cell Biol.* **180**, 931 (2008).
8. S. Mochida, S. Ikeo, J. Gannon, T. Hunt, *EMBO J.* **28**, 2777 (2009).
9. P. V. Castilho, B. C. Williams, S. Mochida, Y. Zhao, M. L. Goldberg, *Mol. Biol. Cell* **20**, 4777 (2009).
10. S. Mochida, T. Hunt, *Nature* **449**, 336 (2007).
11. J. Yu, Y. Zhao, Z. Li, S. Galas, M. L. Goldberg, *Mol. Cell* **22**, 83 (2006).
12. S. Vigneron *et al.*, *EMBO J.* **28**, 2786 (2009).
13. M. Goldberg, personal communication.
14. P. Cohen, A. Knebel, *Biochem. J.* **393**, 1 (2006).
15. Methods are available as supporting material on *Science* Online.
16. J. A. Girault, A. Horiuchi, E. L. Gustafson, N. L. Rosen, P. Greengard, *J. Neurosci.* **10**, 1124 (1990).
17. A. Virsolvy-Vergine *et al.*, *Proc. Natl. Acad. Sci. U.S.A.* **89**, 6629 (1992).
18. L. Gros *et al.*, *Diabetologia* **45**, 703 (2002).
19. Single-letter abbreviations for the amino acid residues are as follows: A, Ala; C, Cys; D, Asp; E, Glu; F, Phe; G, Gly; H, His; I, Ile; K, Lys; L, Leu; M, Met; N, Asn; P, Pro; Q, Gln; R, Arg; S, Ser; T, Thr; V, Val; W, Trp; and Y, Tyr.
20. I. Dulubova *et al.*, *J. Neurochem.* **77**, 229 (2001).
21. E. Kinoshita, E. Kinoshita-Kikuta, K. Takiyama, T. Koike, *Mol. Cell. Proteomics* **5**, 749 (2006).
22. A. W. Murray, *Cell Biol.* **36**, 581 (1991).
23. K. Ohsumi, T. M. Yamamoto, M. Iwabuchi, *Methods Mol. Biol.* **322**, 445 (2006).
24. G. Goshima *et al.*, *Science* **316**, 417 (2007); 10.1126/science.1141314.
25. J. R. Von Stetina *et al.*, *Development* **135**, 3697 (2008).
26. D. Drummond-Barbosa, A. C. Spradling, *Dev. Biol.* **266**, 310 (2004).
27. A. Burgess *et al.*, *Proc. Natl. Acad. Sci. U.S.A.* **107**, 12564 (2010).
28. S. Mangan, A. Zaslaver, U. Alon, *J. Mol. Biol.* **334**, 197 (2003).
29. K. Ishii, K. Kumada, T. Toda, M. Yanagida, *EMBO J.* **15**, 6629 (1996).
30. J. Q. Wu *et al.*, *Nat. Cell Biol.* **11**, 644 (2009).

31. We thank H. Mahbubani, J. Kirk, and L. Egbuniwe for care of frogs and other members of the laboratory for advice and reagents, especially J. Gannon for the antibody to doubly phosphorylated Thr^{14}-Tyr^{15} of Cdk1 (CP 3.2). S.M. was supported by a fellowship from the Japan Society for the Promotion of Science.

Supporting Online Material

www.sciencemag.org/cgi/content/full/330/6011/1670/DC1
Methods
Figs. S1 to S4

27 July 2010; accepted 13 October 2010
10.1126/science.1195689

The Substrate of Greatwall Kinase, Arpp19, Controls Mitosis by Inhibiting Protein Phosphatase 2A

Aicha Gharbi-Ayachi,[1] Jean-Claude Labbé,[1] Andrew Burgess,[1] Suzanne Vigneron,[1] Jean-Marc Strub,[2] Estelle Brioudes,[1] Alain Van-Dorsselaer,[2] Anna Castro,[1]*† Thierry Lorca[1]*†

Initiation and maintenance of mitosis require the activation of protein kinase cyclin B–Cdc2 and the inhibition of protein phosphatase 2A (PP2A), which, respectively, phosphorylate and dephosphorylate mitotic substrates. The protein kinase Greatwall (Gwl) is required to maintain mitosis through PP2A inhibition. We describe how Gwl activation results in PP2A inhibition. We identified cyclic adenosine monophosphate–regulated phosphoprotein 19 (Arpp19) and α-Endosulfine as two substrates of Gwl that, when phosphorylated by this kinase, associate with and inhibit PP2A, thus promoting mitotic entry. Conversely, in the absence of Gwl activity, Arpp19 and α-Endosulfine are dephosphorylated and lose their capacity to bind and inhibit PP2A. Although both proteins can inhibit PP2A, endogenous Arpp19, but not α-Endosulfine, is responsible for PP2A inhibition at mitotic entry in *Xenopus* egg extracts.

Mitotic entry and exit are controlled by activation and inactivation of the cyclin B–Cdc2 protein kinase (*1*). However, maintained phosphorylation of mitotic proteins also requires inhibition of the protein phosphatase 2A (PP2A), the main phosphatase that dephosphorylates mitotic substrates (although a role of protein phosphatase 1 has also been reported in *Xenopus* egg extracts) (*2*–*5*).

The protein kinase Greatwall regulates PP2A activity during mitosis (*2*, *4*, *6*). Depletion of Gwl from mitotic egg extracts induces mitotic exit, whereas depletion of Gwl from interphase egg extracts prevents mitotic entry (*2*–*4*). These phenotypes, as well as the phenotypes observed in Gwl knockdown human cells (*6*), are mediated by PP2A. Although Gwl and PP2A do interact, direct phosphorylation of PP2A by this kinase has not been observed (*2*, *4*), suggesting that Gwl may inhibit PP2A through an intermediary protein. We used biochemical fractionation of cytostatic factor (CSF) meiotic arrested *Xenopus* egg extracts and in vitro phosphorylation by Gwl to identify substrates of this kinase.

We fractionated proteins from interphase extracts on a heparin column. Eluted proteins were precipitated with ammonium sulfate (50 to 70%), resuspended, and fractionated by gel filtration. Samples from the fractions were phosphorylated in vitro with a hyperactive form of human Gwl (K72M mutant) (*7*), and the phosphorylated bands were analyzed by mass spectrometry. Maximal phosphorylation was observed in the gel filtration fractions corresponding to molecular sizes of 30 to 70 kD (Fig. 1A, fraction 3) and 20 to 50 kD (Fig. 1A, fraction 4). These two fractions increased phosphorylation of a band of 20 kD. Forty different proteins were detected in this band by mass spectrometry, among them the cyclic adenosine monophosphate–regulated phosphoprotein 19 (Arpp19), a protein that strongly resembles the small protein α-Endosulfine. The functions of Arpp19 and α-Endosulfine are unclear (*8*, *9*); however, oocytes from *Drosophila* with mutant α-Endosulfine have a prolonged prophase and fail to progress to metaphase (*10*). Cdc2 isolated from these oocytes has normal kinase activity, but the oocytes show a reduced amount of in vivo phosphorylation of mitotic substrates, a phenotype reminiscent of the one observed in Gwl-depleted *Xenopus* egg extracts (*4*). Although by mass spectrometry we identified peptides specific to Arpp19 but not for α-Endosulfine (fig. S1), their sequence similarity indicates that both may be Gwl substrates. We therefore tested glutathione *S*-transferase fusion proteins made from Arpp19 and α-Endosulfine, as possible substrates of Gwl. Both proteins were phosphorylated in vitro by Gwl (Fig. 1B). The endogenous proteins were present in small amounts in *Xenopus* egg extracts, particularly Arpp19, which was very difficult to detect (Fig. 1C). The analysis of the protein sequences of Arpp19 and α-Endosulfine revealed the presence of seven potential serine or threonine phosphorylation sites conserved in both proteins (Fig. 1D). We made individual mutants of Arpp19 in which serine (S) or threonine (T) was mutated to alanine (A) and tested whether they were phosphorylated in vitro by Gwl. All mutants were phosphorylated by Gwl except mutant S62A. Similarly, mutation of this conserved serine of human α-Endosulfine to alanine (S67A) also prevented the phosphorylation of this protein by Gwl (Fig.

[1]Universités Montpellier 2 et 1, Centre de Recherche de Biochimie Macromoléculaire, CNRS UMR 5237, IFR 122, 1919 Route de Mende, 34293 Montpellier cedex 5, France. [2]Institut Pluridisciplinaire Hubert Curien, Strasbourg Cedex, France.

*To whom correspondence should be addressed. E-mail: anna.castro@crbm.cnrs.fr (A.C.); thierry.lorca@crbm.cnrs.fr (T.L.)

†These authors contributed equally to this work.

Ensa are dephosphorylated, presumably by protein phosphatase(s) other than PP2A-B55δ, such as PP1 (*29*, *30*). The threshold for activation of Gwl and entry into mitosis depends on the balance of activities of these as-yet unidentified phosphatases and that of MPF.

References and Notes

1. D. O. Morgan, in *The Cell Cycle: Principles of Control (Primers in Biology)* (New Science Press, London, 2007), p. 297.
2. A. Lindqvist, V. Rodríguez-Bravo, R. H. Medema, *J. Cell Biol.* **185**, 193 (2009).
3. A. Kumagai, W. G. Dunphy, *Cell* **70**, 139 (1992).
4. P. R. Mueller, T. R. Coleman, W. G. Dunphy, *Mol. Biol. Cell* **6**, 119 (1995).
5. S. Y. Kim, E. J. Song, K. J. Lee, J. E. Ferrell Jr., *Mol. Cell. Biol.* **25**, 10580 (2005).
6. S. L. Harvey, A. Charlet, W. Haas, S. P. Gygi, D. R. Kellogg, *Cell* **122**, 407 (2005).
7. G. Pal, M. T. Paraz, D. R. Kellogg, *J. Cell Biol.* **180**, 931 (2008).
8. S. Mochida, S. Ikeo, J. Gannon, T. Hunt, *EMBO J.* **28**, 2777 (2009).
9. P. V. Castilho, B. C. Williams, S. Mochida, Y. Zhao, M. L. Goldberg, *Mol. Biol. Cell* **20**, 4777 (2009).
10. S. Mochida, T. Hunt, *Nature* **449**, 336 (2007).
11. J. Yu, Y. Zhao, Z. Li, S. Galas, M. L. Goldberg, *Mol. Cell* **22**, 83 (2006).
12. S. Vigneron *et al.*, *EMBO J.* **28**, 2786 (2009).
13. M. Goldberg, personal communication.
14. P. Cohen, A. Knebel, *Biochem. J.* **393**, 1 (2006).
15. Methods are available as supporting material on *Science* Online.
16. J. A. Girault, A. Horiuchi, E. L. Gustafson, N. L. Rosen, P. Greengard, *J. Neurosci.* **10**, 1124 (1990).
17. A. Virsolvy-Vergine *et al.*, *Proc. Natl. Acad. Sci. U.S.A.* **89**, 6629 (1992).
18. L. Gros *et al.*, *Diabetologia* **45**, 703 (2002).
19. Single-letter abbreviations for the amino acid residues are as follows: A, Ala; C, Cys; D, Asp; E, Glu; F, Phe; G, Gly; H, His; I, Ile; K, Lys; L, Leu; M, Met; N, Asn; P, Pro; Q, Gln; R, Arg; S, Ser; T, Thr; V, Val; W, Trp; and Y, Tyr.
20. I. Dulubova *et al.*, *J. Neurochem.* **77**, 229 (2001).
21. E. Kinoshita, E. Kinoshita-Kikuta, K. Takiyama, T. Koike, *Mol. Cell. Proteomics* **5**, 749 (2006).
22. A. W. Murray, *Cell Biol.* **36**, 581 (1991).
23. K. Ohsumi, T. M. Yamamoto, M. Iwabuchi, *Methods Mol. Biol.* **322**, 445 (2006).
24. G. Goshima *et al.*, *Science* **316**, 417 (2007); 10.1126/science.1141314.
25. J. R. Von Stetina *et al.*, *Development* **135**, 3697 (2008).
26. D. Drummond-Barbosa, A. C. Spradling, *Dev. Biol.* **266**, 310 (2004).
27. A. Burgess *et al.*, *Proc. Natl. Acad. Sci. U.S.A.* **107**, 12564 (2010).
28. S. Mangan, A. Zaslaver, U. Alon, *J. Mol. Biol.* **334**, 197 (2003).
29. K. Ishii, K. Kumada, T. Toda, M. Yanagida, *EMBO J.* **15**, 6629 (1996).
30. J. Q. Wu *et al.*, *Nat. Cell Biol.* **11**, 644 (2009).

31. We thank H. Mahbubani, J. Kirk, and L. Egbuniwe for care of frogs and other members of the laboratory for advice and reagents, especially J. Gannon for the antibody to doubly phosphorylated Thr^{14}-Tyr^{15} of Cdk1 (CP 3.2). S.M. was supported by a fellowship from the Japan Society for the Promotion of Science.

Supporting Online Material

www.sciencemag.org/cgi/content/full/330/6011/1670/DC1
Methods
Figs. S1 to S4

27 July 2010; accepted 13 October 2010
10.1126/science.1195689

The Substrate of Greatwall Kinase, Arpp19, Controls Mitosis by Inhibiting Protein Phosphatase 2A

Aicha Gharbi-Ayachi,[1] Jean-Claude Labbé,[1] Andrew Burgess,[1] Suzanne Vigneron,[1] Jean-Marc Strub,[2] Estelle Brioudes,[1] Alain Van-Dorsselaer,[2] Anna Castro,[1]*† Thierry Lorca[1]*†

Initiation and maintenance of mitosis require the activation of protein kinase cyclin B–Cdc2 and the inhibition of protein phosphatase 2A (PP2A), which, respectively, phosphorylate and dephosphorylate mitotic substrates. The protein kinase Greatwall (Gwl) is required to maintain mitosis through PP2A inhibition. We describe how Gwl activation results in PP2A inhibition. We identified cyclic adenosine monophosphate–regulated phosphoprotein 19 (Arpp19) and α-Endosulfine as two substrates of Gwl that, when phosphorylated by this kinase, associate with and inhibit PP2A, thus promoting mitotic entry. Conversely, in the absence of Gwl activity, Arpp19 and α-Endosulfine are dephosphorylated and lose their capacity to bind and inhibit PP2A. Although both proteins can inhibit PP2A, endogenous Arpp19, but not α-Endosulfine, is responsible for PP2A inhibition at mitotic entry in *Xenopus* egg extracts.

Mitotic entry and exit are controlled by activation and inactivation of the cyclin B–Cdc2 protein kinase (*1*). However, maintained phosphorylation of mitotic proteins also requires inhibition of the protein phosphatase 2A (PP2A), the main phosphatase that dephosphorylates mitotic substrates (although a role of protein phosphatase 1 has also been reported in *Xenopus* egg extracts) (*2*–*5*).

The protein kinase Greatwall regulates PP2A activity during mitosis (*2*, *4*, *6*). Depletion of Gwl from mitotic egg extracts induces mitotic exit, whereas depletion of Gwl from interphase egg extracts prevents mitotic entry (*2*–*4*). These phenotypes, as well as the phenotypes observed in Gwl knockdown human cells (*6*), are mediated by PP2A. Although Gwl and PP2A do interact, direct phosphorylation of PP2A by this kinase has not been observed (*2*, *4*), suggesting that Gwl may inhibit PP2A through an intermediary protein. We used biochemical fractionation of cytostatic factor (CSF) meiotic arrested *Xenopus* egg extracts and in vitro phosphorylation by Gwl to identify substrates of this kinase.

We fractionated proteins from interphase extracts on a heparin column. Eluted proteins were precipitated with ammonium sulfate (50 to 70%), resuspended, and fractionated by gel filtration. Samples from the fractions were phosphorylated in vitro with a hyperactive form of human Gwl (K72M mutant) (*7*), and the phosphorylated bands were analyzed by mass spectrometry. Maximal phosphorylation was observed in the gel filtration fractions corresponding to molecular sizes of 30 to 70 kD (Fig. 1A, fraction 3) and 20 to 50 kD (Fig. 1A, fraction 4). These two fractions increased phosphorylation of a band of 20 kD. Forty different proteins were detected in this band by mass spectrometry, among them the cyclic adenosine monophosphate–regulated phosphoprotein 19 (Arpp19), a protein that strongly resembles the small protein α-Endosulfine. The functions of Arpp19 and α-Endosulfine are unclear (*8*, *9*); however, oocytes from *Drosophila* with mutant α-Endosulfine have a prolonged prophase and fail to progress to metaphase (*10*). Cdc2 isolated from these oocytes has normal kinase activity, but the oocytes show a reduced amount of in vivo phosphorylation of mitotic substrates, a phenotype reminiscent of the one observed in Gwl-depleted *Xenopus* egg extracts (*4*). Although by mass spectrometry we identified peptides specific to Arpp19 but not for α-Endosulfine (fig. S1), their sequence similarity indicates that both may be Gwl substrates. We therefore tested glutathione *S*-transferase fusion proteins made from Arpp19 and α-Endosulfine, as possible substrates of Gwl. Both proteins were phosphorylated in vitro by Gwl (Fig. 1B). The endogenous proteins were present in small amounts in *Xenopus* egg extracts, particularly Arpp19, which was very difficult to detect (Fig. 1C). The analysis of the protein sequences of Arpp19 and α-Endosulfine revealed the presence of seven potential serine or threonine phosphorylation sites conserved in both proteins (Fig. 1D). We made individual mutants of Arpp19 in which serine (S) or threonine (T) was mutated to alanine (A) and tested whether they were phosphorylated in vitro by Gwl. All mutants were phosphorylated by Gwl except mutant S62A. Similarly, mutation of this conserved serine of human α-Endosulfine to alanine (S67A) also prevented the phosphorylation of this protein by Gwl (Fig.

[1]Universités Montpellier 2 et 1, Centre de Recherche de Biochimie Macromoléculaire, CNRS UMR 5237, IFR 122, 1919 Route de Mende, 34293 Montpellier cedex 5, France. [2]Institut Pluridisciplinaire Hubert Curien, Strasbourg Cedex, France.

*To whom correspondence should be addressed. E-mail: anna.castro@crbm.cnrs.fr (A.C.); thierry.lorca@crbm.cnrs.fr (T.L.)

†These authors contributed equally to this work.

1D). These results indicate that this serine is the Gwl phosphorylation site in both Arpp19 and α-Endosulfine.

We analyzed the effects of Arpp19 and α-Endosulfine added to interphase *Xenopus* egg extracts. Either of these two proteins, if first phosphorylated in vitro by Gwl, promoted rapid mitotic entry as shown by the dephosphorylation of tyrosine 15 of Cdc2 and the phosphorylation of the mitotic substrates, followed by a subsequent exit from mitosis as indicated by the degradation of cyclin A and cyclin B2 (Fig. 1E). In a second experiment, to easily visualize mitotic entry, we prevented cyclin degradation by depleting the anaphase-promoting complex constituent Cdc27. In these extracts, the addition of phosphorylated Arpp19 or α-Endosulfine promoted a rapid entry into mitosis and the maintenance of the mitotic state. Nonphosphorylated protein or the Arpp19 S62A or the α-Endosulfine S67A phosphorylation mutants had no effect (Fig. 2A).

Gwl mediates entry into mitosis through the inhibition of PP2A, and so we suspected that Arpp19 and α-Endosulfine could mediate mitotic entry by directly inhibiting PP2A. However, we could not exclude the possibility that these two proteins also regulate cyclin B–Cdc2 activity to promote entry into mitosis. To determine whether Arpp19 or α-Endosulfine could induce mitotic entry through the regulation of cyclin B–Cdc2 activity, we depleted Cdc25 in interphase egg extracts and analyzed whether the two proteins still induced mitotic entry (*11*). We also depleted Cdc27 to prevent cyclin degradation and to easily visualize mitotic entry in these extracts. Either phospho-Arpp19 or phospho-α-Endosulfine induced entry into mitosis in these extracts where only cyclin A–Cdc2 appeared to be active (Fig. 2B). Thus, Arpp19 and α-Endosulfine are substrates of Gwl that promote mitotic entry, likely through the regulation of PP2A but not through the regulation of cyclin B–Cdc2.

Accordingly, when Gwl was depleted from interphase egg extracts, the addition of α-Endosulfine and Arpp19 still induced mitotic entry, further indicating that they act downstream of Gwl (Fig. 2C). These two proteins promoted entry into mitosis in Gwl-depleted interphase extracts only when they were thio-phosphorylated, indicating that when Gwl is present, dephosphoryl-

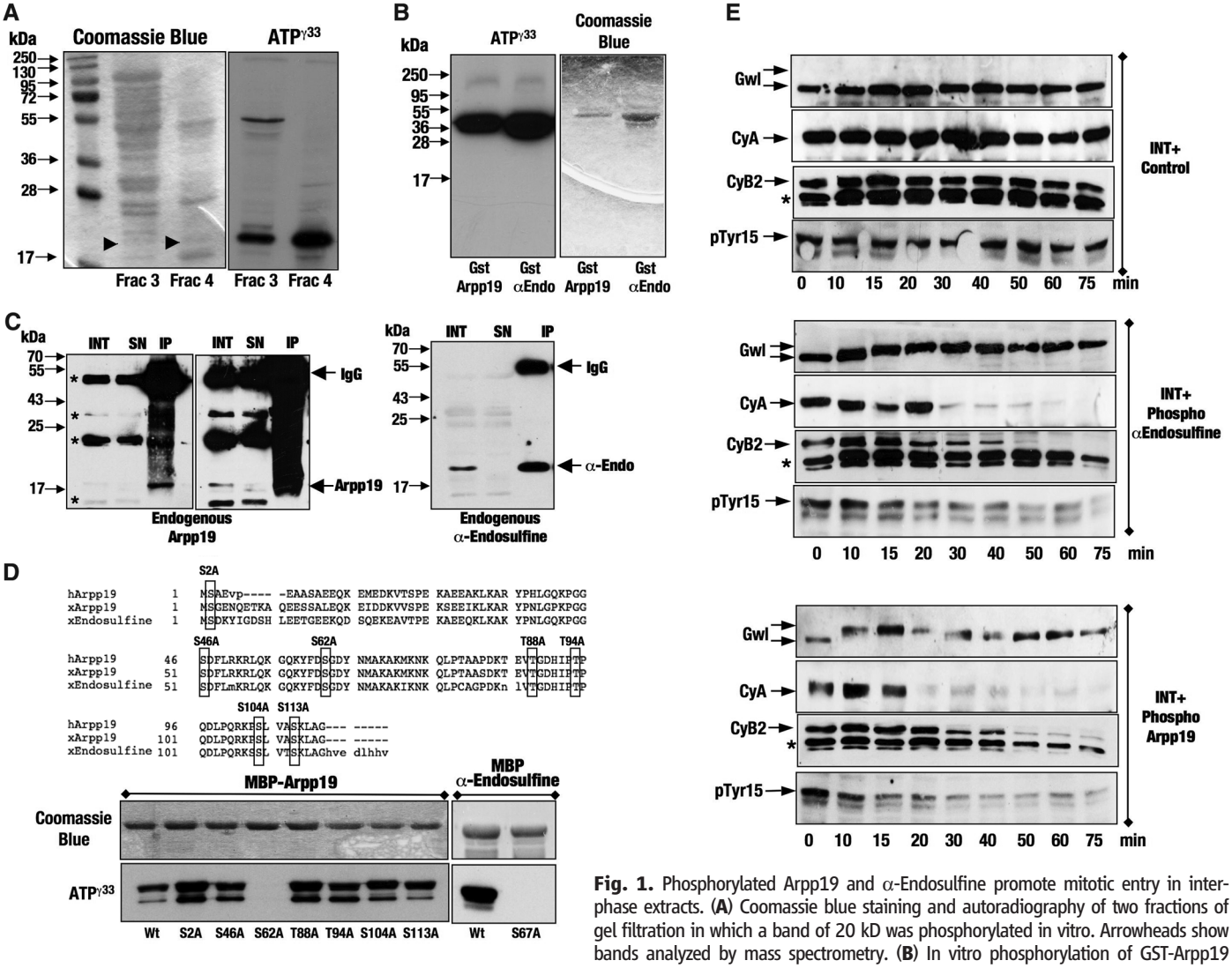

Fig. 1. Phosphorylated Arpp19 and α-Endosulfine promote mitotic entry in interphase extracts. (**A**) Coomassie blue staining and autoradiography of two fractions of gel filtration in which a band of 20 kD was phosphorylated in vitro. Arrowheads show bands analyzed by mass spectrometry. (**B**) In vitro phosphorylation of GST-Arpp19 and GST-α-Endosulfine by Gwl. (**C**) Western blot performed with antibody to full-length human Arpp19 (two exposure times) and to C-terminal *Xenopus* α-Endosulfine showing equal amounts of interphase extract and supernatant [10 μl in Arpp19 immunoprecipitation (IP) and 2 μl in α-Endosulfine IP] and an IP corresponding to 20 μl of interphase extract. To improve detection of endogenous Arpp19, we boiled extract and supernatant before adding Laemmli buffer. (**D**) Protein sequence alignment of human and *Xenopus* Arpp19 and *Xenopus* α-Endosulfine. The conserved S/T sites that were mutated to A are indicated. (**E**) Interphase extracts (INT) were supplemented with phospho-α-Endosulfine or phospho-Arpp19 at a final concentration of 170 ng/μl, or were left untreated (Control). We determined mitotic entry by analyzing the phosphorylation of Gwl, the dephosphorylation of tyrosine 15 on Cdc2, and the abundance of cyclin A and cyclin B2. Nonspecific bands are indicated with an asterisk. Abbreviations for the amino acid residues: A, Ala; C, Cys; D, Asp; E, Glu; F, Phe; G, Gly; H, His; I, Ile; K, Lys; L, Leu; M, Met; N, Asn; P, Pro; Q, Gln; R, Arg; S, Ser; T, Thr; V, Val; W, Trp; and Y, Tyr.

ation of these two substrates is counterbalanced by endogenous Gwl, whereas when Gwl is absent, these two proteins are rapidly dephosphorylated and do not promote or maintain the mitotic state.

Moreover, the addition of thio-phosphorylated Arpp19 or α-Endosulfine to Gwl-depleted CSF extracts also prevented mitotic exit (Fig. 2D), demonstrating that Arpp19 and α-Endosulfine are phosphorylated by Gwl and act downstream of this kinase to promote mitotic entry, possibly by directly inhibiting PP2A. Accordingly, phosphorylation of the Gwl-specific site on Arpp19 and α-Endosulfine (S62/S67) decreased simultaneously with dephosphorylation of Gwl at mitotic exit (Fig. 2E), and it increased again concomitantly with the phosphorylation of this kinase at mitotic entry (Fig. 2F).

To determine whether Arpp19 or α-Endosulfine could bind and inhibit PP2A, we incubated glutathione *S*-transferase (GST)–Arpp19 and GST-α-Endosulfine with interphase or with mitotic egg extracts and tested for association of PP2A with the fusion proteins. GST-α-Endosulfine (moderately) and GST-Arpp19 (very weakly) bound PP2A in interphase egg extracts, in which Gwl is inactive. However, the binding increased (17 times for GST-Arpp19 and twice for GST-α-Endosulfine) in mitotic egg extracts, in which Gwl is fully active, suggesting that the association of these two proteins with the A and C subunits of PP2A is increased by their Gwl-dependent phosphorylation. In support of this idea, the mutation to alanine of the Gwl phosphorylation site S62 in Arrp19 and S67 in α-Endosulfine prevented the binding of either protein to PP2A. However, this association appears not to be exclusively regulated by Gwl-dependent phosphorylation because the α-Endosulfine mutant D66A did not bind

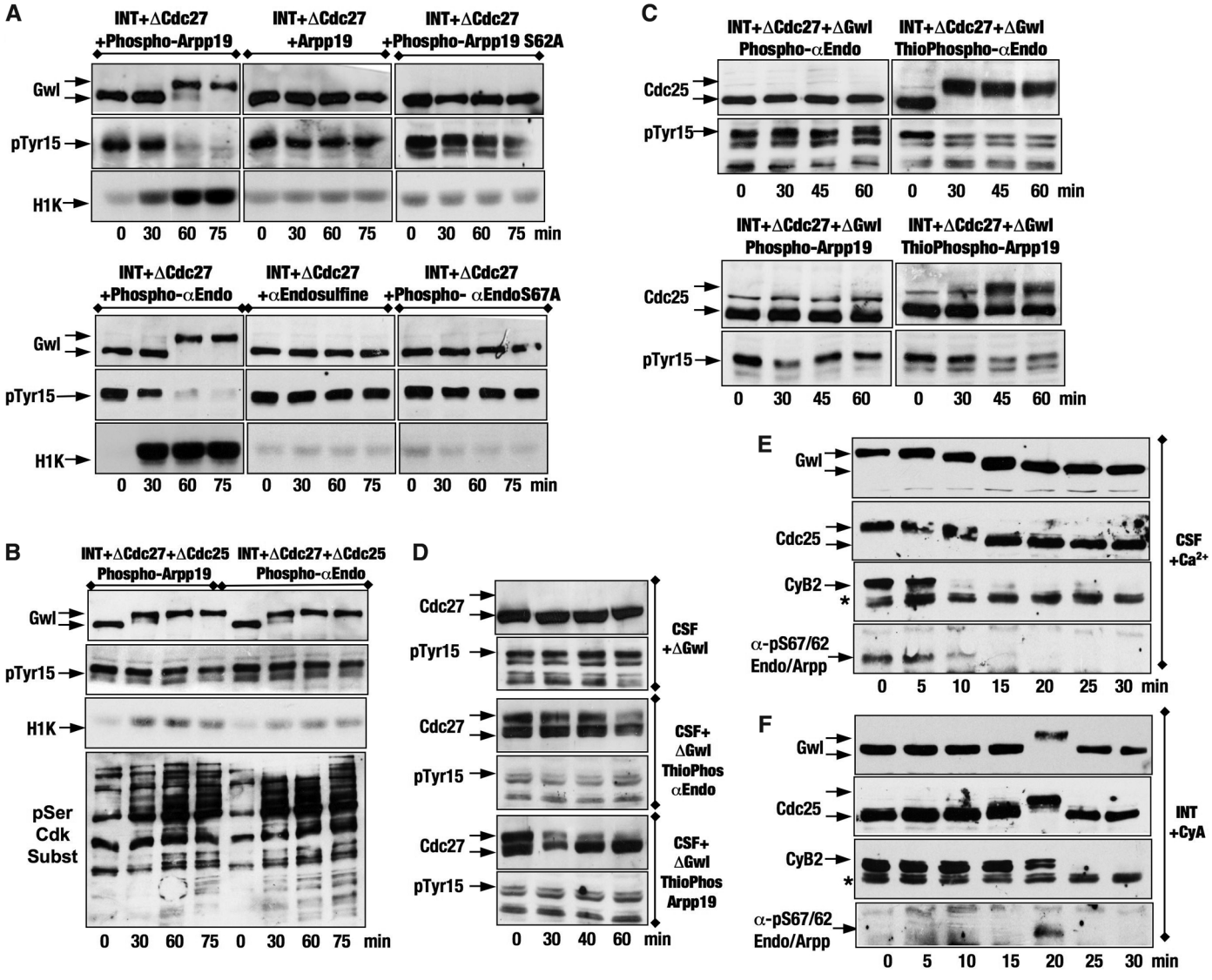

Fig. 2. Addition of thio-phosphorylated Arpp19 and α-Endosulfine rescues the phenotype induced by Gwl depletion in interphase and mitotic egg extracts. (**A**) Interphase extracts were depleted of Cdc27 and supplemented at a final concentration of 170 ng/μl with the proteins GST-Arpp19 and GST-α-Endosulfine phosphorylated or not in vitro by Gwl. The Gwl-phosphorylation mutants Arpp19-S62A and α-Endosulfine-S67A were also used. (**B**) Mitotic entry was analyzed in interphase extracts that were depleted of Cdc27 and Cdc25 and supplemented with phospho-Arpp19 and phospho-α-Endosulfine (final concentration of 170 ng/μl). The phosphorylation of cyclin B-Cdc2 substrates was analyzed with an antibody recognizing the phospho-Serine Cdk consensus motif. (**C**) Interphase extracts were depleted of Cdc27 and Gwl and supplemented with phosphorylated or thio-phosphorylated Arpp19 and α-Endosulfine. (**D**) Mitotic extracts (CSF) were supplemented with thio-phosphorylated Arpp19 or α-Endosulfine and depleted of Gwl. (**E**) Mitotic exit was induced in CSF extracts by the addition of Ca^{2+}, and the amounts of cyclin B2 and phosphorylation of Cdc25, Gwl, and the Gwl-specific sites of Arpp19 and α-Endosulfine were analyzed. (**F**) Interphase extracts were supplemented with cyclin A (final concentration of 60 nM), and the kinetics of the phosphorylation of the indicated proteins as well as the levels of cyclin B2 were analyzed.

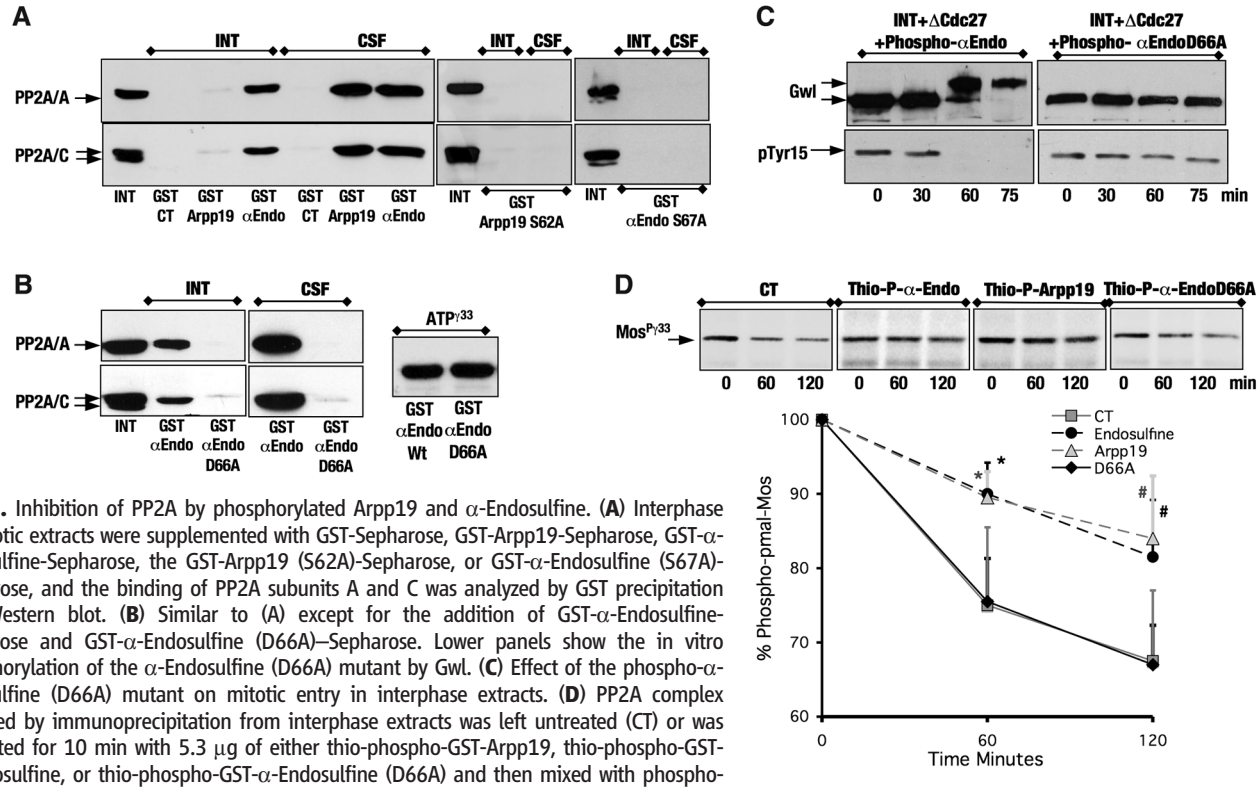

Fig. 3. Inhibition of PP2A by phosphorylated Arpp19 and α-Endosulfine. (**A**) Interphase or mitotic extracts were supplemented with GST-Sepharose, GST-Arpp19-Sepharose, GST-α-Endosulfine-Sepharose, the GST-Arpp19 (S62A)-Sepharose, or GST-α-Endosulfine (S67A)-Sepharose, and the binding of PP2A subunits A and C was analyzed by GST precipitation and Western blot. (**B**) Similar to (A) except for the addition of GST-α-Endosulfine-Sepharose and GST-α-Endosulfine (D66A)–Sepharose. Lower panels show the in vitro phosphorylation of the α-Endosulfine (D66A) mutant by Gwl. (**C**) Effect of the phospho-α-Endosulfine (D66A) mutant on mitotic entry in interphase extracts. (**D**) PP2A complex obtained by immunoprecipitation from interphase extracts was left untreated (CT) or was incubated for 10 min with 5.3 μg of either thio-phospho-GST-Arpp19, thio-phospho-GST-α-Endosulfine, or thio-phospho-GST-α-Endosulfine (D66A) and then mixed with phospho-radiolabeled myelin basic protein–c-Mos fusion protein. At the indicated times, 15 μl of supernatant was analyzed by SDS–polyacrylamide gel electrophoresis and autoradiography. Gels were scanned by a Typhoon Scanner and quantified with Image software. Statistical analysis of the results obtained from two different independent experiments was performed with an unpaired Student's *t* test. The percentage of phosphorylated c-Mos present at each time was expressed as the mean ± SD. Statistical differences between control versus either Arpp19 or α-Endosulfine at the two time points are indicated. $*P < 0.03$; $\#P < 0.04$

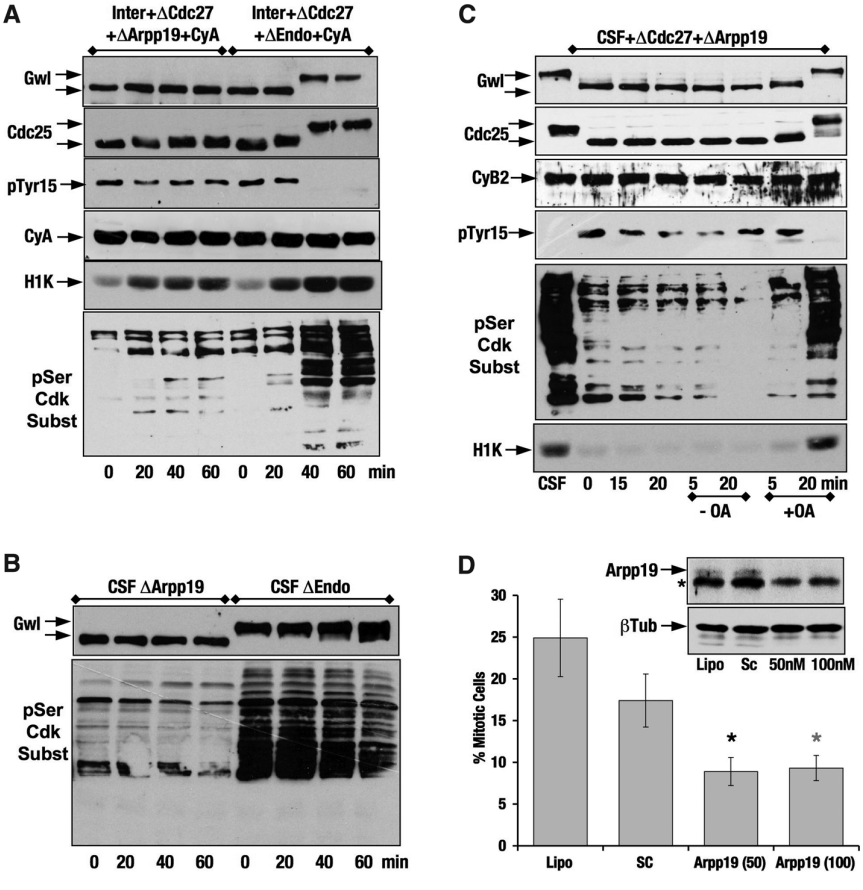

Fig. 4. Endogenous Arpp19 but not α-Endosulfine is required to promote mitotic entry. (**A**) Interphase extracts were depleted of Cdc27 and either Arpp19 or α-Endosulfine and then supplemented with cyclin A. (**B**) Mitotic extracts were depleted of Arpp19 or α-Endosulfine, and the mitotic state was analyzed. (**C**) Mitotic extracts were depleted of Cdc27 and Arpp19 and 20 min later were (+OA) or were not (–OA) supplemented with okadaic acid (final concentration of 0.7 μM), and the mitotic state was analyzed. (**D**) HeLa cells were transfected or not (Lipo) with scrambled small interfering RNA (siRNA) (SC) or 50 or 100 nM of Arpp19 siRNA for 24 hours, then synchronized by thymidine and released into nocodazole (50 ng/ml) for 10 hours. The percentage of mitotic cells was measured by a two-dimensional fluorescence-activated cell sorting (propidium iodide–antibody against phospho serine Cdk) and expressed as the mean ± SD. Statistical differences between scrambled and either 50 or 100 nM Arpp19 siRNA are indicated ($*P < 8.03 \times 10^{-6}$ and $*P < 1.45 \times 10^{-6}$). The cellular levels of endogenous Arpp19 at each condition are shown.

PP2A, although it was normally phosphorylated by Gwl at residue S67 (Fig. 3B). Moreover, the addition of this mutant previously phosphorylated by Gwl into interphase extracts did not induce mitotic entry (Fig. 3C), consistent with the idea that Gwl may inhibit PP2A by promoting the binding of its inhibitors, Arpp19 and α-Endosulfine.

We tested directly the effect of Arpp19 and α-Endosulfine on PP2A activity obtained from immunoprecipitated CSF extracts by assessing dephosphorylation of the cyclin B–Cdc2 substrate c-Mos in vitro in the presence or in the absence of thio-phosphorylated-Arpp19, thio-phosphorylated-α-Endosulfine, and thio-phosphorylated-α-Endosulfine D66A. Thio-phosphorylated-Arpp19 and thio-phosphorylated-α-Endosulfine significantly decreased dephosphorylation of c-Mos by PP2A. Thio-phosphorylated-α-Endosulfine mutant D66A, which does not bind PP2A, had no effect (Fig. 3D).

To test the physiological role of Arpp19 and α-Endosulfine, we depleted interphase extracts of Cdc27 and then depleted them with specific antibodies against Arpp19 or α-Endosulfine (fig. S2), and finally supplemented them with cyclin A. Depletion of Arpp19, but not of α-Endosulfine (Fig. 1C), completely inhibited entry into mitosis (Fig. 4A)—a phenotype that was rescued by adding back this thio-phosphorylated protein (fig. S3). Similarly, only depletion of Arpp19 from CSF extracts caused rapid exit of mitosis (Fig. 4B). This exit appeared to be mediated by a reactivation of PP2A because the inhibition of PP2A with okadaic acid caused these extracts to reenter mitosis (Fig. 4C). Thus, despite the inhibitory effects of both Arpp19 and α-Endosulfine on PP2A, only Arpp19 appears to regulate mitotic entry and exit in *Xenopus* egg extracts. Consistent with this, only Arpp19 is phosphorylated during mitosis (fig. S2) and, despite the presence of larger amounts of endogenous α-Endosulfine than endogenous Arpp19 in *Xenopus* egg extracts, only Arpp19 was identified in our biochemical analysis.

To investigate whether this mechanism was also conserved in human cells, we depleted Arpp19 from human cervical cancer (HeLa) cells using two different sequences of small interfering RNA (siRNA) (fig. S4). Depletion of Arpp19 reduced the number of mitotic cells by 50% compared to that in cells treated with a scramble siRNA, suggesting that Arpp19 also promotes mitotic entry in human cells (Fig. 4D and fig. S4).

Our results demonstrate an essential role of Arpp19 in regulating mitosis and provide a mechanism by which Gwl can influence cell cycle control through regulation of PP2A. Whether Arpp19 might be dephosphorylated at mitotic exit remains to be elucidated. Perhaps other physiological pathways might be regulated by α-Endosulfine–dependent inhibition of PP2A.

References and Notes

1. M. Jackman, C. Lindon, E. A. Nigg, J. Pines, *Nat. Cell Biol.* **5**, 143 (2003).
2. P. V. Castilho, B. C. Williams, S. Mochida, Y. Zhao, M. L. Goldberg, *Mol. Biol. Cell* **20**, 4777 (2009).
3. S. Mochida, S. Ikeo, J. Gannon, T. Hunt, *EMBO J.* **28**, 2777 (2009).
4. S. Vigneron *et al.*, *EMBO J.* **28**, 2786 (2009).
5. J. Q. Wu *et al.*, *Nat. Cell Biol.* **11**, 644 (2009).
6. A. Burgess *et al.*, *Proc. Natl. Acad. Sci. U.S.A.* **107**, 12564 (2010).
7. V. Archambault, X. Zhao, H. White-Cooper, A. T. Carpenter, D. M. Glover, *PLoS Genet.* **3**, e200 (2007).
8. D. Bataille *et al.*, *Cell. Mol. Life Sci.* **56**, 78 (1999).
9. L. Gros *et al.*, *Diabetologia* **45**, 703 (2002).
10. J. R. Von Stetina *et al.*, *Development* **135**, 3697 (2008).
11. T. Lorca *et al.*, *J. Cell Sci.* **123**, 2281 (2010).

12. We thank L. Gros and A. Virsolvy for providing the pBKS-Arpp19, pBKS-α-Endosulfine constructs, and antibodies to human α-Endosulfine and T. Hunt and S. Mochida for the antibody to phosphoS67/62 Endo-Arp. This work was supported by the Ligue Regionale Contre le Cancer (Comité du Gard) and the "Association pour la Recherche sur le Cancer". A.B. and E.B. are "Fondation pour la Recherche Medicale" and "Ligue Nationale Contre le Cancer" fellows, respectively. There is a patent pending that pertains to results presented in this paper.

Supporting Online Material

www.sciencemag.org/cgi/content/full/330/6011/1673/DC1
Materials and Methods
Figs. S1 to S4
References

27 August 2010; accepted 18 October 2010
10.1126/science.1197048

Cholinergic Interneurons Control Local Circuit Activity and Cocaine Conditioning

Ilana B. Witten,[1]* Shih-Chun Lin,[1,2]* Matthew Brodsky,[1]* Rohit Prakash,[1]* Ilka Diester,[1] Polina Anikeeva,[1] Viviana Gradinaru,[1] Charu Ramakrishnan,[1] Karl Deisseroth[1,3,4,5]†

Cholinergic neurons are widespread, and pharmacological modulation of acetylcholine receptors affects numerous brain processes, but such modulation entails side effects due to limitations in specificity for receptor type and target cell. As a result, causal roles of cholinergic neurons in circuits have been unclear. We integrated optogenetics, freely moving mammalian behavior, in vivo electrophysiology, and slice physiology to probe the cholinergic interneurons of the nucleus accumbens by direct excitation or inhibition. Despite representing less than 1% of local neurons, these cholinergic cells have dominant control roles, exerting powerful modulation of circuit activity. Furthermore, these neurons could be activated by cocaine, and silencing this drug-induced activity during cocaine exposure (despite the fact that the manipulation of the cholinergic interneurons was not aversive by itself) blocked cocaine conditioning in freely moving mammals.

Acetylcholine is an important and widely studied neurotransmitter, which acts on a variety of receptors and target cells (*1*–*5*). Pharmacological and genetic studies have elucidated the complex and often opposing influences of the individual subtypes of muscarinic and nicotinic acetylcholine receptors on numerous biological processes, but no study has yet resolved the question of the causal role of cholinergic neurons themselves within a central nervous system tissue (*6*–*11*). Addressing such a question would require a novel paradigm for selective and temporally precise control (activation and inhibition) of cholinergic neurons within living mammalian tissues, because previous investigations have resulted in contradictory findings linked to challenges with specificity and temporal resolution. For example, elegant in vivo pharmacological approaches have shown (*12*–*14*) that cholinergic transmission in the nucleus accumbens (NAc) [a structure involved in natural reward-related behaviors and responses to drugs such as cocaine (*15*–*19*)] is required for reward learning, but novel studies of molecular ablation of cholinergic interneurons within the NAc instead have reported enhanced reward learning (*20*). Cholinergic interneurons within the NAc are particularly intriguing because they constitute less than 1% of the local neural population (*21*), yet they project throughout the NAc and provide its only known cholinergic input (*22*). Relevant cholinergic receptors are expressed locally, and nicotinic and muscarinic pharmacological agonists can exert complex influences on medium spiny neurons (MSNs, which represent >95% of the local neuronal population and constitute the output of the NAc) (*23*–*25*). However, the net effect (if any) of the cholinergic interneurons on any aspect of NAc physiology or behavior is unknown.

We undertook an optogenetic approach to resolve this question by selectively driving or blocking action potential firing in these cells. To

[1]Department of Bioengineering, Stanford University, Stanford, CA 94305, USA. [2]Department of Neurosurgery, Stanford University, Stanford, CA 94305, USA. [3]Department of Psychiatry and Behavioral Sciences, Stanford University, Stanford, CA 94305, USA. [4]Howard Hughes Medical Institute, Stanford University, Stanford, CA 94305, USA. [5]CNC program, Stanford University, Stanford, CA 94305, USA.

*These authors contributed equally to this work.
†To whom correspondence should be addressed. E-mail: deissero@stanford.edu

PP2A, although it was normally phosphorylated by Gwl at residue S67 (Fig. 3B). Moreover, the addition of this mutant previously phosphorylated by Gwl into interphase extracts did not induce mitotic entry (Fig. 3C), consistent with the idea that Gwl may inhibit PP2A by promoting the binding of its inhibitors, Arpp19 and α-Endosulfine.

We tested directly the effect of Arpp19 and α-Endosulfine on PP2A activity obtained from immunoprecipitated CSF extracts by assessing dephosphorylation of the cyclin B–Cdc2 substrate c-Mos in vitro in the presence or in the absence of thio-phosphorylated-Arpp19, thio-phosphorylated-α-Endosulfine, and thio-phosphorylated-α-Endosulfine D66A. Thio-phosphorylated-Arpp19 and thio-phosphorylated-α-Endosulfine significantly decreased dephosphorylation of c-Mos by PP2A. Thio-phosphorylated-α-Endosulfine mutant D66A, which does not bind PP2A, had no effect (Fig. 3D).

To test the physiological role of Arpp19 and α-Endosulfine, we depleted interphase extracts of Cdc27 and then depleted them with specific antibodies against Arpp19 or α-Endosulfine (fig. S2), and finally supplemented them with cyclin A. Depletion of Arpp19, but not of α-Endosulfine (Fig. 1C), completely inhibited entry into mitosis (Fig. 4A)—a phenotype that was rescued by adding back this thio-phosphorylated protein (fig. S3). Similarly, only depletion of Arpp19 from CSF extracts caused rapid exit of mitosis (Fig. 4B). This exit appeared to be mediated by a reactivation of PP2A because the inhibition of PP2A with okadaic acid caused these extracts to reenter mitosis (Fig. 4C). Thus, despite the inhibitory effects of both Arpp19 and α-Endosulfine on PP2A, only Arpp19 appears to regulate mitotic entry and exit in *Xenopus* egg extracts. Consistent with this, only Arpp19 is phosphorylated during mitosis (fig. S2) and, despite the presence of larger amounts of endogenous α-Endosulfine than endogenous Arpp19 in *Xenopus* egg extracts, only Arpp19 was identified in our biochemical analysis.

To investigate whether this mechanism was also conserved in human cells, we depleted Arpp19 from human cervical cancer (HeLa) cells using two different sequences of small interfering RNA (siRNA) (fig. S4). Depletion of Arpp19 reduced the number of mitotic cells by 50% compared to that in cells treated with a scramble siRNA, suggesting that Arpp19 also promotes mitotic entry in human cells (Fig. 4D and fig. S4).

Our results demonstrate an essential role of Arpp19 in regulating mitosis and provide a mechanism by which Gwl can influence cell cycle control through regulation of PP2A. Whether Arpp19 might be dephosphorylated at mitotic exit remains to be elucidated. Perhaps other physiological pathways might be regulated by α-Endosulfine–dependent inhibition of PP2A.

References and Notes

1. M. Jackman, C. Lindon, E. A. Nigg, J. Pines, *Nat. Cell Biol.* **5**, 143 (2003).
2. P. V. Castilho, B. C. Williams, S. Mochida, Y. Zhao, M. L. Goldberg, *Mol. Biol. Cell* **20**, 4777 (2009).
3. S. Mochida, S. Ikeo, J. Gannon, T. Hunt, *EMBO J.* **28**, 2777 (2009).
4. S. Vigneron *et al.*, *EMBO J.* **28**, 2786 (2009).
5. J. Q. Wu *et al.*, *Nat. Cell Biol.* **11**, 644 (2009).
6. A. Burgess *et al.*, *Proc. Natl. Acad. Sci. U.S.A.* **107**, 12564 (2010).
7. V. Archambault, X. Zhao, H. White-Cooper, A. T. Carpenter, D. M. Glover, *PLoS Genet.* **3**, e200 (2007).
8. D. Bataille *et al.*, *Cell. Mol. Life Sci.* **56**, 78 (1999).
9. L. Gros *et al.*, *Diabetologia* **45**, 703 (2002).
10. J. R. Von Stetina *et al.*, *Development* **135**, 3697 (2008).
11. T. Lorca *et al.*, *J. Cell Sci.* **123**, 2281 (2010).

12. We thank L. Gros and A. Virsolvy for providing the pBKS-Arpp19, pBKS-α-Endosulfine constructs, and antibodies to human α-Endosulfine and T. Hunt and S. Mochida for the antibody to phosphoS67/62 Endo-Arp. This work was supported by the Ligue Regionale Contre le Cancer (Comité du Gard) and the "Association pour la Recherche sur le Cancer". A.B. and E.B. are "Fondation pour la Recherche Medicale" and "Ligue Nationale Contre le Cancer" fellows, respectively. There is a patent pending that pertains to results presented in this paper.

Supporting Online Material

www.sciencemag.org/cgi/content/full/330/6011/1673/DC1
Materials and Methods
Figs. S1 to S4
References

27 August 2010; accepted 18 October 2010
10.1126/science.1197048

Cholinergic Interneurons Control Local Circuit Activity and Cocaine Conditioning

Ilana B. Witten,[1]* Shih-Chun Lin,[1,2]* Matthew Brodsky,[1]* Rohit Prakash,[1]* Ilka Diester,[1] Polina Anikeeva,[1] Viviana Gradinaru,[1] Charu Ramakrishnan,[1] Karl Deisseroth[1,3,4,5]†

Cholinergic neurons are widespread, and pharmacological modulation of acetylcholine receptors affects numerous brain processes, but such modulation entails side effects due to limitations in specificity for receptor type and target cell. As a result, causal roles of cholinergic neurons in circuits have been unclear. We integrated optogenetics, freely moving mammalian behavior, in vivo electrophysiology, and slice physiology to probe the cholinergic interneurons of the nucleus accumbens by direct excitation or inhibition. Despite representing less than 1% of local neurons, these cholinergic cells have dominant control roles, exerting powerful modulation of circuit activity. Furthermore, these neurons could be activated by cocaine, and silencing this drug-induced activity during cocaine exposure (despite the fact that the manipulation of the cholinergic interneurons was not aversive by itself) blocked cocaine conditioning in freely moving mammals.

Acetylcholine is an important and widely studied neurotransmitter, which acts on a variety of receptors and target cells (*1*–*5*). Pharmacological and genetic studies have elucidated the complex and often opposing influences of the individual subtypes of muscarinic and nicotinic acetylcholine receptors on numerous biological processes, but no study has yet resolved the question of the causal role of cholinergic neurons themselves within a central nervous system tissue (*6*–*11*). Addressing such a question would require a novel paradigm for selective and temporally precise control (activation and inhibition) of cholinergic neurons within living mammalian tissues, because previous investigations have resulted in contradictory findings linked to challenges with specificity and temporal resolution. For example, elegant in vivo pharmacological approaches have shown (*12*–*14*) that cholinergic transmission in the nucleus accumbens (NAc) [a structure involved in natural reward-related behaviors and responses to drugs such as cocaine (*15*–*19*)] is required for reward learning, but novel studies of molecular ablation of cholinergic interneurons within the NAc instead have reported enhanced reward learning (*20*). Cholinergic interneurons within the NAc are particularly intriguing because they constitute less than 1% of the local neural population (*21*), yet they project throughout the NAc and provide its only known cholinergic input (*22*). Relevant cholinergic receptors are expressed locally, and nicotinic and muscarinic pharmacological agonists can exert complex influences on medium spiny neurons (MSNs, which represent >95% of the local neuronal population and constitute the output of the NAc) (*23*–*25*). However, the net effect (if any) of the cholinergic interneurons on any aspect of NAc physiology or behavior is unknown.

We undertook an optogenetic approach to resolve this question by selectively driving or blocking action potential firing in these cells. To

[1]Department of Bioengineering, Stanford University, Stanford, CA 94305, USA. [2]Department of Neurosurgery, Stanford University, Stanford, CA 94305, USA. [3]Department of Psychiatry and Behavioral Sciences, Stanford University, Stanford, CA 94305, USA. [4]Howard Hughes Medical Institute, Stanford University, Stanford, CA 94305, USA. [5]CNC program, Stanford University, Stanford, CA 94305, USA.

*These authors contributed equally to this work.
†To whom correspondence should be addressed. E-mail: deissero@stanford.edu

express microbial opsin genes specifically in cholinergic interneurons, we employed a transgenic mouse line expressing Cre-recombinase under the choline acetyltransferase (ChAT) promoter (*26*). We stereotaxically injected into the NAc (Fig. 1A) a Cre-inducible adeno-associated virus (AAV) vector carrying the opsin gene fused in-frame with coding sequence for enhanced yellow fluorescent protein (eYFP) (*27*, *28*); the opsin gene encoded either the blue-light gated cation channel channelrhodopsin-2 (ChR2) (*29*) or the yellow-light gated third-generation chloride pump halorhodopsin (eNpHR3.0) (*30*). eYFP expression was specific to neurons that expressed ChAT; moreover, the majority of neurons that expressed ChAT also expressed eYFP (Fig. 1, B and C). Both opsins were expressed on the surface membranes of ChAT neurons (Fig. 1D), and the targeted neurons responded to current injection in a manner corresponding to previously established responses of cholinergic interneurons in the dorsal striatum (Fig. 1E) (*31*). Both the resting membrane potential (V_m) and input resistance (R_{input}) were higher for ChAT neurons (YFP^+ neurons) than for MSNs [identified as YFP^- neurons; table S1; $P < 10^{-4}$ for V_M and $P = 0.004$ for R_{input}, two-tailed t test]. Finally, both opsins were functional in ChAT cells, as eNpHR3.0 drove large hyperpolarizations (Fig. 1F; mean ± SEM: –83.8 ± 11.9 mV, $n = 4$) and ChR2 reliably drove spiking up to 20 to 30 Hz (Fig. 1, G and H).

ChAT interneurons are thought to be tonically active in vivo (3 to 10 Hz) (*32*, *33*), but it has remained mysterious how (or even if) this slow activity in the sparse ChAT cells could be causally involved in affecting local circuit activity or behavior. We used optogenetics to address this question with a combination of slice electrophysiology, in vivo electrophysiology, and freely moving behavior. First, we monitored postsynaptic currents in MSNs (ChR2-eYFP non-expressing cells) in acute NAc slices during optogenetic photostimulation of ChAT cells expressing ChR2-eYFP (Fig. 2A), targeted as in Fig. 1. Stimulating ChAT neurons in this setting increased the frequency of γ-aminobutyric acid type A ($GABA_A$) receptor–mediated inhibitory postsynaptic currents (IPSCs) recorded in MSNs (Fig. 2, B and C). Evoked inhibitory currents were generally synchronized to the light pulse, with a modal latency of 6 ms (Fig. 2D), coupled with a smaller enhancement of asynchronous IPSCs (fig. S1, A to C). Across all recorded cells, the mean frequency of IPSCs observed in the MSNs increased by 525.8 ± 154.3% during light stimulation of the ChAT neurons ($n = 7$; mean ± SEM, $P = 0.01$, paired t test), whereas the mean IPSC amplitude was unaffected ($P > 0.05$, paired t test; $n = 7$, Fig. 2E). This effect was attenuated by the nicotinic antagonist mecamylamine (fig. S3, $n = 5$, $P < 0.05$, paired t test).

We next asked if and how these changes in inhibitory current frequency would translate into changes in MSN spiking in vivo. We recorded neural activity extracellularly with an optrode in the NAc during optogenetic activation of the ChAT interneurons in vivo (Fig. 2F). At sites where single units were not isolated, we observed neural population firing that tracked the light stimulation at 10 Hz but not 100 Hz (fig. S1D), probably representing population spiking across the sparse but synchronously activated ChAT cells in the neighborhood of the electrode. In contrast to these population spikes, the isolated units in the NAc displayed a markedly different response to the optogenetic photostimulation. In agreement with the observed increase in IPSC frequency in MSNs in slices, we observed inhibition of background firing during stimulation of the ChAT cells in vivo (representative cell, Fig. 2G). Across the population, most significantly modulated sites showed a suppression of background firing, although a few responded with an increase in firing (Fig. 2, H and I), consistent with known recurrent inhibition among MSNs and corresponding release from inhibition, during ChAT

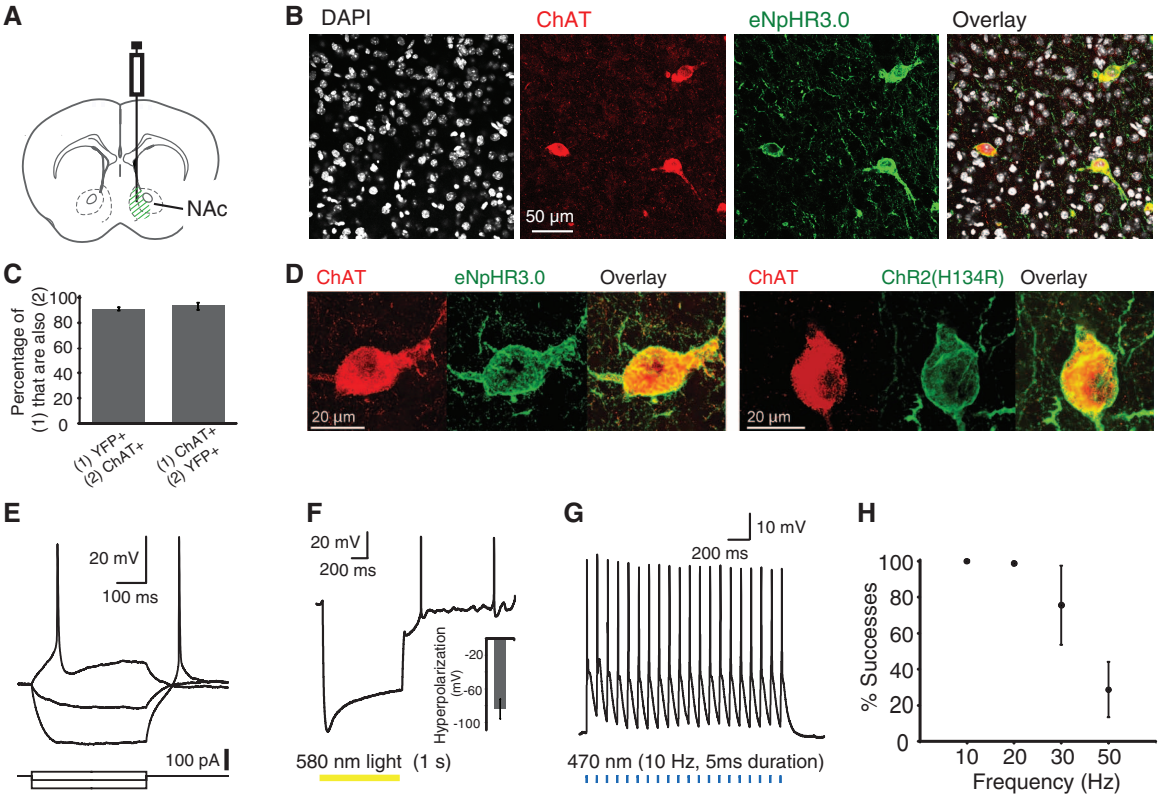

Fig. 1. Specificity, membrane targeting, and functionality of ChR2 and eNpHR3.0 in ChAT interneurons of the NAc. (**A**) Cre-dependent AAV [expressing either eNpHR3.0-eYFP or ChR2(H134R)-eYFP] was injected into the medial portion of the NAc. (**B**) Confocal image of an injected slice demonstrates colocalization of eYFP expression with the ChAT antibody, costained with 4′,6′-diamidino-2-phenylindole (DAPI). (**C**) 91.3 ± 1.3% of neurons that expressed YFP also stained for the ChAT antibody ($n = 418$); 93.5 ± 2.8% of neurons that stained for the ChAT antibody also expressed YFP ($n = 413$). Error bars indicate SEM. (**D**) High-magnification view reveals membrane localization of eNphR3.0-eYFP (left) and ChR2-eYFP (right), costained with ChAT antibody. (**E**) Membrane potential changes induced by current injection in a ChR2-eYFP–expressing ChAT neuron. $V_M = -48$ mV. Current steps: –60, –20, +20 pA. (**F**) Membrane potential changes induced by 1 s of 580-nm light in an eNpHR3.0-eYFP–expressing ChAT neuron (peak hyperpolarization: –103 mV). $V_M = -49$ mV. (Inset) Population-averaged peak hyperpolarization (mean ± SEM: –83.8 ± 11.9 mV; $n = 4$). (**G**) Consecutive action potentials in a ChR2-eYFP–expressing ChAT neuron evoked by a 470-nm pulse train (5 ms pulse width; 10 Hz). (**H**) Average success probability for generating action potentials in ChR2-eYFP–expressing ChAT neurons at different stimulation frequencies ($n = 4$; mean ± SEM; 470-nm pulse train, 5-ms pulse width).

neuron drive, that had been previously exerted by the broader MSN population.

We next explored the consequences of specifically inhibiting ChAT interneurons, employing Cre-dependent eNpHR3.0 expression in vivo. In contrast to what was observed with ChAT neuron excitation, firing of NAc neurons was typically increased in likely MSNs by optogenetic inhibition of the ChAT cells (a representative cell is shown in Fig. 3A). Power spectral analysis revealed a frequency peak in the firing pattern at ~4 Hz in these in vivo recordings (Fig. 3B). Summary data are presented in Fig. 3C; across the population of significantly modulated sites, most neurons were excited by the optogenetic inhibition of ChAT neurons ($n = 17$). We were able to obtain a single-unit recording from a rare putative ChAT interneuron, which was completely shut down by eNpHR3.0 (Fig. 3D) and displayed the long action-potential duration characteristic of ChAT interneurons (*22*) (2.0 ms for this cell, whereas spike durations for MSNs in our recordings ranged from 1.1 to 1.7 ms). Summary data (Fig. 3E) show the dynamics of excitation and inhibition for all recorded sites, illustrating the dominant pattern of excitation (firing increased by 130.5 ± 17.5% in sites that were excited by light).

Finally, we sought to test if this potent NAc control mechanism was relevant to accumbens-dependent reward behavior in freely moving mice. We first tested the effect of acutely administered cocaine on activity of these identified ChAT neurons in acute NAc slices. In ventromedial NAc ChAT cells, cocaine tended to increase spontaneous firing (representative ChAT neuron shown in Fig. 4, A and B). Summary data revealed that cocaine increased firing rates from 0.60 ± 0.41 Hz to 1.74 ± 0.56 Hz at 10 min in ChAT neurons ($n = 7$; $P < 0.005$, paired t test), whereas in the control group of cells receiving only vehicle, firing rates decreased from 0.69 ± 0.24 Hz to 0.09 ± 0.09 Hz over the same time period ($n = 6$; $P < 0.05$ comparing the two groups, two-tailed t test) (Fig. 4C).

We next used eNpHR3.0 to test for causal roles in either this cocaine-induced activity or baseline activity of ChAT cells in the reward-related behavior of cocaine conditioned place preference (CPP), in which animals learn to associate an environment with cocaine. After injecting virus and implanting cannulae bilaterally (Fig. 4D) to silence ChAT neurons during cocaine exposure (Fig. 4E), mice that expressed eNpHR3.0 in the ChAT cells exhibited significantly less cocaine-induced CPP than

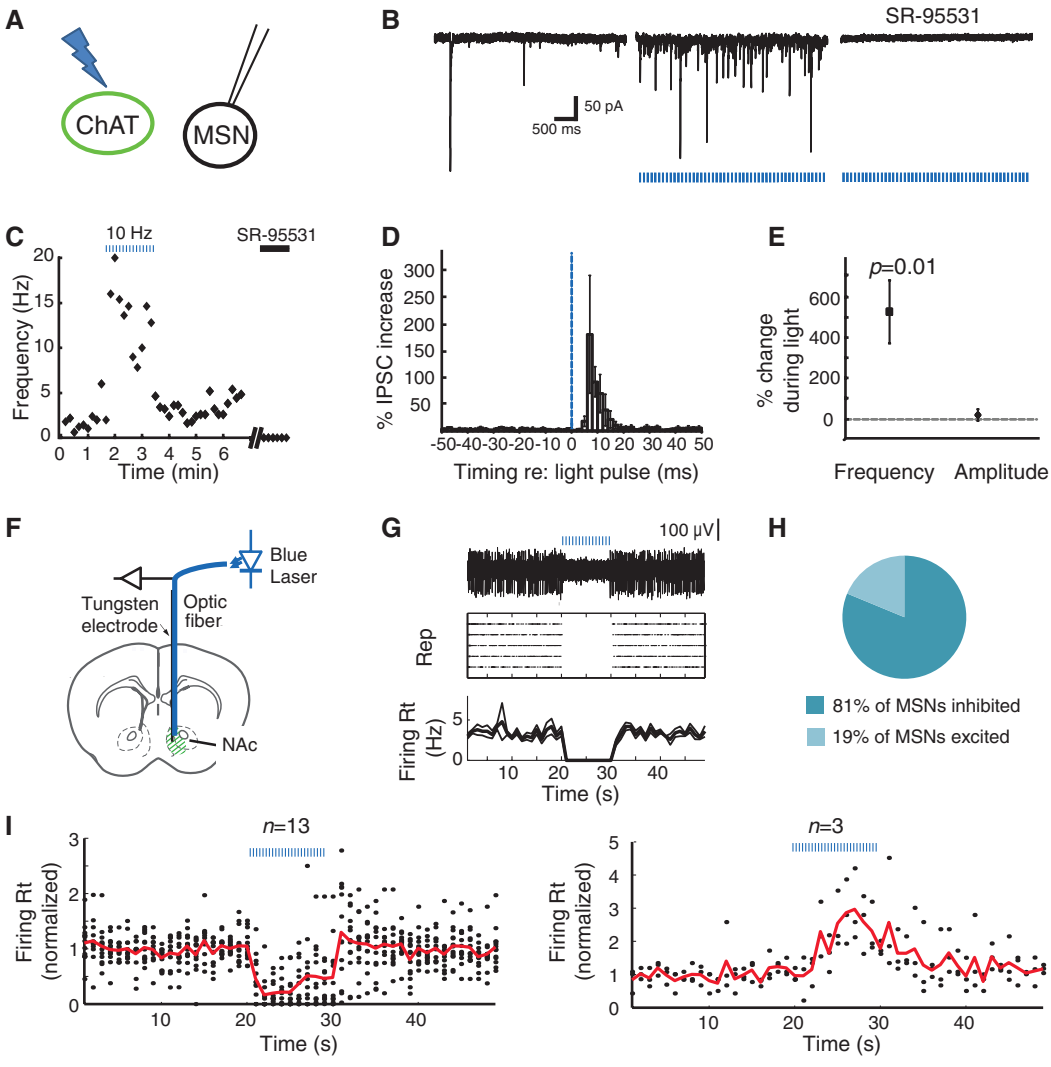

Fig. 2. Optogenetic photoactivation of ChAT interneurons increases frequency of inhibitory currents and suppresses MSN spiking. (**A**) ChAT neurons transduced with ChR2-eYFP were activated with blue light (470 nm) in brain slices, and nearby MSNs (eYFP$^-$ cells) were whole-cell patch-clamped. (**B**) (Left) Spontaneous synaptic currents were observed in an MSN in a slice expressing ChR2-eYFP in ChAT neurons. (Middle) Synaptic currents increased in frequency in response to 470-nm light pulses (5-ms pulse width; 10 Hz). (Right) These currents were blocked by $GABA_A$ receptor antagonist SR-95531 (5 μM) and are thus considered IPSCs. 2,3-dihydroxy-6-nitro-7-sulfamoylbenzo[*f*]quinoxaline-2,3-dione (NBQX) (5 μM) and (RS)-3-(2-Carboxypiperazin-4-yl)-propyl-1-phosphonic acid (RS-CPP) (5 μM) were present in all experiments. (**C**) Time course of IPSC frequencies for this MSN, showing the effect of light pulses (blue dashed bars) and SR-95531 (black bar). (**D**) Average percentage increase in IPSC frequency during the light-on periods (normalized to that of light-off periods) as a function of time relative to light pulses ($n = 6$). The blue dashed line indicates the onset of light pulses; error bars denote SEM. (**E**) Light pulses increased the frequency of IPSCs by 525.8 ± 154.3% ($n = 6$, $P = 0.01$, paired two-tailed t test), whereas the average amplitudes of spontaneous IPSCs were changed by 21.3 ± 28.9% ($P > 0.05$). (**F**) An optrode (optical fiber attached to a tungsten electrode) was stereotaxically positioned in vivo into a NAc that expressed ChR2-eYFP in ChAT cells. (**G**) (Top) Voltage trace of an isolated unit that is inhibited by blue light stimulation. (Middle) Raster plot displaying the response of the same unit to five repetitions of the light stimulation, with each action potential represented by a dot. (Bottom) Average and SEM of the firing rate over time for the same unit. (**H**) Fraction of sites that were inhibited versus excited by light stimulation. (**I**) Population summary of the time course of response to light stimulation for sites that were inhibited (left; $n = 13$ of 16) or excited (right; $n = 3$ of 16) by light. Solid lines represent average firing rate across sites as a function of time; each dot represents the average firing rate of an individual site. All firing rates are normalized to the mean rate before light stimulation. (F to I) Duration of photostimulation, 10 s; pulse duration, 5 ms; wavelength, 470 nm; frequency, 10 Hz. Epochs of light stimulation are represented by blue dashed lines.

did their control (Cre recombinase–negative) littermates that had received the same virus, surgery, and light-delivery protocol [20 mg/kg intraperitoneally (ip), Fig. 4, F and G; $n = 10$ ChAT::Cre$^+$, $n = 12$ ChAT::Cre$^-$ (left panel); $P < 0.01$ for two-tailed t test; three cohorts; see also fig. S2A]. We observed no behavioral effect of inhibiting the ChAT cells in the absence of cocaine, and ChAT neuron inhibition by itself was not aversive, as conditioning with eNpHR3.0 alone did not affect place preference (Fig. 4G, right panel; $n = 9$ ChAT::Cre$^+$, $n = 7$ ChAT::Cre$^-$; $P > 0.05$ for two-tailed t test; three cohorts; fig. S2B; see also fig. S4A for cocaine dose-response curve). Activation of the cells with ChR2 at 10 Hz was not sufficient to drive place preference by itself or enhance cocaine place preference (10 and 20 mg/kg ip, fig. S4, B to D), with our data from ChAT cell inhibition instead demonstrating necessity of these cells. Finally, in control experiments, we found that ChAT neuron inhibition by itself had no effect on mobility or anxiety in the open field (Fig. 4, H and J), and contextual- and auditory-cued fear conditioning were not disrupted by inhibition of the ChAT cells (fig. S5).

Together, these data demonstrate that selectively inhibiting ChAT interneurons in the NAc with high temporal precision has the overall effect of increasing MSN activity and blocking cocaine conditioning in freely moving mammals. These behavioral results do not support conclusions arising from chronic ablation of the cholinergic interneurons (*20*); instead they are more consistent with interpretations arising from faster but less cellularly targeted pharmacological modulation in the NAc (*12*–*14*). Ablation of the cholinergic interneurons might lead to indirect effects, such as a compensatory increase in dopamine in the NAc, which, in turn, could enhance cocaine reward. In fact, a fundamental difference between acute and chronic manipulations could explain clinically relevant apparent contradictions in our understanding of the acetylcholine/dopamine balance in the brain. For example, an acute increase in nicotine (presumably acting on cholinergic receptors) causes a corresponding acute increase in dopamine (*34*), whereas chronic changes in dopamine or acetylcholine levels can cause opposing changes in the levels of the other neuromodulators (*35*), as seen in the dopamine depletion of Parkinson's disease (*36*).

Because cocaine increases dopamine levels in the NAc, the multiple classes of dopamine receptors expressed on the various cell types within the NAc will give rise to substantial complexity. Although the neural encoding of both cocaine and natural stimuli in the NAc is heterogeneous (*37*), the predominant effect of appetitive stimuli may be to decrease activity in the MSNs (inhibitory projection neurons), thereby gating directed behavior through disinhibition of target brain regions. Consistent with this picture, a pause in NAc activity (which we have found that ChAT neurons are well-suited to implement) may be required for reward-related conditioning (*38*, *39*); in contrast, the predominant effect of aversive stimuli may be to increase MSN activity (*40*, *41*). The fact that acute silencing of ChAT interneurons disrupts drug-related learning without affecting conditioning in the absence of drug suggests that control over this microcircuit could be used to selectively disrupt effects of drugs of abuse without affecting appetitive or aversive responses in general, a possibility that would be of substantial clinical benefit. Together, our results point to a powerful role for these sparsely distributed neurons in controlling local circuit activity and implementing behavioral conditioning in freely moving mammals.

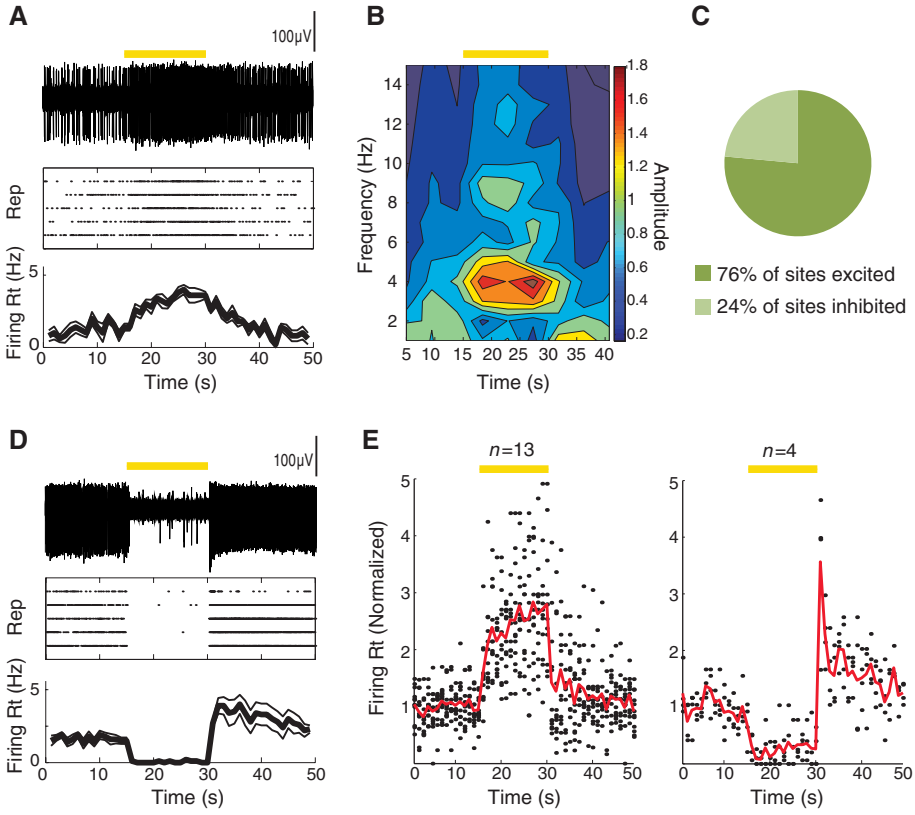

Fig. 3. Optogenetic photoinhibition of ChAT interneurons enhances MSN spiking in vivo. (**A**) (Top) Voltage trace of an isolated unit (recorded from the NAc in vivo) that was excited by optogenetic photoinhibition of the ChAT interneurons with eNpHR3.0. (Middle) Raster plot displaying the response of the same unit to five repetitions of the light stimulation, with each action potential represented by a dot. (Bottom) Average and SEM of the firing rate over time for the same unit. (**B**) Wavelet analysis reveals power of spiking as a function of frequency and time (average across five repetitions) for the same unit as in (A). (**C**) Fraction of sites that were inhibited versus excited by light stimulation. (**D**) Same as (A), for a unit that was inhibited by light stimulation. (**E**) Population summary of the time course of response to light stimulation for sites that were inhibited (left; $n = 13$ of 17) or excited (right; $n = 4$ of 17) by light. Solid lines represent the average firing rate across sites as a function of time; each dot represents the average firing rate of an individual site. All firing rates are normalized to the mean value before light stimulation. (A to E) Duration of photostimulation, 15 s (constant illumination); wavelength, 560 nm. Epochs of light stimulation are represented by yellow bars.

References and Notes

1. J. P. Changeux, *C. R. Biol.* **332**, 421 (2009).
2. M. P. Kilgard, M. M. Merzenich, *Science* **279**, 1714 (1998).
3. J. S. Bakin, N. M. Weinberger, *Proc. Natl. Acad. Sci. U.S.A.* **93**, 11219 (1996).
4. U. Maskos, *Br. J. Pharmacol.* **153** (suppl. 1), S438 (2008).
5. M. R. Picciotto *et al.*, *Nature* **391**, 173 (1998).
6. T. Aosaki *et al.*, *J. Neurosci.* **14**, 3969 (1994).
7. M. L. Furey, P. Pietrini, J. V. Haxby, W. C. Drevets, *Neuropsychopharmacology* **33**, 913 (2008).
8. S. G. Anagnostaras *et al.*, *Nat. Neurosci.* **6**, 51 (2003).
9. S. Ikemoto, B. S. Glazier, J. M. Murphy, W. J. McBride, *Physiol. Behav.* **63**, 811 (1998).
10. M. J. Williams, B. Adinoff, *Neuropsychopharmacology* **33**, 1779 (2008).
11. B. J. Everitt, T. W. Robbins, *Annu. Rev. Psychol.* **48**, 649 (1997).
12. W. E. Pratt, R. C. Spencer, A. E. Kelley, *Behav. Neurosci.* **121**, 1215 (2007).
13. J. A. Crespo, K. Sturm, A. Saria, G. Zernig, *J. Neurosci.* **26**, 6004 (2006).
14. W. E. Pratt, A. E. Kelley, *Behav. Neurosci.* **118**, 730 (2004).
15. F. E. Pontieri, G. Tanda, F. Orzi, G. Di Chiara, *Nature* **382**, 255 (1996).
16. B. T. Chen, F. W. Hopf, A. Bonci, *Ann. N.Y. Acad. Sci.* **1187**, 129 (2010).
17. R. A. Wise, *NIDA Res. Monogr.* **50**, 15 (1984).
18. T. W. Robbins, K. D. Ersche, B. J. Everitt, *Ann. N.Y. Acad. Sci.* **1141**, 1 (2008).
19. E. J. Nestler, G. K. Aghajanian, *Science* **278**, 58 (1997).
20. T. Hikida *et al.*, *Proc. Natl. Acad. Sci. U.S.A.* **98**, 13351 (2001).
21. V. V. Rymar, R. Sasseville, K. C. Luk, A. F. Sadikot, *J. Comp. Neurol.* **469**, 325 (2004).
22. F. M. Zhou, C. J. Wilson, J. A. Dani, *J. Neurobiol.* **53**, 590 (2002).

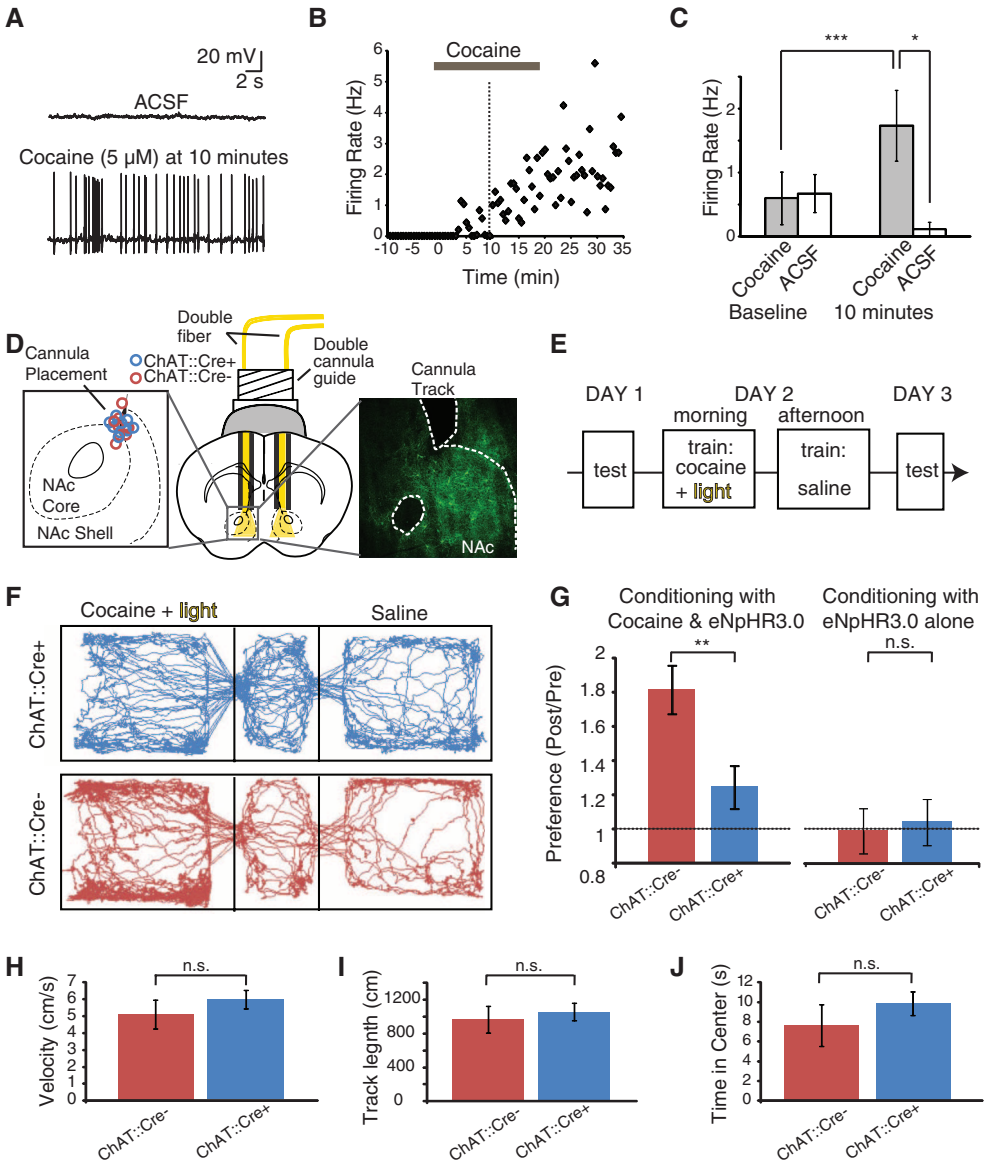

Fig. 4. ChAT interneurons can be activated by cocaine in slice and required for cocaine conditioning in vivo. (**A**) The frequency of spontaneous action potentials in a ChAT neuron increased 10 min after bath application of cocaine (5 μM). ACSF, artificial cerebrospinal fluid. (**B**) Firing rate over time for this ChAT neuron. Horizontal gray bar, application of cocaine; vertical dotted line, 10 min after cocaine application, the time point illustrated in detail in (A) and (C). (**C**) Population data illustrating the cocaine-induced increase in firing in ChAT neurons, comparing the baseline firing rate (averaged over the 2.5 min before cocaine application) with the rate after cocaine infusion (averaged between 10 and 12.5 min after onset of cocaine application; gray bars, cells receiving cocaine; white bars, control cells receiving only ACSF; $P < 0.005$, paired two-tailed t test for cocaine-treated group before versus after cocaine; $P < 0.05$ unpaired two-tailed t test comparing cocaine versus control cells after cocaine or vehicle). (**D**) Schematic illustration of a bilateral cannula system with double fibers inserted to illuminate the medial portion of the NAc. (Left inset) Endpoint of cannula track for all mice used in (H). (Right inset) eYFP expression in NAc of a ChAT::Cre$^+$ mouse injected with Cre-dependent eNpHR3.0-eYFP. (**E**) Conditioning paradigm for cocaine CPP (H). Mice were conditioned with ip cocaine (20 mg/kg), along with ChAT cell inhibition with eNpHR3.0 (wavelength: 590 nm). (**F**) Tracking data from representative ChAT::Cre$^+$ and ChAT::Cre$^-$ mice on the testing day after cocaine conditioning (day 3). On the previous day (day 2), the mice had received cocaine and light in one left chamber, whereas in the other they received saline. The ChAT::Cre$^-$ mouse (but not the ChAT::Cre$^+$ mouse) exhibited a preference for the conditioned chamber. (**G**) (Left) Fold change in time in conditioned chamber during day 3 versus day 1 of cocaine CPP (conditioning with cocaine and light). Comparison of ChAT::Cre$^+$ and ChAT::Cre$^-$ littermates; in both cases injected with Cre-dependent eNpHR3.0 ($n = 10$ ChAT::Cre$^+$, $n = 12$ ChAT::Cre$^-$; $P < 0.01$ for two-tailed t test; three cohorts). (Right) Fold change in time in conditioned chamber during day 3 versus day 1 for conditioning with light alone (no cocaine; $n = 9$ ChAT::Cre$^+$, $n = 7$ ChAT::Cre; $P > 0.05$ for two-tailed t test; three cohorts). Error bars indicate SEM. n.s., not significant. (**H**) Velocity of virus-injected (Cre-dependent eNpHR3.0) and photostimulated ChAT::Cre$^+$ and ChAT::Cre$^-$ mice in the open field ($n = 10$ ChAT::Cre$^+$, $n = 10$ ChAT::Cre$^-$; $P > 0.05$ for two-tailed t test; three cohorts). (**I**) Same as (H) for track length in open field ($n = 10$ ChAT::Cre$^+$, $n = 10$ ChAT::Cre$^-$; $P > 0.05$ for two-tailed t test; three cohorts). (**J**) Same as (H) for time in center of open field ($n = 10$ ChAT::Cre$^+$, $n = 10$ ChAT::Cre; $P > 0.05$ for two-tailed t test; three cohorts). (A to J) *$P < 0.05$; **$P < 0.01$; ***$P < 0.005$.

23. F. M. Zhou, C. Wilson, J. A. Dani, *Neuroscientist* **9**, 23 (2003).
24. T. Koós, J. M. Tepper, *J. Neurosci.* **22**, 529 (2002).
25. M. de Rover, J. C. Lodder, K. S. Kits, A. N. M. Schoffelmeer, A. B. Brussaard, *Eur. J. Neurosci.* **16**, 2279 (2002).
26. Materials and methods are available as supporting material on *Science* Online.
27. H.-C. Tsai *et al.*, *Science* **324**, 1080 (2009); 10.1126/science.1168878.
28. D. Atasoy, Y. Aponte, H. H. Su, S. M. Sternson, *J. Neurosci.* **28**, 7025 (2008).
29. E. S. Boyden, F. Zhang, E. Bamberg, G. Nagel, K. Deisseroth, *Nat. Neurosci.* **8**, 1263 (2005).
30. V. Gradinaru *et al.*, *Cell* **141**, 154 (2010).
31. Y. Kawaguchi, *J. Neurosci.* **13**, 4908 (1993).
32. C. J. Wilson, H. T. Chang, S. T. Kitai, *J. Neurosci.* **10**, 508 (1990).
33. H. Inokawa, H. Yamada, N. Matsumoto, M. Muranishi, M. Kimura, *Neuroscience* **168**, 395 (2010).
34. M. Nisell, M. Marcus, G. G. Nomikos, T. H. Svensson, *J. Neural Transm.* **104**, 1 (1997).
35. A. Hrabovska *et al.*, *Chem. Biol. Interact.* **183**, 194 (2010).
36. B. G. Hoebel, N. M. Avena, P. Rada, *Curr. Opin. Pharmacol.* **7**, 617 (2007).
37. R. M. Carelli, S. A. Deadwyler, *J. Neurosci.* **14**, 7735 (1994).
38. S. A. Taha, H. L. Fields, *J. Neurosci.* **26**, 217 (2006).
39. M. Krause, P. W. German, S. A. Taha, H. L. Fields, *J. Neurosci.* **30**, 4746 (2010).
40. W. A. Carlezon Jr., M. J. Thomas, *Neuropharmacology* **56** (suppl. 1), 122 (2009).
41. L. L. Peoples, M. O. West, *J. Neurosci.* **16**, 3459 (1996).

42. We thank the entire Deisseroth lab for their support. I.B.W. is supported by the Helen Hay Whitney Foundation; S.-C.L. is supported by the National Institute of Neurological Disorders and Stroke; I.D. is supported by DAAD and the Human Frontier Science Program; P.A. is supported by the Stanford Dean's fellowship; V.G. is supported by Bio-X SIGF; K.D. is supported by the Keck, Snyder, Woo, Yu, and McKnight Foundations, as well as by CIRM, the National Institute of Mental Health, and the National Institute on Drug Abuse.

Supporting Online Material

www.sciencemag.org/cgi/content/full/330/6011/1677/DC1
Materials and Methods
Figs. S1 to S5
Tables S1 and S2
References

15 June 2010; accepted 10 November 2010
10.1126/science.1193771

New Genes in *Drosophila* Quickly Become Essential

Sidi Chen, Yong E. Zhang, Manyuan Long*

To investigate the origin and evolution of essential genes, we identified and phenotyped 195 young protein-coding genes, which originated 3 to 35 million years ago in *Drosophila*. Knocking down expression with RNA interference showed that 30% of newly arisen genes are essential for viability. The proportion of genes that are essential is similar in every evolutionary age group that we examined. Under constitutive silencing of these young essential genes, lethality was high in the pupal stage and also found in the larval stages. Lethality was attributed to diverse cellular and developmental defects, such as organ formation and patterning defects. These data suggest that new genes frequently and rapidly evolve essential functions and participate in development.

Essential genes are often portrayed as conserved and ancient (*1*, *2*), whereas younger genes, which exist in only one or a few species, have been considered to be more dispensable and to perform relatively minor organismal functions (*1*–*4*). It is unclear how essential genes arise and how new genes accumulate essential functions. New genes arise continuously through various mechanisms, such as DNA-based duplication, retroposition, and de novo origination (*5*, *6*). When they first arose, new genes were expected to be nonessential because their immediate ancestral species were able to survive without them (Fig. 1A). However, little is known about their phenotypes and degrees of essentiality.

By comparative genomic analysis of 12 closely related *Drosophila* species (*7*), we identified 566 new genes in the *D. melanogaster* genome and dated their evolutionary ages through phylogenetic distributions (*8*) (fig. S1). All these genes originated less than 35 million years (My) after the divergence from *D. willistoni* (*9*), so we called them young genes. To assay their phenotypic effects in viability, we obtained *Drosophila* RNA interference (RNAi) lines targeting these genes (*10*, *11*) and excluded RNAi lines with predicted off-target effects and lines with detectable phenotypes by P-element insertion, resulting in a set of lines targeting 195 young genes. Crosses resulting in constitutive silencing of these genes allowed us to assay the phenotypic effects on viability in the F1 generation (*8*) (fig. S2).

Unexpectedly, 59 of these genes were lethal under constitutive RNAi knockdown (Table 1 and tables S1, S3, and S4). We confirmed lethality in most of the genes (93%) with different driver constructs (table S6, part I). Although the efficiency of gene knockdown by different drivers might vary, the phenotypic consistency indicated a low false-positive rate (<7%), consistent with previous estimates (*10*). Moreover, for the genes with multiple RNAi lines from independent upstream activating sequence–inverted repeat (UAS-IR) constructs or independent transformations that insert into different chromosomal locations, we repeated the crosses with these lines and found that 45 of 47 (96%) genes showed similar viability phenotypes between lines (table S6, part II), ruling out positional effects or construct effects. Furthermore, in deficiency libraries, lines deleting these genes are homozygous lethal, although a deletion block can be large and can contain other genes (*12*). Furthermore, several genes in the list (table S1)—*HP6* (*CG15636*), *CG12842*, and *spn2* (*CG8137*)—were found to be lethal using various gene disruption methods, including P-element disruption, RNAi with independent constructs, and misexpression assays (*13*–*15*). Therefore, we found 59 young genes that are essential for viability (Table 1 and table S1), a conservative number due to false negatives because RNAi does not reduce the mRNA level to zero (*10*). These 59 genes encode diverse protein domains with fundamental molecular and cellular functions, including putative transcription factors and/or nucleic acid–binding proteins, peptidases, G protein–coupled receptors, protease inhibitors, nicotinamide adenine dinucleotide–binding proteins, ribosomal proteins, and molecular chaperones (tables S2 and S8).

The proportion of essential genes in *D. melanogaster* is estimated at ~25 to 35% (*2*, *10*, *16*). We compared the rates of lethality between old genes and young genes using the same gene-silencing methods (*8*). Among randomly chosen old genes, 35% (86 of 245) were essential for viability (Table 1), which was statistically similar to the 30% (59 of 195) essential young genes (two-tailed Fisher's exact test, $P = 0.3$, Table 1). These data suggest that young genes are as essential as old genes in terms of viability.

We analyzed the age distribution of young essential genes by mapping the origination events of these 59 genes onto the *Drosophila* phylogenetic tree (*8*). We found that essential genes emerged throughout the evolutionary period examined (Fig. 1B and table S2). The youngest, *p24-related-2* (*CG33105*), arose within the last 3 My and is thus *D. melanogaster*–specific (table S2). In each age group, the proportion of genes that are essential was around 30% (Table 1), suggesting that whether or not a gene is essential is independent of its age. These data reveal that the proportion of newly arisen essential genes reaches a plateau within a few million years. Reminiscent of the

Table 1. Summary statistics of lethal phenotypes of young genes. (I) Gene age was described in (*8*); age groups 0 to ~3 My and 3 to ~6 My were pooled to increase sample size. A gene was considered essential for viability if it was constitutive RNAi lethal (*8*); fertility is not a subject in this study. (II) Lethality stage of "pupal" includes all substage categories, such as prepupal, early pupal, late pupal, and pharate. "Before pupal" includes multiple larval stages, including early larvae and late larvae. "Other" includes mixed-stage lethal, stage unknown, or stage undefined.

I. Proportion of essential genes (constitutive RNAi lethal)

Young genes

Age (My)	Essential genes	Nonessential genes	Subtotal	Proportion of essential	*P**
0~6	4	9	13	31%	1.00
6~11	25	51	76	33%	0.78
11~25	13	30	43	30%	0.60
25~35	17	46	63	27%	0.24
Total	59	136	195	30%	0.31

Old genes

Age (My)	Essential genes	Nonessential genes	Subtotal	Proportion of essential	Age (My)
>40	86	159	245	35%	>40

II. Stage of lethality

	Young genes		Old genes	
Pupal	47	80%	43	50%
Before pupal	6	10%	38	44%
Other	6	10%	5	6%
Total	59	100%	86	100%
P†	0.0009			

*Two-tailed Fisher's exact test *P* for essential/nonessential young genes in each age group compared with those for old genes; †Two-tailed Fisher's exact test *P* for pupal/non-pupal lethals for young genes compared with those for old genes.

Department of Ecology and Evolution, The University of Chicago, 1101 East 57th Street, Chicago, IL 60637, USA.

*To whom correspondence should be addressed. E-mail: mlong@uchicago.edu

Walsh model, a new duplicate gene can quickly evolve a novel and important function by accumulating advantageous mutations (*17*), especially in the species with large effective population sizes, such as *Drosophila* (*18*). These observations may explain why duplicate genes are as essential as singletons (*19*–*22*), although most genes examined in these mammalian studies are relatively ancient.

We investigated the native gene expression patterns of these genes with *D. melanogaster* life-cycle time-course expression profiling (*23*). Interestingly, most of the 59 genes we identified are highly expressed at the late larval stages (L2 and L3) or during metamorphosis; some genes are also expressed during the embryonic and L1 stages (fig. S4), which suggests that their gene products are subject to transcriptional regulation during the life cycle.

We examined the developmental stages in which lethality occurs under constitutive silencing and found that lethality occurs at various developmental stages (Fig. 2). The vast majority (47 of 59, 80%) of the young essential genes consistently showed lethality during pupation; four new genes (*CG11466*, *CG33459*, *CG6289*, and *CG8358*) showed lethality at larval stage, whereas a few other genes show lethality at both larval and pupal stages, which we termed mixed-stage lethality (Table 1 and tables S1 and S5). About 50% of old genes are lethal during pupation, and the other half are lethal at earlier stages, because many early-stage developmental genes are conserved (*10*) (Table 1). In comparison, young genes are highly enriched in pupal lethals (Table 1; Fisher's exact test, two-tailed, $P = 9 \times 10^{-4}$). These data suggest that new genes have evolved essential functions in larval and pupal development, and frequently regulate development in the pupal stage, with 10% or more regulating the development in the larval or even embryonic stages (table S1) (*13*).

Examination of metamorphosis failures of pupal lethals demonstrated several distinct classes. The majorities (37 of 47, 79%) of pupal lethals were classified as class I (i.e., pharate lethal; complete pharates formed but failed in the final steps of pupal development and/or eclosion), with only a few falling into class II (pupae development aborted at the prepupal or early pupal stage, without proper formation of rudimentary heads or early leg structures) or class III (development failed over multiple stages, including prepupal, early pupal, late pupal and/or complete pharate stages) (tables S1 and S5 and fig. S3). These data suggested that young essential genes tend to play vital roles in middle or late stages of development, with a few cases in early stages.

We applied a tissue-specific loss-of-function (LOF) analysis to wing and notum development to investigate specific underlying defects (*8*). Under tissue-specific RNAi, almost every young essential gene we examined showed visible morphological abnormalities that were distinct in range, position, affected cell type, severity, and penetrance (Fig. 3 and table S7). Several types of canonical cellular and developmental defects were observed: (i) gross morphological defects in the overall shapes of the wing or notum (Fig. 3A and table S7); (ii) cell misdifferentiation or cell fate switching, as seen in loss of bristle cells or ectopic bristles (Fig. 3, B and E); (iii) tissue necrosis or death (Fig. 3C); (iv) tumor formation in the scalar region of the notum or tip of the wing (Fig. 3D and table S7); (v) loss of asymmetric anterior-posterior wing patterning (Fig. 3E), a classical developmental phenotype (*24*); and (vi) a possible signaling defect resembling the Notch phenotype in the wing (Fig. 3F). These data revealed that when the normal expression patterns of these new genes were disrupted, the development of the adult organs was affected. Taken together, knocking down young genes led to stage-specific termination of developmental processes as well as morphological defects. The developmental phenotypes of the lineage-specific genes indicate that different species likely have evolved distinct genetic components for their own development. The young gene HP6 in the *D. melanogaster* subgroup species is one such example (table S1) (*13*).

The vast majority (56 of 59, 95%) of young essential genes were generated through gene duplication, including DNA-based duplication and RNA-based retroposition (Fig. 1, B to D, and table S2). These new duplicates often show novel chimeric gene structures, including new coding regions and untranslated regions (Fig. 1, C and D, fig. S1, and table S2). The protein sequences of these genes have drastically diverged from those of their parental copies, with a median divergence of 47.3% (table S2). A few (3 of 59)

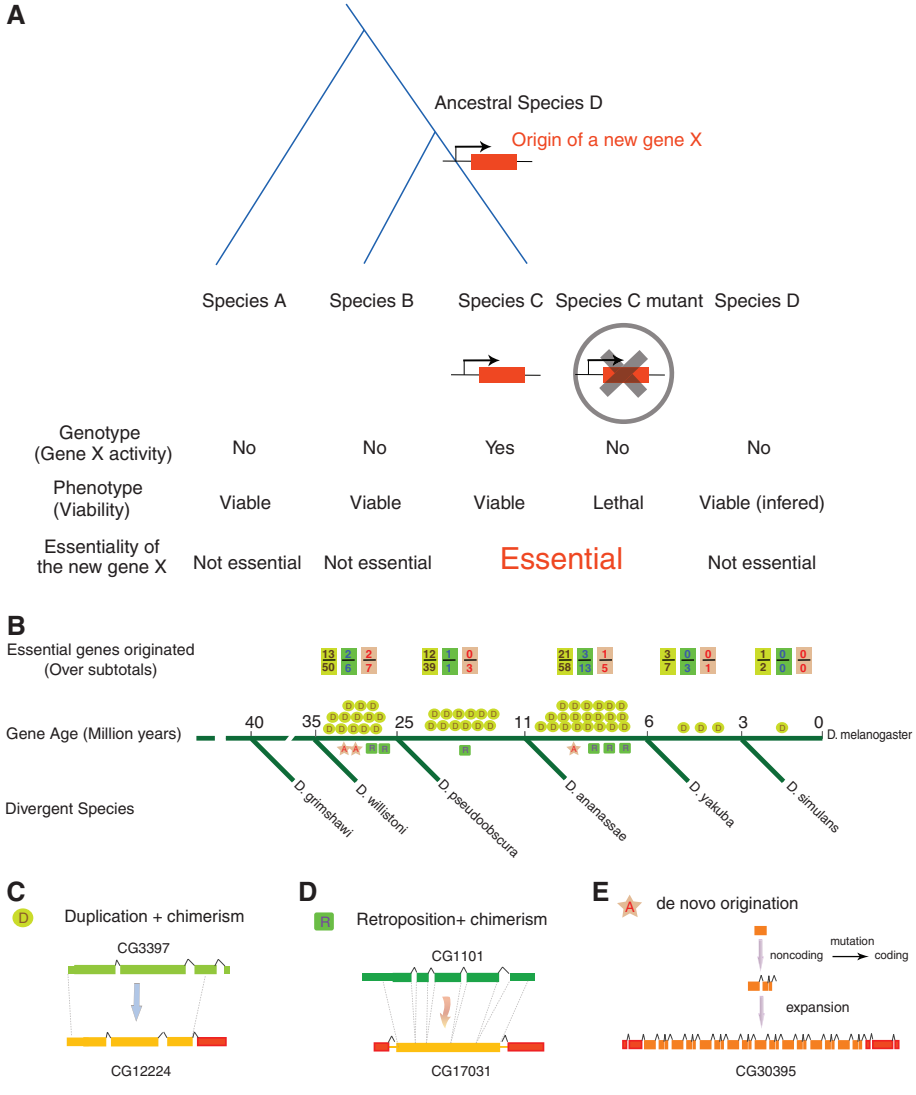

Fig. 1. Origin of new essential genes during recent evolution in *Drosophila*. (**A**) Schematic representation for the hypothesis for the origin of a new essential gene. The ancestral species D is immediately before the new gene X originated. (**B**) Number of young essential genes in major evolutionary periods [D/R and A represent DNA/RNA-based duplicate genes and de novo genes with examples in (**C**) to (**E**), respectively]. The subtotal for a particular mechanism, including both essential and nonessential genes, is also shown as a denominator in B. Green, yellow, red and boxes represent exons in the parental genes, young genes, and recruited chimeric regions, respectively. Dashed lines represent paralogous duplicated regions.

young essential genes originated de novo (Fig. 1, B and E, and table S2). In general, the proportions of new genes that are essential do not differ significantly among the three types of origination mechanisms: 32% (50 of 156) for DNA-based duplication, 26% (6 of 23) for RNA-based retroposition, and 19% (3 of 16) for de novo origination (table S9, $P > 0.4$).

Young essential genes appeared predominantly autosomal (57 of 59), with only two X-linked (table S2). Only 15% (2 of 13) X-linked genes examined were essential for viability, compared with the ~30 to 35% observed for both young and old autosomal genes (fig. S5), which suggests that X-linked genes are less likely to be essential for viability (two-tailed Fisher's exact test, $P = 0.047$).

Sequence evolution (*8*) shows that young essential genes have higher protein substitution rates (fig. S7A; two-tailed Fisher's exact test, $P = 5 \times 10^{-8}$) and higher Ka/Ks ratios (ratios of the rate of amino acid substitution to silent substitution) than their parental genes (fig. S7B; Wilcoxon rank test, $P = 0.03$), likely caused by either relaxation of functional constraint or positive selection. We measured the proportion of substitution under positive selection (α) by comparing between- and within-species variation (*8*). We found that old essential genes were highly constrained with a highly negative α (–1.48) (fig. S8). The essential genes aged 11 to ~35 My have a slightly negative α (–0.32), significantly higher than the previous group (likelihood ratio test, $P < 0.01$) (fig. S8). The youngest essential genes (<11 My) have a positive α (+0.25) (fig. S8), significantly higher than the two previous groups and their parental genes (likelihood ratio tests, $P < 0.01$). These analyses reveal adaptive evolution with young genes and increased purifying selection as genes become older, similar to the pattern of Adh-duplicated new genes (*25*).

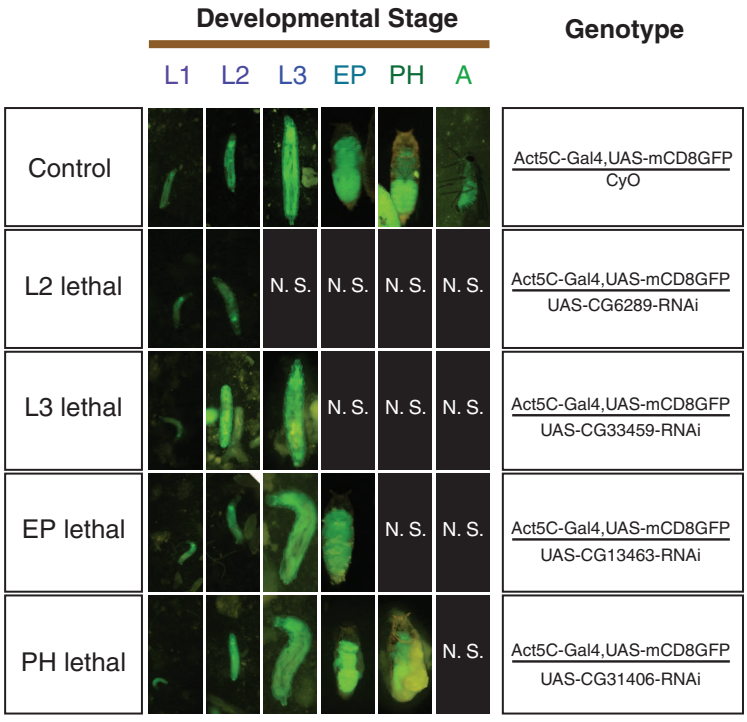

Fig. 2. Staging lethality of gene silencing by fluorescence tracking. Living flies with RNAi–green fluorescent protein dual constructs are shown for six major *D. melanogaster* developmental stages: L1, first instar larva; L2, second instar larva; L3, third instar larva; EP, early pupa; PH, pharate (late pupa); A, adult. (Right) Genotypes of the flies. (Left) Stage of lethality. N.S., no flies of this genotype survived to this stage.

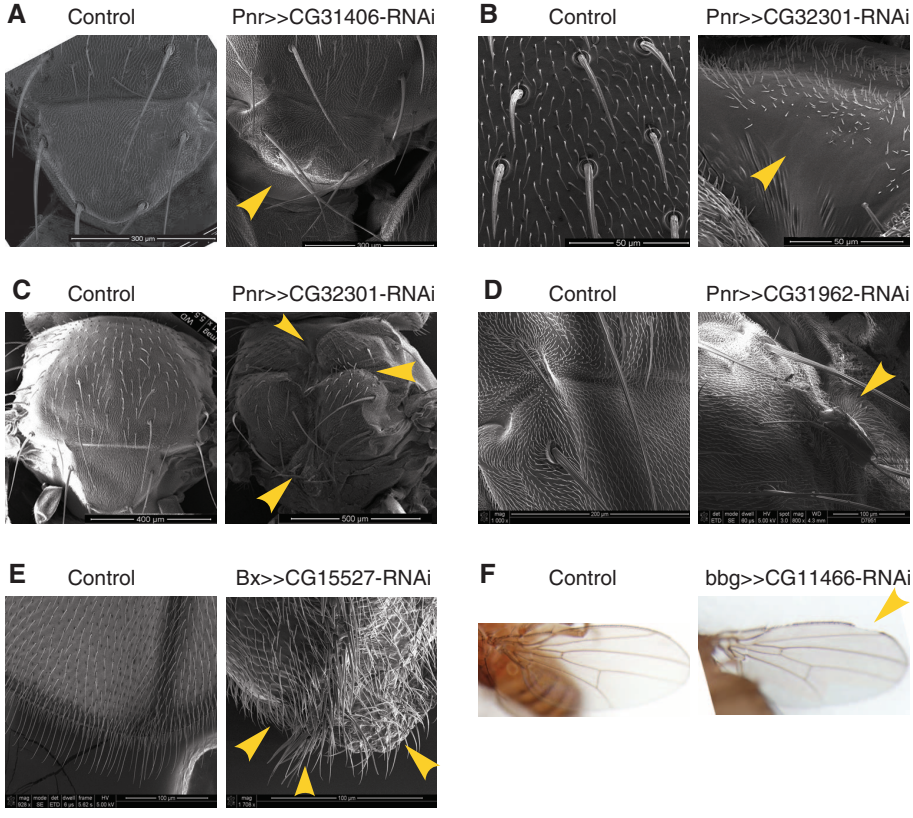

Fig. 3. Representative cellular and developmental defects. Representative tissue-specific LOF of young essential genes leading to (**A**) defects in notum scutellar morphologies, (**B**) irregular bristle patterning and loss of bristles, (**C**) necrosis and tissue death at multiple places in the notum, (**D**) tumor formation at the junction between scutum and scutellum, (**E**) loss of asymmetric patterning with mirror-like wings and ectopic bristles, and (**F**) possible signaling defect with wing notches. Genotypes of flies are shown above each image, with scale bars in the lower right corners. Yellow arrowheads point to particular phenotypic defects.

We finally investigated the viability phenotype of the parental genes with available RNAi lines (table S10) and retrieved the phenotypic information of several additional genes from previous studies (*10*). We summarized the essentiality relationship between parental gene–new gene pairs and found that the parental gene of a young essential gene can be either essential or nonessential, and vice versa (tables S10 and S11). These data suggested that a new essential gene can rise from either an essential or a nonessential parent (given that it represents the ancestral state of essentiality) and that either essential genes or nonessential genes can give rise to each type of gene. These processes appeared to be relatively independent (table S11, Fisher's Exact test, two-tailed, $P = 0.296$).

A previous case study of the sterile phenotype of a paternal-effect gene suggested that genes essential for fertility could arise in 10 My (*26*). Our observation of lethal phenotypes caused by the knockdown of young genes suggested that essential vital genes have been frequently generated in recent evolutionary periods. A new gene might not have become essential immediately after its origination. It, however, can integrate into a vital pathway by interacting with existing genes, and such interaction would be optimized by mutation and selection. This coevolution may lead to the new gene becoming indispensable. This observation is supported by our modeling (*8*) with large-scale interaction data (*27*, *28*), revealing genome-wide interactions of young essential genes with many previously unrelated genes (fig. S6).

The mechanism for the evolution of essentiality would change with the types of new genes. A de novo gene has to evolve essentiality through neofunctionalization because it has no ancestral template. A duplicated gene, generated from an ancestral copy of its parental gene, could become essential from the loss of parents, or from the switch of essentiality from paralogs, or through subfunctionalization (*29*). However, in our data set, the vast majority of the young essential genes have detectable older and conserved paralogs (table S2) and experienced rapid sequence evolution (table S2 and Fig. S7). The prevalent gene structure renovation (table S2), together with the independence between parental gene essentiality and new gene essentiality (table S11), support the neofunctionalization origin of essentiality for most new protein-coding genes, many of which may contribute to the lineage-specific developmental program.

References and Notes

1. J. E. Krebs, E. S. Goldstein, S. T. Kilpatrick, B. Lewin, *Lewin's Essential Genes* (Jones and Bartlett Publishers, Sudbury, Mass., ed. 2nd, 2009)
2. G. L. Miklos, G. M. Rubin, *Cell* **86**, 521 (1996).
3. A. C. Wilson, S. S. Carlson, T. J. White, *Annu. Rev. Biochem.* **46**, 573 (1977).
4. D. M. Krylov, Y. I. Wolf, I. B. Rogozin, E. V. Koonin, *Genome Res.* **13**, 2229 (2003).
5. H. Kaessmann, N. Vinckenbosch, M. Long, *Nat. Rev. Genet.* **10**, 19 (2009).
6. M. Long, E. Betrán, K. Thornton, W. Wang, *Nat. Rev. Genet.* **4**, 865 (2003).
7. A. G. Clark *et al.*; Drosophila 12 Genomes Consortium, *Nature* **450**, 203 (2007).
8. Materials and methods are available as supporting material on *Science* Online.
9. C. A. Russo, N. Takezaki, M. Nei, *Mol. Biol. Evol.* **12**, 391 (1995).
10. G. Dietzl *et al.*, *Nature* **448**, 151 (2007).
11. K. Keleman, T. Micheler, VDRC project members, Personal communication to FlyBase, FBrf0208510: RNAi-phiC31 construct and insertion data submitted by the Vienna Drosophila RNAi Center (2009); http://fb2010_07.flybase.org/reports/FBrf0208510.html.
12. A. L. Parks *et al.*, *Nat. Genet.* **36**, 288 (2004).
13. C. Joppich, S. Scholz, G. Korge, A. Schwendemann, *Chromosome Res.* **17**, 19 (2009).
14. H. Ida *et al.*, *Nucleic Acids Res.* **37**, 1423 (2009).
15. J. L. Mueller, J. L. Page, M. F. Wolfner, *Genetics* **175**, 777 (2007).
16. N. Perrimon, A. Lanjuin, C. Arnold, E. Noll, *Genetics* **144**, 1681 (1996).
17. J. B. Walsh, *Genetics* **139**, 421 (1995).
18. M. Kreitman, J. M. Comeron, *Curr. Opin. Genet. Dev.* **9**, 637 (1999).
19. B. Y. Liao, J. Zhang, *Trends Genet.* **23**, 378 (2007).
20. T. Makino, K. Hokamp, A. McLysaght, *Trends Genet.* **25**, 152 (2009).
21. Z. Su, X. Gu, *J. Mol. Evol.* **67**, 705 (2008).
22. H. Liang, W. H. Li, *Trends Genet.* **23**, 375 (2007).
23. Z. Gauhar *et al.*, Personal communication to FlyBase, FBrf0205914: Drosophila melanogaster life-cycle gene expression dataset and microarray normalisation protocols (2008); http://flybase.org/reports/FBrf0205914.html.
24. J. A. Williams, S. W. Paddock, S. B. Carroll, *Development* **117**, 571 (1993).
25. C. D. Jones, D. J. Begun, *Proc. Natl. Acad. Sci. U.S.A.* **102**, 11373 (2005).
26. B. Loppin, D. Lepetit, S. Dorus, P. Couble, T. L. Karr, *Curr. Biol.* **15**, 87 (2005).
27. L. Giot *et al.*, *Science* **302**, 1727 (2003).
28. S. Griffiths-Jones, *Methods Mol. Biol.* **342**, 129 (2006).
29. M. Lynch, M. O'Hely, B. Walsh, A. Force, *Genetics* **159**, 1789 (2001).

30. We thank C. H. Langley and D. Begun for providing polymorphism data; W. Du, J. Gavin-Smyth, Q. Guo, and M. Guffey for technical assistance and discussion; J. Coyne, M. Kreitman, and X. Ni for critically reading and/or revising the manuscript; and the members of the Manyuan Long laboratory, C. Ferguson, R. Hudson, C. I. Wu, and T. Nagylaki, for valuable discussion. S.C. was supported by University of Chicago Biological Sciences Division Fellowships. This research was supported by National Institutes of Health (R01GM065429-01A1 and R01GM078070-01A1) and National Science Foundation (CAREER Award MCB 0238168) to M.L. Y.E.Z. was also supported by the Searle Funds from Chicago Biomedical Consortium (2009, Spark).

Supporting Online Material

www.sciencemag.org/cgi/content/full/330/6011/1682/DC1
Materials and Methods
Figs. S1 to S8
Tables S1 to S11
References

11 August 2010; accepted 1 November 2010
10.1126/science.1196380

Cytoplasmic Partitioning of P Granule Components Is Not Required to Specify the Germline in *C. elegans*

Christopher M. Gallo,* Jennifer T. Wang,* Fumio Motegi, Geraldine Seydoux†

Asymmetric segregation of P granules during the first four divisions of the *Caenorhabditis elegans* embryo is a classic example of cytoplasmic partitioning of germline determinants. It is thought that asymmetric partitioning of P granule components during mitosis is essential to distinguish germline from soma. We have identified a mutant (*pptr-1*) in which P granules become unstable during mitosis and P granule proteins and RNAs are distributed equally to somatic and germline blastomeres. Despite symmetric partitioning of P granule components, *pptr-1* mutants segregate a germline that uniquely expresses P granules during postembryonic development. *pptr-1* mutants are fertile, except at high temperatures. Hence, asymmetric partitioning of maternal P granules is not essential to specify germ cell fate. Instead, it may serve to protect the nascent germline from stress.

A general characteristic of germ cells is the presence of cytoplasmic RNA-rich granules called germ granules (*1*). In *Caenorhabditis elegans*, germ (P) granules are present in all germ cells except mature sperm, and they segregate asymmetrically with the germline precursors (P blastomeres) during the first embryonic divisions (Fig. 1A) (*2*). Like embryonic germ granules of other organisms, P granules have been hypothesized to harbor the determinants that specify the germline. However, their function and segregation mechanisms are not fully understood (*2*, *3*).

To monitor P granule dynamics, we used confocal microscopy to image live embryos expressing the P granule protein PGL-1 fused to green fluorescence protein (GFP) (*4*). We obtained similar results with GFP fusions to two other P granule proteins PGL-3 and GLH-1 (*5*, *6*). In the live movies, we analyzed granule dynamics (number, size, and movement) and the overall distribution of each protein by quantifying total (granular + diffuse cyto-

Department of Molecular Biology and Genetics, Howard Hughes Medical Institute, Center for Cell Dynamics, Johns Hopkins School of Medicine, 725 North Wolfe Street, PCTB 706, Baltimore, MD 21205, USA.

*These authors contributed equally to this work.
†To whom correspondence should be addressed. E-mail: gseydoux@jhmi.edu

We finally investigated the viability phenotype of the parental genes with available RNAi lines (table S10) and retrieved the phenotypic information of several additional genes from previous studies (*10*). We summarized the essentiality relationship between parental gene–new gene pairs and found that the parental gene of a young essential gene can be either essential or nonessential, and vice versa (tables S10 and S11). These data suggested that a new essential gene can rise from either an essential or a nonessential parent (given that it represents the ancestral state of essentiality) and that either essential genes or nonessential genes can give rise to each type of gene. These processes appeared to be relatively independent (table S11, Fisher's Exact test, two-tailed, $P = 0.296$).

A previous case study of the sterile phenotype of a paternal-effect gene suggested that genes essential for fertility could arise in 10 My (*26*). Our observation of lethal phenotypes caused by the knockdown of young genes suggested that essential vital genes have been frequently generated in recent evolutionary periods. A new gene might not have become essential immediately after its origination. It, however, can integrate into a vital pathway by interacting with existing genes, and such interaction would be optimized by mutation and selection. This coevolution may lead to the new gene becoming indispensable. This observation is supported by our modeling (*8*) with large-scale interaction data (*27*, *28*), revealing genome-wide interactions of young essential genes with many previously unrelated genes (fig. S6).

The mechanism for the evolution of essentiality would change with the types of new genes. A de novo gene has to evolve essentiality through neofunctionalization because it has no ancestral template. A duplicated gene, generated from an ancestral copy of its parental gene, could become essential from the loss of parents, or from the switch of essentiality from paralogs, or through subfunctionalization (*29*). However, in our data set, the vast majority of the young essential genes have detectable older and conserved paralogs (table S2) and experienced rapid sequence evolution (table S2 and Fig. S7). The prevalent gene structure renovation (table S2), together with the independence between parental gene essentiality and new gene essentiality (table S11), support the neofunctionalization origin of essentiality for most new protein-coding genes, many of which may contribute to the lineage-specific developmental program.

References and Notes

1. J. E. Krebs, E. S. Goldstein, S. T. Kilpatrick, B. Lewin, *Lewin's Essential Genes* (Jones and Bartlett Publishers, Sudbury, Mass., ed. 2nd, 2009)
2. G. L. Miklos, G. M. Rubin, *Cell* **86**, 521 (1996).
3. A. C. Wilson, S. S. Carlson, T. J. White, *Annu. Rev. Biochem.* **46**, 573 (1977).
4. D. M. Krylov, Y. I. Wolf, I. B. Rogozin, E. V. Koonin, *Genome Res.* **13**, 2229 (2003).
5. H. Kaessmann, N. Vinckenbosch, M. Long, *Nat. Rev. Genet.* **10**, 19 (2009).
6. M. Long, E. Betrán, K. Thornton, W. Wang, *Nat. Rev. Genet.* **4**, 865 (2003).
7. A. G. Clark *et al.*; Drosophila 12 Genomes Consortium, *Nature* **450**, 203 (2007).
8. Materials and methods are available as supporting material on *Science* Online.
9. C. A. Russo, N. Takezaki, M. Nei, *Mol. Biol. Evol.* **12**, 391 (1995).
10. G. Dietzl *et al.*, *Nature* **448**, 151 (2007).
11. K. Keleman, T. Micheler, VDRC project members, Personal communication to FlyBase, FBrf0208510: RNAi-phiC31 construct and insertion data submitted by the Vienna Drosophila RNAi Center (2009); http://fb2010_07.flybase.org/reports/FBrf0208510.html.
12. A. L. Parks *et al.*, *Nat. Genet.* **36**, 288 (2004).
13. C. Joppich, S. Scholz, G. Korge, A. Schwendemann, *Chromosome Res.* **17**, 19 (2009).
14. H. Ida *et al.*, *Nucleic Acids Res.* **37**, 1423 (2009).
15. J. L. Mueller, J. L. Page, M. F. Wolfner, *Genetics* **175**, 777 (2007).
16. N. Perrimon, A. Lanjuin, C. Arnold, E. Noll, *Genetics* **144**, 1681 (1996).
17. J. B. Walsh, *Genetics* **139**, 421 (1995).
18. M. Kreitman, J. M. Comeron, *Curr. Opin. Genet. Dev.* **9**, 637 (1999).
19. B. Y. Liao, J. Zhang, *Trends Genet.* **23**, 378 (2007).
20. T. Makino, K. Hokamp, A. McLysaght, *Trends Genet.* **25**, 152 (2009).
21. Z. Su, X. Gu, *J. Mol. Evol.* **67**, 705 (2008).
22. H. Liang, W. H. Li, *Trends Genet.* **23**, 375 (2007).
23. Z. Gauhar *et al.*, Personal communication to FlyBase, FBrf0205914: Drosophila melanogaster life-cycle gene expression dataset and microarray normalisation protocols (2008); http://flybase.org/reports/FBrf0205914.html.
24. J. A. Williams, S. W. Paddock, S. B. Carroll, *Development* **117**, 571 (1993).
25. C. D. Jones, D. J. Begun, *Proc. Natl. Acad. Sci. U.S.A.* **102**, 11373 (2005).
26. B. Loppin, D. Lepetit, S. Dorus, P. Couble, T. L. Karr, *Curr. Biol.* **15**, 87 (2005).
27. L. Giot *et al.*, *Science* **302**, 1727 (2003).
28. S. Griffiths-Jones, *Methods Mol. Biol.* **342**, 129 (2006).
29. M. Lynch, M. O'Hely, B. Walsh, A. Force, *Genetics* **159**, 1789 (2001).

30. We thank C. H. Langley and D. Begun for providing polymorphism data; W. Du, J. Gavin-Smyth, Q. Guo, and M. Guffey for technical assistance and discussion; J. Coyne, M. Kreitman, and X. Ni for critically reading and/or revising the manuscript; and the members of the Manyuan Long laboratory, C. Ferguson, R. Hudson, C. I. Wu, and T. Nagylaki, for valuable discussion. S.C. was supported by University of Chicago Biological Sciences Division Fellowships. This research was supported by National Institutes of Health (R01GM065429-01A1 and R01GM078070-01A1) and National Science Foundation (CAREER Award MCB 0238168) to M.L. Y.E.Z. was also supported by the Searle Funds from Chicago Biomedical Consortium (2009, Spark).

Supporting Online Material

www.sciencemag.org/cgi/content/full/330/6011/1682/DC1
Materials and Methods
Figs. S1 to S8
Tables S1 to S11
References

11 August 2010; accepted 1 November 2010
10.1126/science.1196380

Cytoplasmic Partitioning of P Granule Components Is Not Required to Specify the Germline in *C. elegans*

Christopher M. Gallo,* Jennifer T. Wang,* Fumio Motegi, Geraldine Seydoux†

Asymmetric segregation of P granules during the first four divisions of the *Caenorhabditis elegans* embryo is a classic example of cytoplasmic partitioning of germline determinants. It is thought that asymmetric partitioning of P granule components during mitosis is essential to distinguish germline from soma. We have identified a mutant (*pptr-1*) in which P granules become unstable during mitosis and P granule proteins and RNAs are distributed equally to somatic and germline blastomeres. Despite symmetric partitioning of P granule components, *pptr-1* mutants segregate a germline that uniquely expresses P granules during postembryonic development. *pptr-1* mutants are fertile, except at high temperatures. Hence, asymmetric partitioning of maternal P granules is not essential to specify germ cell fate. Instead, it may serve to protect the nascent germline from stress.

A general characteristic of germ cells is the presence of cytoplasmic RNA-rich granules called germ granules (*1*). In *Caenorhabditis elegans*, germ (P) granules are present in all germ cells except mature sperm, and they segregate asymmetrically with the germline precursors (P blastomeres) during the first embryonic divisions (Fig. 1A) (*2*). Like embryonic germ granules of other organisms, P granules have been hypothesized to harbor the determinants that specify the germline. However, their function and segregation mechanisms are not fully understood (*2*, *3*).

To monitor P granule dynamics, we used confocal microscopy to image live embryos expressing the P granule protein PGL-1 fused to green fluorescence protein (GFP) (*4*). We obtained similar results with GFP fusions to two other P granule proteins PGL-3 and GLH-1 (*5*, *6*). In the live movies, we analyzed granule dynamics (number, size, and movement) and the overall distribution of each protein by quantifying total (granular + diffuse cyto-

Department of Molecular Biology and Genetics, Howard Hughes Medical Institute, Center for Cell Dynamics, Johns Hopkins School of Medicine, 725 North Wolfe Street, PCTB 706, Baltimore, MD 21205, USA.

*These authors contributed equally to this work.
†To whom correspondence should be addressed. E-mail: gseydoux@jhmi.edu

plasmic) GFP fluorescence (Figs. 1 and 2; fig. S2, A and B; and movies S1 to S3). P granules behaved differently during interphase and mitosis. During interphase, P granules were in a dynamic equilibrium between growing and shrinking phases (movies S1 to S3), with a bias for shrinking in the anterior and a bias for growing in the posterior. By the end of interphase, 85% of P granules in the anterior had disappeared completely or crossed over to the pos-

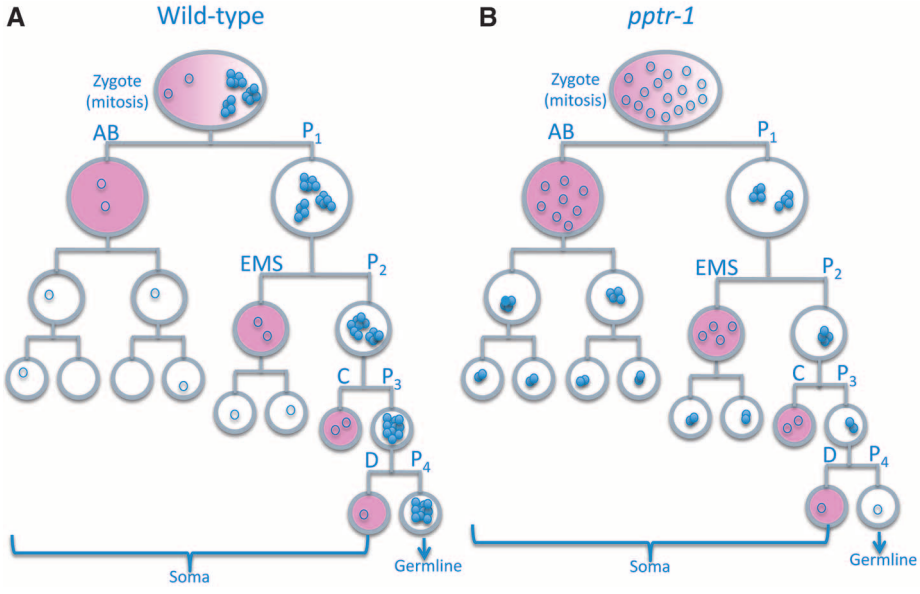

Fig. 1. Segregation of the P granule component PGL-1 in *C. elegans* embryos. (**A**) Abbreviated embryonic lineage showing the divisions that give rise to somatic (AB, EMS, C, and D) and germline (P_1 to P_4) blastomeres. All cells are shown in interphase except for the zygote, which is shown in mitosis. Circles represent PGL-1 molecules; open circles represent PGL-1 diffuse in cytoplasm, and closed circles represent PGL-1 assembled into granules visible by microscopy. Pink is MEX-5, which promotes granule disassembly; localized granule assembly ensures that the majority of PGL-1 segregates with the germline (Fig. 2). (**B**) In *pptr-1* mutants, PGL-1 granules disassemble at each mitosis, and equal numbers of dispersed PGL-1 molecules are segregated to all cells (Fig. 2). During interphase, PGL-1 granules reform in all cells, except in MEX-5–positive somatic blastomeres (pink). Somatic PGL-1 granules are not equivalent to true P granules, because they do not contain P granule–associated mRNAs, which are degraded in somatic lineages (Fig. 3).

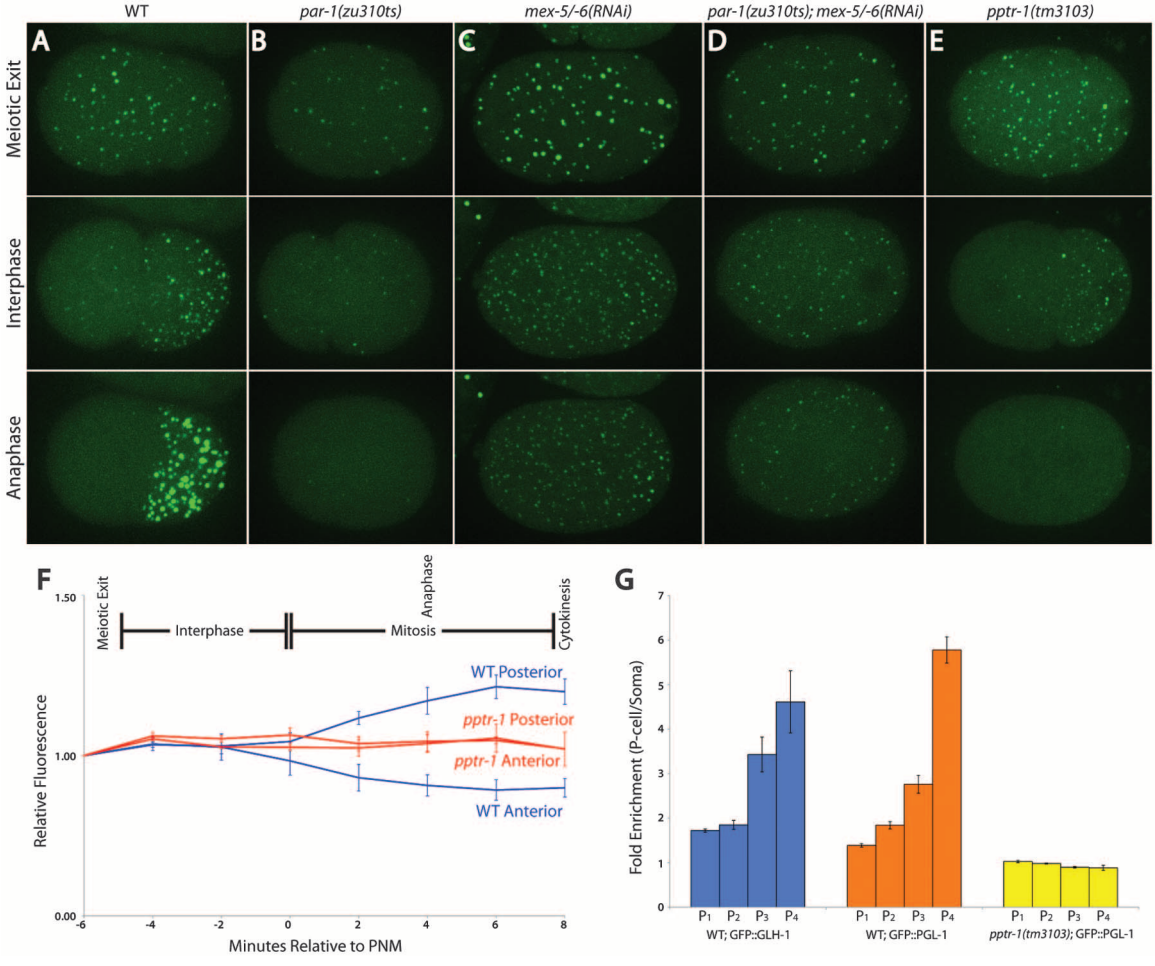

Fig. 2. P granule dynamics require *par-1*, *mex-5/6*, and *pptr-1*. (**A** to **E**) Time-lapse images of zygotes expressing GFP::PGL-1. Images are maximum projections of confocal Z-stacks spanning 8 μm (about half of embryo depth). P granule numbers are shown in fig. S1. MEX-5 and MEX-6 are uniformly distributed in *par-1* embryos, and PAR-1 localizes to a reduced-size posterior domain in *mex-5;mex-6* zygotes (*9*, *10*). (**F**) GFP::PGL-1 levels over time in wild-type and *pptr-1(tm3103)* zygotes. Error bars are SD of mean values from three zygotes. In wild-type embryos, GFP::PGL-1 fluorescence does not decrease in the anterior during interphase, even though the number of visible granules decreases (Fig. 2A), consistent with granule disassembly. During mitosis, GFP::PGL-1 fluorescence and P granule size increase in the posterior (fig. S1), consistent with granule assembly. (**G**) Relative enrichment of GFP::PGL-1 and GFP::GLH-1 in each P blastomere over its somatic sister. Enrichment becomes most pronounced with each division in wild type. No enrichment is observed at any division in *pptr-1* mutants. Error bars are SD from values obtained from three focal planes in three embryos.

terior (15%; n = 41), and the total number of P granules had increased (fig. S1A). Although most granules became restricted to the posterior (Fig. 2A), levels of GFP::PGL-1 fluorescence remained equal in the anterior and posterior halves of the zygote during interphase (Fig. 2F), indicating that GFP::PGL-1 was still present in the anterior cytoplasm although not in discrete granules. During mitosis, P granules grew in size, fused with each other, and decreased in number (Fig. 2A, fig. S1A, and movie S1). GFP::PGL-1 fluorescence decreased in the anterior and increased in the posterior, suggesting that GFP::PGL-1 in the anterior cytoplasm was recruited into the posterior granules (Fig. 2F). Using a photoactivatable Dendra::PGL-1 fusion to permanently label a subpopulation of PGL-1, we confirmed that PGL-1 enrichment in the posterior involves redistribution of existing PGL-1 protein from anterior to posterior with no change in total protein levels (fig. S2D). Dendra::PGL-1 diffuses throughout the embryo and diffuses fastest in the anterior during mitosis (fig. S2, E and G). We conclude that enrichment of PGL-1 in the posterior of the zygote does not depend on synthesis or degradation but correlates with rapid recruitment of cytoplasmic PGL-1 into growing granules during mitosis.

P granule asymmetry requires the polarity regulators PAR-1, MEX-5, and MEX-6 (*7*). PAR-1 is a kinase that segregates with P granules, and MEX-5 and MEX-6 are two redundant RNA binding proteins that segregate opposite P granules in response to PAR-1 asymmetry (*8*). MEX-5 and MEX-6 are inherited by somatic blastomeres and turned over after 1 or 2 cell divisions (*9*). We found that PAR-1 and MEX-5/6 promote P granule assembly and disassembly, respectively. In *par-1* zygotes, where MEX-5/6 are uniformly distributed, most P granules disassembled completely throughout the zygote (Fig. 2B). Complete disassembly was dependent on MEX-5/6: In *par-1;mex-5/6* zygotes and in *mex-5/6* zygotes, P granules remained in a dynamic equilibrium between assembly and disassembly throughout the zygote, and P granule number increased (Fig. 2, C and D, and fig. S1A). Consistent with MEX-5/-6 having a direct role in P granule disassembly, we observed mCherry::MEX-5 on shrinking PGL-1::GFP granules in wild-type embryos (fig. S1B and movie S4). In *mex-5/6* zygotes, we observed large P granules throughout the zygote at meiotic exit and in a small region in the posterior at mitosis (Fig. 2C), consistent with the localization of PAR-1 in *mex-5/6* embryos (*10*). In contrast, in *par-1;mex-5/6* zygotes, P granules were fewer and smaller (Fig. 2D and fig. S1). These results suggest that PAR-1 promotes P granule assembly both directly, by an unknown mechanism most active during mitosis, and indirectly by restricting MEX-5/6 to the anterior [also see (*7*)].

Our observations are consistent with an earlier study (*3*), which also concluded that P granule asymmetry is driven primarily by localized assembly and disassembly rather than by granule movement. That study hypothesized that a local change in the concentration threshold for granule assembly might be sufficient to promote disassembly in the anterior and assembly in the posterior and to enrich PGL-1 in the posterior. Our findings, however, indicate that disassembly during interphase and assembly during mitosis are regulated independently and that preferential segregation of PGL-1 to the germline depends primarily on granule assembly during mitosis.

Consistent with this hypothesis, in an RNA interference (RNAi) screen for genes required for GFP::PGL-1 asymmetry, we identified a gene necessary to assemble P granules during mitosis [see supporting online material (SOM)]. *pptr-1* encodes a regulatory subunit of the phosphatase PP2A [SOM and (*11*)]. In *pptr-1(tm3103)* embryos, GFP::PGL-1 granules disassembled during mitosis (Fig. 2E), and equal levels of diffuse GFP::PGL-1 were inherited by somatic and germline blastomeres at each division (Fig. 2, F and G, fig. S3A, and movie S5). During interphase, GFP::PGL-1 reassembled into granules in the germline daughter but remained diffusely distributed in the somatic daughter until after the next division (after MEX-5 and MEX-6 have turned over). As a result of equal partitioning, GFP::PGL-1 granules became progressively fewer and smaller with each P blastomere (Fig. 1B and fig. S3A). Staining of fixed *pptr-1* embryos with antibodies against core P granule proteins (PGL-1, PGL-3, GLH-1, GLH-2, GLH-4, and the P granule epitope OIC1D4) confirmed that P granules disassemble at each division in *pptr-1* mutants (Fig. 3A and fig. S4). Granules reformed during interphase in each P blastomere but were smaller and fewer than in wild type, consistent with 50% or more loss of P granule components to somatic blastomeres at each division (Fig. 3A). Granules also

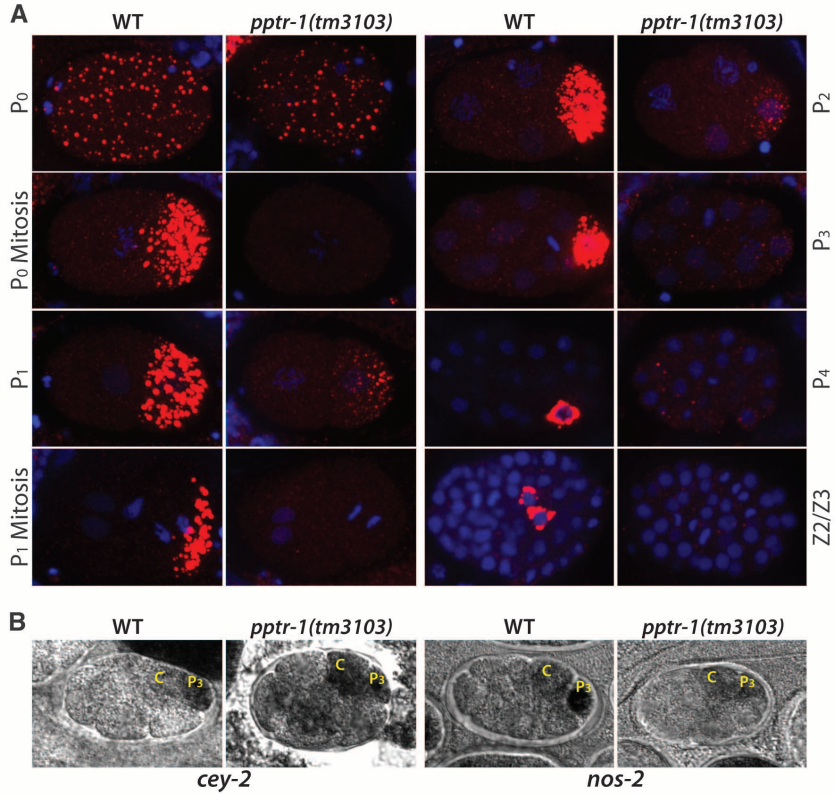

Fig. 3. P granule components are segregated equally to germline and somatic blastomeres in *pptr-1* mutants. (**A**) Fixed wild-type and *pptr-1* embryos stained with 4′,6′-diamidino-2-phenylindole (blue) and OIC1D4 (red). Images are maximum projections of confocal Z-stacks (spanning entire embryo), except for P_4 and Z2/Z3 images, which show single planes. (**B**) Wild-type and *pptr-1* embryos stained for *nos-2* and *cey-2* RNAs (black) by in situ hybridization. In *pptr-1* embryos, *nos-2* and *cey-2* RNAs are present at equal levels in P_3 and C, indicative of symmetric segregation during the P_2 division. In *pptr-1* embryos, as in wild type, *nos-2* and *cey-2* RNA levels are lower in all other blastomeres, indicative of rapid degradation of these RNAs in somatic lineages.

reappeared in somatic cells after the 4-cell stage, in a pattern matching the dynamics of MEX-5/6 turnover (*9*). By the 100-cell stage, only small granules remained, and these were not enriched in the primordial germ cells Z2 and Z3 (Fig. 3A and fig. S4). We also monitored the distribution of two P granule–associated mRNAs, *cey-2* and *nos-2*. In wild-type embryos, *cey-2* and *nos-2* mRNAs segregate preferentially with P granules to the germline blastomeres; lower levels inherited by somatic blastomeres are rapidly degraded after division (*12*, *13*). In *pptr-1* embryos, *cey-2* and *nos-2* mRNAs were equally partitioned to somatic and germline blastomeres but were still degraded in somatic lineages after division (Fig. 3B and fig. S3C). Similarly, after the 30-cell stage, PGL-1 remaining in somatic lineages is degraded by the autophagy machinery in wild-type (*14*) and in *pptr-1* embryos (fig. S3B). We conclude that in *pptr-1* embryos, P granule proteins and RNAs are partitioned equally to somatic and germline blastomeres but behave differently after mitosis in each cell type. In germline blastomeres, P granule components remained stable and were reassembled into granules, albeit of diminishing size and number with each division. In somatic blastomeres, P granule RNAs were rapidly degraded; P granule proteins reassembled into granules after 1 or 2 cell cycles and were turned over after gastrulation.

Segregation of other asymmetric proteins, including PAR-2, PAR-1, and MEX-5, was not affected in *pptr-1* mutants (fig. S5A). Depletion of *mex-5/6* by RNAi in *pptr-1* mutants stabilized P granules in the anterior of the zygote and in somatic blastomeres during interphase but not during mitosis, indicating that MEX-5/6 are active but are not responsible for P granule disassembly during mitosis (fig. S5B). PIE-1 is a transcriptional repressor required to silence transcription in the P lineage (*15*). In the cytoplasm, PIE-1 is enriched on P granules, and this association has been proposed to drive PIE-1's preferential segregation into germline blastomeres (*16*). Consistent with the lack of P granules, in *pptr-1* embryos, GFP::PIE-1 was not enriched on granules during mitosis yet was still asymmetrically segregated (Fig. 4A and fig. S5A). We conclude that *pptr-1* is required specifically for P granule partitioning but is not required for the segregation of other germ plasm components, which can segregate independently of P granules.

If asymmetric partitioning of P granule components is necessary to distinguish germline from somatic blastomeres, then mutants like *pptr-1* should show defects in germline specification. Primordial germ cells do not form in *par-1*, *mex-5/6* mutants, and *mes-1* mutants (which missegregate P granules in the P_2 and P_3 blastomeres), but these mutants also missegregate other factors, notably PIE-1 (*17*, *18*). We found that primordial germ cells form normally in *pptr-1* embryos: By mid-embryogenesis, we detected two cells expressing the germline proteins NOS-1 and PGL-1 as is observed in wild type (*4*, *13*). NOS-1, which is expressed only zygotically, was expressed at the same level in wild-type and *pptr-1* embryos (Fig. 4A). In contrast, PGL-1, which is expressed both maternally and zygotically at this stage, was lower in *pptr-1* embryos, consistent with missegregation of maternal PGL-1 (Fig. 4A). We confirmed that *pptr-1* mutants express PGL-1 zygotically in primordial germ cells using a paternally inherited *pgl-1* transgene (fig. S5C). Consistent with proper germline specification, at 20°C, 100% of *pptr-1* adults (n = 5798) were self-fertile with a full germline. At higher temperatures (24°C and 26°C), however, a minority (~20%) of *pptr-1* adults were sterile (Fig. 4, B and C). Sterile *pptr-1* hermaphrodites had underdeveloped gonads with P granule–positive germ cells but no gametes (Fig. 4B). Stunted gonad development at high temperatures is characteristic of mutants lacking maternal PGL or GLH proteins (*6*, *19*), raising the possibility that the sterility of *pptr-1* mutants is caused by the P granule partitioning defect. Consistent with this hypothesis, we found that, at 20°C, 15% of *pptr-1;pgl-1* double mutants (n = 1191) were sterile, in contrast to the single mutants (1.3%, n = 1959 *pgl-1*; 0%, n = 5798 *pptr-1*). Furthermore, both the sterility and P granule defects of *pptr-1* mutants could be rescued by maternal *pptr-1* but not by zygotic *pptr-1* (Fig. 4C and fig. S6). We conclude that P granule partitioning during embryogenesis is not essential to specify germ cell fate but is required to promote robust germ cell proliferation and differentiation at high temperatures.

Our findings demonstrate that, in *C. elegans*, asymmetric partitioning of P granules during division can be uncoupled from the asymmetric partitioning of other germ plasm components (such as PIE-1) and is not essential to distinguish germline from soma. Even after inheriting equal levels of germ granule components, somatic and germline blastomeres maintain distinct fates. Therefore, why are germ granule components partitioned with the germ plasm? Our results suggest that partitioning increases stress resistance in the nascent germline by maximizing the maternal load of germ granule material inherited by primordial germ cells. In this regard, it is interesting that *pptr-1* also regulates insulin signaling (*10*), a pathway important for stress resistance. Many animals (including mammals) do not possess germ plasm and use inductive interactions to specify the germline. In those animals, germ granules are assembled de novo after germ cell specification (*20*). Our findings suggest that in animals with germ plasm, germ granule assembly is also a consequence, not a cause, of an underlying soma-germline distinction maintained by other factors.

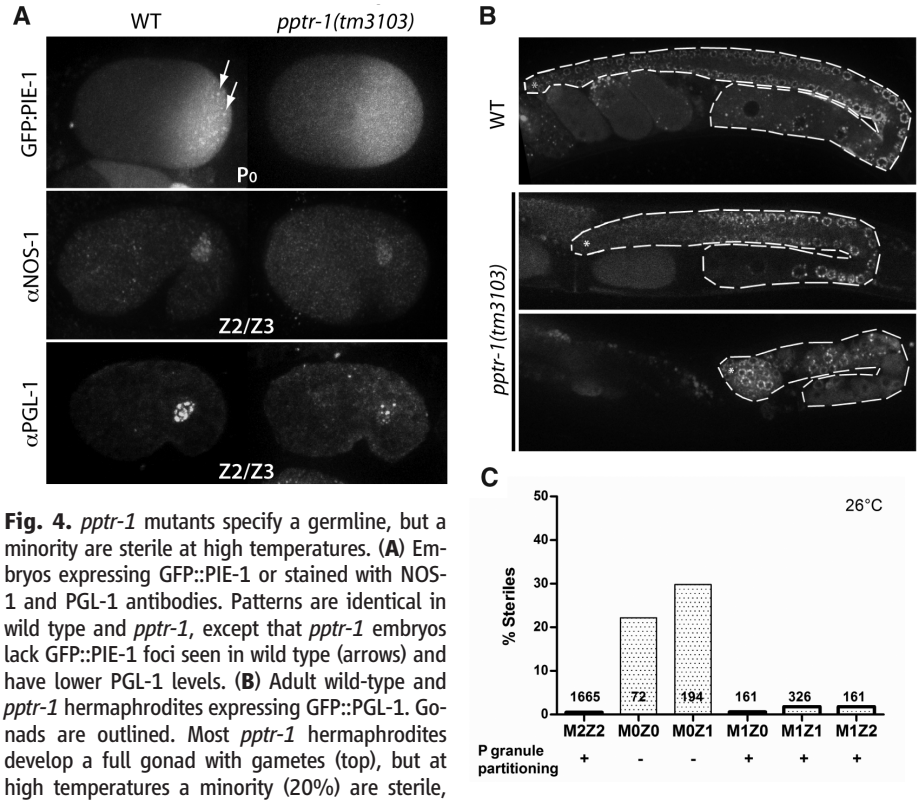

Fig. 4. *pptr-1* mutants specify a germline, but a minority are sterile at high temperatures. (**A**) Embryos expressing GFP::PIE-1 or stained with NOS-1 and PGL-1 antibodies. Patterns are identical in wild type and *pptr-1*, except that *pptr-1* embryos lack GFP::PIE-1 foci seen in wild type (arrows) and have lower PGL-1 levels. (**B**) Adult wild-type and *pptr-1* hermaphrodites expressing GFP::PGL-1. Gonads are outlined. Most *pptr-1* hermaphrodites develop a full gonad with gametes (top), but at high temperatures a minority (20%) are sterile, with no gametes (bottom). Fertile *pptr-1* gonads are smaller than wild type and yield a reduced number of progeny; unlike the P granule defect, however, the brood size defect is partially rescued by zygotic *pptr-1* (fig. S7). (**C**) Percentage of sterile hermaphrodites and total numbers scored. Wild type have two maternal and two zygotic *pptr-1* copies (M2Z2). Mutant *pptr-1* hermaphrodites (M0Z0) were crossed with wild-type males to generate M0Z1, which were allowed to self-fertilize to generate M1Z0, M1Z1, and M1Z2. Only M0Z0 and M0Z1 hermaphrodites show significant sterility, demonstrating maternal requirement. *pptr-1* is also required maternally for P granule partitioning (fig. S3).

References and Notes

1. S. Chuma, M. Hosokawa, T. Tanaka, N. Nakatsuji, *Mol. Cell. Endocrinol.* **306**, 17 (2009).
2. D. Updike, S. Strome, *J. Androl.* **31**, 53 (2010).
3. C. P. Brangwynne *et al.*, *Science* **324**, 1729 (2009).
4. I. Kawasaki *et al.*, *Cell* **94**, 635 (1998).
5. M. E. Gruidl *et al.*, *Proc. Natl. Acad. Sci. U.S.A.* **93**, 13837 (1996).
6. I. Kawasaki *et al.*, *Genetics* **167**, 645 (2004).
7. R. J. Cheeks *et al.*, *Curr. Biol.* **14**, 851 (2004).
8. E. Munro, B. Bowerman, *Cold Spring Harb. Perspect. Biol.* **1**, a003400 (2009).
9. C. M. Schubert, R. Lin, C. J. de Vries, R. H. Plasterk, J. R. Priess, *Mol. Cell* **5**, 671 (2000).
10. A. A. Cuenca, A. Schetter, D. Aceto, K. Kemphues, G. Seydoux, *Development* **130**, 1255 (2003).
11. S. Padmanabhan *et al.*, *Cell* **136**, 939 (2009).
12. G. Seydoux, A. Fire, *Development* **120**, 2823 (1994).
13. K. Subramaniam, G. Seydoux, *Development* **126**, 4861 (1999).
14. Y. Zhang *et al.*, *Cell* **136**, 308 (2009).
15. A. Nakamura, G. Seydoux, *Development* **135**, 3817 (2008).
16. B. R. Daniels, E. M. Perkins, T. M. Dobrowsky, S. X. Sun, D. Wirtz, *J. Cell Biol.* **184**, 473 (2009).
17. P. Gönczy, L. S. Rose, *WormBook* **2005**, 1 (2005).
18. S. Strome, *WormBook* **2005**, 1 (2005).
19. C. Spike *et al.*, *Genetics* **178**, 1973 (2008).
20. N. Kotaja, P. Sassone-Corsi, *Nat. Rev. Mol. Cell Biol.* **8**, 85 (2007).

21. We thank S. H. Kim, S. Strome, E. Voronina, K. Kemphues, K. Bennett, and C. Eckmann for reagents and advice. We also obtained reagents from the National Bioresource Project for the Nematode (Japan), the Caenorhabditis Genetics Center, and the Developmental Studies Hybridoma Bank (USA). This work was supported by NIH grants GM080042 to C.M.G., HD007276 to J.T.W., and HD037047 to G.S. G.S. is a Howard Hughes Medical Institute investigator. Plasmids are supplied under a Materials Transfer Agreement from the Howard Hughes Medical Institute.

Supporting Online Material

www.sciencemag.org/cgi/content/full/science.1193697/DC1
Materials and Methods
Figs. S1 to S7
Table S1
Movies S1 to S5
References

14 June 2010; accepted 3 November 2010
Published online 2 December 2010;
10.1126/science.1193697

Glucose and Weight Control in Mice with a Designed Ghrelin O-Acyltransferase Inhibitor

Brad P. Barnett,[1,2]* Yousang Hwang,[1]* Martin S. Taylor,[1,2]* Henriette Kirchner,[3,7] Paul T. Pfluger,[3] Vincent Bernard,[2] Yu-yi Lin,[2,6] Erin M. Bowers,[1] Chandrani Mukherjee,[1] Woo-Jin Song,[4] Patti A. Longo,[5] Daniel J. Leahy,[5] Mehboob A. Hussain,[4] Matthias H. Tschöp,[3,7] Jef D. Boeke,[2]† Philip A. Cole[1]†‡

Ghrelin is a gastric peptide hormone that stimulates weight gain in vertebrates. The biological activities of ghrelin require octanoylation of the peptide on Ser^3, an unusual posttranslational modification that is catalyzed by the enzyme ghrelin O-acyltransferase (GOAT). Here, we describe the design, synthesis, and characterization of GO-CoA-Tat, a peptide-based bisubstrate analog that antagonizes GOAT. GO-CoA-Tat potently inhibits GOAT in vitro, in cultured cells, and in mice. Intraperitoneal administration of GO-CoA-Tat improves glucose tolerance and reduces weight gain in wild-type mice but not in ghrelin-deficient mice, supporting the concept that its beneficial metabolic effects are due specifically to GOAT inhibition. In addition to serving as a research tool for mapping ghrelin actions, GO-CoA-Tat may help pave the way for clinical targeting of GOAT in metabolic diseases.

The persistent rise in the proportion of overweight individuals in Western society over the past 30 years has been associated with substantial excess morbidity and is widely recognized as a major public health concern. To address this problem, intensive efforts are under way to clarify nutrient-hormone interactions contributing to weight gain. Starting with the isolation of leptin (*1*), a series of hormones acting centrally and peripherally to influence body mass have been discovered. Among these, the gastric peptide hormone acyl ghrelin has generated considerable interest as an important stimulus for weight gain (*2*–*5*) and modulator of glucose homeostasis (*6*–*8*). Various strategies in therapeutic development have been devised to antagonize acyl ghrelin (*9*, *10*), although none has yet emerged as clinically beneficial. Acyl ghrelin has an unusual Ser^3 octanoylation; only acylated ghrelin can bind and activate the growth hormone secretagogue receptor (GHSR-1a). The cDNA for the enzyme responsible for this esterification, ghrelin O-acyltransferase (GOAT), has recently been cloned (*11*, *12*). GOAT has been suggested as a potential therapeutic target for modulating weight gain and glucose control, but this has not yet been directly tested (*9*, *13*). An acyl ghrelin product analog Dap-ghrelin blocks GOAT activity in a microsomal assay (*14*).

We designed bisubstrate analog GO-CoA-Tat based on the theory that if GOAT uses a ternary complex mechanism that templates octanoyl-CoA and ghrelin peptide, then linking the two substrates with a noncleavable bridge could combine the binding energies of the individual ligands without the entropic loss associated with forming the ternary complex (Fig. 1A). A related strategy has been used for other peptide-modifying enzymes, including histone acetyltransferases (HAT) and protein kinases (*15*, *16*). Because we were uncertain about the ghrelin peptide length needed for recognition by GOAT, we selected amino acids 1 to 10 for coupling to octanoyl-CoA to maximize inclusion of highly conserved ghrelin residues. An 11–amino acid oligomer HIV Tat-derived peptide sequence was also attached to the C terminus by an amino-hexanoyl linker to enhance cell penetration. Synthesis of this tripartite compound, GO-CoA-Tat (compound 1), was performed using a solid-phase strategy (Fig. 1B). A set of related analogs (compounds 2 to 6) with different peptide lengths and individual deletion of CoA, octyl, and Tat, respectively, were also synthesized (Fig. 2A) (*17*).

To analyze the cellular effects of GO-CoA-Tat, we generated two human cell lines [in HeLa (epithelial) and HEK (human embryonic kidney)] that stably express GOAT and preproghrelin (see fig. S1A) and show robust production of ghrelin in both its acyl and desacyl forms when grown in medium supplemented with octanoic acid. GO-CoA-Tat but not control compound D4-Tat (tetra-aspartate, to simulate the negative CoA charge, similarly linked to the Tat peptide) inhibited the production of acyl ghrelin but not desacyl ghrelin with a half-maximal inhibitory concentration of ~5 μM (Fig. 1 and fig. S1). Interestingly, maximal inhibition was achieved only after 24 hours of exposure to compound in both preproghrelin/GOAT-transfected HeLa and HEK cells (Fig. 1 and fig. S1). The slow kinetics might result from either atypical enzymatic characteristics or preformed acyl ghrelin stores. To further investigate this delay, we tested GO-CoA-Tat in vitro with recombinant microsomal GOAT (Fig. 2C and fig. S2) using a radioactive assay (*14*). Virtually complete GOAT inhibition was achieved with 100 nM GO-CoA-

[1]Department of Pharmacology and Molecular Sciences, Johns Hopkins University School of Medicine, Baltimore, MD 21205, USA. [2]Department of Molecular Biology and Genetics and High Throughput Biology Center, Johns Hopkins University School of Medicine, Baltimore, MD 21205, USA. [3]Obesity Research Center, Metabolic Diseases Institute, Department of Internal Medicine, University of Cincinnati, Cincinnati, OH 45237, USA. [4]Metabolism Division, Departments of Pediatrics, Medicine, and Biological Chemistry, Johns Hopkins University School of Medicine, Baltimore, MD 21205, USA. [5]Department of Biophysics and Biophysical Chemistry, Johns Hopkins University School of Medicine, Baltimore, MD 21205, USA. [6]Institute of Biochemistry and Molecular Biology, College of Medicine, National Taiwan University, Taipei 100, Taiwan. [7]Department of Pharmacology, German Institute of Human Nutrition, Potsdam-Rehbrücke, Arthur-Scheunert-Allee 114-116, 14558, Nuthetal, Germany.

*These authors contributed equally to this work.
†These authors contributed equally to this work.
‡To whom correspondence should be addressed. E-mail: pcole@jhmi.edu

References and Notes

1. S. Chuma, M. Hosokawa, T. Tanaka, N. Nakatsuji, *Mol. Cell. Endocrinol.* **306**, 17 (2009).
2. D. Updike, S. Strome, *J. Androl.* **31**, 53 (2010).
3. C. P. Brangwynne *et al.*, *Science* **324**, 1729 (2009).
4. I. Kawasaki *et al.*, *Cell* **94**, 635 (1998).
5. M. E. Gruidl *et al.*, *Proc. Natl. Acad. Sci. U.S.A.* **93**, 13837 (1996).
6. I. Kawasaki *et al.*, *Genetics* **167**, 645 (2004).
7. R. J. Cheeks *et al.*, *Curr. Biol.* **14**, 851 (2004).
8. E. Munro, B. Bowerman, *Cold Spring Harb. Perspect. Biol.* **1**, a003400 (2009).
9. C. M. Schubert, R. Lin, C. J. de Vries, R. H. Plasterk, J. R. Priess, *Mol. Cell* **5**, 671 (2000).
10. A. A. Cuenca, A. Schetter, D. Aceto, K. Kemphues, G. Seydoux, *Development* **130**, 1255 (2003).
11. S. Padmanabhan *et al.*, *Cell* **136**, 939 (2009).
12. G. Seydoux, A. Fire, *Development* **120**, 2823 (1994).
13. K. Subramaniam, G. Seydoux, *Development* **126**, 4861 (1999).
14. Y. Zhang *et al.*, *Cell* **136**, 308 (2009).
15. A. Nakamura, G. Seydoux, *Development* **135**, 3817 (2008).
16. B. R. Daniels, E. M. Perkins, T. M. Dobrowsky, S. X. Sun, D. Wirtz, *J. Cell Biol.* **184**, 473 (2009).
17. P. Gönczy, L. S. Rose, *WormBook* **2005**, 1 (2005).
18. S. Strome, *WormBook* **2005**, 1 (2005).
19. C. Spike *et al.*, *Genetics* **178**, 1973 (2008).
20. N. Kotaja, P. Sassone-Corsi, *Nat. Rev. Mol. Cell Biol.* **8**, 85 (2007).

21. We thank S. H. Kim, S. Strome, E. Voronina, K. Kemphues, K. Bennett, and C. Eckmann for reagents and advice. We also obtained reagents from the National Bioresource Project for the Nematode (Japan), the Caenorhabditis Genetics Center, and the Developmental Studies Hybridoma Bank (USA). This work was supported by NIH grants GM080042 to C.M.G., HD007276 to J.T.W., and HD037047 to G.S. G.S. is a Howard Hughes Medical Institute investigator. Plasmids are supplied under a Materials Transfer Agreement from the Howard Hughes Medical Institute.

Supporting Online Material

www.sciencemag.org/cgi/content/full/science.1193697/DC1
Materials and Methods
Figs. S1 to S7
Table S1
Movies S1 to S5
References

14 June 2010; accepted 3 November 2010
Published online 2 December 2010;
10.1126/science.1193697

Glucose and Weight Control in Mice with a Designed Ghrelin O-Acyltransferase Inhibitor

Brad P. Barnett,[1,2]* Yousang Hwang,[1]* Martin S. Taylor,[1,2]* Henriette Kirchner,[3,7] Paul T. Pfluger,[3] Vincent Bernard,[2] Yu-yi Lin,[2,6] Erin M. Bowers,[1] Chandrani Mukherjee,[1] Woo-Jin Song,[4] Patti A. Longo,[5] Daniel J. Leahy,[5] Mehboob A. Hussain,[4] Matthias H. Tschöp,[3,7] Jef D. Boeke,[2]† Philip A. Cole[1]†‡

Ghrelin is a gastric peptide hormone that stimulates weight gain in vertebrates. The biological activities of ghrelin require octanoylation of the peptide on Ser^3, an unusual posttranslational modification that is catalyzed by the enzyme ghrelin O-acyltransferase (GOAT). Here, we describe the design, synthesis, and characterization of GO-CoA-Tat, a peptide-based bisubstrate analog that antagonizes GOAT. GO-CoA-Tat potently inhibits GOAT in vitro, in cultured cells, and in mice. Intraperitoneal administration of GO-CoA-Tat improves glucose tolerance and reduces weight gain in wild-type mice but not in ghrelin-deficient mice, supporting the concept that its beneficial metabolic effects are due specifically to GOAT inhibition. In addition to serving as a research tool for mapping ghrelin actions, GO-CoA-Tat may help pave the way for clinical targeting of GOAT in metabolic diseases.

The persistent rise in the proportion of overweight individuals in Western society over the past 30 years has been associated with substantial excess morbidity and is widely recognized as a major public health concern. To address this problem, intensive efforts are under way to clarify nutrient-hormone interactions contributing to weight gain. Starting with the isolation of leptin (*1*), a series of hormones acting centrally and peripherally to influence body mass have been discovered. Among these, the gastric peptide hormone acyl ghrelin has generated considerable interest as an important stimulus for weight gain (*2*–*5*) and modulator of glucose homeostasis (*6*–*8*). Various strategies in therapeutic development have been devised to antagonize acyl ghrelin (*9*, *10*), although none has yet emerged as clinically beneficial. Acyl ghrelin has an unusual Ser^3 octanoylation; only acylated ghrelin can bind and activate the growth hormone secretagogue receptor (GHSR-1a). The cDNA for the enzyme responsible for this esterification, ghrelin O-acyltransferase (GOAT), has recently been cloned (*11*, *12*). GOAT has been suggested as a potential therapeutic target for modulating weight gain and glucose control, but this has not yet been directly tested (*9*, *13*). An acyl ghrelin product analog Dap-ghrelin blocks GOAT activity in a microsomal assay (*14*).

We designed bisubstrate analog GO-CoA-Tat based on the theory that if GOAT uses a ternary complex mechanism that templates octanoyl-CoA and ghrelin peptide, then linking the two substrates with a noncleavable bridge could combine the binding energies of the individual ligands without the entropic loss associated with forming the ternary complex (Fig. 1A). A related strategy has been used for other peptide-modifying enzymes, including histone acetyltransferases (HAT) and protein kinases (*15*, *16*). Because we were uncertain about the ghrelin peptide length needed for recognition by GOAT, we selected amino acids 1 to 10 for coupling to octanoyl-CoA to maximize inclusion of highly conserved ghrelin residues. An 11–amino acid oligomer HIV Tat-derived peptide sequence was also attached to the C terminus by an amino-hexanoyl linker to enhance cell penetration. Synthesis of this tripartite compound, GO-CoA-Tat (compound 1), was performed using a solid-phase strategy (Fig. 1B). A set of related analogs (compounds 2 to 6) with different peptide lengths and individual deletion of CoA, octyl, and Tat, respectively, were also synthesized (Fig. 2A) (*17*).

To analyze the cellular effects of GO-CoA-Tat, we generated two human cell lines [in HeLa (epithelial) and HEK (human embryonic kidney)] that stably express GOAT and preproghrelin (see fig. S1A) and show robust production of ghrelin in both its acyl and desacyl forms when grown in medium supplemented with octanoic acid. GO-CoA-Tat but not control compound D4-Tat (tetra-aspartate, to simulate the negative CoA charge, similarly linked to the Tat peptide) inhibited the production of acyl ghrelin but not desacyl ghrelin with a half-maximal inhibitory concentration of ~5 μM (Fig. 1 and fig. S1). Interestingly, maximal inhibition was achieved only after 24 hours of exposure to compound in both preproghrelin/GOAT-transfected HeLa and HEK cells (Fig. 1 and fig. S1). The slow kinetics might result from either atypical enzymatic characteristics or preformed acyl ghrelin stores. To further investigate this delay, we tested GO-CoA-Tat in vitro with recombinant microsomal GOAT (Fig. 2C and fig. S2) using a radioactive assay (*14*). Virtually complete GOAT inhibition was achieved with 100 nM GO-CoA-

[1]Department of Pharmacology and Molecular Sciences, Johns Hopkins University School of Medicine, Baltimore, MD 21205, USA. [2]Department of Molecular Biology and Genetics and High Throughput Biology Center, Johns Hopkins University School of Medicine, Baltimore, MD 21205, USA. [3]Obesity Research Center, Metabolic Diseases Institute, Department of Internal Medicine, University of Cincinnati, Cincinnati, OH 45237, USA. [4]Metabolism Division, Departments of Pediatrics, Medicine, and Biological Chemistry, Johns Hopkins University School of Medicine, Baltimore, MD 21205, USA. [5]Department of Biophysics and Biophysical Chemistry, Johns Hopkins University School of Medicine, Baltimore, MD 21205, USA. [6]Institute of Biochemistry and Molecular Biology, College of Medicine, National Taiwan University, Taipei 100, Taiwan. [7]Department of Pharmacology, German Institute of Human Nutrition, Potsdam-Rehbrücke, Arthur-Scheunert-Allee 114-116, 14558, Nuthetal, Germany.

*These authors contributed equally to this work.
†These authors contributed equally to this work.
‡To whom correspondence should be addressed. E-mail: pcole@jhmi.edu

Tat within 5 min (Fig. 2C and fig. S2), suggesting that the delay in reduction of cellular acyl ghrelin levels may reflect a substantial preexisting intracellular reservoir. We also showed that two chemically modified versions of the inhibitor, GO-CoA-Tat-F4BP and GO-CoA-Tat-L5BP, in which Phe[4] or Leu[5], respectively, is replaced with a photoreactive amino acid benzoyl-phenylalanine and each is tagged with a biotin group, can covalently cross-link to recombinant solubilized or microsomal GOAT, providing evidence for direct binding of GO-CoA-Tat (Fig. 2D and fig. S2C). This cross-linking interaction appears to be specific, because it can be blocked by GO-CoA-Tat (Fig. 2D and fig. S2C).

GO-CoA-Tat appears to be a selective GOAT antagonist because at 10 μM, it showed less than 15% inhibition of three acetyl-CoA–utilizing enzymes in vitro, including p300 HAT, p300/CBP-associated factor HAT, and serotonin N-acetyltransferase (fig. S3A). Moreover, GO-CoA-Tat appears nontoxic to cell viability in the concentration range studied and does not antagonize the GHSR-1a receptor (fig. S3, B to G). A broader analysis of GO-CoA-Tat (*1*) and analogs (*2*–*6*) reveals a requirement for at least 10 ghrelin residues, as well as the CoA, octanoyl, and Tat components, respectively, for the most potent cellular inhibition of cellular GOAT (Fig. 2, A and B). These results are consistent with GO-CoA-Tat behaving as a bona fide bisubstrate analog in antagonizing GOAT activity. Furthermore, the requirement for the Tat sequence for inhibitory activity (see compound 6, Fig. 2B) argues that cell penetration is critical, and the compound is not acting on a cell surface receptor.

To examine whether GO-CoA-Tat blocks acyl ghrelin production in mice, we explored the effect of intraperitoneally delivered GO-CoA-Tat at 11 μmol/kg (40 mg per kg of body weight) in wild-type (WT) C57BL6 animals on a medium-chain triglyceride (MCT) diet (*13*). Treatment with GO-CoA-Tat, but not D4-Tat control or vehicle, led to decreased serum levels of acyl ghrelin (Fig. 3A and fig. S4, C and D), with maximum inhibition 6 hours after administration (Fig. 3A). There was

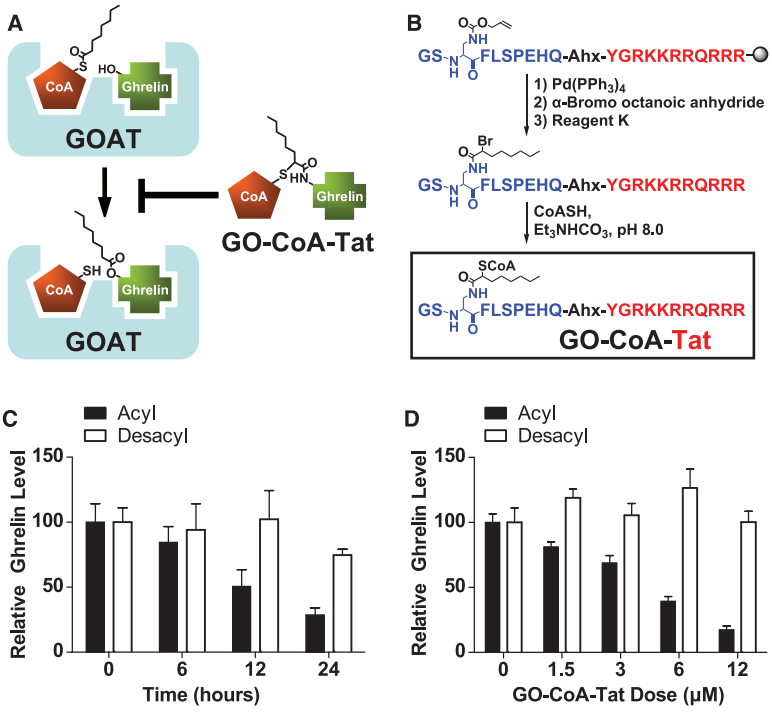

Fig. 1. GO-CoA-Tat is a bisubstrate inhibitor that inhibits GOAT, lowering acyl ghrelin levels. (**A**) Mechanism-based design strategy. Lipid-enzyme interaction, not shown, may also be important. (**B**) Structure of GO-CoA-Tat and synthetic scheme for bisubstrate inhibitors that consist of three components: coenzyme A (CoA), octanoylated ghrelin peptide (GO), and a Tat peptide. Ahx, aminohexanoate. (**C**) Temporal inhibition of acyl but not desacyl ghrelin production by 6 μM GO-CoA-Tat in GOAT/preproghrelin-transfected HeLa cells. (**D**) Dose-response reduction of acyl but not desacyl ghrelin levels by GO-CoA-Tat in GOAT/preproghrelin-transfected HeLa cells after 24 hours of incubation.

Fig. 2. GO-CoA-Tat targets GOAT directly in vitro and in a structure-specific manner. (**A**) Structure of GO-CoA-Tat analogs (1 to 6). (**B**) Acyl and desacyl ghrelin levels after treatment with 6 μM GO-CoA-Tat (1) and analogs (2 to 6) from GOAT/preproghrelin-transfected HeLa cells after 24 hours. (**C**) In vitro acyltransferase inhibition assay (5-min reaction) with microsomal recombinant GOAT. (**D**) Ultraviolet-induced cross-linking of solubilized GOAT by biotin-tagged, benzophenylalanine analogs of GO-CoA-Tat (L5BP, F4BP) (5 μM). Competitor is GO-CoA-Tat at 100 μM. Immunoblots of cross-linked GOAT were visualized with streptavidin; loading was checked with antibody to FLAG.

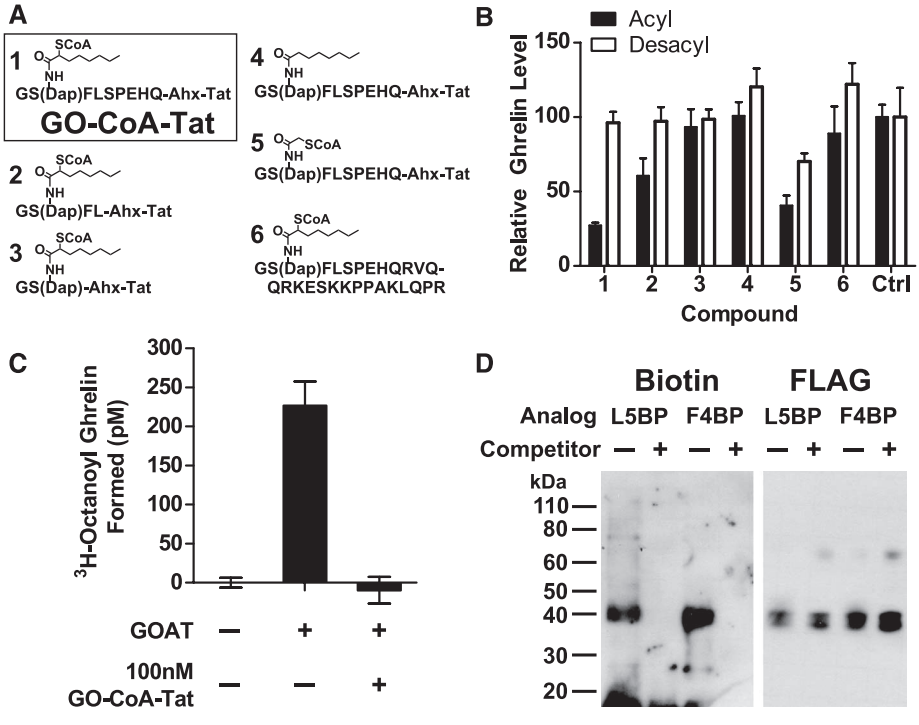

no significant effect on serum levels of desacyl ghrelin (Fig. 3B). Because the average ghrelin levels were found to vary considerably among mice, the statistical significance was most clear when acyl ghrelin was expressed as a percent of the total (Fig. 3C). These results strongly suggest that GO-CoA-Tat targets GOAT in vivo.

We next examined the effect of GO-CoA-Tat on weight gain. WT mice were fed an MCT diet over a 1-month period. These mice were treated every 24 hours with GO-CoA-Tat (11 μmol/kg intraperitoneally) and monitored daily for body mass. In addition, the mice were subjected to quantitative magnetic resonance (QMR) spectroscopy to evaluate the animals' fat and lean mass (*13*). These experiments showed that chronic GO-CoA-Tat treatment in mice prevented the significant weight gain observed in vehicle-treated mice on an MCT-rich high-fat diet (Fig. 3D). Moreover, the QMR measurements showed that, relative to controls, the GO-CoA-Tat–treated animals displayed significantly lower fat mass, but not lean mass (Fig. 3E and fig. S4, A and B).

To investigate the potential for GO-CoA-Tat–induced generalized toxicity as a source of weight loss, we assessed the blood chemistries and blood cell counts in the animals after 1 month of GO-CoA-Tat treatment. These analyses showed no evidence of liver, renal, pancreas, or bone marrow toxicities that could account for weight loss (fig. S5). Notably, GO-CoA-Tat–treated mice displayed lower blood glucose as well as lower levels of insulin-like growth factor 1, which is consistent with endogenous acyl ghrelin modulating the somatotropic axis (fig. S5).

To further understand the effects of GO-CoA-Tat, we studied its effects on body weight and adiposity in ghrelin knockout mice. In contrast to its behavior in WT mice, GO-CoA-Tat did not significantly alter weight, fat, or lean mass in ghrelin knockout mice (Fig. 3, F and G, and fig. S4B). In a separate long-term treatment study, we confirmed that during the course of 1 month of GO-CoA-Tat administration, ghrelin knockout mice gained more weight than otherwise genetically and age-matched WT mice (fig. S6A). Because initial body weights in ghrelin knockout mice were reduced compared with WT mice (19.7 g versus 21.5 g), these data suggest that the GO-CoA-Tat treatment in the WT animals induces functional loss of ghrelin, bringing WT and knockout animals closer together. The food intake in these GO-CoA-Tat–treated WT and ghrelin knockout mice was similar (fig. S6B), suggesting that the weight differences might be caused by differences in metabolic activity as suggested by recent GOAT knockout studies (*13*), although we have not directly tested this. Finally, in an additional WT mouse study, we showed that GO-CoA-Tat slowed weight gain in WT mice fed a high-fat diet. In that study, we observed a relative reduction of fat mass without a change in lean mass, but no effect on food intake (fig. S7). Taken together, these studies suggest that GO-CoA-Tat can specifically reduce acyl ghrelin through GOAT inhibition and thereby prevent weight gain in mice.

It has been reported that acyl ghrelin can influence glucose homeostasis and insulin secretion in pancreatic islet cells (*6–8*, *18–20*), although the precise impact has varied among different studies (*8*, *13*, *20–22*). We pretreated human islet cells with GO-CoA-Tat and showed that these cells displayed a statistically significant increase in insulin response to a glucose challenge when exposed to GO-CoA-Tat (fig. S8). These results suggest that acyl ghrelin plays a direct role in blunting insulin response, similar to what has recently been reported in humans (*22*). To investigate this in vivo, we studied WT mice that received an intraperitoneal glucose challenge of 2.5 g/kg after pretreatment with GO-CoA-Tat. These mice show a significant increase in insulin response (Fig. 4A) that was accompanied by a reduction in blood glucose (Fig. 4B). We repeated this glucose challenge in ghrelin knockout animals, and, under these conditions, GO-CoA-Tat did not have a significant effect compared either to vehicle

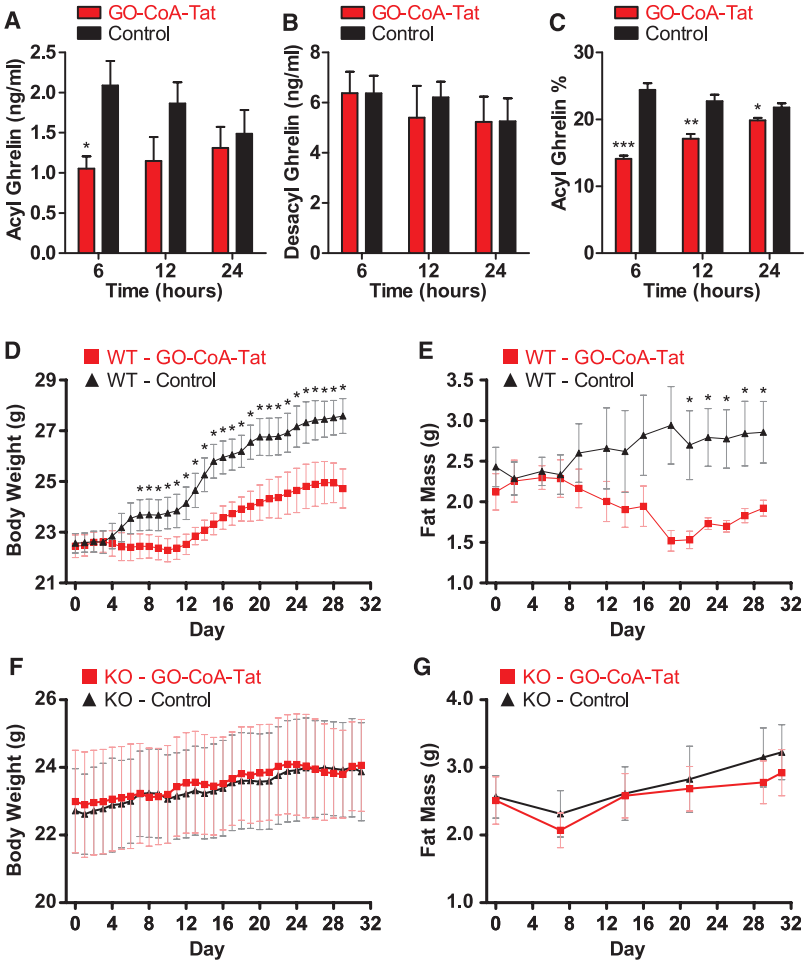

Fig. 3. Effects of GO-CoA-Tat on blood ghrelin and body weight in mice. (**A**) Serum acyl ghrelin levels in WT C57BL6 mice on an MCT diet treated intraperitoneally with 11 μmol/kg GO-CoA-Tat versus D4-Tat control (n = 5) after 6, 12, and 24 hours (*P < 0.05, **P < 0.01, ***P < 0.001, SEM shown). The changes in acyl ghrelin over 24 hours in control animals are neither statistically significant (P > 0.2) nor reproducible in other experiments. (**B**) Serum desacyl ghrelin levels for experiment in (A). (**C**) Percent acyl ghrelin for experiment in (A). (**D**) Body weights in WT C57BL6 mice on an MCT diet treated with 11 μmol/kg GO-CoA-Tat (red, n = 5) or vehicle (black, n = 6) for 1 month (*P < 0.05; conventional ** and *** omitted for clarity, SEM shown). (**E**) Fat mass in WT mice measured by QMR for experiment in (D). (**F**) Body weights in ghrelin knockout C57BL6 mice on an MCT diet treated with 11 μmol/kg GO-CoA-Tat (red, n = 5) or vehicle (black, n = 5) for 1 month (SEM shown). The larger error bars compared with data in (D) likely represent the broader distribution of starting weights. Also note that the scales differ in the two panels, contributing to the larger error bars seen here. (**G**) Fat mass in ghrelin knockout mice measured by QMR for experiment in (F).

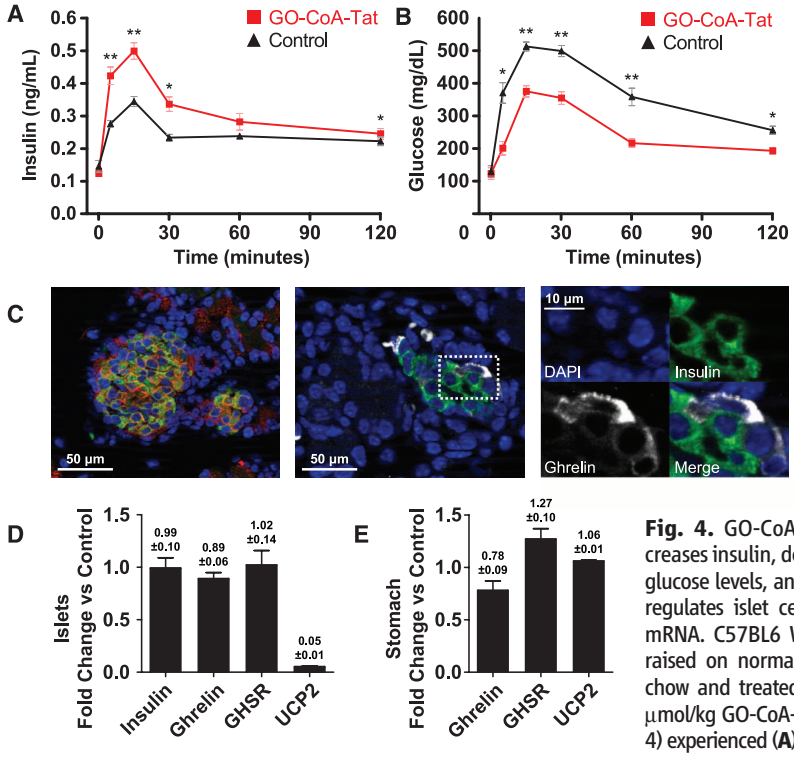

Fig. 4. GO-CoA-Tat increases insulin, decreases glucose levels, and down-regulates islet cell *UCP2* mRNA. C57BL6 WT mice raised on normal mouse chow and treated with 8 μmol/kg GO-CoA-Tat (n = 4) experienced (**A**) a statistically significant increase in insulin secretion and (**B**) a statistically significant decrease in blood glucose as compared with control mice [treated with D4-Tat (n = 4)] when compound was administered 24 hours before intraperitoneal glucose challenge (2.5 g/kg) (*P < 0.05, **P < 0.01, SEM shown). (**C**) Immunohistochemical staining of mouse islets. (Left) Insulin (green), ghrelin receptor (GHSR) (red), and cell nuclei stained with 4′,6′-diamidino-2-phenylindole (blue). (Middle) Staining of islet for ghrelin (white) and insulin (green) demonstrates dual staining and ghrelin-positive and insulin-negative cells. (Right) Close-up of unmerged images in boxed area of middle panel. (**D**) QRT-PCR of islets and (**E**) gastric fundus isolated from mice treated with inhibitor 24 hours before isolation and mRNA expression relative to control (n = 3).

or to its impact on WT animals analyzed in parallel (fig. S9). These data support the hypothesis that GO-CoA-Tat's effects on glucose regulation are mediated by acyl ghrelin inhibition. It is interesting that glucose tolerance tests in GOAT knockout versus WT mice have shown mixed results (*13*, *20*), which may suggest that the acute pharmacologic action of acyl ghrelin inhibition is important for the insulin and glucose response observed here.

To further investigate the connection between GOAT inhibition and insulin regulation, we studied pancreatic islets isolated from mice treated with GO-CoA-Tat. As shown in Fig. 4, the insulin-producing ß cells stained positive for GHSR and islets exhibited a small population of ghrelin-expressing cells, which are distinct from ß cells (Fig. 4C). Quantitative real-time fluorescence polymerase chain reaction (QRT-PCR) of islets isolated from mice treated with GO-CoA-Tat demonstrated a reduction by a factor of 20 in *UCP2* mRNA (encoding uncoupling protein 2, a suppressor of insulin secretion) levels as compared with islets isolated from D4-Tat–treated mice (Fig. 4D) but no change in levels of insulin, ghrelin, or GHSR mRNAs. Additionally, QRT-PCR showed non–statistically significant effects on *UCP2* in the gastric fundus (Fig. 4E). Taken together, these data point to a tissue-specific role for GOAT inhibition in suppressing *UCP2* levels and enhancing insulin release in response to glucose. That GOAT inhibition modulates *UCP2* levels so dramatically further substantiates the connection of acyl ghrelin to obesity and type 2 diabetes (*23*–*25*).

Directly targeting the biosynthesis of the active acyl ghrelin hormone offers several potential advantages over receptor antagonists. First, these enzyme inhibitors may not need to cross the blood-brain barrier, unlike acyl ghrelin receptor blockers, for which many of the key sites of action are in the brain (*2*, *26*). Second, receptor antagonists may drive higher acyl ghrelin formation and increase acyl/desacylin ghrelin ratios (*21*, *26*–*28*) that could be blunted by targeting the biosynthetic pathway. Finally, targeting an enzyme may have advantages over targeting an abundant receptor. Although GOAT inhibitor GO-CoA-Tat has some limitations as a peptide-based agent, we anticipate that future synthetic derivatization will be able to further maximize its pharmacodynamic and/or pharmacokinetic properties. This report lays the foundation for an approach to pharmacologic management of metabolic disorders through targeted GOAT blockade. We note that this strategy also has potential application to the targeting of other GOAT-related mBOAT (membrane bound O-acyl transferase) family members implicated in lipid metabolism and in important cancer-related signaling pathways such as hedgehog and Wnt (*29*).

References and Notes

1. M. Rosenbaum *et al.*, *J. Clin. Endocrinol. Metab.* **81**, 3424 (1996).
2. M. Kojima *et al.*, *Nature* **402**, 656 (1999).
3. M. Tschöp, D. L. Smiley, M. L. Heiman, *Nature* **407**, 908 (2000).
4. A. M. Wren *et al.*, *Diabetes* **50**, 2540 (2001).
5. J. M. Zigman *et al.*, *J. Clin. Invest.* **115**, 3564 (2005).
6. T. Yada *et al.*, *Curr. Diabetes Rev.* **4**, 18 (2008).
7. K. Dezaki, M. Kakei, T. Yada, *Diabetes* **56**, 2319 (2007).
8. Y. Sun, M. Asnicar, P. K. Saha, L. Chan, R. G. Smith, *Cell Metab.* **3**, 379 (2006).
9. O. Gualillo, F. Lago, C. Dieguez, *Trends Pharmacol. Sci.* **29**, 398 (2008).
10. S. C. Lu *et al.*, *Mol. Pharmacol.* **75**, 901 (2009).
11. J. A. Gutierrez *et al.*, *Proc. Natl. Acad. Sci. U.S.A.* **105**, 6320 (2008).
12. J. Yang, M. S. Brown, G. Liang, N. V. Grishin, J. L. Goldstein, *Cell* **132**, 387 (2008).
13. H. Kirchner *et al.*, *Nat. Med.* **15**, 741 (2009).
14. J. Yang, T. J. Zhao, J. L. Goldstein, M. S. Brown, *Proc. Natl. Acad. Sci. U.S.A.* **105**, 10750 (2008).
15. O. D. Lau *et al.*, *Mol. Cell* **5**, 589 (2000).
16. K. Parang *et al.*, *Nat. Struct. Biol.* **8**, 37 (2001).
17. Materials and methods are available as supporting material on *Science* Online.
18. K. Dezaki, H. Sone, T. Yada, *Pharmacol. Ther.* **118**, 239 (2008).
19. R. Granata, A. Baragli, F. Settanni, F. Scarlatti, E. Ghigo, *J. Mol. Endocrinol.* **45**, 107 (2010).
20. T. J. Zhao *et al.*, *Proc. Natl. Acad. Sci. U.S.A.* **107**, 7467 (2010).
21. C. Gauna *et al.*, *J. Clin. Endocrinol. Metab.* **90**, 1055 (2005).
22. J. Tong *et al.*, *Diabetes* **59**, 2145 (2010).
23. C. Y. Zhang *et al.*, *Cell* **105**, 745 (2001).
24. J. W. Joseph *et al.*, *Diabetes* **51**, 3211 (2002).
25. Z. B. Andrews *et al.*, *Nature* **454**, 846 (2008).
26. F. Broglio *et al.*, *J. Clin. Endocrinol. Metab.* **89**, 3062 (2004).
27. H. Ariyasu *et al.*, *Endocrinology* **146**, 355 (2005).
28. W. Zhang, B. Chai, J. Y. Li, H. Wang, M. W. Mulholland, *Endocrinology* **149**, 4710 (2008).
29. K. Hofmann, *Trends Biochem. Sci.* **25**, 111 (2000).

30. We thank M. Shamblott, S. Bhat, A. Chambers, C. Schrum, J. Hembree, N. Forbes, M. Li, J. McClellan, M. Miller, K. O'Donnell-Mendell, J. Jabbari, W. Gibson, J. Liu, and D. Gladowski for advice and assistance; G. Ronnett, J. Liu, and R. Alani for critical reading of the manuscript; and the NIH Common Fund, Pfeiffer Foundation, Kaufman Foundation, and Keck Foundation for financial support. The authors (P.A.C., J.D.B., Y.H., and B.P.B.) and Johns Hopkins University have filed a patent on the GOAT inhibitors described here. The inhibitors have been licensed to the biotechnology company Acylin Therapeutics, Inc. P.A.C., J.D.B., and M.H.T. are on the Scientific Advisory Board and have equity in Acylin Therapeutics. M.H.T. also has equity in and is a member of the Scientific Advisory Boards of Marcadia Biotech, Inc., and Ambrx, Inc.

Supporting Online Material

www.sciencemag.org/cgi/content/full/science.1196154/DC1
Materials and Methods
Figs. S1 to S10
References

6 August 2010; accepted 2 November 2010
Published online 18 November 2010;
10.1126/science.1196154

The Cellular and Physiological Mechanism of Wing-Body Scaling in *Manduca sexta*

H. Frederik Nijhout* and Laura W. Grunert

In animals, appendages develop in proportion to overall body size; when individual size varies, appendages covary proportionally. In insects with complete metamorphosis, adult appendages develop from precursor tissues called imaginal disks that grow after somatic growth has ceased. It is unclear, however, how the growth of these appendages is matched to the already established body size. We studied the pattern of cell division in the tobacco hornworm *Manduca sexta* and found that both the rate of cell division and the duration of growth of the wing imaginal disks depend on the size of the body in which they develop. Moreover, we found that both of these processes are controlled by the level and duration of secretion of the steroid hormone ecdysone. Thus, proportional growth is under hormonal control and indirectly regulated by the central nervous system.

The relative sizes of body parts are among the most characteristic traits of animals (*1*–*3*), and although methods for the analysis of scaling of appendages and other body parts have been described (*3*–*6*), the underlying developmental mechanisms that coordinate the relative sizes of body parts with overall body size remain largely unknown. Body size is determined by genetic and environmental factors. In a constant and optimal environment, insects grow to a characteristic species-specific size. Variation in nutrition and temperature can impose systematic deviations from this species-characteristic size. Increased rearing temperature typically results in smaller body size (*7*–*9*). In the tobacco hornworm *Manduca sexta*, the developmental mechanism underlying this temperature-size interaction is well understood (*8*). Nutrition, too, can have a profound effect on body size (*7*, *10*, *11*); in *Manduca*, variation in nutrition can result in variation in adult body mass by more than a factor of 2 (*12*).

Wings develop internally as imaginal disks. These disks undergo most of their growth after the larva has stopped feeding and growing (*13*, *14*). At this stage, the forewing imaginal disk has a dry mass of 0.12 (±0.03) mg. The dry mass of an adult forewing is 26 (±0.6) mg, so >99% of a wing's growth in mass occurs after the larva has stopped feeding. Small-bodied adults that develop from undernourished larvae have proportionally small wings, as expected. This raises an interesting problem, however, because the wings do not grow at the same time as the body. We sought to identify the mechanism that causes the wing disks to grow less when they develop in a small body than in a large body.

To investigate how control over the proportional growth of wings is exercised, we developed a system that reliably causes *Manduca* individuals to develop to half their normal adult size by taking advantage of the weight at which the endocrine events that culminate in the cessation of growth and metamorphosis are set in motion (the critical weight) in *Manduca*. Critical weight occurs in the middle of the last larval instar (*15*, *16*). The last (fifth) larval instar is divided into the feeding phase, during which the larva grows from about 1.2 g to about 12.5 g, and the wandering phase, during which the larva purges its gut contents in preparation for pupation. In the strain used for this study, the critical weight is about 6.5 g, and larvae enter the wandering stage at about 12.5 g, 2.5 days after passing the critical weight.

When larvae were starved at a weight of 6.5 g, their development time to the wandering stage was identical to that of larvae that were allowed to continue feeding. Such starved larvae developed into normally proportioned adults of about half the mass of normally feeding controls, with wings half the mass of normally feeding controls and having about half the number of cells. Thus, the smaller wing size in adults that developed from undernourished larvae was due to a reduction in cell number in almost exact proportion to the diminution in wing size. Because the number of cells in the diminished wing was half of that in a normal wing, the two must differ by one cell division, on average. We thus sought to determine whether that missing cell division was averaged across the entire development of the wing or whether a cell division was missing at a particular time in development.

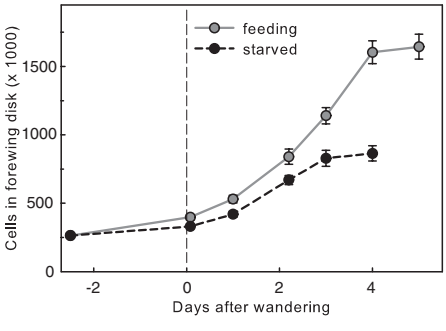

Fig. 1. Growth of forewing imaginal disks during the wandering stage in normally feeding larvae and in larvae starved at 6.5 g (first time point). The wings of starved larvae stopped growing about 1 day before those of normally fed larvae. Each point is the mean of three to five individuals. Error bars show SEM.

In normal development, there are 390,000 (±18,000) cells in the wing disk at the time a larva passes the critical weight, 1.64 million (±91,000) cells at the beginning of the pupal stage, and 8.59 million (±56,000) cells by the time cell division stops and the wing is fully developed. If we assume that all cells of the wing divide, then on average 2.06 cell divisions occur between the critical weight and pupation and 2.38 cell divisions occur between pupation and the fully developed wing.

We examined the pattern of growth of the forewing imaginal disks, beginning at the critical weight. Cell division in the wing disk stops during the fourth day of the wandering stage, about 24 hours before pupation; it resumes again 48 hours after pupation and stops permanently 6 days later. The growth trajectories of forewing disks of normally fed control and starved larvae (Fig. 1) show that the wing disks of starved larvae grew slower than those of fed larvae. The doubling time of cells in the wing disks during the first 3 days of growth in the wandering stage was calculated to be 1.96 days in control larvae and 2.12 days in starved larvae (see supporting online material).

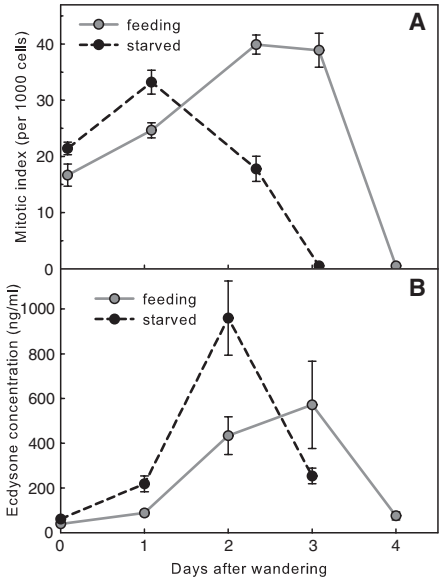

Fig. 2. (**A**) Mitotic index (metaphases per 1000 cells) during the wandering stage of wing imaginal disks of normally fed control larvae and larvae starved at 6.5 g. Each point represents the mean of three to five individuals. (**B**) Ecdysone titers (in 20E equivalents) in the hemolymph during the wandering stage of normally fed control larvae and larvae starved at 6.5 g. Each point represents the mean of five to seven individuals assayed in triplicate. Error bars show SEM.

Department of Biology, Duke University, Durham, NC 27705, USA.

*To whom correspondence should be addressed. E-mail: hfn@duke.edu

In addition to having a lower growth rate, the disks of starved larvae stopped growing a full day before those of normally fed controls (Fig. 1). At the beginning of the wandering stage, the number of cells in the wing disks of starved larvae was 85% of that in controls, and when the disks stopped growing, those from starved larvae had 52% of the number of cells found in controls (Fig. 1). The temporal pattern of mitoses in wing disks during the wandering stage of normally fed and starved larvae (Fig. 2A) shows that cell proliferation was slower after the first day and terminated a day earlier in starved larvae.

In the pupal stage, cell division resumed about 48 hours after pupation, continued for 5 days, and then stopped permanently in both feeding and starved individuals, with no differences in the duration of cell division. Pupae from feeding larvae had 1.64 million (±91,000) cells at the beginning and 8.59 million (±56,000) cells at the end of the growth phase. Pupae from starved larvae had 860,000 (±48,000) cells at the beginning and 4.73 million (±42,000) cells at the end of the growth phase. Thus, in both fed and starved larvae, the number of cells in the developing pupal wing increased by a factor of 5.35 (*t* test: $P_{fed} = 0.197$; $P_{starved} = 0.714$). We conclude that the size difference between the wings of adults produced from fed and starved larvae was almost entirely due to differences in growth during the wandering phase. We estimate that the reduction of the growth rate alone, with an identical duration of growth period, would result in a 74% reduction in wing size. Similarly, a reduction of the growth period by 1 day would result in a 73% reduction in wing size. Therefore, reduced growth rate and development time contribute equally to the reduction of wing size at smaller body size.

We suspected that one or more insect developmental hormones might control the pattern of cellular growth. In *Manduca* and *Precis*, both ecdysone and bombyxin (an insect insulin-like growth factor) are required for growth of the wing imaginal disks in vitro (*13*, *14*). Likewise, in *Drosophila* and other insects, ecdysone and insulin-like growth factors are known to regulate growth and size (*17*–*23*). We examined the profile of ecdysteroid titers during the wandering stage of normally fed and starved *Manduca* larvae (Fig. 2B). In starved larvae, ecdysone secretion stopped earlier and its levels rose higher than in fed larvae.

These findings suggest that the duration of the wandering phase may be determined by the decline in ecdysone, and that high levels of ecdysone reduce the rate of cell division. Declining titers of ecdysone act as timers of developmental events during insect metamorphosis (*24*–*26*), and we examined whether declining ecdysteroids were responsible for terminating the wandering phase. We injected fed larvae with 50 μg of 20-hydroxyecdysone (20E) on days 3 and 4 of the wandering stage, a time when their endogenous ecdysteroids are declining. These injections extended the wandering phase by an average of 18 hours (Fig. 3A).

The resulting adults did not have larger wings than those of saline-injected controls; indeed, contrary to our expectation, their wings were significantly smaller (Fig. 3B), which suggests that the injected 20E inhibited wing growth. In comparison, injections of a human insulin at various times during the wandering stage had no effect on the duration of the wandering phase, nor on the size of the adult wings (*t* test, $P = 0.323$). In *Drosophila*, wing and body size are controlled by both ecdysone and insulin signaling (*17*–*21*), and in Lepidoptera, in vitro culture has revealed that wing disks require both insulin and ecdysone for normal growth; the two act synergistically, and either factor by itself induces only minor growth (*13*, *14*). The fact that insulin injection had no effect on wing size in wandering-stage larvae suggests that insulin was not limiting at this stage and that variation in ecdysone signaling is the only relevant factor. Insulin is typically involved in the regulation of nutrient-dependent growth (*11*, *27*, *28*), and because the wandering-stage larva does not feed, it is possible that insulin does not vary during this stage.

To investigate the possible inhibitory effect of 20E, we ligated larvae behind the head 6 hours after initiation of the wandering stage. Neck ligation isolates the body and wing disks from brain-derived neurosecretory hormones such as bombyxin (the lepidopteran insulin-like growth factor) and the prothoracicotropic hormone (PTTH), which stimulates secretion of ecdysteroids. After waiting 24 hours for endogenous hormones to decay, we injected these larvae with three doses of 20E at 24-hour intervals and compared the sizes of their wing disks to those of saline-injected controls (Fig. 3C). We observed an optimal dosage of about 15 to 20 μg that induced maximal wing growth. Doses below and above this optimum induced substantially less growth in the wing disks.

We conclude that the early termination of the wandering phase in starved larvae was caused by the early decline of ecdysteroid titers, which terminated the growth period of the wing disks. The decrease in the growth rate of the disks during the wandering phase appears to be caused by an elevated titer of ecdysteroids, surpassing the optimal level that promotes growth. This finding suggests that ecdysone levels can modulate tissue growth rates. Our conclusions are further supported

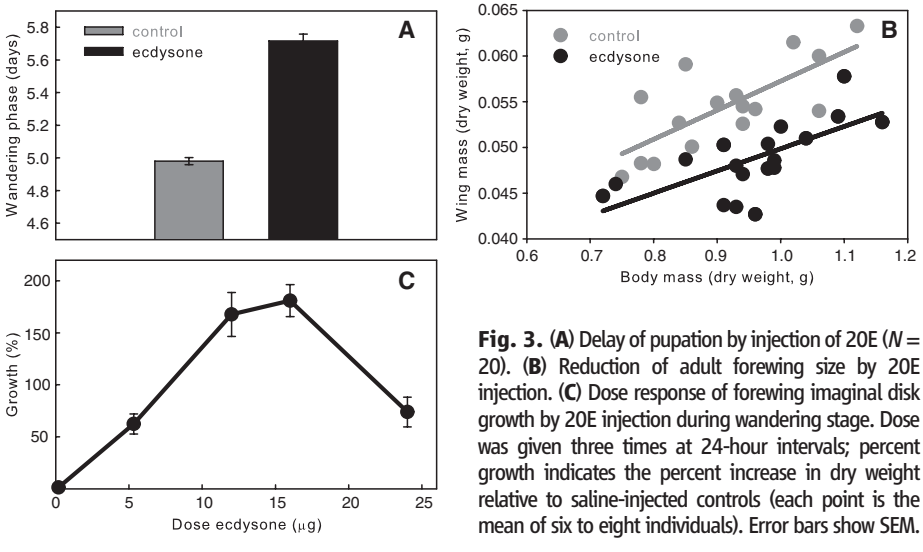

Fig. 3. (**A**) Delay of pupation by injection of 20E ($N = 20$). (**B**) Reduction of adult forewing size by 20E injection. (**C**) Dose response of forewing imaginal disk growth by 20E injection during wandering stage. Dose was given three times at 24-hour intervals; percent growth indicates the percent increase in dry weight relative to saline-injected controls (each point is the mean of six to eight individuals). Error bars show SEM.

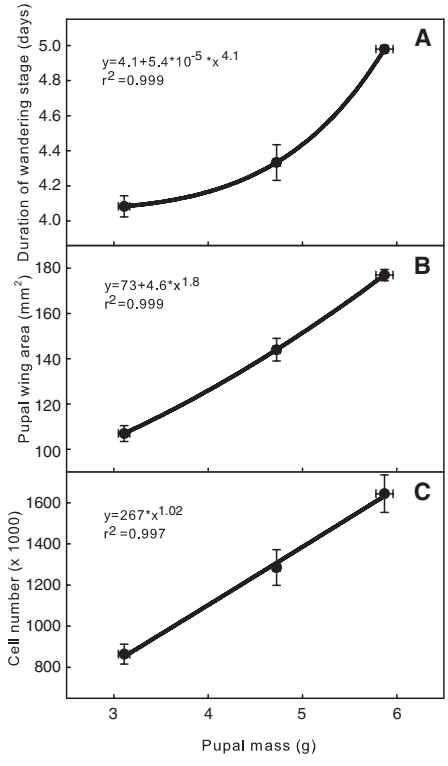

Fig. 4. Larvae starved at 6.5 g, 9.5 g, and allowed to grow normally to 12.5 g produced pupae of 3.1 g, 4.7 g, and 5.9 g, respectively (abscissa). (**A**) Corresponding duration of wandering stage. (**B**) Surface area of pupal wing. (**C**) Cell number in pupal wing before cell division starts ($N = 10$ to 14). Error bars show SEM.

by findings that growth rate and final body size in *Drosophila* are also influenced by ecdysone signaling (*11*, *19*, *20*, *29*). Moreover, different levels of ecdysone signaling are known to have differential effects on tissue growth and differentiation during metamorphosis (*14*, *30*). However, it is puzzling that decreased wing growth in starved larvae is regulated by an increase in ecdysone signaling. In principle, an increase or a decrease on either side of the optimal concentration should have equivalent effects (Fig. 3C). It may be that a decrease in ecdysone signaling cannot be tolerated because other developmental processes occurring during the larval-pupal transformation depend on ecdysone (*30*).

Finally, we examined whether wing disk growth was modulated to be intermediate at intermediate body sizes. We starved larvae at 9.5 g, an intermediate size between 6.5 g and the normal final weight of 12.5 g. Pupal mass, duration of the wandering stage, area of the pupal wing, and cell numbers of the wing at the beginning of the pupal stage were likewise intermediate (Fig. 4). Duration of the wandering stage was a nonlinear function of body size (Fig. 4A), which suggests that body size is the key determinant of the relative roles of development time and rate of cell division in adjusting wing size to body size.

Our results show that the proportional regulation of wing growth to match body size occurs during the wandering stage of the larva, after somatic growth has stopped and before pupation. Furthermore, it depends on the timing and level of ecdysone secretion, which regulates both the duration and rate of growth. Because the brain controls the secretion of ecdysteroids via the production of a tropic neurosecretory hormone, PTTH (*31*), these findings imply that the regulation of proportional growth of wings is, in effect, controlled by the central nervous system. It is still unclear how the central nervous system becomes aware of body size and uses this information to time the pattern of ecdysteroid secretion in the wandering stage. In some insects, body size is measured by abdominal stretch receptors (*32*, *33*), but there is no evidence that such a mechanism operates in *Manduca* (*31*, *34*). Mechanisms that facilitate growth factor sensitivity to body size have been postulated (*4*, *34*) but not yet demonstrated. Elucidating these mechanisms remains one of the great challenges in developmental biology.

References and Notes

1. D. J. Emlen, H. F. Nijhout, *Annu. Rev. Entomol.* **45**, 661 (2000).
2. D. J. Emlen, C. E. Allen, *Integr. Comp. Biol.* **43**, 617 (2003).
3. M. LaBarbera, *Annu. Rev. Ecol. Syst.* **20**, 97 (1989).
4. D. L. Stern, D. J. Emlen, *Development* **126**, 1091 (1999).
5. G. B. West, J. H. Brown, B. J. Enquist, *Science* **276**, 122 (1997).
6. K. Schmidt-Nielsen, *Scaling: Why Is Animal Size So Important?* (Cambridge Univ. Press, Cambridge, 1984).
7. G. Davidowitz, L. J. D'Amico, H. F. Nijhout, *Evol. Ecol. Res.* **6**, 49 (2004).
8. G. Davidowitz, H. F. Nijhout, *Integr. Comp. Biol.* **44**, 443 (2004).
9. D. Atkinson, *Adv. Ecol. Res.* **25**, 1 (1994).
10. J. Colombani *et al.*, *Cell* **114**, 739 (2003).
11. S. Layalle, N. Arquier, P. Léopold, *Dev. Cell* **15**, 568 (2008).
12. H. F. Nijhout, G. Davidowitz, D. A. Roff, *J. Biol.* **5**, 16 (2006).
13. H. F. Nijhout, L. W. Grunert, *Proc. Natl. Acad. Sci. U.S.A.* **99**, 15446 (2002).
14. H. F. Nijhout *et al.*, *Dev. Biol.* **302**, 569 (2007).
15. L. D'Amico, G. Davidowitz, H. Nijhout, *Proc. R. Soc. London Ser. B* **268**, 1589 (2001).
16. G. Davidowitz, L. J. D'Amico, H. F. Nijhout, *Evol. Dev.* **5**, 188 (2003).
17. B. A. Edgar, *Nat. Rev. Genet.* **7**, 907 (2006).
18. A. W. Shingleton, J. Das, L. Vinicius, D. L. Stern, *PLoS Biol.* **3**, e289 (2005).
19. J. Colombani *et al.*, *Science* **310**, 667 (2005); 10.1126/science.1119432.
20. C. K. Mirth, J. W. Truman, L. M. Riddiford, *Curr. Biol.* **15**, 1796 (2005).
21. Y. Kato, L. M. Riddiford, *Development* **100**, 227 (1987).
22. C. K. Mirth, J. W. Truman, L. M. Riddiford, *Development* **136**, 2345 (2009).
23. M. H. Orme, S. J. Leevers, *Cell Metab.* **2**, 277 (2005).
24. T. G. Kingan, M. E. Adams, *J. Exp. Biol.* **203**, 3011 (2000).
25. L. M. Schwartz, J. W. Truman, *Dev. Biol.* **99**, 103 (1983).
26. J. W. Truman, *Am. Zool.* **21**, 655 (1981).
27. J. S. Britton, W. K. Lockwood, L. Li, S. M. Cohen, B. A. Edgar, *Dev. Cell* **2**, 239 (2002).
28. P. Léopold, S. Layalle, *Science* **312**, 1317 (2006).
29. P. E. Caldwell, M. Walkiewicz, M. Stern, *Curr. Biol.* **15**, 1785 (2005).
30. D. T. Champlin, J. W. Truman, *Development* **125**, 2009 (1998).
31. H. F. Nijhout, *Insect Hormones* (Princeton Univ. Press, Princeton, NJ, 1994).
32. H. F. Nijhout, *J. Insect Physiol.* **25**, 277 (1979).
33. H. F. Nijhout, *J. Insect Physiol.* **30**, 629 (1984).
34. H. F. Nijhout, *Dev. Biol.* **261**, 1 (2003).

35. We thank C. Shreve, V. Callier, R. Dilling, K. Preuss, and I. Jalli for assistance and helpful discussions. Supported by NSF grants IOS-0641144 and IOS-0744952.

Supporting Online Material

www.sciencemag.org/cgi/content/full/science.1197292/DC1
Materials and Methods
References

2 September 2010; accepted 4 November 2010
Published online 25 November 2010;
10.1126/science.1197292

Fetal and Adult Hematopoietic Stem Cells Give Rise to Distinct T Cell Lineages in Humans

Jeff E. Mold,[1] Shivkumar Venkatasubrahmanyam,[2]* Trevor D. Burt,[1,3] Jakob Michaëlsson,[4] Jose M. Rivera,[1] Sofiya A. Galkina,[1] Kenneth Weinberg,[5] Cheryl A. Stoddart,[1]† Joseph M. McCune[1]†‡

Although the mammalian immune system is generally thought to develop in a linear fashion, findings in avian and murine species argue instead for the developmentally ordered appearance (or "layering") of distinct hematopoietic stem cells (HSCs) that give rise to distinct lymphocyte lineages at different stages of development. Here we provide evidence of an analogous layered immune system in humans. Our results suggest that fetal and adult T cells are distinct populations that arise from different populations of HSCs that are present at different stages of development. We also provide evidence that the fetal T cell lineage is biased toward immune tolerance. These observations offer a mechanistic explanation for the tolerogenic properties of the developing fetus and for variable degrees of immune responsiveness at birth.

The developing fetal immune system is generally believed to induce immune tolerance after exposure to foreign antigens (*1*). In the mouse, this tolerogenic tendency has been attributed to the absence of a "mature" adaptive immune system before birth (*2*). In the human, however, fetal exposure to foreign antigens, notably maternal alloantigens, can lead to the generation of immune tolerance (*3*–*5*), even though the immune system develops at a substantially earlier developmental stage (*1*, *6*). Recently, we reported that tolerance induction in the human fetus is in part mediated by an abundant population of fetal regulatory T cells (T_{regs}) (*7*), a cell population containing a significantly greater percentage (~15%) of total peripheral $CD4^+$ T cells in the developing human fetus than is found in healthy infants and adults (~5%) (*8*). Unlike adult T cells, we also observed that fetal T cells exhibit enhanced proliferation after exposure to alloantigens and are poised to become T_{regs} upon stimulation, a process dependent on transforming growth factor–β (TGF-β) (*5*).

[1]Division of Experimental Medicine, Department of Medicine, University of California, San Francisco, CA, USA. [2]Center for Biomedical Informatics Research, Stanford University School of Medicine, Stanford, CA, USA. [3]Department of Pediatrics, Division of Neonatology, University of California, San Francisco, CA, USA. [4]Center for Infectious Medicine, Department of Medicine, Karolinska Institutet, Stockholm, Sweden. [5]Division of Hematology, Oncology, and Stem Cell Transplantation, Department of Pediatrics, Stanford University School of Medicine, Stanford, CA, USA.

*Present address: Amgen, 1120 Veterans Boulevard, South San Francisco, CA 94080, USA.
†These authors contributed equally to this work.
‡To whom correspondence should be addressed at the Division of Experimental Medicine, University of California at San Francisco, UCSF Box 1234, SFGH Building 3, San Francisco, CA 94143–1234. E-mail: mike.mccune@ucsf.edu

by findings that growth rate and final body size in *Drosophila* are also influenced by ecdysone signaling (*11*, *19*, *20*, *29*). Moreover, different levels of ecdysone signaling are known to have differential effects on tissue growth and differentiation during metamorphosis (*14*, *30*). However, it is puzzling that decreased wing growth in starved larvae is regulated by an increase in ecdysone signaling. In principle, an increase or a decrease on either side of the optimal concentration should have equivalent effects (Fig. 3C). It may be that a decrease in ecdysone signaling cannot be tolerated because other developmental processes occurring during the larval-pupal transformation depend on ecdysone (*30*).

Finally, we examined whether wing disk growth was modulated to be intermediate at intermediate body sizes. We starved larvae at 9.5 g, an intermediate size between 6.5 g and the normal final weight of 12.5 g. Pupal mass, duration of the wandering stage, area of the pupal wing, and cell numbers of the wing at the beginning of the pupal stage were likewise intermediate (Fig. 4). Duration of the wandering stage was a nonlinear function of body size (Fig. 4A), which suggests that body size is the key determinant of the relative roles of development time and rate of cell division in adjusting wing size to body size.

Our results show that the proportional regulation of wing growth to match body size occurs during the wandering stage of the larva, after somatic growth has stopped and before pupation. Furthermore, it depends on the timing and level of ecdysone secretion, which regulates both the duration and rate of growth. Because the brain controls the secretion of ecdysteroids via the production of a tropic neurosecretory hormone, PTTH (*31*), these findings imply that the regulation of proportional growth of wings is, in effect, controlled by the central nervous system. It is still unclear how the central nervous system becomes aware of body size and uses this information to time the pattern of ecdysteroid secretion in the wandering stage. In some insects, body size is measured by abdominal stretch receptors (*32*, *33*), but there is no evidence that such a mechanism operates in *Manduca* (*31*, *34*). Mechanisms that facilitate growth factor sensitivity to body size have been postulated (*4*, *34*) but not yet demonstrated. Elucidating these mechanisms remains one of the great challenges in developmental biology.

References and Notes

1. D. J. Emlen, H. F. Nijhout, *Annu. Rev. Entomol.* **45**, 661 (2000).
2. D. J. Emlen, C. E. Allen, *Integr. Comp. Biol.* **43**, 617 (2003).
3. M. LaBarbera, *Annu. Rev. Ecol. Syst.* **20**, 97 (1989).
4. D. L. Stern, D. J. Emlen, *Development* **126**, 1091 (1999).
5. G. B. West, J. H. Brown, B. J. Enquist, *Science* **276**, 122 (1997).
6. K. Schmidt-Nielsen, *Scaling: Why Is Animal Size So Important?* (Cambridge Univ. Press, Cambridge, 1984).
7. G. Davidowitz, L. J. D'Amico, H. F. Nijhout, *Evol. Ecol. Res.* **6**, 49 (2004).
8. G. Davidowitz, H. F. Nijhout, *Integr. Comp. Biol.* **44**, 443 (2004).
9. D. Atkinson, *Adv. Ecol. Res.* **25**, 1 (1994).
10. J. Colombani *et al.*, *Cell* **114**, 739 (2003).
11. S. Layalle, N. Arquier, P. Léopold, *Dev. Cell* **15**, 568 (2008).
12. H. F. Nijhout, G. Davidowitz, D. A. Roff, *J. Biol.* **5**, 16 (2006).
13. H. F. Nijhout, L. W. Grunert, *Proc. Natl. Acad. Sci. U.S.A.* **99**, 15446 (2002).
14. H. F. Nijhout *et al.*, *Dev. Biol.* **302**, 569 (2007).
15. L. D'Amico, G. Davidowitz, H. Nijhout, *Proc. R. Soc. London Ser. B* **268**, 1589 (2001).
16. G. Davidowitz, L. J. D'Amico, H. F. Nijhout, *Evol. Dev.* **5**, 188 (2003).
17. B. A. Edgar, *Nat. Rev. Genet.* **7**, 907 (2006).
18. A. W. Shingleton, J. Das, L. Vinicius, D. L. Stern, *PLoS Biol.* **3**, e289 (2005).
19. J. Colombani *et al.*, *Science* **310**, 667 (2005); 10.1126/science.1119432.
20. C. K. Mirth, J. W. Truman, L. M. Riddiford, *Curr. Biol.* **15**, 1796 (2005).
21. Y. Kato, L. M. Riddiford, *Development* **100**, 227 (1987).
22. C. K. Mirth, J. W. Truman, L. M. Riddiford, *Development* **136**, 2345 (2009).
23. M. H. Orme, S. J. Leevers, *Cell Metab.* **2**, 277 (2005).
24. T. G. Kingan, M. E. Adams, *J. Exp. Biol.* **203**, 3011 (2000).
25. L. M. Schwartz, J. W. Truman, *Dev. Biol.* **99**, 103 (1983).
26. J. W. Truman, *Am. Zool.* **21**, 655 (1981).
27. J. S. Britton, W. K. Lockwood, L. Li, S. M. Cohen, B. A. Edgar, *Dev. Cell* **2**, 239 (2002).
28. P. Léopold, S. Layalle, *Science* **312**, 1317 (2006).
29. P. E. Caldwell, M. Walkiewicz, M. Stern, *Curr. Biol.* **15**, 1785 (2005).
30. D. T. Champlin, J. W. Truman, *Development* **125**, 2009 (1998).
31. H. F. Nijhout, *Insect Hormones* (Princeton Univ. Press, Princeton, NJ, 1994).
32. H. F. Nijhout, *J. Insect Physiol.* **25**, 277 (1979).
33. H. F. Nijhout, *J. Insect Physiol.* **30**, 629 (1984).
34. H. F. Nijhout, *Dev. Biol.* **261**, 1 (2003).

35. We thank C. Shreve, V. Callier, R. Dilling, K. Preuss, and I. Jalli for assistance and helpful discussions. Supported by NSF grants IOS-0641144 and IOS-0744952.

Supporting Online Material

www.sciencemag.org/cgi/content/full/science.1197292/DC1
Materials and Methods
References

2 September 2010; accepted 4 November 2010
Published online 25 November 2010;
10.1126/science.1197292

Fetal and Adult Hematopoietic Stem Cells Give Rise to Distinct T Cell Lineages in Humans

Jeff E. Mold,[1] Shivkumar Venkatasubrahmanyam,[2]* Trevor D. Burt,[1,3] Jakob Michaëlsson,[4] Jose M. Rivera,[1] Sofiya A. Galkina,[1] Kenneth Weinberg,[5] Cheryl A. Stoddart,[1]† Joseph M. McCune[1]†‡

Although the mammalian immune system is generally thought to develop in a linear fashion, findings in avian and murine species argue instead for the developmentally ordered appearance (or "layering") of distinct hematopoietic stem cells (HSCs) that give rise to distinct lymphocyte lineages at different stages of development. Here we provide evidence of an analogous layered immune system in humans. Our results suggest that fetal and adult T cells are distinct populations that arise from different populations of HSCs that are present at different stages of development. We also provide evidence that the fetal T cell lineage is biased toward immune tolerance. These observations offer a mechanistic explanation for the tolerogenic properties of the developing fetus and for variable degrees of immune responsiveness at birth.

The developing fetal immune system is generally believed to induce immune tolerance after exposure to foreign antigens (*1*). In the mouse, this tolerogenic tendency has been attributed to the absence of a "mature" adaptive immune system before birth (*2*). In the human, however, fetal exposure to foreign antigens, notably maternal alloantigens, can lead to the generation of immune tolerance (*3*–*5*), even though the immune system develops at a substantially earlier developmental stage (*1*, *6*). Recently, we reported that tolerance induction in the human fetus is in part mediated by an abundant population of fetal regulatory T cells (T_{regs}) (*7*), a cell population containing a significantly greater percentage (~15%) of total peripheral $CD4^+$ T cells in the developing human fetus than is found in healthy infants and adults (~5%) (*8*). Unlike adult T cells, we also observed that fetal T cells exhibit enhanced proliferation after exposure to alloantigens and are poised to become T_{regs} upon stimulation, a process dependent on transforming growth factor–β (TGF-β) (*5*).

[1]Division of Experimental Medicine, Department of Medicine, University of California, San Francisco, CA, USA. [2]Center for Biomedical Informatics Research, Stanford University School of Medicine, Stanford, CA, USA. [3]Department of Pediatrics, Division of Neonatology, University of California, San Francisco, CA, USA. [4]Center for Infectious Medicine, Department of Medicine, Karolinska Institutet, Stockholm, Sweden. [5]Division of Hematology, Oncology, and Stem Cell Transplantation, Department of Pediatrics, Stanford University School of Medicine, Stanford, CA, USA.

*Present address: Amgen, 1120 Veterans Boulevard, South San Francisco, CA 94080, USA.
†These authors contributed equally to this work.
‡To whom correspondence should be addressed at the Division of Experimental Medicine, University of California at San Francisco, UCSF Box 1234, SFGH Building 3, San Francisco, CA 94143–1234. E-mail: mike.mccune@ucsf.edu

Given these observations, we hypothesized that the human fetal T cell compartment may not simply be an "immature" version of the adult T cell compartment, but instead one derived from a separate lineage of T cells that is poised to deliver a tolerogenic response to all antigens encountered in utero.

Although the human fetal T cell compartment begins to develop at approximately 10 gestational weeks (g.w.) (*9*), much of what we know about

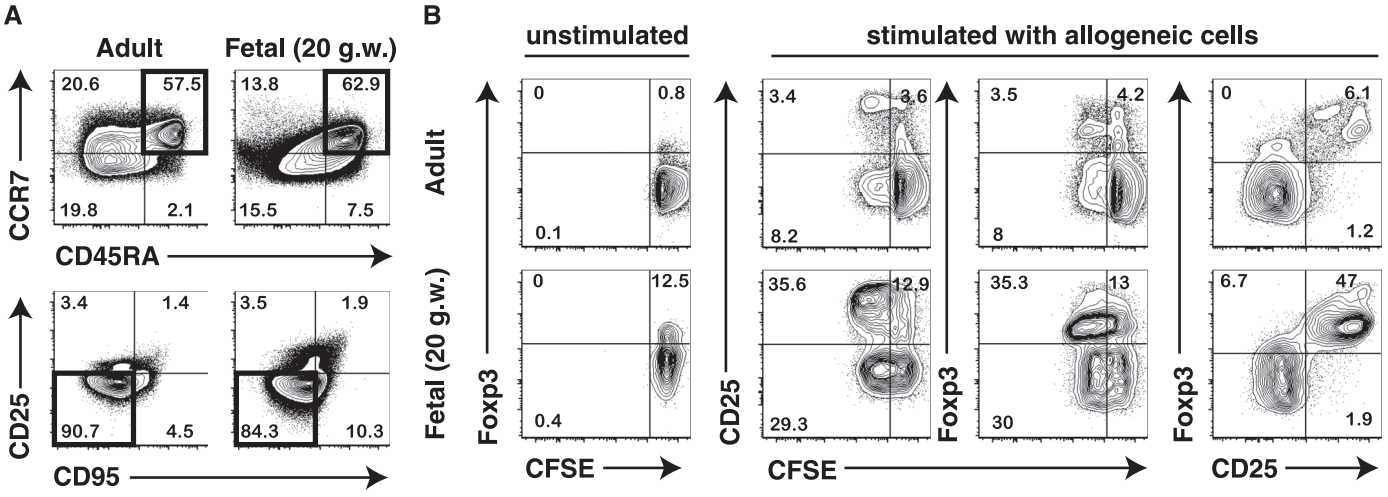

Fig. 1. Fetal naïve CD4$^+$ T cells display functional differences as compared to adult naïve CD4$^+$ T cells. (**A**) Flow cytometric analysis of the phenotype of naïve CD4$^+$ T cells isolated from fetal mLNs (18 to 22 g.w.) and adult PBMCs (25 to 35 years old). Top panels depict initial gating on CD3$^-$CD4$^+$ T cells, showing CD45RA versus CCR7 staining, and bottom panels depict initial gating on CD45RA$^+$CCR7$^+$ cells (highlighted in black in top panels), showing CD95 versus CD25 staining. Cells considered to be "naïve" CD4$^+$ T cells were CD45RA$^+$CCR7$^+$CD25$^-$CD95$^-$ (highlighted in black in bottom panels). Data are representative of at least three independent donors. (**B**) Sorted naïve CD4$^+$ T cells were either left unstimulated or cultured for 6 days in the presence of irradiated allogeneic PBMCs. Proliferation of fetal and adult naïve CD4$^+$ T cells was measured by carboxyfluorescein diacetate succinimidyl ester (CFSE) dilution and analyzed by flow cytometry. T_{reg}s were phenotypically identified by up-regulation of CD25 and $Foxp_3$.

Fig. 2. Fetal and adult naïve CD4$^+$ T cells show significant differences in gene signature. (**A**) Unbiased cluster analysis on the basis of gene expression for fetal (mLN) and adult (PBMC) naïve CD4$^+$ T cells and CD4$^+$CD25$^+$ T_{regs}. (**B** to **D**) Scatterplots of pairwise global gene expression comparisons comparing (B) fetal naïve CD4$^+$ T cells and adult naïve CD4$^+$ T cells, (C) fetal and adult CD4$^+$CD25$^+$ T_{regs}, and (D) CD4$^+$CD25$^+$ T_{regs} and naïve CD4$^+$ T cells (both fetal and adult). Gene expression values are plotted on a log scale. Genes that were differentially expressed between groups (determined using a 5% false discovery rate and a fold change ≥2) are indicated in red and blue. Specific genes that were differentially expressed based on age or subset are highlighted in green.

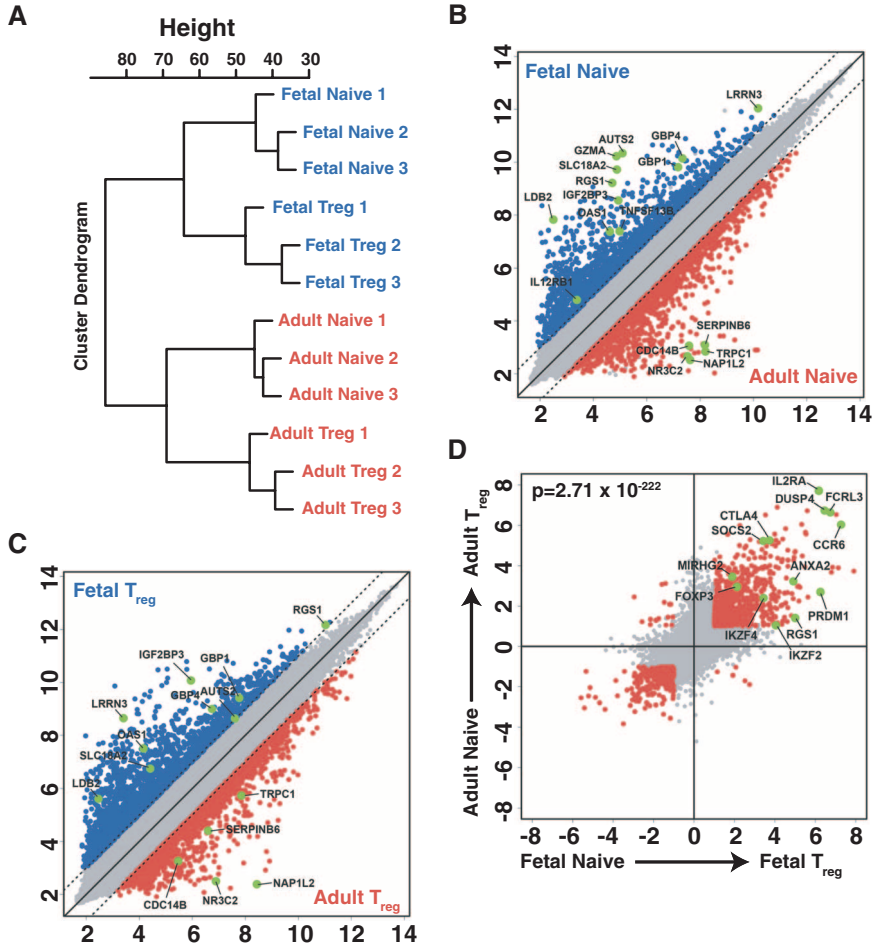

it arises from studies of cord blood obtained at birth. A few reports indicate that the majority of fetal T cells found at mid-gestation (~16 to 24 g.w.) have a surface phenotype comparable to that of conventional naïve T cells found in neonates and in adults (*10*–*12*). To characterize such cells more completely, we analyzed 18- to 22-g.w. fetal $CD4^+$ T cells obtained from mesenteric lymph nodes (mLNs) for the expression of a panel of known surface antigens specific for naïve $CD4^+$ T cells in adults and found that many have a phenotype ($CD45RA^+CCR7^+CD95^-CD25^-$) similar to that of naïve adult $CD4^+$ T cells (Fig. 1A). Next, we assessed the proliferative response of sort-purified fetal and adult naïve T cells to stimulation with allogeneic peripheral blood mononuclear cells (PBMCs) in a primary mixed lymphocyte reaction (MLR). Fetal naïve $CD4^+$ T cells were much more highly responsive to stimulation with allogeneic cells: After 6 days of stimulation, more than 50% had divided as compared to only ~10% of adult naïve $CD4^+$ T cells. Activated fetal naïve $CD4^+$ T cells were also more likely to adopt a T_{reg} fate, as measured by up-regulation of Foxp3 and CD25 (Fig. 1B). Although Foxp3 and CD25 can be transiently expressed by some T cells as a consequence of activation, our previous results indicate that activated fetal T cells exhibit sustained expression of Foxp3 and, unlike adult T cells, are prone to up-regulate Foxp3 even as a result of "spontaneous" activation in tissue culture (*5*, *7*). We have also demonstrated that fetal T_{regs} are capable of suppressing both proliferation and cytokine production, suggesting that their function is similar to that of adult T_{regs} (*5*, *7*).

These findings suggested that fetal and adult naïve $CD4^+$ T cells may be phenotypically similar but functionally distinct. To better define the differences between the two populations, we performed gene expression analysis by microarray on sorted populations of fetal and adult naïve $CD4^+$ T cells (fig. S1) and found substantial differences (Fig. 2, A and B, and table S1). A parallel analysis revealed that many of the same differences that were identified for fetal and adult naïve $CD4^+$ T cells were similar to those found for fetal and adult T_{regs} (Fig. 2, A to C, and table S2). We also noted a substantial overlap in genes that were abundant in both fetal and adult T_{regs}, when compared to fetal or adult naïve T cells, that was consistent with T_{reg} genes identified in previous studies (*13*, *14*) (Fig. 2D and tables S3 and S4). To understand the relative contributions of age and functional phenotype, principal components analysis (PCA) of the different $CD4^+$ T cells was performed. Age (adult versus fetal origin) was the largest PC, accounting for 36.1% of the observed variance, whereas a second PC (functional subtype, naïve versus T_{reg}) accounted for 25.9% (fig. S2). The consistent observation of differential gene expression in fetal and adult T cells (both naïve and T_{reg}) suggests that they represent different lymphocyte populations. As is individually highlighted in each scatterplot (Fig. 2, B and C), this point is illustrated by selected genes that were found to be highly expressed within fetal or adult T cell populations (fig. S3).

We hypothesized that adult and fetal human T cells are different because they are derived from distinct populations of multilineage hematopoietic stem cells (HSCs). Thus, previous work in avian and murine models has demonstrated that fetal and adult HSCs differ in phenotype (*15*), tissue localization (*16*), functional properties (for example, regarding turnover) (*15*, *17*), and developmental potential (*18*–*20*). For example, different populations of HSCs seed the murine and avian thymus during fetal development (*20*, *21*), giving rise to successive waves of thymocytes. In the mouse, the earliest to be found are dendritic epidermal T cells (DETCs), identified by their expression of a specific γδ T cell receptor (TCR) (Vγ3Vδ1) (*18*, *20*). These cells are replaced by a second wave of thymocytes with a diverse array of both TCRγδ and TCRαβ cells, which are then replaced by a third wave of thymocytes at around the time of birth, in which αβ T cells are the primary population.

In similar fashion, human fetal αβ $CD4^+$ T cells may differ from their adult counterparts because they are derived from distinct populations of HSCs. During the course of fetal development in humans, the location of the HSC pool switches from the aorta gonad mesonephros region to the fetal liver and, finally, to the fetal bone marrow (BM), where the majority of HSCs are thought to reside throughout adulthood (*22*). The first wave of thymocytes is derived primarily from HSCs that are present in the fetal liver, whereas thymocytes present at later stages of fetal development and in adults are likely to develop predominantly from BM-derived HSCs (*22*). Thus, besides intrinsic differences between fetal and adult HSC populations, there are also differences in tissue distribution that could contribute to different developmental potential (*23*).

To determine whether distinct HSC populations give rise to distinct lineages of T cells in the human fetus, we isolated total $CD34^+$ hemato-

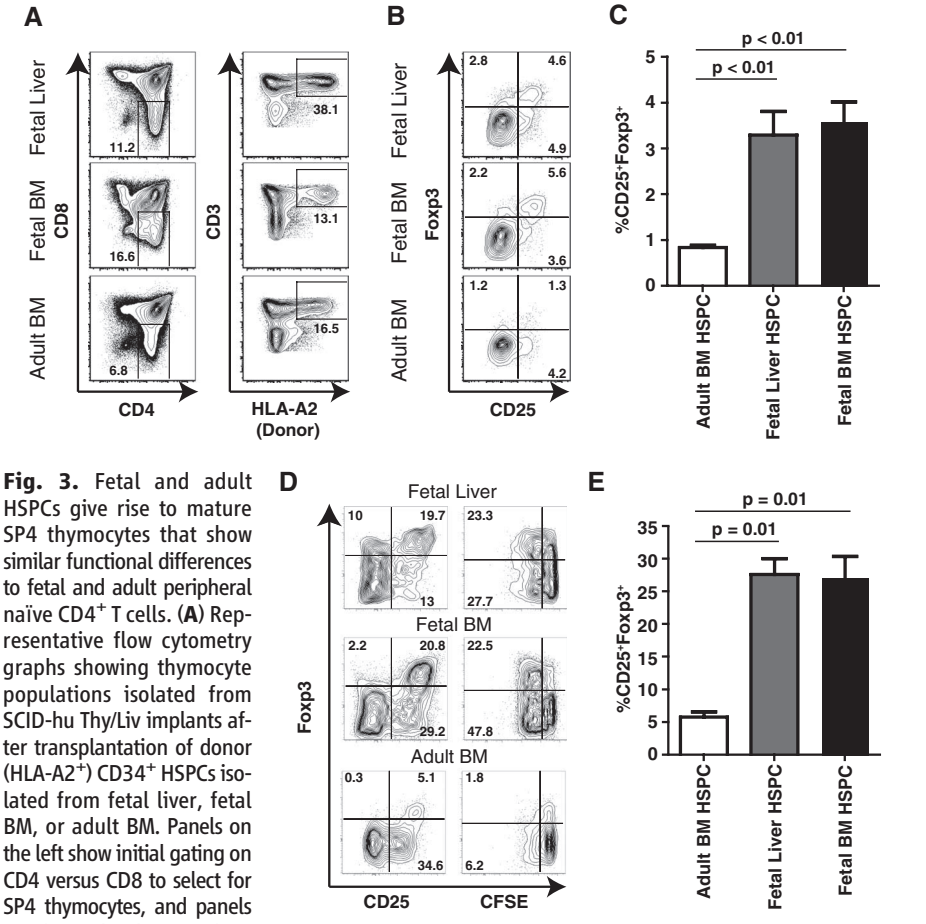

Fig. 3. Fetal and adult HSPCs give rise to mature SP4 thymocytes that show similar functional differences to fetal and adult peripheral naïve $CD4^+$ T cells. (**A**) Representative flow cytometry graphs showing thymocyte populations isolated from SCID-hu Thy/Liv implants after transplantation of donor ($HLA\text{-}A2^+$) $CD34^+$ HSPCs isolated from fetal liver, fetal BM, or adult BM. Panels on the left show initial gating on CD4 versus CD8 to select for SP4 thymocytes, and panels on the right depict subsequent gating on donor-derived ($HLA\text{-}A2^+$) $CD3^+$ mature SP4 thymocytes. (**B**) Flow cytometric analysis of the frequencies of $CD25^+Foxp3^+$ T_{regs} dervied from fetal liver, fetal BM, or adult BM hematopoietic progenitors. (**C**) Quantification of $CD25^+Foxp3^+$ T_{reg} frequencies observed in three to five different thymic implants from each group. (**D**) Flow cytometric analysis of proliferation and Foxp3 expression by SP4 thymocytes derived from fetal liver, fetal BM, or adult BM HSPCs in response to stimulation with irradiated allogeneic PBMCs (7-day stimulation). (**E**) Quantification of the frequencies of $CD25^+Foxp3^+$ T_{regs} after stimulation with allogeneic PBMCs. Data show at least three separate implants for each group. Data in bar graphs represent mean ±SD, and statistical significance was measured by Student's *t* test.

poietic stem/progenitor cells (HSPCs) (including primitive $CD34^+CD38^-$ HSCs and $CD34^+CD38^+$ progenitors with high proliferative potential) from fetal liver (at 18 to 22 g.w.), fetal BM (18 to 22 g.w.), and adult BM (19 to 43 years old) (fig. S4). We used the SCID-hu Thy/Liv mouse model of thymopoiesis to allow these populations of HSPCs to mature into single positive (SP) thymocytes in vivo. SCID-hu Thy/Liv mice were generated by engraftment of fetal thymus and liver from an HLA-A2 donor into the immunodeficient C.B17 *scid/scid* mouse (*24*). The animals were irradiated and then injected with 500,000 HSPCs isolated from HLA-A2–positive fetal liver, fetal BM, adult BM, or vehicle only (n = 5 mice per group) (fig. S4). After 7 to 8 weeks, mature thymocytes were harvested from the Thy/Liv implant. At this time, we were able to identify donor-derived ($HLA\text{-}A2^+$) mature $CD3^+$ thymocytes [$CD3^+CD4^+CD8^+$ (DP), $CD3^+CD4^-CD8^+$ (SP8), and $CD3^+CD4^+CD8^-$ (SP4)] in each of the groups receiving $CD34^+$ HSPCs but not in animals receiving vehicle alone (figs. S4 and S5).

We asked whether fetal and adult HSPCs might differ in their capacity to generate T_{regs} in the thymus, because fetal T cells appear to be predisposed to generating $Foxp3^+$ T_{regs} upon stimulation in vitro, and there is an abundance of T_{regs} in the peripheral tissues of mid-gestation fetuses (*7*, *8*). Both fetal liver and fetal BM-derived HSPCs were found to generate populations of $CD25^+Foxp3^+$ SP4 thymocytes, whereas adult BM-derived HSPCs generated a significantly lower frequency of $CD25^+Foxp3^+$ SP4 thymocytes (Fig. 3, A to C, and fig. S6). Thus, it appears that fetal HSPCs display a heightened capacity to generate T_{regs} during thymic maturation.

The initial observation that prompted our comparison between fetal and adult T cells was the elevated proliferation and differentiation of fetal T cells into T_{regs} after stimulation. To determine whether SP4 thymocytes derived from fetal HSPCs were functionally similar to SP4 thymocytes derived from adult HSPCs, we stimulated whole thymocyte populations in vitro with allogeneic antigen-presenting cells in a primary MLR (at a 1:3 ratio) and thereafter monitored proliferation and Foxp3 expression. SP4 thymocytes derived from fetal HSPCs behaved similarly to peripheral fetal naïve $CD4^+$ T cells, exhibiting robust proliferative responses and a significantly greater expansion of $Foxp3^+$ cells after stimulation as compared to SP4 thymocytes derived from adult HSPCs (Fig. 3, D and E, compare to Fig. 1B). Thus, we conclude that the functional differences observed between fetal and adult naïve T cells in the periphery can be, in part, accounted for by differences in the progenitor populations from which they arise.

We next sought to determine whether the gene signature of T cells derived from fetal HSPCs was different than that of T cells derived from adult HSPCs. To make this comparison, $HLA\text{-}A2^+$ SP4 thymocytes were sorted from SCID-hu Thy/Liv implants injected with fetal liver, fetal BM, or adult BM HSPCs, and microarray analysis was performed using the same platform previously used to test peripheral T cells. This analysis revealed that fetal BM- and fetal liver-derived HSPCs gave rise to SP4 thymocytes that were indistinguishable from one another, indicating that the fetal HSPCs in each of these tissues have similar developmental potential (Fig. 4, A and B, and table S5). In contrast, the transcriptional profile of SP4 thymocytes matured from adult BM-derived HSPCs was vastly different (Fig. 4, A and B, and table S5). Thus, we find that fetal HSPCs and adult HSPCs give rise to mature SP4 thymocytes with profoundly different functional properties and gene expression patterns. These differences are likely to reflect developmental changes in progenitor populations, rather than differences related to compartmentalization of stem cell subsets.

Finally, we sought to determine whether the differences observed in the gene expression patterns of peripheral fetal and adult naïve $CD4^+$ T cells could be explained by differences in the fetal and adult stem cell populations. We performed PCA on both peripheral T cells and HSPC-derived thymocytes to identify the sources of variation in

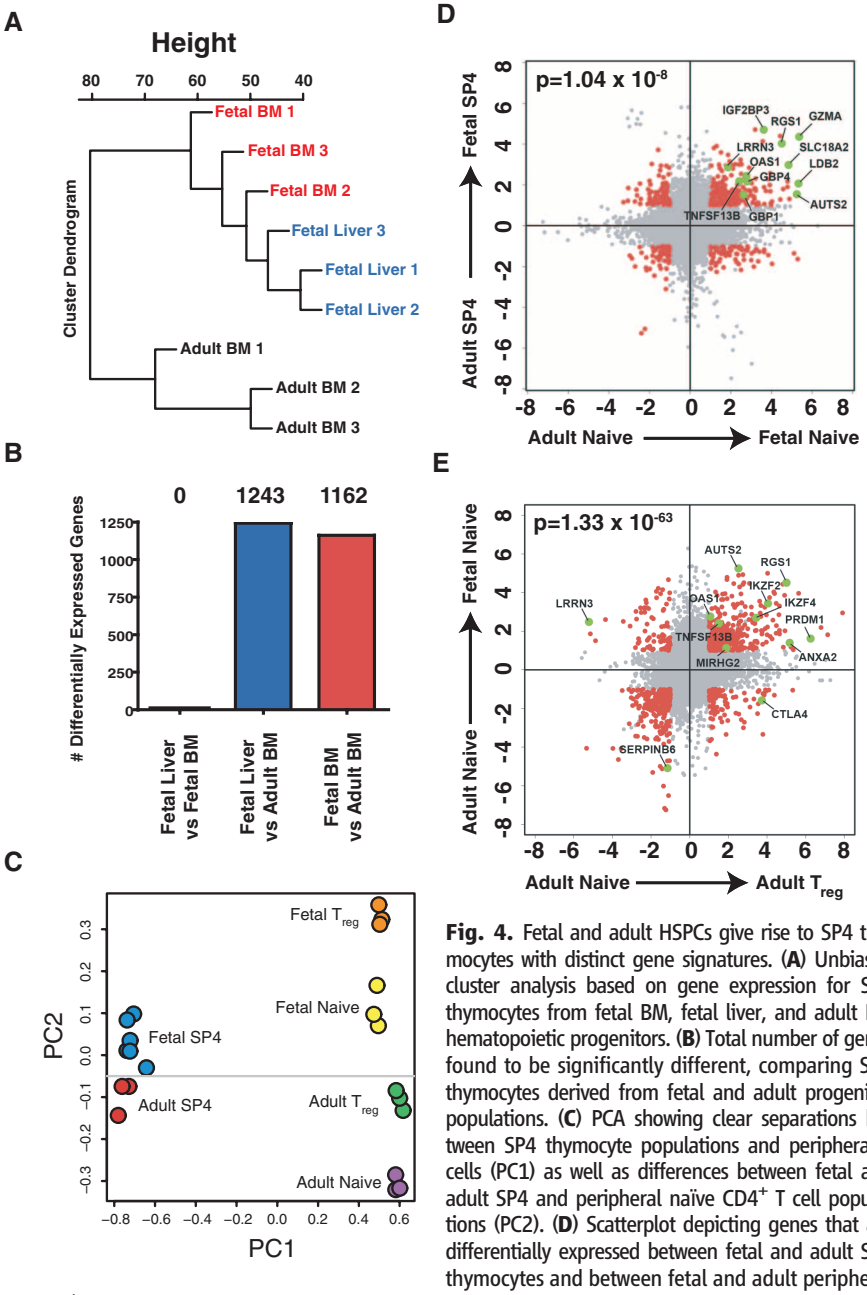

Fig. 4. Fetal and adult HSPCs give rise to SP4 thymocytes with distinct gene signatures. **(A)** Unbiased cluster analysis based on gene expression for SP4 thymocytes from fetal BM, fetal liver, and adult BM hematopoietic progenitors. **(B)** Total number of genes found to be significantly different, comparing SP4 thymocytes derived from fetal and adult progenitor populations. **(C)** PCA showing clear separations between SP4 thymocyte populations and peripheral T cells (PC1) as well as differences between fetal and adult SP4 and peripheral naïve $CD4^+$ T cell populations (PC2). **(D)** Scatterplot depicting genes that are differentially expressed between fetal and adult SP4 thymocytes and between fetal and adult peripheral naïve $CD4^+$ T cells. **(E)** Scatterplot depicting genes that are differentially expressed between adult and fetal naïve T cells and between adult naïve and adult T_{regs}. For both (D) and (E), differential expression was determined using a false discovery rate of ≤5% and a fold change ≥2. The significance of overlap between groups of genes was determined using a chi-squared test for independence.

gene expression and their relative magnitude. In this analysis, developmental stage (thymocytes versus mature T cells) was found to be the most prominent source of variance (PC1, 70.4% of total variance), followed by age (PC2, fetal versus adult, 6.3%) (Fig. 4C). We observed a significant overlap ($P = 1.0 \times 10^{-8}$) between genes that were abundant in both fetal naïve and fetal HSPC-derived SP4 cells (253 probe sets) and genes that were abundant in adult naïve and adult HSPC-derived SP4 cells (79 probe sets) (Fig. 4D). Because fetal naïve cells displayed a propensity to differentiate into T_{regs} as compared to adult naïve T cells, we performed an additional correlation to determine whether fetal and adult naïve T cells shared a common gene signature with T_{regs}. We identified a significant number of genes that were highly expressed in both adult T_{regs} and fetal naïve T cells, but not in adult naïve T cells, some of which have been previously implicated as playing a specific role in determining T_{reg} fate specification (such as IKZ2 and IKZ4) (Fig. 4E and fig. S3). This is also reflected in the PCA performed on all T cell subsets (Fig. 4C), which showed that fetal naïve cells are more closely related to adult T_{regs} than to adult naïve T cells along PC2. We can conclude that fetal T cells are a separate population of cells, distinct from those found in adults, and that this in part reflects differences in the populations of stem cells, which give rise to the T cell compartment across different stages of development.

Our results support the hypothesis that, as in mice and birds (*21*, *25*), in humans the development of the immune system is layered. This hypothesis suggests that hematopoiesis occurs in distinct waves, including an early one that is fetal and a later one that is adult, with each generating distinct populations of cells that may coexist (layer) for a period of time (fig. S7). The propensity for fetal $CD4^+$ T cells to adopt a T_{reg} fate upon stimulation suggests that the initial wave of T cell differentiation may favor a population of T cells whose role is to promote tolerance to self (and potentially foreign) antigens encountered during development. Whether these cells are enriched in a specific T_{reg} precursor, which has been suggested to exist in the adult thymus and periphery in mice (*26*, *27*), remains to be determined. Although the focus of this study has been $CD4^+$ T cells, the fetal peripheral lymphoid tissues contain a full array of hematopoietic cells that have not been extensively studied and may also be distinct from their adult counterparts. For example, although our findings are different from those made in the mouse, the results of our study do not rule out the existence of a comparable population of γδ DETCs in the human fetus. Our findings have broad implications for the understanding of human hematopoiesis and provide a framework for studying a range of biological processes, from infectious diseases to transplantation strategies and immune tolerance.

References and Notes

1. A. M. Silverstein, *Science* **144**, 1423 (1964).
2. R. E. Billingham, L. Brent, P. B. Medawar, *Nature* **172**, 603 (1953).
3. F. H. Claas, Y. Gijbels, J. van der Velden-de Munck, J. J. van Rood, *Science* **241**, 1815 (1988).
4. W. J. Burlingham *et al.*, *N. Engl. J. Med.* **339**, 1657 (1998).
5. J. E. Mold *et al.*, *Science* **322**, 1562 (2008).
6. L. Brent *et al.*, *Immunol. Lett.* **21**, 55 (1989).
7. J. Michaëlsson, J. E. Mold, J. M. McCune, D. F. Nixon, *J. Immunol.* **176**, 5741 (2006).
8. Y. Takahata *et al.*, *Exp. Hematol.* **32**, 622 (2004).
9. B. F. Haynes, M. E. Martin, H. H. Kay, J. Kurtzberg, *J. Exp. Med.* **168**, 1061 (1988).
10. G. Lucivero *et al.*, *Fetal Diagn. Ther.* **6**, 101 (1991).
11. J. A. Byrne, A. K. Stankovic, M. D. Cooper, *J. Immunol.* **152**, 3098 (1994).
12. M. O. Muench, E. M. Pott Bärtsch, J. C. Chen, J. B. Lopoo, A. Bárcena, *Dev. Comp. Immunol.* **27**, 899 (2003).
13. N. Sugimoto *et al.*, *Int. Immunol.* **18**, 1197 (2006).
14. M. Feuerer *et al.*, *Proc. Natl. Acad. Sci. U.S.A.* **107**, 5919 (2010).
15. S. J. Morrison, H. D. Hemmati, A. M. Wandycz, I. L. Weissman, *Proc. Natl. Acad. Sci. U.S.A.* **92**, 10302 (1995).
16. E. D. Zanjani, J. L. Ascensao, M. Tavassoli, *Blood* **81**, 399 (1993).
17. D. E. Harrison, R. K. Zhong, C. T. Jordan, I. R. Lemischka, C. M. Astle, *Exp. Hematol.* **25**, 293 (1997).
18. K. Ikuta *et al.*, *Cell* **62**, 863 (1990).
19. E. Montecino-Rodriguez, H. Leathers, K. Dorshkind, *Nat. Immunol.* **7**, 293 (2006).
20. W. L. Havran, J. P. Allison, *Nature* **335**, 443 (1988).
21. M. Coltey *et al.*, *J. Exp. Med.* **170**, 543 (1989).
22. M. Tavian, B. Péault, *Exp. Hematol.* **33**, 1062 (2005).
23. M. A. Martin, M. Bhatia, *Stem Cells Dev.* **14**, 493 (2005).
24. R. Namikawa, K. N. Weilbaecher, H. Kaneshima, E. J. Yee, J. M. McCune, *J. Exp. Med.* **172**, 1055 (1990).
25. L. A. Herzenberg, L. A. Herzenberg, *Cell* **59**, 953 (1989).
26. D. J. Pennington *et al.*, *Nature* **444**, 1073 (2006).
27. S. Schallenberg, P. Y. Tsai, J. Riewaldt, K. Kretschmer, *J. Exp. Med.* **207**, 1393 (2010).

28. We thank all of the patients who generously donated tissue that was used in these studies. We also thank S. J. Fisher and D. F. Nixon for valuable discussions; A. J. Butte, M. E. Moreno, and G. Kosikova for technical support; and the Gladstone Genomics Core for microarray analysis. Support for this work was provided by grants from NIH to J.M.M. (OD000329 and AI40312) and to K.W. and A. J. Butte (CA049605 and AG033314) and from the Harvey V. Berneking Living Trust. This project has been funded in part with federal funds from the National Institute of Allergy and Infectious Diseases, NIH, under contract no. N01-AI-70002. S.V. is supported by the Deborah Addicott Fellowship for Bioinformatics and Stem Cell Biology. J.M. is supported by the Swedish Research Council. T.D.B. received funding from American Pediatric Society, the American Academy of Pediatrics, and the March of Dimes as a fellow of the Pediatric Scientist Development Program. J.M.M. is a recipient of the NIH Director's Pioneer Award Program, part of the NIH Roadmap for Medical Research, through grant DPI OD00329. The microarray data have been deposited in the Gene Expression Omnibus with accession code GSE25119.

Supporting Online Material

www.sciencemag.org/cgi/content/full/330/6011/1695/DC1
Materials and Methods
Figs. S1 to S7
References

16 August 2010; accepted 5 November 2010
10.1126/science.1196509

NEW PRODUCTS FOCUS: RNAi

siRNA PREMIXES

With FlexiTube siRNA Premix, small interfering RNA (siRNA) for your gene of interest and highly efficient transfection reagent are already premixed and provided in a single tube. FlexiTube siRNA Premix includes a specialized buffer that increases the stability of siRNA-reagent complexes. The ratio of reagent to siRNA in FlexiTube siRNA Premix is preoptimized to provide the highest transfection efficiency and gene knockdown. FlexiTube siRNA Premix is ready-to-use for cell transfection. Simply add to cells and incubate. With FlexiTube siRNA Premix, RNA interference experiments get off to a faster start, as there is no need to optimize siRNA-to-reagent ratio. Tedious optimization experiments involving multiple transfections are minimized or eliminated. Multiple transfections can be performed from a single FlexiTube siRNA Premix, reducing variability, and enabling consistency across experiments and more reliable results.

Qiagen

For info: 800-426-8157 | www.qiagen.com

TRANSFECTION REAGENTS

Effective and nontoxic DNA and small interfering RNA (siRNA) delivery is essential for reliable scientific results. jetPRIME is a new versatile and powerful DNA and siRNA transfection reagent for day-to-day experiments. jetPRIME ensures high DNA transfection efficiency and excellent gene silencing in a variety of adherent cells. jetPRIME is ideal for DNA/siRNA cotransfection and is very gentle to cells since it requires low amounts of nucleic acid and reagent during transfection. The jetPRIME protocol is easy-to-follow and compatible with the use of serum and antibiotics during transfection.

Polyplus Transfection

For info: 508-315-9629 | www.polyplus-transfection.com

siRNA SILENCING KIT

Enabling researchers to perform efficient small interfering RNA (siRNA) silencing (gene knockdown) experiments in small animal models, Invivofectamine 2.0 Reagent and Ambion In Vivo siRNA provide strong and sustained knockdown of in vivo protein expression in an easy-to-use kit. These tools accelerate the use of RNA interference to efficiently study gene function in animal models. Targeted gene silencing has been demonstrated to last for more than three weeks with a single application of Invivofectamine 2.0 Reagent and the positive control Ambion In Vivo siRNA. The new reagents provide a powerful alternative to the conventional use of knockout mouse models, which can take nearly 10 months to develop. Sold as part of a 1 ml starter kit or a 5 ml kit, Invivofectamine 2.0 Reagent and Ambion In Vivo siRNA are synthetic, contain no components of viral origin, and show minimal to no toxicity after extensive initial studies.

Life Technologies (Invitrogen)

For info: 800-955-6288 | www.invitrogen.com

IN VIVO TRANSFECTION KIT

The PEG-Liposome siRNA In Vivo Transfection Kit is designed for in vivo transfection of negatively charged molecules—RNA, DNA, and small proteins. Transfection is one of the major laboratory methods used to introduce DNA and RNA molecules into cells and tissues. This technique makes it possible to cross cellular barriers and deliver a gene or a small interfering RNA (siRNA) into cells for research or therapeutic purposes. The novel PEGylated liposome-based siRNA delivery kit is optimized for directed RNA interference induction by efficient delivery of functional small RNA molecules (siRNA, shRNA, miRNA) into tissues. The liposome component provides in vivo siRNA protection due to efficient siRNA-liposome encapsulation. A remarkable feature of this reagent is reduced innate immune response and low cytotoxicity due to biodegradable PEG modification.

Altogen Biosystems

For info: 800-658-7009 | www.altogen.com/mirna.php

RNA ISOLATION

When working with stored materials, researchers often need to isolate RNA from samples that have been stored as formalin-fixed paraffin-embedded (FFPE) tissue blocks. Although the tissue structure of FFPE samples will have been maintained for histological analysis, damage to the nucleic acid may have occurred through the fixation, embedding, and storage processes impeding measurements of gene expression levels. ExpressArt FFPE RNAready overcomes the limitations associated with RNA degradation and interference from RNA cross-linking in FFPE tissues. The FFPE RNAready kit efficiently isolates and preserves mRNA using a specially developed lysis solution and an innovative universal inhibitor of RNases that displaces tightly bound RNA from high-molecular-weight aggregates. Subsequent treatment with a unique de-modification reagent reverses formalin induced cross-links, resulting in total RNA optimized for reverse transcription reactions and subsequent downstream applications. FFPE RNAready together with ExpressArt RNA amplification TRinucleotide primer technology is now available to amplify microgram quantities of high quality RNA from very small amounts of degraded total RNA, with minimal loss of sequence.

AMSBIO

For info: +44-0-1235-828200 | www.amsbio.com

Electronically submit your new product description or product literature information! Go to www.sciencemag.org/products/newproducts.dtl for more information.

Newly offered instrumentation, apparatus, and laboratory materials of interest to researchers in all disciplines in academic, industrial, and governmental organizations are featured in this space. Emphasis is given to purpose, chief characteristics, and availability of products and materials. Endorsement by *Science* or AAAS of any products or materials mentioned is not implied. Additional information may be obtained from the manufacturer or supplier.

POSITIONS OPEN

Yale

ELECTROPHYSIOLOGY RESEARCH ASSOCIATE

Position available at Yale University School of Medicine for a Ph.D. or M.D. with experience with patch-clamp or intracellular recording to join a multidisciplinary research group studying channel biology and channelopathies. Incumbent will be expected to play a significant role in studies of contribution of ion channels in neuronal electrogenesis in normal and injured neurons. Experience with voltage-gated channels and or DRG neurons is desirable. The position at Postdoctoral or Associate Research Scientist presents a superb opportunity to collaborate with cell and molecular biologists, pharmacologists, and clinicians. Send statement of interest, curriculum vitae, and three letters of reference to: **Stephen G. Waxman, M.D., Ph.D., Director, Neuroscience and Regeneration Research Center, VA Connecticut (127A), 950 Campbell Avenue, West Haven, CT 06516. E-mail: stephen.waxman@yale.edu.** *Women and members of underrepresented minority groups are encouraged to apply. Affirmative Action/Equal Opportunity Employer.*

ASSISTANT PROFESSORSHIPS

California State University, Northridge invites applications for two tenure-track positions in the Department of Biology, starting August 2011. Applicants must have a Ph.D. and postdoctoral experience. Each successful candidate shall develop a vigorous research program involving undergraduate and M.S. students, seek extramural research funding, and demonstrate teaching excellence.

MICROBIOLOGIST: Research interests in prokaryotic systems biology using laboratory-based experimentation with applied or biotechnological applications. Teaching options include general microbiology, applied microbiology, biotechnology, graduate seminar, and introductory biology. Submit to **e-mail: microsearch@csun.edu.**

CELL BIOLOGIST: Candidates specializing in regulatory mechanisms involved in cell signaling, cell growth, cell differentiation, cytoskeleton dynamics, and other physiological processes in eukaryotic cells. Teaching options include introductory biology, physiology, cell biology, and specialty courses in candidate's area of expertise. Submit to **e-mail: cellbiosearch@csun.edu.**

Applicants should submit a cover letter, curriculum vitae, three letters of recommendation, summary of teaching experience, statements of teaching philosophy and research interests, and three publications. Electronic submissions are strongly encouraged. For more information **website: http://www.csun.edu/facultyaffairs/openings/sm/.** Screening will begin on 15 February 2011.

The University is an Equal Opportunity/Affirmative Action Employer and does not discriminate on the basis of race, religion, national origin, sexual orientation, gender, marital status, age, disability, disabled veteran, or Vietnam-era veteran status.

POSTDOCTORAL FELLOWSHIPS in Plant Biotechnology

Queensland University of Technology and the University of Sydney have received funding under the ARC Super Science Fellowships scheme for a collaborative project entitled "Extreme expression: building a platform for industrial plant biotechnology". We are seeking two postdoctoral fellows to join our expert team of investigators who are using a variety of new molecular approaches to explore extreme expression of medical and industrial proteins in plants. One of the positions will be based in Brisbane with **Professor James Dale** in the Centre for Tropical Crops and Biocommodities and the other will be based in Sydney with **Professor Peter Waterhouse** in the Plant Molecular Genetics Group.

Apply through **website: http://www.qut.edu.au/jobs/.**

Job Reference: 10367.

POSITIONS OPEN

OPEN RANK FACULTY POSITIONS
University of Illinois at Urbana-Champaign
Department of Comparative Biosciences

The Department of Comparative Biosciences at the College of Veterinary Medicine, University of Illinois at Urbana-Champaign invites applications for two open positions at the **ASSISTANT, ASSOCIATE,** or **FULL PROFESSOR** level. Candidates must possess a Ph.D. or equivalent degree. Postdoctoral training is preferred. Candidates currently at the Associate or Full Professor rank with federal funding are especially encouraged to apply. The successful candidates will participate in the professional and graduate curricula and develop research programs that complement existing department and campus strengths in developmental and reproductive biology, endocrinology, neuroscience, environmental toxicology, stem cell biology, and cancer biology. Full information about the department is available at **website: http://vetmed.illinois.edu/cb/index.html.** The positions are regular, full-time, 9-month, tenured or tenure-track appointments, and are available August 2011. Salary and rank will be commensurate with qualifications.

Qualified applicants should apply online at **website: https://jobs.illinois.edu.** Applications should include a cover letter including a research statement, curriculum vitae, and contact information for three references. Questions may be directed to **Dr. Jodi Flaws,** chair, **e-mail: jflaws@illinois.edu** or **telephone: 217-333-7933.**

In order to ensure full consideration, applications must be received by February 1, 2011. *Women and minorities are encouraged to apply. The University of Illinois is an Equal Opportunity Employer.*

FACULTY POSITION
Florida Institute of Technology
Department of Biological Sciences

Florida Institute of Technology (**website: http://www.fit.edu**), an independent, technological university located on Florida's east coast, invites applications for an **ASSISTANT** or **ASSOCIATE PROFESSOR** position beginning in fall 2011. Candidates must have a Ph.D. degree, relevant postdoctoral experience, and expertise in cell or molecular biology. They must be prepared to teach undergraduate biochemistry, as well as graduate courses in biotechnology and their area of specialization. Successful candidates are expected to have an active, externally funded research program. Areas of interest include but are not limited to plant biology and large marine vertebrates. Review of applications will begin January 15. *Women and minorities are strongly encouraged to apply.* Submit a cover letter, detailed curriculum vitae, statements of research interests and teaching philosophy, up to three reprints of publications, and contact information for three references to: **Professor Mark B. Bush** (**e-mail: mbush@fit.edu**), **Department of Biological Sciences, Florida Institute of Technology, 150 W. University Boulevard, Melbourne, FL 32901-6975.**

Florida Institute of Technology is an Equal Opportunity/Affirmative Action Employer.

POSTDOCTORAL POSITION at The University of Southern California

Postdoctoral Position in **Dr. Yang Chai**'s laboratory is available immediately for individuals with strong Molecular and Developmental Biology background at the Center for Craniofacial Molecular Biology University of Southern California. The successful applicants will join a large interactive multidisciplinary team of scientists in a strong academic environment focusing on the molecular regulation of craniofacial development. For more details, please visit the **website: http://www.usc.edu/hsc/dental/ccmb.** Send resume to: **Dr. Yang Chai, C/O Ms. Patricia Thompson, e-mail: pathomps@usc.edu.**

DEPARTMENT CHAIR

Department of Population Medicine and Diagnostic Sciences - #13859

The College of Veterinary Medicine at CORNELL UNIVERSITY invites applications for the position of Chair of the Department of Population Medicine and Diagnostic Sciences **(http://www.vet.cornell.edu/popmed/).** The department has academic faculty in Epidemiology, Ambulatory and Production Medicine, and in the Animal Health Diagnostic Center (AHDC). We seek an individual to lead the Department in all aspects of academic activity, including stewardship of personnel and resources. In collaboration with the faculty, the Chair is expected to foster excellence in education, clinical and diagnostic service, and research for the advancement of animal and human health. The Chair provides oversight for the recruitment, retention and professional development of faculty and staff, works closely with the Executive Director of the AHDC to coordinate department and Diagnostic Laboratory functions, participate in fundraising, and is expected to pursue scholarly activities in his/her area of expertise.

Located in the heart of the beautiful Finger Lakes Region of New York State, Cornell University is a center for discovery, academic leadership, and service. Committed to achieving excellence through cultural diversity, we welcome candidates who will create a climate that attracts students of all races, nationalities and genders. The College of Veterinary Medicine also seeks to meet the needs of dual career couples through Cornell's Dual Career Program and membership in the Upstate New York Higher Education Recruitment Consortium **http://www.upstatenyherc.org/home/index.cfm?site_id=671**.

Qualifications: Applicants must hold a veterinary degree or a PhD in a discipline relevant to department interests. For veterinary graduates, there must be evidence of further postgraduate education in the form of diplomate status in a recognized specialty board and/or advanced degrees. The successful candidate will have strong leadership capabilities, a record of active participation in academic affairs, and evidence of balance and excellence in teaching, research and/or clinical activities that are appropriate to the interests of the Department of Population Medicine and Diagnostic Sciences and the College of Veterinary Medicine. Applications will be reviewed beginning 15 January 2011 and continue until the position is filled. Interested individuals are asked to submit curriculum vitae, letter of intent, and the names and addresses of three references to the **Chair of the Search Committee: Professor Doug Antczak, c/o Jill Short, Cornell University, College of Veterinary Medicine, S2-005 Schurman Hall, Ithaca, New York 14853**. Electronic applications are preferred **(pmdschairsearch@cornell.edu)**.

Cornell University

Cornell University is an affirmative action/ equal opportunity employer and educator.

CAL POLY POMONA

DEAN
College of Science

California State Polytechnic University, Pomona (Cal Poly Pomona) invites nominations and applications for the position of Dean of the College of Science. The Dean is the chief academic officer of the College of Science and provides academic leadership for faculty, staff, and students in the college. We seek a scholar with a vision for promoting excellence in undergraduate and graduate teaching, research and other scholarly activities, as well as service. Candidates should have outstanding leadership, management, and interpersonal skills, a record of excellence in teaching and securing extramural funding, and a significant record of department, college, and university service. The successful candidate will be expected to articulate and implement a vision for expanding faculty research productivity in a way that enhances our educational programs. Detailed information about this position may be found online at **http://sci.csupomona.edu/dean_search/**.

One of eight Colleges on the campus, the College of Science has approximately 2,400 undergraduate majors in eight degree programs offered by six academic departments: Biological Sciences, Chemistry, Computer Science, Geological Sciences, Mathematics and Statistics, and Physics. Master's degree programs enrolling approximately 200 students are offered in Biological Sciences, Chemistry, Computer Science, and Mathematics. The College of Science is committed to excellence in teaching and scholarship and is the largest single recipient of extramural funding on campus. Additional information about the College may be found online at **http://sci.csupomona.edu/**.

Cal Poly Pomona, located about 30 miles east of downtown Los Angeles, is one of 23 campuses in The California State University system. The University has an ethnically diverse student population of 20,000. Students are enrolled in 62 undergraduate majors and 19 master's degree programs. Additional information about the University may be found online at **http://www.csupomona.edu/**.

Review of applications will begin on **February 15, 2011** and will continue until the position is filled. The University seeks to fill this position by summer 2011, however, later dates are possible. Applicants must forward (1) a letter of interest, which explains in detail the candidate's administrative philosophy and vision; (2) a curriculum vitae; and (3) the names and contact information of five references to: **Search Committee, Dean of the College of Science, c/o Marissa Martinez, Search Coordinator, Office of the Provost and Vice President for Academic Affairs, California State Polytechnic University, Pomona, 3801 West Temple Avenue, Pomona, California 91768; E-mail: deanscisearch@csupomona.edu.**

California State Polytechnic University, Pomona is an Equal Opportunity, Affirmative Action Employer. Cal Poly Pomona subscribes to all State and Federal regulations and prohibits discrimination based on gender, race, sexual orientation, national origin, disability, marital status, age, religion, or covered veteran's status.

UNIVERSITY of VIRGINIA HEALTH SYSTEM

UNIVERSITY OF VIRGINIA SCHOOL OF MEDICINE DIRECTOR OF ORTHOPAEDIC RESEARCH

The Department of Orthopaedic Surgery at the University of Virginia is seeking a research scientist who has experience with musculoskeletal research. This is a tenure-track position at the Associate or Full Professor rank. Applicants are to have a Ph.D. or equivalent and a record of success in attaining funding as a Principal Investigator on Federal grants such as an RO1 or equivalent. A successful applicant will be expected to establish an independent research program that will attract and maintain Federal ongoing extramural support as well as national recognition for their research. Research areas of experience include cellular genetics, biochemistry, biomechanics or biomedical engineering applied to the musculoskeletal system. The Director is responsible for the overall development and the expansion of the laboratory through his/her research program and by collaboration with investigators from the School of Medicine and the University. As a part of the directorship, the laboratory budget must be managed and balanced.

This position will also mentor junior faculty and post-doctoral personnel with their independent research activities. Oversight of educational symposia and basic science lectures are also expected to foster research collaboration as well as to educate the trainees in fellowships and residencies.

The University of Virginia in Charlottesville offers a unique combination of natural beauty, rich historical and cultural attractions, and close proximity to both a national park and the nation's capitol.

Relevant experience in basic or clinical research with a potential for success in a career in academic medicine is required for the tenure-eligible position. A record of scholarship and a national reputation in clinical education and/or clinical research is required for a tenured position as Full Professor.

The faculty rank and salary compensation will be commensurate with experience and achievement. This position will remain open to applications until filled.

To apply visit https://jobs.virginia.edu and select posting number 0606798 for Full Professor or posting number 0606620 for Associate or Assistant Professor. Complete the candidate profile online and attach a cover letter, CV, a description of their research and their research interests and contact information for three references.

For further information about this position or for questions regarding the application process, please contact:

Cheryl Etelvari
Assistant for Faculty Recruitment for
Mark F. Abel, MD
Lillian T. Pratt Distinguished Professor and Chair
Department of Orthopaedic Surgery
University of Virginia Health System
PO Box 800232
Charlottesville, VA 22901
E-mail: cle4n@virginia.ed
Telephone: 434-982-0893

The University of Virginia is an Equal Opportunity/Affirmative Action Employer. Women and members of under represented groups are encouraged to apply.

FONDATION
BETTENCOURT
SCHUELLER

2010
LILIANE BETTENCOURT PRIZE FOR LIFE SCIENCES

BRUNO
LEMAITRE

THE 2010 LILIANE BETTENCOURT PRIZE for Life Sciences has been awarded to the outstanding leader of modern immunobiology, Bruno Lemaitre, Professor of Genetics at the Ecole Polytechnique Fédérale de Lausanne, Switzerland.

Bruno Lemaitre's research interest is focused on innate immunity and particularly on mechanisms of microbial infection and host defense response. By using genetic and genomic approaches of the fruit fly Drosophila model, he demonstrated that Imd and Toll pathways are involved in antimicrobial responses in insects and that they allow to discriminate the responses to infection by Gram-negative and Gram-positive bacteria and fungi. He identified also the bacterial determinants recognized by these pathways as well as bacteria that can infect Drosophila through the digestive tract and initiate a potent innate immune response.

Currently, Bruno's group explores the mechanisms that make the gut an efficient and interactive barrier despite its constant interactions with microbes. This fundamental knowledge generated on Drosophila immunity will have a great impact on our understanding of mammalian, in particular human immunity.

THE 2010 LILIANE BETTENCOURT PRIZE for Life Sciences of €250,000 is an essential part of the Bettencourt Schueller Foundation's commitment to Biomedical Research. It aims to support a top-level European researcher under the age of 45, along with his or her team, to pursue their work in the field of Life Science. The international Jury for the Award is chaired by Professor Pierre Corvol, Administrator of the Collège de France, member of the American Academy of Arts and Sciences and of the French Academy of Sciences.

The Bettencourt Schueller Foundation was created in 1987 by Mrs. Liliane Bettencourt, in memory of her father, the late Eugène Schueller, founder of L'Oréal. Its mission is to encourage entrepreneurship in Sciences, Arts and Social Commitment.
The Foundation Bettencourt Schueller dedicates around 55 % of its total budget to finance scientific education and to directly support researchers.

Fondation
Bettencourt Schueller
27-29, rue des Poissonniers
92200 Neuilly-sur-Seine – France
www.fondationbs.org
Contact: mw@fondationbs.org

Max-Planck-Institut für Immunbiologie

Max Planck Institute of Immunobiology

The **Max Planck Institute (MPI) of Immunobiology** in Freiburg, Germany is offering

Postdoctoral positions

in the Laboratory of Chromatin Regulation (Head: Dr. Asifa Akhtar). The positions are available for an initial two-year appointment with the possibility of extension.

The research focus of the Akhtar laboratory includes mechanisms underlying chromatin and epigenetic regulation. The lab mainly uses dosage compensation of the male X chromosome in fruit flies as a model system employing multidisciplinary approaches such as genetics, biochemistry, functional genomics as well as cell biology and structural biology. Furthermore, we are currently expanding our efforts to explore conservation of function in mammalian models.

We are looking for enthusiastic, highly-motivated, science-driven and experienced postdoctoral fellows to join our team to unravel the molecular mechanisms that regulate gene expression.

Applicants should have a PhD or equivalent doctoral degree with at least 3 years of proven research experience in molecular biology, biochemistry and/or high-throughput analysis. Prior experience working in Drosophila or mouse models is highly encouraged. Candidates must have a strong publication record. Furthermore, the ability to work in a team, communication skills and experience in the supervision of graduate students are an asset.

The MPI in Freiburg is an international research institute at the cross-road of Southern Germany, Switzerland and France. The working language is English. State-of-the-art infrastructure and service units, including transgenesis, mass spectrometry, proteomics, flow cytometry, fly and imaging facilities are available.

Salaries will be according to postdoctoral fellowships of the Max-Planck-Society or TVöD and will commensurate with experience. A childcare facility is directly attached to the Institute. Women are especially encouraged to apply; handicapped applicants with equal qualifications will be given preferential treatment.

Please send your application, including a statement of research interests, a CV and three references indicating the reference number **021110** to Ms. Weigold at **weigold@immunbio.mpg.de.**

Deadline for applications is **31st January 2011.**

SCHOOL OF MEDICINE
INDIANA UNIVERSITY

Faculty Position
Department of Pharmacology and Toxicology

The Department of Pharmacology and Toxicology at Indiana University School of Medicine in Indianapolis invites applications from outstanding individuals for a faculty position at the **Assistant or Associate Professor** level. A Ph.D. and/or M.D. degree with at least 3 years of postdoctoral research experience and a strong track record of academic achievement is required. Successful applicants will be expected to establish a vigorous research program supported by extramural funding and participate in teaching/mentoring of graduate and medical students. Outstanding candidates working in all areas of molecular and cellular signaling are invited to apply. Preference will be given to candidates with research interests and experiences that complement or strengthen our existing programs (**http://pharmtox.iusm.iu.edu**), particularly apoptosis, drug action and resistance, epigenetics and gene regulation, and host-pathogen interactions. Startup package includes a highly competitive salary, generous startup funds and ample laboratory space, plus access to exceptional core facilities in a highly interactive scientific environment with many multidisciplinary centers (**http://www.medicine.iu.edu/research**).

The search committee will begin considering applications immediately and continue until the position is filled. Interested individuals should send a cover letter, curriculum vitae, a summary of past research accomplishment and future plans (2-3 pages), and the names and addresses of 3 references via electronic format to: **Chair of the Search Committee, Department of Pharmacology and Toxicology, IU School of Medicine** at **phtxjobs@iupui.edu**.

IU is an EEO/AA Employer, M/F/D.

Julius-Maximilians-
UNIVERSITÄT WÜRZBURG

JULIUS-MAXIMILIANS-UNIVERSITÄT WÜRZBURG, GERMANY

ZINF IMIB

YOUNG INVESTIGATOR / GROUP LEADER

The Research Centre for Infectious Diseases (ZINF) of the University of Würzburg seeks a new group leader for its young investigator program. We are interested in researchers with postdoctoral experience and international recognition in the general fields of microbiology, cell biology, parasitology, immunology, or host-pathogen interactions. Candidates using emerging imaging and sequencing technologies to study new aspects of pathogenesis are preferred, but all outstanding scientists are encouraged to apply.

The successful candidate will be appointed for a period of 5+2 years. Salary (E14/15) will be commensurate with training and experience. The position includes laboratory operating expenses and salaries for additional personnel (postdoc, graduate student, and technician), and laboratory space in a recently finished 9,000 m^2 state-of-the-art research building with bio-containment, molecular imaging, high-throughput genomics, and animal facilities. The building is specifically designed to foster collaborative research, and houses eight additional young investigator groups as well as laboratories run by faculty members. See **www.infektionsforschung.uni-wuerzburg.de** for more information. Informal inquiries about the posts can be made to Profs. Jörg Vogel (joerg.vogel@uni-wuerzburg.de) or Matthias Frosch (mfrosch@hygiene.uni-wuerzburg.de).

Interested individuals should send, by **February 15, 2011**, a one-page description of research interests and future directions; CV including list of publications; the names of three academic references. We may request short-listed candidates to submit a more detailed research proposal. Preference will be given to handicapped persons in case of otherwise equal aptitude. The University aims at increasing the proportion of female employees. Applications from qualified women are therefore particularly welcome. Applications should be addressed to the spokesperson of ZINF, Prof. Dr. Matthias Frosch and sent **via mail** to kristina.schaeffer@uni-wuerzburg.de.

NUS National University of Singapore

Positions in Environmental Biology/Biodiversity Studies

Associate Professor/Assistant Professor
Department of Biological Sciences

The Department of Biological Sciences, National University of Singapore (NUS), invites applications for two tenure-track faculty positions at the Assistant/Associate Professorship level in Environmental Biology/Biodiversity Studies. Candidates with research background in relevant fields are invited to apply but we are particularly interested in applications from climate change biologists, environmental modellers, ecotoxicologists, urban ecologists, aquatic microbial and algal biodiversity/ecologists.

An interest in tropical environments will be an advantage. Candidates should have a PhD. with relevant postdoctoral experience, an outstanding publication record, and a strong commitment to both teaching and research. Successful applicants will join a growing Environmental Biology group within a diverse and highly successful Department of Biological Sciences. The Department has 60 full-time faculty members and over 260 graduate students from 16 countries. Facilities and research support are world-class. NUS currently ranks high in the Times Higher Education World University Rankings. Please visit our website at www.dbs.nus.edu.sg/ for further details of the Department and its research and teaching programs. Competitive salary and perks will be offered.

Interested candidates should forward a letter of intent describing their career goals, research plans, teaching interests, curriculum vita and arrange for three reference letters directly sent to:

Chair, Environmental Biology Search Committee (c/o Ms Lisa Lau)
Department of Biological Sciences
National University of Singapore
14 Science Drive 4
Singapore 117543
Fax: (65) 6779 5671; Email: dbsjobs@nus.edu.sg

Closing date of application: 15 March 2011

AAAS is here – helping scientists achieve career success.

Every month, over 400,000 students and scientists visit ScienceCareers.org in search of the information, advice, and opportunities they need to take the next step in their careers.

A complete career resource, free to the public, *Science* Careers offers a suite of tools and services developed specifically for scientists. With hundreds of career development articles, a grants and scholarships database, webinars and downloadable booklets filled with practical advice, a community forum providing real-time answers to career questions, and thousands of job listings in academia, government, and industry, *Science* Careers has helped countless individuals prepare themselves for successful careers.

As a AAAS member, your dues help AAAS make this service freely available to the scientific community. If you're not a member, join us. Together we can make a difference.

To learn more, visit **aaas.org/plusyou/sciencecareers**

AAAS + U = Δ

NIFA

UNITED STATES DEPARTMENT OF AGRICULTURE
NATIONAL INSTITUTE OF FOOD AND AGRICULTURE

The National Institute of Food and Agriculture (NIFA) in the Department of Agriculture (USDA) was recently reorganized to a structure with four Institutes. Each of the Institutes is co-led by an Assistant Director and a Principal Scientist. The Assistant Director provides leadership for the administration of programs that comprise the Institute. The Principal Scientist provides the scientific leadership to programs assigned to the Institute. More information about NIFA can be found at **http://www.nifa.usda.gov/**. NIFA is seeking to fill the following four Principal Scientist positions, as either permanent **(PERM)**, term **(TERM)**, or under an **Intergovernmental Personnel Act (IPA)** appointment:

Principal Scientist of the Institute of Bioenergy, Climate, and Environment (PERM) (NIFA-SL: 10-06)
Principal Scientist of the Institute of Bioenergy, Climate, and Environment (TERM) (NIFA-SL: 10-07)

Principal Scientist of the Institute of Food Production and Sustainability (PERM) (NIFA-SL:10-08)
Principal Scientist of the Institute of Food Production and Sustainability (TERM) (NIFA-SL: 10-09)

Principal Scientist of the Institute of Food Safety and Nutrition (PERM) (NIFA-SL: 10-10)
Principal Scientist of the Institute of Food Safety and Nutrition (TERM) (NIFA-SL:10-11)

Principal Scientist of the Institute of Youth, Family, and Community (PERM) (NIFA-SL: 10-12)
Principal Scientist of the Institute of Youth, Family, and Community (TERM) (NIFA-SL:10-13)

Principal Scientist positions are Senior Level (SL) positions. The Federal salary ranges from $119,554 to $179,700. A copy of each job announcement may be located on the Office of Personnel Management web page at **http://www.usajobs.opm.gov/**. As specified in each job announcement, applicants must meet mandatory qualifications and address specific technical qualifications. Veterans preference applies, and U.S. citizenship is required. The job announcements listed above identify these four positions as a Permanent or a Term position (which is a competitive appointment for a period of more than one year but not more than four years). Candidates applying for permanent and term appointments should clearly identify in your application the type(s) of appointment desired, indicate the corresponding vacancy announcement number(s), and submit the documents required in the job announcements through USAJOBS.

In addition, NIFA will consider filling these positions under an **Intergovernmental Personnel Act (IPA)** appointment. The IPA allows for a temporary assignment (detail) of skilled employees from local, State and Indian tribal government, institutions of higher education and other eligible organizations to Federal Government agencies. IPAs remain employees of their permanent organizations; appointments can be made for up to two years and may be extended an additional two years under specific conditions. Cost of the assignment (including salary, benefits, relocation cost, travel and per diem expenses) are negotiated between participating organizations. **Applicants applying only for an IPA appointment should submit a resume and address the specific technical qualifications identified for the position(s). To obtain the technical qualifications and/or receive additional information relating to IPA appointments contact Rhonda Pratt (301-504-1475)**.

All applications must be received by **January 31, 2011**. For more information about the application process, contact **Deborah Crump (301-504-1448)**. To learn more about NIFA, contact **Betty Lou Gilliland (202-720-5506)**.

KUANG-CHI INSTITUTE
OF ADVANCED TECHNOLOGY
深圳光启高等理工研究院

Kuang-Chi Institute of Advanced Technology (Kuang-Chi Institute) is a non-profit Research Institute sponsored by government, industry and venture capitals. The mission of Kuang-Chi Institute is to conduct breakthrough science with direct implementation in a broad range of applications, execute cutting-edge technology in order to turn dreams into reality and bridge the gap between science and human life. Kuang-Chi Institute attracts distinctive scientists from different countries featuring highly qualified collaborative cross-disciplinary research with prestigious world recognized partner universities and research organizations, and a globe vision.

Multiple Research Faculty and Postdoctoral Fellowship Positions

The Kuang-Chi Institute invites applications for more than **50 research faculty** (Ref: RF-2010/2011-310) and **50 postdoctoral fellow** (Ref: RF-2010/2011-311) positions in all areas of science and technology, including: Applied Mathematics, Applied Physics, Biomedical Engineering, Computer Science and Technology, Electrical and Electronic Engineering, Materials Science and Engineering, Mechanical Engineering, Statistics, Scientific Computing, and etc.

Research Faculty
The research faculty should be committed to excellence in research and collaborate with other faculty members on interdisciplinary methodological and applied research. Applicants should be research active and have a proven accomplishment. A highly competitive salary, **up to 600,000 RMB per annum**, commensurate with qualifications and experience will be offered. Generous annual bonus and comprehensive health insurance benefit will also be offered.

Postdoctoral Fellow
Postdoctoral fellows are expected to devote themselves to full-time research. Applicants should therefore hold a doctoral degree and have a desire to develop skills in interdisciplinary methodological and applied research as well as in building strong collaborations. A highly competitive salary, **up to 250,000 RMB per annum**, commensurate with qualifications and experience will be offered. Generous annual bonus and comprehensive health insurance benefit will also be offered.

Application Procedure
To apply, please send a cover letter, a full CV, a research statement, and contact details of three references as a package to **search@kuang-chi.org**. All applications will be reviewed immediately, and early submissions are encouraged. Please refer to web: **http://www.kuang-chi.org** for more information.

Meeting a 21st Century Grand Challenge: Water Sustainability

A multidisciplinary cluster hiring initiative at The University of Iowa

The lack of adequate access to clean water is a global crisis affecting more than a billion people worldwide. Population growth, climate change, land use and energy choices, and global poverty have caused precipitous changes in water quantity, availability, and quality. Unless we can overcome or adapt to these driving forces, future generations will inherit a legacy of declining and degraded water resources.

Meeting this challenge will require expertise in and collaboration among a wide range of disciplines, including economics, policy, and law as well as the natural sciences and engineering. That's why **The University of Iowa is assembling a multidisciplinary faculty alliance** on water sustainability, bringing together faculty from the Colleges of Liberal Arts and Sciences, Public Health, Law, and Engineering; the Graduate College; and the Public Policy Center.

The **Water Sustainability Initiative** (**http://watersustainability.uiowa.edu**) is part of a comprehensive program in sustainability announced by UI President Sally Mason—a **vision for national leadership** in sustainability education, research, and outreach. It builds on a solid foundation of existing UI strengths including the Iowa Flood Center, academic strengths in cognate areas of sustainable energy and clean air, the Office of Sustainability, and an undergraduate Certificate in Sustainability.

The University is establishing ten new tenure track faculty positions, based in various academic departments, to be filled by individuals who will contribute additional expertise in teaching, research, and service to this faculty alliance (or "cluster"). Together, these faculty will create new knowledge as well as unique educational and research opportunities for students interested in a sustainable water future.

Currently, the University is recruiting five tenure track assistant professors in the following areas: (1) communications and/or policy related to water pollution, legislation, conflicts, rights, and water use (based in Communication Studies, Political Science, or Journalism and Mass Communication); (2) hydrogeology with required interest in groundwater, and possible related interests in water pollution, environmental/hydrologic sciences, and sustainability (based in Geoscience); (3) sustainability and surface water resources with complementary strengths in geoinformatics, land use science, environmental policy, biogeography, or health geography (based in Geography); (4) large scale intelligent systems related to water sustainability with expertise in computational intelligence, modeling, simulation, control theory, communications, sensor networks, knowledge discovery, and intelligent integration of information from diverse sources (based in Electrical and Computer Engineering); and (5) environmental health with an emphasis on water sustainability, with possible research interests in analytical chemistry/toxicology/water-borne contaminants, health implications of climate change, epidemiology of water-borne diseases, or rural safety and health related to water quality and quantity (based in Occupational and Environmental Health).

Come help us meet the challenge! Potential applicants may contact the **Office of the Provost** by phone (**319-335-3565**) or via e-mail (**provost-office@uiowa.edu**), or see the initiative's web site (**http://watersustainability.uiowa.edu**) for more information.

The University of Iowa is an Equal Opportunity and Affirmative Action Employer. We strongly encourage women and minorities to apply.

Jiangsu Academy of Agricultural Sciences

Seeking Distinguished Scientists in Various Agriculture Areas

Jiangsu Academy of Agricultural Sciences (JAAS) is a professional agricultural research and extension institution that has been established since 1932. JAAS ranks at the top of provincial agricultural academies in China in terms of the comprehensive strength in agriculture. JAAS's headquarter and main research facilities are located in Nanjing, Jiangsu, China.

Currently, there are 3 distinguished full professor positions available for application in the following areas: breeding, food processing, bioenergy, facility agriculture, and large-scale farming for modern animal husbandry. Applicants should have a faculty position already beyond the assistant professor level in a university or the equivalent position in a research institution. In addition, all candidates should demonstrate excellent records of research accomplishment and have a command of bilingual language for English and Chinese, both in spoken and written.

Successful applicants will be offered a competitive package, including sufficient laboratory space, startup funding, relocation fee and competitive salary commensurate with experience, in addition to a housing allowance, and other employee benefit. Applicants can go to www.jaas.ac.cn for application details.

In addition, more information for other regular faculty positions from JAAS relevant to a variety of disciplines in agriculture is also available at www.jaas.ac.cn.

Contact information

E-mail: rsc-gbk@jaas.ac.cn; Tel: 086-25-84390037

a place of mind
THE UNIVERSITY OF BRITISH COLUMBIA

TENURE TRACK BIOLOGY INSTRUCTOR

University of British Columbia, Vancouver BC, Canada

The Departments of Botany and Zoology seek candidates to fill a tenure-track Instructor position to teach in the Biology Undergraduate Program in the general areas of cell and molecular biology. Candidates must hold a PhD in relevant areas of the life sciences, have an integrative approach to biology, and be committed to improving biology teaching. Postdoctoral teaching and/or research experience is preferred.

The successful candidate will demonstrate evidence of outstanding teaching, expertise in the subject area, and the ability to contribute to ongoing curriculum and course development.

Duties of the position might include the development and coordination of tutorials for a cell biology class (over 1000 students), as well as contributing to lab and lecture teaching in cell and molecular biology at introductory and advanced levels. Instructors will participate in course and curriculum development, and in training and supervision of graduate student teaching assistants.

Application packages should consist of a cover letter, curriculum vitae, and the names of at least three individuals who have agreed to provide letters of reference. The CV must include a summary of teaching experience, a statement of teaching philosophy, an outline of teaching interests and evidence of teaching effectiveness (such as teaching evaluations). Candidates are particularly encouraged to highlight previous experience in fostering the education of students from diverse backgrounds. Please submit application packages either as a single pdf file to biology.searchcommittee@ubc.ca or by mail to:

Biology Instructor Search Committee; Attention: Jessica Sui, Department of Botany. University of British Columbia, 3529 - 6270 University Blvd., Vancouver BC V6T 1Z4.

Screening of applications will begin January 17, 2011, with appointments anticipated to begin on or after July 1, 2011.

The University of British Columbia hires on the basis of merit and is committed to employment equity. All qualified persons are encouraged to apply; however, priority will be given to Canadian citizens and permanent residents of Canada.

GRANTS

HUMAN FRONTIER SCIENCE PROGRAM (HFSP)

12 quai Saint-Jean, 67080 STRASBOURG Cedex, FRANCE

CALL FOR LETTERS OF INTENT FOR INNOVATIVE FRONTIER RESEARCH GRANTS: AWARD YEAR 2012

The Human Frontier Science Program supports **international** preferably **intercontinental** collaborations in basic life science research with emphasis placed on **innovative** and **interdisciplinary** approaches to fundamental investigations. Applications are invited for grants to support frontier approaches to understanding **complex mechanisms of living organisms**. Applicants are expected to develop **novel** lines of research distinct from their ongoing research. Preliminary results are not required.

There are two types of Grant: Young Investigators' Grants are for teams of scientists who are **all** within 5 years of establishing an independent laboratory and within 10 years of obtaining their PhDs. **Program Grants** are for independent scientists at all stages of their careers. The participation of younger scientists is especially encouraged.

Grants provide 3 years support for 2-4 member teams, with not more than one member from any one country, unless critical for the **innovative** nature of the project, which is an important selection criterion. Applicants may establish a local or national interdisciplinary collaboration as a component of an international team but will be considered as 1.5 team members for budgetary purposes. Awards depend on team size and successful teams will receive up to $450,000 per year. The principal applicant must be located in one of the member countries (Australia, Canada, the European Union, France, Germany, India, Italy, Japan, New Zealand, Norway, the Republic of Korea, Switzerland, the United Kingdom and the United States) but co-investigators may be located in any country.

Guidelines and further instructions are available on the HFSP web site (www.hfsp.org). International teams of scientists must first submit a letter of intent online via the web site. Specific enquiries: grant@hfsp.org

Deadlines: Compulsory pre-registration, via the website: March 22, 2011
Submission of Letters of Intent: March 31, 2011

POSITIONS OPEN

Guangdong University of Technology (GDUT), Guangzhou, China, Invites Applications and Nominations for the Positions of 8 Deans

Guangdong University of Technology is located in Guangzhou, in south China. It is a key multi-disciplinary university of Guangdong Province with a history of over 50 years, offering a wide range of courses in engineering, science and technology, business management, liberal arts and law, with major emphasis on the study of engineering.

With the University's rapid development, we are seeking candidates for 8 faculties' dean positions at professor levels to work in the fields of (1)Faculty of Electromechanical Engineering, (2)Faculty of Automation, (3)Faculty of Chemical Engineering and Light Industry, (4)Faculty of Materials and Energy, (5)Faculty of Information Engineering, (6)Faculty of Physics and Optoelectronic Engineering, (7)School of Art and Design, (8) School of Foreign Languages . The student population of most of the above said faculties and schools exceed 3000, with teaching staff number exceeding 100. Besides, Faculty of Electromechanical Engineering, Faculty of Automation, Faculty of Chemical Engineering and Light Industry, and Faculty of Materials and Energy are privileged to offer doctoral programs, which are the key programs of Guangdong Province and are supported by Guangdong "211 project" fund.

We offer competitive compensation and benefits to the selected candidates. The maximum annual income and the maximum R&D fee can be RMB1000,000 and RMB10,000,000 respectively. We also provide the selected candidates a 100M^2 apartment, and for those who need to buy an apartment in Guangzhou, a housing package of RMB300,000-500,000 is offered.

Candidates should have a PhD degree, an outstanding track record in Higher Education field, the confidence and ability to build up a world-class faculty (requirements to overseas candidates and to candidates for School of Arts Design and School of Foreign Languages can be discussed).

Interested and qualified individuals should provide a cover letter and a resume with signature in person before 31 March 2011.

Contact information:
Contact person: Ms Zhiying Zeng
Telephone : 0086-20-39322792 Fax: 0086-20-39322208
Email: gdutyzzp@gdut.edu.cn
Address: Human Resource Department, Guangdong University of Technology, No. 100 Waihuan Xi Road, Guangzhou Higher Education Mega Center, Panyu District, Guangzhou, P.R China.
Postcode: 510006

5-year Individual Researcher Position ~Yamanaka-Balzan Award~

Center for iPS Cell Research and Application (CiRA),
Kyoto University
Director: Shinya Yamanaka

CiRA invites applications for a 5-year individual researcher position with research expenses. In September 2010, the International Balzan Prize Foundation awarded Prof. Yamanaka because of his efforts to generate iPS cells from somatic cells. Based on this award, CiRA have established the "Yamanaka-Balzan Award" to support a young researcher who could contribute to the research on the mechanisms of direct reprogramming and further application of iPS cell technology. The position allows the selected researcher to conduct iPS cell research for 5 years with research expenses, 100,000 Swiss francs/year. Faculty title will depend on her/his achievements and experience.

Please refer to our website for details:
http://www.cira.kyoto-u.ac.jp/e/employment.html

Work Place: CiRA, Kyoto University, Japan

Qualifications: Researcher with less than 10 years of research experience since obtaining Ph.D. (As of October 2010)

Job Conditions: [Term] 5 years (from April 1st, 2011)[Salary] In accordance with Kyoto University Regulations [Research expense] 100,000 Swiss francs/year

*Other necessary human resources or equipments is provided from CiRA, separately.

How to apply: Applicants should mail CV, list of research achievements and some other required documents to the postal address listed below by January 13. Please see our website for details and download the forms. (Applying by e-mail is not acceptable.)

Contact: Tetsuya Ishii
Head of the Research Management Office
Center for iPS cell Research and Application (CiRA), Kyoto University
(53 Kawara-cho, Shogoin, Sakyo-ku, Kyoto, Japan 606-8507)
E-mail: **collaboration@cira.kyoto-u.ac.jp**

Visit our ENHANCED WEBSITE!

Revealing your vision to employers is our job. We're your source for connecting with top employers in industry, academia, and government. We're the experts and entry point to the latest and most relevant career information across the globe.

Our newly designed website offers a set of tools that reveal career opportunities and your personal potential. Whether you're seeking a new job, career advancement in your chosen field, or ways to stay current on industry trends, *Science* Careers is your window to a limitless future.

Improved Website Features:

- Relevant Job E-mail Alerts
- Improved Resume Uploading
- Content Specific Multimedia Section
- Facebook Profile

Job Search Functionality:

- Save and Sort Jobs
- Track Your Activity
- Search by Geography
- Enhanced Job Sorting

Your Future Awaits.

Science Careers

From the journal *Science* AAAS

ScienceCareers.org

POSITIONS OPEN

ASSISTANT PROFESSORS IN ECOLOGY AND NEUROBIOLOGY
Department of Biology
University of Nevada, Reno

The Biology Department at the University of Nevada, Reno (UNR) has targeted EECB (ecology, evolution, and conservation biology) and neurobiology as strategic foci for growth and is seeking:

An ECOLOGIST—Assistant Professor (tenure-track)

The ecology position is open with regard to area of specialization. The department's areas of research excellence include conservation biology, conservation and evolutionary genetics, behavioral ecology, and evolutionary ecology. Our EECB faculty are well funded by diverse sources, including NSF and NIH.

A NEUROBIOLOGIST—Assistant Professor (tenure-track)

The neurobiology position is open to researchers investigating any fundamental neurobiological topic using cellular, genetic, or molecular approaches. The successful applicant will expand our core group of NSF and NIH funded neuroscientists. Excellent support facilities include microscopy, genomics, and proteomics cores. Early career faculty who conduct biomedically related research at UNR can apply for NIH-IDeA program career development support.

Applicants for both positions should have expertise that complements and expands the research capacity of the department. The successful candidates will be provided with competitive startup packages and will be expected to maintain nationally recognized, extramurally funded research programs. The Department has 765 majors, 45 M.S. and Ph.D. students, and 24 state-funded faculty. In addition, a new interdisciplinary program in Neuroscience supports 114 majors. Reno sits on the eastern flank of the Sierra Nevada in close proximity to desert and montane field sites and to Lake Tahoe, and it was recently rated one of the best small cities in the United States for overall quality of life. Applicants should apply online at **website: http://www.unrsearch.com,** where they should submit an application letter, curriculum vitae, a statement of research plans, a statement of teaching interests and philosophy, and contact information for three references. Applications received by 21 January 2010 will receive full consideration. The start date is 1 July 2011 for both positions.

Equal Employment Opportunity/Affirmative Action. Women and underrepresented groups are encouraged to apply.

ASSISTANT PROFESSORS

The Department of Biological Sciences (**website: http://biology.uark.edu**) at The University of Arkansas solicits applications for two tenure-track Assistant Professors. (1) **MICROBIOLOGIST** working in any area of microbiology (**position No. Y11929**). (2) **PLANT BIOLOGIST** using photosynthetic organisms to explore topics including but not limited to systematics, developmental/physiological genetics or molecular ecology (**position No. Y11928**). Successful candidates must have a Ph.D. and postdoctoral experience, will be expected to establish an extramurally supported research program, supervise graduate and undergraduate research, and teach at the graduate and undergraduate levels. Review of completed applications will begin January 31, 2011, and will continue until the positions are filled. Applications should include curriculum vitae, a statement of current and future research plans, teaching interests, and three letters of recommendation. Application materials should be sent or electronically sent to the appropriate search committee chair: **Dr. Mack Ivey** (**e-mail: mivey@uark.edu**) for Microbiologist or **Dr. Jeffrey Silberman** (**e-mail: jeff@uark.edu**) for Plant Biologist. **Department of Biological Sciences, 601 SCEN, 1 University of Arkansas, Fayetteville, AR 72701.** *The University of Arkansas is an Equal Opportunity/Affirmative Action Employer. Applicants must have proof of legal authority to work in the United States at the time of hire. All applicants are subject to public disclosure under the Arkansas Freedom of Information Act.*

TENURE-TRACK FACULTY POSITION
Department of Chemistry and Biochemistry
Utah Science, Technology and Research (USTAR) Initiative
Utah State University

The USTAR initiative and the Department of Chemistry and Biochemistry at Utah State University, invite applications for a tenure-track position at any rank. Candidates must have a Ph.D. in Chemistry, Biochemistry, or a related field, with an established research track record in either academia or industry. The successful applicant is expected to maintain and expand a research program related to health therapeutics or disease diagnostics via chemical or biochemical approaches. Preference will be given to candidates with research programs in the areas of medicinal, synthetic, or bioanalytical chemistry that complement the USTAR Veterinary Diagnostics and Infectious Disease (VDID) research program. The position is funded by the USTAR initiative, a statewide program that aims to promote commercialization of technologies at the state universities. Applicants should submit curriculum vitae, a concise description of future research projects and their relevance to the goals of VDID, associated major research infrastructure needs, and the names and e-mail addresses of three references at **website: http://jobs.usu.edu** (**REQ ID 052439**). Evaluation of applications will begin January 15 and will continue until the position is filled. For further information, please visit our **website: http://www.chem.usu.edu.** *Utah State University is an Equal Opportunity/Affirmative Action Employer committed to assembling a diverse faculty. Women and members of minority groups are strongly encouraged to apply.*

POSTDOCTORAL AND RESEARCH ASSISTANT POSITIONS
Bioinformatics and Genomics of Gene Regulation
University of Texas Southwestern Medical Center at Dallas

Seeking individuals with a Ph.D. or Master's degree in bioinformatics, computational biology, or genomics to study gene regulation on a global scale in the laboratory of **Dr. W. Lee Kraus.** Candidates should be proficient in programming and analysis of genomic data sets, and have experience working with biological systems. The Kraus laboratory has a number of exciting ongoing projects related to the genomics of signal-regulated gene expression (visit our laboratory site and view us on PubMed). The University of Texas Southwestern Medical Center provides a dynamic, collaborative, integrative, and cutting-edge research and training environment.

Candidates should submit curriculum vitae or resume, brief statement of interests and accomplishments, and a list of three references by **e-mail: lee.kraus@utsouthwestern.edu.** Successful applicants will receive competitive pay and benefits.

University of Texas Southwestern Medical Center is an Equal Opportunity/Affirmative Action Employer.

AQUATIC ECOLOGY POSTDOCS

The U.S. Environmental Protection Agency (USEPA) Office of Research and Development's National Center for Environmental Assessment seeks applications for several postdoctoral positions focused on quantifying relationships between physical, chemical, and biological stressors and the condition of valued biological resources. The successful applicant will be part of a vibrant team that is studying stressors related to energy production (mountaintop mining, biofuels) and urbanization to inform environmental decision-makers about the probable causes of biological impairments in aquatic ecosystems. Examples of our work can be viewed at **website: http://www.epa.gov/caddis.**

These are three-year, federal appointments in Arlington, Virginia. Salary is approximately $62,000 to $75,000 commensurate with qualifications, plus benefits. *Citizenship restrictions apply.* Additional information and application instructions may be found at **website: http://www.epa.gov/ncea,** or by contacting **Jeffrey Frithsen, e-mail: frithsen.jeff@epa.gov.** Application deadline is January 7, 2011. *The USEPA is an Equal Opportunity Employer.*

ASSISTANT/ASSOCIATE PROFESSOR
Neuroscience

The Division of Basic Biomedical Sciences at the Sanford School of Medicine of The University of South Dakota invites applications for a tenure-track faculty position at the Assistant or Associate Professor level. Applicants must have a Ph.D. and/or M.D., or equivalent degree, and postdoctoral experience. Successful candidates will be expected to develop an independent, externally funded research program. Candidates must have technical expertise in functional magnetic resonance imaging and should develop a research program that complements and interacts with existing strengths in the Division. Preference will be given to candidates working in areas related to stress and trauma, brain injury and recovery, learning and memory, neurodegenerative disorders, or addiction, though additional areas will be considered. The successful candidate will also be expected to participate in teaching undergraduate, graduate, and medical students. Excellent startup funds, state-funded salary commensurate with experience, and modern research facilities in the new Lee Medical Building, Vermillion, South Dakota will be provided. Application should include curriculum vitae, a summary of past research and teaching experience, a statement of research interests and future plans, as well as three letters of reference. All materials should be sent to The University of South Dakota online employment **website: https://yourfuture.sdbor.edu.** Review of applications will begin on January 17, 2011 and continue until position is filled. *Women and minorities are encouraged to apply. Affirmative Action/Equal Opportunity Employer.*

REHABILITATION COORDINATOR, Colton, California, advises on rehab options; monitors progress; assesses patient rehab needs/goals; coordinates resources and support. 8am–5pm. B.S. behavioral science/psychology. $56,285 per year plus benefits. Resumes to: **Recruitment & Employment Office, Reche Canyon Rehabilitation Center a DBA of Reche Canyon Convalescent Center, Attn: Job Ref #: REC86195, P.O. Box 56625 Atlanta, GA 30303.**

UNIVERSITY COLLEGE CORK

Applications are invited for the post of: **PROFESSORSHIP** in Plant Biology.

Salary: €113,604–€145,953.

For full details, see **website: http://www.ucc.ie/hr/vacancies/academic.**

Closing Date: Monday 31 January 2011.

MARKETPLACE

Preclinical research customized for you.

Your responsive CRO partner, delivering customized solutions and adaptability to changing needs.

MPI Research is the CRO that defines responsiveness, moving your drug development program forward with customized solutions for all your preclinical research. From discovery services to safety evaluation, including analytical and bioanalytical support, you can count on MPI Research for quick quotes, frequent updates, rapid turnaround, and scientific rigor. At every stage, and on every level, we adapt to your most exacting needs.

Explore the breadth of capabilities that make us your responsive CRO at www.MPIResearch.com.

MPI RESEARCH

Customized. Responsive. On-Time.™

Fusing nanotechnology with biotechnology, Toray DNA microarrays are 100 times more sensitive than conventional technologies, allowing for more microscopic measurements than ever before. Toray continues to develop next-generation bio-tools to enable faster, more accurate medical diagnoses, detect microorganisms for soil decontamination, and bring new value to life. ***The right chemistry, the right answers.***

Find new BLOOD RNA markers!

miRNA Analysis of Serum/Plasma

Analysis service for comprehensive gene expression from blood samples is started!
miRNA in serum/plasma now receives much attention as a new candidate of biomarkers in the biological research, clinical study, toxicology and drug discovery.
The combination of our novel miRNA extraction technique and the highly sensitive microarray ***3D-Gene***™ will bring you exciting new discovery.

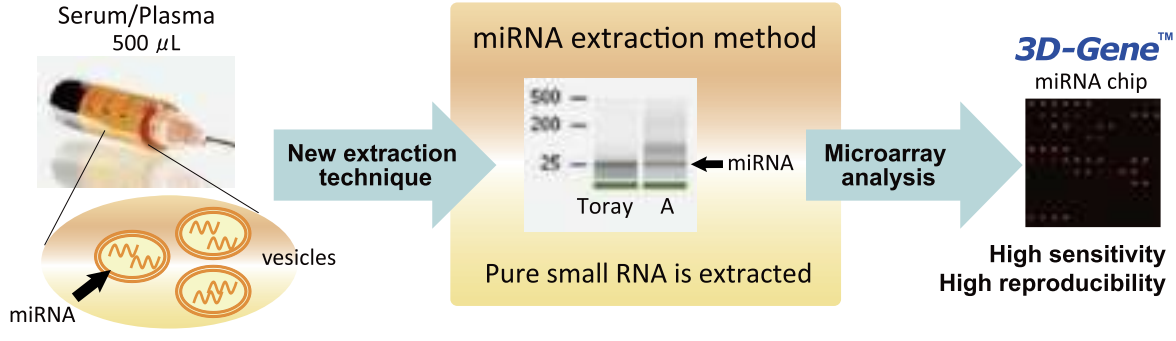

miRNA in commercially available healthy control serum (10 mixed) or Tumor A patient serum (6 mixed) was analyzed by ***3D-Gene***™.

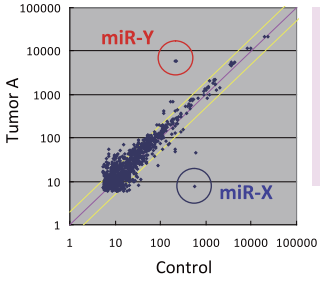

miR-X : Association with multiple cancers has been reported.
- Lung, ovary, gastrointestinal cancer
- Inhibitory effects on oncogenes

miR-Y : No report about cancer association.
- Target and mechanism is also unknown.

Known marker detection & novel marker finding

Toray Industries, Inc.
1-1, Nihonbashi-Muromachi 2-chome, Chuo-ku, Tokyo 103-8666, JAPAN
http://www.3d-gene.com

'TORAY'
Innovation by Chemistry

GE Healthcare
Life Sciences

Thank you ECL™ Plus, you've been great.

For every success there's a successor. It's called progress. So while we knew we had something special in Amersham™ ECL Plus, our Western blotting team was quietly working on the next generation of detection reagent. The result: a new substrate that operates with superior levels of sensitivity, signal intensity and stability than even its famous predecessor, making it an excellent choice for CCD imagers. **Welcome to ECL Prime.**

Signal intensity sustained at higher antibody dilutions

Ab dilution		Amersham ECL Prime		Amersham ECL Plus	
Primary	**Secondary**	10 µg	156 ng	10 µg	156 ng
1:3000	1:300 000				
1:10 000	1:500 000				

Comparison of Amersham ECL Prime and Amersham ECL Plus detection of ß-catenin in NIH 3T3 whole cell lysates using different dilutions of rabbit anti-ß-catenin and HRP-conjugated anti-rabbit IgG.

Find out more about Amersham ECL Prime at www.gelifesciences.com/eclprime

imagination at work

Any sample, any application — no limits

Maximize success with QIAGEN sample technologies

- Innovative, room-temperature sample collection and stabilization
- DNA, RNA, and protein purification from any sample
- Hands-free automated sample preparation
- Reliable genetic, epigenetic, and gene expression analysis from FFPE samples
- Whole genome and transcriptome amplification to overcome sample limitations

Contact QIAGEN today or visit www.qiagen.com/sample-technologies

QIAGEN®

Sample & Assay Technologies

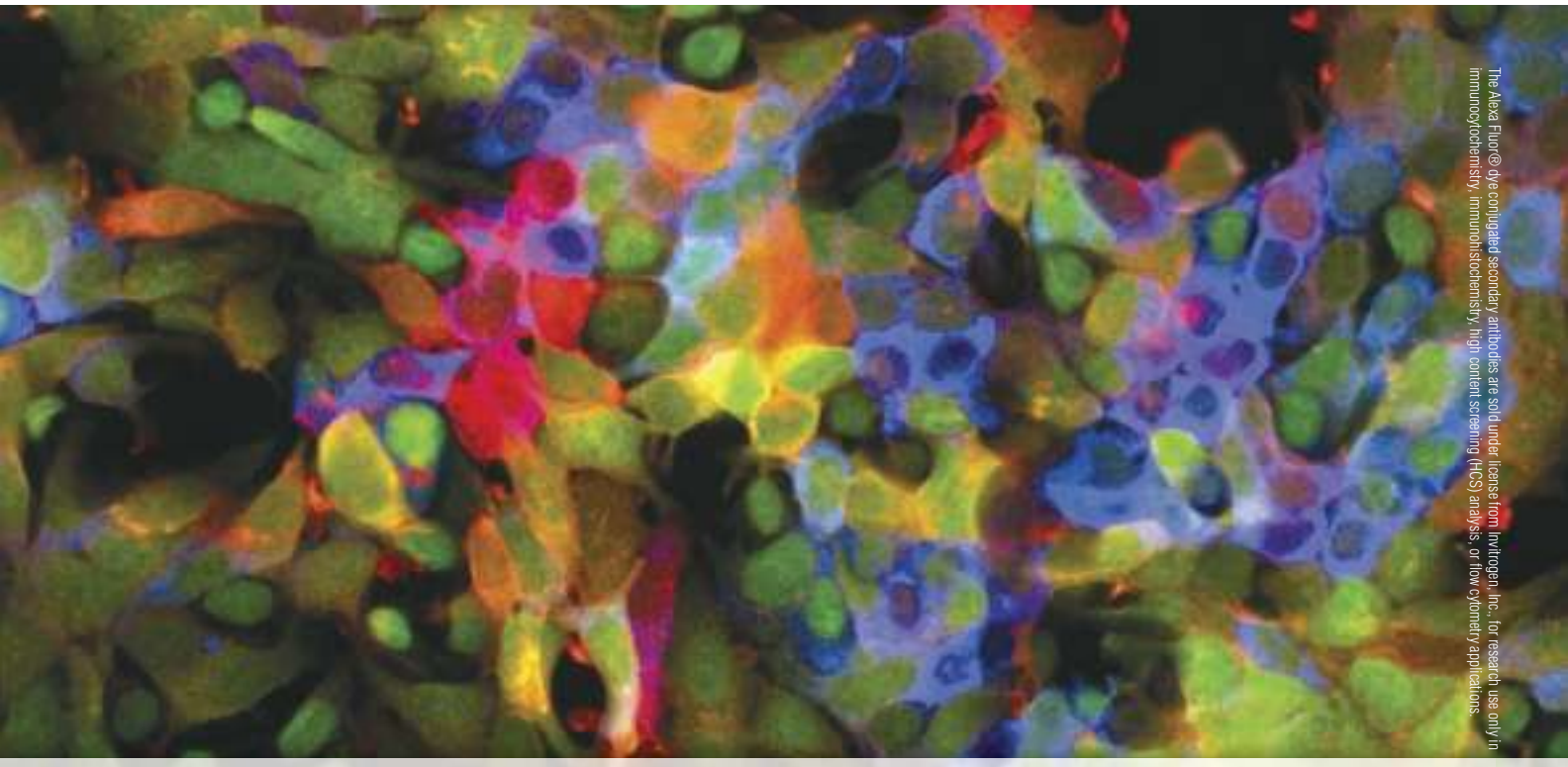

The Alexa Fluor® dye conjugated secondary antibodies are sold under license from Invitrogen, Inc., for research use only in immunocytochemistry, immunohistochemistry, high content screening (HCS) analysis, or flow cytometry applications.

PathScan® Signaling Nodes Multiplex IF Kit

from Cell Signaling Technology

Immunofluorescent analysis of MCF7 (human breast adenocarcinoma) cells insulin-treated for 5 minutes, using PathScan® Signaling Nodes Multiplex IF Kit #8999.

PathScan® Signaling Nodes Multiplex IF Kit #8999 from Cell Signaling Technology provides a novel multiplex assay to simultaneously assess signaling through key pathway nodes (activated-Akt, p44/42, and S6 Ribosomal Protein) using automated imaging or laser scanning high content platforms, or manual immunofluorescence microscopy. The kit provides reagents necessary to perform 100 assays (based on 100 µl assay volume).

- The kit allows the analysis of multiple pathway endpoints within a single sample, saving time and reagents.
- The kit is produced and optimized in-house with the highest quality antibodies, providing you with the greatest possible specificity and sensitivity.
- Technical support is provided by our in house IF group who developed the product and knows it best.

#8999 Kit Targets	Detection Dye	$Ex_{(max)}$ (nm)	$Em_{(max)}$ (nm)
Phospho-Akt (Ser473)	Alexa Fluor® 555	555	565
Phospho-p44/42 (Erk1/2) (Thr202/Tyr204)	Alexa Fluor® 488	495	519
Phospho-S6 Ribosomal Protein (Ser235/236)	Alexa Fluor® 647	650	665

for quality products you can trust...

www.cellsignal.com

Cell Signaling TECHNOLOGY®

Orders (toll-free) 1-877-616-2355 | **Technical support** (toll-free) 1-877-678-8324 support@cellsignal.com | **Inquiries** info@cellsignal.com | **Environmental Commitment** eco.cellsignal.com

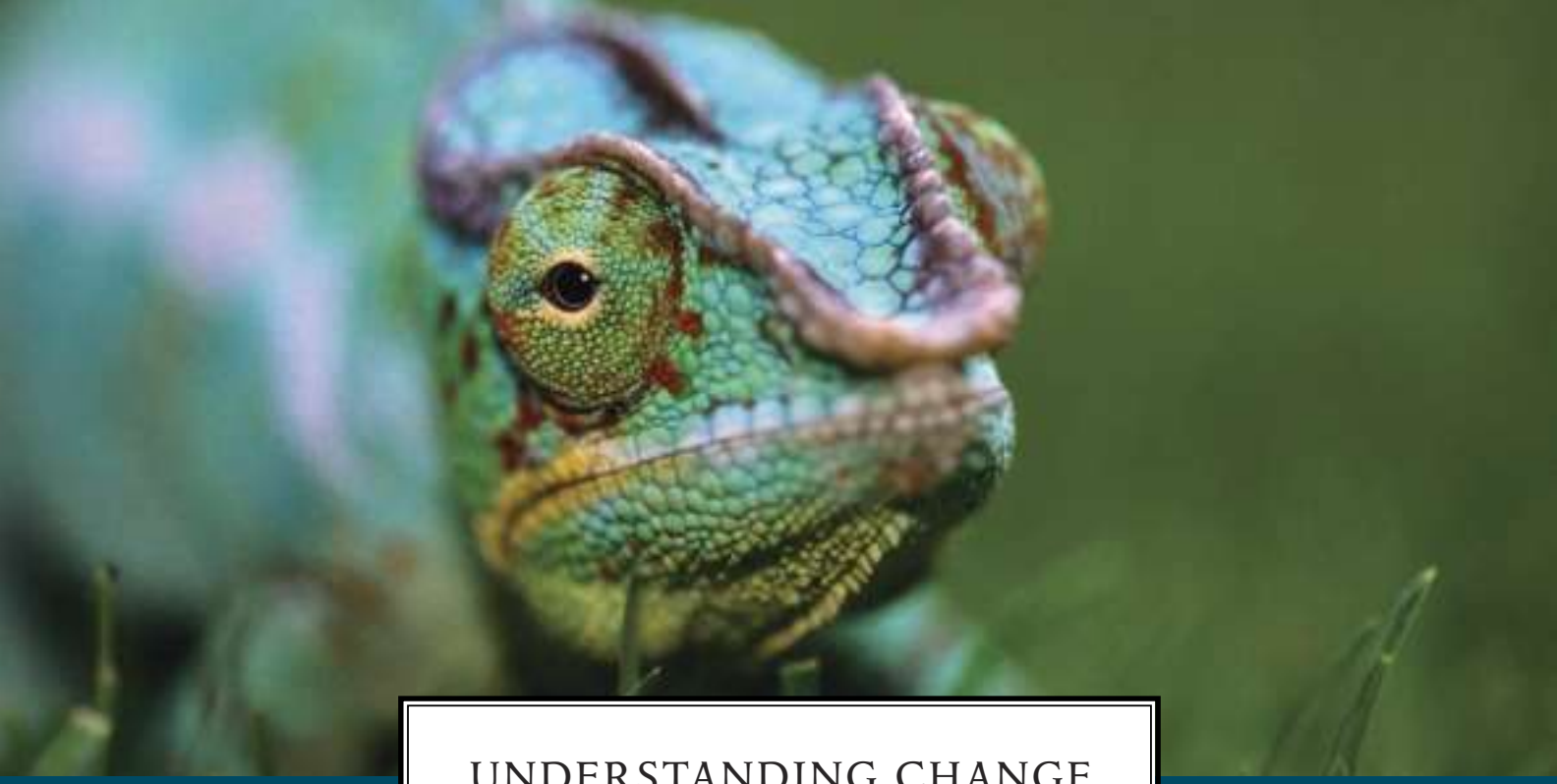

UNDERSTANDING CHANGE

New tools to advance epigenetics research

For over 35 years, New England Biolabs has been committed to understanding the mechanisms of restriction and methylation of DNA. This expertise in enzymology has recently led to the development of a suite of validated products for epigenetics research. These unique solutions to study DNA methylation are designed to address some of the challenges of the current methods. EpiMark™ validated reagents simplify epigenetics research and expand the potential for biomarker discovery.

Simplify DNA methylation analysis with MspJI

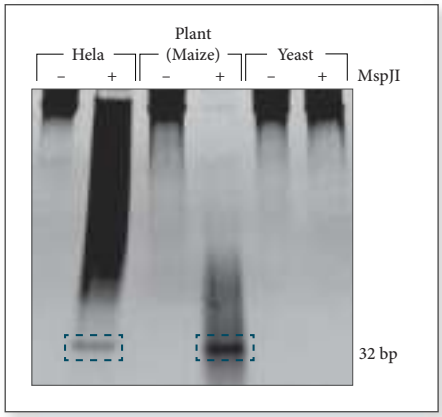

MspJI recognizes methylated and hydroxymethylated DNA and cleaves out 32 bp fragments for sequencing analysis. Overnight digestion of 1 µg of genomic DNA from various sources with or without MspJI is shown. Note: Yeast DNA does not contain methylated DNA, therefore no 32-mer is detected.

EpiMark™ validated products include:

- Newly discovered methylation-dependent restriction enzymes
- A novel kit for 5-hmC and 5-mC analysis and quantitation
- Methyltransferases
- Histones
- Genomic DNAs

To learn how these products can help you to better understand epigenetic changes, visit neb.com/epigenetics.

NEW ENGLAND BioLabs® Inc.
enabling technologies in the life sciences

Bioidentify.

Introducing the MISSION® 3'UTR Lenti GoClone.

Take the guess work out of your miRNA target validation!

You can now validate the 3'UTR target of your favorite miRNA with a functional, versatile and quantitative assay. Sigma Life Science and SwitchGear Genomics Inc., have partnered to offer you a collection of lentiviral constructs, each with a unique human 3'UTR cloned downstream of an optimized *Renilla* luciferase. Identify and validate the 3'UTR target of your favorite miRNA with the powerful new MISSION 3'UTR Lenti GoClone!

wherebiobegins.com/lentigoclone

biosilencing

华大基因 BGI

Premier Scientific Partner

Genomics Solutions

de novo
Whole Genome Resequencing
Exome
Target region
RNA-Seq
Metagenomics
Epigenomics
Microbes

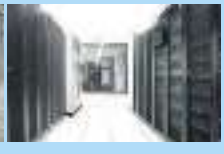

Sequencing & Computing Platforms

- **137** Illumina HiSeq 2000
  27 Applied Biosystems SOLiD 4 System
- Supercomputing centers with a total of
  102 T flops
  20 TB memory
  10 PB storage

Bioinformatics Centre

- **1000** professionals

Email: tech@genomics.cn
Web: www.genomics.cn

BGI, as the premier scientific partner, establishes collaborations worldwide to accelerate the innovation and development of genomics research and applications in healthcare, agriculture, bioenergy and related areas.

Based on the powerful infrastructure and acknowledged research background, our goal is to partner with researchers and scientists, make leading-edge genomics accessible to the global research community and deliver more discoveries.

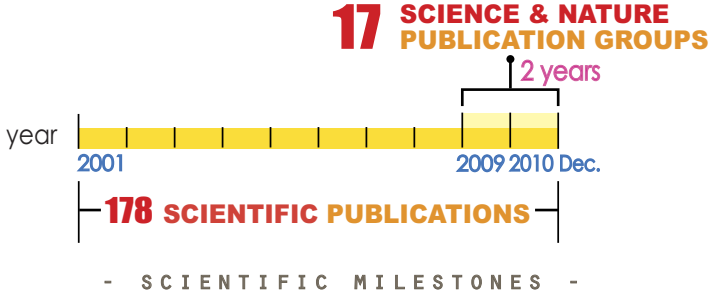

- SCIENTIFIC MILESTONES -

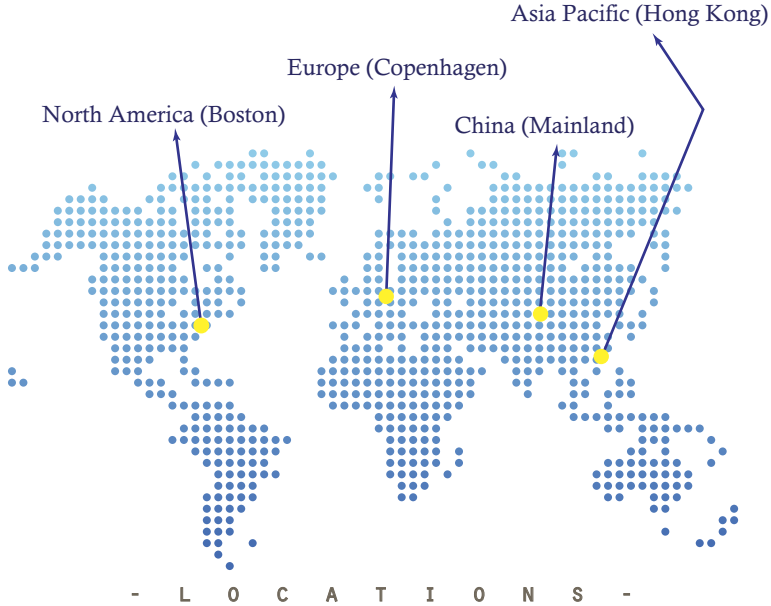

- LOCATIONS -

'Tis the season of giving (and getting)

Give *Science* with full AAAS benefits. Get our special gift rate and our new shirt!

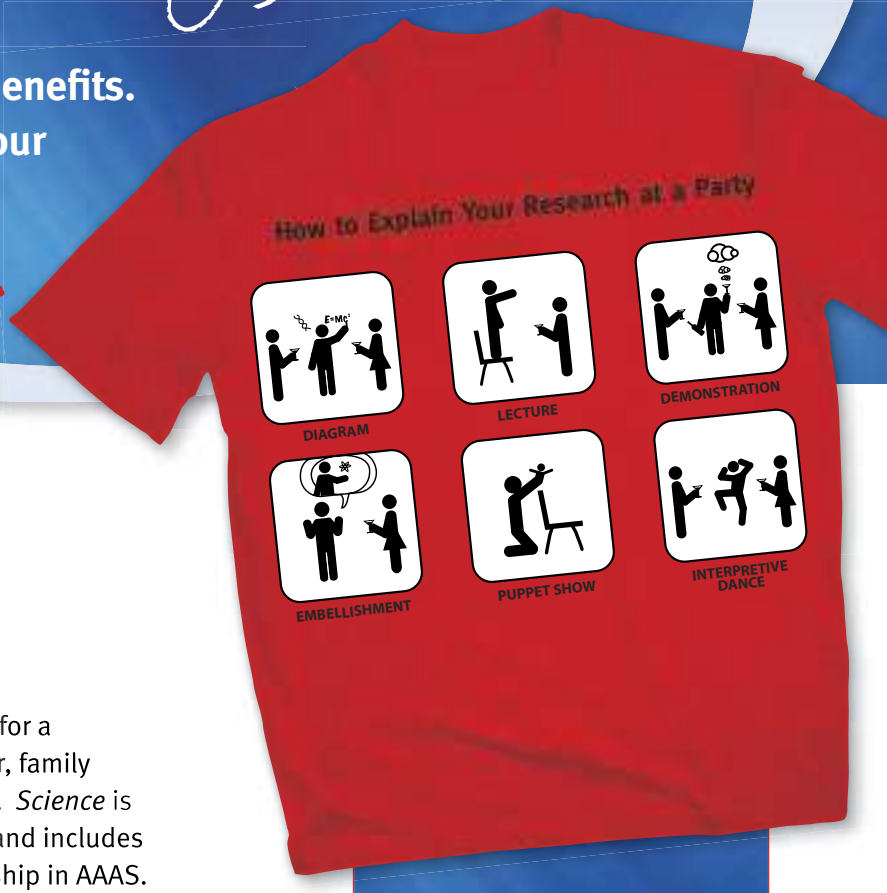

$99 Professional gift rate
(reg. $146)

$50 Postdoc/Student gift rate
(reg. $99/$75)

Make the holidays happier for a promising young researcher, family member, friend, or student. *Science* is the gift that lasts all year—and includes all the benefits of membership in AAAS.

Get our new "Explain Your Research" shirt—FREE! With its playful graphics, it makes just the right fashion statement at holiday gatherings, and other social events all year long.

You'll enjoy something else as well: the satisfaction of helping to support AAAS and our international, public policy, and educational programs—the ones that advance science and serve society. Happy holidays, indeed!

A $22.50 value—yours FREE when you give *Science!*

AAAS + U = Δ

Detail on back

Order now: visit promo.aaas.org/holiday or call 866-434-2227.

Please order at least two weeks before the holiday you're celebrating, so we have time to send your gift recipient a letter announcing your gift. Non-U.S. recipients may receive *Science* Digital edition at the special gift rate. Check online for print edition rates. $74 allocated to *Science* for Professional memberships, $50 for Postdoc/Student memberships. Please allow 4 weeks for receipt of first issue. Prices valid through 3/1/11.

Science
AAAS

SBS 17TH ANNUAL CONFERENCE & EXHIBITION

Advancing the Science of Drug Discovery

Gaylord Palms Resort and Convention Center
March 27–31, 2011 | Orlando, Florida, USA

Learn more and register at SLAS.org/events/sbs11

Some of the Many Reasons to Attend SBS 2011:

- **15 Diverse Scientific Sessions Organized Into Three Tracks:**
  - » Innovation in the Screening Sciences
  - » Translational Research
  - » Sequenced Genomes: Reducing Opportunities to Practice
- **Engaging Keynote Presentations**
  From SBS Achievement Award winner Robert J. Lefkowitz, M.D., Duke University, and SBS Accomplishment Award winner Brian Shoichet, Ph.D., University of California, San Francisco
- **Enhanced Exhibit Hall Hours and Schedule**
  Allowing for a thriving exhibit floor with leading companies from around the world
- **SLAS Smart-Savers Discount Program**
  Offering extraordinary discounts on flights, registration, hotel accommodations, and more
- **Enhanced SLAS Career Connections**
  Providing a forum for job seekers and employers to connect and career coaches offering free coaching services to participants by appointment
- **SLAS New Product Award Designation**
  Recognizing up to three of the best and most promising new products launched on the exhibit floor

Register Today at SLAS.org/events/sbs11

slas SOCIETY FOR LABORATORY AUTOMATION AND SCREENING
An International Community Advancing Scientific Research and Discovery Through Laboratory Technology

The Society for Laboratory Automation and Screening (SLAS) is a new non-profit scientific organization uniting the Society for Biomolecular Sciences (SBS) and the Association for Laboratory Automation (ALA). The SLAS mission is to be the preeminent global organization providing forums for education and information exchange to encourage the study of, and improve the science and practice of, laboratory automation and screening.

Society for Biomolecular Sciences SBS | ALA Association for Laboratory Automation

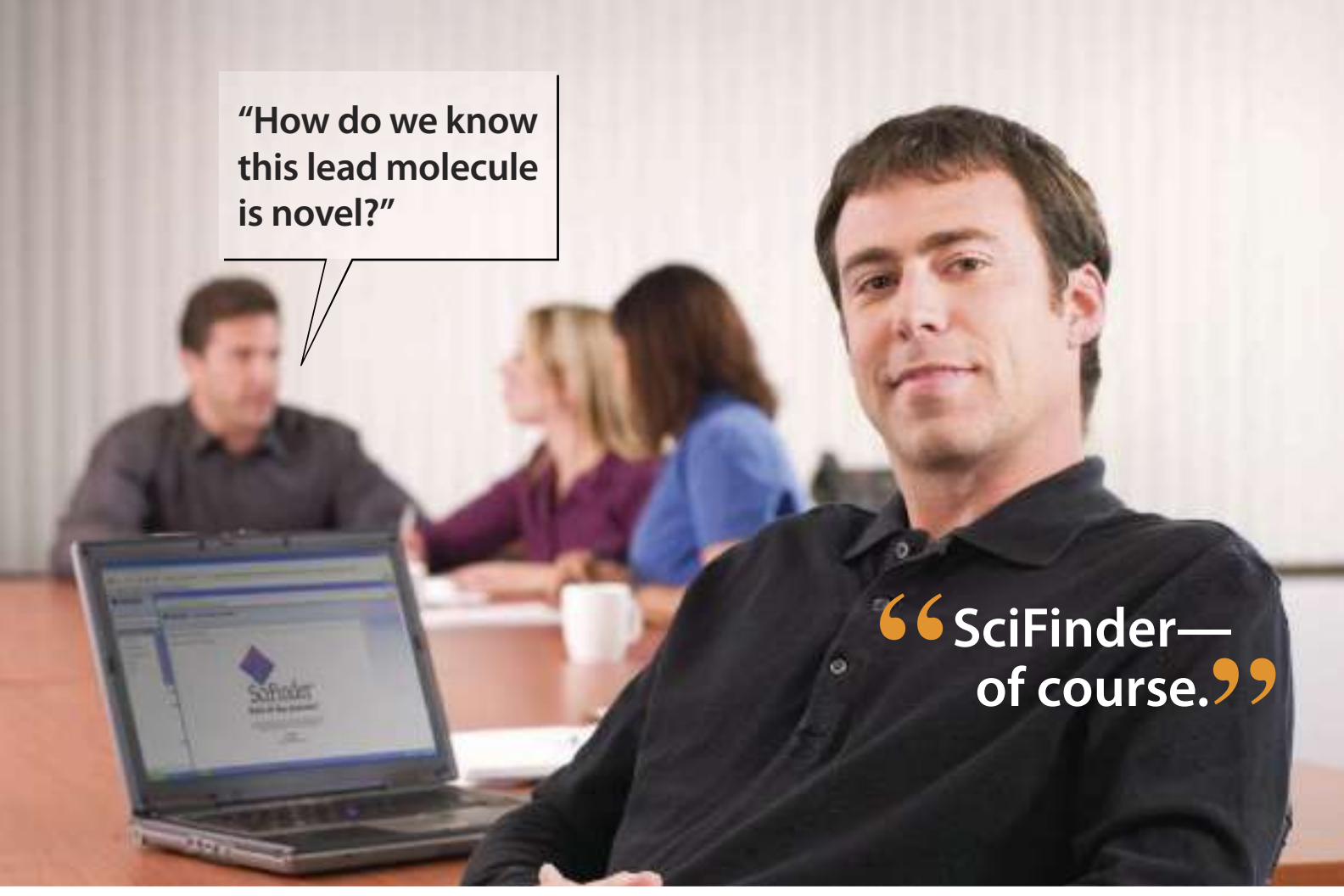

Need to assess the novelty of substances?
SciFinder is the answer.

It includes CAS REGISTRY,SM the most comprehensive substance information available, integrated with relevant journal articles and patents.

Give your research team the highest quality and most timely scientific information resource.

Make SciFinder an essential part of your research process.

For more information about SciFinder, visit www.cas.org or e-mail help@cas.org.

an essential

SciFinder®—Part of the process.™

CAS | SciFinder®

www.cas.org

CAS is a division of the American Chemical Society

MBL Biological Discovery in Woods Hole

Founded in 1888 as the Marine Biological Laboratory

Substantial financial assistance is available for many of our courses!

2011 Courses

Analytical & Quantitative Light Microscopy
May 4 - May 13

Biology of the Inner Ear
August 7 - August 27

Biology of Parasitism: Modern Approaches
June 17 - August 6

BioMedical Informatics
1st Session: May 29 - June 4
2nd Session: September 18 - September 24

Embryology: Concepts & Techniques in Modern Developmental Biology
June 4 - July 17

Frontiers in Reproduction: Molecular & Cellular Concepts & Applications
April 30 - June 12

Frontiers in Stem Cells and Regeneration
October 2 - October 8

Gene Regulatory Networks for Development
October 11 - October 22

Methods in Computational Neuroscience
July 31 - August 28

Microbial Diversity
June 11 - July 28

Molecular Biology of Aging
July 24 - August 13

Molecular Mycology: Current Approaches to Fungal Pathogenesis
August 3 - August 19

Neural Systems & Behavior
June 4 - July 31

Neurobiology
June 4 - July 31

Neuroinformatics
August 13 - August 28

Optical Microscopy & Imaging in the Biomedical Sciences
October 11 - October 21

Physiology: Cell & Computational Biology
June 11 - July 31

Strategies and Techniques for Analyzing Microbial Population Structures
August 3 - August 13

Summer Program in Neuroscience, Ethics, & Survival (SPINES)
June 18 - July 16

Workshop on Molecular Evolution
July 24 - August 3

Zebrafish Development & Genetics
August 7 - August 21

FOR MORE INFORMATION CONTACT:
Admissions Coordinator; admissions@mbl.edu;
(508) 289-7401, MBL, 7 MBL Street,
Woods Hole, MA 02543

www.mbl.edu/education

The MBL is an Equal Opportunity/Affirmative Action Institution.

abcam®

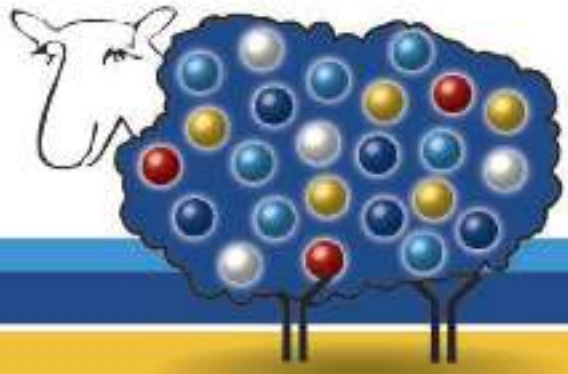

New Stem Cell Marker Panels

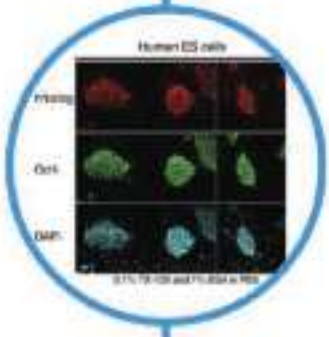

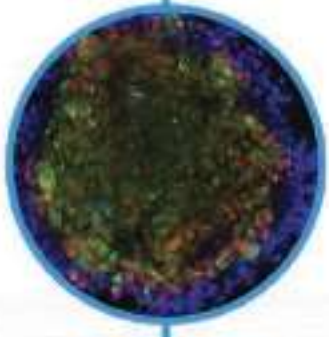

New data available

- **Human Embryonic Stem Cell Marker Panel (ab93085)**
  Oct3/4 , Nanog, SSEA3, SSEA4, Tra-1-60

- **Mouse Embryonic Stem Cell Marker Panel (ab93757)**
  Oct3/4, Nanog, SOX2, SSEA1, Lin28

- **Human Mesenchymal Stromal Cell Marker Panel (ab93758)**
  CD44, CD90 , CD29 , CD105, CD45.

We have complimented our existing range of over 12,000 stem cell products with brand new stem cell marker panels. These combinations allow the definitive validation and characterization of cultured or newly derived embryonic and mesenchymal stem cell lines. The panels contain five antibodies to well known markers, with citations, reviews, optimal dilutions and also, negative controls in the mesenchymal range.

www.abcam.com

Abcam in the USA
Abcam Inc
1 Kendall Square, Ste 341
Cambridge,
MA 02139-1517
USA

Tel: +1-517-228-2272
Tollfree: +1-888-77-ABCAM
Fax: +1-866-739-5864

Abcam in Europe
Abcam plc
330 Cambridge Science Park
Milton Road
Cambridge
CB4 0FL
UK

Tel: +44-(0)1223-696000
Fax: +44-(0)1223-771600

Abcam in Japan
Abcam KK
1-16-8 Nihonbashi
Kakigaracho,
Chuo-ku
Tokyo 103-0014
Japan

Tel: +81-(0)3-6231-0940
Fax: +81-(0)3-6231-0941

Abcam in Hong Kong
Abcam (Hong Kong) Ltd
Unit 225A & 225B, 2/F
Core Building 2
1 Science Park West Avenue
Hong Kong Science Park
Hong Kong

Tel: (852)-2603-6023
Fax: (852)-3016-1688

NEW PRODUCTS FOCUS: RNAi

siRNA PREMIXES

With FlexiTube siRNA Premix, small interfering RNA (siRNA) for your gene of interest and highly efficient transfection reagent are already premixed and provided in a single tube. FlexiTube siRNA Premix includes a specialized buffer that increases the stability of siRNA-reagent complexes. The ratio of reagent to siRNA in FlexiTube siRNA Premix is preoptimized to provide the highest transfection efficiency and gene knockdown. FlexiTube siRNA Premix is ready-to-use for cell transfection. Simply add to cells and incubate. With FlexiTube siRNA Premix, RNA interference experiments get off to a faster start, as there is no need to optimize siRNA-to-reagent ratio. Tedious optimization experiments involving multiple transfections are minimized or eliminated. Multiple transfections can be performed from a single FlexiTube siRNA Premix, reducing variability, and enabling consistency across experiments and more reliable results.

Qiagen

For info: 800-426-8157 | www.qiagen.com

TRANSFECTION REAGENTS

Effective and nontoxic DNA and small interfering RNA (siRNA) delivery is essential for reliable scientific results. jetPRIME is a new versatile and powerful DNA and siRNA transfection reagent for day-to-day experiments. jetPRIME ensures high DNA transfection efficiency and excellent gene silencing in a variety of adherent cells. jetPRIME is ideal for DNA/siRNA cotransfection and is very gentle to cells since it requires low amounts of nucleic acid and reagent during transfection. The jetPRIME protocol is easy-to-follow and compatible with the use of serum and antibiotics during transfection.

Polyplus Transfection

For info: 508-315-9629 | www.polyplus-transfection.com

siRNA SILENCING KIT

Enabling researchers to perform efficient small interfering RNA (siRNA) silencing (gene knockdown) experiments in small animal models, Invivofectamine 2.0 Reagent and Ambion In Vivo siRNA provide strong and sustained knockdown of in vivo protein expression in an easy-to-use kit. These tools accelerate the use of RNA interference to efficiently study gene function in animal models. Targeted gene silencing has been demonstrated to last for more than three weeks with a single application of Invivofectamine 2.0 Reagent and the positive control Ambion In Vivo siRNA. The new reagents provide a powerful alternative to the conventional use of knockout mouse models, which can take nearly 10 months to develop. Sold as part of a 1 ml starter kit or a 5 ml kit, Invivofectamine 2.0 Reagent and Ambion In Vivo siRNA are synthetic, contain no components of viral origin, and show minimal to no toxicity after extensive initial studies.

Life Technologies (Invitrogen)

For info: 800-955-6288 | www.invitrogen.com

IN VIVO TRANSFECTION KIT

The PEG-Liposome siRNA In Vivo Transfection Kit is designed for in vivo transfection of negatively charged molecules—RNA, DNA, and small proteins. Transfection is one of the major laboratory methods used to introduce DNA and RNA molecules into cells and tissues. This technique makes it possible to cross cellular barriers and deliver a gene or a small interfering RNA (siRNA) into cells for research or therapeutic purposes. The novel PEGylated liposome-based siRNA delivery kit is optimized for directed RNA interference induction by efficient delivery of functional small RNA molecules (siRNA, shRNA, miRNA) into tissues. The liposome component provides in vivo siRNA protection due to efficient siRNA-liposome encapsulation. A remarkable feature of this reagent is reduced innate immune response and low cytotoxicity due to biodegradable PEG modification.

Altogen Biosystems

For info: 800-658-7009 | www.altogen.com/mirna.php

RNA ISOLATION

When working with stored materials, researchers often need to isolate RNA from samples that have been stored as formalin-fixed paraffin-embedded (FFPE) tissue blocks. Although the tissue structure of FFPE samples will have been maintained for histological analysis, damage to the nucleic acid may have occurred through the fixation, embedding, and storage processes impeding measurements of gene expression levels. ExpressArt FFPE RNAready overcomes the limitations associated with RNA degradation and interference from RNA cross-linking in FFPE tissues. The FFPE RNAready kit efficiently isolates and preserves mRNA using a specially developed lysis solution and an innovative universal inhibitor of RNases that displaces tightly bound RNA from high-molecular-weight aggregates. Subsequent treatment with a unique de-modification reagent reverses formalin induced cross-links, resulting in total RNA optimized for reverse transcription reactions and subsequent downstream applications. FFPE RNAready together with ExpressArt RNA amplification TRinucleotide primer technology is now available to amplify microgram quantities of high quality RNA from very small amounts of degraded total RNA, with minimal loss of sequence.

AMSBIO

For info: +44-0-1235-828200 | www.amsbio.com

Electronically submit your new product description or product literature information! Go to www.sciencemag.org/products/newproducts.dtl for more information.

Newly offered instrumentation, apparatus, and laboratory materials of interest to researchers in all disciplines in academic, industrial, and governmental organizations are featured in this space. Emphasis is given to purpose, chief characteristics, and availability of products and materials. Endorsement by *Science* or AAAS of any products or materials mentioned is not implied. Additional information may be obtained from the manufacturer or supplier.

INTRODUCING

AAAS **Member**Central

The exclusive new website for the AAAS member community.

AAAS MemberCentral is a new website focused on helping you — the scientists, engineers, educators, students, policymakers, and concerned citizens who make up the AAAS community — connect like never before.

On MemberCentral you can contribute to discussion groups or blogs, participate in a webinar, or share photos of your field research. You can exchange ideas, learn about your fellow members, and gain fresh insights into issues that matter to you the most. MemberCentral is also an easy access point for a wide variety of other AAAS membership benefits, like discounts on cars and books, travel opportunities, and more.

Experience MemberCentral for yourself. Visit MemberCentral.aaas.org today and log in using your *Science* online username and password.

AAAS

MemberCentral.aaas.org

Efficiency Expert.

3500 Series Genetic Analyzer

Every lab needs one.

Are you that type? Always looking for ways to simplify and streamline lab processes—like, for example, the cumbersome and imprecise chores of handling and tracking consumables? Well, with a revolutionary new suite pre-formulated, ready-to-use, RFID-trackable consumables, the 3500 Series Genetic Analyzer *is* that type, too. Just snap in and run.

Make it Yours.

Easy-to-Use Consumables

Control at Your Fingertips

Quality-Assured Data

www.appliedbiosystems.com/3500Series

applied biosystems™
by life technologies™